Structures and Internal Dynamics of Cyclic Molecules Studied by Microwave Spectroscopy and Quantum Chemistry

Von der Fakultät für Mathematik, Informatik und Naturwissenschaften der RWTH Aachen University zur Erlangung des akademischen Grades eines Doktors der Naturwissenschaften genehmigte Dissertation

vorgelegt von

Vinh Van M. Sc.

aus Boppard

Berichter: Universitätsprofessor Dr. rer. nat. Wolfgang Stahl

Universitätsprofessor Dr. rer. nat. Arne Lüchow

Tag der mündlichen Prüfung: 07.03.2017

This work is dedicated to my parents and Janine George.

The work of this thesis has been prepared in the time between November 2013 and November 2016 in the group of Prof. Dr. Wolfgang Stahl at the Institute of Physical Chemistry of the RWTH Aachen University. Some of the presented results are already published. Parts of the work were financially supported by the Fonds der Chemischen Industrie (FCI) and by the RWTH Start-up.

Summary

In the first part of this thesis, conformational analyses of four odorant molecules with non-planar five-membered ring systems were realized using a combination of quantum chemical calculations and microwave spectroscopy. The gas phase structures of odorant molecules are the basis to understand the structure-odor relationship since the sense of smell starts from gas phase molecules. The knowledge of aromas is important to understand the sense of smelling and to create new flavors. The class of five-membered non-planar rings was chosen because its conformational landscape has two different types of stable geometries, the *twist* and the *envelope* structure.

Two different conformers and one ^{34}S-isotopologue were assigned for the molecule 2-methyltetrahydrothiophene, which is a natural flavor compound found in wine and brandy. The molecule 2-methyltetrahydrofuran is an eco-friendly solvent and biofuel component as well as a natural flavor molecule in fish sauce and earth almond. Here, its experimental heavy atom positions of its most stable conformer were determined using isotopic substitution. The molecule 2-methyl-1,3-dithiolane can be found in the roasting aroma of meat and peanut oil. Coffee furanone (2-methyltetrahydrofuran-3-one) is an important volatile compound of the coffee aroma and also a natural flavor in tomato and pork. For these two molecules, the most stable conformer was assigned and compared with quantum chemical calculations.

First, sulfur-containing molecules mostly have different olfactory properties compared to their oxygen analogons. Second, functional groups might have different influence on the ring structure. Therefore, the structures of the studied odorant molecules were compared together with 2-methyltetrahydrothiophen-3-one, 2-methylcyclopentanone, and methylcyclopentane using Cremer-Pople parameters. Stable *twist* conformers with similar geometries and olfactory properties were found for 2-methyltetrahydrothiophen-3-one and its related molecules coffee furanone and 2-methylcyclopentanone. On the other hand, stable *envelope* conformers only exist for 2-methyltetrahydrofuran, 2-methyl-1,3-dithiolane, and methylcyclopentane. Finally, most of the calculated transition states have (near-)*envelope* geometries.

In the second part of this thesis, the effect of multiple internal rotations in the class of planar five-membered ring systems was investigated. Microwave spectroscopy is an outstanding tool to study this effect due to its high resolution and extremely high accuracy. The intramolecular dynamics and couplings of internal rotation obtained by microwave spectroscopy are much more accurate than the chemical accuracy of modern quantum chemistry. Therefore, these experimental results can be used for benchmarks. The knowledge of these large amplitude motions is essential in astrophysics to identify new molecules in the interstellar medium. The results can also be used in atmospheric chemistry as references.

The investigated series of seven molecules starts with molecules with two equivalent methyl rotors – 2,5-dimethylthiophene and 2,5-dimethylfuran. Similar torsional barriers like in the monomethyl derivatives 2-methylthiophene and 2-methylfuran were found. Crowded spectra were investigated in the molecule 2-acetyl-5-methylfuran. In this molecule, two conformers with two inequivalent methyl rotors were assigned. A dramatic change of one barrier purely due to steric effects of the different conformers was determined. The molecule 4,5-dimethylthiazole was chosen to study the effect of coupled large amplitude motions on the torsional barrier. Together with first results on 2,4-dimethylthiazole, it could be verified that the coupling of internal rotations reduced drastically the torsional barriers. Additionally, the hyperfine structures due to quadrupole coupling were assigned. The molecule 1,2,5-trimethylpyrrole has three internal rotations and quadrupole coupling. Due to the electronic effects, the barriers of the two equivalent methyl groups are twice as high as calculated for 2,5-dimethylpyrrole. On the other hand, the barrier of the N-methyl group has a value below 10 cm^{-1}, which is smaller than the one of N-methylpyrrole.

Finally, the rotational spectra of the first, to the best of my knowledge, molecule with four internal rotations – 2,3,4,5-tetramethylthiophene – was studied and assigned. Here, the spectra were highly crowded due to 25 torsional species and unusual barriers were determined. However, these barriers could be verified by the results of the other studied molecules with internal rotations.

Zusammenfassung

Im ersten Teil dieser Arbeit wurden Konformationsanalysen von vier Duftstoffmolekülen mit nicht-planaren Fünfringsystemen durchgeführt, indem eine Kombination aus quantenchemischen Berechnungen und Mikrowellenspektroskopie verwendet wurde. Die Gasphasenstrukturen von Duftstoffen sind wichtig, um ein Verständnis der Struktur-Duft-Beziehung zu erhalten, da die Geruchswahrnehmung mit Molekülen in der Gasphase beginnt. Die Kenntnis der Aromen ist eine Grundlage um den Geruchssinn zu verstehen und neue Düfte zu kreieren. Die Klasse der nicht-planaren Fünfringe wurde gewählt, da ihr Konformationsraum zwei verschiedene Typen von stabilen Konformeren bietet – die *Twist*- und *Envelope*-Geometrie.

Zwei Konformere und ein ^{34}S-Isotopolog des Moleküls 2-Methyltetrahydrothiophens, das ein Naturduftstoff in Wein und Brandy ist, wurden zugeordnet. Das Sauerstoffanalogon 2-Methyltetrahydrofuran ist sowohl ein umweltfreundliches Lösungsmittel und eine Biotreibstoffkomponente als auch ein natürlicher Duftstoff in Fischsauce und in der Tigernuss. In dieser Arbeit wurden die experimentellen Atompositionen in der Schweratom-Mikrowellenstruktur des stabilsten Konformers mittels Isotopensubstitution bestimmt. Das Molekül 2-Methyl-1,3-dithiolan kann in den Röstaromen von Fleisch und Erdnussöl gefunden werden. Kaffee-Furanon (2-Methyltetrahydrofuran-3-on) ist eine wichtige flüchtige Komponente des Kaffeearomas und auch ein Duftstoff in Tomaten und Schweinefleisch. Bei diesen beiden Molekülen wurde das jeweils stabilste Konformer identifiziert und mit quantenchemischen Ergebnissen verglichen.

Schwefelhaltige Moleküle haben meistens andere olfaktorische Eigenschaften (Geruchseigenschaften) als ihre Sauerstoffanalogen. Des Weiteren können funktionelle Gruppen verschiedene Einflüsse auf die Ringstruktur haben. Deshalb wurden die Strukturen der untersuchten Duftstoffmoleküle mit 2-Methyltetrahydrothiophen-3-on, 2-Methylcyclopentanon und Methylcyclopentan verglichen, indem die Cremer-Pople Parameter verwendet wurden. Hierbei wurden stabile *Twist*-Konformere mit ähnlicher Struktur und olfaktorischen Eigenschaften für 2-Methyltetrahydrothiophen-3-on, Kaffee-Furanon und 2-Methylcyclopentanon gefunden. Andererseits existieren stabile *Envelope*-Konformere nur für 2-Methyltetrahydrofuran, 2-Methyl-1,3-dithiolan und Methylcyclopentan. Auch zeigen die meisten simulierten Übergangsstrukturen (nahezu) *Envelope*-Strukturen.

Der zweite Teil dieser Arbeit beschäftigt sich mit den Effekten von multiplen internen Rotationen für die Molekülklasse der planaren Fünfringsysteme. Mikrowellenspektroskopie ist wegen seiner sehr hohen Auflösung und Genauigkeit ein exzellentes Werkzeug, um diesen Effekt zu untersuchen. Die mittels Mikrowellenspektroskopie bestimmten intramolekularen Dynamiken und Kopplungen in Form von interner Rotation sind genauer als die aktuelle chemische Genauigkeit von modernen quantenchemischen

Berechnungen. Daher können diese Ergebnisse als Benchmark verwendet werden. Das Wissen über diese großamplitudigen Bewegungen ist essentiell im Bereich der Astrophysik für die Entdeckung neuer Moleküle im interstellaren Raum. Weiter können die Ergebnisse auch in der Atmosphärenchemie als Referenzen herangezogen werden.

Die untersuchte Serie, bestehend aus 7 Molekülen, startet mit den Molekülen 2,5-Dimethylthiophen und 2,5-Dimethylfuran mit jeweils zwei äquivalenten Methylrotoren. Hier wurden ähnliche Torsionsbarrieren wie in den Monomethyl-Derivaten 2-Methylthiophen und 2-Methylfuran gefunden. Dichte Rotationsspektren wurden im Molekül 2-Acetyl-5-methylfuran beobachtet und zwei Konformere mit jeweils zwei inäquivalenten Methylrotoren wurden identifiziert. Hier wurde festgestellt, dass beide Konformere sich stark in einer Torsionsbarriere unterscheiden. Dies lässt sich allein durch sterische Effekte erklären. Das Molekül 4,5-Dimethylthiazol wurde ausgewählt, um den Einfluss von gekoppelten internen Rotationen auf die Torsionsbarriere zu untersuchen. Zusammen mit den ersten Ergebnissen für 2,4-Dimethylthiazol konnte bestätigt werden, dass die Kopplung zu einer drastischen Reduktion der Barrieren führt. Zusätzlich wurden die Hyperfeinstrukturen durch Quadrupolkopplung aufgeklärt. Drei interne Rotationen mit zusätzlicher Quadrupolkopplung wurden im Molekül 1,2,5-Trimethylpyrrol untersucht. Die Torsionsbarrieren für die zwei äquivalenten Methylrotoren sind wegen elektronischen Effekten doppelt so groß wie die, die für 2,5-Dimethylpyrrol berechnet wurden. Andererseits ist hier die Barriere des N-Methylrotors mit weniger als 10 cm^{-1} kleiner als im Molekül N-Methylpyrrol.

Zum Abschluss wurde das nach bestem Wissen erste jemals untersuchte Molekül mit vier internen Methylrotoren – 2,3,4,5-Tetramethylthiophen – gemessen und zugeordnet. Sehr dichte Rotationsspektren aufgrund der vielen Torsionsspezien wurden beobachtet und ungewöhnliche Barrieren wurden hier bestimmt. Diese Barrieren konnten aber durch die hier untersuchte Molekülserie erklärt werden.

Acknowledgements

I am very grateful to Prof. Dr. Wolfgang Stahl for the opportunity to write my thesis under his guidance and for the accomplishment of a familiar atmosphere in his group. I would like to thank him for his contagious passion for microwave spectroscopy and the given scientific freedom to let me choose my research projects and also the way of their realization.

I would like to thank Dr. Ha Vinh Lam Nguyen for constructive advice and her endless support in improving articles. I am also very thankful to her for giving me the opportunity to visit several laboratories in foreign countries such as the National Institute of Standards and Technology (NIST), USA, the synchrotron Soleil, France, and the Laboratoire Interuniversitaire des Systèmes Atmosphériques (LISA), France.

Many thanks to Arne Philipps for the synthesis of 2,3,4,5-tetramethylthiophene and the opportunity to study the first molecule with four internal rotors in microwave spectroscopy.

Without my colleagues Raphaela Kannengießer, Dr. Lilian Wijaya Sutikdja, Dr. Halima Mouhib, Lynn Ferres, and Konrad Eibl, the office and the laboratory would not have felt like a big family. I thank Atef Jabri and Isabelle Kleiner for successful collaborations. Also, I would like to thank Daniela Lucht for her support in administration.

I also thank Prof. Dr. Arne Lüchow for his assistance as co-adviser of this dissertation and all members of his group, expecially Kaveh Haghighi Mood and Christoph Schulte, for their advice in quantum chemistry.

I would like to thank the Fonds der Chemischen Industrie (FCI) for a doctoral scholarship and the financial support which had also allowed me to visit a summer school and several conferences. I also acknowledge the Jülich Aachen Research Alliance (JARA) and the IT center of the RWTH Aachen University in cooperation with the FZ Jülich for the computing resources in the project JARA0124.

Finally, I would particularly like to thank my parents for their never ending encouragement and for their many sacrifices allowing me go to an university in spite of their own hard times in life. I thank Janine George for always supporting and motivating me.

During this thesis, I supervised several students' research projects and bachelor theses. I would like to thank all these students for their help.

- Students' research projects: Laura Hoppe Alvarez and Jonas Bruckhuisen
- Bachelor theses: Christina Dindic, Judith Schütt, and Chu Suchiao

Supervised students' projects used in this thesis

Some of the following projects were used in this thesis:

- Laura Hoppe Alvarez,
  "Internal Rotation and Quadrupole Coupling in 2,4-Dimethylthiazole"
  (Students' research project, September 2016)
- Jonas Bruckhuisen,
  "Microwave Spectroscopic and Quantum Chemical Investigations on 2,5-Dimethylfuran"
  (Students' research project, June 2016)
- Christina Dindic,
  "Quantum Chemical and Microwave Spectroscopic Studies on 2-Methyltetrahydrothiophene"
  (Bachelor thesis, July 2014)
- Judith Schütt,
  "Microwave Spectroscopic and Quantum Chemical Investigations
  on Dimethylcyclopropane-1,1-dicarboxylate"
  (Bachelor thesis, July 2015)

Parts of this thesis used for conference contributions

Some of the results were already presented at international conferences:

30.08 – 03.09.16 **V. Van**, W. Stahl, and H.V.L. Nguyen
Josef Plíva Prize Talk: *Coupled Internal Rotations in Five-Membered Rings*
PRAHA 2016 – The 24th International Conference on High Resolution
Molecular Spectroscopy in Prague, Czech Republic

20. – 24.07.16 **V. Van**, W. Stahl, and H.V.L. Nguyen
Two Equivalent Methyl Internal Rotations in 2,5-Dimethylthiophene
Investigated by Microwave Spectroscopy
ISMS 2016 – The 71th International Symposium on Molecular Spectroscopy
in Urbana-Champaign, USA

24. – 28.08.15 **V. Van**, W. Stahl, and H.V.L. Nguyen
The Internal Rotation of Four Methyl Groups in Tetramethylthiophene
HRMS 2015 – The 24th Colloquium on High Resolution
Molecular Spectroscopy in Dijon, France

22. – 26.06.15 **V. Van**, W. Stahl, and H.V.L. Nguyen
Conformational Transformation of Five-Membered Rings:
The Gas Phase Structures of 2-Methyltetrahydrofuran
ISMS 2015 – The 70th International Symposium on Molecular Spectroscopy
in Urbana-Champaign, USA

27.11.14 **V. Van**, W. Stahl, and H.V.L. Nguyen
Conformational Transformation of Five-Membered Rings:
The Gas Phase Structures of 2-Methyltetrahydrothiophene and 2-Methyltetrahydrofuran
5th Scientific Meeting Aachen–Namur in Namur, Belgium

02. – 06.09.14 **V. Van**, H.V.L. Nguyen, and W. Stahl
Gas Phase Structures of 2-Methyltetrahydrothiophene
Investigated by Rotational Spectroscopy
BOLOGNA 2014 – The 23rd International Conference on High Resolution
Molecular Spectroscopy in Bologna, Italy

Parts of this thesis used for publications

Some of the results are already published in:

(4) **V. Van**, W. Stahl, and H.V.L. Nguyen
The structure and torsional dynamics of two methyl groups in 2-acetyl-5-methylfuran as observed by microwave spectroscopy
ChemPhysChem **17**, 3223 – 3228 (2016). DOI: 10.1002/cphc.201600757

(3) **V. Van**, W. Stahl, and H.V.L. Nguyen
The heavy atom microwave structure of 2-methyltetrahydrofuran
J. Mol. Struc., **1123**, 24 – 29 (2016). DOI: 10.1016/j.molstruc.2016.05.078

(2) **V. Van**, W. Stahl, and H.V.L. Nguyen
Two equivalent methyl internal rotations in 2,5-dimethylthiophene investigated by microwave spectroscopy
Phys. Chem. Chem. Phys. **17**, 32111 – 32114 (2015). DOI: 10.1039/c5cp03513a
Inside front cover *Phys. Chem. Chem. Phys.* **48/2015**. DOI: 10.1039/C5CP90220G

(1) **V. Van**, C. Dindic, H.V.L. Nguyen, and W. Stahl
Conformational Transformations of Sulfur-Containing Rings: 2-Methyltetrahydrothiophene Gas-Phase Structures
ChemPhysChem **16**, 291 – 294 (2015). DOI: 10.1002/cphc.201402727
Front cover *ChemPhysChem* **2/2015** DOI: 10.1002/cphc.201590006
Cover profile *ChemPhysChem* **2/2015** DOI: 10.1002/cphc.201402895

Other publications

(5) A. Jabri, **V. Van**, H.V.L. Nguyen, W. Stahl, and I. Kleiner
Probing the Methyl Torsional Barriers of the *E* and *Z* Isomers of Butadienyl Acetate by Microwave Spectroscopy
ChemPhysChem **17**, 2660 – 2665 (2016). DOI: 10.1002/cphc.201600265

(4) A. Jabri, **V. Van**, H. V. L. Nguyen, H. Mouhib, F. Kwabia Tchana, L. Manceron, W. Stahl, and I. Kleiner
Laboratory microwave, millimeter wave and far-infrared spectra of dimethyl sulfide
A&A **589**, A127 (2016). DOI: 10.1051/0004-6361/201628074

(3) H.V.L. Nguyen, A. Jabri, **V. Van**, and W. Stahl
Methyl Internal Rotation in the Microwave Spectrum of Vinyl Acetate
J. Phys. Chem. A **118**, 12130 – 12136 (2014). DOI: 10.1021/jp5075829

(2) H.V.L. Nguyen, **V. Van**, W. Stahl, and I. Kleiner
The effects of two internal rotations in the microwave spectrum of ethyl methyl ketone
J. Chem. Phys. **140**, 214303 (2014). DOI: 10.1063/1.4878412

(1) H. Mouhib, **V. Van** and W. Stahl
Sulfur-Containing Flavors: Gas Phase Structures of Dihydro-2-methyl-3-thiophenone
J. Phys. Chem. A **117**, 6652 – 6656 (2013). DOI: 10.1021/jp4041748

Contents

CHAPTER 1

Introduction

Microwave spectroscopy explores the molecular structure and dynamics of isolated molecules or complexes in the gas phase. Over the past years, it has helped to obtain new insights in the fields of astronomy and nuclear physics since Fourier transform microwave spectroscopy has an unrivalled resolution and precision. The investigations of complexes like water clusters allow to study the nature and cooperativity of hydrogen bonds and to understand the process of solvation. [1] The high sensitivity of this type of rotational spectroscopy enables to detect isotopologues in their natural abundance like ^{18}O with 0.2% and to determine absolute atom positions of molecules in the gas phase. Large amplitude motions such as inversion tunneling and internal rotation can be precisely determined due to their characteristic pattern in the observed spectrum. Also magnetic and electric interactions like nuclear quadrupole coupling can be investigated to determine the nature of chemical bonds and the electronic environment in the molecule. [2]

The purposes of this dissertation can be divided into two goals:

A. Structure Determination of Non-Planar Ring Molecules

The first purpose is to explore the structure of odorant molecules with non-planar five-membered ring systems since the sense of smell starts from gas phase molecules. To get a better understanding of the structure-odor relationship, the class of five-membered non-planar rings was chosen since its conformational landscape has only two different types of stable geometries, the *twist* and the *envelope* structure (see Chapter 4). Usually, sulfur-containing molecules like mercaptans (R-SH) and thioethers (R-S-R') are mostly intensely bad-smelling compared to their oxygen analogons. In order to understand and explain this phenomenon in more details, it is important to answer the questions, how molecular shapes of the odorant molecules and the receptor fit together or how strong their interaction via hydrogen bonds are. For this purpose, gas phase structures of sulfur- and oxygen-containing odorants are needed. The molecules studied in this thesis are shown in Figure 1.1 together with 2-methyltetrahydrothiophen-3-one (**1**) [3], which can be found in coffee, whiskey, wine [4] and roasted peanuts [5].

Some of these volatile heterocyclic flavor substances can be found in the Maillard reaction which is known to create roasting aromas when food is browned. [6, 7] The knowledge of composition of these aromas is important to understand the aroma production during food cooking and to create new fla-

vors. 2-Methyltetrahydrothiophene (**2**) is a natural flavor compound found in wine [8] and brandy [9]. This molecule is also a volatile product after thermal degradation of vitamin B_1, which provides a better understanding of the progress of nutrient loss. [10] 2-Methyltetrahydrofuran (**3**) is in the principles of Green Chemistry an eco-friendly solvent and biofuel component, which is derived from renewable resources. [11] Additionally, it is a natural flavor molecule in fish sauce [12] and earth almond [13]. 2-Methyl-1,3-dithiolane (**4**) is a volatile sulfur-containing flavor substance and can be found in the roasting aroma of meat [14] and peanut oil [15]. 2-Methyltetrahydrofuran-3-one (**5**) is also called coffee furanone and is an important volatile compound of the complex coffee aroma. [16, 17] It can also be found as natural flavor in tomato [18] and pork [19]. The investigated odorant molecules are compared to other odorant molecules of the same class.

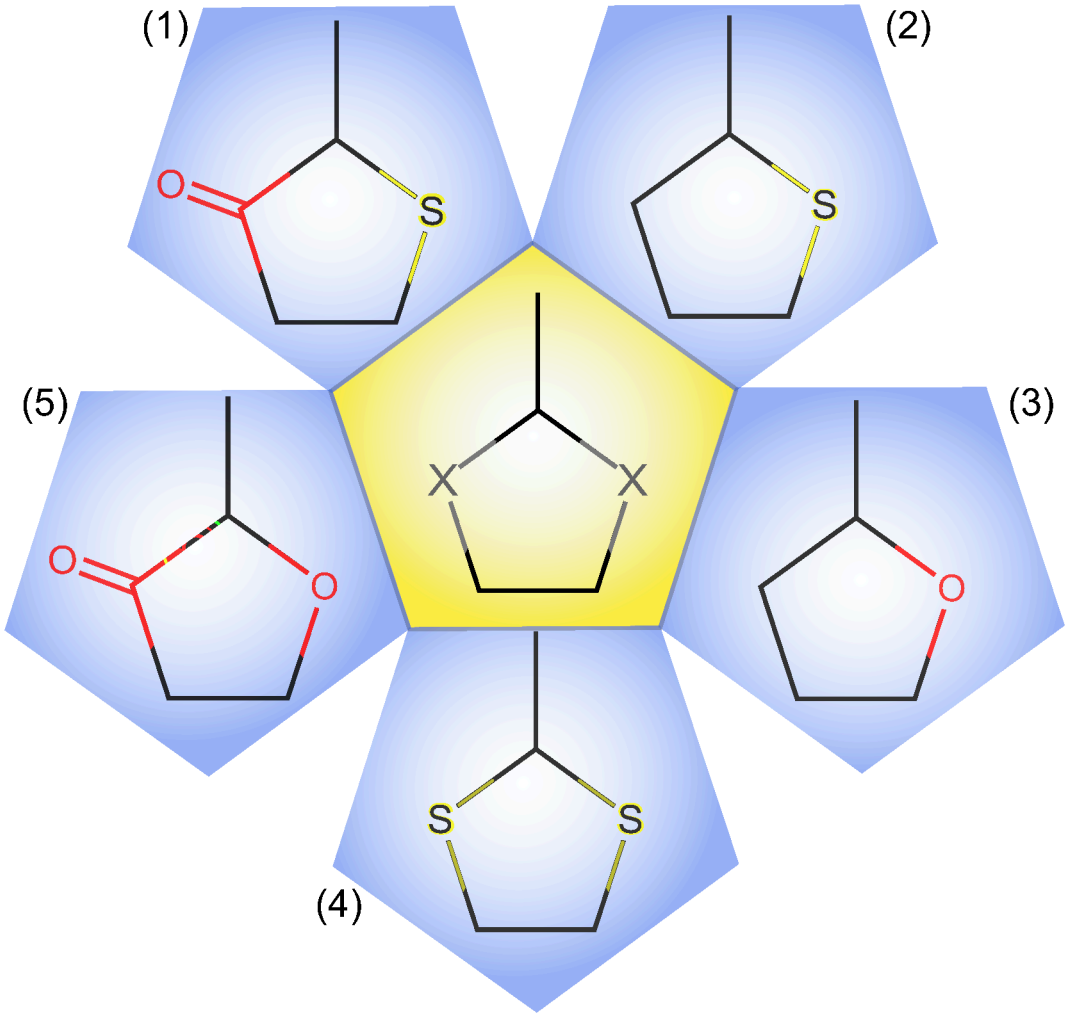

Figure 1.1. Odorant molecules with non-planar five-membered heterocyclic compounds. 2-Methyltetrahydrothiophen-3-one (**1**) [3], 2-methyltetrahydrothiophene (**2**), 2-methyltetrahydrofuran (**3**), 2-methyl-1,3-dithiolane (**4**), and coffee furanone (2-methyltetrahydrofuran-3-one, **5**).

B. Multiple Internal Rotations of Methyl Groups in Planar Ring Systems

The second purpose is to investigate the effect of multiple internal rotations in the class of planar five-membered ring systems as shown in Figure 1.2. Microwave spectroscopy is an outstanding tool to study this effect due to its high resolution and extremely high accuracy. Since torsional barriers are small (0.1 – 10 kJ·mol^{-1}) and experimental results obtained by microwave spectroscopy are much more precise than the chemical accuracy of modern quantum chemistry, they are very important for benchmarks. Especially, it is a big challenge for quantum chemistry when these large amplitude motions are coupled. The knowledge of these intramolecular dynamics is essential in astrophysics to identify new molecules in the interstellar medium.

The goal was to study the rotational spectra of the first, to the best of my knowledge, molecule with four internal rotations – 2,3,4,5-tetramethylthiophene (**6**). For this goal, first the related molecule 2,5-dimethylthiophene (**7**) with two equivalent methyl rotors is investigated. Together with the literature on the monomethyl derivatives 2-methylthiophene [20] and 3-methylthiophene [21], a first hint of the torsional barriers is obtained. Second, crowded spectra with fewer torsional components in the molecule 2-acetyl-5-methyl-furan (**9**) are investigated to verify if it is possible to assign such crowded spectra. Third, the first results on 2,3,4,5-tetramethylthiophene (**6**) suggested one surprising low barrier height. Therefore, the molecule 4,5-dimethylthiazole (**10**) was chosen and studied to verify the effect of coupled large amplitude motions on the torsional barrier. Finally, the molecule 1,2,5-trimethylpyrrole (**11**) with three internal rotations and quadrupole coupling was studied to check the capability of the assignment program to treat complex internal effects. Altogether with this set of studied molecules, the foundation is created to measure and assign the first molecule with four internal rotations.

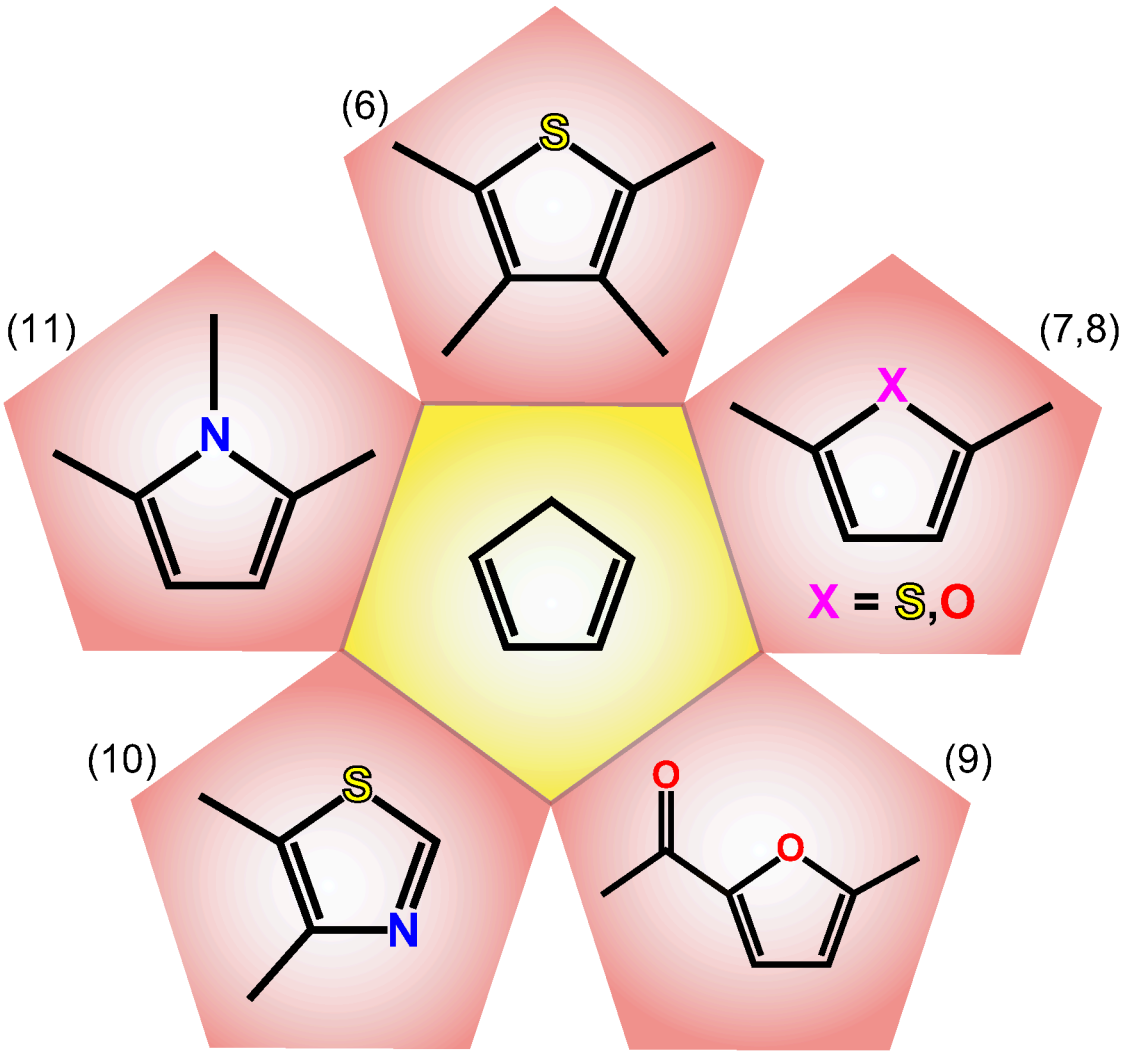

Figure 1.2. Multiple internal rotations in planar five-membered rings. 2,3,4,5-tetramethylthiophene (**6**), 2,5-dimethylthiophene (**7**), 2,5-dimethylfuran (**8**), 2-acetyl-5-methylfuran (**9**), 4,5-dimethylthiazole (**10**), and 1,2,5-trimethylpyrrole (**11**).

CHAPTER 2

Methods

2.1 Experimental methods

The measurements of all microwave spectra throughout this thesis were performed using the **m**olecular **b**eam-**F**ourier **t**ransform **m**icro**w**ave (**MB-FTMW**) technique. The two MB-FTMW spectrometers in Aachen and Paris are working in the frequency ranges 2 to 26.5 GHz and 26.5 to 40.0 GHz, respectively. Details of the spectrometers are described in Refs. [22–24].

Depending on the vapor pressure of the sample, two methods are applied to create a mixture of approx. 1% of the sample in helium as a carrier gas. In the first case, the pipe cleaner method (method A) is used when the vapor pressure is lower than 10 Torr. Here, some drops of the liquid substance were put on a 5 cm piece of a pipe cleaner and placed inside a steel tube close to the nozzle. A helium stream at a pressure of approximately 200 kPa flowed over the substance on the pipe cleaner and the helium-substance mixture was expanded into the cavity.

In the second case for molecules with high vapor pressure ($>$ 10 Torr; method B), the substance was placed in a Schlenk tube, degasified and conveyed into a gas container. In the next step, the container was filled with helium until a mixture of approx. 1% of the sample in helium and 1.5 bar was obtained.

All molecules except 2,3,4,5-tetramethylthiophene were commmercially purchased from Alfa Aesar GmbH & Co KG, Karlsruhe, Germany, TCI Deutschland GmbH, Eschborn, Germany, or Sigma Aldrich Chemie GmbH, Munich, Germany. The molecules are listed in Table 2.1. Since the stated purity was over 95% for all purchased molecules, the samples were used without further purification. The sample of 2,3,4,5-tetramethylthiophene was synthesized by Arne R. Philipps, Institute of Organic Chemistry, RWTH Aachen University.

At the beginning of the investigations, broadband scans were recorded in the frequency range of several GHz for an overview of the rotational spectra. Here, every 250 kHz overlapping spectra were recorded automatically with the same numbers of repetitions. In the next step, each observed rotational transition was remeasured in the high resolution mode with a number of repetitions depending on the signal-to-noise ratio.

Table 2.1. Investigated molecules and their properties.

molecule[a]	supplier	purity	method[b]	vapor pressure[c]	CAS
MTTP	TCI	$\geq 98\%$	A	10.9 Torr	1795-09-1
MTHF	Alfa Aesar	$\geq 99\%$[e]	B	96.8 Torr	96-47-9
MDT	Alfa Aesar	$\geq 99\%$	A	1.58 Torr	5616-51-3
COFFEE	TCI	$\geq 98\%$	A	6.56 Torr	3188-00-9
DMTP	Alfa Aesar	$\geq 98\%$	A	8.98 Torr	638-02-8
DMF	Alfa Aesar	$\geq 98\%$	B	57.1 Torr	625-86-5
AMF	TCI	$\geq 97\%$	A	0.301 Torr	1193-79-9
DMTA	TCI	$\geq 97\%$	A	3.46 Torr	3581-91-7
TMP	TCI	$\geq 98\%$	A	1.73 Torr	930-87-0
TMTP	synthesized[d]		A	0.501 Torr	14503-51-6
CPC	TCI	$\geq 98\%$	A	2.73 Torr	6914-71-2

[a]abbreviations: 2-methyltetrahydrothiophene (MTTP); 2-methyltetrahydrofuran (MTHF); 2-methyl-1,3-dithiolane (MDT); 2-methyltetrahydrofuran-3-one (coffee furanone) (COFFEE); 2,5-dimethylthiophene (DMTP); 2,5-dimethylfuran (DMF); 2-acetyl-5-methylfuran (AMF); 4,5-dimethylthiazole (DMTA); 1,2,5-trimethylpyrrole (TMP); 2,3,4,5-tetramethylthiophene (TMTP); dimethylcyclopropane-1,1-dicarboxylate (CPC).[b] method A: pipe cleaner; method B: gas container. [c] predicted values at a temperature of 25°C as given by SciFinder [25], [d] synthesized by Arne R. Philipps, Institute of Organic Chemistry, RWTH Aachen University, [e] stabilized with 150 – 400 ppm BHT (butylated hydroxytoluene).

2.2 Quantum chemical calculations

The GAUSSIAN09 package [26] was used for the quantum chemical part in this thesis. For the conformational analysis, all possible starting geometries were created and optimized at the MP2/6-311++G(d,p) level of theory. This level was chosen, since the yielded rotational constants are in good agreement to the experimental values for other heterocyclic molecules [27].

In the next step, geometry optimizations were performed at various levels of theory using the methods HF, MP2, B3LYP, M06-2X, and CCSD in combination with different basis sets to check for convergence of the obtained geometries. Harmonic frequency calculations at the same level of theory were carried out to verify, whether the optimized geometries are true minima or saddle points. Using the Berny algorithm [28], first order transition states of non-planar rings were optimized to understand the intramolecular conversion of these molecules.

Potential energy curves were calculated at various levels of theory by varying the dihedral angle of the internal rotor, while all other geometry parameters were optimized. By parameterization of the corresponding energies using a one-dimensional Fourier expansion, the contributions of V_3 and higher order terms could be recognized. This approach gave a first hint of the barrier height due to internal rotation. Using the geometries with the highest energy in the potential energy curves, transition states of the internal rotation were optimized with the Berny algorithm [28] to calculate the barrier heights due to internal rotation more precisely. Two-dimensional potential energy surfaces (PESs) were calculated to determine the conformational landscape or to study the coupling between two methyl groups.

When possible, anharmonic frequency calculations were performed to obtain the centrifugal distortion constants and the rotational constants B_0 of the vibrational ground state. The specific quantum chemical calculations for a given molecule are described separately in each chapter.

These simulations were performed with computing resources from the IT center of the RWTH Aachen University in cooperation with the FZ Jülich granted by the JARA-HPC under the project jara0124.

CHAPTER 3

Theory

Microwave spectroscopy studies the geometrical structure and dynamics of molecules in the gas phase. Here, electromagnetic radiation in the frequency range of 1 GHz to 1000 GHz is used to observe rotational transitions. The frequency to excite a rotational transition corresponds to the energy between two energy levels. These rotational energy levels depend on the geometry of the molecule. In the next section, a introduction of the rotation of a rigid body is given. Here, three principal moments of inertia are sufficient to completely determine its rotational energy levels. However, this model needs to be extended for many molecules due to additional effects like centrifugal distortion, large amplitude motions, and quadrupole coupling. These effects can lead to shifts of the frequency and additional splittings in the rotational spectra. In the case of ^{14}N quadrupole coupling, the hyperfine structure has small splittings of a few kHz, while, on the other hands, low torsional barriers due to internal rotation can lead to splittings in the range of several GHz. One purpose of this dissertation is to explore the effects of multiple large amplitude motions in the form of coupled internal rotations. Therefore, the effect of internal rotations is shortly described in Section 3.2 and compared to a rigid molecule. In the last section, the structure determination using isotopic substitution is explained.

3.1 Asymmetric top molecules

In classical mechanic, the vector of the angular momentum $\vec{P}$ [29] of a rigid molecule is described as

$$\vec{P} = I \cdot \vec{\omega}. \tag{3.1}$$

Here, $\vec{\omega}$ is the vector of the angular velocity

$$\vec{\omega} = \begin{pmatrix} \omega_x \\ \omega_y \\ \omega_z \end{pmatrix} \tag{3.2}$$

and I is the moment of inertia tensor

$$I = \begin{pmatrix} I_{xx} & I_{xy} & I_{xz} \\ I_{yx} & I_{yy} & I_{yz} \\ I_{zx} & I_{zy} & I_{zz} \end{pmatrix}. \tag{3.3}$$

The off-diagonal elements of this tensor are defined as

$$I_{\alpha\beta} = -\sum_{i=1}^{n} m_i \cdot \alpha_i \cdot \beta_i,$$

while the diagonal elements can be written as

$$I_{xx} = \sum_{i=1}^{n} m_i(y_i^2 + z_i^2),\ I_{yy} = \sum_{i=1}^{n} m_i(x_i^2 + z_i^2), \text{ and } I_{zz} = \sum_{i=1}^{n} m_i(x_i^2 + y_i^2)$$

with n as the number of particles, m_i as the mass of a particle i, and x_i, y_i, and z_i as its coordinates relative to a Cartesian coordinate system with the center of mass as the origin. In this coordinate system the kinetic energy of translation and of rotation can be separated. The kinetic energy of rotation is described by

$$T = \frac{1}{2}\vec{\omega}^{\intercal} \cdot I \cdot \vec{\omega} = \frac{1}{2}\vec{P}^{\intercal} \cdot I^{-1} \cdot \vec{P} \tag{3.4}$$

with the transposed vectors $\vec{\omega}^{\intercal}$ and $\vec{P}^{\intercal}$.

$$\vec{\omega}^{\intercal} = \begin{pmatrix} \omega_x & \omega_y & \omega_z \end{pmatrix}$$

The Cartesian coordinate system can be transformed into a principal axis system. Here, the off-diagonal elements vanish (see Equation 3.5). The diagonal elements are called principal moments of inertia.

$$I = \begin{pmatrix} I_a & 0 & 0 \\ 0 & I_b & 0 \\ 0 & 0 & I_c \end{pmatrix} \tag{3.5}$$

The advantage of the principal axis system is the simplicity to invert the moment of inertia tensor I:

$$I^{-1} = \begin{pmatrix} \frac{1}{I_a} & 0 & 0 \\ 0 & \frac{1}{I_b} & 0 \\ 0 & 0 & \frac{1}{I_c} \end{pmatrix}. \tag{3.6}$$

The rotational constants are defined as $A = \frac{h}{8\pi^2 I_a}$, $B = \frac{h}{8\pi^2 I_b}$, and $C = \frac{h}{8\pi^2 I_c}$ with the convention $I_a \leq I_b \leq I_c$. The general Hamiltonian H of an asymmetric molecule is:

$$H = \frac{P_a^2}{2I_a} + \frac{P_b^2}{2I_b} + \frac{P_c^2}{2I_c} \tag{3.7}$$

with P_a, P_b, and P_c as the angular moment operators in the principal axes a, b, and c.

3.2 Internal rotation

The effect of large amplitude motion in the form of internal rotation is described shortly in this section and is also compared to a rigid molecule. More detailed information can be found in the article "Mikrowellenspektroskopische Bestimmung von Rotationsbarrieren freier Moleküle" by H. Dreizler [30]. A summary of the important effects due to internal rotation of this article is given here. Internal rotation is a rotation of a part of the molecule, called top, with respect to the frame of the molecule. Here, only the internal rotation of methyl groups as tops are considered. This kind of large amplitude motion leads to splittings which depend on the barrier heights of the internal rotation. When internal rotation is observable, the dimensions of the angular velocity vector $\vec{\omega}$ and the moment of inertia tensor I increase by one per internal rotor. As an example, $\vec{\omega}$ and I are given for two internal rotors n, numbered 1 and 2:

$$\vec{\omega} = \begin{pmatrix} \omega_a \\ \omega_b \\ \omega_c \\ \omega_1 \\ \omega_2 \end{pmatrix} \tag{3.8}$$

and

$$I = \begin{pmatrix} I_a & 0 & 0 & \lambda_{a,1} I_{\alpha,1} & \lambda_{a,2} I_{\alpha,2} \\ 0 & I_b & 0 & \lambda_{b,1} I_{\alpha,1} & \lambda_{b,2} I_{\alpha,2} \\ 0 & 0 & I_c & \lambda_{c,1} I_{\alpha,1} & \lambda_{c,2} I_{\alpha,2} \\ \lambda_{a,1} I_{\alpha,1} & \lambda_{b,1} I_{\alpha,1} & \lambda_{c,1} I_{\alpha,1} & I_{\alpha,1} & 0 \\ \lambda_{a,2} I_{\alpha,2} & \lambda_{b,2} I_{\alpha,2} & \lambda_{c,2} I_{\alpha,2} & 0 & I_{\alpha,2} \end{pmatrix}. \tag{3.9}$$

Here, $\lambda_{i,n} = \cos(\angle(g_n, i))$, $i = a, b, c$ is the direction cosine of the internal rotation axis g_n with respect to the principal axes and $I_{\alpha,n}$ is the moment of inertia of the internal rotor n. While the moment of inertia tensor I for a rigid molecule and the one for a molecule with internal rotation look similar (compare Equation 3.5 and 3.9), the inverse moment of inertia tensors are quite different due to the off-diagonal elements in the moment of inertia tensor I of a molecule with internal rotation:

$$\frac{1}{2} \cdot I^{-1} = \begin{pmatrix} 1/2I_a + Z_{aa} & Z_{ab} & Z_{ac} & -Q_{a,1} & -Q_{a,2} \\ Z_{ba} & 1/2I_b + Z_{bb} & Z_{bc} & -Q_{b,1} & -Q_{b,2} \\ Z_{ca} & Z_{cb} & 1/2I_c + Z_{cc} & -Q_{c,1} & -Q_{c,2} \\ -Q_{a,1} & -Q_{b,1} & -Q_{c,1} & F_1 & F_{12} \\ -Q_{a,2} & -Q_{b,2} & -Q_{c,2} & F_{12} & F_2 \end{pmatrix}. \tag{3.10}$$

The tensor elements of Equation 3.10 are:

$$Z_{ij} = Z_{ji} = \frac{\lambda_{i,1}\lambda_{j,1} I_{\alpha,1}^2}{I_i I_j} \cdot F_1 + \left(\frac{\lambda_{j,1} I_{\alpha,1} \lambda_{i,2} I_{\alpha,2}}{I_i I_j} + \frac{\lambda_{i,1} I_{\alpha,1} \lambda_{j,2} I_{\alpha,2}}{I_i I_j}\right) \cdot F_{12} + \frac{\lambda_{i,2}\lambda_{j,2} I_{\alpha,2}^2}{I_i I_j} \cdot F_2$$

$$Q_{i,1} = \frac{\lambda_{i,1} I_{\alpha,1}}{I_i} \cdot F_1 + \frac{\lambda_{i,2} I_{\alpha,2}}{I_i} \cdot F_{12}$$
$$Q_{i,2} = \frac{\lambda_{i,1} I_{\alpha,1}}{I_i} \cdot F_{12} + \frac{\lambda_{i,2} I_{\alpha,2}}{I_i} \cdot F_2.$$

Using the expression

$$\begin{pmatrix} F_1 & F_{12} \\ F_{12} & F_2 \end{pmatrix} = \frac{1}{2} \cdot \begin{pmatrix} I_{\alpha,1}(1 - \sum_i \frac{\lambda_{i,1}^2 I_{\alpha,1}}{I_i}) & \sum_i \frac{\lambda_{i,1}\lambda_{i,2} I_{\alpha,1} I_{\alpha,2}}{I_i} \\ \sum_i \frac{\lambda_{i,1}\lambda_{i,2} I_{\alpha,1} I_{\alpha,2}}{I_i} & I_{\alpha,2}(1 - \sum_i \frac{\lambda_{i,2}^2 I_{\alpha,2}}{I_i}) \end{pmatrix}^{-1}, \tag{3.11}$$

the remaining tensor elements are obtained as

$$\begin{aligned} F_1 &= \frac{1}{2} \cdot I_{\alpha,2}(1 - \sum_i \frac{\lambda_{i,2}^2 I_{\alpha,2}}{I_i}) \cdot W \\ F_2 &= \frac{1}{2} \cdot I_{\alpha,1}(1 - \sum_i \frac{\lambda_{i,1}^2 I_{\alpha,1}}{I_i}) \cdot W \\ F_{12} &= -\frac{1}{2} \cdot W \cdot \sum_i \frac{\lambda_{i,1} I_{\alpha,1} \lambda_{i,2} I_{\alpha,2}}{I_i} \end{aligned} \tag{3.12}$$

with

$$W = \left[I_{\alpha,1}(1 - \sum_i \frac{\lambda_{i,1}^2 I_{\alpha,1}}{I_i}) \cdot I_{\alpha,2}(1 - \sum_i \frac{\lambda_{i,2}^2 I_{\alpha,2}}{I_i}) - (\sum_i \frac{\lambda_{i,1}\lambda_{i,2} I_{\alpha,1} I_{\alpha,2}}{I_i})^2 \right]^{-1}.$$

Due to the off-diagonal elements in Equation 3.9, the result of the inversion of the moment of inertia tensor I is not a tensor with its inverse elements anymore (compare with Equation 3.6).

First, a distinction has to be made between F_n (Equation 3.12) and $F_{n,0}$ for the internal rotor $n = 1, 2$:

$$F_{n,0} = \frac{1}{2 \cdot I_{\alpha,n}}. \tag{3.13}$$

Second, the rotational constants A, B, and C of a rigid molecule differ from the ones of a molecule with internal rotation. In the last case, the rotational constants change to $A' = \frac{1}{2I_a} + Z_{aa}, B' = \frac{1}{2I_b} + Z_{bb}$, and $C' = \frac{1}{2I_c} + Z_{cc}$. Equation 3.10 can be written as

$$\frac{1}{2} \cdot I^{-1} = \begin{pmatrix} A' & Z_{ab} & Z_{ac} & -Q_{a,1} & -Q_{a,2} \\ Z_{ba} & B' & Z_{bc} & -Q_{b,1} & -Q_{b,2} \\ Z_{ca} & Z_{cb} & C' & -Q_{c,1} & -Q_{c,2} \\ -Q_{a,1} & -Q_{b,1} & -Q_{c,1} & F_1 & F_{12} \\ -Q_{a,2} & -Q_{b,2} & -Q_{c,2} & F_{12} & F_2 \end{pmatrix}. \tag{3.14}$$

The kinetic energy of rotation $T = \frac{1}{2}\vec{P}^{\intercal} \cdot I^{-1} \cdot \vec{P}$ can be written as

$$\begin{aligned} T = &(\frac{P_a^2}{2I_a} + \frac{P_b^2}{2I_b} + \frac{P_c^2}{2I_c}) \\ &+ F_1(p_1 - \Pi_1)^2 + F_2(p_2 - \Pi_2)^2 \\ &+ F_{12}\{(p_1 - \Pi_1)(p_2 - \Pi_2) + (p_2 - \Pi_2)(p_1 - \Pi_1)\} \end{aligned} \tag{3.15}$$

with

$$\Pi_n = \sum_i \frac{\lambda_{i,n} I_{\alpha,n}}{I_i} \cdot P_i.$$

When the internal rotors are methyl groups, the symmetry of a methyl group is assumed to be C_3 with unchanged bond lengths and angles while rotating. The potential of one methyl group has three equivalent minima as shown in Figure 3.1. The barrier height is called V_3 and the potential is approximated as

$$V(\varphi) = \frac{V_3}{2}[1 - \cos(3\varphi)]. \tag{3.16}$$

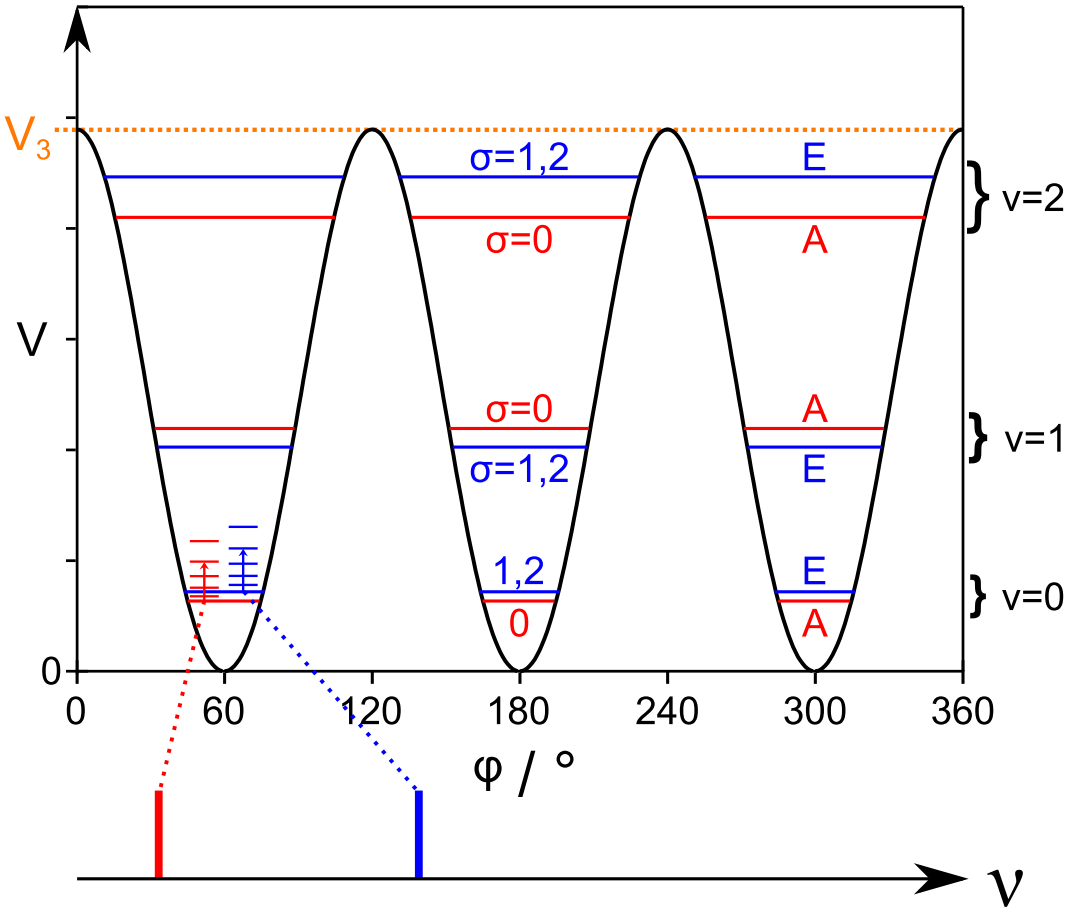

Figure 3.1. V_3 potential curve of a methyl rotor with its schematic rotational-torsional energy diagram. On the left, the rotational energy levels of the A and E species of the torsional level v=0 are given. At the bottom, the spectrum of the two rotational transition of different species is shown. This figure is a modified version from [29].

The barrier height depends mainly on steric and electronic effects and varies in a wide range. The prediction of torsional barriers is still difficult even with state-of-the-art quantum chemical methods because of the small energy differences.

Due to one internal rotor, each torsional energy level with the quantum number v splits into a A and E species. These species have different symmetry and can be represented by the numbers $\sigma = 0, 1, 2$. Here, the planar rotor wave function $e^{i(3k+\sigma)\varphi}$ with $k \in \mathbb{Z}$ and the torsional angle φ has corresponding transformation properties to the A species ($\sigma = 0$) and the doubly degenerated E species ($\sigma = 1, 2$). A transition between the rotational energy levels of these species is forbidden. The rotational transitions of different torsional species have different frequencies due to centrifugal distortion. A splitting of each rotational transition into a doublet for one internal rotor can be observed. In the case of two internal rotors, each rotational transition splits into four torsional species if both rotors are equivalent. Otherwise five torsional species can be observed when the two internal rotors are inequivalent (more details can be found in the Chapters 10 and 12 of the respective molecules).

The Hamiltonian H is the sum of the kinetic energy T and a potential energy term V. The potential energy for two methyl rotors can be estimated as

$$\begin{aligned} V(\varphi_1, \varphi_2) = {} & \frac{V_{3,1}}{2}[1 - \cos(3\varphi_1)] + \frac{V_{3,2}}{2}[1 - \cos(3\varphi_2)] \\ & + V_{cc} \cdot \cos(3\varphi_1)\cos(3\varphi_2) + V_{ss} \cdot \sin(3\varphi_1)\sin(3\varphi_2) \\ & + V_{cs} \cdot \cos(3\varphi_1)\sin(3\varphi_2) + V_{sc} \cdot \sin(3\varphi_1)\cos(3\varphi_2). \end{aligned} \tag{3.17}$$

With this, the Hamiltonian H of an asymmetric molecule with two internal rotations can be described as

$$\begin{aligned} H = {} & A' \cdot P_a^2 + B' \cdot P_b^2 + C' \cdot P_c^2 \\ & + \frac{1}{2} \cdot \sum_{i \neq j} (Z_{ij} + Z_{ji})(P_i \cdot P_j + P_j \cdot P_i) \\ & + F_1 \cdot p_1^2 + \frac{V_{3,1}}{2}[1 - \cos(3\varphi_1)] \\ & + F_2 \cdot p_2^2 + \frac{V_{3,2}}{2}[1 - \cos(3\varphi_2)] \\ & + F_{12}(p_1 \cdot p_2 + p_2 \cdot p_1) \\ & + V_{cc} \cdot \cos(3\varphi_1)\cos(3\varphi_2) + V_{ss} \cdot \sin(3\varphi_1)\sin(3\varphi_2) + \ldots \\ & - 2 \sum_n \sum_i Q_{i,n} \cdot P_i \cdot p_n. \end{aligned} \tag{3.18}$$

The Hamiltonian can be separated into different terms:

$$H = H_R + H_{RR} + H_{T,1} + H_{T,2} + H_{TT} + H_{RT}$$

with $H_R + H_{RR}$ as the Hamiltonian of the overall rotation, $H_{T,1}$ and $H_{T,2}$ as the ones of the internal rotation of the rotor 1 and 2, H_{TT} as the Hamiltonian of the top-top interaction, and H_{RT} as the interaction between the internal rotations and the overall rotation. H_{RR} is an additional term of the overall rotation due to the off-diagonal elements in I^{-1}.

The terms $H_{T,1}$, $H_{T,2}$, and H_{TT} can be separated into a kinetic and a potential part:

$$\begin{aligned} H_{T,n} &= H_{T,n,\text{kin.}} + H_{T,n,\text{pot.}} \\ &= F_n \cdot p_n^2 + \frac{V_{3,n}}{2}[1 - \cos(3\varphi_n)] \\ H_{TT} &= H_{TT,\text{kin.}} + H_{TT,\text{pot.}} \\ &= F_{12}(p_1 \cdot p_2 + p_2 \cdot p_1) \\ &+ V_{cc} \cdot \cos(3\varphi_1)\cos(3\varphi_2) + V_{ss} \cdot \sin(3\varphi_1)\sin(3\varphi_2). \end{aligned}$$

As shown in Equation 3.12 and also for 2,5-dimethylthiophene (Chapter 10), F_{12} depends only on the direction cosines, moments of inertia of the internal rotors, and the principal moments of inertia of the entire molecule. Therefore, only the potential interactions parameters V_{cc} and V_{ss} or higher order terms are free parameters to describe the top-top interaction. However, sometimes F_{12} can be used as an effective parameter since not all potential top-top interaction parameters are available in the program codes to fit rotational spectra as shown for 4,5-dimethylthiazole (Chapter 13).

Inertial defect

The inertial defect can help to determine the barrier heights of internal rotation in planar molecules. For a planar molecule like benzene without any out-of-plane atoms, the relation of its equilibrium moments of inertia I_i^e is

$$I_c^e - I_a^e - I_b^e = 0 \tag{3.19}$$

with the axis c perpendicular to the molecular plane. Due to vibrational effects, this relation is unequal zero, the value is called inertial defect Δ_c [29]:

$$I_c^v - I_a^v - I_b^v = \Delta_c \tag{3.20}$$

with I_i^v as effective moments of inertia. In the case of planar molecules with a methyl group as internal rotor, the inertial defect includes also the out-of-plane hydrogen atoms of this methyl group. Here, Δ_c can give a hint of the torsional barrier of the methyl group for small barriers. The value of $|\Delta_c|$ decreases when the torsional barrier decreases. For high barriers, the value of $|\Delta_c|$ increases and stays the same at the point when its value corresponds to the moment of inertia I_α of a methyl group. Therefore, no hint for the torsional barriers with high hindering potentials can be obtained from the inertial defect.

3.3 Nuclear quadrupole coupling

Some of the molecules in this thesis have a ^{14}N atom. Therefore, this section gives a short introduction to quadrupole coupling. Detailed information can be found in chapter IX of the book "Microwave Molecular Spectra" by W. Gordy and R. L. Cook [29] and are summarized here.

The nuclear quadrupole coupling is an interaction between an electronic field gradient and a nonspherical distribution of a nuclear charge. Only nuclei with a nuclear spin $I \geq 1$ have a nonspherical distribution of its nuclear charge and therefore a nuclear quadrupole moment. An electronic field gradient arises only when the electronic charge is also nonspherical around the nucleus with a nuclear quadrupole moment. The nuclear quadrupole coupling forces the nuclear spin axis to precess because it tends to align the nuclear spin in the same direction as the electric field gradient.

In a microwave spectrum, the nuclear quadrupole coupling causes splittings which are called hyperfine structure. These hyperfine structures depend on the rotational state and contain experimental determinable information about the electronic environment of the nuclei with a quadrupole moment.

The electric energy in classical electrostatics is described as

$$E = \int \rho_n V d\tau_n \tag{3.21}$$

with ρ_n as the density of the nuclear charge, the static potential V, and the volume element $d\tau_n = dXdYdZ$. When V is expressed as a Taylor expansion, the electric energy can be written as a sum of terms with monopole, dipole, quadrupole interactions and higher order interactions (page 394 of [29]):

$$\begin{aligned}
E &= E_{monopole} + E_{dipole} + E_{quadrupole} + \ldots \\
&= V_0 \int \rho_n d\tau_n \\
&+ \left(\frac{\partial V}{\partial X}\right)_0 \int X_n \rho_n d\tau_n + \left(\frac{\partial V}{\partial Y}\right)_0 \int Y_n \rho_n d\tau_n + \left(\frac{\partial V}{\partial Z}\right)_0 \int Z_n \rho_n d\tau_n \\
&+ \frac{1}{2}\left(\frac{\partial^2 V}{\partial X^2}\right)_0 \int X_n^2 \rho_n d\tau_n + \frac{1}{2}\left(\frac{\partial^2 V}{\partial Y^2}\right)_0 \int Y_n^2 \rho_n d\tau_n + \frac{1}{2}\left(\frac{\partial^2 V}{\partial Z^2}\right)_0 \int Z_n^2 \rho_n d\tau_n \\
&+ \frac{1}{2}\left(\frac{\partial^2 V}{\partial X \partial Y}\right)_0 \int X_n Y_n \rho_n d\tau_n + \frac{1}{2}\left(\frac{\partial^2 V}{\partial X \partial Z}\right)_0 \int X_n Z_n \rho_n d\tau_n + \frac{1}{2}\left(\frac{\partial^2 V}{\partial Y \partial Z}\right)_0 \int Y_n Z_n \rho_n d\tau_n \\
&+ \ldots
\end{aligned} \tag{3.22}$$

The dipole term E_{dipole} vanishes because ρ_n is a symmetric function. In a body-fixed system with z along the spin axis, the integrals of the cross terms in $E_{quadrupole}$ vanish due to the rotational symmetry about

the spin axis and the quadrupole energy $E_{quadrupole}$ can be expressed as

$$E_{quadrupole} = \frac{1}{4}\left[\left(\frac{\partial^2 V}{\partial x^2}\right)_0 + \left(\frac{\partial^2 V}{\partial y^2}\right)_0\right]\int \rho_n (r_n^2 - z_n^2) d\tau_n + \frac{1}{2}\left(\frac{\partial^2 V}{\partial z^2}\right)_0 \int \rho_n z_n^2 d\tau_n \tag{3.23}$$

with z along the spin axis and $r_n^2 = x_n^2 + y_n^2 + z_n^2$. Using the fact, that the charge giving rise to the field gradient is zero over the nuclear volume (described by Laplace's equation $\nabla^2 V = 0$), the quadrupole energy $E_{quadrupole}$ can be simplified to

$$E_{quadrupole} = \frac{1}{4}\left(\frac{\partial^2 V}{\partial z^2}\right)_0 eQ^* \tag{3.24}$$

with the elementary charge e and the intrinsic nuclear quadrupole moment

$$Q^* = \frac{1}{e}\int \rho_n (3z_n^2 - r_n^2) d\tau_n.$$

The quantum number F as total angular momentum of the molecule is introduced as coupling of the nuclear spin I and the rotational angular momentum J. The angular momentum quantum numbers F and M_F can have following values:

$$F = J+I, J+I-1, J+I-2, ..., |J-I| \tag{3.25}$$

and

$$M_F = F, F-1, F-2, ..., -F. \tag{3.26}$$

The eigenvalues of $\mathbf{F}^2$ and the component F_Z along a space-fixed axis are determined as follows:

$$\begin{aligned} \langle F, M_F | \mathbf{F}^2 | F, M_F \rangle &= \hbar^2 \cdot F(F+1) \\ \langle F, M_F | F_Z | F, M_F \rangle &= \hbar \cdot M_F. \end{aligned} \tag{3.27}$$

In quantum mechanics, the nuclear quadrupole coupling can be illustrated as coupled system of two angular momenta. Using a first-order pertubation, the quadrupole energy E_Q of a rigid asymmetric rotor [31, 32] is given as

$$E_Q = \frac{2}{J(J+1)} Y(J,I,F) \sum_i \chi_{ii} \langle P_i^2 \rangle \tag{3.28}$$

with the Casimir function

$$Y(J,I,F) = \frac{\frac{3}{4}C(C+1) - I(I+1)J(J+1)}{2(2J+3)(2J-1)I(2I-1)}$$

and

$$C = F(F+1) - J(J+1) - I(I+1).$$

Here, χ_{ii} ($i = a,b,c$) are the quadrupole coupling constants. Due to the relation

$$\chi_{aa} + \chi_{bb} + \chi_{cc} = 0, \tag{3.29}$$

only two coupling constants are independent. Usually, the quadrupole coupling constants χ_{aa} and $\chi_{-} = \chi_{bb} - \chi_{cc}$ in the principal axis system and in the I^r representation can be determined from spectroscopic measurements.

Due to symmetry, no off-diagonal quadrupole coupling constants can be determined in the first-order approximation for rigid molecules. [33] In the case of internal rotation however, it is possible to determine the off-diagonal element χ_{ab} for a molecule like 4,5-dimethylthiazole (Chapter 13) with a mirror plane along the *ab*-plane using the equation [34]

$$E_Q = \frac{2}{J(J+1)} Y(J,I,F)[\chi_{aa}\langle P_a^2\rangle + \chi_{bb}\langle P_b^2\rangle + \chi_{cc}\langle P_c^2\rangle + \chi_{ab}\langle P_a P_b + P_b P_a\rangle]. \tag{3.30}$$

3.4 Structure determination using isotopic substitution

Usually, the structural information obtained with microwave spectroscopy are condensed in the three rotational constants *A*, *B*, and *C*. When information on the bond lengths and dihedral angles is needed, a method to determine the experimental atom position in a molecule was developed by Kraitchman [35]. The structure determination is based on the assumption that isotopologues have the same bond distances and angles. Each isotopologue has a slightly different set of rotational constants and frequency shifts of its rotational spectra. The isotopologue with the highest natural abundance is called parent species. The principal axis system of the parent species is already given in Equation 3.5 with no off-diagonal elements and the centers of mass as origin. When only one isotope is substituted in this molecule, this isotopologue has the following moments of inertia tensor I' in the coordinate system of the parent species [29]:

$$I' = \begin{pmatrix} I'_{aa} & I'_{ab} & I'_{ac} \\ I'_{ba} & I'_{bb} & I'_{bc} \\ I'_{ca} & I'_{cb} & I'_{cc} \end{pmatrix} = \begin{pmatrix} I_a + \mu(b^2+c^2) & -\mu \cdot a \cdot b & -\mu \cdot a \cdot c \\ -\mu \cdot b \cdot a & I_b + \mu(a^2+c^2) & -\mu \cdot b \cdot c \\ -\mu \cdot c \cdot a & -\mu \cdot c \cdot b & I_c + \mu(a^2+b^2) \end{pmatrix} \tag{3.31}$$

with

$$\mu = \frac{M \cdot \Delta m}{M + \Delta m}.$$

Here, M is the total mass of the parent species and Δm the change of the mass due to the isotopic substitution. Both isotopologues can have different principal axis systems with different center of mass and alignments of the axes except the isotopic substituent is located at the center of mass. When the rotational constants of a single substituted isotopologue is known, the atom position of its substituted

isotope can be determined with the assumption that the parent species and its isotopologues have the same atom positions. So the different sets of rotational constants are purely due to the different mass of one isotope. Together with the information of this change of the mass and the moments of inertia of the parent species, the assigned moments of inertia of one isotopologue yield the atom position of the substituted isotope as given by

$$|a| = \sqrt{\frac{\Delta P_a}{\mu}\left(1+\frac{\Delta P_b}{I_a - I_b}\right)\left(1+\frac{\Delta P_c}{I_a - I_c}\right)} \tag{3.32}$$

$$|b| = \sqrt{\frac{\Delta P_b}{\mu}\left(1+\frac{\Delta P_c}{I_b - I_c}\right)\left(1+\frac{\Delta P_a}{I_b - I_a}\right)} \tag{3.33}$$

$$|c| = \sqrt{\frac{\Delta P_c}{\mu}\left(1+\frac{\Delta P_a}{I_c - I_a}\right)\left(1+\frac{\Delta P_b}{I_c - I_b}\right)} \tag{3.34}$$

with

$$\Delta P_a = \frac{1}{2}\cdot(-\Delta I_a + \Delta I_b + \Delta I_c)$$
$$\Delta P_b = \frac{1}{2}\cdot(-\Delta I_b + \Delta I_c + \Delta I_a)$$
$$\Delta P_c = \frac{1}{2}\cdot(-\Delta I_c + \Delta I_a + \Delta I_b)$$

and

$$\Delta I_i = I_i' - I_i \text{ for } i = a, b, c.$$

With these equations, the atom positions of all assigned single substituted isotopologues can be determined. For a complete microwave structure, all different single substituted isotopologues have to be assigned since one assigned isotopologue yields only one atom position. The sign of the coordinates can be obtained by comparison with quantum chemical calculations.

Part I

Structure Determination of Non-Planar Ring Molecules

CHAPTER 4

Conformational Landscape

The simplest non-planar five-membered ring is cyclopentane. Two stable conformers exist for this molecule. [36] In the *envelope* structure, one atom is out of the ring plane (atom 1 in Figure 4.1). The ring plane is defined by the dihedral angle $\varphi = \angle(C_2,C_3,C_4,C_5)$. The *envelope* flap is given by the plane C_2-C_1-C_5 (blue plane in Figure 4.1). To illustrate this geometry, the opening angle of the *envelope* can be described by $\gamma = \angle(C_1,C_5,C_2,C_3)$ or $\gamma' = \angle(C_1,C_2,C_5,C_4)$. If the ring plane is perfectly planar ($\varphi = 0$), only one opening angle is required because $\gamma = \gamma'$.

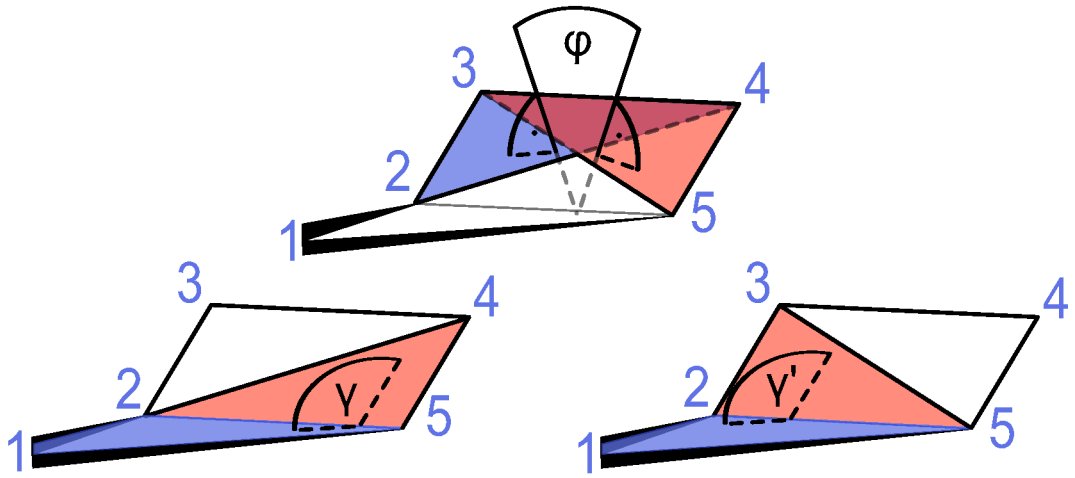

Figure 4.1. The *envelope* conformation of cyclopentane. The atom C_1 is out of the ring plane C_2-C_3-C_4-C_5 and is part of the *envelope* flap (blue plane). The geometry can be described by the dihedral angles φ, γ, and γ'. If the ring structure is not distorted, $\varphi = 0$ and $\gamma = \gamma'$.

While the *envelope* structure has C_s symmetry (for $\gamma = \gamma'$), the undistorted *twist* structure has C_2 symmetry. This structure can be illustrated as an *envelope* geometry with a *twisted* ring plane (see Figure 4.2). Here, the atoms C_3 and C_4 of the former ring plane are moved in opposite directions below and above the *envelope* flap. The *twist* geometry can be illustrated using the angle α which describes the *twist* angle between the vector C_3-C_4 and the *envelope* fold C_2-C_1-C_5. In the perfect *twist* geometry, the *envelope* fold C_2-C_1-C_5 bisects the vector C_3-C_4. Similar to the *envelope* structure, an opening angle is defined by the angle $\beta = \angle(C_1,C_2,C_5,C_4)$ or $\beta' = \angle(C_1,C_5,C_2,C_3)$. $\beta = \beta'$, when the *twist* geometry is ideal.

These characterizations are picturesque descriptions of the *envelope* and the *twist* structure. If the geometry is distorted, a more general definition of the geometry is needed. For this purpose, Cremer-Pople parameters are used (see next section).

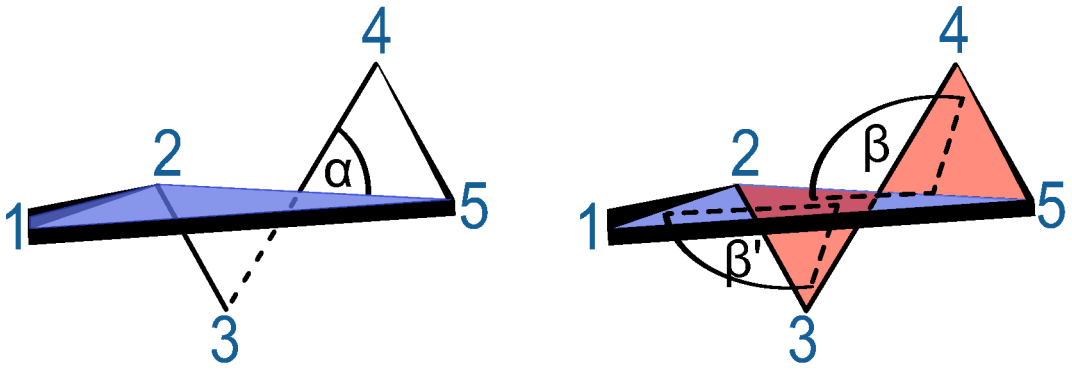

Figure 4.2. The *twist* conformation of cyclopentane using the same perspective as in Figure 4.1. The *envelope* fold is given as the blue plane (compare with Figure 4.1). The *twisted* conformation is illustrated by the angles α, β, and β'.

Cremer-Pople puckering parameters for five-membered rings

The Cremer-Pople puckering parameters [37] give a general characterization of ring geometries including distorted structures. The conformational space for a five-membered ring is defined by two parameters. The puckering amplitude $q_2 \geq 0$ describes the magnitude of the puckering of the ring and is zero for a planar ring. The second parameter, the phase angle ϕ_2 has a value between 0 and 360°. It describes the distribution of an *envelope* and a *twist* structure in the studied geometry. Starting by $\phi_2 = 0$, changing ϕ_2 by $\pm 36°$ leads to the next *envelope* structure. On the other hand, the *twist* structures are shifted from the *envelope* structure by $\phi_2 = \pm 18°$. The directions of the atoms above and below the ring plane changes sign every $\phi_2 = \pm 180°$.

The orientation of a ring substituent like a methyl group is described by the angle δ with values between 0 and 180°. [38] δ defines the angle between the mean plane of the puckered ring and the bond of the methyl group. The orientations of the methyl group are classified as *axial* ($0° \leq \delta \leq 30°$ or $150° \leq \delta \leq 180°$) and *equatorial* ($60° \leq \delta \leq 120°$). For all other values, the orientation is called *inclinal*. $\delta = 90°$ corresponds to a parallel orientation of the mean ring plane and the ring substituent, while $\delta = 0°$ or 180° means a perpendicular orientation. Using the program RING [39], the Cremer-Pople puckering parameters of geometries obtained by quantum chemical calculations and isotopic substitutions can be calculated.

The Cremer-Pople puckering parameters for five-membered rings can be illustrated with the model of Altona and Sundaralingam [40], as shown in Figure 4.3.

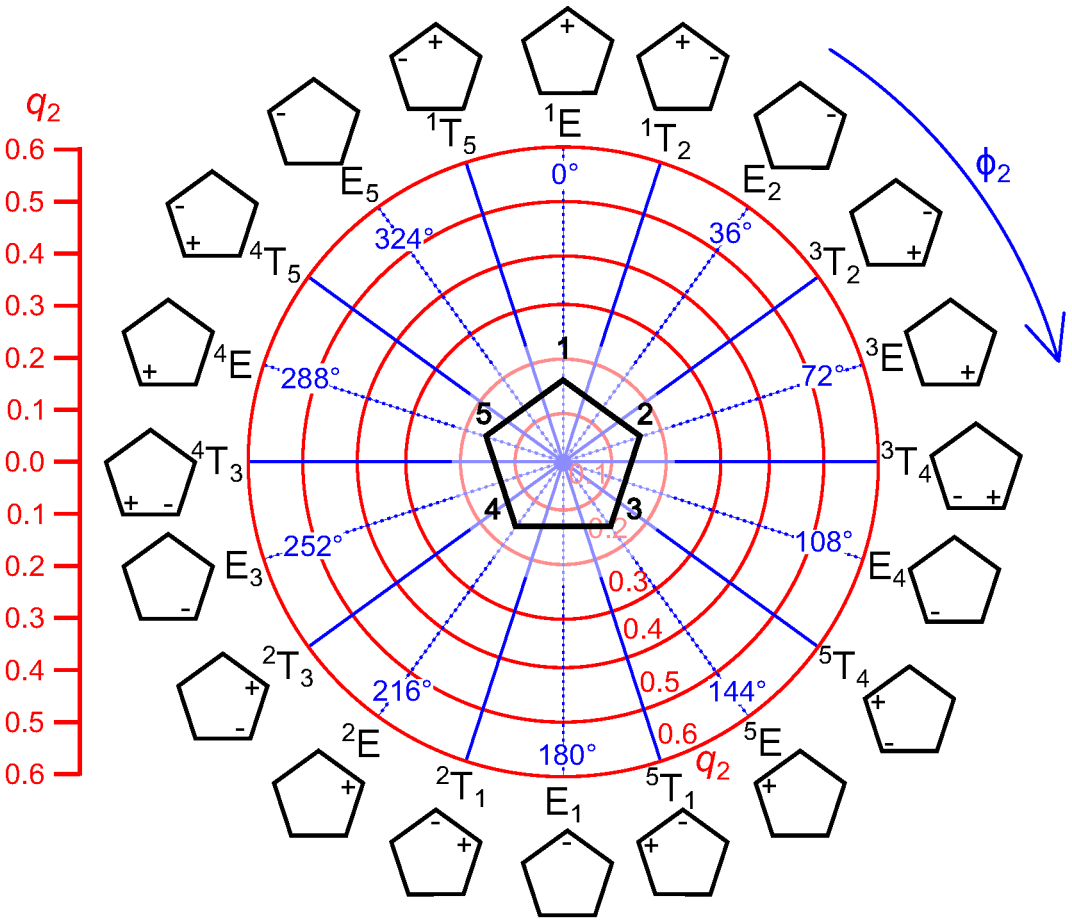

Figure 4.3. Conformational landscape of cyclopentane described by the Cremer-Pople parameters q_2 (puckering amplitude) and ϕ_2 (phase angle). The nomenclature is based on the ***Twist*** or ***Envelope*** geometry and alters every $\phi_2 = 18°$. The numbers in the name indicates the positions of the corresponding atoms above (+) and below (−) the ring plane. At the center, the ring is planar and $q_2 = 0$.

CHAPTER 5

2-Methyltetrahydrothiophene

Parts of this chapter have already been published in:

Vinh Van, Christina Dindic, Ha Vinh Lam Nguyen, and Wolfgang Stahl
Conformational Transformations of Sulfur-Containing Rings: 2-Methyltetrahydrothiophene Gas-Phase Structures [41]
ChemPhysChem **16**, 291-294 (2015). DOI: 10.1002/cphc.201402727
Front cover *ChemPhysChem* **2/2015** DOI: 10.1002/cphc.201590006
Cover profile *ChemPhysChem* **2/2015** DOI: 10.1002/cphc.201402895

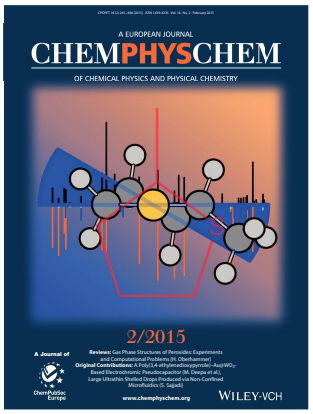

Vinh Van performed the quantum chemical calculations, the measurements, the spectral analysis, and co-wrote the manuscript. Christina Dindic helped with the measurements and the spectral analysis in her bachelor thesis under the supervision of Vinh Van. Ha Vinh Lam Nguyen and Wolfgang Stahl discussed and co-wrote the manuscript. Parts of this chapter are reproduced from Ref. [41] with permission from John Wiley and Sons.

5.1 Introduction

Volatile heterocyclic flavor substances are of interest to understand the aroma production during food cooking. For example, the Maillard reaction is known to create desirable aromas in browned food under heating. The educts of this reaction are amino acids and reducing compounds; the products are mixtures of flavor substances. In 1995, Umano *et al.* [6] reported on the formation of odor compounds by heating D-glucose and L-cysteine as a Maillard model, where thiophenes are important sulfur-containing products. Here, the gas phase conformations of 2-methyltetrahydrothiophene (MTTP), a product of the aforementioned Maillard reaction, were studied. MTTP is a five-membered heterocyclic molecule with a stereo center. The substance is also found as natural flavor in Petite Arvine wine [8] and Chinese brandy [9]. In 1984, Hartman *et al.* [10] identified this molecule in the volatile products after thermal degradation of vitamin B_1, which provides a better understanding of the progress of nutrient loss. Under molecular beam conditions, several *twist* conformations of MTTP are expected to be observe, which are linked by *envelope* transition states. The *twist* conformations often appear as the most stable structures

in many other five-membered rings [3, 42, 43].

5.2 Quantum chemical calculations

At the beginning, several starting geometries were created and optimized at the MP2/6-311++G(d,p) level using the GAUSSIAN09 package [26]. The start geometries are based on the structures of the two conformers of the prototype molecule cyclopentane [36]. Quantum chemistry was used since it is a helpful tool to assign rotational spectra. The optimized geometries are reasonable estimations to start the spectral assignment. On the other hand, experimental parameters obtained by microwave spectroscopy are useful for benchmark calculations to improve the parameters in some quantum chemical calculations [44]. Additionally, harmonic frequency calculations were performed to verify the nature of the stationary points.

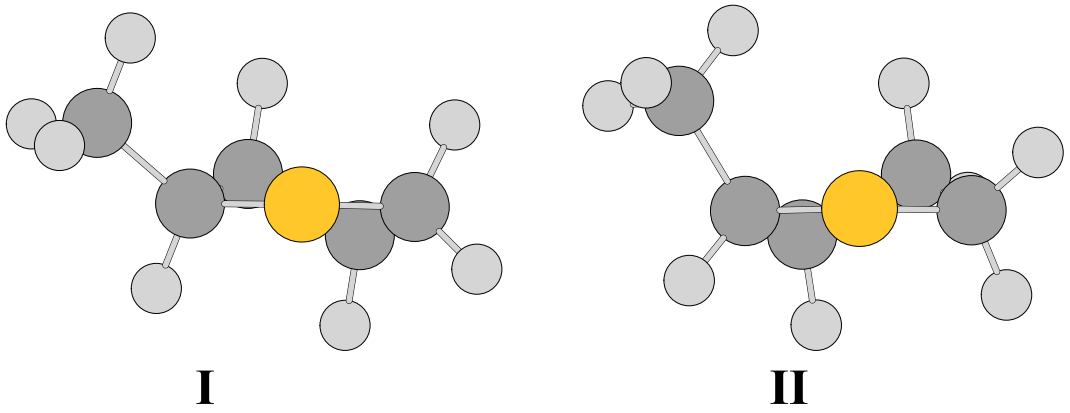

Figure 5.1. Optimized geometries of conformer I and II calculated at the MP2/6-311++G(d,p) level. The energy difference between conformer II and the more stable conformer I is 0.99 kJ·mol^{-1}. [41]

The geometry optimizations yielded two *twist* conformers (I and II) as shown in Figure 5.1. In general, the geometry of five-membered rings can be described by the Cremer-Pople parameters (see Section 5.3). First, a more picturesque description will be given here: The *twist* conformations can be described by the angle α between the C_5-S-C_2 plane and the C_4-C_3 vector as shown in Figure 5.2. Furthermore, the angles β and β' between the C_5-S-C_2 plane and the *twisted* planes C_4-C_3-C_2 and C_5-C_4-C_3, respectively, are needed for the characterization.

β and β' are equal if the *twist* geometry is not distorted. To check for convergence of the geometries, the structures of conformer I and II (see Figure 5.1) were re-optimized at different levels of theory using various combinations with the HF, DFT, MP2, and CCSD methods and different basis sets. The Cartesian coordinates are given in Table 17.1; the rotational constants and dipole moment components are given in Table 17.2 and Table 17.3 for conformer I and II, respectively.

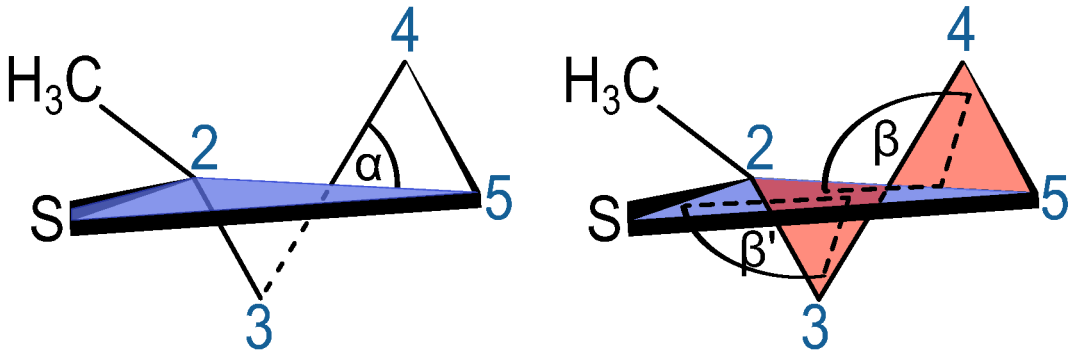

Figure 5.2. Definitions of the angles α, β, and β' in the *twisted* conformation of MTTP. [41]

Two transition states (TS1 and TS2) were optimized using the Berny algorithm [28] to understand the conversion between the stable conformers I and II. Contrary to the chemical intuition, optimized geometries of the transition states do not show a planar ring structure. Depending on the orientation of the methyl group, *envelope* conformations with more or less pronounced distortion were found and visualized in Figure 5.3. The Cartesian coordinates are given in Table 17.4. These transition states were subsequently re-optimized at different levels of theory. The intramolecular conversion is shown in Figure 5.4.

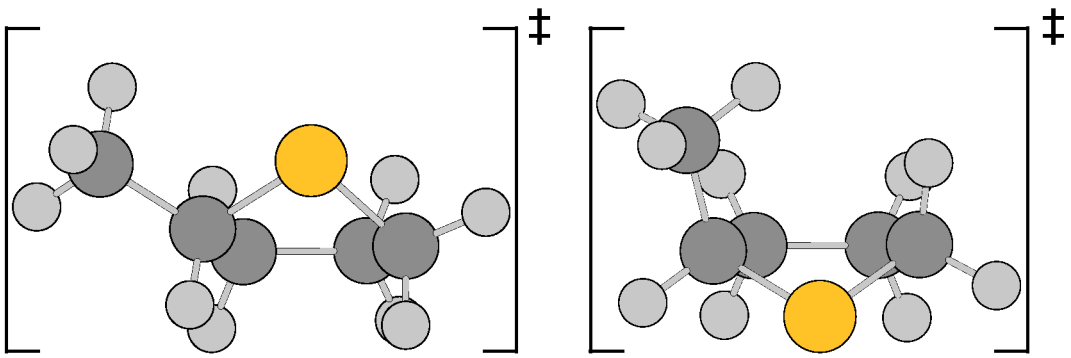

Figure 5.3. The transition states TS1 (methyl group in *equatorial* position) and TS2 (methyl group in *axial* position, 1.43 kJ·mol^{-1} higher in energy than TS1) with *envelope* structures where the sulfur atom indicates the *envelope* flap. [41]

If the methyl group is in the *axial* orientation (TS2), the ring plane (described by the dihedral angle $\varphi = \angle(C_5,C_4,C_3,C_2)$) is less distorted than in the case of the *equatorial* orientation (TS1). Normally, the geometry of an *envelope* conformation can be described sufficiently by the position of the out-of-plane atom. Here, since the ring plane is distorted ($\varphi \neq 0$), two dihedral angles $\gamma = \angle(S,C_2,C_5,C_4)$ and $\gamma' = \angle(S,C_5,C_2,C_3)$ given in Figure 5.5 are additionally required to define the flap angle of the *envelope*. The rotational constants and angles φ, γ, and γ' of TS1 and TS2 are given in Table 17.5 and 17.6.

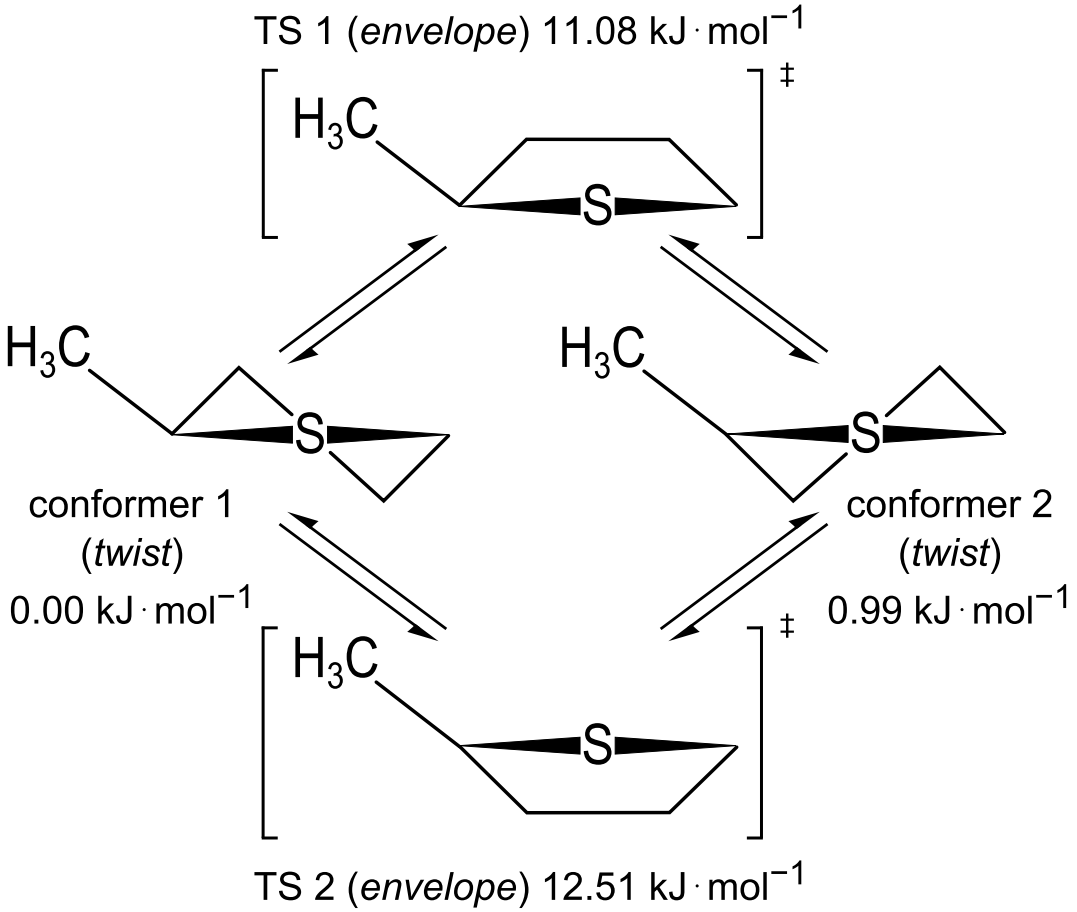

Figure 5.4. Intramolecular conversion between two stable *twist* conformers and the corresponding *envelope* transition states. The energies are related to the lowest energetic conformer I with its absolute energy E = −593.6422076 Hartree. [41]

The transition state showing a planar ring structure was obtained while φ and γ' were kept fixed to zero and all other parameters were allowed to relax. Harmonic frequency calculations yielded two imaginary frequencies. This second order transition state is 20.63 kJ·mol^{-1} higher in energy than the first order one TS1.

As illustrated in Figure 5.4, the two stable conformers of MTTP have an energy difference of only 0.99 kJ·mol^{-1}. Therefore, both are expected to be observable under molecular beam conditions. At the beginning of the spectroscopic studies, a broadband scan was recorded in the frequency range from 9 to 14 GHz, where overlapping spectra were automatically taken by a step width of 0.25 MHz. Afterwards, all lines were remeasured in the high resolution mode of the spectrometer. They appeared as doublets due to the Doppler effect.

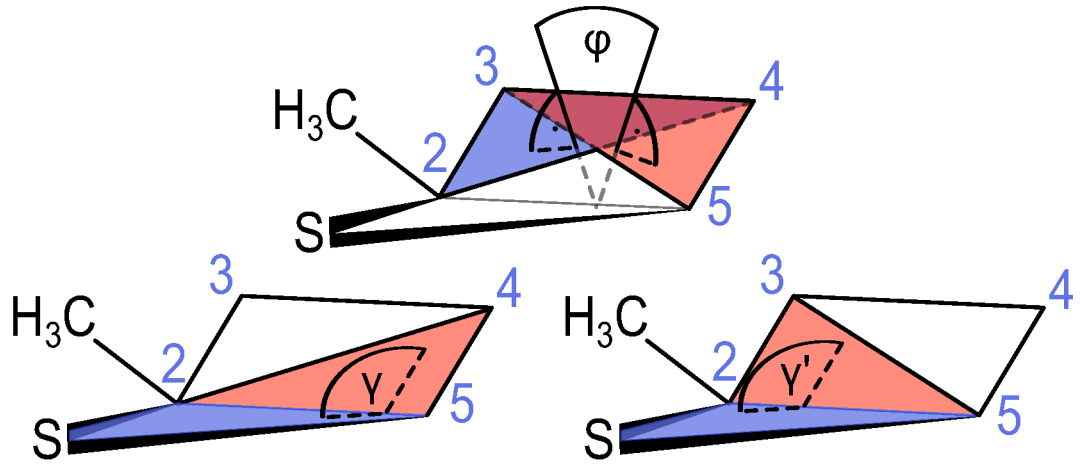

Figure 5.5. The *envelope* conformation is described by the dihedral angles φ, γ, and γ'. If the ring structure is not distorted, $\varphi = 0$ and $\gamma = \gamma'$. [41]

5.3 Cremer-Pople puckering parameters

The Cremer-Pople puckering parameters [37] were calculated for both conformers and the transition states using the program RING [39] to characterize the ring geometries in more detail. The explanation of these parameters are given in Chapter 4. The calculated geometry of conformer I has a *twist* structure ($^3T_4$) and the methyl substituent is in an *inclinal* orientation with $q_2 = 0.45$, $\phi_2 = 88.7°$, and $\delta = 58.2°$. Conformer II has a *twist* structure ($^4T_3$) with a little more contribution of the *envelope* structure ^4E. In contrast to conformer I, the methyl substituent of conformer II has an *axial* orientation with $q_2 = 0.45$, $\phi_2 = 276.2°$, and $\delta = 23.7°$. The *axial* orientation is higher in energy than the *inclinal* orientation due to steric effects.

The lower energy transition state TS1 is almost a 1:1 mixture of the *twist* structure $^1T_5$ with more contribution of the *envelope* structure ^1E. The methyl group is in an *equatorial* position. The Cremer-Pople puckering parameters of TS1 are $q_2 = 0.52$, $\phi_2 = 350.8°$, and $\delta = 63.7°$. On the other hand, the transition state TS2 has a near-*envelope* structure (E_1) with $q_2 = 0.50$, $\phi_2 = 177.2°$, and $\delta = 13.3°$. Here, the methyl group is in an *axial* orientation. All conformers and transition states are illustrated in Figure 5.6.

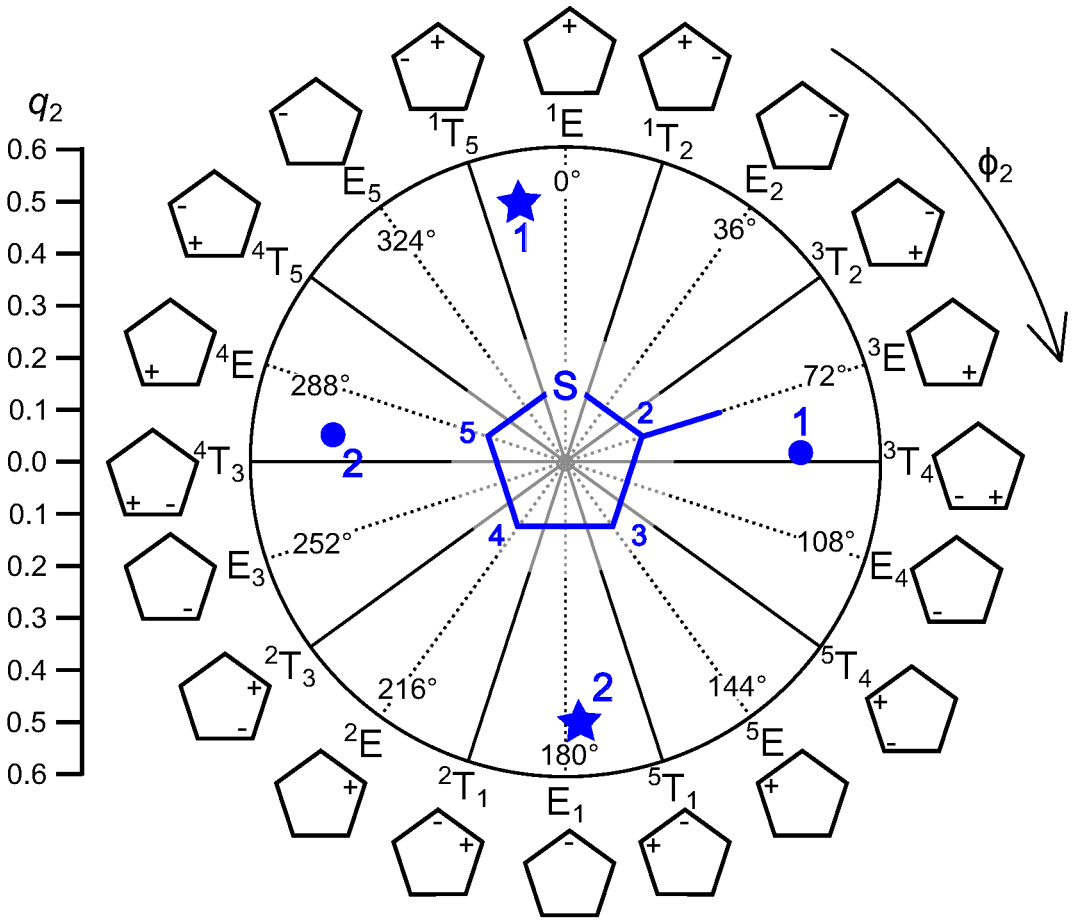

Figure 5.6. Conformational landscape of MTTP using the Cremer-Pople parameters q_2 (puckering amplitude) and ϕ_2 (phase angle) based on the model of Altona and Sundaralingam [40]. The nomenclature is based on the ***Twist*** or ***Envelope*** geometry and the positions of the atoms which are above (+) and below (−) the ring plane. At the center, $q_2 = 0$ corresponds to a planar ring. Stable conformations are illustrated as dots and transition states as stars.

5.4 Microwave spectroscopy

The microwave spectrum was predicted with the program XIAM [45] using the rotational constants calculated at the MP2/6-311++G(d,p) level. The dipole moment components suggested a spectrum with much stronger *b*-type transitions for both conformers (see Table 17.2). For the assignment of conformer I the transitions $2_{12} \leftarrow 1_{01}$, $3_{03} \leftarrow 2_{12}$, and $3_{13} \leftarrow 2_{02}$ were used. By trial and error, these transitions could be assigned and they were the most intense transitions in the scan. Afterwards, more *b*-type transitions were found and added to the fit. The attempt to assign *a*-type transitions was surprisingly successful although the dipole moment component in *a*-direction was calculated to be small. All measured *a*-type transitions were much stronger than expected. The calculated *c*-dipole moment component was zero and accordingly, no *c*-type transitions could be observed. In total, 42 *a*-type and 101 *b*-type transitions were fitted to a standard deviation of 1.7 kHz, within the experimental accuracy of 2 kHz. All fitted transitions are listed in Table 17.7, the molecular parameters are given in Table 5.1.

Quantum chemically, conformer I should be the most stable one, which is confirmed by the experiment, since all transitions assigned to conformer I are quite strong. From the experience, the rotational spectrum of the ^{34}S-isotopologue of the most stable conformer can be observed in natural abundance of about 4.3%. The assignment process followed the steps carried out for conformer I. In total, 75 *a*- and *b*-type transitions of the ^{34}S-isotopologue were assigned. The frequency list is given in Table 17.8, the molecular parameters also in Table 5.1. The *A* and *B* rotational constants are almost the same as those of the main isotopologue; the *C* constant is appreciably lower.

After conformer I and its ^{34}S-isotopologue were assigned, many lines remained in the scan, which might belong to conformer II. The assignment was started with the same *b*-type transitions $2_{12} \leftarrow 1_{01}$, $3_{03} \leftarrow 2_{12}$, and $3_{13} \leftarrow 2_{02}$, which could be easily identified. For conformer II, 9 *a*- and 68 *b*-type transitions were assigned and fitted to an excellent standard deviation of 1.1 kHz. The transition frequencies are listed in Table 17.9, the fitted parameter also in Table 5.1.

It is possible to calculate the r_s position of the sulfur atom with respect to the center of mass (isotopic shift) with the ^{34}S isotopic species. Using Kraitchman's equations [35], the ^{32}S coordinates were found to be $|a| = 0.101(15)$ Å, $|b| = 1.2511(12)$ Å, $|c| = 0.056(27)$ Å. The errors are estimated with Costain's method [46]. The position of the sulfur atom is in excellent agreement with the calculated results of $a = 0.1003$ Å, $b = -1.2282$ Å, $c = -0.0589$ Å (see Table 17.1).

Table 5.1. Molecular parameters of conformer I, conformer II, and the ^{34}S-isotopologue of conformer I obtained using the program XIAM.

Par.[a]	Unit	^{32}S-Conformer I	^{34}S-Conformer I	^{32}S-Conformer II
A	GHz	4.225 235 990(81)	4.123 695 34(16)	3.789 899 843(97)
B	GHz	2.790 053 737(51)	2.789 652 53(12)	3.008 622 018(74)
C	GHz	1.848 361 318(52)	1.828 567 48(11)	2.031 137 229(73)
Δ_J	kHz	0.259 71(53)	0.2615(21)	0.5337(20)
Δ_{JK}	kHz	0.1197(13)	0.1220(28)	−0.7783(13)
Δ_K	kHz	1.1338(12)	1.0727(30)	1.8994(16)
δ_J	kHz	0.062 70(21)	0.062 17(54)	0.087 59(20)
δ_K	kHz	0.314 38(82)	0.3155(23)	0.235 42(67)
σ[b]	kHz	1.7	1.8	1.1
N[c]		143	75	77

[a] All parameters refer to the principal axis system. Watson's A reduction in I^r representation was used. [b] Standard deviation of the fit. [c] Number of lines.

5.5 Discussion

The experimental rotational constants were compared with those from quantum chemical calculations. Best agreements could be found at the CCSD/cc-pVTZ level for both conformers I and II, as shown in Tables 17.2 and 17.3. For conformer I, the HF method in combination with various basis sets provided rotational constants with better agreement than calculations using the MP2 and B3LYP methods, which is very probably due to error compensation. Conversely, the MP2 method yielded better agreement for conformer II. The methyl group in MTTP undergoes internal rotation and causes A-E splittings of all rotational lines. [47] The barrier heights are calculated to be 1349 cm^{-1} and 1268 cm^{-1} for conformer I and II, respectively, which are rather high. Accordingly, A-E splittings are only observable for a few transitions. Since these splitting are very small, the effect of internal rotation was not taken into account.

5.6 Conclusion

The conformational analysis of MTTP with quantum chemical calculations yielded two stable *twist* conformers (I and II) and two *envelope* transition states. The microwave spectra of both conformers as well as the ^{34}S-isotopologue of conformer I were assigned. Molecular parameters like the rotational, centrifugal distortion constants, and the position of the sulfur atom in respect to the center of mass of conformer I could be determined with very high accuracy. The observed spectra were reproduced within the experimental accuracy of 2 kHz. This study confirms that the *twist* and *envelope* structures of stable conformers and transition states, respectively, are energetically favorable as also found in some related five-membered rings.

5.7 Acknowledgements

Christina Dindic is gratefully acknowledged for her help in the assignment and measurements as part of her bachelor thesis under the supervision of Vinh Van. Financial funds were provided by the Land Nordrhein-Westfalen, the Start-up project and the undergraduate fond of the RWTH Aachen University and of the Université de Paris Est Créteil. Vinh Van thanks the Fonds der Chemischen Industrie (FCI) for a Ph.D. fellowship. Free computer time was provided by the IT Center of the RWTH Aachen University.

CHAPTER 6

2-Methyltetrahydrofuran

This chapter has already been published in:

Vinh Van, Wolfgang Stahl, and Ha Vinh Lam Nguyen
The heavy atom microwave structure of 2-methyltetrahydrofuran [48]

J. Mol. Struc., **1123**, 24-29 (2016).
DOI: 10.1016/j.molstruc.2016.05.078

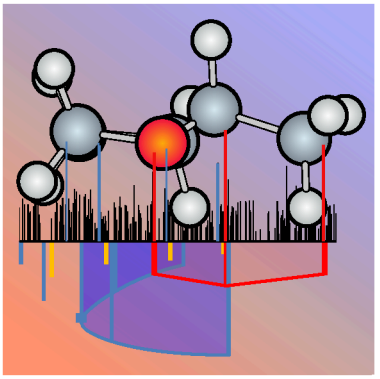

Vinh Van performed the quantum chemical calculations, the measurement, the spectral analysis, and co-wrote the manuscript. Ha Vinh Lam Nguyen and Wolfgang Stahl discussed and co-wrote the manuscript. This chapter is reproduced from Ref. [48] with permission from Elsevier.

6.1 Introduction

Rotational spectroscopy in the gas phase has increasingly been applied to determine the structure of medium-sized molecules, which often exhibit complex conformational landscapes [49–51]. The support of quantum chemistry becomes a helpful tool, where *ab initio* structures can be taken as references for a comparison of the experimental and calculated molecular parameters. On the other hand, quantum chemical calculations at different levels of theory often differ in a wide range, whereas atomic positions determined by rotational spectroscopy are highly precise [52], in particular when using the molecular beam Fourier transform microwave (MB-FTMW) technique. With high sensitivity and excellent experimental accuracy, it is possible to observe singly substituted isotopologues such as ^{13}C, ^{34}S, ^{15}N, and ^{18}O in natural abundances. Comparisons of experimentally and computationally derived molecular parameters can therefore validate the quality of various theoretical methods in characterizing the studied system.

Here, the heavy atom r_s-structure of 2-methyltetrahydrofuran (MTHF) was studied by MB-FTMW spectroscopy and compared with results from quantum chemistry. MTHF is a promising environmentally friendly solvent and biofuel component, which is derived from renewable resources. Following the prin-

ciples of Green Chemistry, MTHF has been evaluated as an eco-friendly substance in various fields like organometallics [53], metathesis [54], and biosynthesis [55]. The methyl group in MTHF exhibits internal rotation with a rather high barrier of 13.12 kJ·mol^{-1} (i.e. 1097 cm^{-1}) calculated at the CCSD(T)/6-311++G(d,p) level of theory. In the experimental spectrum, narrow torsional splittings only occur in a few transitions with high J values.

6.2 Quantum chemical calculations

6.2.1 Geometry optimizations

Several starting geometries of MTHF were created based on the structures of two conformers of cyclopentane used as a prototype [36]. Geometry optimizations were performed at the MP2/6-311++G(d,p) level of theory using the GAUSSIAN09 package [26]. This level was chosen, since it yielded rotational constants which were close to the experimental values for other heterocyclic molecules [27,41]. Only the (*S*)-configuration was considered, because enantiomers cannot be distinguished using the experimental setup in Aachen. The geometry optimizations signified two *envelope* conformers, called the *equatorial* and the *axial* conformer. Harmonic frequency calculations at the same level of theory were also carried out to decide, whether the optimized geometries are true minima or saddle points. Anharmonic frequency calculations resulted in the quartic centrifugal distortion constants (shown in Table 6.1) and the rotational constants B_0 of the vibrational ground state. The *equatorial* conformer is illustrated in Figure 6.1; the Cartesian coordinates of both conformers are given in Table 17.10.

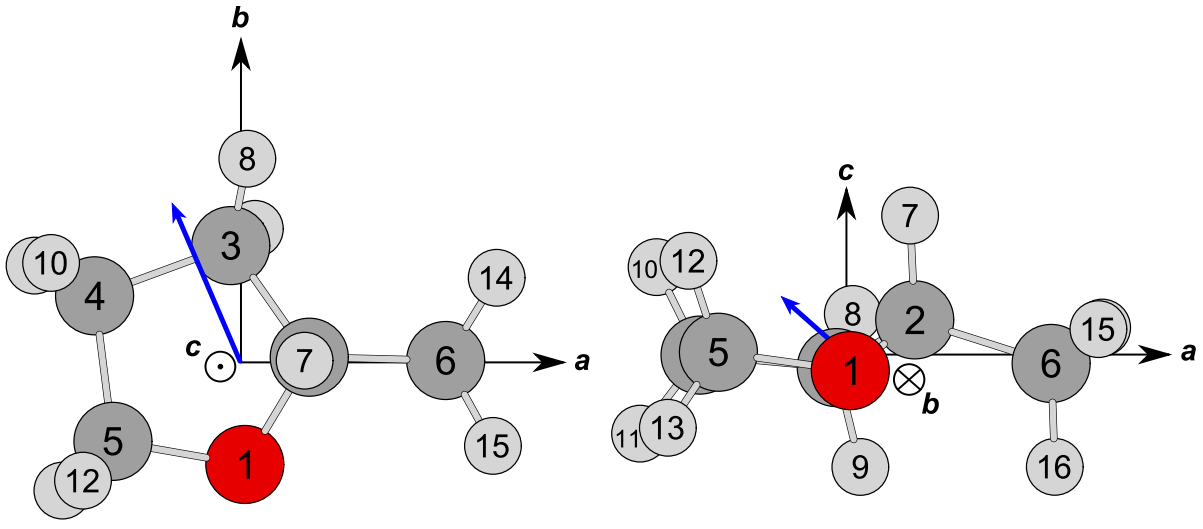

Figure 6.1. The optimized geometry in the principal axes of inertia of the most stable conformer of MTHF calculated at the MP2/6-311++G(d,p) level of theory. Left-hand side: view along the *c*-axis; right-hand side: view along the *b*-axis. The circled dot and cross indicate that the axis direction points out of and into the paper plane, respectively. The blue arrow presents the dipole moment vector. [48]

The *envelope* conformations can be described by the ring plane determined by the O, C_3, C_4, C_5 atoms, and the *envelope* fold determined either by C_2, O, C_3, C_4 or C_2, C_3, O, C_5, as depicted in Figure 6.2. The dihedral angle $\varphi = \angle(O,C_5,C_4,C_3)$ of the ring plane is zero and both angles $\gamma = \angle(C_2,O,C_3,C_4)$ and $\gamma' = \angle(C_2,C_3,O,C_5)$ of the *envelope* fold are equal, if the ring structure is not distorted. Similar to the case of methylcyclopentane, the *equatorial* orientation of the methyl group is lower in energy than the *axial* orientation due to steric effects, where the hydrogen atoms in the methyl group are closer to the hydrogen atoms of the ring. The *equatorial* conformer was afterwards re-optimized at different levels of theory using the HF, DFT, MP2, and CCSD methods and various basis sets. The calculated rotational constants are listed in Table 17.11. If not otherwise stated, all values given in this chapter will refer to the MP2/6-311++G(d,p) level of theory.

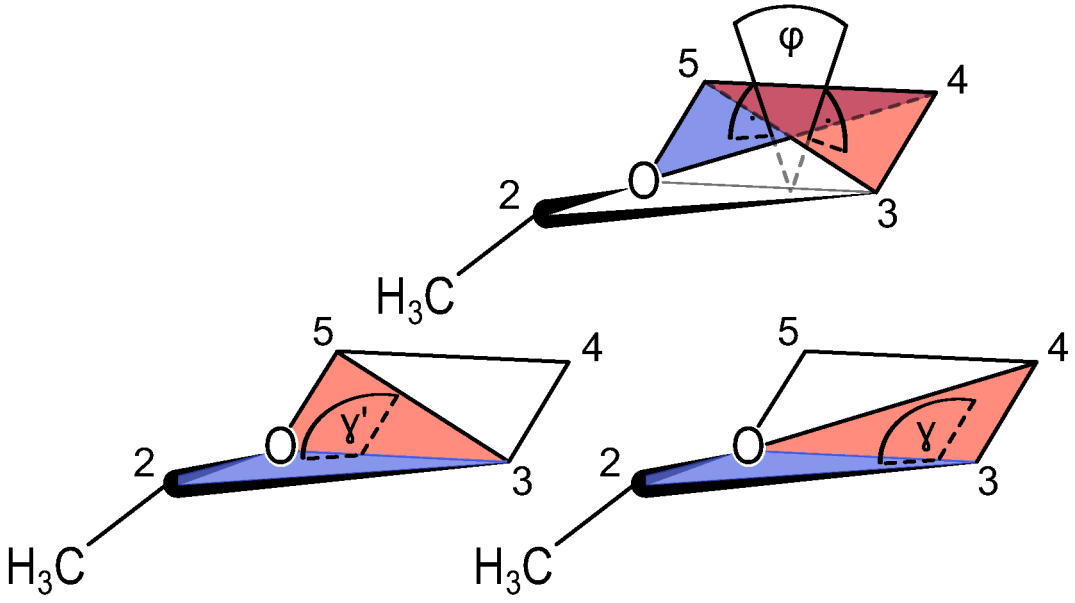

Figure 6.2. The *envelope* conformation is described by the dihedral angles $\varphi = \angle(O,C_5,C_4,C_3)$ of the ring plane and two angles $\gamma = \angle(C_2,O,C_3,C_4)$ and $\gamma' = \angle(C_2,C_3,O,C_5)$, which describe the *envelope* flap. If the ring structure is not distorted, $\varphi = 0$ and $\gamma = \gamma'$. [48]

6.2.2 Transition states

Using the Berny algorithm [28], two transition states (called $^2T_3$ and E_1) were found. The ring structures in both $^2T_3$ and E_1 are slightly distorted. The transition state energies were obtained from single-point calculations at the CCSD(T)/6-311++G(d,p) level of theory using the geometries optimized at the MP2/6-311++G(d,p) level. The *envelope* transition state E_1 is 2.00 kJ·mol^{-1} higher in energy than the *twist* configuration $^2T_3$. Their Cartesian coordinates are given in Table 17.10. Figure 6.3 indicates the intramolecular conversion between the stable conformers via $^2T_3$ and E_1. Since $^2T_3$ is only 0.10 kJ·mol^{-1} higher in energy than the *axial* conformer, the barrier to convert the *axial* conformer into the *equatorial* conformer via $^2T_3$ is very low.

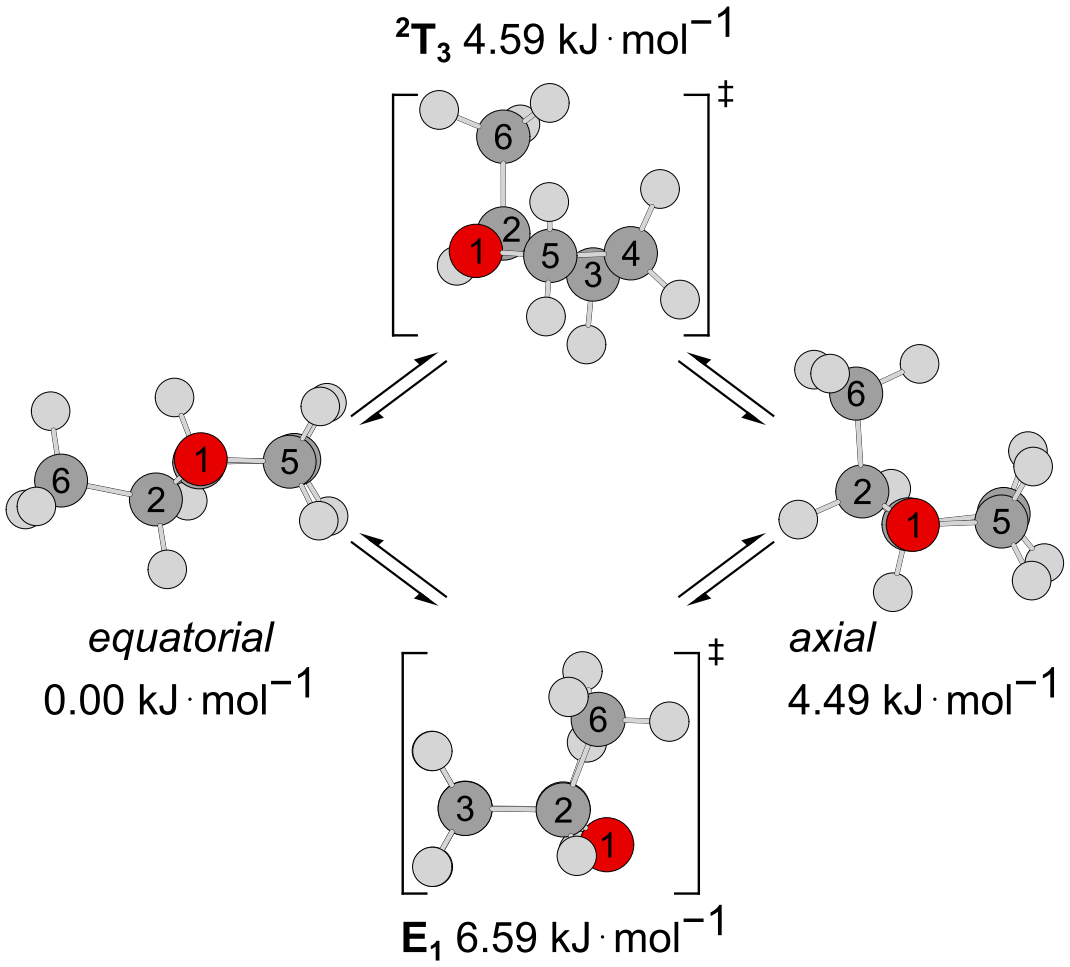

Figure 6.3. The intramolecular conversion between two stable *envelope* conformers (*equatorial* and *axial*) via one *twist* ($^2T_3$) and one *envelope* (E_1) transition state. The energies calculated at the CCSD(T)/6-311++G(d,p) level are related to the lowest energetic *equatorial* conformer with its absolute energy E = −271.1307051 Hartree. $^2T_3$ is only 0.10 kJ·mol^{-1} higher in energy than the stable *axial* conformer. This facilitates the conversion from the *axial* conformer to the *equatorial* conformer. The perspectives were chosen to illustrate the atoms above and below the ring plane. [48]

6.2.3 Cremer-Pople puckering parameters

The Cremer-Pople puckering parameters [37] for both conformers and the transition states are calculated using the program RING [39] to characterize the ring geometries in more detail. The orientation of the methyl group as a ring substituent is described by the angle δ between the mean plane of the puckered ring and the bond of the methyl group [38].The explanation to these parameters are given in Chapter 4. Figure 6.4 illustrates possible conformations based on the model of Altona and Sundaralingam [40]. The calculated as well as the experimental geometry of the *equatorial* conformer has the *envelope* structure E_2 with significant contribution of the *twist* structure $^1T_2$, and the methyl substituent in *equatorial* orientation with $q_2 = 0.39$, $\phi_2 = 32.4°$, and $\delta = 67.7°$ as well as $q_2 = 0.40$, $\phi_2 = 27.48°$, and $\delta = 68.5°$, respectively. The *axial* conformer is a 1:1 mixture of the *envelope* structure ^2E and the *twist* structure $^2T_3$

and has the methyl substituent in *axial* orientation with $q_2 = 0.38$, $\phi_2 = 226.6°$, and $\delta = 10.1°$. The *axial* orientation is higher in energy than the *equatorial* orientation due to steric effects. The lower energy transition state $^2T_3$ has a more pronounced *twist* structure with $q_2 = 0.38$, $\phi_2 = 242.4°$, and $\delta = 13.1°$, whereas the transition state E_1 has an *envelope* structure with $q_2 = 0.36$, $\phi_2 = 179.5°$, and $\delta = 17.1°$. In both of them, the methyl group is in *axial* orientation.

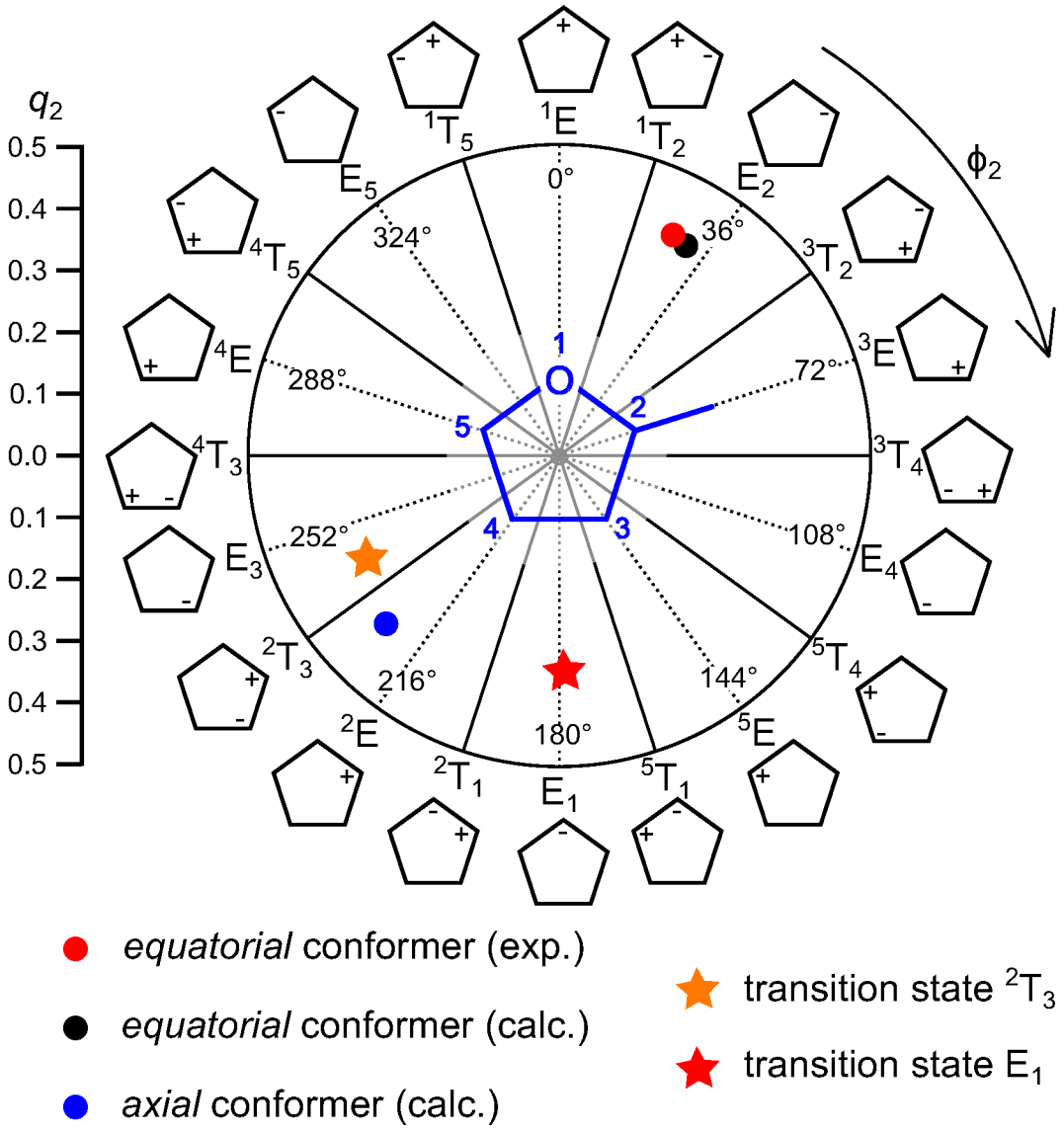

Figure 6.4. Conformational landscape of MTHF using the Cremer-Pople parameters q_2 (puckering amplitude) and ϕ_2 (phase angle). The nomenclature is based on the ***Twist*** or ***Envelope*** geometry and the positions of the atoms which are above (+) and below (−) the ring plane. At the center, $q_2 = 0$ corresponds to a planar ring. Stable conformations are illustrated as dots and transition states as stars. [48]

6.3 Microwave spectroscopy

6.3.1 Measurements

MTHF was purchased from Alfa Aesar GmbH & Co. KG, Karlsruhe, Germany with a stated purity of 99% and stabilized with approximately 150 – 400 ppm BHT (butylated hydroxytoluene). Additional purification was not necessary, since the vapor pressure of BHT is too low for an observation in the gas phase under the same conditions. The rotational spectra were measured with a MB-FTMW spectrometer operating in the frequency range 2 – 26.5 GHz. A detailed description is given in Refs. [22, 23]. A gas mixture of 1% substance in helium at a total pressure of 60 – 110 kPa was expanded through the nozzle into the cavity.

A broadband scan from 8.8 to 12.4 GHz was recorded, which consists of automatically taken overlapping spectra with 50 co-added decays per each at a step width of 0.25 MHz. The scan indicates positions of the rotational transitions, which were remeasured afterwards at higher resolution. The typical line widths are 10 – 40 kHz; the measurement accuracy of isolated lines is approximately 2 kHz. Figure 6.5 illustrates some portions of a typical broadband scan and a high resolution spectrum.

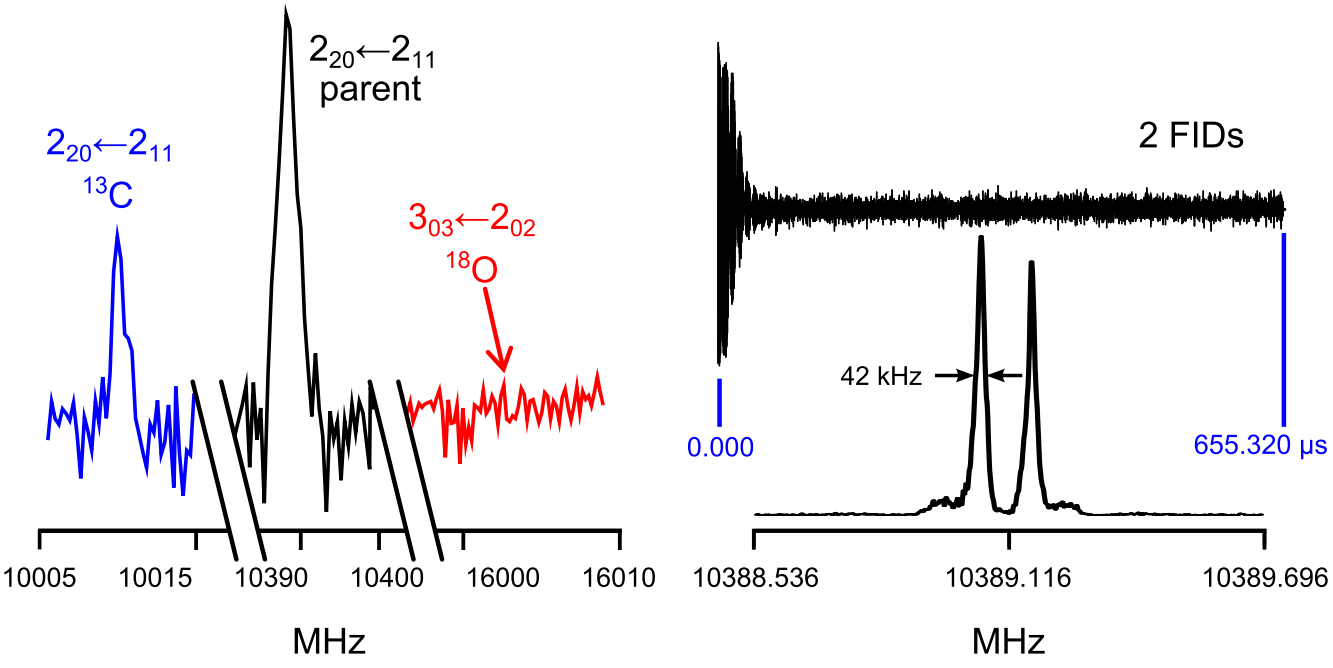

Figure 6.5. Left diagram: Some portions of a typical broadband scan, where overlapping spectra are automatically taken at a step width of 0.25 MHz with 50 co-added decays per each spectrum. The relative intensities on a logarithmic scale of the main, ^{13}C-, and ^{18}O-isotopologue are indicated. Right diagram: A high resolution spectrum of the $2_{20} \leftarrow 2_{11}$ transition obtained after two co-added free induction decays (FIDs) with a line width of approximately 42 kHz. The splitting is due to the Doppler effect. [48]

6.3.2 Spectral assignment

The *axial* conformer is not expected to be observable in the spectrum because (i) there is an energy difference of 4.59 kJ·mol^{-1} between the two stable conformers of MTHF (calculated at the CCSD(T)/6-311++G(d,p) level of theory). The *axial* conformer is thus too high in energy to be observed under molecular beam conditions, where the rotational temperature is very low (about 2 K) and (ii) the intramolecular conversion from the *axial* conformer to the *equatorial* conformer has a very low barrier of only 0.10 kJ·mol^{-1} (see Section 6.2.2).

After assigning the *equatorial* conformer, all attempts to assign the *axial* conformer failed. Therefore, it is expected that (i) in the supersonic expansion only the *equatorial* conformer exists due to collisional conformational relaxation and (ii) the remaining lines with much weaker intensity belong to vibrationally excited states occurring from ring puckering effects. Only the assignment procedure of the *equatorial* conformer is thus given here.

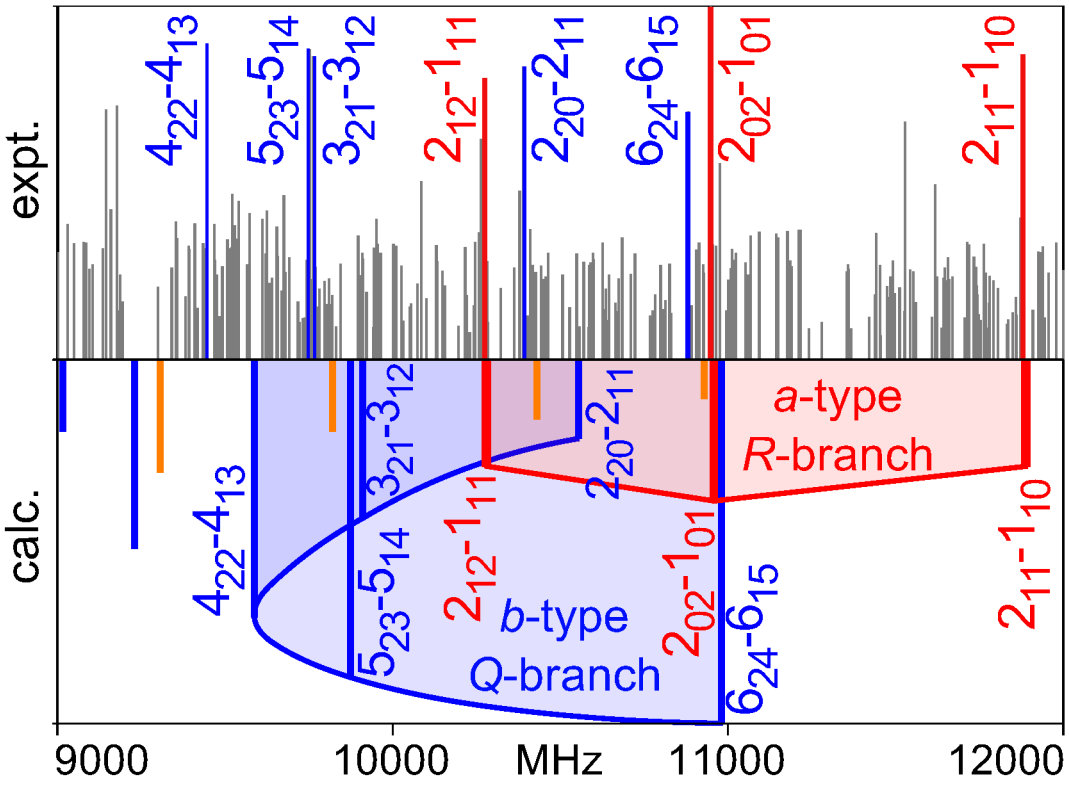

Figure 6.6. a) Upper trace: Experimental broadband scan in the frequency range from 9000 to 12000 MHz. Three *a*-type *R*-branch transitions $2_{12} \leftarrow 1_{11}$, $2_{02} \leftarrow 1_{01}$, and $2_{11} \leftarrow 1_{10}$ of the parent species of the *equatorial* conformer are marked in red, some assigned *b*-type *Q*-branch transitions in blue. b) Lower trace: Predicted spectrum of the *equatorial* conformer using the rotational constants calculated at the MP2/6-311++G(d,p) level of theory. The calculated *a*-, *b*-, and *c*-type transitions are colored in red, blue, and orange, respectively. [48]

Parent species

The calculated dipole moment components were $|\mu_a| = 0.69$ D, $|\mu_b| = 1.60$ D, and $|\mu_c| = 0.62$ D. Correspondingly, strong b-type and medium intense a- and c-type transitions were expected. Nevertheless, at the beginning a-type transitions were sought due to their characteristic pattern, which could be often assigned readily in the spectrum. At a rotational temperature of about 2 K of the molecular beam, transitions with low J and K values are usually of highest intensity. Therefore, the assignment was started with the a-type R-branch transitions $2_{12} \leftarrow 1_{11}$, $2_{02} \leftarrow 1_{01}$, and $2_{11} \leftarrow 1_{10}$. They were indeed three of the most intense lines in the broadband scan as can be recognized in Figure 6.6. The assignment of these lines fixed the B and C rotational constants. To determine the A rotational constant, the b-type Q-branch transitions $2_{20} \leftarrow 2_{11}$, $3_{21} \leftarrow 3_{12}$, $4_{22} \leftarrow 4_{13}$, and $5_{23} \leftarrow 5_{14}$ were taken into account (also given in Figure 6.6). Afterwards, further lines up to $J = 15$ (including c-type transitions) could be measured and assigned. The molecular parameters were fitted using the XIAM program [45] and summarized in Table 6.1; the frequency list is given in Table 17.12.

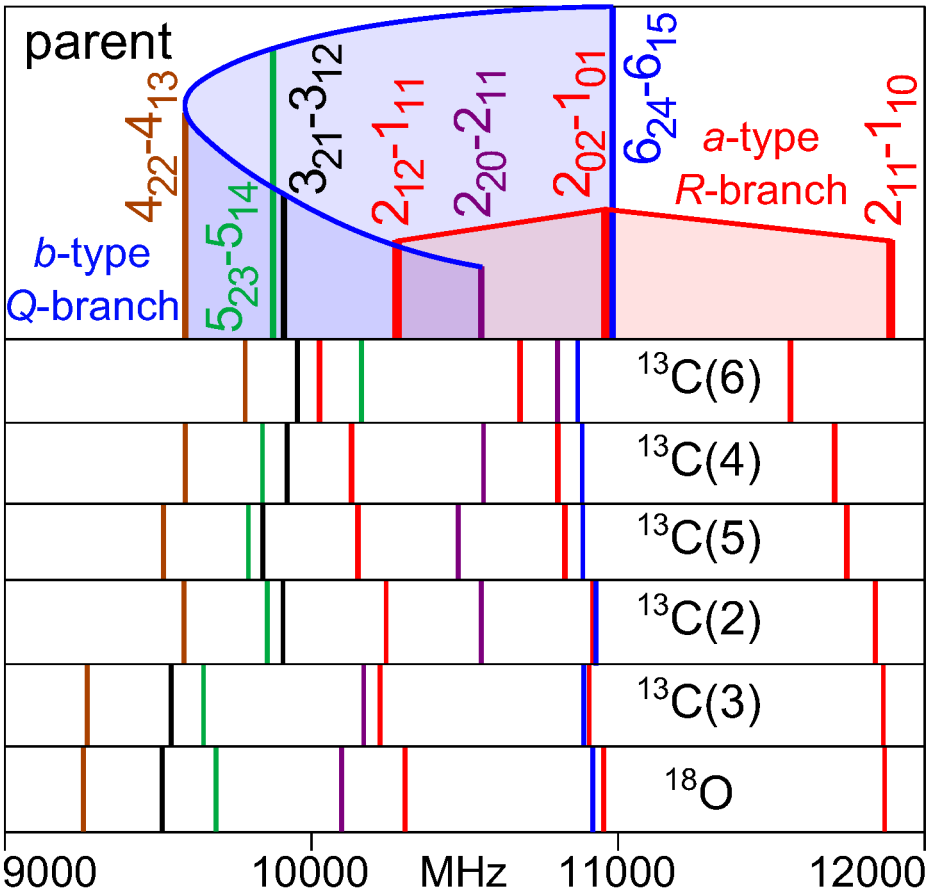

Figure 6.7. Predicted spectra of the ^{13}C and ^{18}O-isotopologues compared to that of the parent species using the rotational constants calculated at the MP2/6-311++G(d,p) level. The substituted ^{13}C atom is numbered according to Figure 6.1. [48]

Table 6.1. Molecular parameters of the *equatorial* conformer of MTHF as obtained by the XIAM program compared to the values calculated at the MP2/6-311++G(d,p) level of theory. Fit I and II include rotational transitions with $J \leq 15$. In contrast to Fit I, Fit II does not take into account the sextic centrifugal distortion constants. Fit III, on the other hand, only consists of transitions up to $J = 6$.

Par.[a]	Unit	Fit I (J $\leq$ 15)	Fit II (J $\leq$ 15)	Fit III (J $\leq$ 6)	Calc.[b]
A	GHz	6.591 568 23(22)	6.591 568 21(25)	6.591 568 14(18)	6.649
B	GHz	3.170 370 175(84)	3.170 369 95(14)	3.170 370 550(94)	3.172
C	GHz	2.367 116 054(88)	2.367 116 45(14)	2.367 115 98(11)	2.367
Δ_J	kHz	0.3312(13)	0.3340(21)	0.3368(20)	0.257
Δ_{JK}	kHz	0.0641(35)	0.0822(45)	0.0703(58)	0.761
Δ_K	kHz	2.855(20)	2.756(21)	2.787(14)	0.849
δ_J	kHz	0.058 81(44)	0.055 33(36)	0.060 16(89)	0.057
δ_K	kHz	0.5322(69)	0.5516(59)	0.580(10)	0.561
H_{JK}	Hz	−0.788(96)			
H_{KJ}	Hz	2.83(35)			
h_{JK}	Hz	0.331(46)			
h_K	Hz	−2.84(55)			
σ^c	kHz	2.2	3.6	1.4	
N^d		111	111	72	

[a] All parameters refer to the principal axis system. Watson's A reduction in I^r representation was used. [b] Vibrational ground state rotational constants and centrifugal distortion constants obtained by anharmonic frequency calculation at the MP2/6-311++G(d,p) level. [c] Standard deviation of the fit. [d] Number of lines.

^{13}C-Isotopologues

After the most intense transitions were assigned to the *equatorial* conformer, a large number of lines with low to medium intensities remained in the scan. These transitions probably belong to the ^{13}C-isotopologues of MTHF in their natural abundances of 1%. By changing the mass of a ^{12}C atom to that of a ^{13}C atom, the rotational constants of the respective ^{13}C isotopologue could be obtained. The same transitions were used as mentioned in Section 6.3.2 for the assignment process. Since the line density was quite high, a script was used which automatically generates XIAM inputs and fits to simplify the assignment. The calculated frequencies were close to those of the respective transitions of the main isotopologue, as can be recognized in Figure 6.7. The calculated and experimental *a*-type *R*-branch frequencies differed by less than 10 MHz, whereas the *b*-type *Q*-branch is shifted by approximately 160 MHz in the spectra of all isotopologues. For all ^{13}C-isotopologues, the rotational constants and four quartic centrifugal distortion constants could be determined with high accuracy, as summarized in Table 6.2; the frequency lists are given in the Tables 17.13, 17.14, 17.15, 17.16, and 17.17.

Table 6.2. Molecular parameters of different isotopologues of the *equatorial* conformer as obtained by the XIAM program. The atoms are numbered according to Figure 6.1.

Par.[a]	Unit	^{18}O(1)	^{13}C(2)	^{13}C(3)	^{13}C(4)	^{13}C(5)	^{13}C(6)
A	GHz	6.396 230 1(30)	6.579 709 64(61)	6.461 874 41(69)	6.551 074 31(70)	6.534 237 52(71)	6.590 287 55(61)
B	GHz	3.169 660 61(63)	3.157 134 42(33)	3.170 004 30(43)	3.123 729 13(38)	3.134 655 51(41)	3.080 863 83(37)
C	GHz	2.342 294 27(70)	2.361 308 76(29)	2.349 944 23(31)	2.336 116 89(36)	2.340 129 97(37)	2.317 011 45(35)
Δ_J	kHz	0.332(29)	0.3318(69)	0.3355(82)	0.329(12)	0.3235(76)	0.3143(72)
Δ_K	kHz	2.53(53)	3.021(51)	2.781(53)	2.696(55)	2.610(59)	2.997(50)
δ_J	kHz	0.060 16[b]	0.0665(30)	0.0663(35)	0.0553(27)	0.0496(44)	0.0513(48)
δ_K	kHz	0.580[b]	0.596(26)	0.662(39)	0.544(27)	0.709(43)	0.617(56)
σ[c]	kHz	3	2.3	2.3	2.8	2.4	3
N[d]		14	33	31	37	30	37

[a] Molecular parameters. [b] Can not be fitted. Fixed to the value of the main isotopologue. [c] Standard deviation of the fit. [d] Number of lines.

^{18}O-Isotopologue

The natural abundance of the ^{18}O-isotopologue is 0.2%. Its rotational transitions, therefore, did not appear in the scan like those of the ^{13}C-isotopologues. Figure 6.5 visualizes the relative intensities of the parent species, ^{13}C-, and ^{18}O-isotopologues in the broadband scan. Whereas the *b*-type transitions mentioned in Section 6.3.2 were discarded here, the same *a*-type *R*-branch transitions $2_{12} \leftarrow 1_{11}$, $2_{02} \leftarrow 1_{01}$, and $2_{11} \leftarrow 1_{10}$ as well as three other *a*-type lines $3_{13} \leftarrow 2_{12}$, $3_{03} \leftarrow 2_{02}$, and $3_{12} \leftarrow 2_{11}$ were searched, since *a*-type transition frequencies could, in general, be much better predicted.

Scans of $\pm$5 MHz around the predicted frequencies with overlapping spectra of 750 co-added decays per each and a step width of 0.2 MHz were performed. In total, 14 transitions could be found and fitted. The quartic centrifugal distortion constants Δ_J and Δ_K were well determined, whereas the δ_J and δ_K were fixed. The frequency list for the ^{18}O-isotopologue is given in Table 17.18, the fitted molecular parameters are in Table 6.2.

Internal rotation

The methyl group in MTHF undergoes internal rotation and causes A-E splittings of all rotational lines. [47] The barrier to internal rotation is calculated using various method-basis set combinations, as given in Table 17.11. The CCSD(T)/6-311++G(d,p) level of theory yields a barrier of 13.12 kJ·mol^{-1} (1097 cm^{-1}), which is rather high. The splittings, if resolvable, were expected to be very small, in the order of a few tens of kHz. In the experimental spectrum, only a few transitions at high *J* values show A-E splittings. A typical spectrum with observable splitting is given in Figure 6.8. The torsional splittings of 23 rotational transitions were observable. Nevertheless, due to the small splittings, no reasonable fit including internal rotation was obtained. Furthermore, very small splittings often appear too large after Fourier transformation. The barrier to internal rotation was not well determined, and the standard deviation was four times larger than the measurement accuracy.

Therefore, the effect of internal rotation in MTHF was completely neglected. It should be noted that the A-E splittings are larger for excited torsional states, and the barrier to internal rotation could be much better determined if transitions from the excited torsional states were included. Unfortunately, these states are not observable in a supersonic jet.

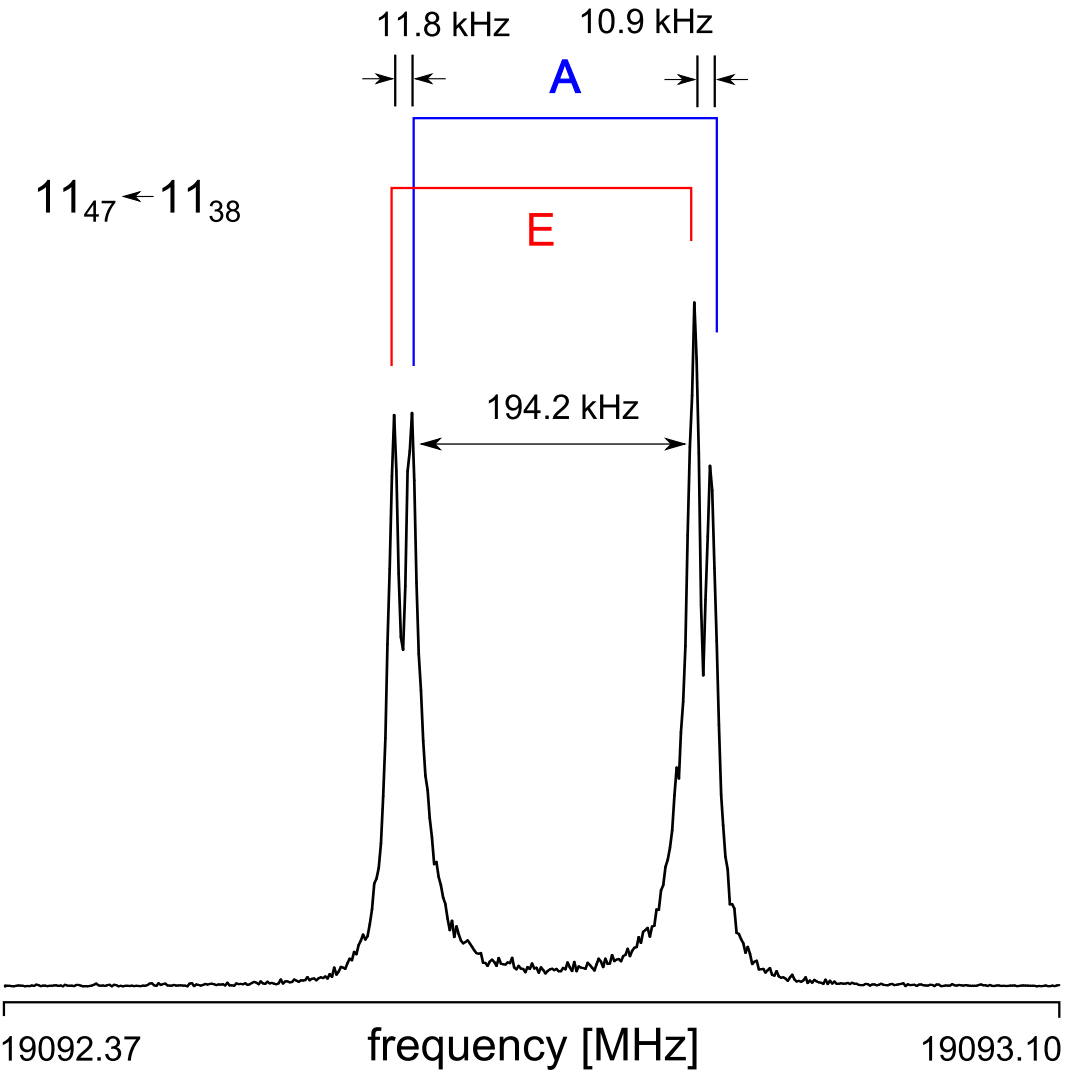

Figure 6.8. A typical spectrum of the $11_{47} \leftarrow 11_{38}$ transition of the parent species of MTHF, which shows an A-E splitting due to internal rotation of the methyl group. The line width is approximately 50 kHz (FWHH). For this spectrum 130 FIDs were co–added. [48]

6.4 Results of the fits and discussion

For the *equatorial* conformer, the rigid rotor fit including 111 rotational transitions has a standard deviation of 2.2 kHz, which is within the measurement accuracy. However, four sextic centrifugal distortion constants are needed to achieve this fit quality, while only transitions with $J \leq 15$ are included. Omitting these constants increases the standard deviation to 3.6 kHz, as shown in Fit II in Table 6.1. By taking into account only transitions with $J \leq 6$, the standard deviation decreases to 1.4 kHz (Fit III, also in Table 6.1). As mentioned in Section 6.3.2, the internal rotation of the methyl group causes splittings of about 20 kHz for some high J transitions. In such cases, the E component is neglected and only the A component is included in the fit. This approximate treatment partly explains the increase of the standard deviation of the fit, when transitions with $J > 6$ are considered. It might also be the reason that some

sextic centrifugal distortion constants improve the fit. The quartic centrifugal distortion constants are in a normal order of magnitude for molecules with comparable rotational constants, and there is no indication for an unusual floppiness of the molecule. The constants obtained from anharmonic frequency calculations are close to the experimental values for Δ_J, δ_J, and δ_K. The deviations for Δ_{JK}, Δ_K, and all sextic centrifugal distortion constants are remarkable, probably due to the effects of small vibration rotation interactions which have been taken into account in the calculations for these constants.

The experimentally deduced rotational constants are compared with those from quantum chemical calculations and listed in Table 17.11. Because the experimental constants B_0 refer to the ground vibrational state (r_0 structure), whereas the theoretical constants B_e refer to the equilibrium geometry (r_e structure), the values usually agree only within 1%. The best agreement is found at the B3LYP/cc-pVQZ level of theory. The MP2 method in combination with triple zeta basis sets provides excellent results for the B and C rotational constants but a larger deviation for the A rotational constant. The M06-2X functional is specifically designed for taking into account long-range dispersive interactions and yields also good results in this case. The rotational constants of the ground vibrational state are predicted by anharmonic frequency calculations, as given in Table 6.1. At the MP2/6-311++G(d,p) level of theory, the calculated A rotational constant agrees well with the experimental values; on the other hand, the B and C constants are much worse comparing to the results from geometry optimizations (see Table 17.11).

6.5 Determination of the heavy atom microwave structure

The structure determination can be performed using the experimentally deduced rotational constants of the parent species and the ^{13}C and ^{18}O-isotopologues. The isotopic shifts allow to calculate the heavy atom (carbon and oxygen) positions with respect to the center of mass of the parent species using Kraitchman's equations [35] as implemented in the program KRA and EVAL, which are available from the PROSPE database [56]. The uncertainties are calculated using Costain's rule, saying that the uncertainty is inversely proportional to the center of mass distance [46]. The signs of the atom coordinates have been taken from the coordinates calculated at the MP2/6-311++G(d,p) level. This determined r_s structure is in excellent agreement with the vibrationally averaged structure (r_z) calculated by anharmonic frequency calculations, as shown in Figure 6.9. The Cartesian coordinates of the r_z geometry are given in Table 17.10.

Table 6.3. Experimental heavy atom positions of the *equatorial* conformer obtained by isotopic substitutions and using Kraitchmann's equations implemented in the program KRA [56]. The atoms are numbered according Figure 6.1.

	|a|/Å	|b|/Å	|c|/Å
O1	0.104(15)	1.0792(14)	0.1747(86)
C2	0.7290(21)	0.051(30)	0.3774(40)
C3	0.140(11)	1.2464(12)	0.039(39)
C4	1.54132(97)	0.6932(22)	0.104(15)
C5	1.3428(12)	0.8240(19)	0.118(13)
C6	2.15737(70)	0.018(83)	0.123(13)

The experimental atom positions, bond lengths, angles, and dihedral angles are indicated in Table 6.3 and Table 6.4. By regarding both, Figure 6.7 and Figure 6.9, the frequency shifts from the parent transitions increase with the distance of the substituted carbon atom to the center of mass.

The microwave structure yields the experimental ring plane dihedral angle φ as well as the *envelope* fold angles, which characterize the *envelope* structure of MTHF as mentioned in Section 6.2. The ring plane is indeed distorted by $\varphi = -6.48(21)^\circ$, resulting in a 'near-*envelope*' conformation of the observed conformer. The *envelope* fold angles are $\gamma = 135.715(48)^\circ$ and $\gamma' = 139.950(54)^\circ$. These values reasonably agree with the calculated angles of $\varphi = -3.66^\circ$, $\gamma = 137.46^\circ$, and $\gamma' = 139.90^\circ$. The experimental Cremer-Pople parameters $q_2 = 0.40$, $\phi_2 = 27.5^\circ$, and $\delta = 68.5^\circ$ show that the *equatorial* conformer has a more *twist* character (see Figure 6.4) than the structure calculated at the MP2/6-311++G(d,p) level of theory ($q_2 = 0.39$, $\phi_2 = 32.4^\circ$ and $\delta = 67.7^\circ$).

Table 6.4. Experimental bond lengths, bond angles, and dihedral angles of the *equatorial* conformer obtained using the program EVAL [56].

Bond lengths / Å		**Bond angles / °**		**Dihedral angles / °**	
O1-C2	1.404(21)	O1-C2-C3	105.54(89)	C5-C4-C3-C2	−18.26(13)
C2-C3	1.536(21)	C2-C3-C4	102.34(94)	C4-C3-C2-C6	157.13(18)
C3-C4	1.5132(86)	C3-C4-C5	104.07(20)	C4-C3-C2-O1	39.483(67)
C4-C5	1.5304(23)	C4-C5-O1	107.01(23)	C3-C4-C5-O1	−6.48(21)
O1-C5	1.498(12)	C5-O1-C2	102.49(68)	C4-C5-O1-C2	31.081(70)
C2-C6	1.5139(41)	O1-C2-C6	105.8(30)	C5-O1-C2-C3	−43.334(58)
		C3-C2-C6	117.4(32)	C5-O1-C2-C6	−168.49(31)
				C5-O1-C3-C2	135.715(48)
				C4-C3-O1-C2	−139.950(54)

6.6 Conclusion

Geometry optimizations of MTHF using quantum chemical calculations yielded two stable conformers (*equatorial* and *axial*); both of them have an *envelope* structure. The intramolecular conversion from the *axial* conformer to the energetically more favorable *equatorial* conformer can occur via two transition states; one has an *envelope* and the other one a *twist* structure. In the microwave spectra recorded using the MB-FTMW technique, only the *equatorial* conformer could be observed. Rotational transitions of all heavy atom isotopologues were assigned, resulting in highly accurate rotational constants, centrifugal distortion constants, and the heavy atom positions with respect to the center of mass. The observed spectra could be reproduced within the measurement accuracy of 2 kHz.

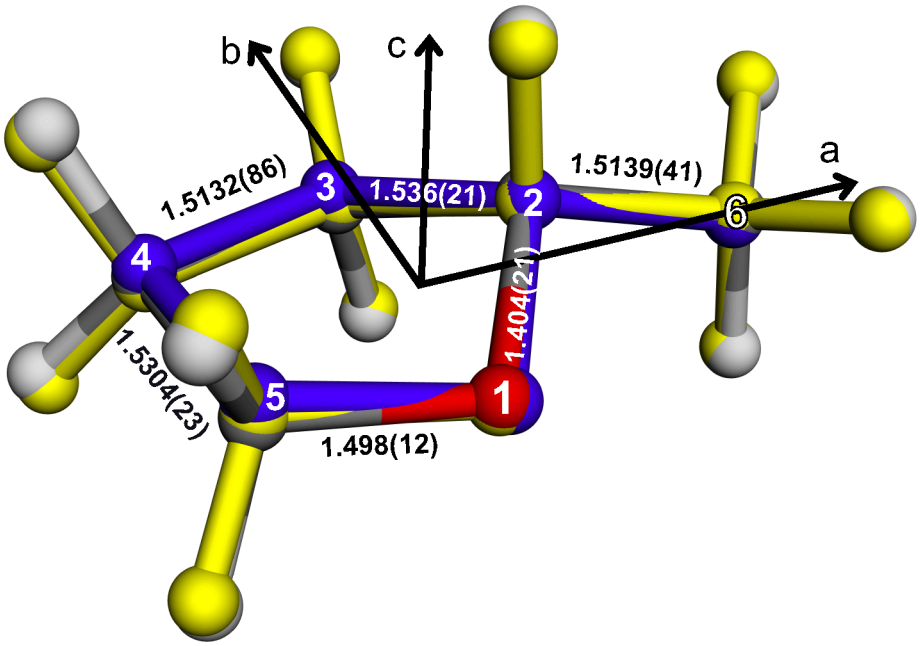

Figure 6.9. Comparison of the r_s microwave structure of MTHF (in blue) determined by heavy atom substitutions with atom positions (carbon in gray, oxygen in red) of the vibrationally averaged geometry calculated by anharmonic frequency calculations at the MP2/6-311++G(d,p) level of theory. Additionally, the atom positions of the equilibrium geometry at the MP2/6-311++G(d,p) level are given in yellow. The indicated experimental bond lengths are given in Å. Note that the further away the carbon atom is from the center of mass, the larger the frequency shift is from the parent transition (see Figure 6.7 for comparison). [48]

CHAPTER 7

2-Methyl-1,3-Dithiolane

7.1 Introduction

Volatile sulfur-containing heterocyclic molecules are important flavor substances as well as raw materials for perfumes. Sulfur-containing odorants of the chemical classes mercaptans (R-SH) and thioethers (R-S-R') are intensely bad-smelling, especially in high concentrations, while the oxygen analogons, alcohols (R-OH) and ethers (R-O-R'), are usually less perceptible and have in many cases a much more pleasant odor. Until now, the reason for this phenomenon has not yet been completely understood. An explanation by Fischer that the sulfur-containing substances are recognized by human smelling receptors by the 'lock and key' model [57] is not satisfactory, since almost no remarkable changes of the molecular structures could be found between the oxygen- and the sulfur-containing analogons. Hydrogen bonds from sulfur-containing substances are also much weaker than those from oxygen-containing molecules. [58] Furthermore, the typical odors of sulfur-containing molecules cannot be imitated by sulfur-free substances which have similar molecular geometry and charge distribution. Therefore, one assumption is that sulfur-containing substances bind reversible bonds directly between the sulfur atoms with the protein in the human receptor, which is not possible in the respective oxygen analogons. In order to understand and explain this phenomenon in more details, it is important to answer the questions, how molecular shapes fit together or how strong and how directional hydrogen bonds are. For this purpose, gas phase structures of sulfur-containing odorants are needed, since the sense of smell starts from gas phase molecules. A huge number of oxygen-containing odorants were investigated in the gas phase, including the studies on linalool [59], a main component of lavender oil, on fruit esters such as isoamyl acetate (banana odor) [60], ethyl valerate (green apple) [61] as well as on cassyrane (blackcurrant) [27]. Considerably fewer gas phase investigations on sulfur-containing odorants have been carried out, even though they are often the odor compounds found in nature. Some examples are cat ketone [62], 2-methyltetrahydrothiophen-3-one [3], and methyl isopropyl sulfide [63].

Here, the gas phase structures of 2-methyl-1,3-dithiolane (MDT) is studied. For this investigation, a combination of quantum chemical calculations and microwave spectroscopy in a supersonic expansion is used.

7.2 Quantum chemical calculations

7.2.1 Geometry optimizations

MDT is a five-membered heterocyclic molecule with two sulfur atoms in the ring structure and a methyl group. At the beginning, several starting geometries were created based on the structures of the two different conformers of cyclopentane [36]. Geometry optimizations were first performed at the MP2/6-311++G(d,p) level of theory using the GAUSSIAN09 package [26] in order to search for stable conformers. Quantum chemistry is a powerful tool to understand microwave spectra. The optimized geometries and molecular parameters of stable conformers give a reasonable estimation to start the spectral assignment. Conversely, experimental parameters obtained with high accuracy by microwave spectroscopy can be used for benchmark calculations. For example, in the study of Grimme *et al.* [44], the experimental data of isoamyl acetate [60], diisopropyl ketone [64], and triethyl amine [65] were necessary to validate the quantum chemical results.

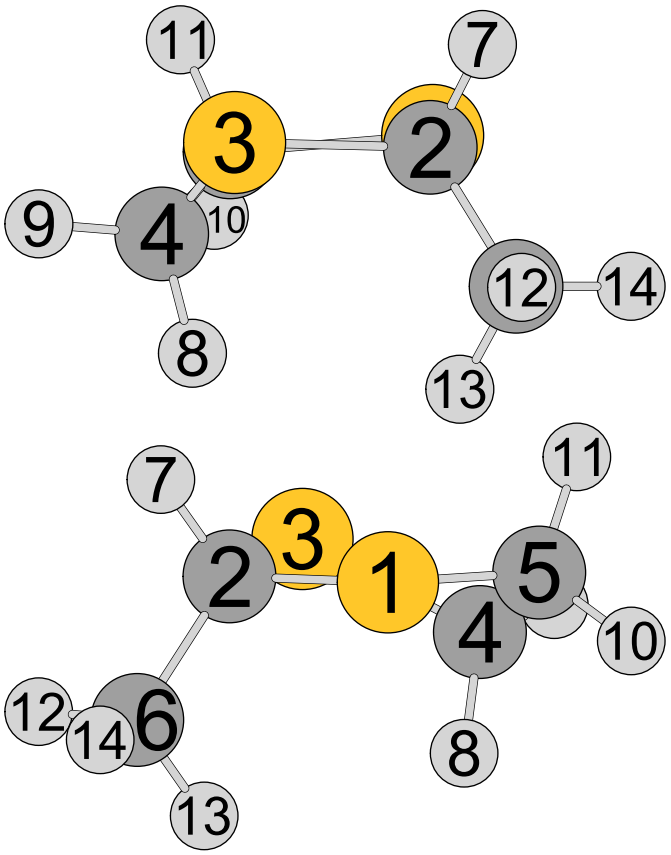

Figure 7.1. Optimized geometry of conformer I of MDT calculated at the M06-2X/cc-pVQZ level of theory from two perspectives since the geometry is a mixture of the *envelope* structure E_4 and the *twist* structure $^3T_4$.

The MP2/6-311++G(d,p) level of theory was chosen, since it led to acceptable rotational constants for other heterocyclic molecules [3,27]. It is also used quite often in the spectroscopic community [66–68]. The Cartesian coordinates are given in Table 17.19. Anharmonic frequency calculations were carried out at the same level of theory to obtain centrifugal distortion constants and to verify, whereas the optimized geometries are true minima or saddle points.

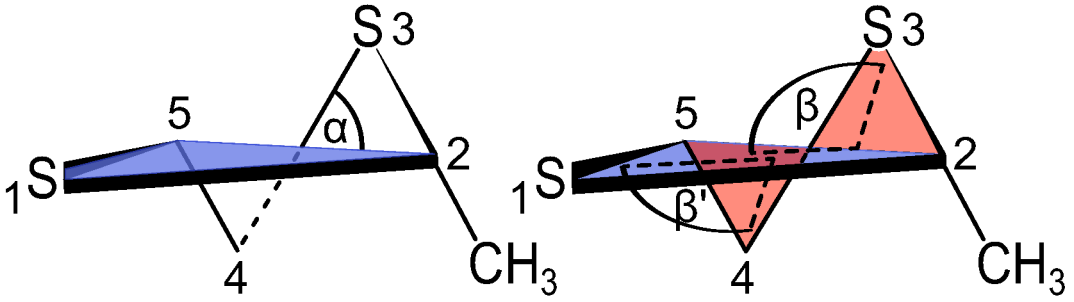

Figure 7.2. Definitions of the angles α, β, and β' in the *twist* conformation of MDT.

Quantum chemical calculations were redone at different levels of theory using various combinations of the HF, DFT, MP2, and CCSD methods and different basis sets including correlation consistent and Pople basis sets. Here, a few levels of theory yield two optimized conformers as given in Table 17.20. While two *twist* conformers were obtained at the M06-2X/cc-pVQZ level, only one near-*envelope* conformer was optimized at MP2/6-311++G(d,p) level. The most stable conformer at the M06-2X/cc-pVQZ level is visualized in Figure 7.1 and is a mixture of the *twist* structure $^3T_4$ and *envelope* structure E_4. The *twist* conformation can be described by the angle α between the ring plane C_5-S_1-C_2 and the vector S_3-C_4 as shown in Figure 7.2. Additionally, it is characterized by the angles β and β' between the ring plane C_5-S_1-C_2 and the *twisted* planes C_5-C_4-S_3 and C_2-S_3-C_4, respectively. β and β' are equal, if the ring structure is not distorted. On the other hand, the conformer obtained at the MP2/6-311++G(d,p) level has more contribution of the *envelope* structure E_4 (for comparison see Figure 7.3).

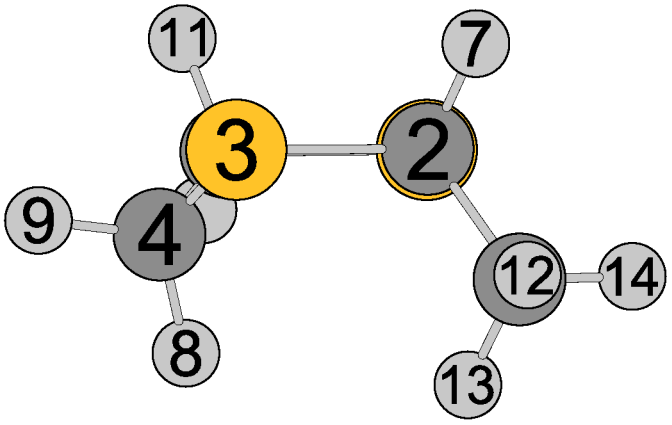

Figure 7.3. Optimized geometry of MDT calculated at the MP2/6-311++G(d,p) level of theory from the perspective of the *envelope* structure E_4.

The Cartesian coordinates of the stable conformers and transition states are given in Table 17.19 and 17.21 or Table 17.22 and 17.23 for the MP2/6-311++G(d,p) and M06-2X/cc-pVQZ level, respectively. A general characterization of the ring geometry is given in Section 7.2.4 using the Cremer-Pople puckering parameters [37]. If not stated else, all values given from now on as well as all calculations will refer to the MP2/6-311++G(d,p) level of theory.

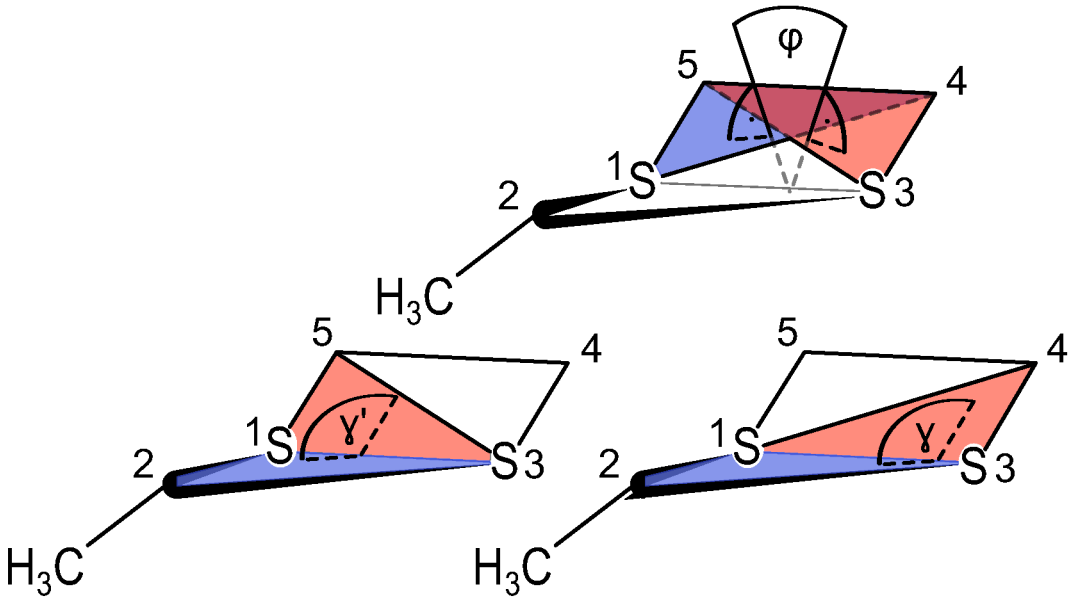

Figure 7.4. The *envelope* conformation is described by the dihedral angles φ, γ, and γ'. The angle $\varphi = \angle(S_1,C_5,C_4,S_3)$ is also the angle between the normal vectors of the blue and the red plane in the upper figure.

7.2.2 Transition states

Two transition states of MDT (TS1 and TS2) were optimized using the Berny algorithm [28] to understand the intramolecular conversion. Contrary to chemical intuition, the optimized geometries of the transition states do not show a planar ring structure. Two *envelope* conformations with different orientations of the methyl group were found. These transition states were also re-optimized at different levels of theory subsequently. When the *envelope* geometry is not disturbed, the *envelope* conformation can be described only by the position of the out-of-plane atom. In this case, the ring plane, described by the dihedral angle $\varphi = \angle(S_1,C_5,C_4,S_3)$, is perfect planar ($\varphi = 0$). Consequently, the two dihedral angles $\gamma = \angle(C_2,S_1,S_3,C_4)$ and $\gamma' = \angle(C_2,S_3,S_1,C_5)$, which define the flap angle of the *envelope*, have the same value. The angles are illustrated in Figure 7.4. A general characterization of the ring geometry is given in Section 7.2.4. The intramolecular conversion is shown in Figure 7.5.

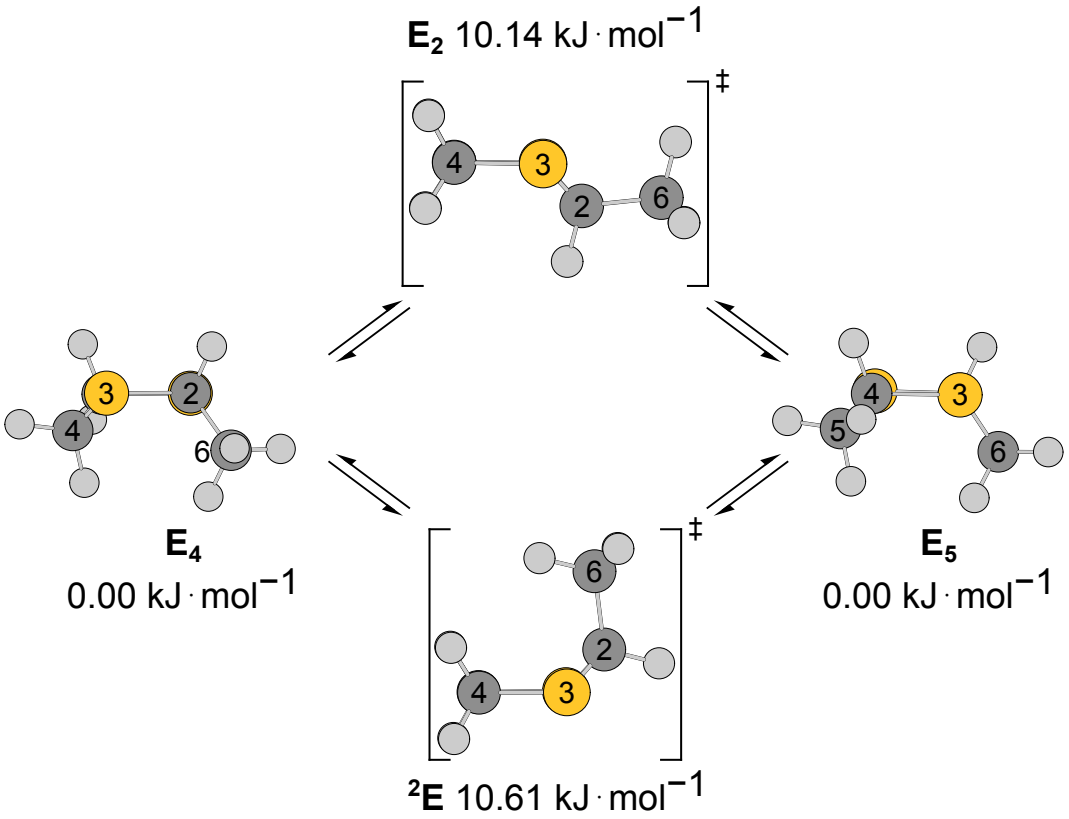

Figure 7.5. Intramolecular conversion between the stable *twist* conformers E_4 and E_5 (enantiomers) and the *envelope* transition states calculated at the MP2/6-311++G(d,p) level of theory. The energies are related to the lowest energetic conformer I with its absolute energy $E = -952.1096318$ Hartree.

7.2.3 Internal rotation

The methyl group in MDT undergoes internal rotation and causes A-E splittings of all rotational lines in the microwave spectrum. [47] The barriers to internal rotation are calculated to be 1650 cm^{-1}. This barrier is high and therefore, splittings due to internal rotation are not expected to be resolved with the resolution of the spectrometer.

7.2.4 Cremer-Pople puckering parameters

The calculated Cremer-Pople puckering parameters (see Chapter 4) verify that all conformations have an *envelope* geometry. The transitions states are located near $\phi_2 = 36°$ and 216° (^{2}E and E_2), while the stable conformer is located around $\phi_2 = 108°$ (E_4). The methyl substituent of the transition state E_2 has an *equatorial* orientation with $q_2 = 0.54$, $\phi_2 = 36.00°$, and $\delta = 70.50°$, while the transition state ^{2}E has an *axial* orientation of the methyl group with $q_2 = 0.55$, $\phi_2 = 216.00°$, and $\delta = 5.90°$. Conformer I (E_4) has an *axial* orientation of the methyl group with $q_2 = 0.52$, $\phi_2 = 108.39°$, and $\delta = 150.30°$. In Figure 7.6, the conformations are illustrated based on the model of Altona and Sundaralingam [40].

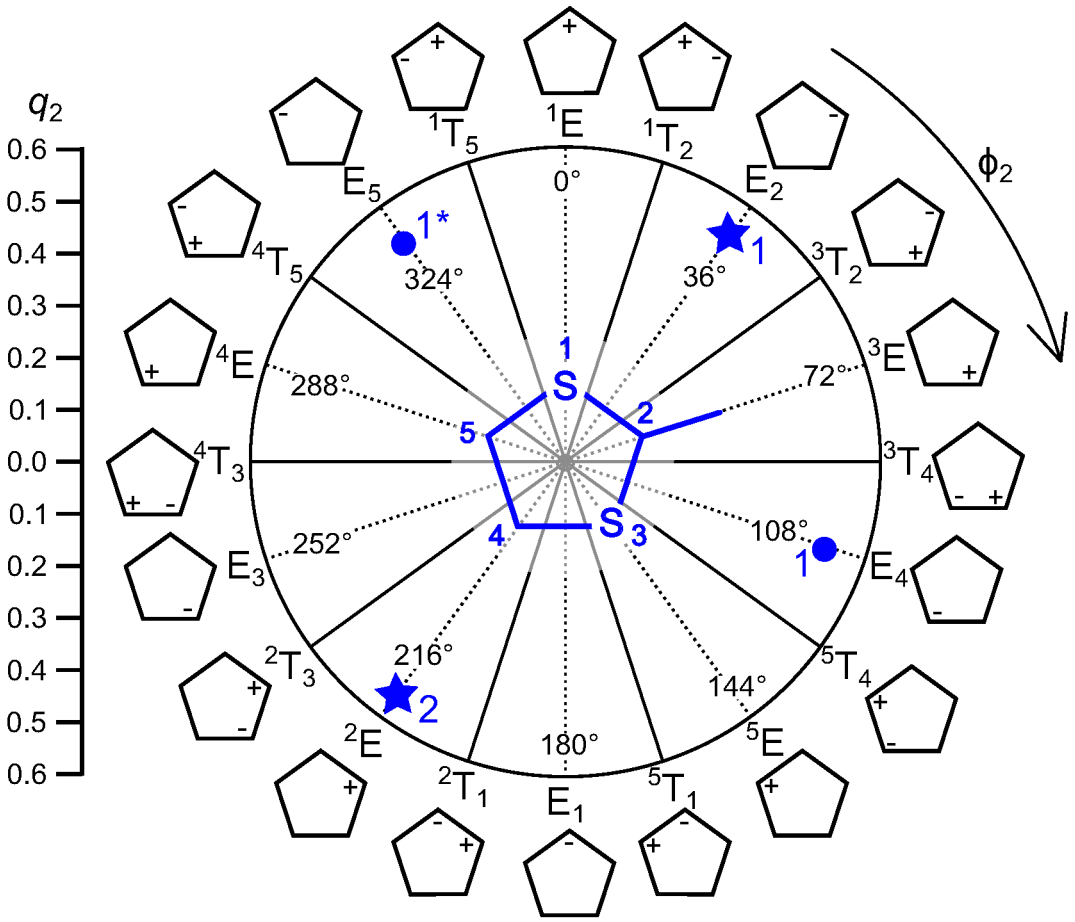

Figure 7.6. Conformational landscape of MDT using the Cremer-Pople parameters q_2 (puckering amplitude) and ϕ_2 (phase angle). The nomenclature is based on the ***Twist*** or ***Envelope*** geometry and the positions of the atoms which are above (+) and below (−) the ring plane. At the center, $q_2 = 0$ corresponds to a planar ring.

7.3 Microwave spectroscopy

7.3.1 Measurements

At the beginning, a broadband scan was recorded in the frequency range from 9 to 14 GHz. Overlapping spectra were automatically taken with a step width of 0.25 MHz. Afterwards, all lines were remeasured in the high resolution mode of the spectrometer. Here, the lines appear as doublets due to the Doppler effect. The measurement accuracy of isolated lines is estimated to be 2 kHz.

7.3.2 Spectral assignment

The stable conformer of MDT is a near oblate top with a Ray's asymmetry parameter κ of 0.903. The microwave spectrum was predicted with the program XIAM [45] using the rotational constants calculated at the MP2/6-311++G(d,p) level of theory. The dipole moment components suggested a spectrum with strong *b*- and *c*-type transitions and weak *a*-type transitions ($|\mu_a| = 0.12$ D, $|\mu_b| = 0.80$ D, and $|\mu_c| = 0.80$ D). Furthermore, transitions with low J and K values are often more intense in the molecular beam rotational spectrum. Based on the prediction of a near oblate top spectrum, the *a*- and *b*-type transitions of the *Q*- and *R*-branches are almost not separated in the broadband scan. Therefore, the clearly separated *c*-type transitions $2_{11} \leftarrow 1_{01}$, $2_{20} \leftarrow 1_{10}$, and $2_{21} \leftarrow 1_{11}$ and the separated *b*-type transition $2_{20} \leftarrow 1_{11}$ were chosen as a starting point for the assignment as shown in Figure 7.7. Using these lines, it was possible to assign the remaining lines. Additional transitions, which were not covered in the broadband scan, were predicted and could be found in the frequency range up to 40 GHz. Subsequently, the highly dense *a*- and *b*-type transitions of the *Q*- and *R*-branches could be assigned. All fitted transitions are listed in Table 17.24. The fitted molecular parameters can be found in Table 7.1.

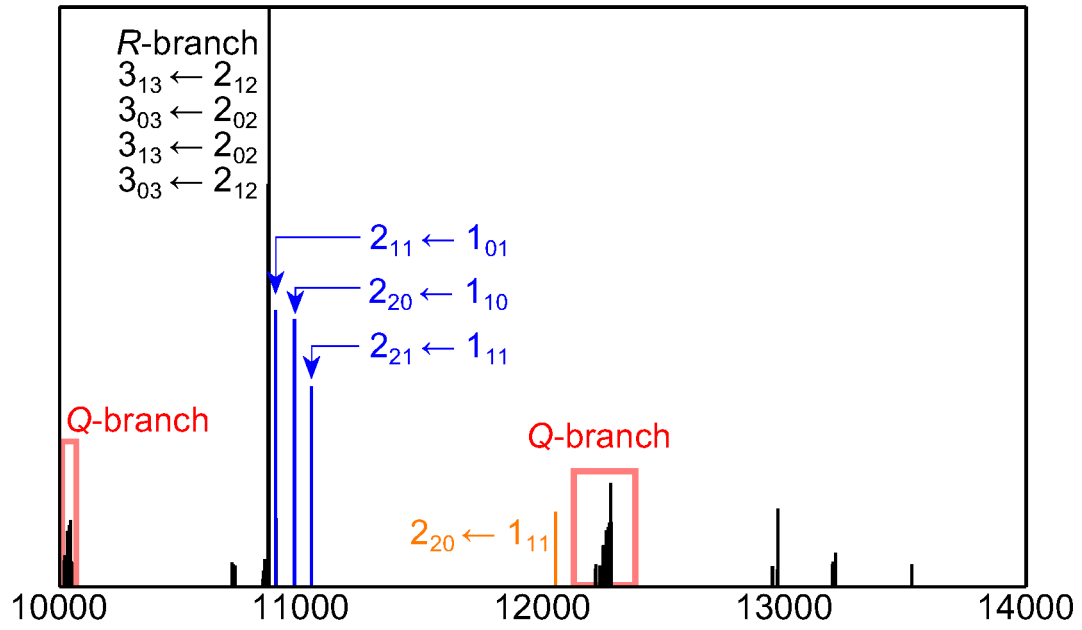

Figure 7.7. Experimental broadband scan in the frequency range from 10000 to 14000 MHz. Three *c*-type *R*-branch transitions $2_{11} \leftarrow 1_{01}$, $2_{20} \leftarrow 1_{10}$, and $2_{21} \leftarrow 1_{11}$ are marked in blue and two *Q*-branches with high density of lines are illustrated in red. Only in the high resolution spectra, the splittings of the strongest line into different rotational transitions were observable.

7.4 Results of the fit and discussion

The rotational and centrifugal distortion constants of MDT were determined with very high accuracy. In total, 136 transitions were fitted to an excellent standard deviation of 1.5 kHz, which is within the experimental accuracy of the spectrometer. Watson's S reduction in I^r representation was used. The experimentally deduced rotational constants were compared with those from quantum chemical calculations. The best agreement could be found with the method M06-2X, as shown in Table 17.20. The barrier to internal rotation of the methyl group was calculated to be higher than 1650 cm^{-1}. In agreement with this calculation, no torsional splittings were observed. All rotational transitions in the broadband scan were assigned to the observed conformer. Therefore, only one conformer is observable in the molecular beam.

Table 7.1. Molecular parameters of conformer I obtained by the program XIAM.

Par.[a]	Unit	Fit	Calc.[b]
A	GHz	2.779 190 37(14)	2.761
B	GHz	2.705 487 270(73)	2.698
C	GHz	1.624 829 803(60)	1.598
D_J	kHz	0.5982(12)	0.896
D_{JK}	kHz	−0.4194(55)	−2.323
D_K	kHz	0.4574(48)	2.247
d_1	kHz	−0.154 94(39)	−0.246
d_2	kHz	−0.140 00(23)	−0.071
σ^c	kHz	1.5	
N[d]		136	
κ		0.872	

[a] All parameters refer to the principal axis system. Watson's S reduction in I^r representation was used. [b] Calculated at the MP2/6-311++G(d,p) level using anharmonic frequency calculation. The rotational constants refer to the vibrational ground state. [c] Standard deviation of the fit. [d] Number of lines.

7.5 Conclusion

The conformational analysis using quantum chemical calculations yielded one stable conformer of 2-methyldithiolane with near-*envelope* geometry and two transition states with *envelope* structures at the MP2/6-311++G(d,p) level. The microwave spectra of the near-*envelope* conformer was assigned and could be reproduced within the experimental error of 2 kHz. In contrast to the molecule 2-methyltetrahydrothiophene (see Chapter 5) with two *twist* geometries, MDT has a near-*envelope* structure like 2-methyltetrahydrofuran (see Chapter 6).

CHAPTER 8

Coffee Furanone (2-Methyltetrahydrofuran-3-one)

8.1 Introduction

Coffee is a very popular drink in the daily life of millions of people in many countries. As a first hot beverage in the morning for many people, several methods were investigated and created to obtain the best quality of this popular drink including different extraction techniques and roasting processes. The coffee aroma is quite complex with more than 800 volatile compounds. [16] Since the bean roasting and the brewing of coffee have many process parameters to create the desired aroma, the composition of the volatile aroma has been widely studied. [17, 69]

In this chapter, the gas phase structure of one of the volatile aroma compounds, coffee furanone (2-methyltetrahydrofuran-3-one), is investigated since the sense of smell starts from gas phase molecules. Coffee furanone is a five-membered heterocyclic molecule and can be found as natural flavor in tomato [18] and pork [19]. It was also identified in the Maillard reaction which is known to create important roasting aromas when food is browned. [7]

This study is based on a combination of quantum chemical calculations and microwave spectroscopy in a supersonic expansion to understand the gas phase of this important coffee aroma compound.

8.2 Quantum chemical calculations

8.2.1 Geometry optimizations

Coffee furanone is a five-membered heterocyclic molecule with an oxygen atom in the ring structure, a carbonylic group, and a methyl group. Several starting geometries were created to calculate rotational constants based on the structures of the two different conformers of cyclopentane [36] similar to the molecules 2-methyltetrahydrothiophene, 2-methyltetrahydrofuran, and 2-methyl-1,3-dithiolane of the previous chapters. Geometry optimizations were performed at the MP2/6-311++G(d,p) level of theory

using the GAUSSIAN09 package [26]. The optimized geometries and their molecular parameters give a reasonable estimation to start the spectral assignment. Harmonic frequency calculations were carried out at the same level of theory to verify, whereas the optimized geometries are true minima or saddle points. Anharmonic frequency calculations were performed to obtain centrifugal distortion constants.

Quantum chemical calculations were redone at different levels of theory using various combinations of the HF, DFT, MP2, and CCSD methods and different basis sets. Two *twist* conformers were obtained at the MP2/6-311++G(d,p) level. The most stable conformer I is visualized in Figure 8.1 and has the *twist* structure $^{3}T_{4}$ while conformer II has the *twist* structure $^{4}T_{3}$ as shown in Figure 8.2. A general characterization of the ring geometry is given in the Section 8.2.3 using the Cremer-Pople puckering parameters [37]. The rotational constants calculated at different levels of theory are listed in Table 17.25 and 17.26 for conformer I and II, respectively. The Cartesian coordinates are given in Table 17.27.

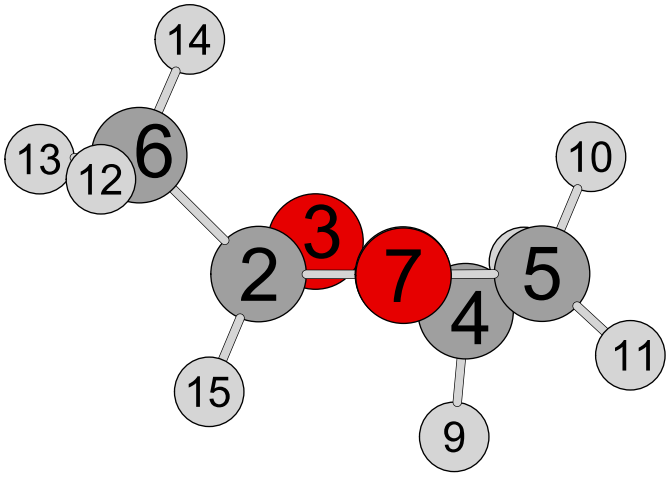

Figure 8.1. Optimized geometry of conformer I of coffee furanone calculated at the MP2/6-311++G(d,p) level of theory from the perspective of the *twist* structure $^{3}T_{4}$.

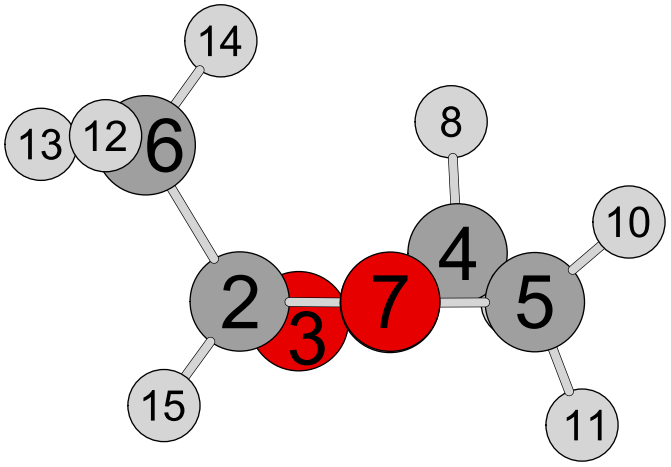

Figure 8.2. Optimized geometry of conformer II of coffee furanone calculated at the MP2/6-311++G(d,p) level of theory from the perspective of the *twist* structure $^{4}T_{3}$ (4.34 kJ·mol^{-1} higher in energy than conformer I).

8.2.2 Internal rotation

The large amplitude motion of the methyl group in coffee furanone causes A-E splittings of all rotational lines in the microwave spectrum. [47] These splittings depend on the torsional barrier. These barriers to internal rotation are calculated to be 1020 cm^{-1} and 1120 cm^{-1} for conformer I and conformer II, respectively. Therefore, splittings due to internal rotation of the methyl group are expected to be too small to be resolved with the resolution of the spectrometer.

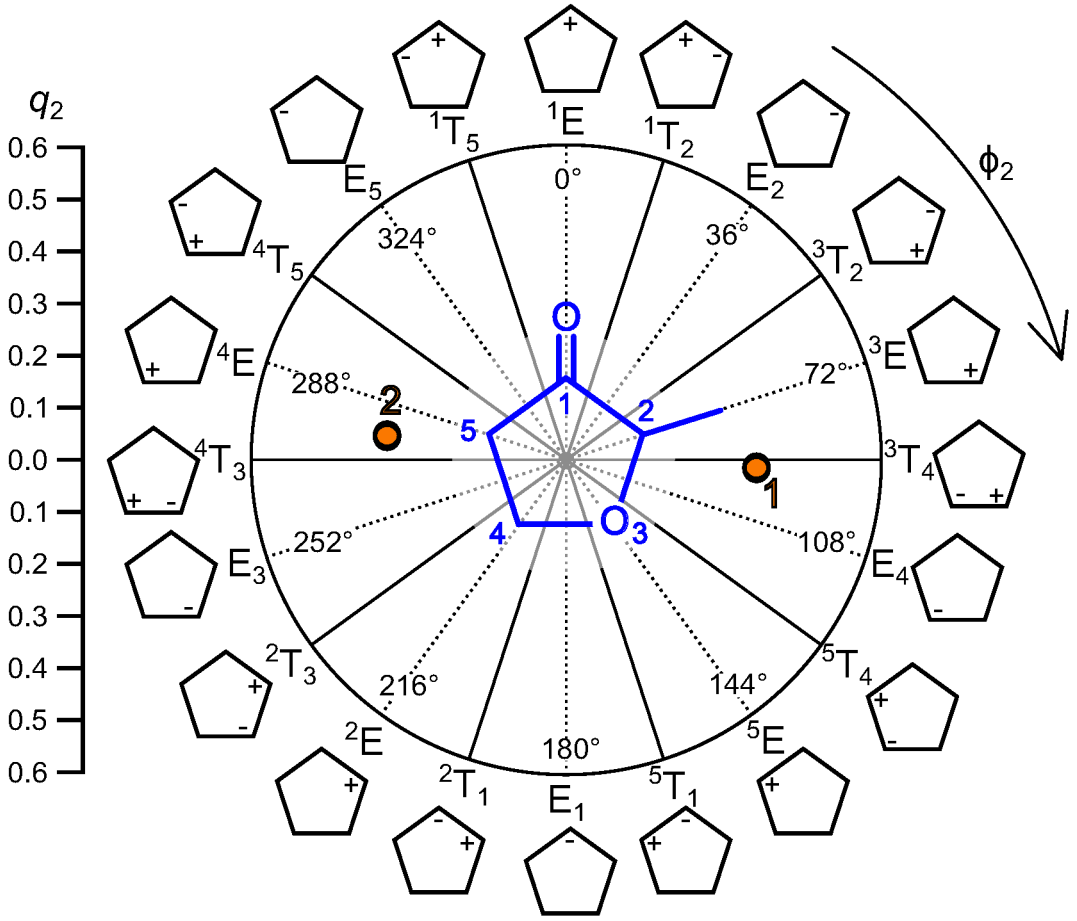

Figure 8.3. Conformational landscape of coffee furanone using the Cremer-Pople parameters q_2 (puckering amplitude) and ϕ_2 (phase angle). The nomenclature is based on the ***Twist*** or ***Envelope*** geometry and the positions of the atoms which are above (+) and below (−) the ring plane. At the center, $q_2 = 0$ corresponds to a planar ring.

8.2.3 Cremer-Pople puckering parameters

The Cremer-Pople puckering parameters [37] were calculated for both conformers to characterize their ring geometries. The parameters describe the conformational space of a five-membered ring using the puckering amplitude q_2 and the phase angle ϕ_2 (see Chapter 4). The orientation of the methyl group is described by the angle δ between the mean plane of the puckered ring and the bond of the methyl group. [38] The calculated geometry of conformer I is a *twist* structure (^{3}T$_4$) and the methyl substituent

is in an *inclinal* orientation with $q_2 = 0.38$, $\phi_2 = 92.3°$, and $\delta = 53.6°$. Conformer II is also a *twist* structure ($^4T_3$) with a little more contribution of the *envelope* structure ^4E. In contrast to conformer I, the methyl substituent of conformer II has an *axial* orientation with $q_2 = 0.35$, $\phi_2 = 277.6°$, and $\delta = 25.2°$. In Figure 8.3, both conformers are illustrated based on the model of Altona and Sundaralingam [40].

8.3 Microwave spectroscopy

8.3.1 Measurements

For an overview of the rotational spectra, a broadband scan was recorded in the frequency range from 9 to 14 GHz with a step width of 0.25 MHz. Afterwards, all lines were remeasured with more repetitions to obtain isolated doublet lines due to the Doppler effect. The measurement accuracy of isolated lines is estimated to be 2 kHz.

8.3.2 Spectral assignment

First, the most stable conformer I of coffee furanone was searched in the broadband scan. The microwave spectrum was predicted with the program XIAM [45] using the rotational constants calculated at the MP2/6-311++G(d,p) level of theory. The dipole moment components suggested a spectrum with strong *a*-type transitions and medium *b*- and *c*-type transitions ($|\mu_a| = 2.25$ D, $|\mu_b| = 0.62$ D, and $|\mu_c| = 0.34$ D). Furthermore, transitions with low J and K values are often more intense in the molecular beam rotational spectrum. The assignment was started with the *a*-type transitions $3_{13} \leftarrow 2_{12}$ and $3_{03} \leftarrow 2_{02}$ as well as the *b*-type transition $3_{03} \leftarrow 2_{12}$ and $3_{13} \leftarrow 2_{02}$. Additional transitions, which were not covered in the broadband scan, were predicted and assigned in the frequency range of the spectrometer. All measured transitions are listed in Table 17.28. The fitted molecular parameters can be found in Table 8.1. All strong lines in the broadband scan can be assigned to conformer I. However, still half of the rotational transitions remain unassigned. All attempts to assign conformer II were unsuccessful so far.

8.4 Results of the fit and discussion

The rotational and centrifugal distortion constants of coffee furanone were determined with very high accuracy. In total, 120 transitions were fitted to a standard deviation of 2.8 kHz, which is near the experimental accuracy of the spectrometer. Watson's A reduction in I^r representation was used. The barrier to internal rotation of the methyl group was calculated to be higher than 1000 cm^{-1}. In agreement to this calculation, no torsional splittings were observed. A high number of transitions are still unassigned. So far, all attempts to assign the second conformer failed. While the use of a script was successful to assign

the isotopologues of 2-methyltetrahydrofuran, it failed to fit more than five rotational transitions of the second conformer using brute force. Here, all possible combinations of observed molecular signals were tried to fit.

Table 8.1. Molecular parameters of conformer I of coffee furanone under molecular beam conditions obtained by the program XIAM.

Par.[a]	Unit	Fit	Calc.[b]
A	GHz	3.539 555 98(21)	3.501
B	GHz	3.111 023 37(14)	3.094
C	GHz	1.796 248 83(14)	1.787
Δ_J	kHz	0.2922(31)	0.291
Δ_{JK}	kHz	−0.2793(30)	0.017
Δ_K	kHz	1.4498(31)	0.923
δ_J	kHz	0.088 56(50)	0.080
δ_K	kHz	0.1213(15)	0.260
σ^c	kHz	2.8	
N[d]		120	

[a] All parameters refer to the principal axis system. Watson's A reduction in I^r representation was used. [b] Ground state rotational constants and centrifugal distortion constants obtained by anharmonic frequency calculation at the MP2/6-311++G(d,p) level of theory. [c] Standard deviation of the fit. [d] Number of lines.

8.5 Conclusion

The conformational analysis yielded two stable conformers of coffee furanone, both with *twist* structures. The microwave spectra of conformer I ($^3T_4$) were assigned and could be reproduced almost within the experimental accuracy of 2 kHz. Compared to other five-membered heterocyclic molecules with a methyl group, coffee furanone has similar conformers and transition states as the flavor molecules 2-methyltetrahydrothiophene, 2-methylcyclopentanone, and 2-methyltetrahydrothiophen-3-one.

CHAPTER 9

Characterization of Non-Planar Rings

9.1 Introduction

The knowledge of gas phase structures of odorant molecules is important for the understanding of the structure-odor relationship since the sense of smell starts from gas phase molecules. Some of these volatile heterocyclic flavor substances can be found in the Maillard reaction which is known to create roasting aromas when food is browned. [6, 7] The knowledge of the composition of these aromas is important to understand the aroma production during food cooking and to create new flavors. The prototype molecule cyclopentane has two stable conformers, one with a *twisted* and the other one with an *envelope* structure. [36] Here, the conformational landscape of the investigated five-membered non-planar rings has only two different types of stable geometries, the *twist* and the *envelope* structure (see Chapter 4). Sulfur-containing molecules mostly have different olfactory properties compared to their oxygen analogons. To investigate this phenomenon, gas phase structures of sulfur- as well as oxygen-containing odorants are needed. Functional groups might have different influence on the ring structure. Therefore, a comparison of the structure of odorant molecules with non-planar five-membered ring systems will be given here. The molecules are listed in Table 9.1. Additionally, the two molecules 2-methylcyclopentanone (**6**) [42] and methylcyclopentane (**7**) are compared here due to their similar chemical structure.

Table 9.1. Comparison of non-planar odorant molecules.

molecule	natural odorant compound in	reference
2-Methyltetrahydrothiophen-3-one (**1**)	coffee, whiskey, wine [4], roasted peanuts [5]	[3]
2-Methyltetrahydrothiophene (**2**)	wine [8], brandy [9], degradation of vitamin B_1 [10]	Chapter 5
2-Methyltetrahydrofuran (**3**)	fish sauce [12], earth almond [13]	Chapter 6
2-Methyl-1,3-dithiolane (**4**)	roasting aroma of meat [14], peanut oil [15]	Chapter 7
Coffee Furanone (**5**)	coffee [16, 17], tomato [18], pork [19]	Chapter 8

9.2 Comparison

All molecules except 2-methyl-1,3-dithiolane (**4**) and methylcyclopentane (**7**) are chiral. The configurations of these molecules were chosen in a way that all molecules have comparable structures.

2-Methyltetrahydrothiophen-3-one

In a microwave spectroscopic study, Mouhib *et al.* [3] reported on two stable *twist* conformers in 2-methyltetrahydrothiophen-3-one (**1**). Here, the carbonyl and the thioether group co-exist in the ring. The carbonyl group is in the ring plane and the thioether groups is off the plane. The intramolecular conversion is shown in Figure 9.1. It is an interesting question which group dominantly determines the ring structure.

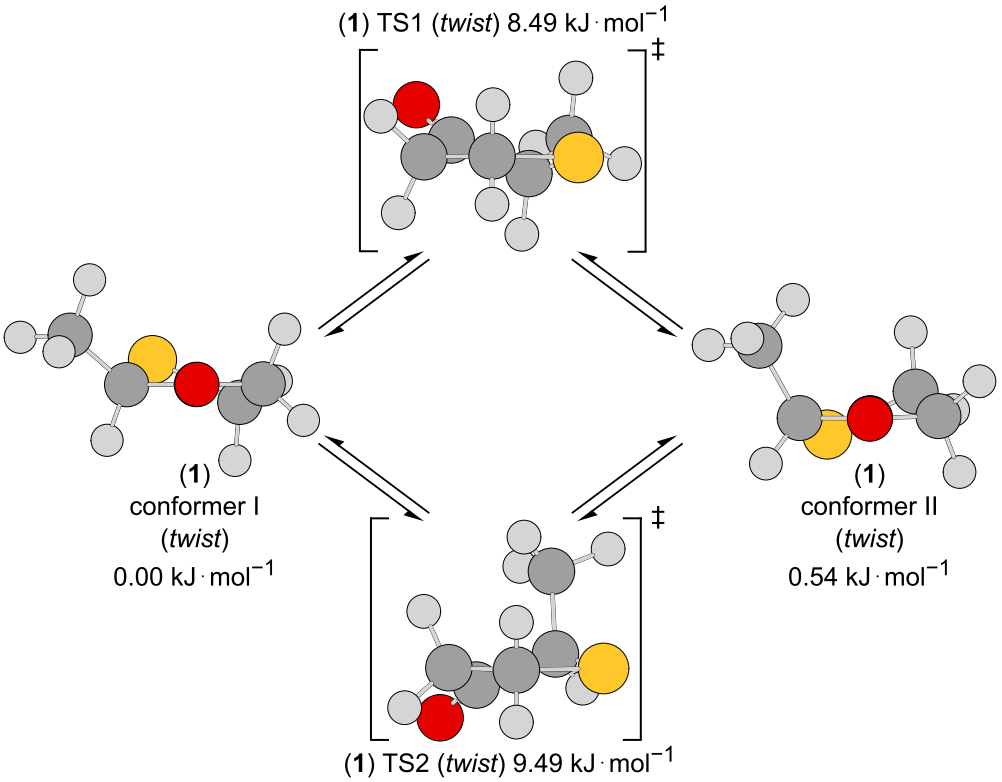

Figure 9.1. Optimized geometries of the stable *twist* conformers I and II as well as the *envelope* transition states TS1 and TS2 of 2-methyltetrahydrothiophen-3-one (**1**) calculated at the MP2/6-311++G(d,p) level of theory. The energies are given relative to the energy of conformer I ($E = -667.527749$ Hartree). [3]

2-Methyltetrahydrothiophene

Therefore, one functional group was removed to study its influence in more detail. When the carbonyl group is exchanged by a methylene group, the molecule 2-methyltetrahydrothiophene (**2**) is obtained (see Chapter 5). Here, also two stable *twist* conformers were observed and transitions states with near-

envelope geometries and disturbed ring planes were calculated. In contrast to 2-methyltetrahydrothiophen-3-one (**1**), the thioether group is now in the ring plane. For this reason, the carbonyl group clearly dominates the thioether group, which acts like a normal methylen group in the ring of 2-methyltetrahydrothiophen-3-one (**1**).

2-Methyltetrahydrofuran

Next, the thioether group in 2-methyltetrahydrothiophene (**2**) is exchanged by a smaller ether group in 2-methyltetrahydrofuran (**3**) to study its effect on the ring structure (see Chapter 6). Two stable *envelope* conformers were calculated. Only the most stable conformer was observed due to the small barrier to convert the conformer with higher energy into the most stable ones. In 2-methyltetrahydrothiophene (**2**), the thioether group has a dominant influence on the ring structure. In contrast, the methyl group of 2-methyltetrahydrofuran (**3**) affects the ring structure much stronger than the ether group. Two different transition states were found; the most stable one has a *twisted* geometry while the other has an *envelope* structure. Altogether, the stable conformers of 2-methyltetrahydrofuran (**3**) have *envelope* structures while the transitions states have a *twist* as well as an *envelope* structure. The most stable near-*envelope* conformer of 2-methyltetrahydrofuran (**3**) was verified by its heavy atom microwave structure (see Chapter 6).

2-Methyl-1,3-dithiolane

In 2-methyl-1,3-dithiolane (**4**), two thioether groups are present (see Chapter 7). Here, the conformational analysis with quantum chemical calculations yielded only one stable conformer. This is in agreement with the experimental microwave spectra, in which the near-*envelope* conformer was assigned and could be reproduced within the experimental error. Two transition states with *envelope* structures were calculated. In contrast to 2-methyltetrahydrothiophene (**2**) with two *twist* geometries, 2-methyl-1,3-dithiolane (**4**) has a near-*envelope* structure like 2-methyltetrahydrofuran (**3**). While the ring atom attached to the methyl group is off the ring plane in 2-methyltetrahydrofuran (**3**), this is not the case for 2-methyl-1,3-dithiolane (**4**).

Coffee Furanone (2-Methyltetrahydrofuran-3-one)

When the thioether group in 2-methyltetrahydrothiophen-3-one (**1**) is exchanged by an ether group, 2-methyltetrahydrofuran-3-one, also called coffee furanone (**5**), is obtained (see Chapter 8). Here, the conformational analysis yielded two stable conformers with *twist* structures. The microwave spectrum of one conformer was assigned while transitions of the second conformer might remain in the spectra. Coffee furanone (**5**) has similar *twist* conformers as 2-methyltetrahydrothiophen-3-one (**1**) and 2-

methyltetrahydrothiophene (**2**).

2-Methylcyclopentanone

2-Methylcyclopentanone (**6**) is also a related molecule of 2-methyltetrahydrothiophen-3-one (**1**) and 2-methyltetrahydrofuran-3-one (**5**), where the (thio)ether group is exchanged by a methylene group. Its rotational spectra are reported in Ref. [42]. Two stable *twist* conformers were obtained by quantum chemical calculations and are shown in Figure 9.2. Ring structures similar to those in 2-methyltetrahydrothiophen-3-one (**1**), 2-methyltetrahydrothiophene (**2**), and coffee furanone (**5**) were found. Two transition states with near-*envelope* structures can be observed (see also Figure 9.2). The transition state with the methyl group and the flap on the same side of the ring plane (TS1) is 1.84 kJ·mol^{-1} lower in energy than that with the methyl group and the flap on the opposite site (TS2), similar to the case of 2-methyltetrahydrothiophene (**2**). The ring plane of TS1 is more distorted than that of TS2, where the angle φ is nearly zero. The angle of the *envelope* flap is larger than the one of the transition states of 2-methyltetrahydrothiophene (**2**). The Cartesian coordinates of the stable conformers are given in Table 17.29 and of the transition states in Table 17.30. The results of the geometry optimizations at different levels of theory are given in Table 17.31 and 17.32 for the stable conformers as well as in Table 17.33 and 17.34 for the transition states.

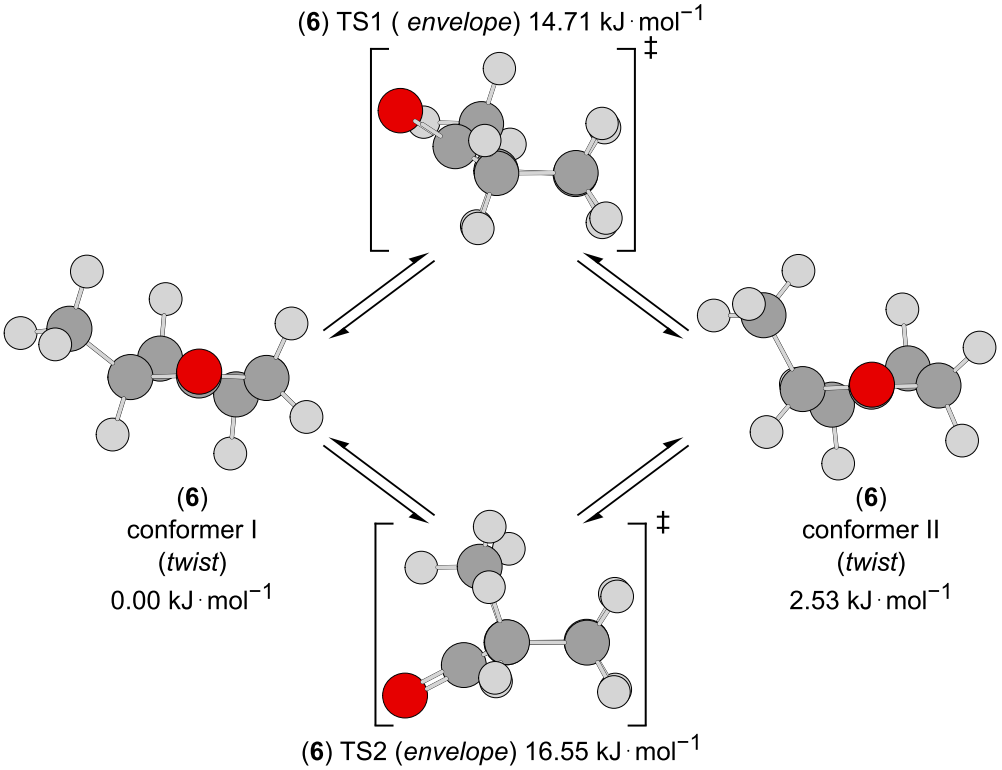

Figure 9.2. Optimized geometries of the stable *twist* conformers I and II as well as the *envelope* transition states TS1 and TS2 of 2-methylcyclopentanone (**6**) calculated at the MP2/6-311++G(d,p) level of theory. The energies are given with respect to the energy of conformer I ($E = -309.056582$ Hartree).

Methylcyclopentane

In contrast to the just mentioned molecules, methylcyclopentane (**7**) has no functional group in the ring structure at all. Quantum chemical calculations yielded two *envelope* (conformer I and II) as well as two *twist* conformers (conformer III/III*), which exist as an enantiomeric pair as shown in Figure 9.3. In the *envelope* conformers, the methyl group is attached on the top of the flap while it is attached to the center of the ring plane in conformers III/III*. Obviously, the methyl group has an influence on the ring structure like the carbonyl group in 2-methylcyclopentanone (**6**) or the thioether group in 2-methyltetrahydrothiophene (**2**). The most stable conformer I has an *envelope* structure with the methyl group in *equatorial* position. The *envelope* conformer with the methyl group in *axial* position is 1.09 kJ·mol^{-1} higher in energy. The ring plane is perfectly planar ($\varphi = 0$) for the conformers I and II. The *twist* conformers III/III* are higher in energy than the *envelope* conformers.

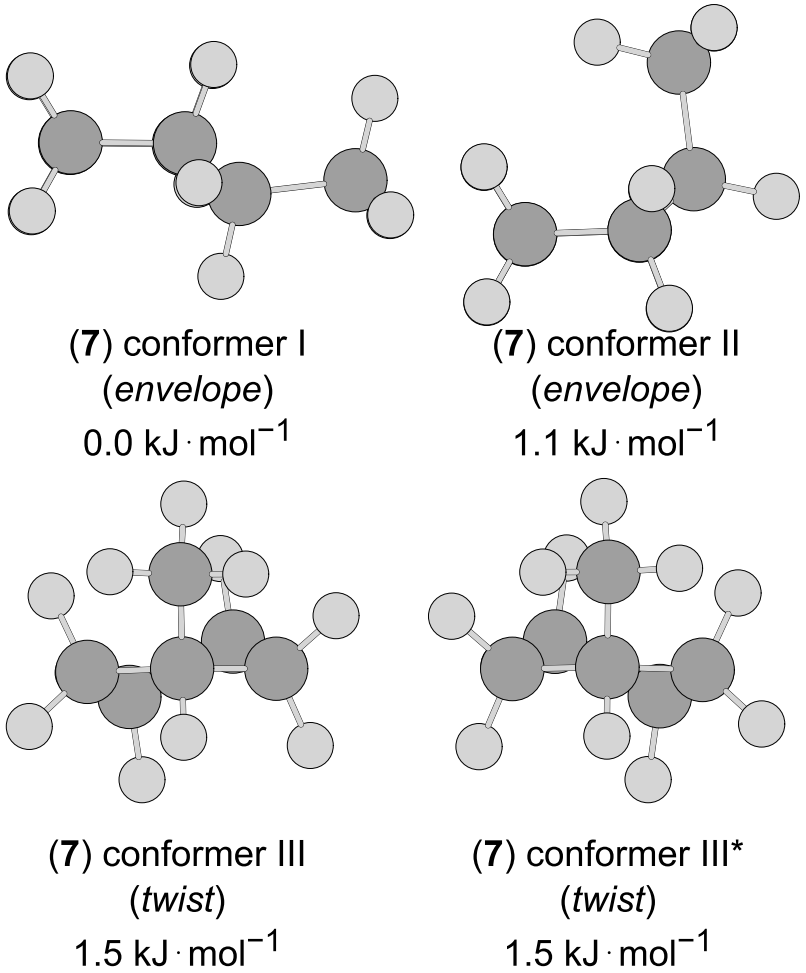

Figure 9.3. Optimized geometries of the stable *envelope* conformers I and II as well as the *twist* conformers III and III* (enantiomers) of methylcyclopentane (**7**) calculated at the MP2/6-311++G(d,p) level of theory. The energies are given with respect to the energy of conformer I ($E = -235.164855$ Hartree).

Additionally, four transition states (TS1/1* and TS2/2*) were found and are shown in Figure 9.4. They exist as two enantiomeric pairs and exhibit *envelope* structures, where, in contrast to the stable conformers I and II, the methyl group is not attached to the flap. The transition states TS1/1* have the methyl group in 3-position to the flap. In constrast, the transition states TS2/2* have the methyl group neighboring to the flap (2-position). The Cartesian coordinates of the stable conformers are given in Table 17.35 and of the transition states in Table 17.36. The results of the geometry optimizations at different levels of theory are given in Table 17.37 and 17.38 for the stable conformers as well as in Table 17.39 for the transition state.

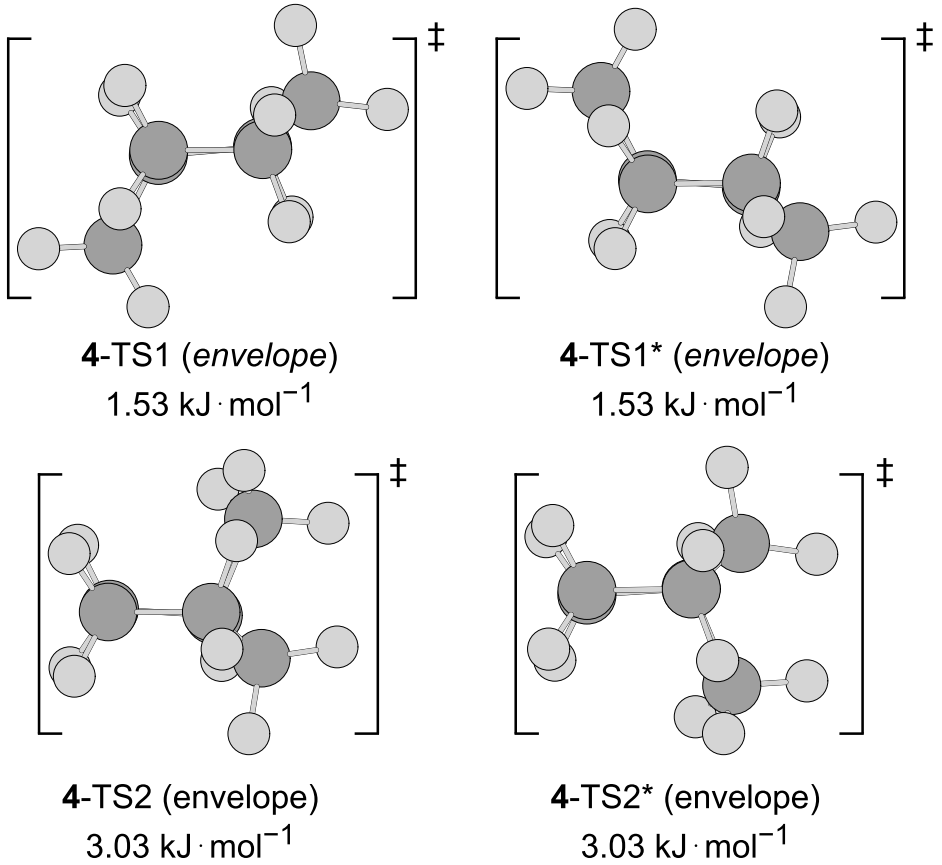

Figure 9.4. Optimized geometries of the *envelope* transition states TS1, TS1*, TS2, and TS2* of methylcyclopentane (**7**) calculated at the MP2/6-311++G(d,p) level of theory. They exist as two enantiomeric pairs. The energies are given with respect to the energy of conformer I ($E = -235.164855$ Hartree).

A summary of the characterizing angles (see Chapter 4) and energies for the *twist* and *envelope* structures of all molecules is given in Table 9.2. Additional characterizing angles calculated at several levels of theory are given in Table 17.40, 17.41, and 17.42.

Table 9.2. Comparison of the stable conformers and transition states of 2-methyltetrahydrothiophen-3-one (**1**), 2-methyltetrahydrothiophene (**2**), 2-methyltetrahydrofuran (**3**), 2-methyl-1,3-dithiolane (**4**), coffee furanone (**5**), 2-methylcyclopentanone (**6**), and methylcyclopentane (**7**) using the characterizing angles α (*twist* angle) and $\beta^{(\prime)}$ (opening angle) for the *twist* and φ (ring plane) and $\gamma^{(\prime)}$ (*envelope* flap) for the *envelope* structure calculated at the MP2/6-311++G(d,p) level of theory (see Chapter 4). ΔE is the energy in kJ·mol^{-1} with respect to the most stable conformer.

	(**1**)	(**2**)	(**3**)	(**4**)	(**5**)	(**6**)	(**7**)		(**4**)	(**7**)	(**3**)
Conformer I (*twist*)								**Conformer I (*envelope*)**			
α / °	26.10	27.83			24.93	24.79		φ / °	0.20	0.03	−3.66
β' / °	30.62	37.71			32.04	34.11		γ' / °	−130.78	−138.16	−139.90
β / °	34.57	36.17			32.60	29.68		γ / °	−130.92	−138.18	−137.46
Conformer II (*twist*)							**III/III* (*twist*)**	**Conf. II (*envelope*)**			**Conf. III**
α / °	−25.01	−27.55	26.52	–	−23.24	−24.00	∓27.15	φ / °	–	0.00	−6.38
β' / °	27.94	34.10	35.74	–	27.93	30.07	33.13/35.84	γ' / °	–	−138.71	139.29
β / °	35.72	39.33	32.72	–	32.74	31.53	35.81/33.11	γ / °	–	−138.71	143.52
ΔE	0.54	0.99	0.94	–	3.85	2.53	1.50	ΔE	–	1.09	4.36
Transition state I (*envelope*)								**Transition state I (*twist*)**			
φ / °		9.28		0.00		3.50	±5.96	α / °			23.75
γ' / °		−135.43		−132.12		−147.31	±140.14	β' / °			27.87
γ / °		−141.06		−132.12		−149.53	±136.25	β / °			33.10
ΔE		11.08		12.48		14.71	1.53	ΔE			4.47
Transition state II (*envelope*)											
φ / °		−2.75	−0.29	0.00		−1.16	∓4.21				
γ' / °		140.07	141.53	132.25		152.07	138.23/140.94				
γ / °		138.41	141.72	132.25		152.80	140.94/138.23				
ΔE		12.51	6.88	12.80		16.55	3.03				

9.3 Cremer-Pople puckering parameters

All molecules were compared using Cremer-Pople puckering parameters [37] and are illustrated with the model of Altona and Sundaralingam [40] in Figure 9.5 for the stable conformers. Here, the molecules 2-methyltetrahydrothiophen-3-one (**1**), coffee furanone (**5**), 2-methylcyclopentanone (**6**), and 2-methyltetrahydrothiophene (**2**) have *twist* conformers with similar geometries. The first three molecules have a carbonyl group and similar olfactory properties. On the other hand, 2-methyltetrahydrofuran (**3**), 2-methyl-1,3-dithiolane (**4**), and methylcyclopentane (**7**) have stable *envelope* conformers.

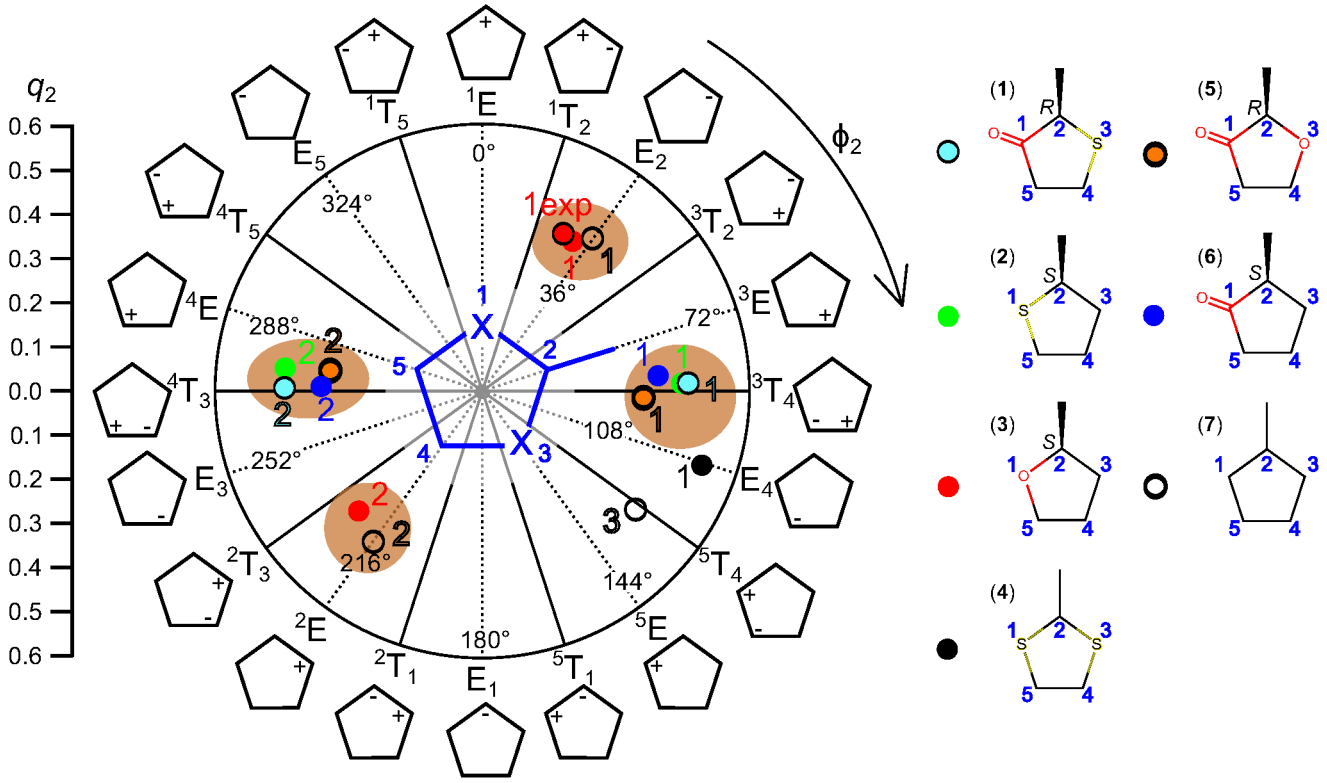

Figure 9.5. Stable conformers of the compared molecules, illustrated in the conformational landscape of five-membered heterocyclic molecules using the Cremer-Pople parameters q_2 (puckering amplitude) and ϕ_2 (phase angle). The nomenclature is based on the ***Twist*** or ***Envelope*** geometry and the positions of the atoms which are above (+) and below (−) the ring plane. At the center, $q_2 = 0$ corresponds to a planar ring. The conformers are numbered in energetic order.

In Figure 9.6, the transition states are shown. Most of them have (near-)*envelope* geometries and are located at $\phi_2 = 0$ and 180° (^{1}E and E$_1$ structure). Additionally, the Cremer-Pople puckering parameters are summarized for all molecules in Table 9.3.

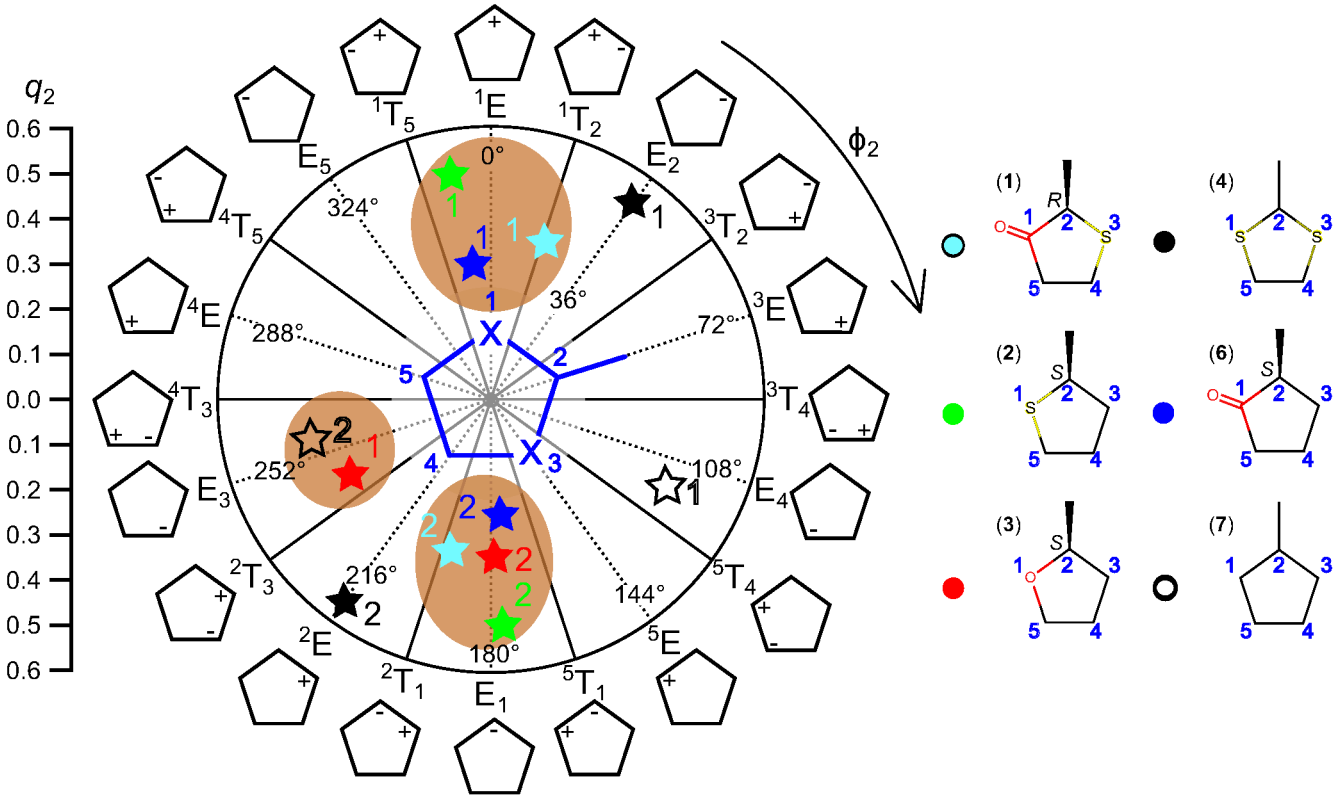

Figure 9.6. Transition states of the compared molecules, illustrated in the conformational landscape of five-membered heterocyclic molecules using the Cremer-Pople parameters q_2 (puckering amplitude) and ϕ_2 (phase angle). The nomenclature is based on the ***Twist*** or ***Envelope*** geometry and the positions of the atoms which are above (+) and below (−) the ring plane. At the center, $q_2 = 0$ corresponds to a planar ring. The transition states are numbered in energetic order. No transition states could be optimized for coffee furanone (**5**).

Table 9.3. Comparison of the stable conformers and transition states of 2-methyltetrahydrothiophen-3-one (**1**), 2-methyltetrahydrothiophene (**2**), 2-methyltetrahydrofuran (**3**), 2-methyl-1,3-dithiolane (**4**), coffee furanone (**5**), 2-methylcyclopentanone (**6**), and methylcyclopentane (**7**) using the Cremer-Pople parameters q_2 (puckering amplitude), ϕ_2 (phase angle), and δ (angle between the mean plane of the puckered ring and the bond of the methyl group) calculated at the MP2/6-311++G(d,p) level of theory.

	(**1**)	(**2**)	(**3**)	(**4**)	(**5**)	(**6**)	(**7**)	
Conformer I								
q_2	0.47	0.45	0.39	0.52	0.38	0.40	0.43	
ϕ_2	87.39	88.68	32.40	108.39	92.33	85.48	36.04	
	$^3T_4$	$^3T_4$	E_2	E_4	$^3T_4$	$^3T_4$	E_2	
δ	58.70	58.20	67.70	150.30	53.60	61.10	71.00	
	inclinal	inclinal	equatorial	axial	inclinal	equatorial	equatorial	
Conformer II								**III**
q_2	0.46	0.45	0.38		0.35	0.38	0.42	0.43
ϕ_2	271.20	276.20	226.63		277.60	271.84	216.00	128.73
	$^4T_3$	$^4T_3$	(^2E)/ $^2T_3$		$^4T_3$	$^4T_3$	^2E	$^5T_4$
δ	21.30	23.70	10.10		25.20	20.20	6.30	37.20
	axial	axial	axial		axial	axial	axial	inclinal
Transition state I								
q_2	0.37	0.52	0.38	0.54		0.30	0.43	
φ	18.63	350.76	242.43	36.00		353.58	115.76	
	$^1T_2$	^1E/($^1T_5$)	E_3/($^2T_3$)	E_2		^1E/($^1T_5$)	(E_4)/ $^5T_4$	
δ	62.30	63.70	13.10	70.50		57.90	45.10	
	equatorial	equatorial	axial	equatorial		inclinal	inclinal	
Transition state II								
q_2	0.35	0.50	0.36	0.55		0.27	0.41	
ϕ_2	195.63	177.20	179.54	216.00		177.63	257.75	
	$^2T_1$	E_1	E_1	^2E		E_1	E_3	
δ	16.70	13.30	17.10	5.90		20.20	15.70	
	axial	axial	axial	axial		axial	axial	

9.4 Conclusion

Stable *twist* conformers with similar geometries were found for 2-methyltetrahydrothiophen-3-one (**1**) and its related molecules coffee furanone (**5**) and 2-methylcyclopentanone (**6**). These three molecules have a carbonyl group as well as similar olfactory properties. Also, 2-methyltetrahydrothiophene (**2**) has similar conformers as shown in Figure 9.5. In the most energetically favorable conformer of 2-methyltetrahydrothiophene (**2**) and 2-methylcyclopentanone (**6**), the methyl group and the neighboring methylene group are on the same side of the C-S-C and C-(C=O)-C plane, respectively.

On the other hand, stable *envelope* conformers exist only for 2-methyltetrahydrofuran (**3**), 2-methyl-1,3-dithiolane (**4**), and methylcyclopentane (**7**). Most of the transition states have *envelope* and near-*envelope* geometries. The lowest energetic transition states of 2-methyltetrahydrothiophen-3-one (**1**), 2-methyltetrahydrothiophene (**2**), and 2-methylcyclopentanone (**6**) have the methyl group and the *envelope* flap on the same side of the ring plane.

Part II

Multiple Internal Rotations of Methyl Groups in Planar Ring Systems

CHAPTER 10

2,5-Dimethylthiophene

Two equivalent rotors and C_{2v} frame symmetry

Parts of this chapter have already been published in:

Vinh Van, Wolfgang Stahl, and Ha Vinh Lam Nguyen
Two equivalent methyl internal rotations in 2,5-dimethylthiophene investigated by microwave spectroscopy [70]

Phys. Chem. Chem. Phys. **17**, 32111 – 32114 (2015).
DOI: 10.1039/c5cp03513a
Inside front cover *Phys. Chem. Chem. Phys.* **48/2015**.
DOI: 10.1039/C5CP90220G

Vinh Van performed the quantum chemical calculations, the measurements, the spectral analysis, and co-wrote the manuscript. Ha Vinh Lam Nguyen and Wolfgang Stahl produced the group theory and co-wrote the manuscript. Parts of this chapter are reproduced from Ref. [70] with permission from the PCCP Owner Societies.

10.1 Introduction

Monomethyl derivatives of unsaturated heterocyclic five-membered rings have been widely studied by microwave spectroscopy. The barriers to internal rotation of the methyl group cover a wide range from low barriers such as in 2-methylthiazole (**1**) [71], N-methylpyrrole (**2**) [72], and 4-methylisothiazole (**3**) [73] to intermediate barriers like in 4-methyloxazole (**4**) [74], 2-methylfuran (**5**) [75], and 3-methylfuran (**6**) [76], as well as 2-methylthiophene (**7**) [20] and 3-methylthiophene (**8**) [21] as summarized in Figure 10.1. To the best of my knowledge, no microwave investigations on the rotational spectra of dimethyl substituted unsaturated heterocyclic five-membered rings are available. Here, 2,5-dimethylthiophene (DMTP) was studied with the aim to determine the torsional barriers of two equivalent methyl tops. A comparison of the experimental results with state of the art quantum chemical calculations will also be discussed.

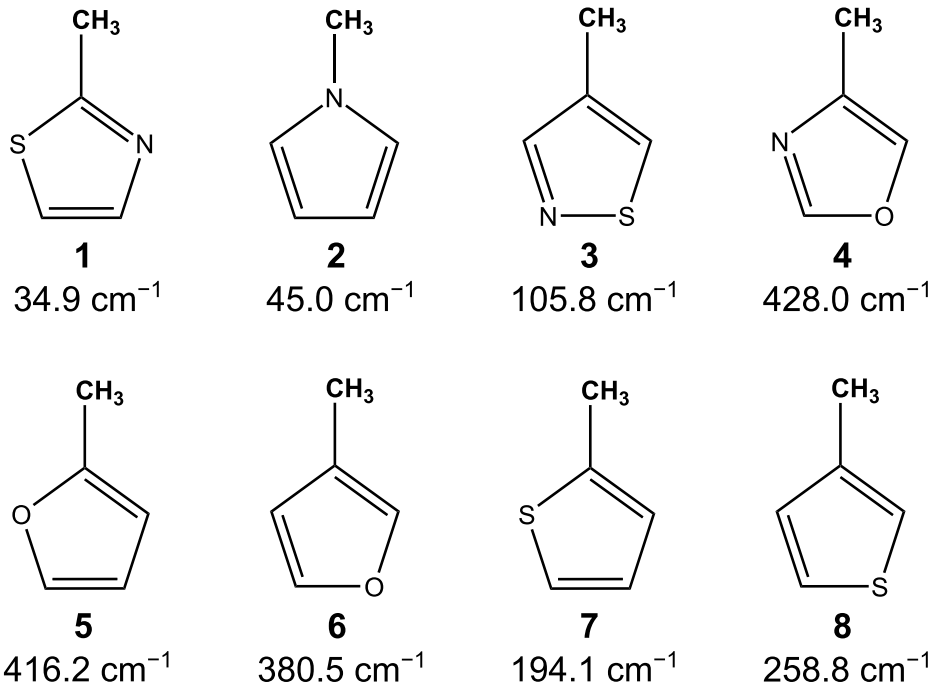

Figure 10.1. Barriers to internal rotation of some monomethyl unsaturated heterocyclic five-membered rings. [70]

10.2 Quantum chemical calculations

In DMTP, two conjugated double bonds force the thiophene frame to planarity, and thus only one conformer is possible. [77] However, the orientations of the two methyl groups in the equilibrium, which determine the molecular symmetry (C_{2v}, C_2, or C_s), remain questionable. In a previous electron diffraction study [78], one of the C–H bonds of the methyl groups is *cis* with respect to the S–C bond, which is in contrast to their quantum chemical calculations at the HF/3-21G(d) level. Here, much higher levels of theory are applied to study this observation.

Potential energy curves were obtained by varying the dihedral angle $\varphi_1 = \angle(S_{15},C_{12},C_{10},H_4)$ in a step width of 1°, while all other geometry parameters were optimized (for atom numbers see Figure 10.2). Calculations were performed using the GAUSSIAN09 package [26] with the MP2, B3LYP, and M06-2X methods and various basis sets. Three potential energy curves calculated with the cc-pVTZ basis set are shown in Figure 10.3. The V_3 potentials possess negligible contributions of higher order terms, which can be clearly recognized through the Fourier coefficients indicated in Table 17.43. The energy minima show a C_{2v} symmetry, where a hydrogen atom of each methyl group is antiperiplanar to the sulfur atom. The two methyl groups are thus equivalent. Full geometry optimizations and harmonic frequency calculations yielded similar results (see Figure 10.2), which are also in agreement with the calculations given in Ref. [78]. The Cartesian coordinates are given in Table 17.44.

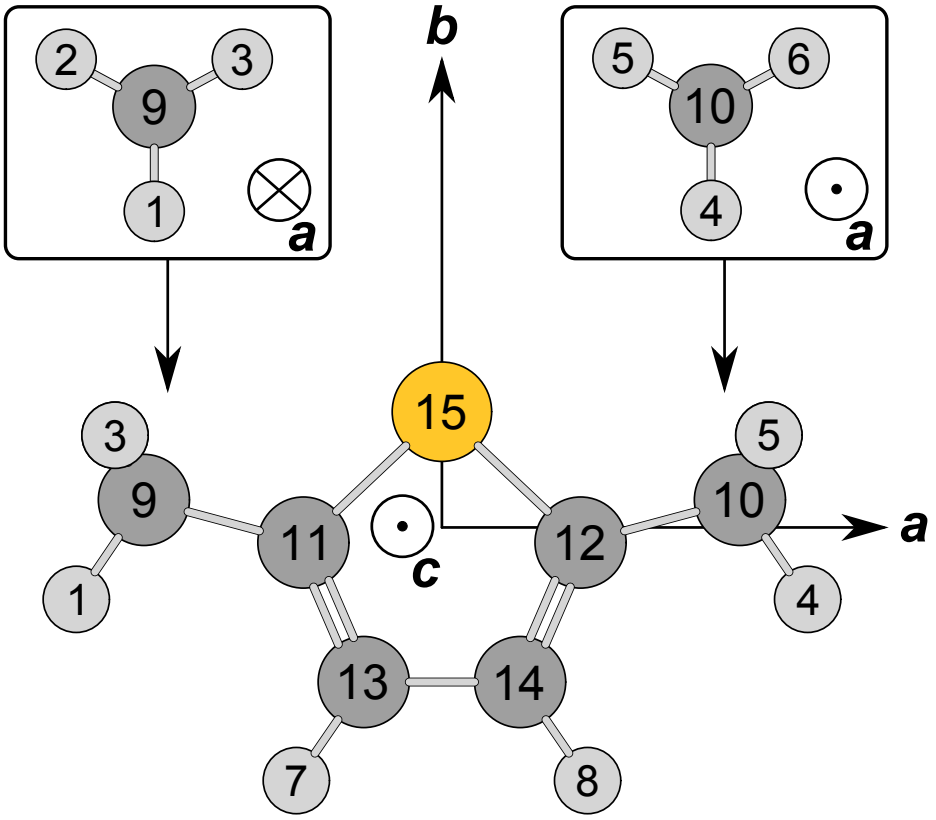

Figure 10.2. The molecular geometry of DMTP calculated at the MP2/cc-pVTZ level of theory given in its principal axes of inertia. The direction of the axes into and out of the paper plane is indicated by an encircled cross or dot, respectively. [70]

To study the coupling between the two methyl tops, a potential energy surface (PES) was calculated at the MP2/6-311++G(d,p) level of theory by varying the dihedral angles φ_1 and $\varphi_2 = \angle(S_{15},C_{11},C_9,H_1)$ in a step width of 10°, as given in Figure 10.4. The corresponding energies were parameterized with a two-dimensional Fourier expansion based on terms representing the correct symmetry; the Fourier coefficients are listed in Table 17.45. No significant coupling between the two tops could be observed. A similar situation was found for the PES calculated at the B3LYP/6-311++G(d,p) level (visualized in Figure 10.4). However, the energy minima are broader; the contribution of cross terms is smaller, as can also be recognized in Table 17.45.

Geometry optimizations to a first order transition state of one methyl group using the Berny algorithm [28] at various levels of theory were used to calculate the barriers to internal rotation. The calculated rotational constants, angles between an internal rotor axis and the principal axes, as well as the V_3 potentials are summarized in Table 17.46. The angle $\angle(i_2,a)$ for the second rotor is $\pi - \angle(i_1,a)$, whereas $\angle(i_1,n) = \angle(i_2,n)$ for $n = b,c$. The geometry optimizations and harmonic frequency calculations at the MP2/6-311++G(d,p) level yielded one imaginary vibrational mode, which is a bending mode of the planar thiophene frame. Stating stable planar ring systems as unstable is a well-known behavior found at this level of theory, which has been reported for benzene and arenes [79].

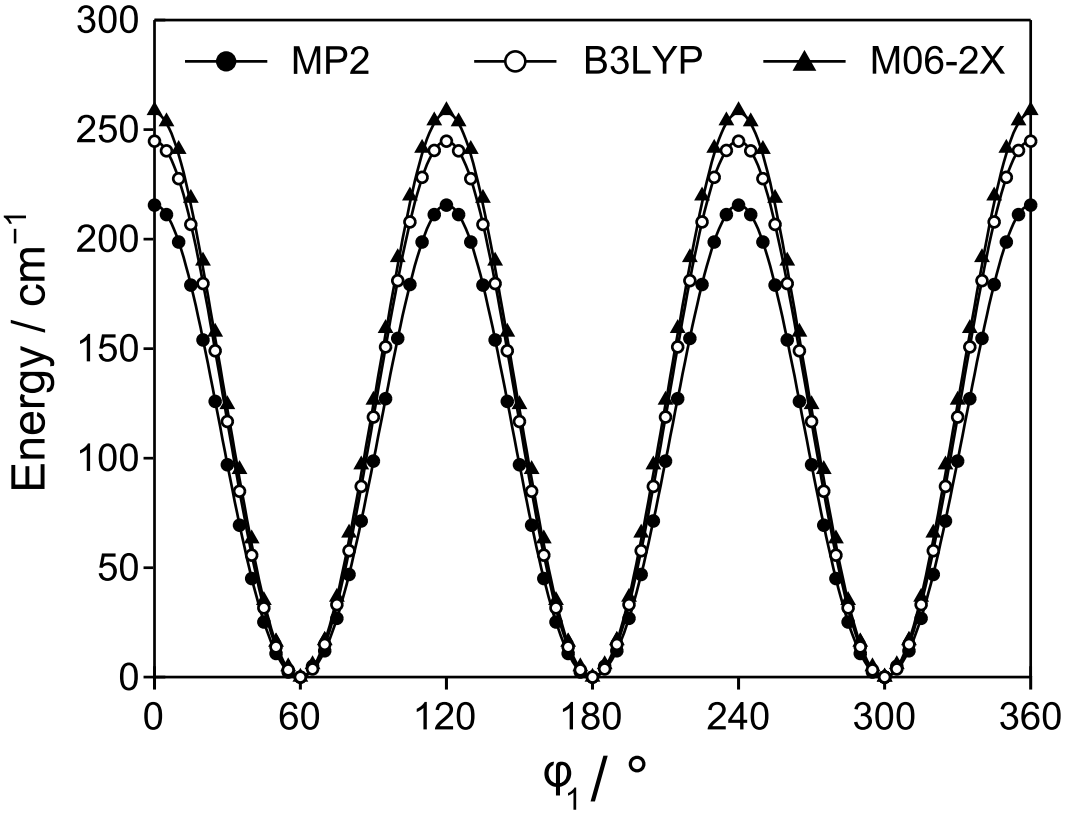

Figure 10.3. The potential energy curves obtained by rotating one methyl group around the C_{12}-C_{10} bond (for atom number see Figure 10.2). The dihedral angle $\varphi_1 = \angle(S_{15},C_{12},C_{10},H_4)$ was varied in a step width of 1°. The basis set cc-pVTZ was used in combination with the MP2, B3LYP, and M06-2X methods. Relative energies are given with respect to the absolute minima of E = −630.646179 Hartree (MP2), −631.761983 Hartree (B3LYP), and −631.617104 Hartree (M06-2X). [70]

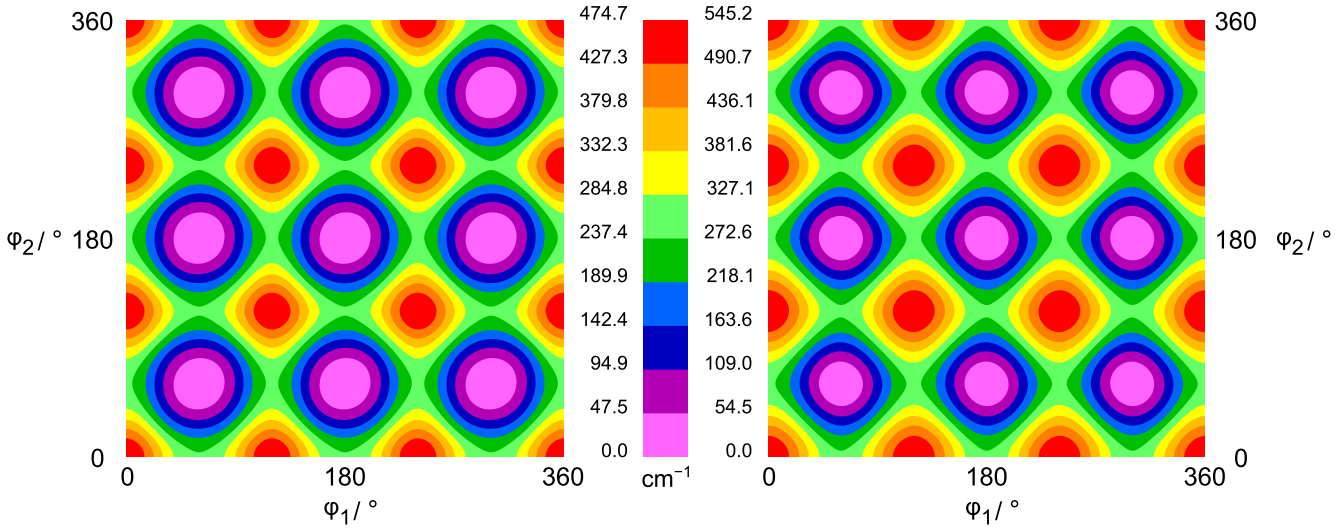

Figure 10.4. The potential energy surface of 2,5-dimethylthiophene calculated with the methods MP2 (left hand side) and B3LYP (right hand side) and the basis set 6–311++G(d,p) obtained by rotating the two methyl groups. No significant coupling was observed. [70]

10.3 Group theory

10.3.1 Symmetry labels

DMTP has a C_{2v} frame symmetry and two equivalent methyl rotors. It is well known that the molecular symmetry group of such a system is G_{36} with the character table given in Table 10.1. There are different symmetry labels in use which arise from different product decompositions of G_{36}. Probably, the earliest method is based on the direct product $C_{3v}^{-} \times C_{3v}^{+}$, and the symmetry species of G_{36} are labeled with the labels of both subgroups C_{3v}^{-} and C_{3v}^{+} [47] as given in column S3 of Table 10.1. Using the permutation-inversion group formalism, Bunker and Jensen [80] derived a character table of acetone, where the different species are denoted by their degeneracy letter A, E, G and a running index (shown in column S2 of Table 10.1).

Table 10.1. Character table of the molecular symmetry group G_{36} of DMTP.

$\mathbf{G_{36}}$ [a]			**E**	$\mathbf{a^{-1}}$	**ab**	$\mathbf{ab^{-1}}$	**P**	**bP**	**Q**	**aQ**	**R**	
Equiv. rot.[b]			R^0	R^0	R^0	R^0	R_b^π	R_b^π	R_a^π	R_a^π	R_c^π	
S1[c]	**S2**[d]	**S3**[e]	[f] 1	4	2	2	3	6	3	6	9	**wt**[g]
(00)·A_1	A_1	A_1A_1	1	1	1	1	1	1	1	1	1	36
(00)·B_1	A_2	A_2A_1	1	1	1	1	−1	−1	1	1	−1	28
(00)·A_2	A_3	A_1A_2	1	1	1	1	1	1	−1	−1	−1	36
(00)·B_2	A_4	A_2A_2	1	1	1	1	−1	−1	−1	−1	1	28
(12)·A'	E_1	EA_1	2	−1	2	−1	0	0	2	−1	0	16
(12)·A''	E_2	EA_2	2	−1	2	−1	0	0	−2	1	0	16
(11)·A	E_3	A_1E	2	−1	−1	2	2	−1	0	0	0	20
(11)·B	E_4	A_2E	2	−1	−1	2	−2	1	0	0	0	12
(01)·A	G	EE	4	1	−2	−2	0	0	0	0	0	64

[a] **a** = (1 2 3), **b** = (4 5 6), **P** = (1 4)(2 5)(3 6)(7 8)(9 10)(11 12)(13 14), **Q** = (1 4)(2 6)(3 5)(7 8)(9 10)(11 12)(13 14)*, **R** = (2 3)(5 6)*, for atom numbers see Figure 10.2. [b] Equivalent rotations of the Four-group. [c] Symmetry labels based on the semi-direct product $(C_3^{\mathrm{I}} \times C_3^{\mathrm{I}}) \ltimes C_{2v}$, see Ref. [81]. [d] Symmetry labels according to Ref. [80]. [e] Symmetry labels based on the direct product $C_{3v}^{-} \times C_{3v}^{+}$, see Ref. [47]. [f] Row between S3 and wt: number of elements in the respective class. [g] Spin statistical weight.

A third labeling scheme (column S1) is preferred, for which G_{36} is written as the semi-direct product $(C_3^{\mathrm{I}} \times C_3^{\mathrm{I}}) \ltimes C_{2v}$, as reported by Ezra [81]. The theoretical background was described in detail also by Altmann [82]. The direct product $C_3^{\mathrm{I}} \times C_3^{\mathrm{I}}$ of the two intrinsic (superscript I) C_3 groups of the internal rotors, which is an invariant subgroup of G_{36}, decomposes into four orbits under C_{2v} (Table 10.2). One representative of each orbit forms the first part of the symmetry label, e.g. (01). The numbers σ = 0, 1, 2 represent the three symmetry species A, E_a, E_b, respectively, of the group C_3 and correspond to

the transformation properties of the C_3-adapted planar rotor wave functions $e^{i(3k+\sigma)\varphi}$ with $k \in \mathbb{Z}$ and the torsional angle φ. Each orbit is associated with its little co-set. They form subgroups of C_{2v}. The symmetry species of the little co-sets provide the second part of the new symmetry labels.

Table 10.2. Orbits of the species of $(C_3^{\mathrm{I}} \times C_3^{\mathrm{I}})$ under C_{2v}.

orbit (σ_1, σ_2)	little co-set
(00)	C_{2v}
(11), (22)	C_2
(12), (21)	C_s
(01), (10), (02), (20)	C_1

10.3.2 Nuclear spin statistics

The total wave function $\psi_{\mathrm{tot}} = \psi_{\mathrm{el}} \cdot \psi_{\mathrm{vib}} \cdot \psi_{\mathrm{rotors}} \cdot \psi_{\mathrm{ns}}$ must obey the Pauli principle, i.e. it changes sign under an odd number of fermion permutations (here protons) and retains sign under an even number of permutations. It belongs thus either to the species $(00)\cdot\mathrm{A}_1$ or $(00)\cdot\mathrm{A}_2$. There are 256 nuclear spin functions arising from 8 protons in DMTP with the representation

$$\Gamma_{ns} = 36\ (00)\cdot\mathrm{A}_1 + 28\ (00)\cdot\mathrm{B}_2 + 10\ (12)\cdot\mathrm{A}' + 6\ (12)\cdot\mathrm{A}'' + 10\ (11)\cdot\mathrm{A} + 6\ (11)\cdot\mathrm{B} + 32\ (01)\cdot\mathrm{A}.$$

The spin weights (column wt in Table 10.1) are determined by counting the number of allowed total wave functions for $\Gamma_{el} = \Gamma_{vib} = (00)\cdot\mathrm{A}_1$.

10.3.3 Selection rules

The dipole moment vector in space fixed coordinates is invariant under pure permutation operations but changes sign under inversion. Therefore, it transforms as $\Gamma_\mu = (00)\cdot\mathrm{A}_2$. In the vibronic ground state, transitions between two rotorsional levels i and j are allowed, if $\Gamma_i \times \Gamma_\mu \times \Gamma_j \supset (00)\cdot\mathrm{A}_1$. The resulting four torsional components of two different b-type transitions, namely K_aK_c: ee $\leftrightarrow$ oo and eo$\leftrightarrow$ oe (e = even, o = odd) along with their spin statistical weights are given in Table 10.3. They are determined by correlation with the molecular symmetry group C_{2v}(M) of the hypothetical rigid DMTP. If the quantum numbers K_a and K_c are known, the torsional state can be labeled conveniently by the first part (σ_1,σ_2) of the full symmetry label. This abbreviated notation will be used throughout this chapter.

Table 10.3. Spin statistical weights of torsional components of allowed transitions of DMTP.

ee ↔ oo transitions			wt	eo ↔ oe transitions			wt
(00)·A_1	↔	(00)·A_2	36	(00)·B_1	↔	(00)·B_2	28
(12)·A'	↔	(12)·A''	16	(12)·A'	↔	(12)·A''	16
(11)·A	↔	(11)·A	20	(11)·B	↔	(11)·B	12
(01)·A	↔	(01)·A	64	(01)·A	↔	(01)·A	64

10.4 Microwave spectroscopy

10.4.1 Spectral analysis

The results of the quantum chemical calculations have shown that DMTP does not possess dipole moment components in *a*- and *c*-direction. Only *b*-type transitions are thus expected, which is in agreement with the group theoretical results (see Section 10.3.3). In the first step, the *b*-type rigid-rotor spectrum was predicted using the rotational constants calculated at the MP2/cc-pVTZ level. Based on this prediction, a broadband scan in the frequency range from 8.5 to 12.0 GHz was measured, where overlapping spectra in a step width of 0.25 MHz were automatically recorded. In the next step, all lines were remeasured at higher resolution.

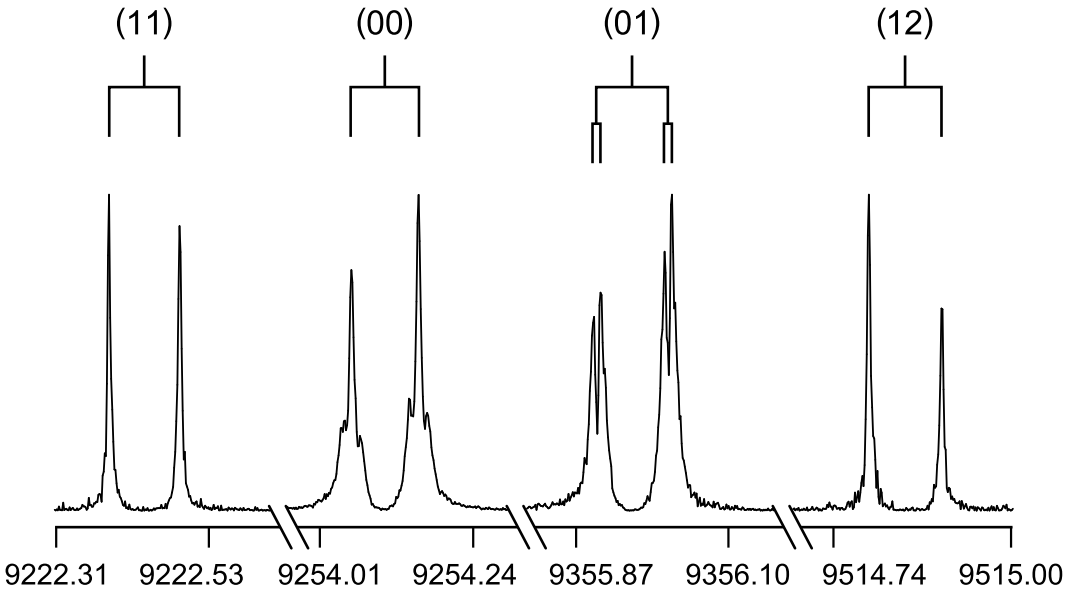

Figure 10.5. Typical spectra of the four torsional species (00), (01), (11), and (12) of the $3_{21} \leftarrow 3_{12}$ transition of DMTP (in MHz). The experimental resolution is 2 kHz, the typical line width 10 kHz (FWHH). The larger splittings indicated by brackets are due to the Doppler effect; the smaller brackets indicate splittings of unknown origin. For these spectra, 21–614 decays were co-added. The intensities are normalized. [70]

Table 10.4. Molecular parameters of DMTP obtained by the program XIAM. Only the (00) species is fitted in Fit I, whereas all four species are taken into account in Fit II – IV. In Fit II, the parameters V_{cc} and F_{12} are not fitted. While in Fit III the kinetic coupling parameter F_{12} is fitted, the potential coupling parameter V_{cc} is fitted instead in Fit IV.

Par.[a]	Unit	Fit I	Fit II	Fit III	Fit IV	Calc.[b]
A	GHz	4.972 243 62(42)	4.965 008(18)	4.965 007 00(89)	4.965 008 0(11)	4.941
B	GHz	1.746 964 78(26)	1.746 947 8(23)	1.746 947 35(13)	1.746 947 95(13)	1.743
C	GHz	1.313 380 08(20)	1.313 336 2(15)	1.313 336 823(81)	1.313 336 180(81)	1.298
D_J	kHz	0.0642(26)	0.082(19)	0.063 90(97)	0.0671(11)	0.062
D_{JK}	kHz	0.2328(89)	0.146(64)	0.1774(35)	0.1582(36)	0.178
D_K	kHz	3.1944(97)	0.892(73)	0.8998(43)	0.9173(43)	0.797
d_1	kHz	−0.0196(14)	0.0228(88)	−0.018 39(51)	0.018 35(50)	−0.017
d_2	kHz	−0.002 14(23)	0.30(16)	−0.001 63(14)	0.1033(88)	−0.001
V_3	cm^{-1}		247.90(60)	247.956 10(30)	242.148(41)	241.2
I_α	$uÅ^2$		3.1650(78)	3.164 42(39)	3.163 85(45)	3.1587
V_{cc}	cm^{-1}				−3.607(15)	2.3
∠(i,a)[c]	°		14.61(14)	14.5931(78)	14.597(78)	14.9
∠(i,b)	°		75.39(14)	75.4069(78)	75.403(78)	75.1
∠(i,c)	°		90.00(fixed)	90.00(fixed)	90.00(fixed)	89.96
F_{12}	GHz		−4.825(derived)	−7.320(12)	−4.826(derived)	−4.784
D_{pi2J}	kHz		−0.6(43)[d]	−2.77(25)	−2.49(23)	
D_{pi2K}	kHz		−101(84)[d]	−99.0(42)	−96.3(45)	
D_{pi2-}	kHz		3.7(33)[d]	1.97(19)	2.73(18)	
σ[e]	kHz	2.6	32.4	1.9	1.9	
N[f]		41	157	157	157	

[a] All parameters refer to the principal axis system. Watson's S reduction and I^r representation were used. [b] Vibrational ground state rotational constants and centrifugal distortion constants obtained by anharmonic frequency calculation at the MP2/6-311++G(d,p) level. [c] The angle ∠(i_2,a) for the second rotor is derived from the relation $\pi - \angle(i_1,a)$. [d] These parameters can be no longer well-determined while F_{12} or V_{cc} are not fitted.[e] Standard deviation of the fit. [f] Number of lines.

At the beginning, the transitions $2_{20} \leftarrow 2_{11}$, $3_{21} \leftarrow 3_{12}$, and $4_{22} \leftarrow 4_{13}$ as well as $2_{21} \leftarrow 2_{12}$ and $3_{22} \leftarrow 3_{13}$ were considered. They were not the most intense transitions in the scan but their positions could be predicted quite precisely. After these transitions had been assigned and fitted, further lines in the scan were added to the fit. Afterwards, transitions outside the scan region were also included. The results are given as Fit I in Table 10.4. A prediction considering the internal rotation of both methyl groups was then carried out using the program XIAM [45]. The angles $\angle(i_1,n)$ and $\angle(i_2,n)$, n = *a, b, c*, as well as the initial V_3 potential were taken from the values calculated at the MP2/cc-pVTZ level. Supported by the intensities from the spin statistical weights, the (01), (11), and (12) species in the scan were successfully assigned. The splittings were up to 0.5 GHz. Finally, further torsional transitions up to $J = 7$ and $K_a = 5$ were measured to increase the data set.

A typical high resolution spectrum of the four torsional components is visualized in Figure 10.5. In many transitions, the (00) and the (01) species indicate additional small splittings of about 10 kHz. These splittings are probably due to spin–spin or spin–rotation coupling of the protons. However, for the (01) species, another explanation is possible. In G_{36} molecules, the (01) and the (10) species are degenerate. Under the influence of centrifugal distortion, this degeneracy could be lifted if rotations about axes other than *a*, *b*, and *c* are considered. [83] Nevertheless, since the splittings are small and no theory is available for spin–spin and spin–rotation couplings of molecules with 8 protons like DMTP, nor for the effect mentioned above, no support for this argument can be given.

10.4.2 Top-top interaction

An energy level diagram to illustrate the splitting is given in Figure 10.6. When no top-top interaction is present, the torsional species (11) and (12) are degenerated since the methyl groups are equivalent. The reason for the splitting is the kinetic top-top interaction F_{12} and a potential top-top interaction (here: V_{cc}). The (11)–(12) splittings are not small. Therefore, a fit without using any top-top interaction leads to a high standard deviation of 32.4 kHz, as shown in Fit II in Table 10.4. A fit using the kinetic coupling parameter F_{12} was carried out in Fit III in Table 10.4 because the PES in Section 10.2 shows negligible potential top–top interaction. The standard deviation drops to an excellent value of 1.9 kHz just due to an additional parameter. However, the value of F_{12} differs largely compared to the value obtained from *ab initio* calculation as well as to the value derived from the fitted moments of inertia of the entire molecule and of the methyl groups. Here, F_{12} is used as an effective parameter since it is already determined by the direction cosines, the moments of inertia of the internal rotors, and the moments of inertia of the entire molecule as described in Equation 3.12 (see Section 3.2) as

$$F_{12} = -\frac{1}{2} \cdot \left[I_{\alpha,1}(1 - \sum_i \frac{\lambda_{i,1}^2 I_{\alpha,1}}{I_i}) \cdot I_{\alpha,2}(1 - \sum_i \frac{\lambda_{i,2}^2 I_{\alpha,2}}{I_i}) - (\sum_i \frac{\lambda_{i,1}\lambda_{i,2} I_{\alpha,1} I_{\alpha,2}}{I_i})^2 \right]^{-1} \sum_i \frac{\lambda_{i,1} I_{\alpha,1} \lambda_{i,2} I_{\alpha,2}}{I_i}.$$

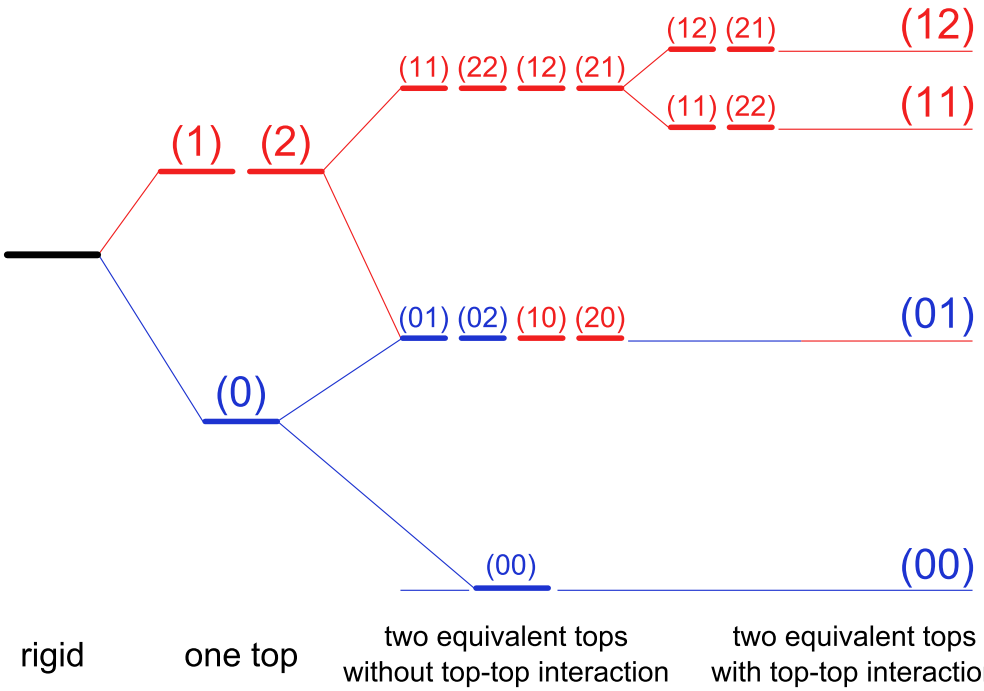

Figure 10.6. Schematic energy level diagram to illustrate the splittings due to internal rotation. Left-hand side: rigid molecule; middle: splittings into a (0) and a (1) species due to the internal rotation of one methyl top; right-hand side: splittings into a (00), a doubly degenerated (01), a (11) and a (12) species due to the internal rotations of two equivalent methyl tops. The (11) and (12) species are not degenerated due to top-top interaction. [70]

Instead, a fit using the potential coupling parameter V_{cc} was carried out in Fit IV in Table 10.4. Here, the derived value of F_{12} is reasonable and the value of V_{cc} is well determined. Therefore, the parameter V_{cc} is preferred, instead of F_{12}, to describe the additional (potential) top-top interaction since the kinetic top-top interaction is already determined by the direction cosines, the moments of inertia of the internal rotors, and the moments of inertia of the entire molecule. However, F_{12} can be fitted in addition to V_{cc} as an effective parameter when the internal rotors are highly coupled as shown for 4,5-dimethylthiazole in Chapter 13. The parameter F_{12} is used here as a compensation for the potential top-top interaction terms, which are not available in XIAM. Possible missing terms are V_{sc} and V_{cs} or higher order terms as given in

$$\begin{aligned} V(\varphi_1,\varphi_2) = &\frac{V_{3,1}}{2}[1-\cos(3\varphi_1)] + \frac{V_{3,2}}{2}[1-\cos(3\varphi_2)] \\ &+ V_{cc}\cdot\cos(3\varphi_1)\cos(3\varphi_2) + V_{ss}\cdot\sin(3\varphi_1)\sin(3\varphi_2) \\ &+ V_{cs}\cdot\cos(3\varphi_1)\sin(3\varphi_2) + V_{sc}\cdot\sin(3\varphi_1)\cos(3\varphi_2). \end{aligned}$$

10.5 Results of the fits and discussion

In total, 157 torsional components were fitted to a standard deviation of 1.9 kHz, which is within the measurement accuracy. The rotational and centrifugal distortion constants were well determined. The V_3 potential, the moment of inertia I_α, the angles δ between the internal rotation axes and the principal a-axis, the potential coupling between the two rotors V_{cc}, and the three higher order parameters D_{pi2J}, D_{pi2K}, and $D_{\mathrm{pi2-}}$ were also fitted as linear combinations of the two tops. The results are given as Fit IV in Table 10.4; the frequency list is in Table 17.47.

The experimental rotational constants were compared with those from quantum chemical calculations. The best agreements was found with the method M06-2X, followed by MP2 and B3LYP, as shown in Table 17.46. The smallest Pople basis set shows better agreement than bigger basis sets, which is probably the result of error compensation.

The calculated barriers to internal rotation vary in a wide range between 215.5 cm^{-1} and 405.2 cm^{-1}, but they are still in the same order of magnitude as the experimental V_3 potential of 242.1 cm^{-1}. The HF method overestimates the barrier by more than 100 cm^{-1}, whereas the MP2 method underestimates the barrier by up to 30 cm^{-1}. The Dunning basis sets yield better results than the Pople ones. The barrier of 241.2 cm^{-1} calculated at the MP2/6-311++G(d,p) level matches the experimental value best.

The barriers of DMTP are closer to the value found for the mono-substituted molecule (8) rather than that of (7), which has a more similar structure (see Figure 10.1). In molecules with other hetero atoms (oxygen or nitrogen) or with two hetero atoms, the barrier changes significantly. No rule to predict the methyl barriers in unsaturated heterocyclic five-membered rings exists so far. Unlike in alkyl acetates where the barrier remains largely invariant at approximately 100 cm^{-1}, this value cannot be easily predicted when electronic effect exists, e.g. by the presence of double bonds. In unsaturated acetates [84, 85], π-electron conjugation, extending from the double bond to the ester group, is possible, which causes significantly different barriers.

For unsaturated rings with conjugated double bonds like DMTP, it is mostly probable that this electronic system influences the barrier heights. However, more investigations have to be performed to confirm this speculation and moving towards a more precise prediction of the methyl barriers.

10.6 Conclusions

The spectrum of DMTP recorded under molecular beam conditions was successfully assigned using a combination of FT microwave spectroscopy, group theory, and quantum chemistry. The rotational constants obtained by geometry optimizations at different levels of theory are in good agreement with the experimental values. A C_{2v} equilibrium structure was calculated, where one hydrogen atom of each methyl group is antiperiplanar to the sulfur atom, and the two methyl groups are thus equivalent. They undergo internal rotations with a barrier height of 242.148(41) cm^{-1}, which is in reasonable agreement with the calculated barrier.

CHAPTER 11

2,5-Dimethylfuran

Two equivalent rotors and C_{2v} frame symmetry

Vinh Van performed the measurements and the spectral analysis. Jonas Bruckhuisen helped with the measurements and the spectral analysis in his students' project under the supervision of Vinh Van.

11.1 Introduction

The limits and decreasing accessibility of fossil fuel resources are currently in strong contrast to the growing needs of humanity on petroleum. Moreover, the concerns on their effects on the environment such as global warming are demanding renewable sources. It has been shown since a decade that the conversion of biomass such as hexose (e.g. fructose or glucose) into liquid fuels is a promising way to produce renewable liquid fuel with 2,5-dimethylfuran (DMF) as the most attractive product [86, 87]. In comparison to ethanol, the only renewable liquid fuel that is produced in large quantities up to now, DMF is particularly suitable because of its nearly ideal boiling point (92 – 94°C) and its high research octane number (RON = 119) [88]. The energy content of 31.5 MJ/L is similar to that of gasoline (35 MJ/L) and 40% greater than that of ethanol (23 MJ/L) [89]. Furthermore, it is immiscible with water and easier to blend with gasoline than ethanol.

Despite its widespread use, nothing is known about the gas phase molecular structure of DMF and its internal dynamics. Therefore, DMF is studied here by molecular beam Fourier transform microwave spectroscopy with quantum chemical calculations as a helpful support to obtain this important information. From the structural point of view, DMF is a derivative of furan with two methyl substitutions on the second and the fifth ring position. The methyl groups are thus equivalent. Concerning the internal dynamics, when starting this work, splittings arising from the internal rotations of the two equivalent methyl groups were expected and could be resolved. The program XIAM treats such large amplitude motion problems and was used to reproduce the experimental spectrum. The results will be compared.

11.2 Quantum chemical calculations

11.2.1 Geometry optimization

Similar to the case of furan, DMF is planar because of the π-electron delocalization of two conjugated double bonds. This constrain confines the structural analysis to only one starting geometry. Geometry optimizations were performed on this initial form using the HF, B3LYP, M06-2X, MP2, and CCSD methods in combination with various Pople and Dunning basis sets [90–96] as implemented in the GAUSSIAN09 package [26] to check for convergence. The fully optimized structure at the MP2/6-311++G(d,p) level of theory is shown in Figure 11.1 in its principal axes of inertia. The nuclear Cartesian coordinates are given in Table 17.48 in the Appendix. The rotational constants are summarized in Table 17.49.

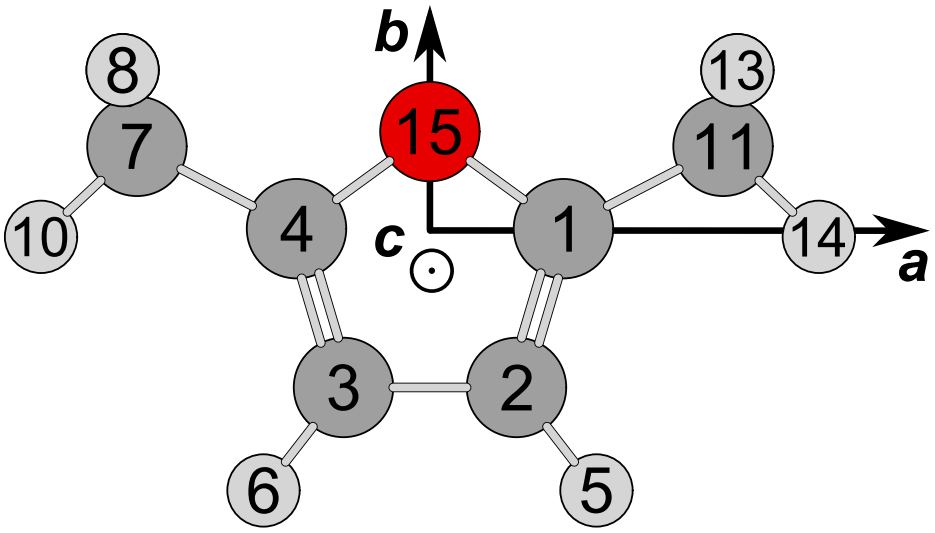

Figure 11.1. The optimized geometry of DMF at the MP2/6-311++G(d,p) level of theory given in its principal axes of inertia. The direction of the perpendicular c-axis pointing out of the paper plane is indicated by an encircled dot.

11.2.2 Methyl internal rotations

DMF has a C_{2v} symmetry and two equivalent methyl rotors. The rotational transitions of such a molecule split into four torsional components, which can be labeled as (00), (01), (11), and (12) by writing G_{36} as the semi-direct product $(C_3^{\mathrm{I}} \times C_3^{\mathrm{I}}) \ltimes C_{2v}$, as introduced in the group theory (Section 10.3) of 2,5-dimethylthiophene (DMTP). There, C_3^{I} is the intrinsic (superscript I) C_3 group of an internal rotor, which is an invariant subgroup of G_{36}. The notation (00), (01), (11), and (12) is used throughout this chapter.

The torsional splittings mainly depend on the orientations of the methyl groups in the molecule and the barriers hindering the internal rotation. While the orientations of the methyl groups can be often well-calculated by geometry optimizations, predicting the barrier heights is a much more difficult task. The predicted values vary in a wide range and depend strongly on the level of theory in use [70, 97]. A level that yields reasonable value for a methyl group may fail for another methyl group, even in the same molecule [98]. High level quantum chemical methods such as diffusion quantum Monte Carlo and coupled cluster are not necessary in best agreement with the experiments [99]. On the other hand, results from quantum chemical calculations often give the correct order of magnitude (low, intermediate, or high) of the barrier heights, which is sufficient to start the spectral assignment.

For DMF, the barrier heights of the equivalent methyl groups were calculated by geometry optimizations to a first order transition state of one methyl group using the Berny algorithm [28] at various levels of theory. The angles between the internal rotor axes and the *a*-principal axis as well as the calculated V_3 potential are also summarized in Table 17.49 in the Appendix.

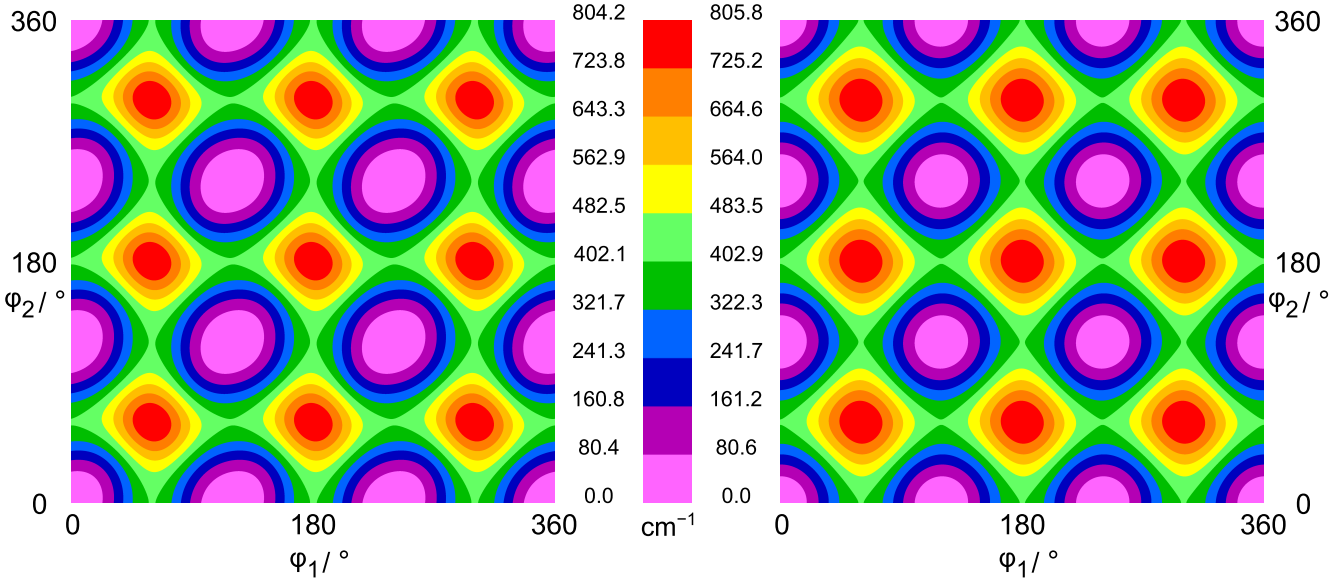

Figure 11.2. The potential energy surface of DMF depending on the dihedral angles $\varphi_1 = \angle(C_3,C_4,C_7,H_8)$ and $\varphi_2 = \angle(C_2,C_1,C_{11},H_{12})$ calculated at the MP2/6–311++G(d,p) level (left) and at the B3LYP/6–311++G(d,p) level (right). φ_1 and φ_2 were varied in a grid of 10°, while all other parameters were optimized.

11.2.3 Potential energy surface

No significant potential coupling between the two methyl groups was observed in the two-dimensional Fourier expansion terms of the potential energy surfaces. Here, two-dimensional potential energy surfaces (2D-PES) depending on φ_1 and φ_2 were calculated at the MP2/6-311++G(d,p) and B3LYP/6-311++G(d,p) level of theory to study the coupling between the two methyl rotors (see Figure 11.2 and Table 17.50 in the Appendix). The dihedral angles φ_1 and φ_2 were varied in a grid of 10°. Due to

symmetry, only data points in the range from φ_1 and $\varphi_2 = 0°$ to 120° were needed. The corresponding energies were parameterized with a two-dimensional Fourier expansion based on terms representing the correct symmetry. The Fourier coefficients are listed in Table 17.50. Using these Fourier coefficients, the PES were drawn as a contour plot illustrated in Figure 11.2. The PES exhibits almost no potential coupling terms between φ_1 and φ_2.

11.3 Microwave spectrum

The rotational spectra of DMF were measured using a molecular beam Fourier transform microwave spectrometer covering the frequency range 2 – 26.5 GHz [22, 23]. DMF was purchased from Alfa Aesar GmbH & Co KG, Karlsruhe, Germany, and used without further purification. The stated purity is more than 98%. DMF is a clear, volatile liquid with a boiling point of 92 – 94°C (at 1013 mbar). Its vapor pressure of approximately 50 hPa at 20°C is high. Therefore, the measurement process is simplified. For all measurements, a gas mixture containing 1% DMF in helium at a total pressure of 60 to 110 kPa was used.

The spectrometer can be operated in two different modes, the high resolution mode and the scan mode. In the high resolution mode, all lines appear as doublets due to the Doppler effect. The molecular transition frequency is the center frequency. The splitting depends on both, the center frequency and the velocity of the molecular beam. The estimated measurement accuracy is better than 2 kHz [100]. In the scan mode, a series of overlapping spectra are automatically recorded and only the presence of lines is indicated in the broadband scan.

As mentioned in Section 11.2.2, DMF belongs to the molecular symmetry group G_{36}, which is the same group as of 2,5-dimethylthiophene. Therefore, the selection rules for 2,5-dimethylthiophene (Section 10.3.3) can be applied directly to DMF, and only *b*-type transitions were expected in the spectrum. This is in agreement with the results from quantum chemical calculations, which predict dipole moment components of 0.00 D, 0.31 D, and 0.00 D in *a*-, *b*-, and *c*-direction, respectively at the MP2/6-311++G(d,p) level of theory.

In the first step, the *b*-type rigid-rotor spectrum was predicted with the program XIAM [45] using the rotational constants also calculated at the MP2/6-311++G(d,p) level. Only the (00) torsional state was taken into account. Based on the prediction, several discontinuous broadband scans from 9.0 to 16.0 GHz were measured, where overlapping spectra in a step size of 0.25 MHz were automatically taken. In the next step, all lines were remeasured in the high resolution mode of the spectrometer. Because only *b*-type transitions are present and the dipole moment of 0.31 D in *b*-direction is quite low, the measurements for DMF are significantly more extensive than usual.

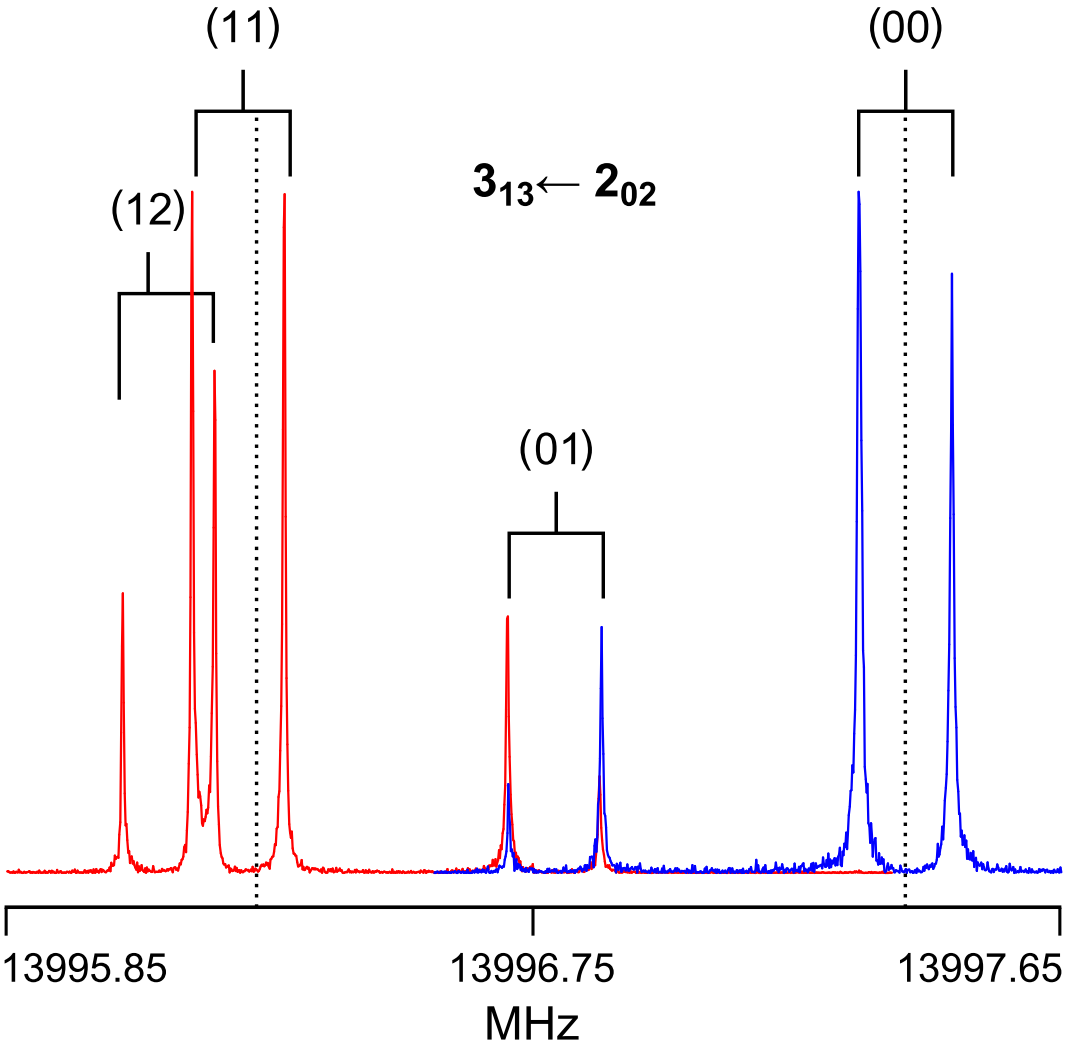

Figure 11.3. Two spectra at high resolution showing the torsional species (00), (01), (11), and (12) of the $3_{13} \leftarrow 2_{02}$ transition of DMF. The measurement accuracy is 2 kHz, the frequencies are given in MHz. The splittings indicated by brackets are due to the Doppler effect. The polarization frequency of each measurement is given as dashed lines. The red and blue spectra were obtained after 153 and 203 co-added decays, respectively. The intensities are normalized.

At the beginning of the analysis of the spectra, the *R*-branch $2_{12} \leftarrow 1_{01}$ and $3_{13} \leftarrow 2_{02}$ transitions as well as the *Q*-branch $3_{21} \leftarrow 3_{12}, 4_{22} \leftarrow 4_{13}$ and $5_{23} \leftarrow 5_{14}$ transitions were assigned readily, because the prediction was sufficiently accurate. These five transitions fixed all three rotational constants and enabled to predict and measure further rigid-rotor lines outside the broadband scans. The rigid-rotor fit including 27 rotational transitions are given in Fit I of Table 11.1; all of them are the (00) torsional species.

In the next step, a prediction considering the internal rotation of both methyl groups was carried out, where each rotational transition splits into four torsional components. The angles between the internal rotor axes and the principal axes of inertia as well as the V_3 potential were taken from the values calculated at the MP2/6-311++G(d,p) level.

Based on the frequencies given in this prediction and supported by the intensities calculated with the spin statistical weights by group theory for 2,5-dimethylthiophene (see Section 10.3), the (01), (11), and (12) torsional species were successfully assigned. Because most of the splittings were only up to a few MHz, all torsional components were observable in one or two high resolution measurements. A typical spectrum with all four torsional components is illustrated in Figure 11.3. In total, 107 torsional components of 30 rotational transitions up to $J = 8$ were measured and fitted with the program XIAM to increase the data set and to obtain molecular parameters with higher accuracy.

Table 11.1. Spectroscopic constants of DMF referred to the PAM system.

Par.[a]	Unit	Fit I	Fit II	Calc.[b]
A	GHz	6.161 466 31(27)	6.160 684 46(18)	6.053
B	GHz	2.130 780 71(14)	2.130 807 355(74)	2.120
C	GHz	1.615 040 51(11)	1.614 989 170(64)	1.602
D_J	kHz	0.1218(20)	0.1206(12)	0.117
D_{JK}	kHz	−0.2681(99)	−0.2932(59)	−0.296
D_K	kHz	3.658(45)	3.346(32)	3.329
d_1	kHz	−0.039 65(84)	−0.038 68(43)	−0.038
d_2	kHz	−0.002 21(27)	−0.002 03(15)	−0.002
V_3	cm^{-1}		439.176(11)	404.1
F_0	GHz		159.4[c]	159.4
∠(i,a)	°		27.254(11)	27.32
∠(i,b)	°		62.746(11)	62.68
∠(i,c)	°		90.0[d]	90.00
σ[e]	kHz	1.1	1.4	
N[f]		27	107	

[a] All parameters refer to the principal axis system. Watson's S reduction in I^r representation was used. [b] Ground state rotational constants and centrifugal distortion constants obtained by anharmonic frequency calculation at the MP2/6-311++G(d,p) level of theory. [c] Fixed to the *ab initio* value. [d] Fixed due to symmetry. [e] Standard deviation of the fit. [f] Number of lines.

11.4 Results of the fits and discussion

In total, 107 torsional components were fitted using the program XIAM to a standard deviation of 1.4 kHz, which is within the measurement accuracy of the spectrometer. The rotational constant A, B, and C, the centrifugal distortion constants D_J, D_{JK}, D_K, d_1, and d_2, the V_3 potentials, and the angles between the internal rotation axes and the a-principal axis were determined with very high accuracy, while the rotational constants of the two equivalent tops F_0 was kept fixed. In agreement with the results of quantum chemical calculations given in Section 11.2.3, no potential coupling terms are needed to achieve this fit quality. The results of the fit are given in the fourth column of Table 11.1 (Fit II). The list of frequencies fitted along with the residuals, is given in Table 17.51.

The program XIAM is suitable to analyze the spectrum of DMF to measurement accuracy. Quantum chemical calculations performed at different levels of theory are consistent. The predicted rotational constants are in good agreement with the experimental values (see Table 17.49), despite the fact that the quantum chemical data refer to the equilibrium structure, whereas the experimental data yield rotational constants for the ground vibrational state and no corrections have been made. The only exception is the calculation at the MP2/6-311++G(d,p) level of theory, where anharmonic frequency calculations are available and provide the ground state r_0 structure. The B_0 and C_0 rotational constants were calculated perfectly. On the contrary, the A_0 constant is not better than the A_e values obtained at some levels of theory (see Table 17.49), which is probably due to error compensations. The predicted centrifugal distortion constants at the MP2/6-311++G(d,p) level are in almost exact agreement with the experimental values. Since the planar five-membered ring frame of DMF is quite rigid, all centrifugal distortion constants are small.

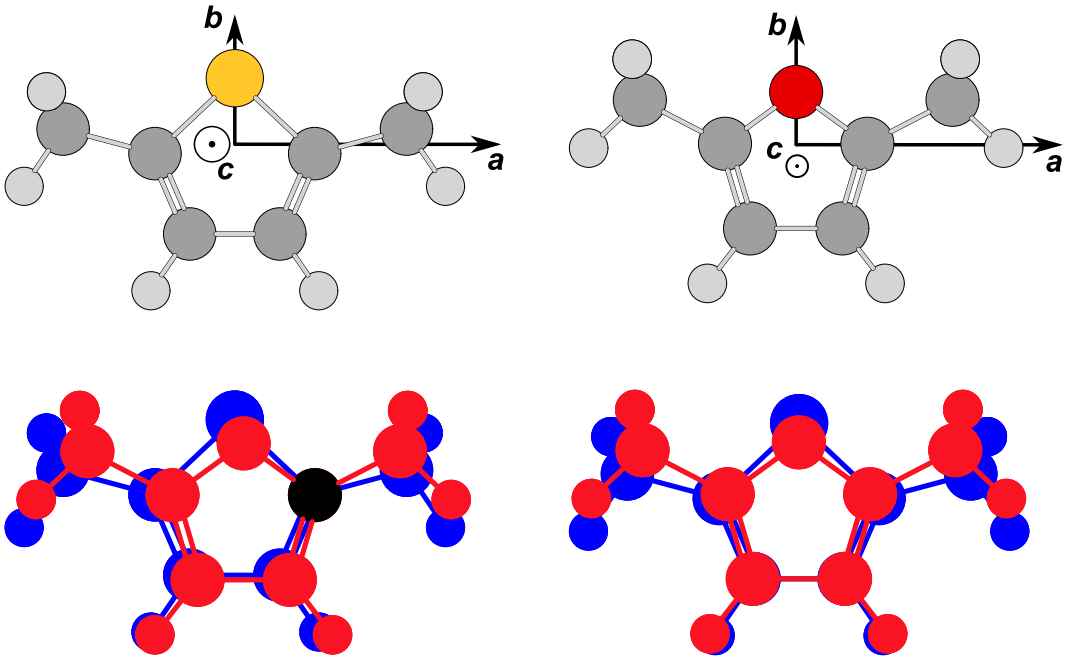

Figure 11.4. The conformer of 2,5-dimethylthiophene (DMTP) (top left) and of DMF (top right) calculated at the MP2/6-311++G(d,p) level of theory given in its principal axes of inertia. The direction of the axes out of the paper plane is indicated by an encircled dot. In the lower trace are the superpositions of both conformers given (red: DMF, blue: DMTP).Bottom left: aligned at the frame atom given in black; bottom right: aligned at the principal axes of inertia showing that (i) the sulfur atom in 2,5-dimethylthiophene is located higher on the *b*-axis than the oxygen atom in DMF and (ii) the angles $\angle(i,a)$ of the molecules differ by 12.7°.

The experimental V_3 potentials of approximately 439.176(11) cm^{-1} is much higher than the value of 242.148(41) cm^{-1} of the sulfur analogon 2,5-dimethylthiophene (DMTP, see Table 10.4). The same trend was observed for the monomethyl derivatives of furan and thiophene, 2-methylfuran (416.2 cm^{-1}) [75] versus 2-methylthiophene (194.1 cm^{-1}) [20] and 3-methylfuran (380.5 cm^{-1}) [76] versus 3-methylthiophene (258.8 cm^{-1}) [21]. Furthermore, it is possible to compare the angles between the internal rotor

axes and the a-principal axis, because 2,5-dimethylthiophene and DMF have parallel principal axes of inertia. The $\angle(i,a)$ angle of 27.254(11)° in DMF is significantly larger than the value of 14.597(78)° found for 2,5-dimethylthiophene (see Table 10.4). Because the sulfur atom is larger, the ring is stretched along the *b*-axis and pushes the methyl groups in the opposite direction, as visualized in Figure 11.4, in which the optimized conformer for both molecules at the MP2/6-311++G(d,p) level are superimposed.

The V_3 potentials calculated using the MP2, M06-2X, and B3LYP methods are between 362.2 cm^{-1} and 421.6 cm^{-1}, in the same order of magnitude as the experimental value. Using the HF method, this value is always overestimated by about 100 cm^{-1} and is in the range between 500 – 600 cm^{-1}.

The inertial defect $\Delta_c = I_c - I_a - I_b = -6.280$ u$Å^2$ confirms that the heavy atom skeleton is planar with two pairs of hydrogen atoms out of plane. This value is essentially the same as found in 2,5-dimethylthiophene ($\Delta_c = -6.275$ u$Å^2$) and other rings containing two methyl groups with comparable barrier heights, e.g. 3,5-dimethylbenzaldehyde ($\Delta_c = -6.245$ u$Å^2$) [101] and the two conformers of 2-acetyl-5-methylfuran ($\Delta_c = -6.469$ and -6.508 u$Å^2$ for the *trans* and *cis* conformers, respectively) [98].

11.5 Conclusion

The only conformer of 2,5-dimethylfuran present under molecular beam conditions was assigned using a combination of Fourier transform microwave spectroscopy and quantum chemistry. Highly accurate molecular parameters were determined using the program XIAM. The rotational spectrum could be reproduced to measurement accuracy, which is better than 2 kHz. Splittings arising from the internal rotations of the two methyl groups with a barrier height of 439.176(11) cm^{-1} were completely resolved. The angles between the internal rotor axes and the *a*-principal axis of DMF differ by 12.7° compared to those of the sulfur-analogon 2,5-dimethylthiophene.

CHAPTER 12

2-Acetyl-5-Methylfuran

Two inequivalent rotors and C_s frame symmetry

Parts of this chapter have already been published in:

Vinh Van, Wolfgang Stahl, and Ha Vinh Lam Nguyen
The structure and torsional dynamics of two methyl groups in 2-acetyl-5-methylfuran as observed by microwave spectroscopy [98]

ChemPhysChem **17**, 3223 – 3228 (2016).
DOI: 10.1002/cphc.201600757

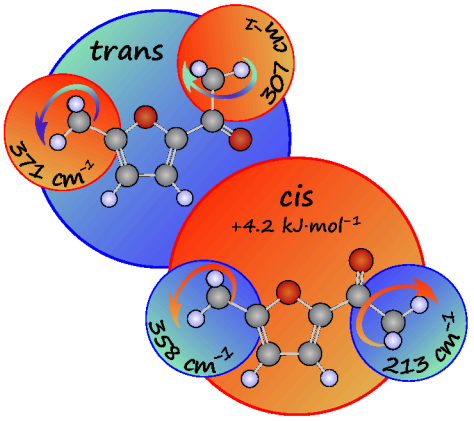

Vinh Van performed the quantum chemical calculations, the measurements, the spectral analysis, and co-wrote the manuscript. Ha Vinh Lam Nguyen and Wolfgang Stahl discussed and co-wrote the manuscript. Parts of this chapter are reproduced from Ref. [98] with permission from John Wiley and Sons.

12.1 Introduction

Volatile heterocyclic substances are responsible for the aroma during food cooking. For example, the Maillard reaction is known to create desirable aromas in browned food under heating. To understand and explain the smell in more detail, it is important to answer the questions how molecular shapes fit together and how strong and how directional hydrogen bonds are. For this purpose, gas-phase structures and information on molecular internal dynamics of the Maillard reaction products are needed, since the sense of smell starts from gas-phase molecules. Among these products, 2-acetyl-5-methylfuran (AMF) arises from reactions between amino acids and reducing sugars, and produces aroma in cooked food. [7] It was also identified as natural flavor in Chinese liquors [102], smoked salmon [103], and roasted coffee beans [104].

Spectroscopically, AMF is a derivative of furan with an acetyl substituent on the 2-position and a methyl substituent on the 5-position. When starting this work, splittings arising from the internal rotations of both methyl groups were expected to be resolvable. The barrier heights of such large amplitude motions (LAM) are mainly determined by steric and electronic effects. While the steric influence is rather local, the electronic contribution can arise from quite distant sources in the molecule, especially when conjugated double bonds and/or aromatic systems are involved. Predicting torsional barriers is challenging because chemical intuition often fails and quantum chemical calculations are still rather inaccurate. [70, 99] On the other hand, microwave spectroscopy yields highly accurate torsional barriers. Moreover, this chapter will show that two different AMF conformers exist, in which at least the acetyl methyl group is exposed to different steric environments, while the ring methyl group is almost unaffected. In contrast to the molecules 2,5-dimethylthiophene and 2,5-dimethylfuran with two equivalent methyl groups, the two inequivalent methyl groups lead to splittings of each rotational transition into five torsional components instead of four as shown in Figure 12.1. [47]

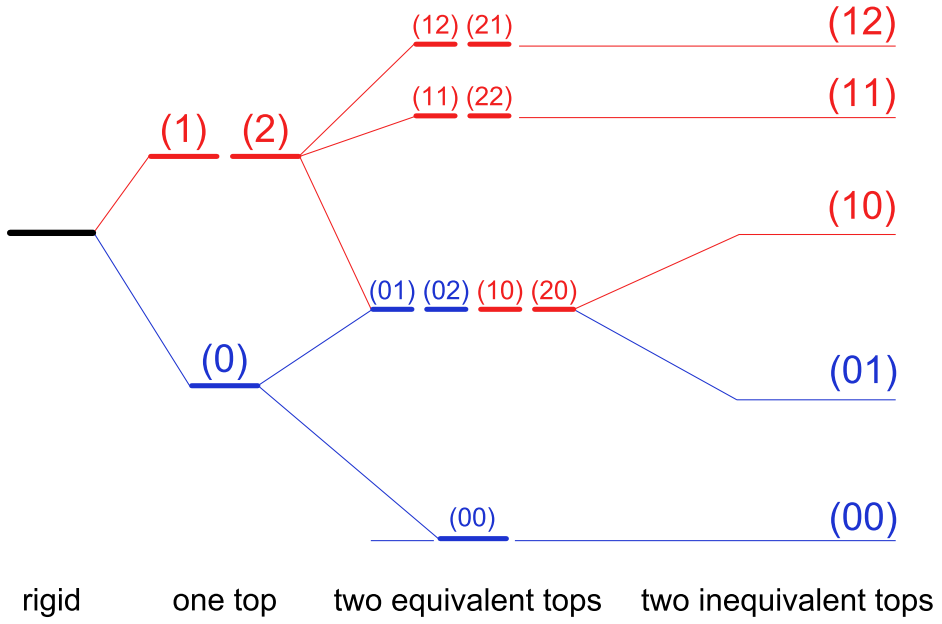

Figure 12.1. Schematic energy level diagram to illustrate the internal rotation splittings. Left-hand side: rigid molecule; second: splittings into a (0) and a (1) species due to the internal rotation of a methyl top; third: splittings into a (00), a doubly degenerated (01), a (11) and a (12) species due to the internal rotations of two equivalent methyl tops; right-hand side: splittings into a (00), a (01), a (10), a (11) and a (12) species due to the internal rotations of two inequivalent methyl tops.

12.2 Quantum chemical calculations

From the structural point of view, AMF is rather rigid because the conjugated double bonds in the five-membered ring force the furan frame to be planar. Therefore, the conformational landscape is solely determined by a rotation about the C_4-C_{12} bond (for atom numbering, see Figure 12.2). By varying the dihedral angle $\varphi_1 = \angle(O_{11},C_4,C_{12},O_{13})$ in a grid of 2° while all other geometry parameters were opti-

mized at the MP2/6-311++G(d,p) level of theory by using the GAUSSIAN09 package [26], a potential energy curve with two minima was obtained. The calculated energies were parameterized by means of a Fourier expansion with the corresponding coefficients given in Table 17.52 in the Appendix. The potential energy curve obtained by using these Fourier coefficients is depicted in Figure 12.3. Geometries at the minima were fully reoptimized by using the HF, B3LYP, M06-2X, MP2, and CCSD methods in combination with various Pople and Dunning basis sets [90–96] to compare the rotational constants and to check for convergence. The predicted rotational constants are collected in Table 17.53 and 17.54. If not otherwise stated, all values given in this chapter were calculated at the MP2/6-311++G(d,p) level of theory. Figure 12.2 shows the fully optimized conformers; their Cartesian coordinates are given in Table 17.55. With zero-point energy correction, the conformer at $\varphi_1 = 180°$, called the *trans* conformer henceforth, is 4.19 kJ·mol^{-1} lower in energy than the so-called *cis* conformer ($\varphi_1 = 0°$).

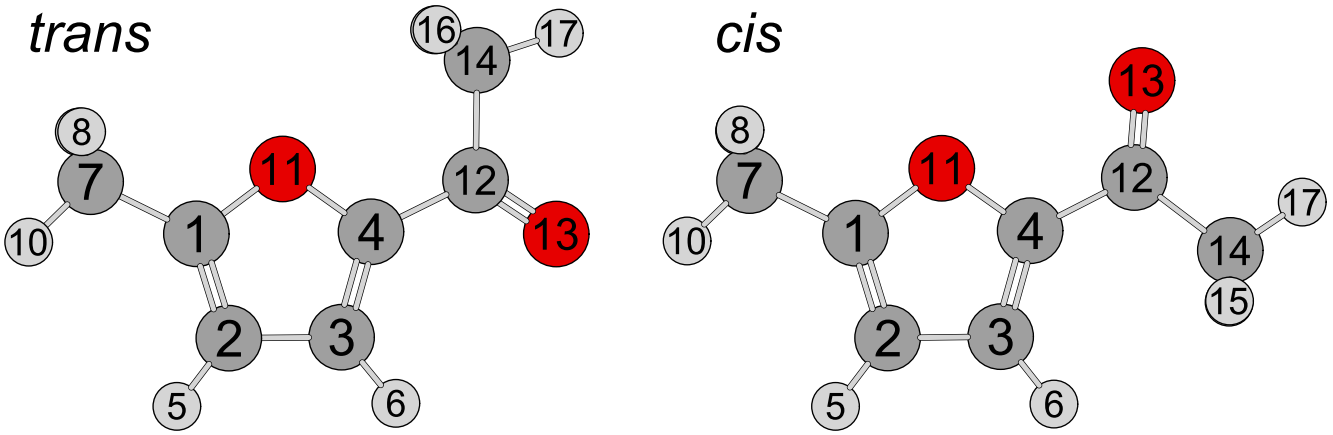

Figure 12.2. Two conformers of AMF optimized at the MP2/6-311++G(d,p) level of theory. [98]

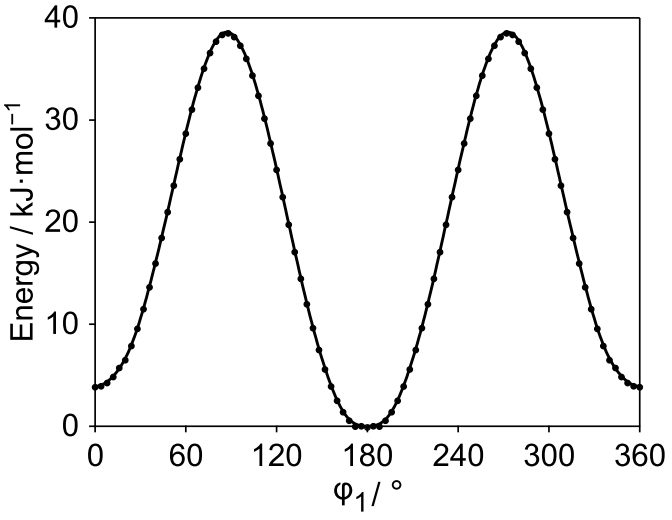

Figure 12.3. The potential energy curve obtained by rotating the acetyl group about the C_4-C_{12} bond. The dihedral angle $\varphi_1 = \angle(O_{11},C_4,C_{12},O_{13})$ was varied in a grid of 2° and optimized at the MP2/6-311++G(d,p) level of theory. Relative energies are given with respect to the lowest energy configuration at $E = -420.930421$ Hartree. The *trans* conformer is located at $\varphi_1 = 180°$, the *cis* conformer at 0°. [98]

In spite of its relatively simple structure, the internal dynamics of AMF is challenging because of the LAMs of two inequivalent methyl groups, which cause all rotational transitions to split into quintets. [47] The barrier heights of the ring and acetyl methyl groups were calculated by varying the dihedral angles $\varphi_2 = \angle(C_2,C_1,C_7,H_8)$ and $\varphi_3 = \angle(O_{13},C_{12},C_{14},H_{15})$, respectively, in a grid of 2°. A rotation of 120° was sufficient due to the threefold symmetry of the methyl groups. The potential energy curves of the ring methyl group are shown in Figure 12.4; the corresponding coefficients are listed in Table 17.56 and 17.57. For the *trans* conformer, V_3 potentials of 340 cm^{-1} for the ring methyl group and 241 cm^{-1} for the acetyl methyl group with no significant V_6 contributions were found. The respective values for the *cis* conformer are 334 and 207 cm^{-1}.

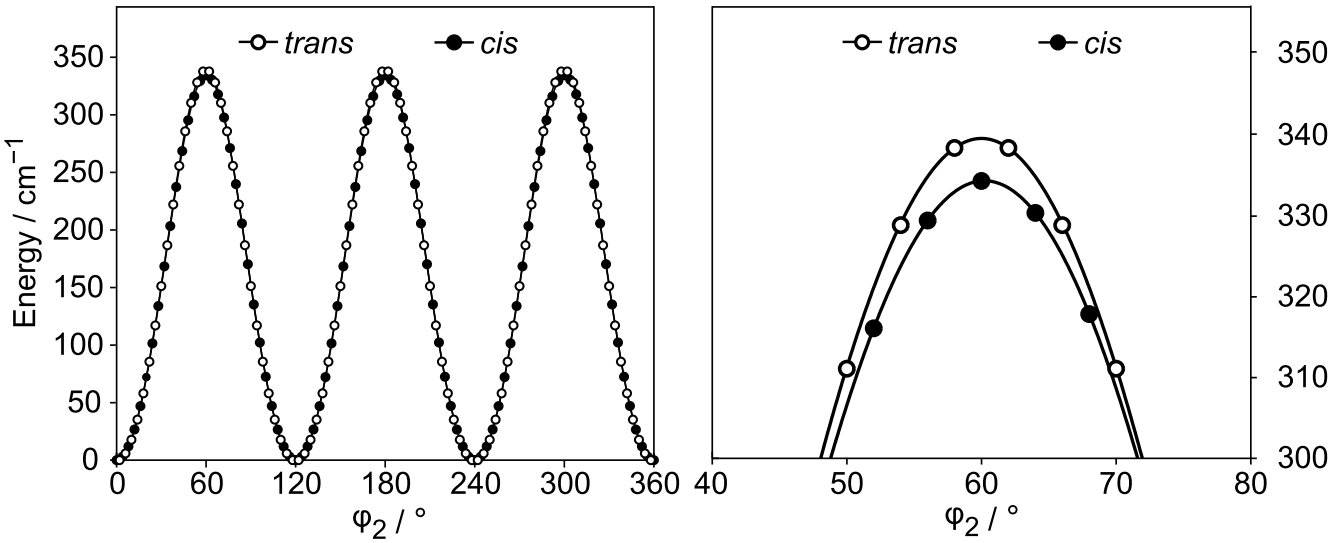

Figure 12.4. The potential energy curves of the *trans* and the *cis* conformer of AMF obtained by rotating the ring methyl group about the C_1-C_7 bond (for atom numbering see Figure 12.2). The dihedral angle $\varphi_2 = \angle(C_2,C_1,C_7,H_8)$ was varied in a grid of 2°, while all other molecular parameters were optimized at the MP2/6-311++G(d,p) level. Relative energies with respect to the lowest energy conformations with the absolute energies $E = -420.930421$ Hartree and -420.928812 Hartree for the *trans* and the *cis* conformer, respectively, were used. The barrier heights are 340 cm^{-1} for the *trans* conformer and 334 cm^{-1} for the *cis* conformer. [98]

The potential energy curves for the rotation of the acetyl methyl groups are depicted in Figure 12.5. Here, V_6 contributions were expected for the *trans* conformer due to a more symmetrical environment of the acetyl methyl rotor in relation to both oxygen atoms. Unfortunately, an unusual discontinuity occurred in the minimum regions of the potential curves of this conformer during the rotation of the acetyl methyl group. Therefore, the data set cannot be fitted well. By comparing the two geometries at the discontinuity, it was found that (i) only the methyl group was twisted, while all other dihedral angles remain the same, and (ii) one hydrogen atom approaches the eclipse position of the oxygen atom at this location. The barrier height of 241 cm^{-1}, obtained from $E(60°) - E(120°)$ is essentially the same as the energy difference between the optimized minimum and the transition state.

As an alternative, geometry optimizations to a first-order transition state of the methyl groups were performed at various levels of theory by using the Berny algorithm to calculate the barriers to internal rotations. [28] The V_3 potentials predicted at different levels of theory and the angles between the internal rotor axes and the principal axes are summarized in Table 17.53 and 17.54.

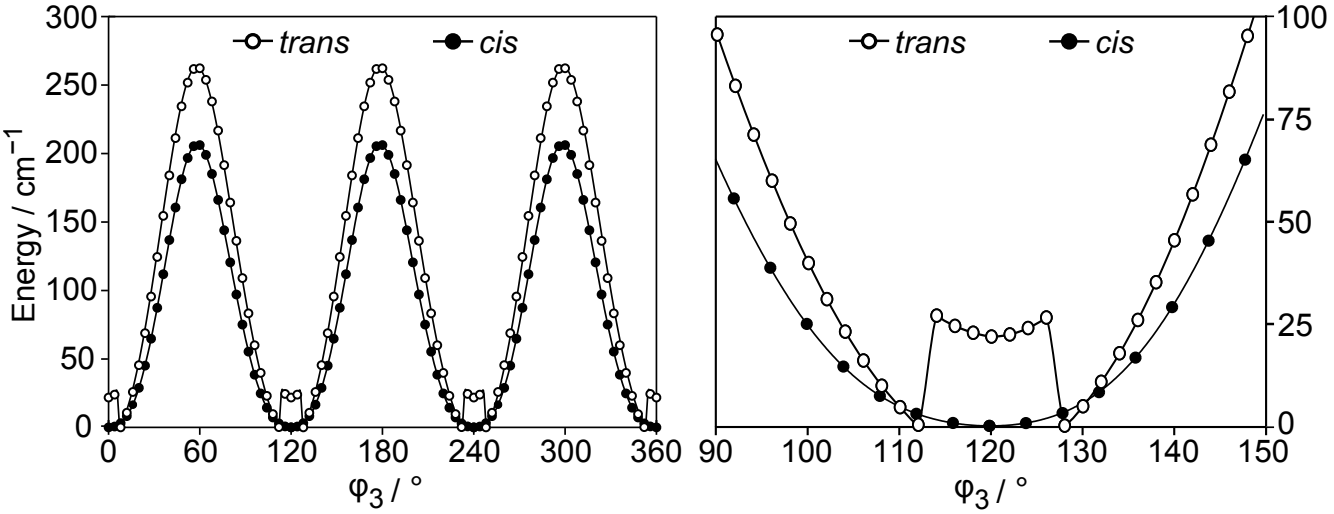

Figure 12.5. The potential energy curves of the *trans* and the *cis* conformer of AMF obtained by rotating the acetyl methyl group about the C_{12}-C_{14} bond (for atom numbering see Figure 12.2). The dihedral angle $\varphi_3 = \angle(O_{13},C_{12},C_{14},H_{15})$ was varied in a grid of 2°, while all other molecular parameters were optimized at the MP2/6-311++G(d,p) level. Relative energies with respect to the lowest energy conformations with the absolute energies $E = -420.930421$ Hartree and -420.928812 Hartree for the *trans* and the *cis* conformer, respectively, are given. The barrier height is 207 cm^{-1} for the *cis* conformer. For the *trans* conformer, an unusual discontinuity occurred in the minimum regions, as can be recognized on an enlarged scale (right). [98]

Finally, a 2D potential energy surface (PES) depending on φ_2 and φ_3 was obtained by varying these two dihedral angles in a grid of 10° to study the coupling between the two LAMs of the methyl groups. Due to symmetry, only data points in the range from φ_2 and $\varphi_3 = 0 - 120°$ were needed. The potential energies were parameterized with a 2D Fourier expansion based on terms representing the correct symmetry of the angles φ_2 and φ_3. The corresponding coefficients are given in Table 17.58. The PES illustrated in Figure 12.6 exhibits almost no potential coupling terms between φ_2 and φ_3 for both conformers.

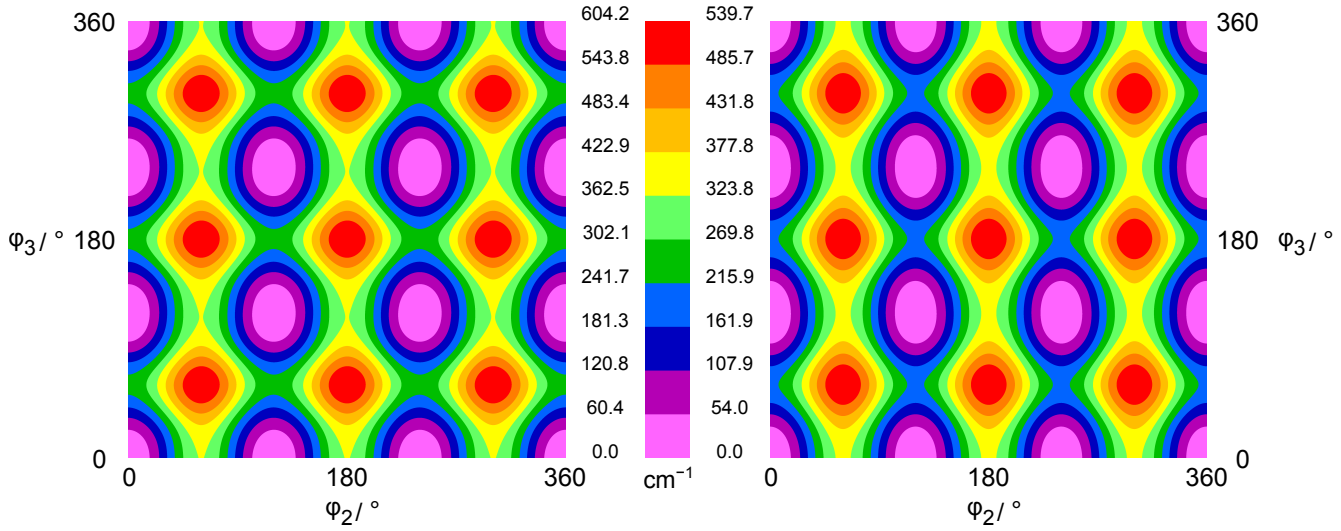

Figure 12.6. The potential energy surface in dependence on the dihedral angles $\varphi_2 = \angle(C_2,C_1,C_7,H_8)$ and $\varphi_3 = \angle(O_{13},C_{12},C_{14},H_{15})$ of the *trans* (left) and the *cis* conformer (right) of AMF calculated at the MP2/6–311++G(d,p) level of theory. φ_2 and φ_3 were varied in a grid of 10°, while all other parameters were optimized. Due to symmetry, only data points in the range from $\varphi_2 = 0°$ to 120° and $\varphi_3 = 0°$ to 120° were needed. The relative energy maxima are 604.2 cm^{-1} (7.2 $kJ \cdot mol^{-1}$) and 539.7 cm^{-1} (6.5 $kJ \cdot mol^{-1}$) for the *trans* and the *cis* conformers, respectively. The corresponding energies were parameterized with a two-dimensional Fourier expansion based on terms representing the correct symmetry of the angles φ_2 and φ_3. The Fourier coefficients are given in Table 17.58. [98]

12.3 Microwave spectroscopy

The assignment was started with the spectrum of the most stable *trans* conformer, which has dipole moment components of 4.14, 1.67, and 0.00 D in the *a*-, *b*-, and *c*-directions, respectively. Only *a*- and *b*-type transitions were expected in the spectrum, and *a*-type lines should be more intense. The selection rules for *a*-type lines are K_aK_c: ee↔eo and oo↔oe and those for *b*-type lines are K_aK_c: ee↔oo and oe↔eo (e = even, o = odd). [29] At the beginning, the internal rotation effects were neglected and AMF was considered as a rigid rotor. A prediction by the program XIAM [45] indicated a relatively dense spectrum in the frequency range from 9.0 to 13.0 GHz. A broadband scan was recorded in this region, whereby overlapping spectra in a step size of 0.25 MHz were automatically recorded. Figure 12.7 shows a portion of the scan. All lines indicated in the scan were remeasured at higher resolution. A typical high resolution spectrum is shown in Figure 12.8.

The $J = 5 \leftarrow 4$ *a*-type transitions with $K_a = 0$, 1 and the *b*-type $6_{06} \leftarrow 5_{15}$ and $7_{07} \leftarrow 6_{16}$ as well as $4_{14} \leftarrow 3_{03}$, $5_{15} \leftarrow 4_{04}$ and $6_{16} \leftarrow 5_{05}$ transitions were readily assigned. Each transition splits into five torsional components ($\sigma_1\sigma_2$) = (00), (01), (10), (11), and (12) because of the LAMs of the two methyl groups. [47] The notations σ_1 and σ_2 refer to the ring-methyl and acetyl-methyl rotors, respectively. The assignment of these lines enabled to predict and find further (00) transitions.

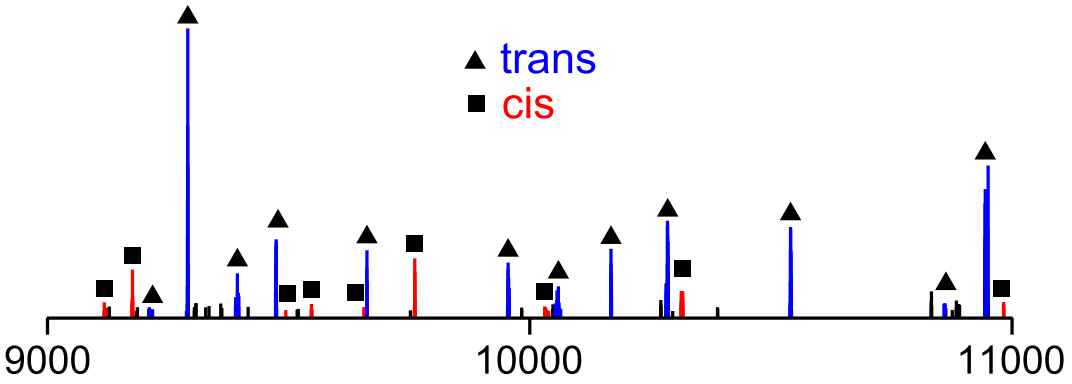

Figure 12.7. A portion of the broadband scan from 9000 to 11000 MHz of AMF showing that (i) transitions of the *trans* conformer (▲) are much more intense than those of the *cis* conformer (■), and (ii) only a few unassigned lines are present in the spectrum. [98]

In the next step, the methyl internal rotations were taken into consideration and a two-top spectrum was predicted using the rotational constants from the rigid-rotor fit. The angles δ between the internal rotor axes and the principal *a* axis as well as the V_3 potentials were obtained from *ab initio* calculations. The LAM splittings are relatively small (up to 20 MHz), which simplified the assignment. Some rotational transitions exhibited very small splittings down to a few kilohertz. The assignment of these transitions was quite challenging because different torsional species could not be easily distinguished. Finally, 280 torsional transitions with $J \leq 10$ were assigned and fitted to a standard deviation of 2.4 kHz by using XIAM. The results of the fits are given in Table 12.1.

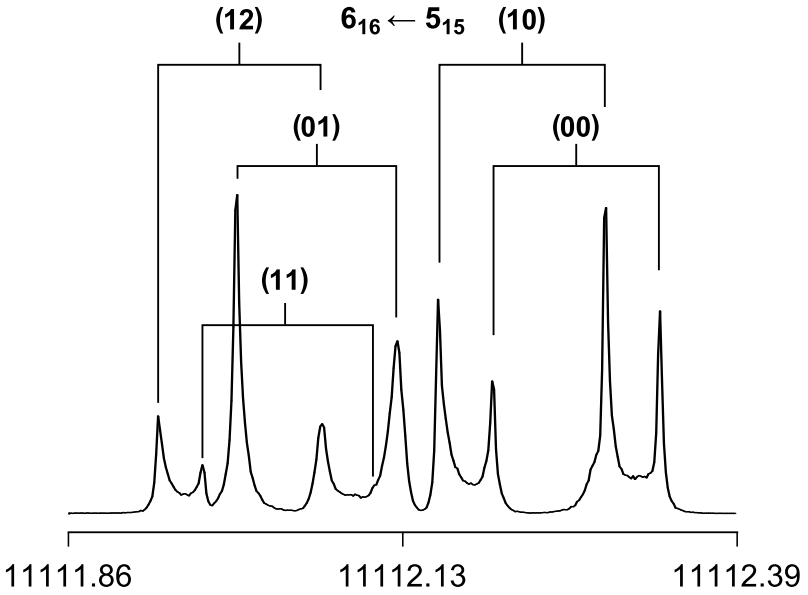

Figure 12.8. A typical spectrum of the $6_{16} \leftarrow 5_{15}$ transition of the *trans* conformer of AMF with its torsional (00), (10), (01), (11), and (12) species. The frequency is in MHz, the line width approximately 13 – 25 kHz (FWHH), corresponding to a measurement accuracy of 2 kHz. The splittings indicated by brackets are due to the Doppler effect. For this spectrum 2000 decays were co-added. [98]

After the *trans* conformer was assigned, many lines with low intensities remained in the scan, which presumably belong to the *cis* conformer with calculated dipole moment components of 2.26, 4.04, and 0.00 D in the *a*-, *b*-, and *c*-directions, respectively. Also in this case, the spectrum contains only *a*- and *b*-type transitions and *b*-type lines should be more intense. Surprisingly, the $J = 5 \leftarrow 4$ and $6 \leftarrow 5$ *a*-type transitions could be assigned first and they were more intense than most of the *b*-type lines. For the *cis* conformer, 105 torsional transitions up to $J = 8$ were measured and fitted to a standard deviation of 2.6 kHz (see Table 12.1). The frequency lists of the *trans* and *cis* conformers are available in Table 17.59 and 17.60.

Table 12.1. Molecular parameters of the *trans* and the *cis* conformer of AMF as obtained by the program XIAM. Top 1 refers to the ring methyl group, top 2 to the acetyl methyl group. The frequency lists are given in Table 17.59 and 17.60.

Par.[a]	Unit	*trans*	*cis*
A	GHz	3.699 650 628(73)	3.913 857 2(37)
B	GHz	1.125 952 913(72)	1.095 561 67(24)
C	GHz	0.872 880 211(49)	0.865 502 61(12)
D_J	kHz	0.035 11(28)	0.0294(20)
D_{JK}	kHz	−0.0392(29)	−0.050(17)
D_K	kHz	1.10(17)	0.783(71)
d_1	kHz	−0.010 66(20)	−0.0066(14)
d_2	kHz	−0.001 24(16)	0.00[b]
$V_{3,1}$	cm^{-1}	369.78(25)	356.47(39)
$F_{0,1}$	GHz	159.40(11)	159.16(16)
$\angle(i_1,a)$	°	143.601(34)	146.523(69)
$\angle(i_1,b)$	°	126.399(34)	123.477(69)
$\angle(i_1,c)$[c]	°	90.00	90.00
$V_{3,2}$	cm^{-1}	307.78(59)	212.71(30)
$F_{0,1}$	GHz	160.51(39)	159.87(24)
$\angle(i_2,a)$	°	75.154(31)	−41.012(15)
$\angle(i_2,b)$	°	165.154(31)	48.988(15)
$\angle(i_2,c)$[c]	°	90.00	90.00
$D_{pi2J,2}$	kHz	40.36(47)	18.78(34)
$D_{pi2K,2}$	kHz	−206.5(61)	−343(24)
σ[d]	kHz	2.4	2.6
N[e]		280	105

[a] All parameters are given with one standard uncertainty in parentheses. Watson's S reduction in I^r representation was used. [b] Not fitted, set to zero. [c] Fixed due to symmetry. [d] Standard deviation of the fit. [e] Number of lines.

Table 12.2. Molecular parameters of the *trans* and the *cis* conformer of AMF as obtained by the program XIAM while F_0 values are fixed to those calculated at the MP2/6-311++G(d,p) level of theory. Top 1 refers to the ring methyl group, top 2 to the acetyl methyl group.

Par.[a]	Unit	*trans*	MP2[b]	B3LYP[b]	*cis*	MP2[b]	B3LYP[b]
A	GHz	3.699 651 44(76)	3.638	3.678	3.913 830 50(86)	3.843	3.893
B	GHz	1.125 952 983(75)	1.120	1.115	1.095 561 29(27)	1.089	1.084
C	GHz	0.872 880 084(48)	0.866	0.865	0.865 502 36(14)	0.858	0.857
D_J	kHz	0.034 94(29)	0.034	0.035	0.0298(24)	0.030	0.031
D_{JK}	kHz	−0.0396(30)	−0.044	−0.043	−0.060(19)	−0.031	−0.024
D_K	kHz	1.60(16)	0.737	0.762	0.865(86)	0.715	0.721
d_1	kHz	−0.010 79(21)	−0.010	−0.010	−0.0063(16)	−0.008	−0.008
d_2	kHz	−0.001 24(17)	−0.001	−0.001	0.00[c]	−0.0003	−0.0001
$V_{3,1}$	cm^{-1}	369.514(38)	339.9	323.4	356.502(55)	334.4	313.0
$F_{0,1}$ [c]	GHz	159.3	159.3	158.8	159.2	159.2	159.0
$\angle(i_1,a)$	°	143.588(34)	143.11	143.65	146.526(54)	146.36	146.74
$\angle(i_1,b)$	°	126.422(34)	126.89	126.35	123.474(54)	123.64	123.26
$\angle(i_1,c)$[d]	°	90.00	90.00	90.00	90.00	90.00	90.00
$V_{3,2}$	cm^{-1}	303.967(41)	241.4	165.1	210.510(11)	206.8	87.1
$F_{0,2}$ [c]	GHz	158.0	158.0	160.0	158.1	158.1	159.9
$\angle(i_2,a)$	°	74.9581(86)	78.59	77.74	−40.928(11)	−44.48	−43.79
$\angle(i_2,b)$	°	164.9581(86)	168.59	167.74	49.072(11)	45.52	46.21
$\angle(i_2,c)$[d]	°	90.00	89.99	90.00	90.00	90.00	90.00
$D_{pi2J,2}$	kHz	41.34(47)			20.55(31)		
$D_{pi2K,2}$	kHz	−174.4(42)			−174.8(30)		
σ[e]	kHz	2.5			3.2		
N[f]		280			105		

[a] All parameters are given with one standard uncertainty in parentheses. Watson's S reduction in I^r representation was used. [b] Vibrational ground state rotational constants and centrifugal distortion constants obtained by anharmonic frequency calculation at the MP2/6-311++G(d,p) and B3LYP/6-311++G(d,p) level of theory, respectively. [c] Fixed. [d] Fixed due to symmetry. [e] Standard deviation of the fit. [f] Number of lines.

12.4 Results and discussion

The three linear combinations of the rotational constants $B_J = \frac{1}{2}(B+C)$, $B_K = A - \frac{1}{2}(B+C)$, $B_- = \frac{1}{2}(B-C)$ and the centrifugal distortion constants D_J, D_{JK}, D_K, d_1, and d_2 were determined with very high accuracy for both conformers. The V_3 potentials, the angles δ between the internal rotor axes and the principal *a*-axis, the internal rotation constants, and two higher order parameters D_{pi2J} and D_{pi2K} were also fitted.

The experimentally deduced rotational constants were compared with those from quantum chemical calculations. The best agreement was found with the DFT method using the M06-2X and B3LYP functionals for the *trans* and the *cis* conformer, respectively, as shown in Table 17.53 and 17.54. All levels of theory yield quite reasonable *B* and *C* rotational constants, while the *A* rotational constant has larger deviations. All predicted rotational constants reported in Table 17.53 and 17.54 refer to the equilibrium r_e structure, and the experimentally deduced rotational constants to the vibrational ground state r_0 structure. Theoretical rotational constants of the r_0 structure can be obtained by anharmonic frequency calculations (Table 12.2). Surprisingly, they show larger deviations to the experimental values compared to those of the r_e structure. This is probably due to error compensations.

Because of the strong correlation between V_3 and F_0 in the fit shown in Table 12.1, a fit with F_0 fixed to the *ab initio* values was carried out in Table 12.2. The V_3 terms, which depend on the assumed values of F_0, as well as the higher order parameters D_{pi2J} and D_{pi2K}, change slightly. The V_6 term cannot be fitted independently, because only transitions in the torsional ground state are available, and set to zero. Since the *ab initio* results predict no significant V_6 contributions (see Section 12.2), the experimental values of the V_3 terms are expected to be sufficiently accurate.

The calculated centrifugal distortion constants obtained by anharmonic frequency calculations with the MP2 and B3LYP methods and the 6-311++G(d,p) basis set are in good agreement with the experimental values, except for the parameter D_K of the *trans* conformer (see Table 12.2). Since the planar five-membered ring frame of AMF is quite rigid, all centrifugal distortion constants are small. A relatively strong correlation between the parameters B_K and D_K was identified in the fit of the *trans* conformer if F_0 is fixed to its *ab initio* value (see Table 17.61 in the Appendix). This correlation weakens slightly if F_0 is fitted (as in the fit shown in Table 12.1; for the correlation matrix see Table 17.62), and the D_K value is closer to the predicted value. The correlation matrices of the cis conformer are given in Table 17.63 and 17.64.

The barrier heights of the ring-methyl top are 369.78(25) and 356.47(39) cm^{-1} for the *trans* and the *cis* conformer, respectively, which are very similar. Obviously, the orientation of the acetyl group does not significantly affect the torsional barrier of the ring methyl group. On the other hand, the barrier heights

are clearly lower than that of 2-methylfuran (416.2 cm^{-1}) [75], and this shows that the presence of the acetyl group with its negative mesomeric effect and the possibility for an extended π-conjugation might decrease the barrier of the ring methyl group as shown in Figure 12.9. This effect was also found for the sulfur derivatives.

The barrier to internal rotation of the acetyl-methyl top is quite different in the two conformers. A value of 307.78(59) cm^{-1} for the *trans* and 212.71(30) cm^{-1} for the *cis* conformer were found. From many previous investigations, it is known that the torsional barrier of the acetyl methyl group in ketones depends strongly on the substitution at the other side of the carbonyl group (Figure 12.10). [105][15–21] This behavior in ketones, where the substituent on the other side of the carbonyl group causes the acetyl-methyl barrier to vary over a wide range without any apparent trends, is in strong contrast to the acetates, which can be divided into classes with predictable barrier heights. [97]

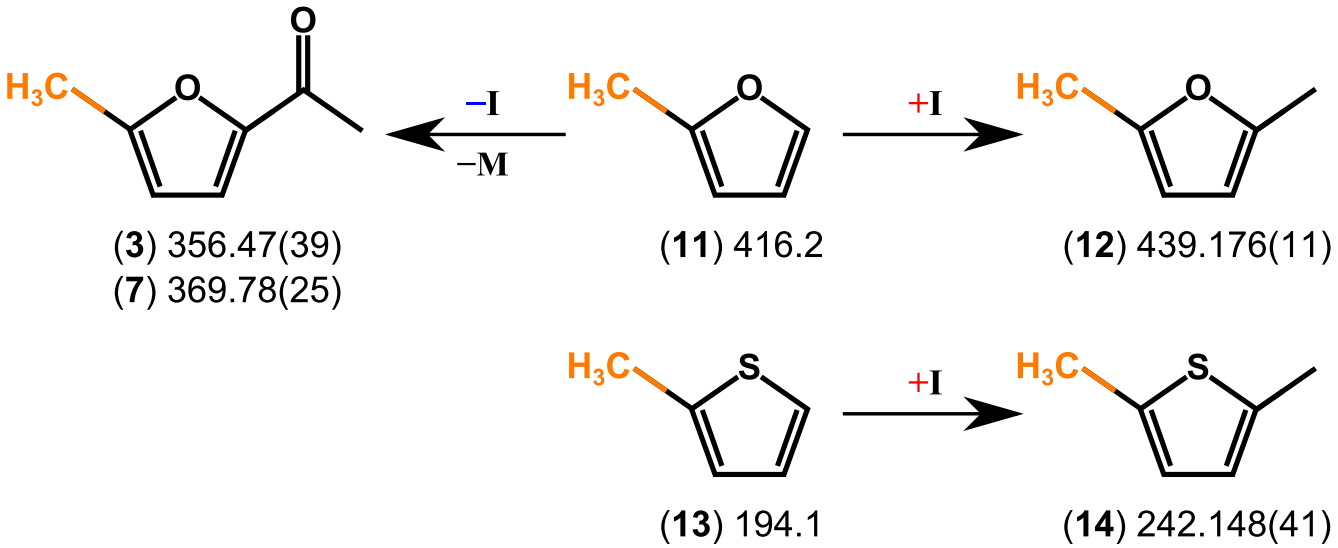

Figure 12.9. Influence of mesomeric and inductive effects on the barrier heigths for the (**3**) *cis* and (**7**) *trans* conformer of AMF (this chapter), the furan derivatives (**11**) 2-methylfuran [75] and (**12**) 2,5-dimethylfuran (see Chapter 11) as well as the thiophene derivatives (**13**) 2-methylthiophene [20] and (**14**) 2,5-dimethylthiophene (see Chapter 10).

For example in α,β-saturated alkyl acetates, the barrier to internal rotation is approximately 100 cm^{-1} and remains largely invariant. [106, 107] This value cannot be easily predicted when an electronic effect exists, for example, due to the presence of double bonds or lone electron pairs, which can contribute in a conjugated system. In unsaturated acetates such as vinyl acetate [84] and isopropenyl acetate [85], π-electron conjugation, extending from the vinyl double bond to the ester group, is possible. The barriers are significantly different and also differ from those found for saturated acetates. In some acetamides, such as *N*-ethylacetamide [108] and *N,N*-diethylacetamide [99], the barriers of the acetyl methyl group are strongly affected by the electronic effect of the lone electron pair and the substituents attached to the nitrogen atom. Even though AMF is different from other ketones because of the aromatic ring, the barrier height in its both conformers is not unusually larger or smaller. Similar to the cases of

N,N-diethylacetamide [99] and methyl vinyl ketone [109], the barrier height of the acetyl-methyl rotor depends strongly on the orientation of the substituent on the other side of the carbonyl group. Further conclusions cannot be drawn since too few examples of ketones are available at the moment.

The torsional barriers of the ring methyl group calculated at different levels of theory are 297 – 501 cm^{-1} and 283 – 477 cm^{-1} for the *trans* and the *cis* conformer, respectively, which are on the same order of magnitude as the experimental V_3 potentials. For the acetyl-methyl top, 162 – 349 cm^{-1} were found for the *trans* and 71 – 311 cm^{-1} for the *cis* conformer. The best agreement between the calculated and experimental barriers was found for both conformers and both methyl groups at the M06-2X/6-311++G(3df,2pd) level of theory (see Table 17.53 and 17.54).

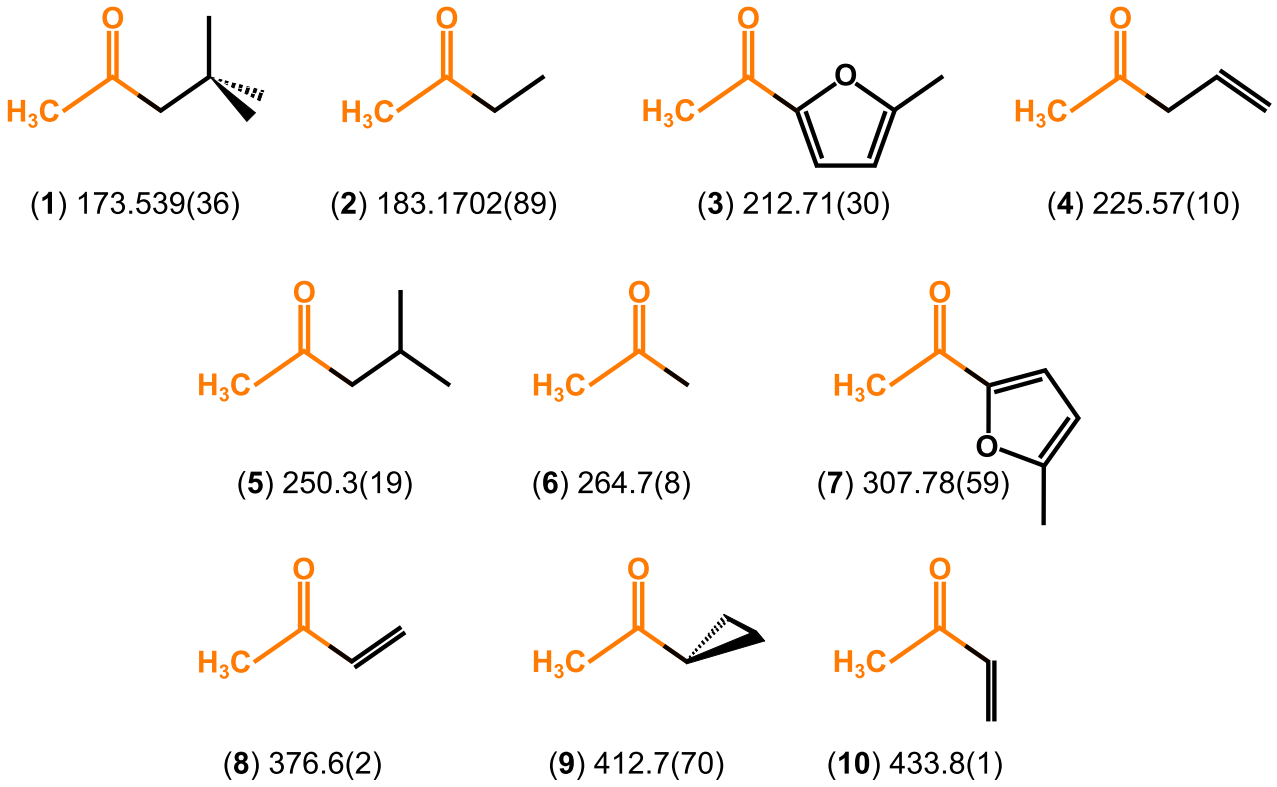

Figure 12.10. Torsional barriers of the acetyl methyl groups in ketones (in cm^{-1}). Methyl neopentyl ketone (**1**) [105], ethyl methyl ketone (**2**) [110], *cis*-AMF (**3**, this chapter), allyl acetone (**4**) [111], methyl isobutyl ketone (**5**) [112], acetone (**6**) [113], *trans*-AMF (**7**, this chapter), *syn*-methyl vinyl ketone (**8**) [109], cyclopropyl methyl ketone (**9**) [114], *anti*-methyl vinyl ketone (**10**) [109]. [98]

The inertial defects $\Delta_c = I_c - I_a - I_b = -6.469$ and -6.580 u$Å^2$ of the *trans* and *cis* conformers, respectively, confirm that the heavy-atom skeleton is planar with two pairs of hydrogen atoms out of plane. These values are almost the same as that found in other planar molecules containing two methyl groups with comparable barrier heights, for example, methyl acetate ($\Delta_c = -6.315$ u$Å^2$) [115] and the *syn* and *anti* conformers of 3,4-dimethylbenzaldehyde ($\Delta_c = -6.452$ and -6.469 u$Å^2$, respectively) [101].

12.5 Conclusion

Two conformers of AMF exhibiting internal rotations of two nonequivalent methyl groups were successfully assigned under molecular-beam conditions by means of a combination of Fourier transform microwave spectroscopy and quantum chemistry. The above-mentioned intramolecular dynamics causes splittings of all rotational transitions into five different torsional species. The torsional barriers of the ring-methyl top are similar in both conformers, whereas those of the acetyl methyl group are quite different, probably because of electronic rather than steric effects. Quantum chemical calculations yielded reasonable structural parameters, but the predicted barrier heights are not yet sufficiently accurate.

CHAPTER 13

4,5-Dimethylthiazole

Two inequivalent rotors, ^{14}N quadrupole coupling, and C_s frame symmetry

13.1 Introduction

Thiazole is a five-membered heterocyclic compound that contains a sulfur atom and a nitrogen atom in the ring. It exists as the basic structure element in a variety of organic compounds such as vitamin B_1, epothilone, and clomethiazole. It is also a precursor in the production of fungicides, drugs (e.g. alagebrium), and dyes. Thiazole derivatives participate in several biosyntheses as required for the formation of thiamine, where the sulfur element is extracted from cysteine. Whereas thiazoles are well-represented in biomolecules, its related compound oxazoles, where the sulfur atom is replaced by an oxygen atom, are not.

Thiazole and its monomethyl derivatives have been studied thoroughly by microwave spectroscopy (see Figure 13.1). Whereas their structures are proved to be relatively rigid, the internal dynamics arising from the internal rotation of the substituted methyl group is unpredictable. [71, 74, 116–119] It is particularly interesting to compare the hindering potentials of the methyl internal rotation, which strongly depends on the position of the methyl substituent. While changing the methyl group from the 4- (**2**) [117] to the 5-position (**3**) [118] does not significantly influence the hindering potential (357.6 cm^{-1} and 332.0 cm^{-1}, respectively), it decreases drastically to one tenths in 2-methylthiazole (**1**, 34.9 cm^{-1}) [71]. The same trend can be recognized in the related oxazole compounds, where the hindering potentials are 252.0 cm^{-1}, 428.3 cm^{-1}, and 478.2 cm^{-1} for 2- (**5**) [119], 4- (**6**) [74], and 5-methyloxazole (**7**) [119], respectively. It is also notable by comparing (**1**) and (**5**), (**2**) and (**6**), as well as (**3**) and (**7**), that substitution of oxygen by sulfur significantly reduces the hindering potential. An explanation for these observations is the aromatic character of azole rings. Thiazoles are characterized by larger π-electron delocalization than the corresponding oxazoles and have therefore greater aromaticity. This aromaticity is evidenced by the chemical shift of the ring protons in ^{1}H-NMR spectroscopy, which is between 7.27 and 8.77 ppm. It clearly indicates a strong diamagnetic ring current. The calculated π-electron density marks the 5-position as the primary site for electrophilic substitution and the 2-position as the site for nucleophilic substitution. [120]

It is an interesting question, how the hindering potentials are influenced if two positions in the thiazole ring are substituted by methyl groups. This induced to study 4,5-dimethylthiazole (**4**) (DMTA). To the best of my knowledge, only one dimethyl substituted five-membered heterocyclic compound, 2,5-dimethylthiophene [70], has been studied by microwave spectroscopy so far. DMTA is the first molecule and will be a part of the studies on dimethyl derivatives of azoles.

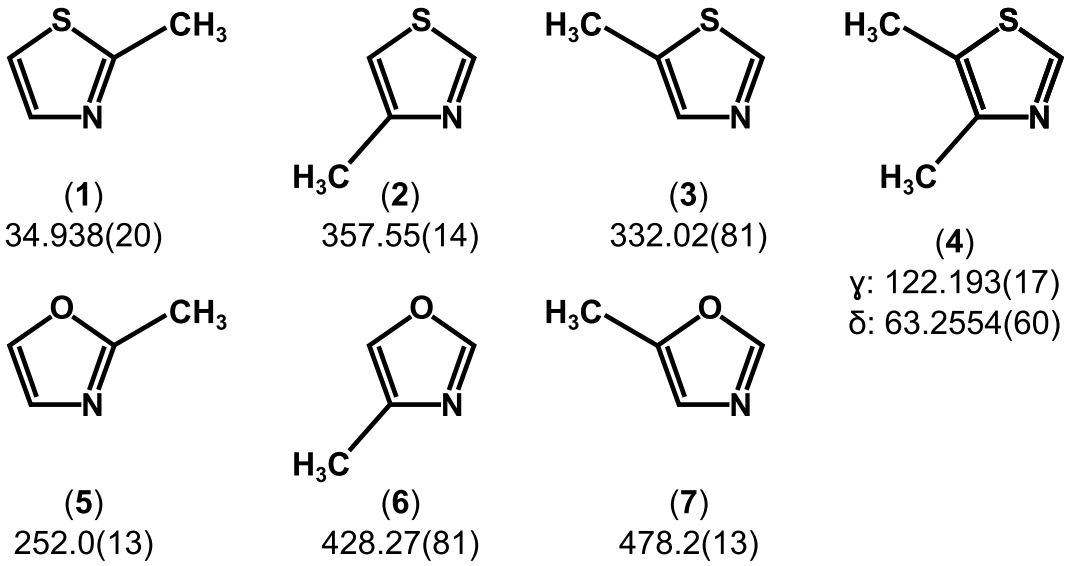

Figure 13.1. Methyl torsional barriers in thiazoles and oxazoles (in cm^{-1}). (**1**) 2-methylthiazole [71], (**2**) 4-methylthiazole [117], (**3**) 5-methylthiazole [118], (**4**) 4,5-dimethylthiazole (this chapter), (**5**) 2-methyloxazole [119], (**6**) 4-methyloxazole [74], (**7**) 5-methyloxazole [119].

13.2 Quantum chemical calculations

13.2.1 Geometry optimization

As other thiazole rings, DMTA is planar and aromatic because of the π-electron delocalization of the two conjugated double bonds. This constrain confines the structural analysis to have only one starting geometry. Fully geometry optimizations were performed on this initial forms using the HF, B3LYP, M06-2X, MP2, and CCSD methods in combination with various Pople and Dunning basis sets [90–96] as implemented in the GAUSSIAN09 package [26]. The optimized conformer at the MP2/6-311++G(d,p) level of theory is shown in Figure 13.2 in its principal axes of inertia. The nuclear Cartesian coordinates of the fully optimized geometry is given in Table 17.65 in the Appendix. Harmonic frequency calculations were carried out to verify the stationary point whether it is a saddle point or a true minimum geometry.

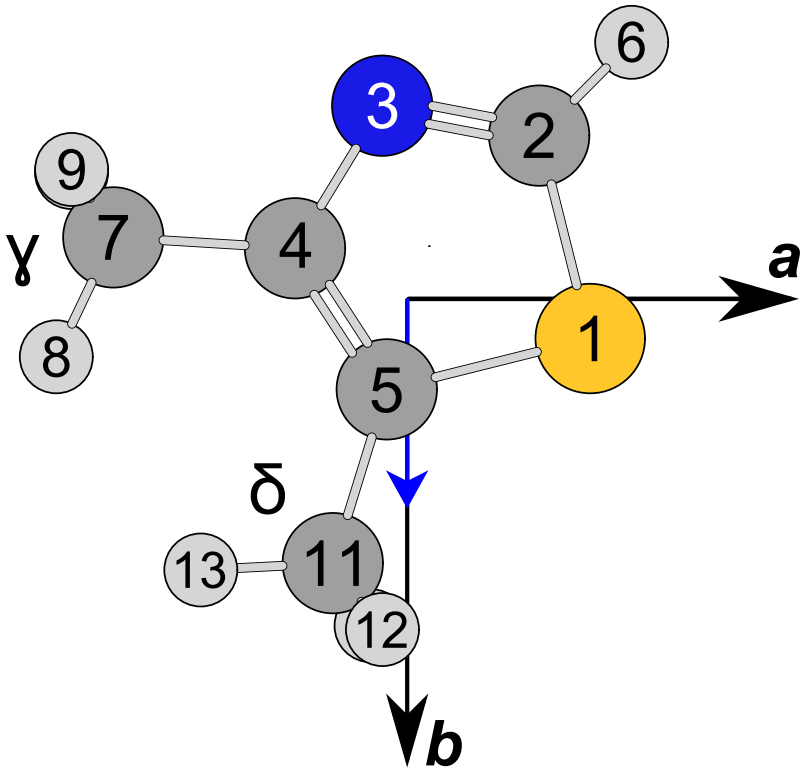

Figure 13.2. The atom numbers and structure calculated at the MP2/6-311++G(d,p) level of theory of the only conformer of 4,5-dimethylthiazole and its dipole moment (in blue), as viewed along the *c*-principal axis, illustrating that: (i) all heavy atoms are located on the *ab*-plane and (ii) the dipole moment is almost exactly parallel to the *b* principal axis. Torsional splittings are observed for both methyl groups (called γ and δ).

13.2.2 ^{14}N nuclear quadrupole coupling constants

DMTA contains one ^{14}N nucleus with a nuclear spin of I = 1 and, therefore, nuclear quadrupole coupling will result in a hyperfine pattern for each rotational line. The splittings depend on the nuclear quadrupole coupling constants (NQCCs). From the optimized structure at the MP2/6-311++G(d,p) level, a single point electric field gradient calculation was carried out at the B3PW91/6-311+(d,p) level of theory using a calibration factor of eQ/h = 4.599(12) MHz a.u.$^{-1}$ [121]. This combination is a proven method for the prediction of NQCCs in π-conjugated amides in particular and might be also suitable for systems like DMTA. The calculation results in a nuclear quadrupole coupling tensor with the diagonal elements $\chi_{aa} = 0.8070$ MHz, $\chi_{bb} = -3.2397$ MHz, $\chi_{cc} = 2.4327$ MHz, as well as the off-diagonal elements $\chi_{ab} = -2.1512$ MHz, $\chi_{ac} = 0.0117$ MHz, and $\chi_{bc} = 0.0028$ MHz.

13.2.3 Methyl internal rotation

DMTA has a C_s frame symmetry and two inequivalent methyl rotors, which are called the γ and δ methyl group, as illustrated in Figure 13.2. The rotational transitions of such a molecule split into five torsional components $(\sigma_1\sigma_2)$ = (0 0), (0 $\pm$1), ($\pm$1 0), ($\pm$1 $\pm$ 1), and ($\pm$1 $\mp$ 1). [47] Here the torsional states are labeled by the torsional symmetries σ_1 and σ_2 of the γ and δ methyl group, respectively. The notation (00), (01), (10), (11), and (12), respectively, will be used throughout this chapter.

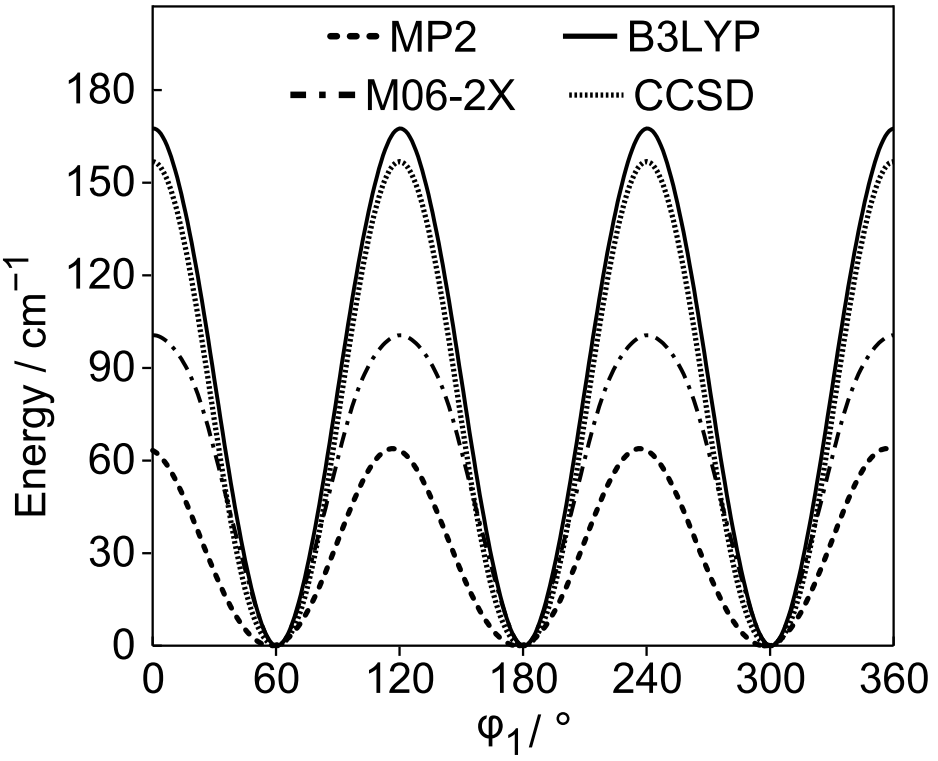

Figure 13.3. The potential energy curve corresponding to a rotation of the γ methyl group calculated using the MP2, B3LYP, M06-2X, and CCSD methods in combination with the 6-311++G(d,p) basis set. The dihedral angle $\varphi_1 = \angle(N_3,C_4,C_7,H_8)$ is varied over a grid of 2°. Energy values relative to the energetically lowest conformation with E_{min} = −646.4816118 (MP2), −647.7803704 (B3LYP), −647.6327793 (M06-2X), and −646.5253342 Hartree (CCSD) are used.

The torsional splittings mainly depend on the orientations of the methyl groups in the molecule and the barriers hindering the internal rotation. While the orientations of the methyl groups can be often well-calculated by geometry optimizations, predicting the barrier heights is a much more difficult task. The predicted values vary in a wide range and depend strongly on the used level of theory. [70, 97] However, the results from quantum chemical calculations often have the correct order of magnitude of the barrier heights, which is sufficient to start the spectral assignment.

For DMTA, the barrier heights of the γ and δ methyl groups were calculated by varying the dihedral angles $\varphi_1 = \angle(N_3,C_4,C_7,H_8)$ and $\varphi_2 = \angle(S_1,C_5,C_{11},H_{12})$, respectively, over a grid of 2° (for atom numbering see Figure 13.2), while all other geometry parameters were optimized with the MP2, B3LYP, M06-2X, and CCSD methods in combination with the 6-311++G(d,p) basis set. A rotation of only 120° was sufficient due to the three-fold symmetry of the methyl groups. The potential energy curves corresponding to the γ methyl group are depicted in Figure 13.3, which all have negligible V_6 contributions. The Fourier coefficients are available in Table 17.66 in the Appendix. The barrier heights are quite different and vary from 60 cm^{-1} to 170 cm^{-1}.

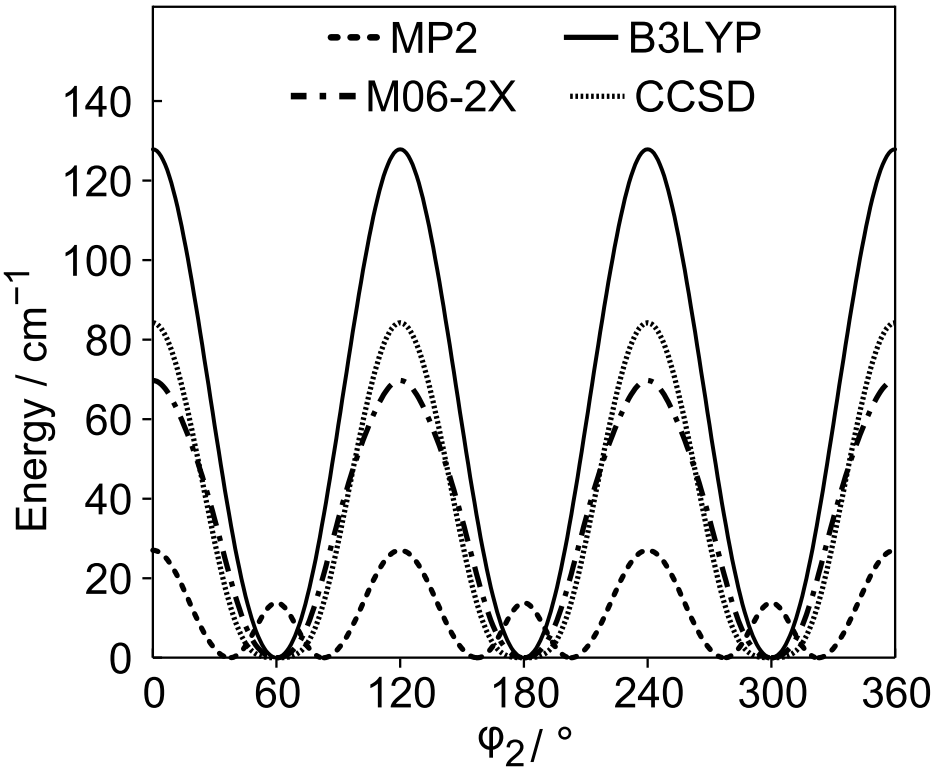

Figure 13.4. The potential energy curve corresponding to a rotation of the δ methyl group calculated using the MP2, B3LYP, M06-2X, and CCSD methods in combination with the 6-311++G(d,p) basis set. The dihedral angle $\varphi_2 = \angle(S_1,C_5,C_{11},H_{12})$ is varied over a grid of 2°. Energy values relative to the energetically lowest conformation with E_{min} = −646.4816118 (MP2), −647.7803704 (B3LYP), −647.6327793 (M06-2X), and −646.5253342 Hartree (CCSD) are used.

In the case of the δ methyl group, the potential energy curves predicted by the B3LYP, M06-2X, and CCSD methods (illustrated in Figure 13.4) indicate normal three-fold potentials with no V_6 contributions. On the other hand, the MP2 method predicts a considerable V_6 contribution of about 52%. The corresponding potential curve shows clearly six minima. The Fourier coefficients are given in Table 17.67 in the Appendix. Also for the δ methyl group, the calculated barrier heights are quite different and vary from 25 cm^{-1} to 130 cm^{-1}.

As an alternative, geometry optimizations to a first order transition state of the methyl groups were performed at various levels of theory using the Berny algorithm [28] to calculate the barrier heights. The rotational constants and angles between the internal rotor axes and the principal axes obtained from geometry optimizations as well as the V_3 potentials from the transition state calculations are collected in Table 17.68.

In addition, two-dimensional potential energy surfaces (2D-PES) depending on φ_1 and φ_2 are calculated at the same levels of theory to study the coupling between the two methyl rotors. The dihedral angles φ_1 and φ_2 were varied over a grid of 10°. The corresponding energies were parameterized with a two-dimensional Fourier expansion based on terms representing the correct symmetry. The Fourier coefficients are listed in Table 17.69 in the Appendix. Using these Fourier coefficients, the PES were drawn as a contour plot depicted in Figure 13.5. All PES (especially that predicted with the MP2 method) indicate significant coupling between the two rotors, as will be revisited in the discussion.

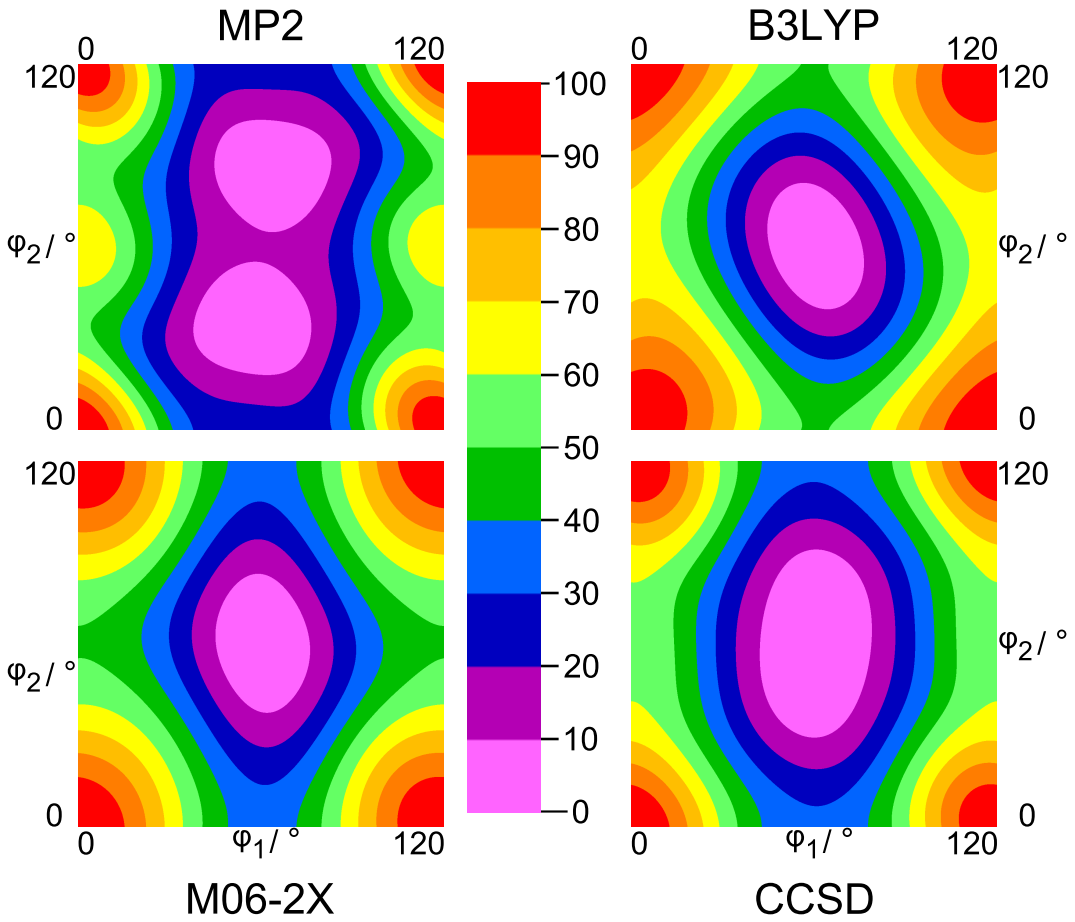

Figure 13.5. The potential energy surface of DMTA calculated with the MP2 (top left), B3LYP (top right), M06-2X (bottom left), and CCSD (bottom right) method and the basis set 6-311++G(d,p) and obtained by rotating the γ and δ methyl groups in a step width of 10° around the dihedral angles $\varphi_1 = \angle(N_3,C_4,C_7,H_8)$ and $\varphi_2 = \angle(S_1,C_5,C_{11},H_{12})$.

13.3 Microwave spectrum

13.3.1 Experimental setup

The sample of DMTA was purchased from TCI Deutschland GmbH, Eschborn, Germany with a stated purity of over 97% and used without further purification. The rotational spectra were measured using a COBRA-type pulsed molecular beam Fourier transform microwave spectrometer covering the frequency range from 2 to 26.5 GHz described in Refs. [22, 23]. The sample was placed on a piece of pipe cleaner as carrier material, which was subsequently inserted in a stainless steel tube close to the nozzle. Helium at a pressure of approximately 200 kPa was flowed over the sample and the resulting mixture was expanded into the Fabry-Pérot cavity. After Fourier transformation, each rotational transition splits by the Doppler effect due to the molecular beam expansion in the coaxial arrangement of the supersonic jet and resonator axes. The rest frequency is calculated as the arithmetic mean of the frequencies of the Doppler components. The line widths are approximately $15 - 30$ kHz; the estimated measurement accuracy is better than 2.2 kHz.

13.3.2 Spectral analysis

The dipole moment components predicted at the MP2/6-311++G(d,p) level of theory are -0.02 D, 1.81 D, and 0.03 D in *a*-, *b*-, and *c*-direction, respectively. Because of the negligible components in *a*- and *c*-direction, a pure *b*-type spectrum was expected for DMTA.

Preliminary calculations of the spectrum using a rigid-rotor Hamiltonian were based on the rotationtal constants calculated at the MP2/6-311++G(d,p) level of theory (see Table 17.68). A broadband scan in the frequency range 9.0 – 13.25 GHz was automatically recorded by overlapping spectra in a step size of 0.25 MHz. It reveals a very dense spectrum, which makes the assignment quite challenging. First, the *b*-type $(J+1)_{0,(J+1)} \leftarrow J_{1,J}$, $(J+1)_{1,(J+1)} \leftarrow J_{0,J}$, and $(J+1)_{1,J} \leftarrow J_{2,(J-1)}$ lines with J ranging from 2 to 4 were searched. The (00) torsional state of these transitions could be identified by trial and error, which allowed to predict further (00) lines quite well.

Each rotational line shows a hyperfine structure, as can be seen in Figure 13.6, due to the quadrupole coupling of the ^{14}N nucleus. As a next step, this effect was taken into account. Using the NQCCs calculated in Section 13.2.2, the hyperfine structure of the (00) torsional state were readily assigned. A fit using the rigid-rotor model with centrifugal distortion correction and first order approximation for the quadrupole coupling yielded molecular parameters with sufficient accuracy.

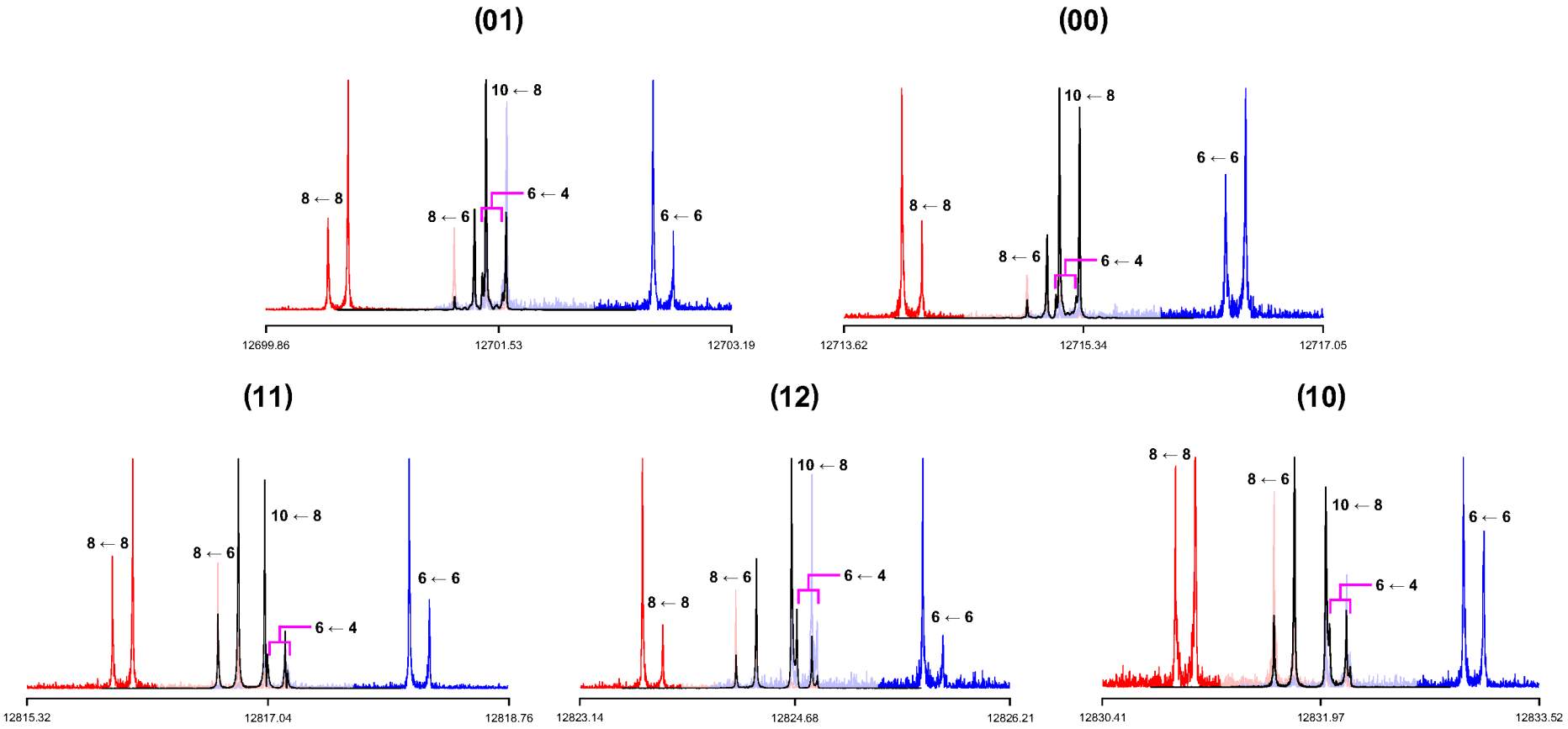

Figure 13.6. Typical high resolution spectra of the $4_{14} \leftarrow 3_{03}$ transition of DMTA. Each torsional species splits into five quadrupole components; the quadrupole components are given by $F' \leftarrow F$. Three spectra were recorded for each torsional species and can be distinguished by different colors. For each spectrum, 50 decays were co-added.

After excluding all (00) lines, an amount of approximately four times the assigned lines remain in the broadband scan. They belong to the other torsional species arising from the internal rotations of the two methyl groups. The program XIAM [45] was used to predict the torsional splittings. The initial values of the angles between the internal rotor axes and the principal axes of inertia as well as the hindering potentials were taken from *ab initio* calculation at the MP2/6-311++G(d,p) level of theory; those of the rotational constants, centrifugal distorsion constants, and NQCCs from the rigid-rotor fit. The (01) and (10) species were assigned by trial and error, and a satisfactory fit including the (00), (01), and (10) torsional species with their hyperfine components was obtained, but it was not possible to assign any (11) and (12) transitions with this fit.

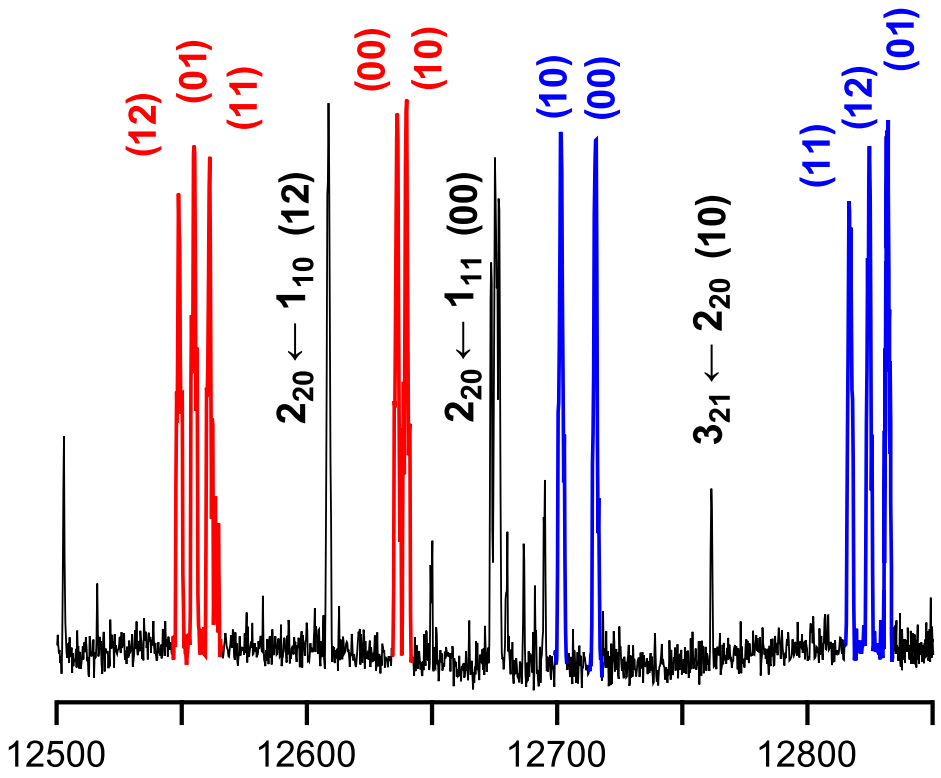

Figure 13.7. A portion of the spectrum of DMTA showing the five torsional components (00), (10), (01), (11), and (12) of the $4_{04} \leftarrow 3_{13}$ (in red) and $4_{14} \leftarrow 3_{03}$ (in blue) rotational transitions. Other lines (in black) are marked with their torsional species and rigid rotor quantum numbers J, K_a, K_c. The lines are broadened or split because of the quadrupole coupling arising from the ^{14}N nucleus.

As can be seen as an example in Figure 13.7, where a portion of the broadband spectrum with the $4_{04} \leftarrow 3_{13}$ and $4_{14} \leftarrow 3_{03}$ rotational transitions is illustrated, the splittings of the (01), (11), and (12) torsional species are rather small for some transitions, resulting in a triplet pattern. For those transitions, the (00) and (10) transitions are also close and they often appear in the spectrum as doublets. This gave an opportunity to start the identification of the (11) and (12) lines, where transitions with doublet structure of (00) and (10) were searched, the corresponding (01) line was found, and the neighboring lines in the triplets as (11) and (12) were identified.

The first attempts to fit all five torsional species in a global fit did not yield satisfactory results, and it was not possible to assign any further (11) and (12) species in this fit. In the course of fitting, the (01) had to be excluded, and only the (00) and (10) species together with the (11) or (12) species were used in two separated fits to determine the δ methyl group and to assign this torsional species.

It was possible to extend considerably the assignment of the (11) and (12) torsional species with these fits. The hyperfine structure analysis was also straightforward for these species. All five torsional species were subsequently fitted in a global fit. After many trials, the standard deviations were still close to 1 MHz. This pointed out that a parameter for the coupling between the two methyl groups is required. Fitting the top-top coupling parameter V_{cc}, which includes the cosinus terms of the two tops, reduces this deviation to 25 kHz.

13.4 Discussion

A total of 40 rotational transitions with 113 torsional and 415 hyperfine components were fitted to a standard deviation of 24.4 kHz using the program XIAM. The rotational constants, centrifugal distortion constants, and nuclear quadrupole coupling constants were obtained with high accuracy. The analysis of the nitrogen hyperfine patterns is based on the first order Hamiltonian

$$H_{NQ} = 2\frac{Y(I,J,F)}{J(J+1)}\left[\chi_{aa}\langle P_a^2\rangle + \chi_{bb}\langle P_b^2\rangle - (\chi_{aa}+\chi_{bb})\langle P_c^2\rangle + \chi_{ab}\langle P_aP_b + P_bP_a\rangle\right],$$

where brackets $\langle\rangle$ denote the expectation values of various combinations of angular momentum components and $Y(I,J,F)$ is the Casimir function [34]. In rigid rotors, the expectation value $\langle P_aP_b + P_bP_a\rangle$ vanishes and the determination of χ_{ab} is not possible within the first order approximation. In the case of DMTA, because of the methyl internal rotations, the Coriolis terms are non-zero and the determination of χ_{ab} becomes feasible.

The experimentally deduced rotational constants agree within 2% with those predicted at different levels of theory (see Table 17.68). The V_3 hindering potentials, angles between the internal rotation axes and the a-principal axis, the higher order parameters D_{pi2K}, D_{pi2J} and D_{pi2-}, and the top-top coupling term V_{cc} were fitted as internal rotation parameters. The V_3 hindering potentials of the γ and the δ methyl group are: 122.193(17) cm^{-1} and 63.2554(60) cm^{-1}, respectively; the V_{cc} term is $-4.7472(33)$ cm^{-1}.

Table 13.1. Molecular parameters of the only conformer of DMTA observed under molecular beam conditions obtained by the program XIAM. The γ methyl group is numbered with $n = 1$ and the δ methyl group with $n = 2$.

Par.[a]	Unit	Fit I	Fit II	Fit III	Fit IV	Calc.[b]
A	GHz	3.200 630 11(56)	3.188 267(20)	3.187 844(36)	3.187 118 3(31)	3.162
B	GHz	2.473 312 66(35)	2.457 105(26)	2.459 137 20(37)	2.457 491 2(22)	2.432
C	GHz	1.411 671 172(77)	1.411 633 25(25)	1.411 629 84(20)	1.411 631 90(49)	1.399
D_J	kHz	0.2907(80)	−0.0325(51)	0.0190(74)	0.125(33)	0.122
D_{JK}	kHz	1.390(28)	1.621(56)	1.464(27)	0.91(13)	0.416
D_K	kHz	0.410(23)	−0.622(83)	−0.802(27)	−0.66(15)	−0.105
d_1	kHz	−0.2263(46)		−0.0387(44)	−0.075(21)	−0.044
d_2	kHz	−0.097 23(99)	−0.0313(23)	−0.0457(11)	−0.0410(69)	0.003
$V_{3,1}$	cm^{-1}			122.58(44)	122.193(17)	64.3
$F_{0,1}$	GHz			155.67(55)	154.592(24)	159.8
$\angle(i_1,a)$	°			173.9065(38)	175.088 30(70)	176.11
$\angle(i_1,b)$	°			96.0935(38)	94.911 70(70)	93.89
$\angle(i_1,c)$	°			90.00[c]	90.00[c]	89.84
$D_{pi2J,1}$	kHz			55.52(72)	45.85(95)	
$D_{pi2K,1}$	kHz			−187(66)		
$D_{pi2-,1}$	kHz			101.8(78)	90.7(11)	
$V_{3,2}$	cm^{-1}		61.33(11)		63.2554(60)	27.2
$F_{0,2}$	GHz		159.75(25)		163.624(16)	160.4
$\angle(i_2,a)$	°		108.976 30(50)		108.955 80(10)	108.47
$\angle(i_2,b)$	°		18.976 30(50)		18.955 80(10)	18.49
$\angle(i_2,c)$	°		90.00[c]		90.00[c]	89.34
$D_{pi2J,2}$	kHz		81(11)		−70.67(21)	
$D_{pi2K,2}$	kHz		−637.2(61)		−539.1(12)	
$D_{pi2-,2}$	kHz		154(10)			
F_{12}	GHz				−0.6097(27)	0.88
V_{cc}	cm^{-1}				−4.7472(33)	5.5
χ_{aa}	MHz	0.6213(21)	0.5692(81)	0.6630(23)	0.586(13)	0.807
χ_{-}	MHz	−5.7494(24)	−5.699 54(93)	−5.7918(26)	−5.712(16)	−5.672
χ_{ab}	MHz		−2.188(23)	−2.166(93)	−2.231(27)	−2.151
σ^d	kHz	2.2	10.3	2.4	24.4	
N[e]		108	200	182	415	

[a] All parameters refer to the principal axis system. Watson's S reduction in I^r representation was used. [b] Ground state rotational constants and centrifugal distortion constants obtained by anharmonic frequency calculations at the MP2/6-311++G(d,p) level of theory. [c] Fixed due to symmetry. [d] Standard deviation of the fit. [e] Number of lines.

The results of the fits are given in Table 13.1 and the observed transitions and frequencies are listed in Table 17.70. The standard deviation of the global fit IV is 24.4 kHz which is still 12 times the estimated measurement accuracy (2 kHz), but is surprisingly good if considering the relatively low hindering potentials of both methyl groups and the possible strong coupling between them. Larger deviations have been found in many one-top problems with higher barriers treated by the program XIAM, i.a. ethyl acetate (101.606(23) cm^{-1}, 85.3 kHz) [106], allyl acetate (98.093(12) cm^{-1}, 54.0 kHz) [107], and vinyl acetate (151.492(34) cm^{-1}, 92.3 kHz) [84]. If top-top coupling is possible, as in the case of pinacolone, the standard deviation determined by XIAM is even worse (121.532(57) cm^{-1}, 1155.8 kHz) [122]. XIAM appears to work better in this case. Attempts to reduce the deviation in the fit of DMTA by fitting other parameters available in the program XIAM failed. In Table 13.1, the reasons for the high standard deviation can be pinned (1) to the δ methyl group with the lower barrier and (2) to the coupling. Here, the rigid rotor fit I as well as the one-top fit III can determine the rotational constants, the quartic centrifugal distortion constants, the quadrupole coupling, and the γ methyl group to an excellent standard deviation of 2.2 kHz and 2.4 kHz, respectively. However, the one-top fit II has a higher standard deviation of 10.3 kHz due to the small barrier height and the orientation of the δ methyl group. XIAM should work well for small barriers as well when the internal rotor is orientated along one principal axis as shown for 1,2,5-trimethylpyrrole in Chapter 14. Finally, the two top fit IV has a standard deviation of 24.4 kHz due to the high coupling between both methyl groups manifested in the (11) and (12) torsional species. The deviation is much larger than the measurement accuracy. A reason could be due to the limited amount of available potential top-top interaction parameters. An indicator is the fitted kinetic coupling constant F_{12}, which usually is already determined by the direction cousines, the moments of inertia of the internal rotors, and the moments of inertia of the entire molecule as given in Section 3.2 Equation 3.12. Here, the standard deviation increases over 110 kHz without fitting F_{12}. It is notable that the γ methyl group points almost along the *a*-principal axis with an angle of only 4.91170(70)°. Therefore, other top-top coupling parameters including the sinus terms such as V_{ss} cannot be fitted.

Using the experimentally deduced V_3 potentials and the potential cross term V_{cc}, a 2D-PES was drawn using the equation

$$\begin{aligned} V(\varphi_1,\varphi_2) =& 63.2554\ cm^{-1}\cdot\frac{1}{2}[1-cos(3\varphi_1)] + 122.193\ cm^{-1}\cdot\frac{1}{2}[1-cos(3\varphi_2)] \\ & - 4.7472\ cm^{-1}\cdot cos(3\varphi_1)\cdot cos(3\varphi_2) \end{aligned}$$

as depicted in Figure 13.8. Here, also the influence of the parameter V_{cc} is shown. Negative values increase the barriers of the lowest energy path for each methyl group. Vice versa, the barriers decrease when V_{cc} increases. The experimentally deduced PES is most similar to that predicted at the B3LYP/6-311++G(d,p) level illustrated in Figure 13.5.

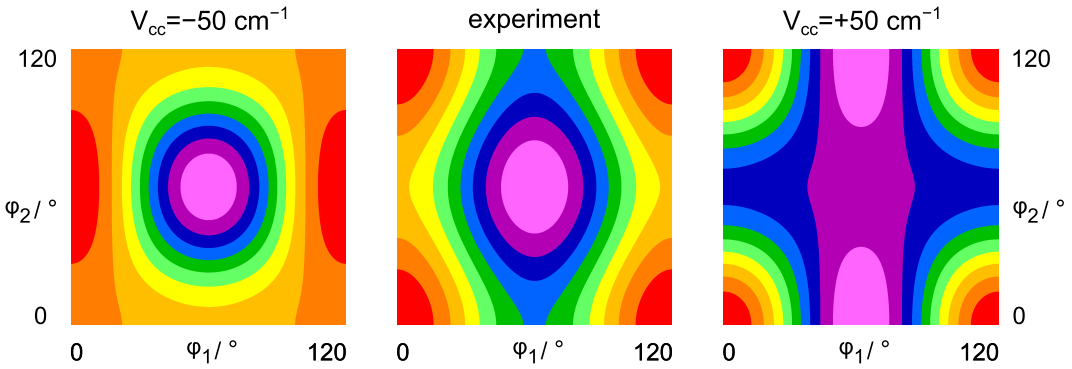

Figure 13.8. Potential energy surface based on the experimental values of the barrier heights of the methyl groups and the coupling term V_{cc} in the center. The influences of a negative and a positive coupling term V_{cc} on the potential energy surface are given on the left and the right hand side, respectively. The energy ranges are 187.8 cm^{-1} for the experimental PES (center) and 223.9 cm^{-1} for the PES on the left and right hand side.

One the other hand, the calculated barrier heights are a big challenge for quantum chemistry since the coupling of the methyl groups is hard to compute. Even in the range of the chemical accuracy in theoretical calculations, the variations of the barrier heights at different levels of theory are large: The barrier height of the γ methyl group is between $16-272$ cm^{-1} (experimental: 122.193(17) cm^{-1}) and of the δ methyl group is between $24-174$ cm^{-1} (experimental: 63.2554(60) cm^{-1}). Some levels of theory even switch the high and low barrier methyl groups. The V_3 potentials of 122.2 cm^{-1} and 63.3 cm^{-1} of the γ and the δ methyl group, respectively, are considerably different to the values of 357.6 cm^{-1} of 4-methylthiazole [117] and 332.0 cm^{-1} of 5-methylthiazole [118].

13.5 Conclusion

The rotational spectra of 4,5-dimethylthiazole with five torsional species and additional quadrupole hyperfine splittings were successfully assigned under molecular beam conditions using a combination of FT microwave spectroscopy and quantum chemistry. In total, 25 components of each rotational transition were identified and highly accurate molecular parameters were determined. In contrast to the monomethyl derivatives (357.6 cm^{-1} in 4-methylthiazole (**1**) [117] and 332.0 cm^{-1} in 5-methylthiazole (**2**) [118]), the barrier heights of 4,5-dimethylthiazole decrease drastically just due to the coupling between the two methyl groups (122.193(17) cm^{-1} for the γ methyl group and 63.2554(60) cm^{-1} for the δ methyl group).

CHAPTER 14

1,2,5-Trimethylpyrrole

Three rotors (two inequivalent rotors), ^{14}N quadrupole coupling, and C_s frame symmetry

14.1 Introduction

From the spectroscopic perspective, the molecule 1,2,5-trimethylpyrrole (**1**) is fascinating due to three methyl tops – one methyl group with a very low barrier and two equivalent methyl groups with high torsional barriers – as well as additional hyperfine splittings due to quadrupole coupling. Since the coupling of the two methyl groups in 4,5-dimethylthiazole (see previous chapter) leads to surprisingly small torsional barriers, this effect will be investigated in 1,2,5-trimethylpyrrole (TMP). Here, a coupling of three methyl groups is expected. This molecule is also used to check the capability of the assignment program XIAM to treat complex internal dynamics. TMP is an intermediate stage in the assignment of 2,3,4,5-tetramethylthiophene with four internal rotors in the next chapter.

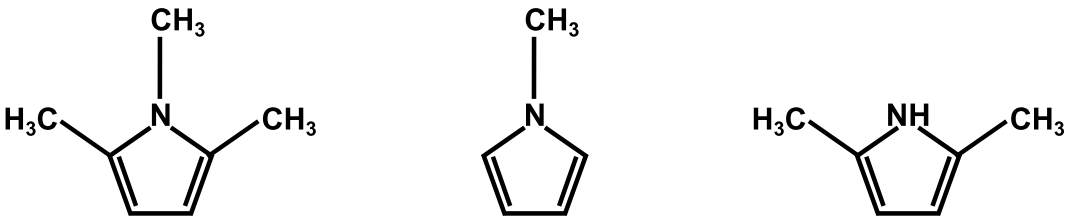

(1) **(2)** 45.0 cm^{-1} **(3)** 291.9 cm^{-1}

Figure 14.1. 1,2,5-trimethylpyrrole (**1**) and the torsional barriers of the related molecules N-methylpyrrole (**2**) [72] and 2,5-dimethylpyrrole (**3**) (calculated at the MP2/6-311++G(d,p) level).

When simple chemical intuition is applied and TMP is compared to related molecules, similar torsional barriers like in the molecules N-methylpyrrole (**2**) [72] and 2,5-dimethylpyrrole (**3**) might be expected. The molecules are shown in Figure 14.1. The microwave spectroscopic investigation of the molecule N-methylpyrrole (**2**) [72] can serve as a starting point for the barrier height of the N-methyl group in TMP. On the other hand, no experimental torsional barrier of the two equivalent methyl groups is available. Therefore, the calculated torsional barrier of 2,5-dimethylpyrrole (**3**) at the MP2/6-311++G(d,p) level can be used since quantum chemistry yields reasonable barriers for the related molecules 2,5-dimethylthiophene (see Chapter 10) and 2,5-dimethylfuran (see Chapter 11). However, at the end of this

chapter, this molecule will show that this simple chemical intuition can not be applied here.

14.2 Quantum chemical calculations

TMP has a planar pyrrole frame because of two conjugated double bonds. Using the GAUSSIAN09 package [26], full geometry optimizations and harmonic frequency calculations were performed at different levels of theory using the HF, B3LYP, M06-2X, MP2, and CCSD methods in combination with various Pople and Dunning basis sets [90–96]. The optimized conformer is shown in Figure 14.2 in its principal axes of inertia. The nuclear Cartesian coordinates of the fully optimized geometry at the MP2/6-311++G(d,p) level of theory are available in Table 17.71. The rotational constants, the angles between the internal rotor axes and the principal axes as well as the V_3 potentials for the two different types of methyl tops calculated at different levels of theory are summarized in Table 17.72.

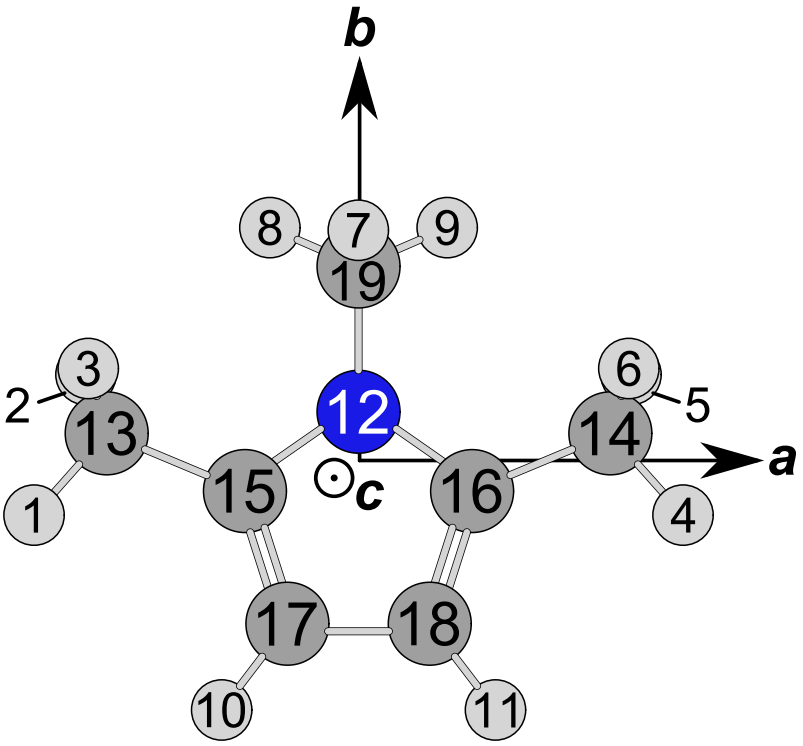

Figure 14.2. The stable conformer of TMP calculated at the MP2/6-311++G(d,p) level of theory given in its principal axes of inertia. The direction of the *c*-axis out of the paper plane is indicated by a circle.

The methyl tops lead to splittings of all rotational transitions. These splittings depend on the barrier heights. Theoretical torsional barriers of the N-methyl top were calculated by rotating the methyl group about the N_{12}-C_{19}-bond (for atom numbers see Figure 14.2). The potential energy curves were obtained by varying the dihedral angle $\varphi_1 = \angle(C_{15},N_{12},C_{19},H_7)$ in a step width of 2° while all other geometry parameters were optimized. A rotation of only 60° was sufficient due to the C_3 symmetry of the methyl group and the C_s symmetry of the frame. The potential energy curves are shown in Figure 14.3. A clear V_6 character is observable, which is also indicated through the Fourier coefficients in Table 17.73. The

calculated barrier heights vary between 20 cm^{-1} and 90 cm^{-1}. Additionally, geometry optimizations to a first order transition state of the N-methyl group were performed to calculate the torsional barriers more precisely using the Berny algorithm [28].

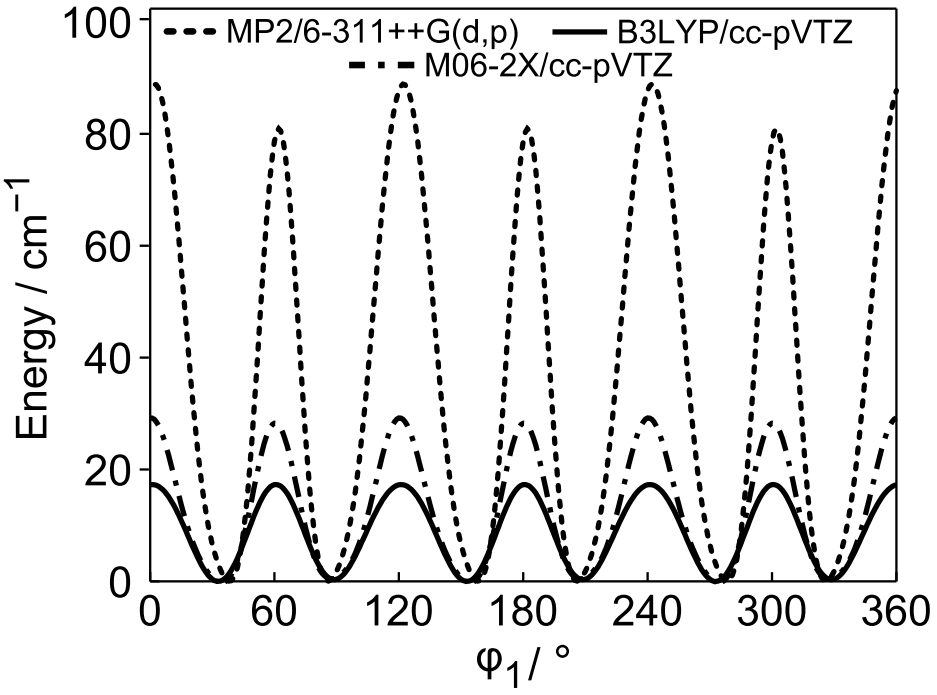

Figure 14.3. The potential energy curves obtained by rotating the N-methyl group about the N_{12}-C_{19} bond (for atom number see Figure 14.2). The dihedral angle $\varphi_1 = \angle(C_{15},N_{12},C_{19},H_7)$ was varied in a step width of 2° at the MP2/6-311++G(d,p) level and with the B3LYP and M06-2X methods and the basis set cc-pVTZ. Relative energies with respect to the stable conformations with their absolute energies $E = -327.1936361$ (MP2), -328.2352476 (B3LYP), and -328.0813684 Hartree (M06-2X) are given.

To calculate the barrier heights of the two equivalent methyl tops, geometry optimizations to a first order transition state of one of these methyl groups were performed at various levels of theory using the Berny algorithm [28].

Finally, two different 2D potential energy surfaces (PESs) were calculated at the MP2/6-311++G(d,p) level of theory to study the coupling between the methyl internal rotors by varying the dihedral angles φ_1 and $\varphi_2 = \angle(N_{12},C_{16},C_{14},H_4)$ or φ_2 and $\varphi_3 = \angle(N_{12},C_{15},C_{13},H_1)$ in a step width of 10°. The corresponding energies were parameterized with a two-dimensional Fourier expansion based on terms representing the correct symmetry of the angles φ_1, φ_2, and φ_3. The Fourier coefficients are listed in Table 17.74 and 17.75. No significant coupling between the different tops could be observed, as shown in Figure 14.4 and 14.5.

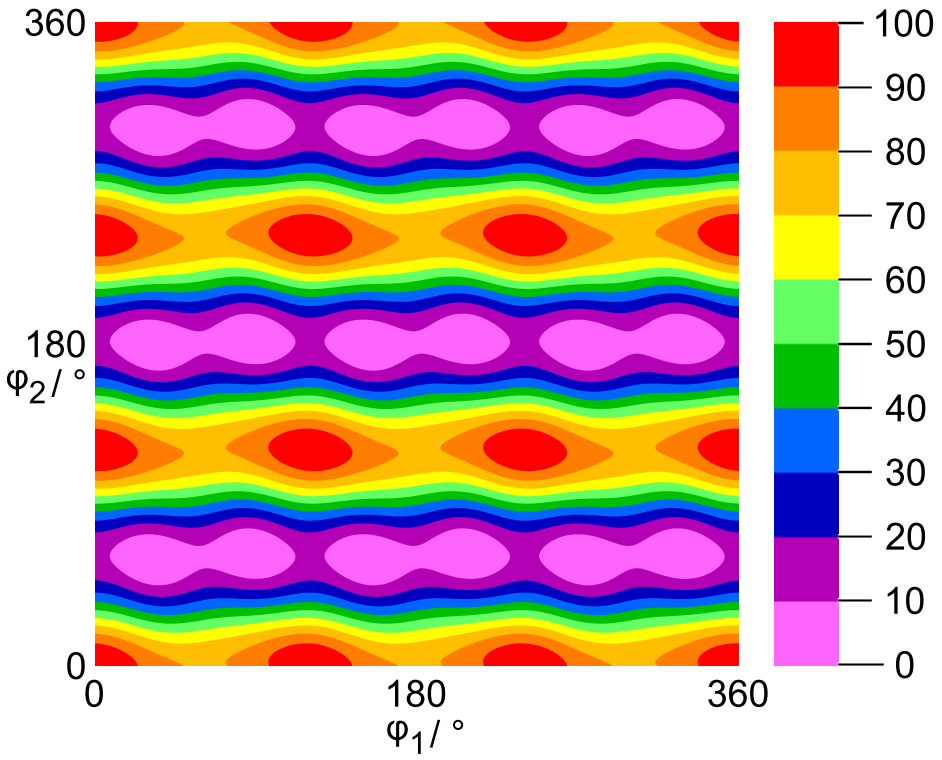

Figure 14.4. The potential energy surface of TMP calculated at the MP2/6–311++G(d,p) level of theory obtained by rotating the nitrogen and one carbon methyl group in a step width of 10° about the dihedral angles $\varphi_1 = \angle(C_{15},N_{12},C_{19},H_7)$ and $\varphi_2 = \angle(N_{12},C_{16},C_{14},H_4)$. Relative energies with respect to the stable conformer with its absolute energy $E = -327.1936361$ Hartree are given. The energy range is 10.08 kJ·mol^{-1}.

For the prediction of the quadrupole hyperfine structure, a single point electric field gradient calculation at the B3PW91/6-311+(d,p) level of theory was carried out using a calibration factor of $eQ/h = 4.599(12)$ MHz a.u.$^{-1}$ [121]. For this purpose, the structure optimized at the MP2/6-311++G(d,p) level was used. This combination works well for the prediction of nuclear quadrupole coupling constants (NQCCs) in π-conjugated amides and 4,5-dimethylthiazole (see Chapter 13). The calculation results in the nuclear quadrupole coupling tensor with the diagonal elements χ_{aa} = 1.2000 MHz, χ_{bb} = 2.0723 MHz, χ_{cc} = −3.2723 MHz, as well as the off-diagonal elements χ_{ab} = −0.0003 MHz, χ_{ac} = −0.0008 MHz, and χ_{bc} = 0.2854 MHz.

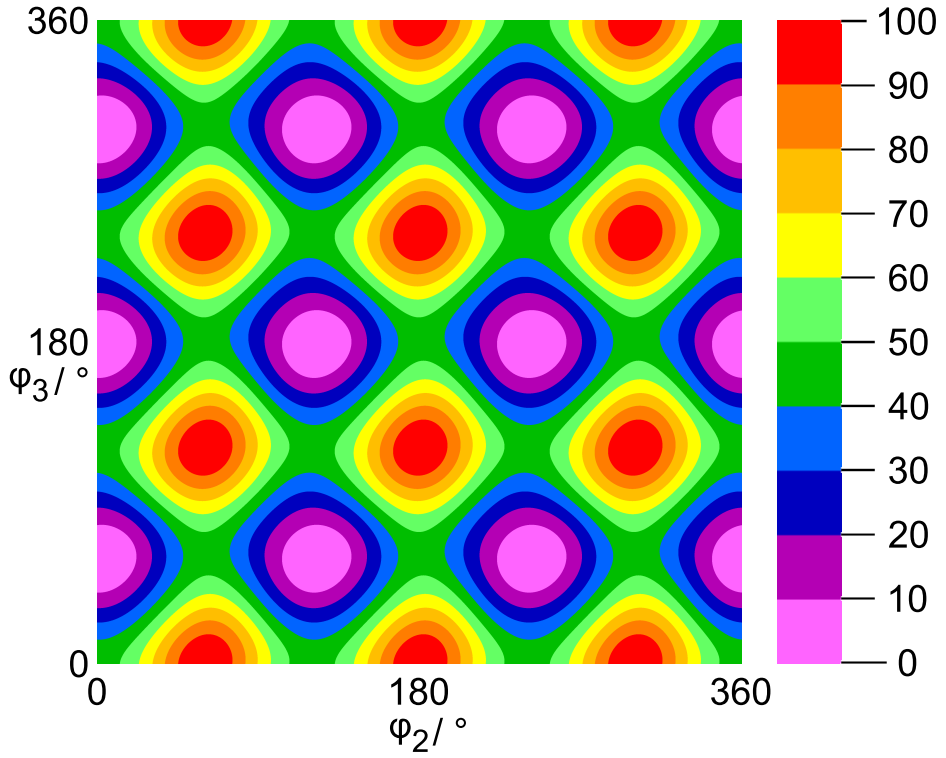

Figure 14.5. The potential energy surface of TMP calculated at the MP2/6–311++G(d,p) level of theory obtained by rotating both carbon methyl groups in a step width of 10° about the dihedral angles $\varphi_2 = \angle(N_{12},C_{16},C_{14},H_4)$ and $\varphi_3 = \angle(N_{12},C_{15},C_{13},H_1)$. Relative energies with respect to the stable conformer with its absolute energy $E = -327.1936361$ Hartree are given. The energy range is 17.31 kJ·mol^{-1}.

14.3 Microwave spectroscopy

The quantum chemical calculations at the MP2/6-311++G(d,p) level have suggested that TMP possesses a dipole moment only in *b*-direction (dipole moment components of 0.00 D, 2.33 D, and 0.04 D in *a*-, *b*-, and *c*-direction).

In the first step, a broadband scan in the frequency range from 8.8 to 14.1 GHz was recorded based on a prediction of a *b*-type rigid-rotor spectrum with the program XIAM [45] using the rotational constants calculated at the MP2/6-311++G(d,p) level. Here, overlapping spectra in a step width of 0.25 MHz were automatically recorded.

As shown in Figure 14.6, torsional splittings of each rotational transition into 10 components were expected. The notation σ_1 of the torsional component ($\sigma_1\sigma_2\sigma_3$) refers to the N-methyl group, while σ_2 and σ_3 refer to the two equivalent methyl groups. The first approach to study TMP was to treat such a molecule as a rigid rotor. Here, the *b*-type transitions $3_{13} \leftarrow 2_{02}$ and $4_{14} \leftarrow 3_{03}$ as well as $5_{14} \leftarrow 5_{05}$ were chosen for the assignment.

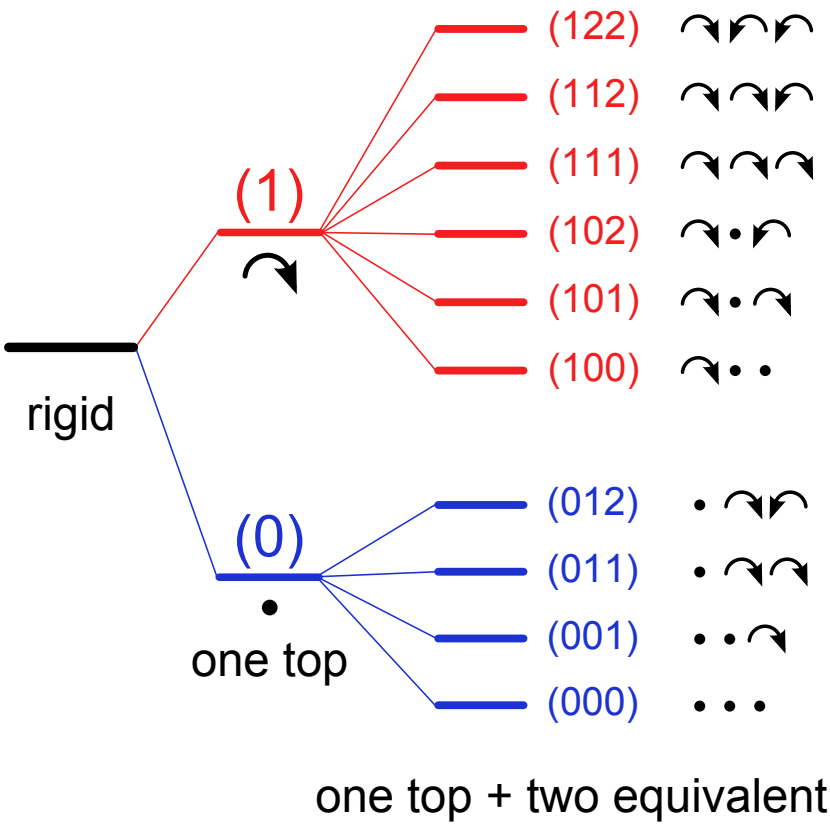

Figure 14.6. Schematic energy level diagram to illustrate the splittings due to the internal rotations in TMP. Left-hand side: splittings into a (0) and a (1) torsional species due to the internal rotation of one methyl top; right-hand side: splittings into 10 torsional species due to the internal rotations of three tops including two equivalent methyl groups.

In the next step, the hyperfine splittings due to the ^{14}N nucleus and the torsional components of the two equivalent methyl rotors with high barriers were considered. Only few additional torsional splittings due to the high barrier of the two equivalent methyl groups were observed. This indicates a very high barrier for these two methyl groups.

To treat the low barrier of the N-methyl group, its splittings were predicted for different barrier heights in a range of 0 to 200 cm^{-1} as shown in Figure 14.7. Here, the importance of good starting values for the assignment of low barrier heights is illustrated. In general, the torsional splittings increase when the barrier decreases. A calculated deviation of 50 cm^{-1} is reasonable for barriers higher than 150 cm^{-1} since the prediction does not change significantly. On the other hand, the same deviation leads to frequency shifts up to several GHz for a barrier below 50 cm^{-1}. These shifts are sometimes larger than the complete range of the broadband scan.

Unfortunately, the calculated barrier height of 92 cm^{-1} at the MP2/6-311++G(d,p) level, which is commonly used in the microwave spectroscopic community, has a deviation of about 90% compared to the experimental value. However, the barrier was successfully assigned due to the hint of the inertia defect,

which indicates one very small and two high torsional barriers. In the (100) species, additional splittings smaller than the hyperfine structure were identified as torsional splittings of the two equivalent methyl groups with a high barrier. In total, three kinds of splittings were observed as shown in Figure 14.8: (i) the splittings due to the N-methyl group in the range of several GHz due to a very small torsional barrier below 10 cm^{-1}; (ii) the hyperfine splittings due to the quadrupole coupling of the ^{14}N nucleus in the range of a few MHz; and (iii) the very small splittings due to the equivalent methyl groups in the range of a few kHz. An example of these splittings is shown in Figure 14.9.

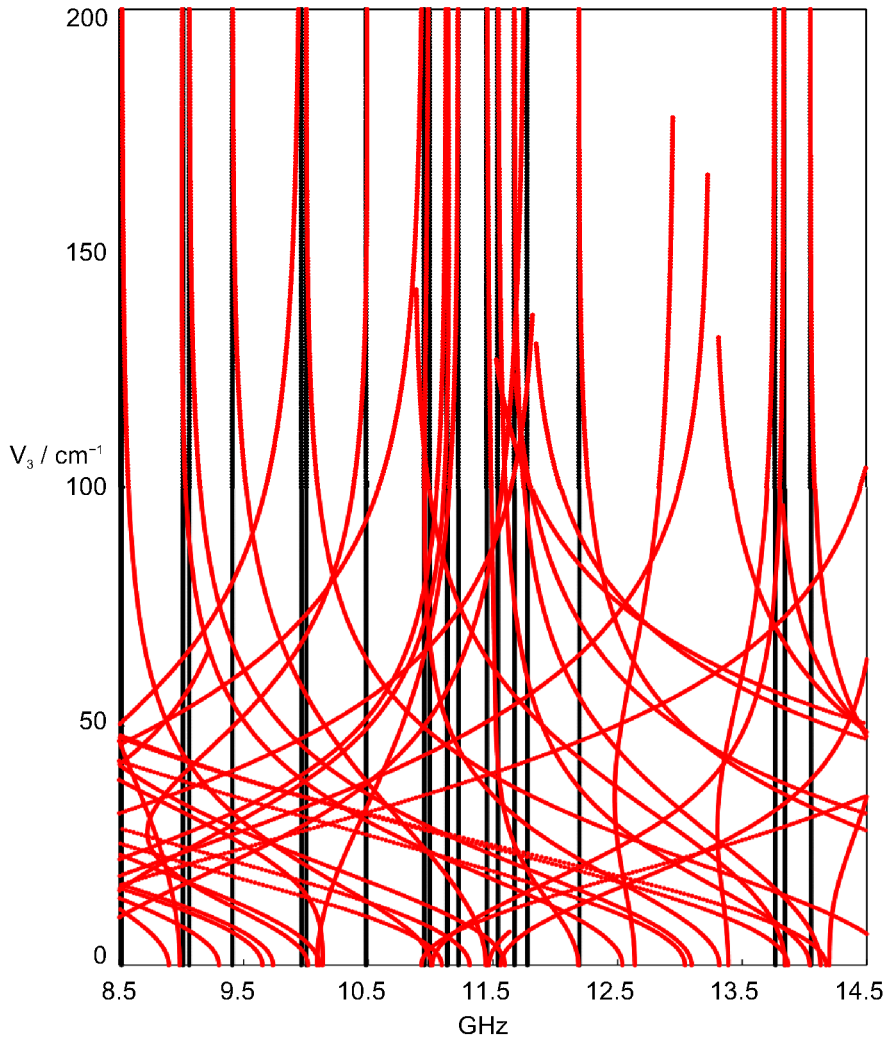

Figure 14.7. Predicted rotational spectrum of TMP as a theoretical one top molecule depending on the barrier height of the N-methyl group. The black lines indicates the (000) species and the red lines the (100) species.

In the last step, further transitions up to $J = 7$ were predicted in the complete frequency range of the spectrometer and measured to increase the data set and to obtain molecular parameters with higher accuracy.

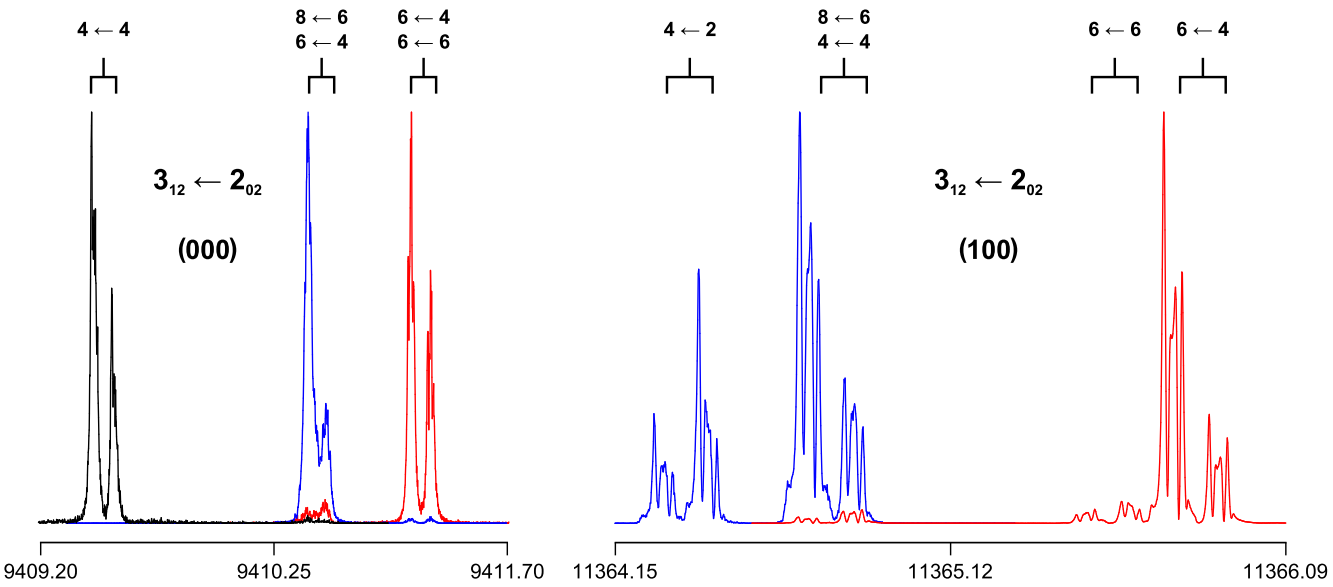

Figure 14.8. Typical spectra of the torsional species (000) and (100) of the $3_{12} \leftarrow 2_{02}$ transition of TMP. The experimental resolution is 1.9 and 3.5 kHz for the (1XX) and (000) species, respectively, the typical line width is approximately 7 – 55 kHz (FWHH). The splitting indicated by brackets is due to the Doppler effect. Additional splittings of the torsional species (100) are due to the internal rotation of the two equivalent methyl groups. For this spectrum 1436 – 4000 decays were co-added.

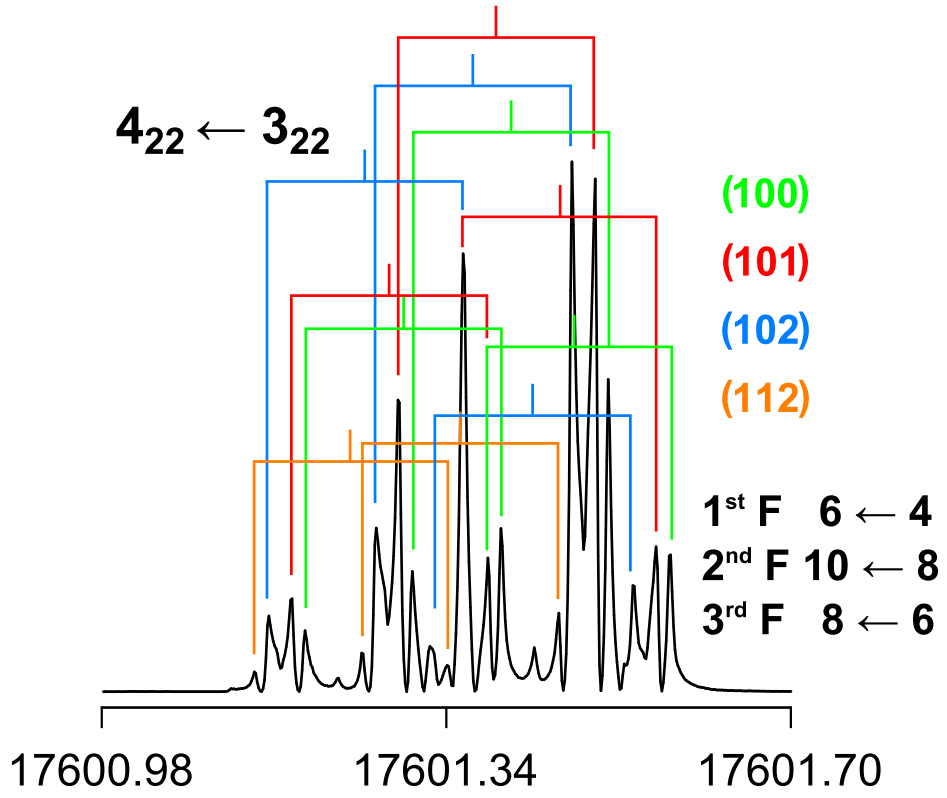

Figure 14.9. Additional splittings in the torsional species (100) of the $4_{22} \leftarrow 3_{22}$ transition of TMP due to the two equivalent methyl groups. The splitting indicated by brackets is due to the Doppler effect. Each color represents a torsional species with the quadrupole components $F' \leftarrow F$: $6 \leftarrow 4$, $10 \leftarrow 8$, and $8 \leftarrow 6$ in ascending frequency order.

Table 14.1. Molecular parameters of TMP under molecular beam conditions obtained by the program XIAM. Top 1 refers to the N-methyl group, top 2 to one of the two equivalent carbon methyl groups.

Par.[a]	Unit	Fit I	Fit II
A	GHz	3.317 736 05(87)	3.317 746 7(14)
B	GHz	1.982 579 71(32)	1.982 556 66(67)
C	GHz	1.271 192 50(18)	1.271 193 83(30)
D_J	kHz	0.0178(24)	−0.7866(57)
D_{JK}	kHz	0.590(21)	2.018(31)
D_K	kHz	−0.879(57)	−1.131(74)
d_1	kHz		0.5474(32)
d_2	kHz		0.1234(17)
$V_{3,1}$	cm^{-1}		8.826 20(10)
$I_{\alpha,1}$	$uÅ^2$		3.188[b]
$\angle(i_1,a)$	°		90.00[c]
$\angle(i_1,b)$	°		0.00[c]
$\angle(i_1,c)$	°		90.00[c]
$D_{pi2J,1}$	MHz		1.117 66(22)
$D_{pi2K,1}$	MHz		−1.106 75(60)
$D_{pi2-,1}$	MHz		1.120 78(20)
$V_{3,2}$	cm^{-1}		693.14(74)
$I_{\alpha,2}$	$uÅ^2$		3.188[b]
$\angle(i_2,a)$	°		16.63(29)
$\angle(i_2,b)$	°		73.37(29)
$\angle(i_2,c)$	°		90.00[c]
χ_{aa}	MHz	1.1839(33)	1.1844(44)
χ_{-}	MHz	5.2549(46)	5.2581(54)
σ[d]	kHz	4.6	10.9
N[e]		76	355

[a] All parameters are given with one standard uncertainty in parentheses. Watson's S reduction in I^r representation was used. [b] Fixed. [c] Fixed due to symmetry. [d] Standard deviation of the fit. [e] Number of lines.

14.4 Results of the fits and discussion

Using the program XIAM, 355 components were fitted in Fit II to a standard deviation of 11 kHz (see Table 14.1). The frequencies of the different components are given in Table 17.76. The standard deviation is much larger than the experimental resolution of the spectrometer. Possible reasons are the very small barrier height of the N-methyl group and the complex structure of the spectra, especially for the (1XX) species. Fit I treats only the (000) torsional species. Here, a standard deviation of 4.6 kHz was achieved. This value is reasonable since these rotational transitions have broad lines because the splittings into the torsional species (000), (001), (011), and (012) components were only observable for a few transitions.

The (000) torsional species has an experimental resolution of 3.5 kHz while the one of the (1XX) species is 1.9 kHz.

The calculated barriers to internal rotation of the N-methyl group are between 8 – 95 cm^{-1}. In the case of the two equivalent methyl groups, the range of the barrier is 576 – 764 cm^{-1}. While the chemical accuracy of the last prediction is reasonable to assign the high barrier, small barrier heights require more precise predictions since the torsional splittings changes more at low barriers than at high barriers.

14.5 Conclusion

1,2,5-trimethylpyrrole was successfully assigned under molecular beam conditions using a combination of FT microwave spectroscopy and quantum chemistry. Even though the barrier of the two equivalent methyl groups is high and nearly no splittings were observable in the (000) species, the very small barrier of the N-methyl group leads to observable splittings in the (100) species. This allowed the determination of the internal rotation of the two equivalent methyl groups. Highly accurate molecular parameters were determined. In contrast to the expectation as well as to the predictions, the barrier height of the N-methyl top is smaller than the one of N-methylpyrrole (45.0 cm^{-1} [72]). Another surprise was the barrier height of the two equivalent methyl groups. While the calculated torsional barrier of 2,5-dimethylpyrrole is 291.9 cm^{-1}, the same methyl groups in TMP have barriers heights, which are twice as high. Here, just the change from secondary to tertiary azoles has a big influence on the barrier height.

CHAPTER 15

2,3,4,5-Tetramethylthiophene

Four rotors (two sets of two equivalent rotors) and C_{2v} frame symmetry

15.1 Introduction

In microwave spectroscopy, three aspects increase the complexity of rotational spectra. First, when a molecule has a large number of conformers with very small energy differences to the most stable one, the density of transitions in the spectra increases. Second, splittings of rotational transitions can be observed due to nuclear quadrupole coupling. Third, large amplitude motions lead to splittings depending on the barrier height of the motion. Here, the complexity of rotational spectroscopy due to the last effect is presented, when four methyl internal rotations with small barriers are present. The barriers to internal rotation of methyl groups are mainly influenced by steric and electronic effects. Predicting torsional barriers is challenging because quantum chemical calculations are still rather inaccurate for these small energy differences. Also, there are no reliable rules to predict barrier heights and often chemical intuition fails completely. On the other hand, microwave spectroscopy yields highly accurate torsional barriers. The molecule 2,3,4,5-tetramethylthiophene (TMTP) will show that coupled motions also have an effect on the barrier height. In this molecule, four methyl rotors as two sets of two equivalent methyl rotors lead to splittings of each rotational transition into 25 torsional species.

In literature, a barrier of 194.1 cm^{-1} was found for the monomethyl derivative 2-methylthiophene (**1**) [20] while in 3-methylthiophene (**2**) [21] a barrier of 258.8 cm^{-1} was determined. The dimethyl derivative 2,5-dimethylthiophene (**3**) [70] has a similar barrier of 248.0 cm^{-1}. This chapter will show that one barrier of TMTP is drastically smaller. In 4,5-dimethylthiazole (**4**) , the barriers changed largely compared to its monomethyl derivatives due to the coupling of the two methyl groups. The barriers due to internal rotation of 332.0 cm^{-1} in 5-methylthiazole (**5**) [118] and 357.6 cm^{-1} in 4-methylthiazole (**6**) [117] are much higher than the corresponding ones in 4,5-dimethylthiazole with barriers of 122.2 cm^{-1} and of 63.3 cm^{-1} (see Chapter 13).

However, TMTP will show at the end of this chapter that only one barrier is influenced by this effect while the other potential has a similar barrier height as its monomethyl derivative. All the mentioned molecules are summarized in Figure 15.1.

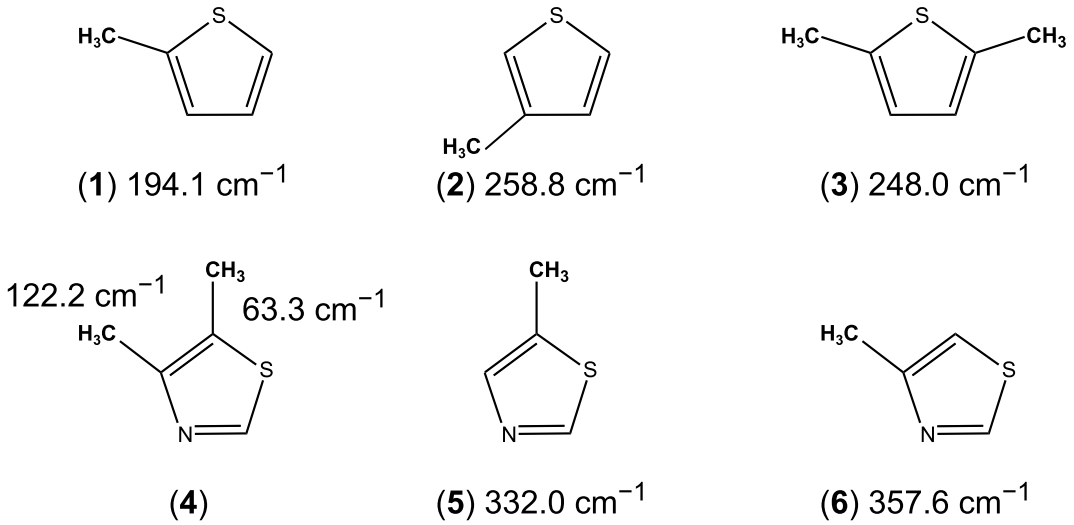

Figure 15.1. Torsional barriers of methyl groups in planar five-membered rings of 2-methylthiophene (**1**) [20], 3-methylthiophene (**2**) [21], 2,5-dimethylthiophene (**3**) [70], 4,5-dimethylthiazole (**4**) (see Chapter 13), 5-methylthiazole (**5**) [118], and 4-methylthiazole (**6**) [117].

15.2 Quantum chemical calculations

The geometrical structure of the thiophene frame in TMTP is planar due to the two conjugated double bonds. However, the challenge for quantum chemical calculations is the lowest energy orientation of the four methyl groups because strong couplings between them, similar to four connected gearwheels, are expected. Full geometry optimizations and harmonic frequency calculations were performed with the GAUSSIAN09 package [26] at different levels of theory using the HF, B3LYP, M06-2X, MP2, and CCSD methods in combination with various Pople and Dunning basis sets [90–96]. The optimized conformers of the methods MP2, B3LYP, and M06-2X with the basis set 6-311++G(d,p) are shown in Figure 15.2.

For simplification, the equivalent methyl groups in the position 2 and 5 will be called the top methyl groups and the ones in position 3 and 4 the bottom methyl groups. MP2 and B3LYP suggested a C_2 symmetry but the orientation of the top methyl groups are different. In the case of the methods M06-2X and CCSD, the suggestion is a C_s symmetry with similar orientation of the top methyl groups. This is in agreement with the method B3LYP. However, the orientations of the bottom methyl groups are different. The nuclear Cartesian coordinates of the fully optimized geometries are given in Table 17.77 and 17.78 in the Appendix. The molecular parameters calculated at different levels of theory are listed in Table 17.79.

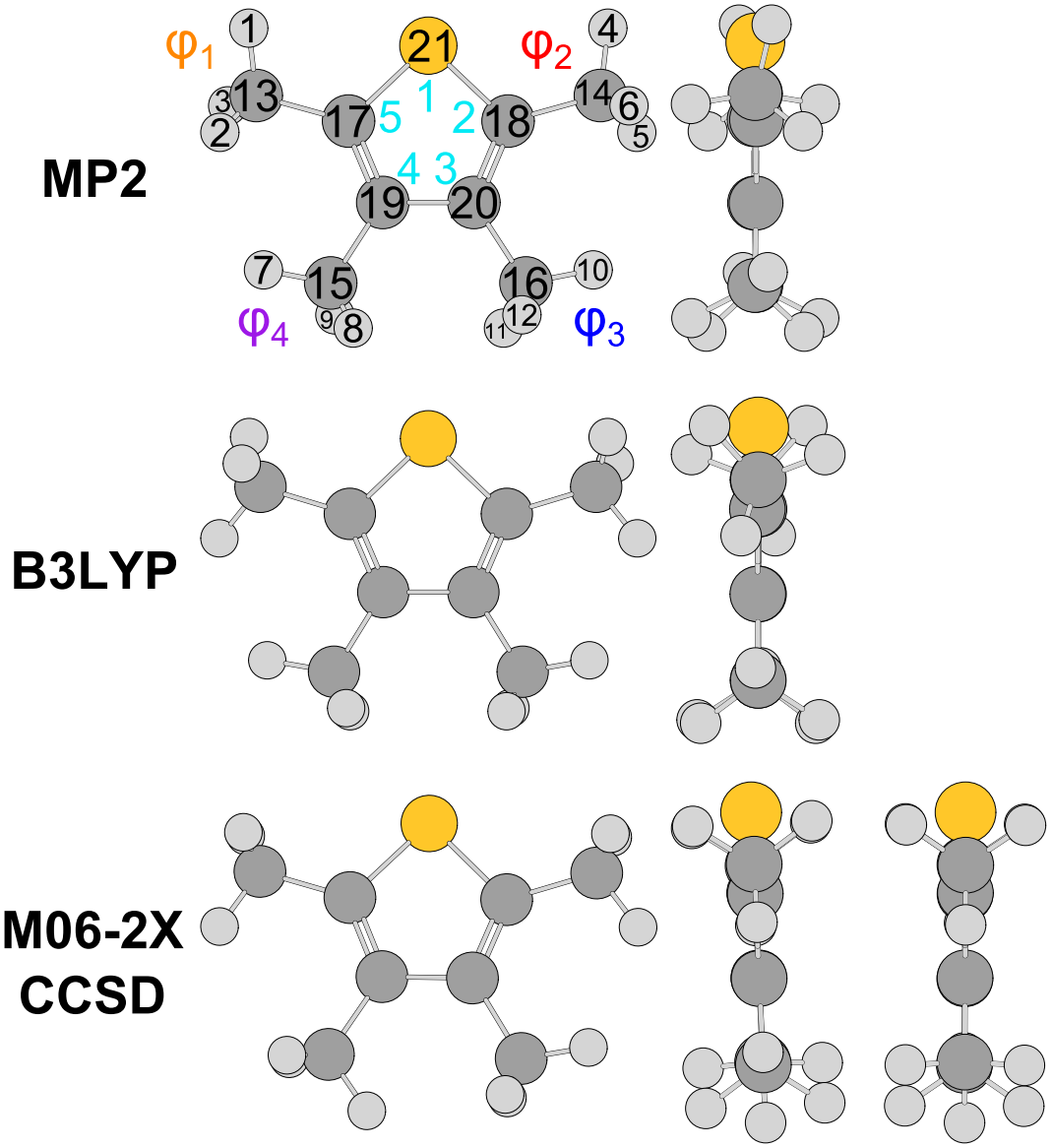

Figure 15.2. The stable conformer of TMTP calculated using the MP2, B3LYP and M06-2X method with the basis set 6-311++G(d,p) from two perspectives (three at the M06-2X level). The conformer at the CCSD/6-311++G(d,p) level has the same geometry as the one at the M06-2X/6-311++G(d,p) level. The positions of the methyl groups are labelled as numbers in cyan.

Next, potential energy curves were calculated to understand the different orientation of the methyl groups and to get an idea of the barrier heights due to internal rotation. The methyl groups lead to splittings of all rotational transitions. The splittings depend on the barrier heights. The potential energy curves of the methyl groups were calculated by varying the dihedral angles $\varphi_1 = \angle(S_{21},C_{17},C_{13},H_1)$ (or $\varphi_2 = \angle(S_{21},C_{18},C_{14},H_4)$) and $\varphi_3 = \angle(C_{18},C_{20},C_{16},H_{10})$ (or $\varphi_4 = \angle(C_{17},C_{19},C_{15},H_7)$), respectively (for atom numbers see Figure 15.2). A step width of 5° was used and only a rotation of 120° was calculated due to the C_3 symmetry of the methyl group. All other geometry parameters were optimized. The calculations were performed with the methods MP2, B3LYP and M06-2X and the basis set 6-311++G(d,p). The potential energy curves of the top methyl group are shown in Figure 15.3. The barrier heights vary

between 15 cm^{-1} and 95 cm^{-1} for different levels of theory. While the curves obtained with the methods MP2 and M06-2X have similar shapes, the energy curve with the method B3LYP has more V_6 character and a bigger shift in the position of the minima.

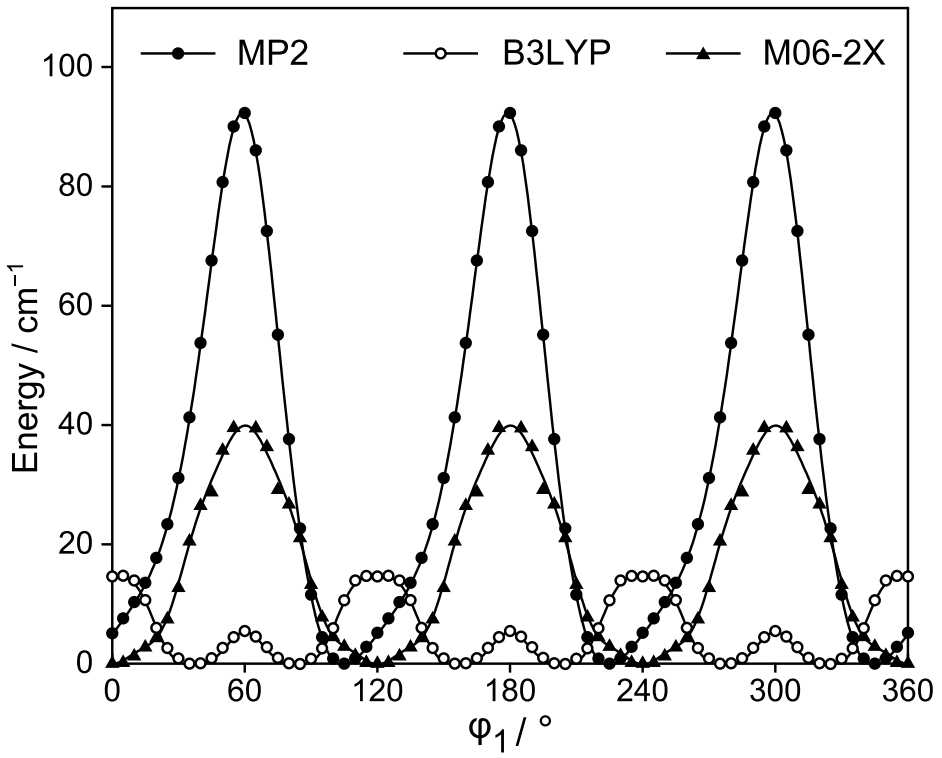

Figure 15.3. The potential energy curves obtained by rotating the top methyl group about the C_{13}-C_{17} bond (for atom number see Figure 15.2). The dihedral angle $\varphi_1 = \angle(S_{21},C_{17},C_{13},H_1)$ was varied in a step width of 5° with the MP2, B3LYP, and M06-2X methods and the basis set 6-311++G(d,p). Relative energies with respect to the stable conformations with their absolute energies $E = -708.8464766$ Hartree (MP2), -710.3828904 Hartree (B3LYP), and -710.1949805 Hartree (M06-2X) are given.

A reason for the different energy curves can be found in Figure 15.4. Here, the optimized dihedral angles of the other methyl groups are shown when the dihedral angle $\varphi_1 = \angle(S_{21},C_{17},C_{13},H_1)$ of the methyl group in 5-position was varied. This is similar to the lowest energy pathway of a four-dimensional potential energy surface for the rotation of all four methyl groups. While the MP2 method shows a big dependence on the equivalent methyl group in 2-position, the B3LYP method prefers to couple with the vicinal inequivalent methyl group in 4-position.

In case of the bottom methyl groups, the barrier heights are higher and more similar for the different levels of theory as shown in Figure 15.5. Using the methods B3LYP and M06-2X and the basis set 6-311++G(d,p), three clear minima are located at $\varphi_2 = 60°$, 180°, and 300°. However, the coupling shown in Figure 15.6 is much larger for the bottom methyl group compared to the top methyl group.

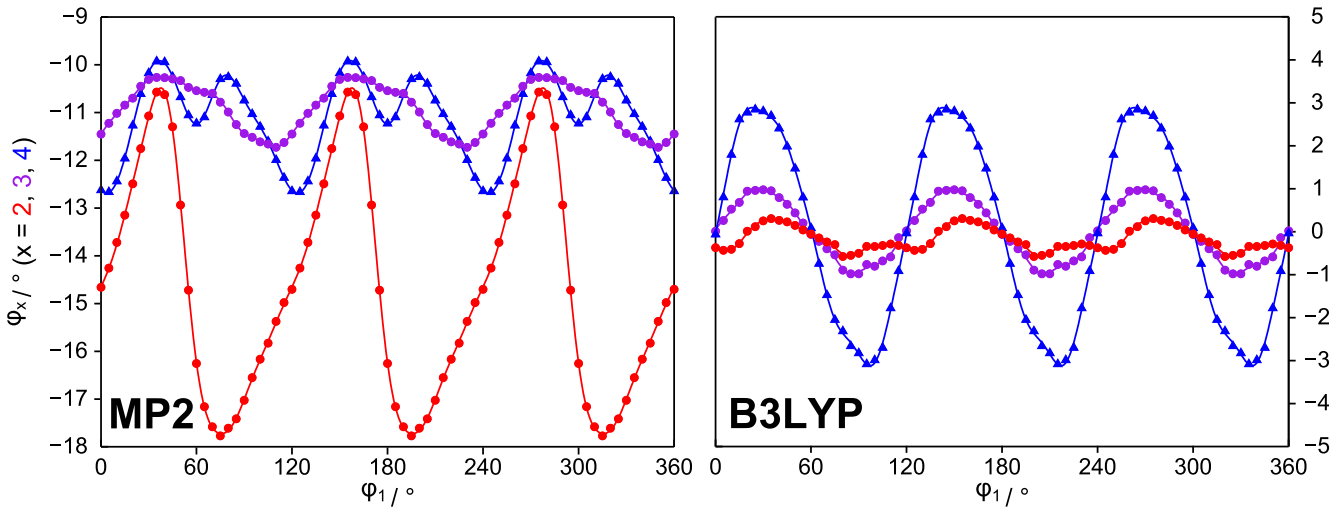

Figure 15.4. The dihedral angles of the methyl groups in the positions 2 (red, $\varphi_2 = \angle(S_{21},C_{18},C_{14},H_4)$), 3 (purple, $\varphi_3 = \angle(C_{18},C_{20},C_{16},H_{10})$), and 4 (blue, $\varphi_4 = \angle(C_{17},C_{19},C_{15},H_7)$), and when the top methyl group in 5-position is rotated about the C_{13}-C_{17} bond (for atom number see Figure 15.2). The dihedral angle $\varphi_1 = \angle(S_{21},C_{17},C_{13},H_1)$ was varied in a step width of 5° with the MP2, B3LYP, and M06-2X methods and the basis set 6-311++G(d,p).

Additional barrier heights were calculated using the Berny algorithm [28] at various levels of theory. Here, geometry optimizations to a first order transition state of the top and the bottom methyl group, respectively, were performed.

The potential energy curves suggest large couplings between the methyl groups. Therefore, two dimensional potential energy surfaces (PESs) were calculated for all possible combinations of the rotations of two methyl groups. Since the potentials of the inequivalent methyl groups are too different, only the PESs of the equivalent methyl groups are shown here. As given in Figure 15.7, the surfaces of the top methyl groups are completely different for the methods MP2 and B3LYP with the basis set 6-311++G(d,p). Here, the challenge of these small barriers for quantum chemical calculations can be seen. In the case of the bottom methyl groups, the surfaces are similar due to the higher barrier as shown in Figure 15.8.

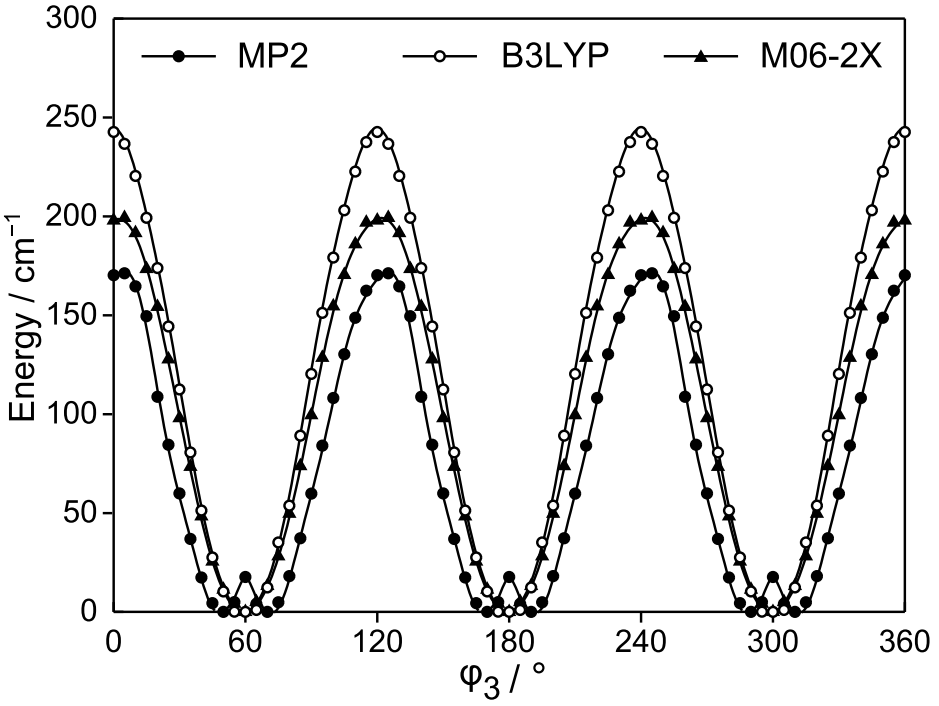

Figure 15.5. The potential energy curves obtained by rotating the bottom methyl group about the C_{16}-C_{20} bond (for atom number see Figure 15.2). The dihedral angle $\varphi_3 = \angle(C_{18},C_{20},C_{16},H_{10})$ was varied in a step width of 5° with the MP2, B3LYP, and M06-2X methods and the basis set 6-311++G(d,p). Relative energies with respect to the stable conformations with their absolute energies $E = -708.8464766$ Hartree (MP2), -710.3828904 Hartree (B3LYP), and -710.1949805 Hartree (M06-2X) are given.

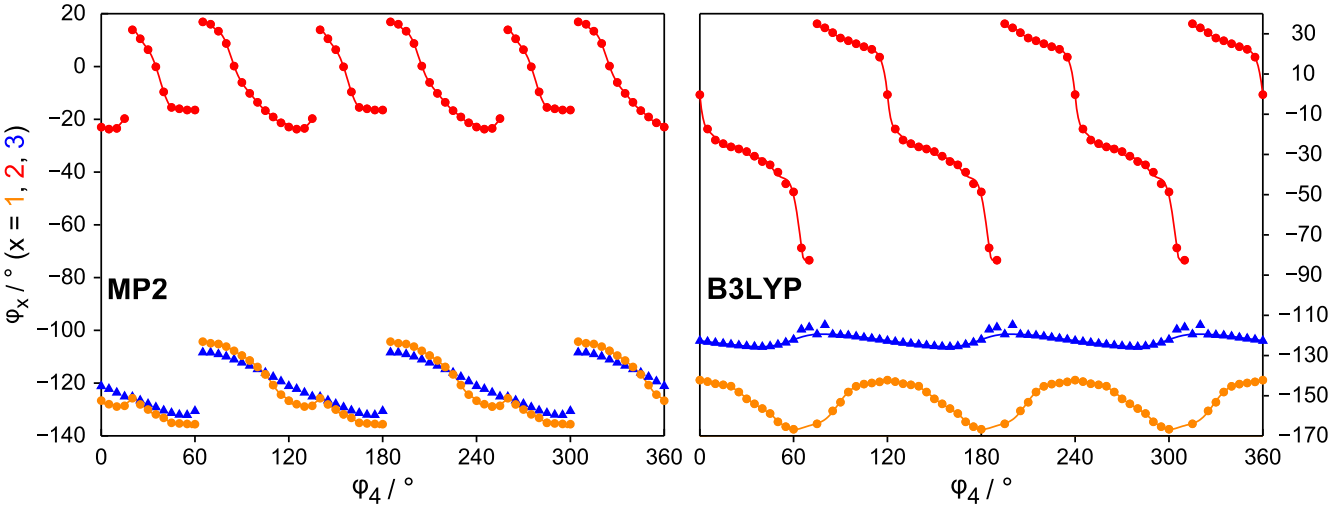

Figure 15.6. The dihedral angles of the methyl groups in the positions 2 (red, $\varphi_2 = \angle(S_{21},C_{18},C_{14},H_4)$), 4 (blue, $\varphi_4 = \angle(C_{17},C_{19},C_{15},H_7)$), and 5 (orange, $\varphi_1 = \angle(S_{21},C_{17},C_{13},H_1)$) when the top methyl group in 3-position is rotated about the C_{16}-C_{20} bond (for atom number see Figure 15.2). The dihedral angle $\varphi_3 = \angle(C_{18},C_{20},C_{16},H_{10})$ was varied in a step width of 5° with the MP2, B3LYP, and M06-2X methods and the basis set 6-311++G(d,p).

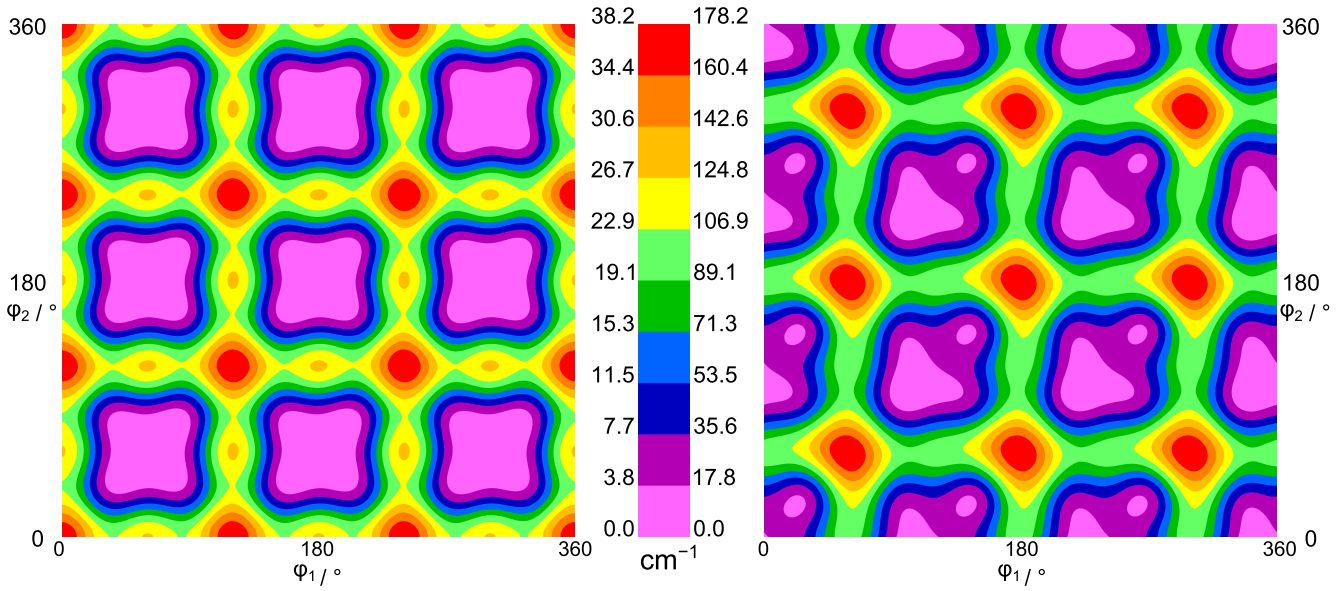

Figure 15.7. The potential energy surface of TMTP calculated with the method B3LYP (left) and MP2 (right) and the basis set 6–311++G(d,p) by rotating both top methyl groups in a step width of 10° about the dihedral angles $\varphi_1 = \angle(S_{21},C_{17},C_{13},H_1)$ and $\varphi_2 = \angle(S_{21},C_{18},C_{14},H_4)$. Relative energies with respect to the stable conformer are given with their absolute energies $E = -710.3828904$ Hartree and -708.8464766 Hartree for the methods B3LYP and MP2, respectively.

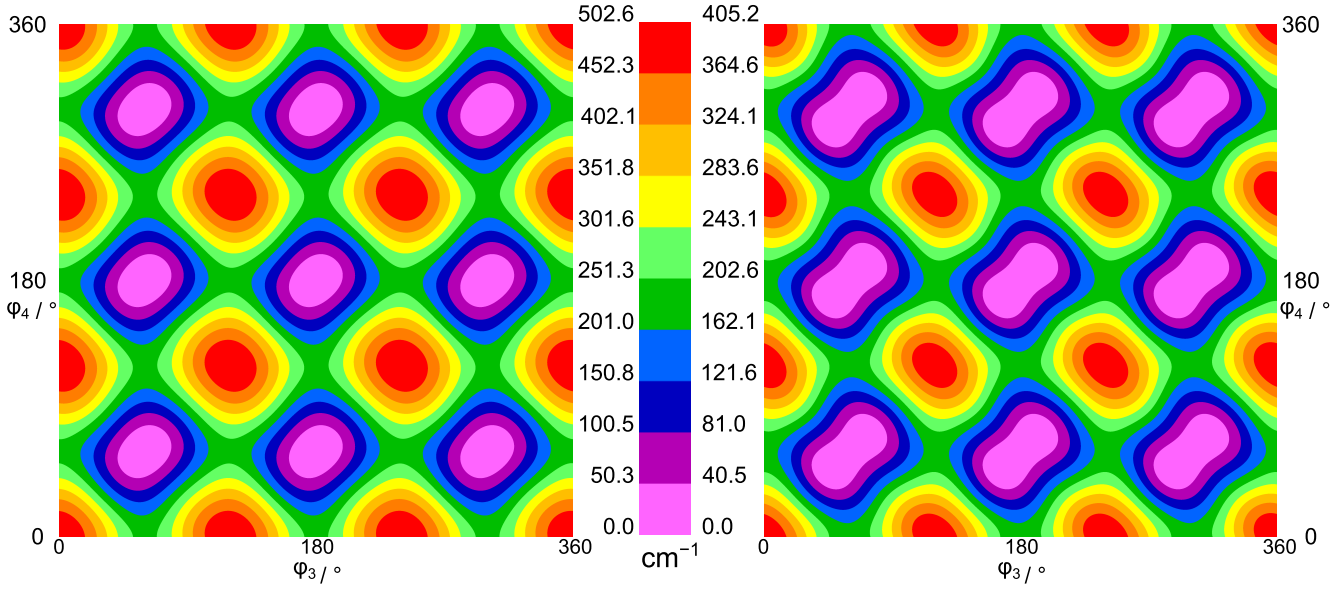

Figure 15.8. The potential energy surface of TMTP calculated with the method B3LYP (left) and MP2 (right) and the basis set 6–311++G(d,p) by rotating both bottom methyl groups in a step width of 10° about the dihedral angles $\varphi_3 = \angle(C_{18},C_{20},C_{16},H_{10})$ and $\varphi_4 = \angle(C_{17},C_{19},C_{15},H_7)$. Relative energies with respect to the stable conformer are given with their absolute energies $E = -710.3828904$ Hartree and -708.8464766 Hartree for the methods B3LYP and MP2, respectively.

15.3 Microwave spectroscopy

15.3.1 Group Theory

TMTP has a C_{2v} frame symmetry and two sets of two equivalent methyl rotors. The molecular symmetry group of this system is G_{324} which can be written as the semi-direct product $(C_3^I \times C_3^I \times C_3^I \times C_3^I) \ltimes C_{2v}$. W. Stahl has constructed the character table based on this formalism as reported by Altmann [82] and Ezra [81]. The character table with 36 classes is given in Table 15.1. The direct product $C_3^I \times C_3^I \times C_3^I \times C_3^I$ of the four intrinsic (superscript I) C_3 groups of the internal rotors is an invariant subgroup of G_{324}. This direct product decomposes into 25 orbits under C_{2v} (Table 15.2). The symmetry labels are based on one representative of each orbit as the first part. The symmetry species of the little co-sets are used as second part of the symmetry labels. The notations σ_1 and σ_2 of the torsional component $(\sigma_1\sigma_2\sigma_3\sigma_4)$ refer to the top methyl groups, while σ_3 and σ_4 refer to the bottom methyl groups. The inequivalent methyl groups in the *cis* positions have the combination σ_2 and σ_3 (or σ_1 and σ_4). In the *trans* positions, the inequivalent methyl groups of the labels σ_2 and σ_4 (or σ_1 and σ_3) are combined.

Nuclear spin statistics

The total wave function $\psi_{tot} = \psi_{el} \cdot \psi_{vib} \cdot \psi_{rotors} \cdot \psi_{ns}$ must change sign under an odd number of fermion permutations (here protons) and retains sign under an even number of permutations as given by the Pauli principle. It belongs thus to the species $(0000)\cdot A_1$. In total, $2^{12} = 4096$ nuclear spin functions arise from 12 protons in TMTP.

Table 15.1. Character table of $G_{324} = (C_3^{\mathrm{I}} \times C_3^{\mathrm{I}} \times C_3^{\mathrm{I}} \times C_3^{\mathrm{I}}) \rtimes C_{2v}$.

G_{324}^{a}	**E**	**a**	**c**	**ab**	**ac**	**ad**	**cd**	**ab^2**	**ac^2**	**ad^2**	**cd^2**	**abc**	**ac^{2}d^2**	**ab^{2}d**	**ab^{2}c**	**acd**	**abc^2**	**ac^{2}d**	**acd^2**	**abcd**	**ab^{2}cd**	**abcd^2**	**abc^{2}d^2**	**ab^{2}cd^2**	**ab^{2}c^{2}d**	**P**	**aP**	**cP**	**acP**	**ac^{2}P**	**R**	**aR**	**cR**	**acR**	**ac^{2}R**	**Q**
S1^{b}	^{c}1	4	4	2	4	4	2	2	4	4	2	4	4	4	4	4	4	4	4	2	4	4	2	2	2	9	18	18	18	18	9	18	18	18	18	81
(0000).A$_1$	1	1	1	1	1	1	1	1	1	1	1	1	1	1	1	1	1	1	1	1	1	1	1	1	1	1	1	1	1	1	1	1	1	1	1	1
(0000).A$_2$	1	1	1	1	1	1	1	1	1	1	1	1	1	1	1	1	1	1	1	1	1	1	1	1	1	1	1	1	1	1	-1	-1	-1	-1	-1	-1
(0000).B$_1$	1	1	1	1	1	1	1	1	1	1	1	1	1	1	1	1	1	1	1	1	1	1	1	1	1	-1	-1	-1	-1	-1	1	1	1	1	1	-1
(0000).B$_2$	1	1	1	1	1	1	1	1	1	1	1	1	1	1	1	1	1	1	1	1	1	1	1	1	1	-1	-1	-1	-1	-1	-1	-1	-1	-1	-1	1
(0011).A	2	2	-1	2	-1	-1	-1	2	-1	-1	2	-1	-1	-1	-1	-1	-1	2	2	-1	-1	2	-1	2	2	2	2	-1	-1	-1	0	0	0	0	0	0
(0011).B	2	2	-1	2	-1	-1	-1	2	-1	-1	2	-1	-1	-1	-1	-1	-1	2	2	-1	-1	2	-1	2	2	-2	-2	1	1	1	0	0	0	0	0	0
(1100).A	2	-1	2	-1	-1	-1	2	2	-1	-1	2	-1	-1	2	2	-1	-1	-1	-1	-1	2	-1	-1	2	2	2	-1	2	-1	-1	0	0	0	0	0	0
(1100).B	2	-1	2	-1	-1	-1	2	2	-1	-1	2	-1	-1	2	2	-1	-1	-1	-1	-1	2	-1	-1	2	2	-2	1	-2	1	1	0	0	0	0	0	0
(1111).A	2	-1	-1	-1	-1	-1	-1	2	2	2	2	2	-1	-1	-1	2	-1	-1	-1	-1	-1	-1	2	2	2	2	-1	-1	-1	2	0	0	0	0	0	0
(1111).B	2	-1	-1	-1	-1	-1	-1	2	2	2	2	2	-1	-1	-1	2	-1	-1	-1	-1	-1	-1	2	2	2	-2	1	1	1	-2	0	0	0	0	0	0
(1122).A	2	-1	-1	-1	2	2	-1	2	-1	-1	2	-1	2	-1	-1	-1	2	-1	-1	2	-1	-1	-1	2	2	2	-1	-1	2	-1	0	0	0	0	0	0
(1122).B	2	-1	-1	-1	2	2	-1	2	-1	-1	2	-1	2	-1	-1	-1	2	-1	-1	2	-1	-1	-1	2	2	-2	1	1	-2	1	0	0	0	0	0	0
(0012).A’	2	2	-1	2	-1	-1	2	2	-1	-1	-1	-1	2	-1	-1	2	-1	-1	-1	2	2	-1	2	-1	-1	0	0	0	0	0	2	2	-1	-1	-1	0
(0012).A”	2	2	-1	2	-1	-1	2	2	-1	-1	-1	-1	2	-1	-1	2	-1	-1	-1	2	2	-1	2	-1	-1	0	0	0	0	0	-2	-2	1	1	1	0
(1200).A’	2	-1	2	2	-1	-1	2	-1	-1	-1	2	2	-1	-1	-1	-1	2	-1	-1	2	-1	2	2	-1	-1	0	0	0	0	0	2	-1	2	-1	-1	0
(1200).A”	2	-1	2	2	-1	-1	2	-1	-1	-1	2	2	-1	-1	-1	-1	2	-1	-1	2	-1	2	2	-1	-1	0	0	0	0	0	-2	1	-2	1	1	0
(1212).A’	2	-1	-1	2	-1	2	2	-1	2	-1	-1	-1	-1	-1	2	-1	-1	-1	2	2	-1	-1	2	-1	2	0	0	0	0	0	2	-1	-1	-1	2	0
(1212).A”	2	-1	-1	2	-1	2	2	-1	2	-1	-1	-1	-1	-1	2	-1	-1	-1	2	2	-1	-1	2	-1	2	0	0	0	0	0	-2	1	1	1	-2	0
(1221).A’	2	-1	-1	2	2	-1	2	-1	-1	2	-1	-1	-1	2	-1	-1	-1	2	-1	2	-1	-1	2	2	-1	0	0	0	0	0	2	-1	-1	2	-1	0
(1221).A”	2	-1	-1	2	2	-1	2	-1	-1	2	-1	-1	-1	2	-1	-1	-1	2	-1	2	-1	-1	2	2	-1	0	0	0	0	0	-2	1	1	-2	1	0
(0001).A	4	4	1	4	1	1	-2	4	1	1	-2	1	-2	1	1	-2	1	-2	-2	-2	-2	-2	-2	-2	-2	0	0	0	0	0	0	0	0	0	0	0
(0100).A	4	1	4	-2	1	1	4	-2	1	1	4	-2	1	-2	-2	1	-2	1	1	-2	-2	-2	-2	-2	-2	0	0	0	0	0	0	0	0	0	0	0
(0101).A	4	1	1	-2	1	-2	-2	-2	4	-2	-2	-2	1	1	-2	-2	1	1	-2	-2	1	1	4	-2	4	0	0	0	0	0	0	0	0	0	0	0
(0102).A	4	1	1	-2	4	-2	-2	-2	1	-2	-2	1	-2	-2	1	1	-2	-2	1	4	1	1	-2	4	-2	0	0	0	0	0	0	0	0	0	0	0
(0110).A	4	1	1	-2	-2	1	-2	-2	-2	4	-2	-2	1	-2	1	-2	1	-2	1	-2	1	1	4	4	-2	0	0	0	0	0	0	0	0	0	0	0
(0111).A	4	1	-2	-2	-2	-2	-2	-2	1	1	4	-2	-2	1	1	1	4	1	1	4	1	-2	-2	-2	-2	0	0	0	0	0	0	0	0	0	0	0
(0112).A	4	1	-2	-2	1	-2	4	-2	-2	1	-2	1	1	-2	4	1	1	1	-2	-2	-2	1	-2	-2	4	0	0	0	0	0	0	0	0	0	0	0
(0120).A	4	1	1	-2	-2	4	-2	-2	-2	1	-2	1	-2	1	-2	1	-2	1	-2	4	1	1	-2	-2	4	0	0	0	0	0	0	0	0	0	0	0
(0121).A	4	1	-2	-2	-2	1	4	-2	1	-2	-2	1	1	4	-2	1	1	-2	1	-2	-2	1	-2	4	-2	0	0	0	0	0	0	0	0	0	0	0
(0122).A	4	1	-2	-2	1	1	-2	-2	-2	-2	4	4	1	1	1	-2	-2	1	1	-2	1	-2	4	-2	-2	0	0	0	0	0	0	0	0	0	0	0
(1101).A	4	-2	1	-2	-2	-2	-2	4	1	1	-2	1	4	1	1	-2	-2	1	1	4	-2	1	-2	-2	-2	0	0	0	0	0	0	0	0	0	0	0
(1102).A	4	-2	1	-2	1	1	-2	4	-2	-2	-2	-2	-2	1	1	4	1	1	1	-2	-2	1	4	-2	-2	0	0	0	0	0	0	0	0	0	0	0
(1112).A	4	-2	-2	-2	1	1	4	4	1	1	-2	1	-2	-2	-2	-2	1	1	1	-2	4	1	-2	-2	-2	0	0	0	0	0	0	0	0	0	0	0
(1201).A	4	-2	1	4	1	-2	-2	-2	-2	1	-2	1	1	1	-2	1	1	-2	4	-2	1	-2	-2	-2	4	0	0	0	0	0	0	0	0	0	0	0
(1202).A	4	-2	1	4	-2	1	-2	-2	1	-2	-2	1	1	-2	1	1	1	4	-2	-2	1	-2	-2	4	-2	0	0	0	0	0	0	0	0	0	0	0
(1211).A	4	-2	-2	4	1	1	-2	-2	1	1	4	-2	1	1	1	1	-2	-2	-2	-2	1	4	-2	-2	-2	0	0	0	0	0	0	0	0	0	0	0

^{a} **a** = (1 2 3), **b** = (4 5 6), **c** = (7 8 9), **d** = (10 11 12), **P** =(1 4)(2 5)(3 6)(7 10)(8 11)(9 12)(13 14)(15 16)(17 18)(19 20), **Q** = (2 3)(5 6)(8 9)(11 12)*, **R** = **PQ** = (1 4)(2 6)(3 5)(7 10)(8 12)(9 11)(13 14)(15 16)(17 18)(19 20)*, the identity operator is **E** = **a**^{3} = **b**^{3} = **c**^{3} = **d**^{3} = **P**^{2} = **Q**^{2} = **R**^{2}, for atom numbers see Figure 15.2. ^{b} Symmetry labels based on the semi-direct product $(C_3^{\mathrm{I}} \times C_3^{\mathrm{I}} \times C_3^{\mathrm{I}} \times C_3^{\mathrm{I}}) \rtimes C_{2v}$. ^{c} Row after S1: number of elements in the respective class.

Table 15.2. Orbits of the irreducible representations of $(C_3^{\mathrm{I}} \times C_3^{\mathrm{I}} \times C_3^{\mathrm{I}} \times C_3^{\mathrm{I}})$ under C_{2v}.

orbit	little co-group
(0000)	C_{2v}
(0001), (0010), (0002), (0020)	C_1
(0011), (0022)	C_2
(0012), (0021)	$C_s(\sigma_v)$
(0100), (1000), (0200), (2000)	C_1
(0101), (1010), (0202), (2020)	C_1
(0102), (1020), (0201), (2010)	C_1
(0110), (1001), (0220), (2002)	C_1
(0111), (1011), (0222), (2022)	C_1
(0112), (1021), (0221), (2012)	C_1
(0120), (1002), (0210), (2001)	C_1
(0121), (1012), (0212), (2021)	C_1
(0122), (1022), (0211), (2011)	C_1
(1100), (2200)	C_2
(1101), (1110), (2202), (2220)	C_1
(1111), (2222)	C_2
(1102), (1120), (2201, (2210)	C_1
(1112), (1121), (2221, (2212)	C_1
(1122), (2211)	C_2
(1200), (2100)	$C_s(\sigma_v)$
(1201), (2110), (2102), (1220)	C_1
(1202), (2120), (2101), (1210)	C_1
(1211), (2111), (2122), (1222)	C_1
(1212), (2121)	$C_s(\sigma_v)$
(1221), (2112)	$C_s(\sigma_v)$

Selection rules

Due to the fact that the dipole moment vector in space fixed coordinates is invariant under pure permutation operations but changes sign under inversion the dipole moment vector transforms as $\Gamma_\mu = (0000) \cdot \mathrm{A}_2$. Transitions between two rotorsional levels i and j are allowed in the vibronic ground state, if $\Gamma_i \times \Gamma_\mu \times \Gamma_j \supset (0000) \cdot \mathrm{A}_1$. The resulting 25 torsional components of two different b-type transitions, namely $K_a K_c$: ee $\leftrightarrow$ oo and eo$\leftrightarrow$ oe (e = even, o = odd) along with their spin statistical weights are given in Table 15.3. They were determined by correlation with the molecular symmetry group C_{2v}(M) of the hypothetical rigid TMTP. The different torsional species and their spin statistical weights are illustrated in Figure 15.9.

Table 15.3. Spin statistical weights of the torsional components of the allowed transitions in TMTP.

ee ↔ oo transitions			wt	eo ↔ oe transitions			wt
(0000).A_1	↔	(0000).A_2	136	(0000).B_1	↔	(0000).B_2	120
(0011).A	↔	(0011).A	72	(0011).B	↔	(0011).B	56
(1100).A	↔	(1100).A	72	(1100).B	↔	(1100).B	56
(1111).A	↔	(1111).A	20	(1111).B	↔	(1111).B	12
(1122).A	↔	(1122).A	20	(1122).B	↔	(1122).B	12
(0012).A’	↔	(0012).A”	64	(0012).A’	↔	(0012).A”	64
(1200).A’	↔	(1200).A”	64	(1200).A’	↔	(1200).A”	64
(1212).A’	↔	(1212).A”	16	(1212).A’	↔	(1212).A”	16
(1221).A’	↔	(1221).A”	16	(1221).A’	↔	(1221).A”	16
(0001).A	↔	(0001).A	256	(0001).A	↔	(0001).A	256
(0100).A	↔	(0100).A	256	(0100).A	↔	(0100).A	256
(0101).A	↔	(0101).A	128	(0101).A	↔	(0101).A	128
(0102).A	↔	(0102).A	128	(0102).A	↔	(0102).A	128
(0110).A	↔	(0110).A	128	(0110).A	↔	(0110).A	128
(0111).A	↔	(0111).A	64	(0111).A	↔	(0111).A	64
(0112).A	↔	(0112).A	64	(0112).A	↔	(0112).A	64
(0120).A	↔	(0120).A	128	(0120).A	↔	(0120).A	128
(0121).A	↔	(0121).A	64	(0121).A	↔	(0121).A	64
(0122).A	↔	(0122).A	64	(0122).A	↔	(0122).A	64
(1101).A	↔	(1101).A	64	(1101).A	↔	(1101).A	64
(1102).A	↔	(1102).A	64	(1102).A	↔	(1102).A	64
(1112).A	↔	(1112).A	32	(1112).A	↔	(1112).A	32
(1201).A	↔	(1201).A	64	(1201).A	↔	(1201).A	64
(1202).A	↔	(1202).A	64	(1202).A	↔	(1202).A	64
(1211).A	↔	(1211).A	32	(1211).A	↔	(1211).A	32

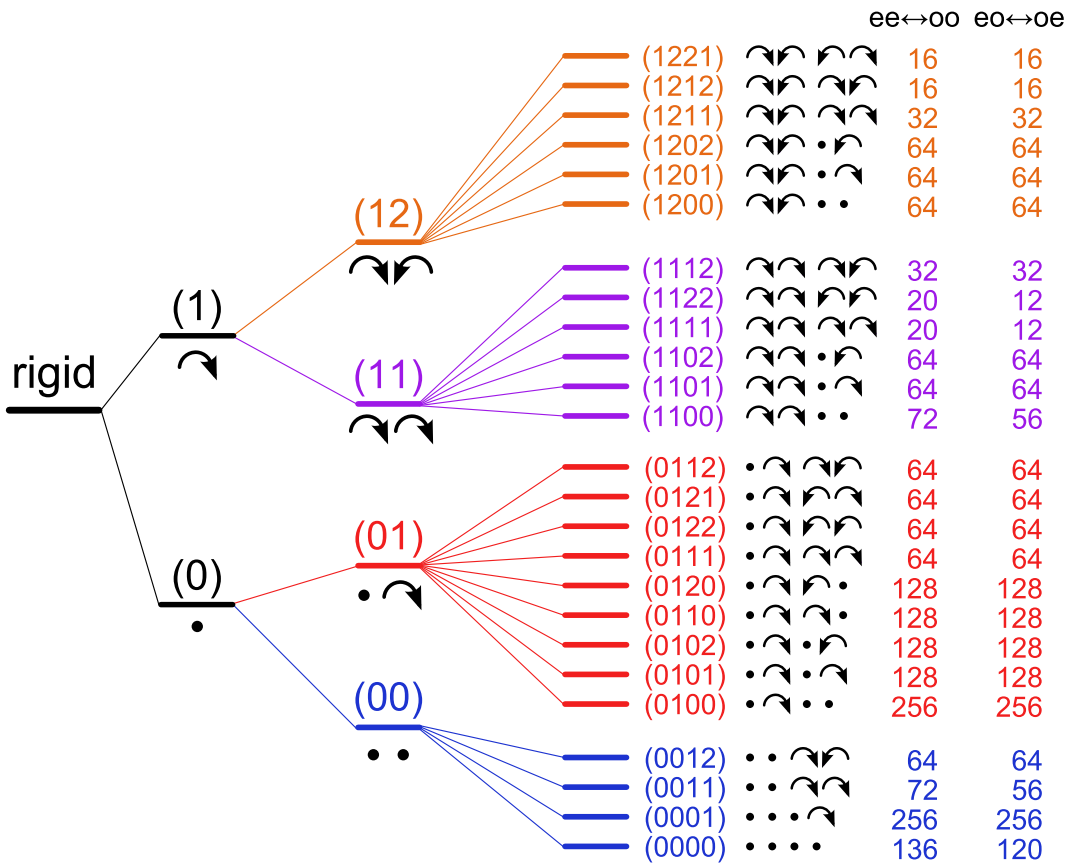

Figure 15.9. Schematic energy level diagram to illustrate the splittings due to internal rotation. Left-hand side: rigid molecule; second: splittings into a (0) and a (1) species due to the internal rotation of one methyl group; third: splittings into a (00), a doubly degenerated (01), a (11) and a (12) species due to the internal rotations of two equivalent methyl groups; fourth: splittings into 25 torsional species due to the internal rotations of four methyl groups as two sets of two equivalent methyl groups; right-hand side: spin weights of the *b*-type transitions.

15.3.2 Spectral analysis

First, a broadband scan with overlapping spectra in a step width of 0.25 MHz was recorded in the frequency range from 8.5 to 15.0 GHz. This frequency range was chosen based on a prediction of a *b*-type rigid-rotor spectrum with the program XIAM [45] using the rotational constants calculated at the MP2/6-311++G(d,p) level. In agreement with the group theory and quantum chemical calculations, only *b*-type transitions were expected in the spectrum.

The usual approach to assign molecules with internal rotations is a rigid-rotor treatment of the rotational spectra. In the case of TMTP however, this approach was unrewarding due to the large number of different torsional species and the density of the rotational transitions in the broadband scan. It was recognized that the predicted rotational transitions of the (0000)-species at the MP2/6-311++G(d,p) level were always located in frequency ranges with high line density. However, the obtained rigid-rotor fit was not accurate to predict the transitions. An example for the high density of lines is shown in Figure 15.10

for 13 torsional components.

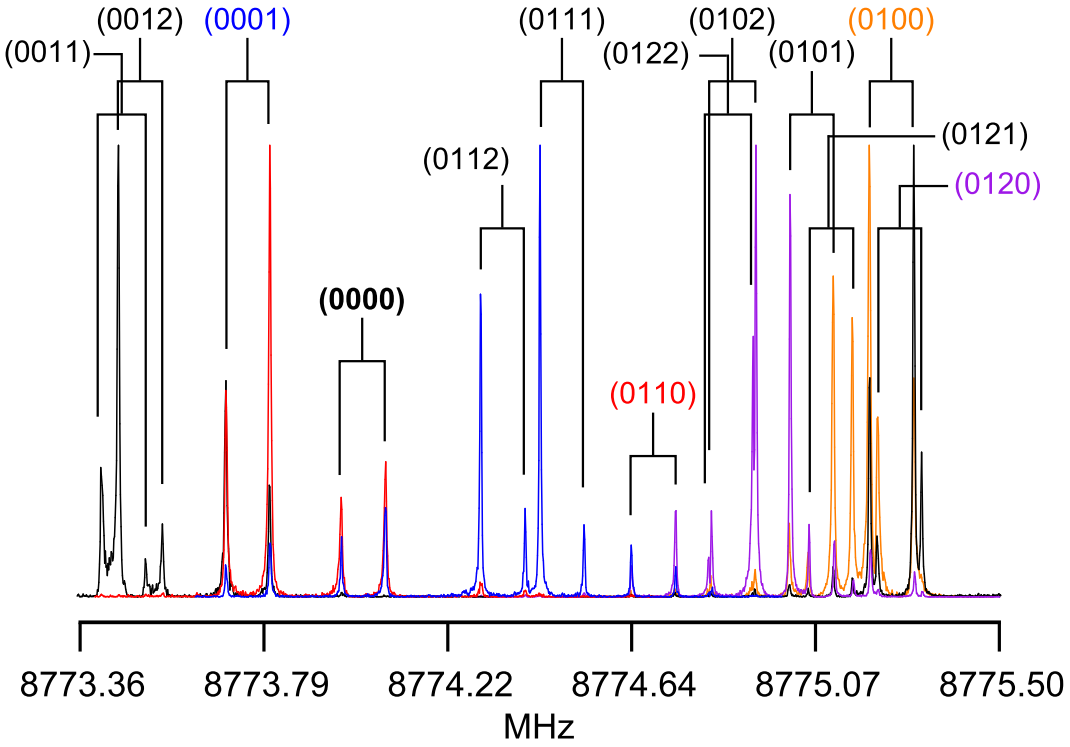

Figure 15.10. Typical spectra of 13 torsional species of the $5_{05} \leftarrow 4_{14}$ transition of TMTP. The additional splitting indicated by brackets is due to the Doppler effect. For this figure, six high resolution measurements marked by different colors are combined. The intensities of the lines are not comparable since they are highly dependent on the polarization frequency.

Several spectra with all torsional species were predicted while the barrier heights of both kinds of methyl groups were varied. With this approach, the possible range of the splittings for the different methyl tops could be limited. By consideration of the spin weights, the splittings were predicted only for the species with the highest spin weights – the (0001)-species of the bottom methyl group and the (0100)-species of the top methyl group (see Figure 15.9). The spin statistical weight of the (0000)-species is half of the one of the (0001)-species. Therefore, all transitions with high intensities used in the rigid-rotor fit must belong to the (0001)-species. With this knowledge, the (0001)-species was assigned due to the small splittings and due to the expected medium barrier height. At the beginning, the *b*-type transitions $5_{05} \leftarrow 4_{14}$, $6_{06} \leftarrow 5_{15}$, $7_{07} \leftarrow 6_{16}$, and $8_{08} \leftarrow 7_{17}$ were identified. Using this one-top fit containing only the (0001)-species, the (0000)-species was searched and assigned. The next step was the assignment of the inequivalent methyl top using the (0100)-species. This process was challenging because the barrier height was unexpectedly low. Additionally, the behavior of the (0100)-species as a function of the barrier height was critical. On the one hand, the rotational transitions of the (0100)-species have several possible matching barrier heights for the same frequency as shown in Figure 15.11. On the other hand, the observed lines have possible matching rotational transitions at different frequencies. By variation of the barrier heights for a number of rotational transitions, matches were only found for a single value of the barrier height. Therefore, a V_3 barrier near 50 cm^{-1} was identified for the top methyl group.

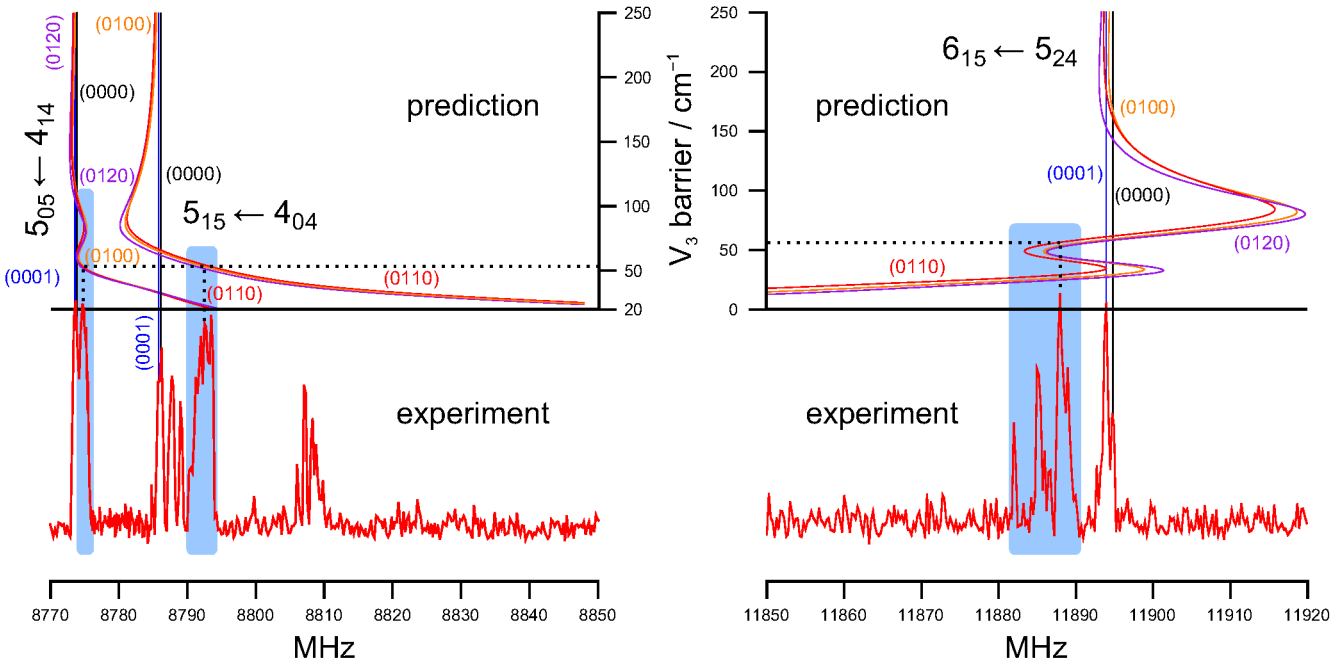

Figure 15.11. Approach to assign the (0100)-species using three different rotational transitions. Top: calculated frequencies of the (0100)-, (0110)- and (0120)-species for different values of the barrier heights. Bottom: experimental broadband scan. The correct matches for all three rotational transitions are marked in the blue boxes and by the dashed line at the barrier height of about 50 cm^{-1}.

After that, successively tries were taken to assign the two-top torsional species using four different two-rotor fits (2 two-inequivalent rotor fits for the species (0110) and (0120) or (0101) and (0102); 2 two-equivalent rotor fits for the species (1100) and (1200) or (0011) and (0012)). The prediction of the (0011)- and (0012)-species were accurate and these species could be easily assigned. For the two-inequivalent rotor fits however, the same approach as in the case of 4,5-dimethylthiazole (see Section 13.3.2) was used since the predictions were off by several to hundreds of MHz. Due to the significant coupling of the methyl groups, the prediction was not accurate and the (0100)-species had to be excluded from the fit. The species (0110) and (0120) as well as the species (0101) and (0102) were assigned from scratch using the parameters obtained for the (0100)-species as starting values. With this method, also the (0111)- and (0122)-species were assigned starting from the two-equivalent rotor fit of the bottom methyl groups. In total, five separated fits were needed to fit the assigned species since some coupling parameters are missing in XIAM. All of the fits are accurate and can predict the transitions precisely. However, the remaining unassigned species could not be predicted using these fits due to the interaction between the methyl groups. An example for the high coupling is the fact that the species (1100) and (1200) could not be assigned even though the species (1000) was well determined. The reasons are: (i) their intensities are low as determined by the spin weights and (ii) the predictive power is low since the coupling is high. Here, the coupling between up to four methyl groups needs to be considered. The current XIAM code as well as all other programs to treat internal rotation are not suitable for four methyl tops. Also, no kinetic or potential coupling parameters for more than two rotors are available. The six

torsional species (1111), (1112), (1122), (1211), (1212), and (1221) are not expected to be observable since their intensities are too low. This was determined by the spin statistical weights. In total, 11 of 25 torsional components were already assigned. As future work, it is planned to implement coupling parameters for more than two rotors and to modify the XIAM code to treat four methyl tops. The goal is to assign the remaining torsional species.

15.4 Results of the fits and discussion

The rigid-rotor fit of the (0000) torsional species has an excellent standard deviation of 2.6 kHz. The two-top fit of the two equivalent bottom methyl groups corresponds to a theoretical 3,4-dimethylthiophene, in which the other methyl groups of TMTP are assumed to be rigid. Here, the torsional transitions of the (0001), (0011), and (0012) species were used. This two-top fit also has an excellent standard deviation of 4.0 kHz, as given in Table 15.4. These standard deviations are within the measurement accuracy of the spectrometer. However, the issues in this molecule already start with the one-top fit of the top methyl group using the transitions of the (0100) species. Since its barrier is low and its internal rotor axis is not orientated parallel to a principal axis, parameters in XIAM are missing for a better fit. The remaining 2 two-top fits correspond to a hypothetical 2,3-dimethylthiophene (*cis*) and to a 2,4-dimethylthiophene (*trans*). Here, the torsional species (0110) and (0120) in the *cis* and the (0101)- and (0102)-species in the *trans* fit were successfully assigned. However, in these fits the (0100) species had to be excluded to obtain a reasonable prediction of further transitions of the torsional species (0110) and (0120) or (0101) and (0102). With these five fits, all torsional species with high intensities are already assigned. The intensities were determined by their spin statistical weights. Additionally, the torsional species (0111) and (0122) were successfully assigned in a three-top fit of a hypothetical 2,3,4-trimethylthiophene. Here, the standard deviation of 52.4 kHz is 20 times larger than the measurement accuracy. However, the torsional species are assumed to be correctly assigned since only transitions were used, in which the splittings are higher than the standard deviation. Also new transitions, which are not in the frequency range of the broadband scan, were accurately predicted. For example, the transition shown in Figure 15.10 was not used for the assignment of the different torsional species. However, the final predictions were accurately to identify the correct sequence of its torsional species. An indicator for the quality of the fits is the fact that the torsional barriers, the internal rotor angles as well as the higher order terms D_{pi2J}, D_{pi2K}, and D_{pi2-} have similar values even though different torsional species were fitted. In each fit, the three rotational constants A, B, and C, as well as the V_3 potentials, and the angles between the internal rotation axes were determined with very high accuracy. All fitted parameters are given in Table 15.4. A list of all frequencies along with their residuals is given in Table 17.80. The reasons for the high standard deviations are missing parameters to describe the high potential coupling between the different methyl groups in TMTP. This was already recognized for 4,5-dimethylthiazole (see Chapter 13). Only one kinetic (F_{12}) and one potential top-top interaction parameter ($V_{c_1c_2}$) for two rotors are available

in XIAM but kinetic interaction parameters like F_{13}, F_{23},...,F_{34} as well as potential interaction parameters for up to four rotors like $V_{c_1c_3}$,$V_{c_2c_3}$,...,$V_{c_1c_2c_3}$, $V_{c_1c_2c_4}$,...,$V_{c_1c_2c_3c_4}$ are needed here.

The experimentally deduced rotational constants were compared with those calculated by quantum chemistry. Since the frame of TMTP is rigid, the rotational constants, especially the rotational constants B and C were excellently calculated at all levels of theory. The best agreement was found at the B3LYP/6-311++G(3df,2pd) level of theory as shown in Table 17.79. The rotational constant A has larger deviations for all levels of theory. It should be noted that the quantum chemical data in Table 17.79 refer to the equilibrium structure whereas the experimental data refer to the ground vibrational state.

The calculated barriers to internal rotation of the top methyl groups vary in a wide range from 15 – 103 cm^{-1}. The range of the bottom methyl groups is from 164 – 265 cm^{-1}. The B3LYP method predicts the barrier of the bottom methyl groups quite well, whereas the MP2 method underestimates the barrier by up to 90 cm^{-1}. On the other hand, the MP2 method overestimates the barrier of the top methyl groups by up to 50 cm^{-1}.

The barrier of 54.471(81) cm^{-1} of the top methyl groups in TMTP is surprisingly smaller than the barrier of 194.1 cm^{-1} in the monomethyl derivative 2-methylthiophene (**1**) [20] as well as the barrier of 248.0 cm^{-1} in the dimethyl derivative 2,5-dimethylthiophene (**3**) [70]. However, the barrier of the top methyl groups in TMTP (54.471(81) cm^{-1}) is in good agreement with the unusually low barrier of 63.3 cm^{-1} of the γ-rotor in 4,5-dimethylthiazole (**4**) (see Chapter 13). On the other hand, the barrier of 245.236(74) cm^{-1} of the bottom methyl groups in TMTP is in good agreement with the barrier of 258.8 cm^{-1} found in 3-methylthiophene (**2**) [21]. In 4,5-dimethylthiazole (**4**), the corresponding δ-rotor has a smaller barrier of 122.2 cm^{-1} due to its different electronic environment because of the nitrogen nucleus.

Table 15.4. Molecular parameters of TMTP under molecular beam conditions obtained by the program XIAM. Top 1 refers to the top methyl group, top 2 to the bottom methyl group.

Parameter[a]	Unit	rigid	2top bottom	1top top	2top *cis*	2top *trans*	3top bottom	calc.[b]
A	GHz	1.831412 13(58)	1.831 114 41(60)	1.808 538 0(19)	1.819 763 0(21)	1.819 756 7(24)	1.819 607 1(42)	1.782
B	GHz	1.386 904 50(28)	1.386 515 90(41)	1.385 752 3(16)	1.386 113 5(17)	1.386 112 7(20)	1.385 917 2(33)	1.384
C	GHz	0.800 078 06(18)	0.800 072 65(15)	0.800 071 03(63)	0.800 072 59(44)	0.800 072 31(51)	0.800 069 45(85)	0.794
Δ_J	kHz	0.0070(22)	−0.0736(33)	−0.0503(94)				0.034
Δ_{JK}	kHz	0.279(16)	0.5215(88)		0.235(21)	0.187(26)	0.219(45)	0.010
Δ_K	kHz	0.166(16)						0.096
δ_J	kHz		−0.0399(18)	−0.0252(51)				0.014
δ_K	kHz	0.103(12)						0.016
$V_{3,1}$	cm^{-1}			53.774 33(20)	53.942 10(10)	53.937 19(20)	54.471(81)	15
$F_{0,1}$	GHz			160.00[c]	160.00[c]	160.00[c]	160.00[c]	
∠(i_1,a)	°			16.346 70(40)	16.882 60(40)	163.150 40(40)	16.8456(11)	16.89
∠(i_1,b)	°			73.653 30(40)	73.117 40(40)	73.150 40(40)	73.1544(11)	73.12
∠(i_1,c)	°			90.00[d]	90.00[d]	90.00[d]	90.00[d]	90.58
$D_{pi2J,1}$	kHz			−81.33(44)	−80.03(49)	−81.30(56)	−80.09(98)	
$D_{pi2K,1}$	kHz			391.44(77)	447.89(74)	448.93(87)	436.1(19)	
$D_{pi2-,1}$	kHz			−99.15(52)	−98.92(62)	−101.20(72)	−99.2(14)	
$V_{3,2}$	cm^{-1}		246.252(11)		244.7623(92)	244.635(12)	245.236(74)	246
$F_{0,2}$	GHz		160.00[c]		160.00[c]	160.00[c]	160.00[c]	
∠(i_2,a)	°		56.4921(62)		56.9829(65)	56.0926(76)	57.029(13)	58.20
∠(i_2,b)	°		146.4921(62)		146.9829(65)	146.0926(76)	147.029(13)	148.20
∠(i_2,c)	°		90.00[d]		90.00[d]	90.00[d]	90.00[d]	90.23
$D_{pi2J,2}$	kHz		66.02(79)		69.0(74)	77.5(85)	62.5(76)	
$D_{pi2K,2}$	kHz		−162.3(13)		192(12)	−205(14)	−168(13)	
$D_{pi2-,2}$	kHz		65.20(88)		68.2(85)	76.6(97)	59.1(85)	
F_{12}	GHz		3.892(97)		−1.684(16)	3.519(21)	−1.434(29)	
V_{cc}	cm^{-1}						5.35(79)	
σ[e]	kHz	2.6	4.0	14.3	20.7	23.2	52.4	
species: N[f]		(0000): 33[g]	(0001): 45 (0011): 26 (0012): 26	(0100): 30	(0110): 33 (0120): 29	(0101): 26 (0102): 26	(0111): 29 (0122): 26	

[a] All parameters are given with one standard uncertainty in parentheses. Watson's A reduction and I^r representation was used. [b] Vibrational ground state rotational constants and centrifugal distortion constants obtained by anharmonic frequency calculation at the B3LYP/6-311++G(d,p). [c] Fixed. [d] Fixed due to symmetry. [e] Standard deviation of the fit. [f] Fitted torsional species and their number of lines. [g] All other fits include the (0000) species.

15.5 Conclusion

Highly accurate molecular parameters were determined for 2,3,4,5-tetramethylthiophene under molecular beam conditions. In total, 11 of 25 torsional components were successfully assigned using a combination of group theory, microwave spectroscopy, and quantum chemistry. Unusual potential barriers were found. The assignment was only possible due to the predicted spin statistical weights obtained by group theory because the number of torsional components is large. On the one hand, the barrier height of the bottom methyl groups with a value of 245.236(76) cm^{-1} is similar to the monomethyl derivative 3-methylthiophene with a barrier of 258.8 cm^{-1} [21]. On the other hand, the barrier height of the top methyl groups with a value of 54.471(81) cm^{-1} is unexpectedly lower than the barrier of 194.1 cm^{-1} in the monomethyl derivative 2-methylthiophene [20] as well as the barrier of 248.0 cm^{-1} in the dimethyl derivative 2,5-dimethylthiophene [70]. Like in the case of 4,5-dimethylthiazole, the barrier heights drop drastically just due to the coupling of vicinal methyl groups (see Chapter 13). The coupling of the methyl groups in this molecule can be depicted as a motion of four connected gearwheels. Usually, all molecular parameters and all torsional components can be described by assigning only the three torsional species (0000), (0100), and (0001). Since the coupling of the methyl groups is so large, even the 11 assigned species cannot be fitted in a global fit nor can they predict the remaining species accurately. However, both barrier heights and the angles of all methyl internal rotor axes are well determined. Therefore, TMTP is the prototype molecule to observe four coupled internal rotors and the effects of their interaction.

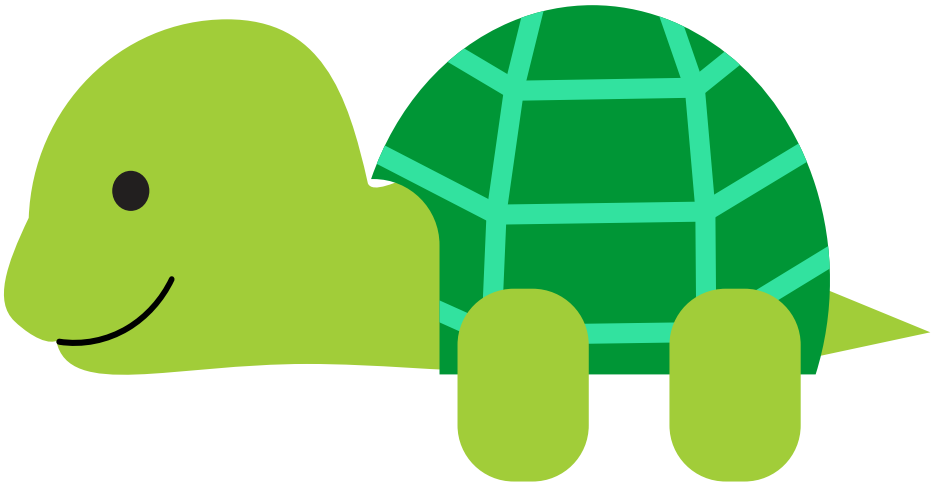

Figure 15.12. The molecule TMTP is similar to a turtle due to a rigid thiophene-frame as its shell and the two sets of two equivalent methyl groups as its arms and legs.

CHAPTER 16

Dimethylcyclopropane-1,1-Dicarboxylate

Two equivalent rotors and C_2 frame symmetry

Vinh Van performed the spectral analysis, parts of the measurements and co-wrote the manuscript. Judith Schütt helped with the quantum chemical calculations and the measurements in her bachelor thesis under the supervision of Vinh Van. Ha Vinh Lam Nguyen and Wolfgang Stahl produced the group theory and co-wrote the manuscript.

16.1 Introduction

Microwave spectroscopic studies on a series of methyl esters CH_3-O(C=O)-**R** have shown that the barrier to internal rotation of the methoxy methyl group **C**H_3O- is fairly invariant. The smallest member in this series, methyl formate (**R** = H), has a barrier height of 399 cm^{-1} [123]. For the following compounds methyl acetate (**R** = CH_3, 424.581(56) cm^{-1}) [115], methyl propionate (**R** = C_2H_5, 428.537(15) cm^{-1}) [124], methyl butyrate (**R** = C_3H_7, 425.1 cm^{-1}) [125], methyl valerate (**R** = C_4H_9, 417.7 cm^{-1}) [126], and methyl hexanoate (**R** = C_5H_{11}, 414.0 cm^{-1}) [127], the barrier height is approximately 420 ± 10 cm^{-1}. The continuous decrease of the barrier from methyl propionate to methyl hexanoate might be an artifact arising from the coupling of the methyl internal rotation and a low-lying vibration of the alkyl chain.

For a better understanding of the barrier heights in methyl esters, it is important to investigate esters with non-linear carbon chains **R**. Here, the microwave studies on the structure and internal dynamics of dimethylcyclopropane-1,1-dicarboxylate (CPC) is presented, with the chemical formula given in Figure 16.1, supplemented by quantum chemical calculations. CPC has two methyl carboxylate groups CH_3-O(C=O)-, which are bridged via a cyclopropane ring. In other molecules possessing two carbonyl groups such as malonaldehyde [128] and 2-methylmalonaldehyde [129], the lowest energy conformer exhibits a C_s structure with an OH...O=C intramolecular hydrogen bond closing a six-membered ring. It is also the case found in the conformational analysis and near-infrared induced rotamerization of malonic acid in an argon matrix. [129] This structure (called form I in Ref. [129]) is accompanied by two other conformers (called form II and III), which are slightly higher in energy. Because in CPC no hydrogen is available for an intramolecular hydrogen bond, a structure similar to form II or form III in Ref. [129]

might be energetically more favorable. As the following sections will show, the interesting and rather rare C_2 structure similar to form III in Ref. [129] is present in the most stable conformer of CPC, where the two methoxy methyl groups are equivalent. The orientation of the cyclopropane ring is rather rigid; the structure was reported for cyclopropanecarboxylic acid using microwave spectroscopy and isotopic substitutions. [130]

This chapter is divided into sections dealing with: (1) the conformational landscape of CPC obtained by quantum chemistry, (2) the theory of the molecular symmetry group G_{18} of CPC composed of the group C_2 of the frame with two C_{3v} methyl internal rotors, (3) microwave spectroscopy with experimental details, spectral assignments, and the fit using the program XIAM, and (4) a brief discussion of the theoretical and experimental results.

16.2 Quantum chemical calculations

The conformational landscape of CPC is determined by four dihedral angles: $\varphi_1 = \angle(O_{18}, C_{13}, C_{17}, C_{14})$, $\varphi_2 = \angle(O_{19}, C_{14}, C_{17}, C_{13})$, $\varphi_3 = \angle(C_{11}, O_{18}, C_{13}, C_{17})$, and $\varphi_4 = \angle(C_{12}, O_{19}, C_{14}, C_{17})$, corresponding to the rotations about the C_{13}-C_{17}, C_{14}-C_{17}, C_{13}-O_{18}, and C_{14}-O_{19} bonds, respectively. These angles were varied over a grid of 60° in order to create starting geometries, which were optimized using the GAUSSIAN09 program package [26] at the MP2/6-311++G(d,p) level of theory, leading to six conformers. Harmonic frequency calculations confirm that they are all stable conformers rather than saddle points. The most stable conformer (called conformer I) depicted in Figure 16.1 has a C_2 molecular symmetry. The rotational constants, energies relative to that of conformer I, and the dihedral angles φ_i (i = 1 – 4) of all conformers are summarized in Table 16.1. Their Cartesian coordinates are available in Table 17.81.

Table 16.1. The rotational constants A, B, and C in GHz and the dihedral angles $\varphi_1 = \angle(O_{18}, C_{13}, C_{17}, C_{14})$, $\varphi_2 = \angle(O_{19}, C_{14}, C_{17}, C_{13})$, $\varphi_3 = \angle(C_{11}, O_{18}, C_{13}, C_{17})$, and $\varphi_4 = \angle(C_{12}, O_{19}, C_{14}, C_{17})$ in degrees, relative energies in kJ·mol^{-1} with respect to conformer I with its absolute energy $E = -572.285795$ Hartree, and dipole moment components in Debye of six conformers of CPC calculated at the MP2/6-311++G(d,p) level of theory (for atom numbering see Figure 16.1).

Conf.	A	B	C	ΔE	φ_1	φ_2	φ_3	φ_4	μ_a	μ_b	μ_c
I	1.438	0.975	0.681	0.00	−36.73	−36.73	−178.78	−178.78	0.00	−1.60	0.00
II	1.832	0.812	0.632	4.31	−39.75	158.76	−179.38	174.84	−1.91	0.53	1.89
III	2.342	0.711	0.596	10.78	154.20	154.20	174.83	174.82	0.00	3.95	0.00
IV	1.414	1.024	0.820	28.79	−20.57	−60.60	−177.21	−2.94	−2.49	0.16	2.50
V	1.666	0.911	0.743	34.00	61.58	−171.83	−0.02	−175.85	4.81	0.68	4.13
VI	1.295	1.122	0.994	59.58	−44.01	−43.99	−11.77	−11.81	0.00	0.30	0.00

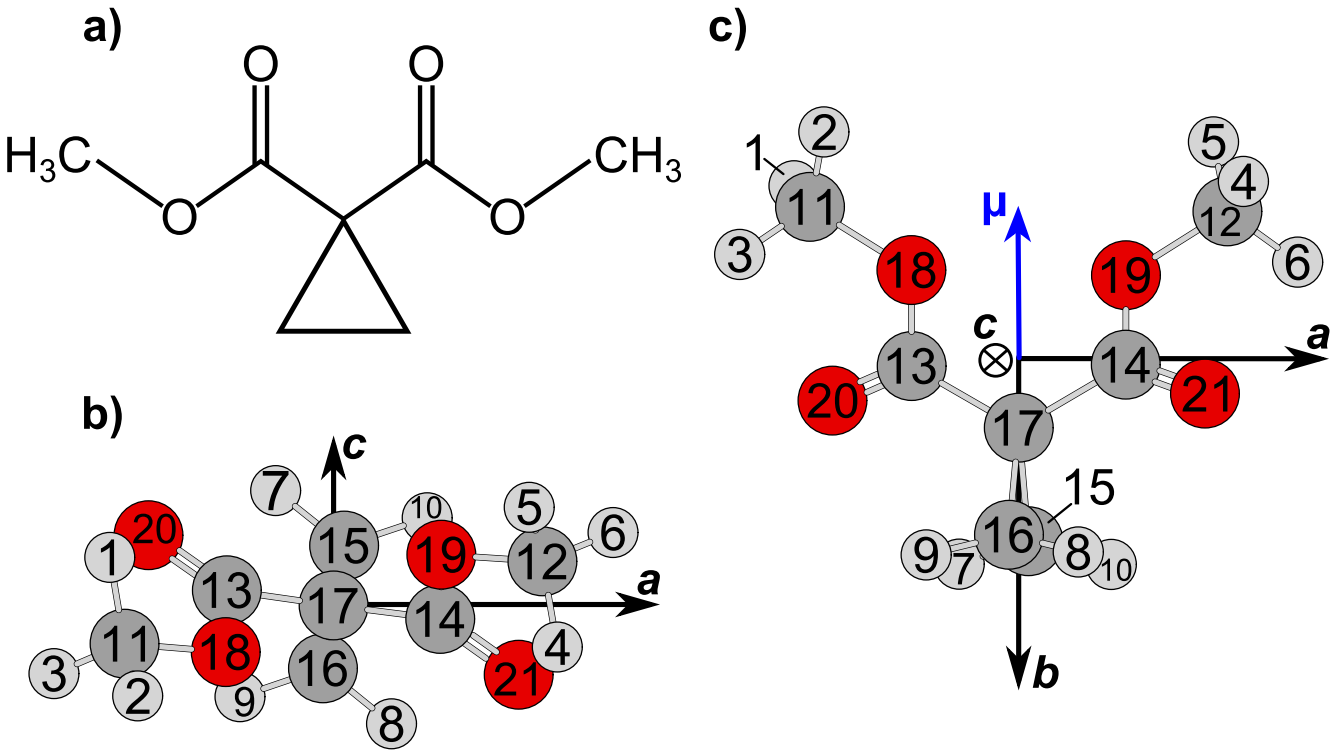

Figure 16.1. (a) The chemical formula of CPC. (b) The atom numbers and the structure of the most stable conformer of CPC calculated at the MP2/6-311++G(d,p) level of theory, as viewed along the *b*-principal axis, illustrating: (i) the C_2 symmetry and (ii) that the *a*-axis almost coincides with a line connecting C_{13} and C_{14}. (c) View along the *c*-principal axis, which points into the paper plane, as indicated by an encircled cross, showing: (i) a classic diester structure and (ii) the dipole moment (in blue) located along the *b*-principal axis.

The rotations about the C_{13}-O_{18} and C_{14}-O_{19} bonds (by varying φ_3 and φ_4) create *trans* and *cis* conformations of the ester groups. In agreement with previous investigations on esters [84, 97, 106] and results from the conformational analysis of malonic acid [129] as well as other theoretical works [131], *cis* esters are stable conformations; however, they possess rather high energies. Three *cis* conformers (conformer IV, V, and VI) were found; all of them are more than 18 kJ·mol^{-1} higher in energy than the three *trans* conformers (conformer I, II, and III, see Figure 16.2). They cannot be observed under molecular beam conditions, where the rotational temperature is in the order of a few Kelvin. Among the *trans* conformers, the relative energies of 4.31 and 10.78 kJ·mol^{-1} of conformer II and III, respectively, are already quite considerable. Therefore, only conformer I is expected to be observable in the microwave spectrum. Notably, the structure of conformer II is similar to form II in Ref. [129], and conformer III also has C_2 symmetry.

From the microwave spectroscopic investigations on a series of acetates, it is known that the barrier to internal rotation of the acetyl methyl group is low (about 100 cm^{-1}). [107, 115] Some of the quantum chemical calculations confirm the high flexibility of the C-C bond between the α-carbon and the carboxylate group (the C_{13}-C_{17} and C_{14}-C_{17} bonds in the case of CPC). [61, 132] Since two of such bonds

are present in CPC, a potential energy surface (PES) was calculated at the MP2/6-311++G(d,p) level of theory to study the torsional behavior of these bonds. The dihedral angles φ_1 and φ_2 were varied over a step width of 10°, while all other geometry parameters were allowed to relax with the starting values of 180° for φ_3 and φ_4 to assure *trans* conformations. The resulting PES has high symmetry, where the geometries represented by (φ_1, φ_2), $(-\varphi_1, -\varphi_2)$, (φ_2, φ_1), and $(-\varphi_2, -\varphi_1)$ possess the same potential energy. Therefore, only a quarter of the full PES had to be calculated. The potential energies were parameterized using a two-dimensional Fourier expansion based on terms with the correct symmetry of the angles φ_1 and φ_2. The corresponding coefficients are given in Table 17.82. Using these Fourier coefficients, the PES was drawn as a contour plot given in Figure 16.3.

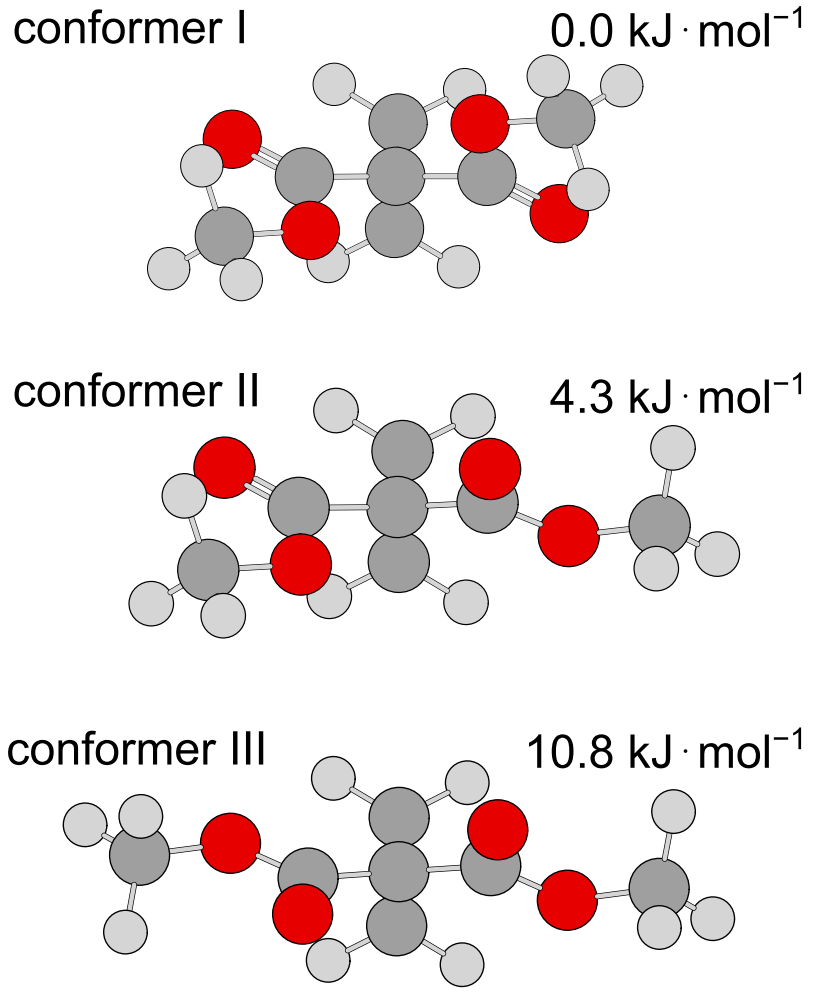

Figure 16.2. The three *trans* conformers of CPC calculated at the MP2/6-311++G(d,p) level of theory as viewed along the *b*-principal axis. Relative energies are given with respect to conformer I with its absolute energy $E = -572.285795$ Hartree.

Because of the C_2 symmetry of conformer I, the two methyl groups are equivalent. They undergo internal rotations with the same three-fold hindering potential. The barrier height was calculated by varying the dihedral angle $\varphi_5 = \angle(H_1,\ C_{11},\ O_{18},\ C_{13})$ over a grid of 2°, whereas all other parameters were optimized. Due to the symmetry of the methyl group, only a rotation of 120° was needed. The data were parametrized with the expansion

$$V = V_0 + \frac{V_3}{2} \cdot \cos(3\alpha) + \frac{V_6}{2} \cdot \cos(6\alpha).$$

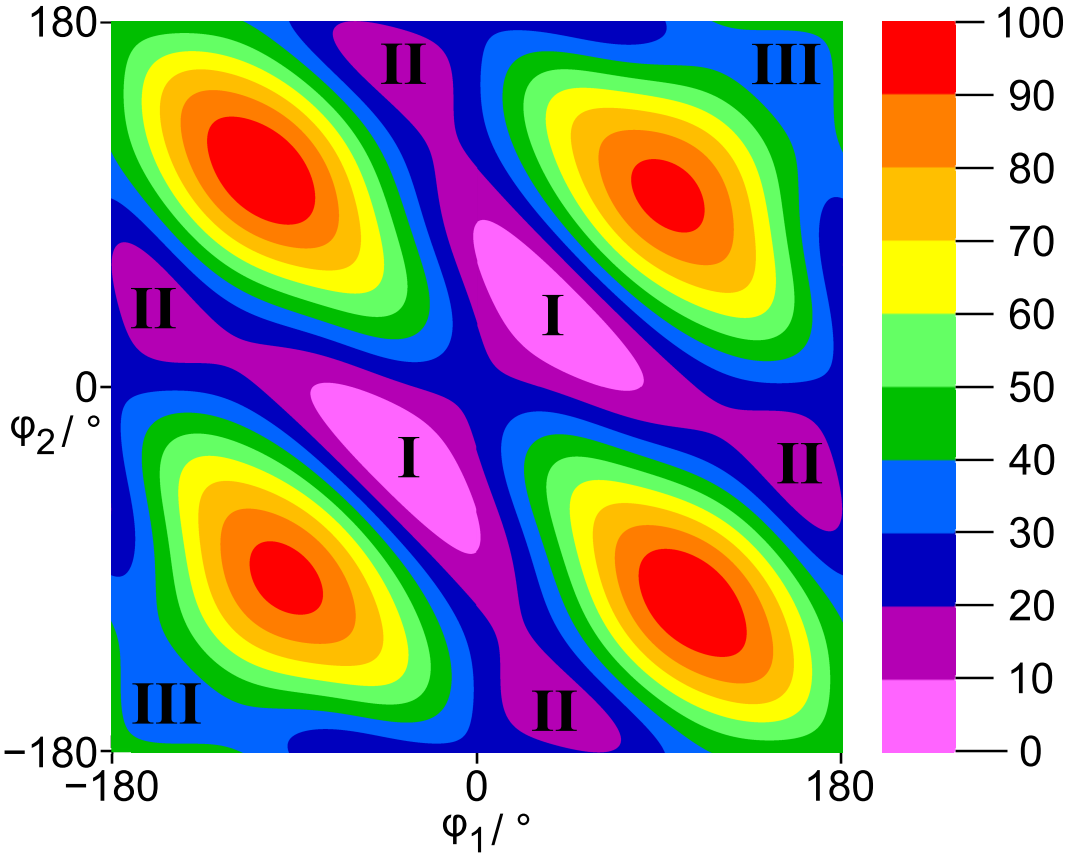

Figure 16.3. The potential energy surface of CPC calculated at the MP2/6–311++G(d,p) level of theory obtained by varying the dihedral angles $\varphi_1 = \angle(O_{18},C_{13},C_{17},C_{14})$ and $\varphi_2 = \angle(O_{19},C_{14},C_{17},C_{13})$ in a step width of 10°, corresponding to the rotations of the carboxylate groups. The dihedral angles $\varphi_3 = \angle(C_{11},O_{18},C_{13},C_{17})$ and $\varphi_4 = \angle(C_{12},O_{19},C_{14},C_{17})$ were allowed to relax with a starting value of 180°. The global energy minimum and maximum are $E = -572.285795$ Hartree and -572.272977 Hartree, respectively.

The potential energy curves calculated at the MP2/6–311++G(d,p) and B3LYP/6–311++G(d,p) levels of theory are given in Figure 16.4, the Fourier coefficients in Table 17.83. The offset V_0 was determined to be -572.284700042 Hartree, $V_3 = 237.2$ cm^{-1}, $V_6 = 3.4$ cm^{-1}. The V_6 contribution is almost negligible.

To study the coupling between the two methyl rotors, a PES was calculated as a function of the dihedral angles $\varphi_5 = \angle(H_1, C_{11}, O_{18}, C_{13})$ and $\varphi_6 = \angle(H_4, C_{12}, O_{19}, C_{14})$ in a grid of 10°, as given in Figure 16.5. Only calculations for one ninth of the full PES are needed due to the C_3 symmetry of the two tops. Clearly, no significant coupling could be observed as shown in Table 17.84.

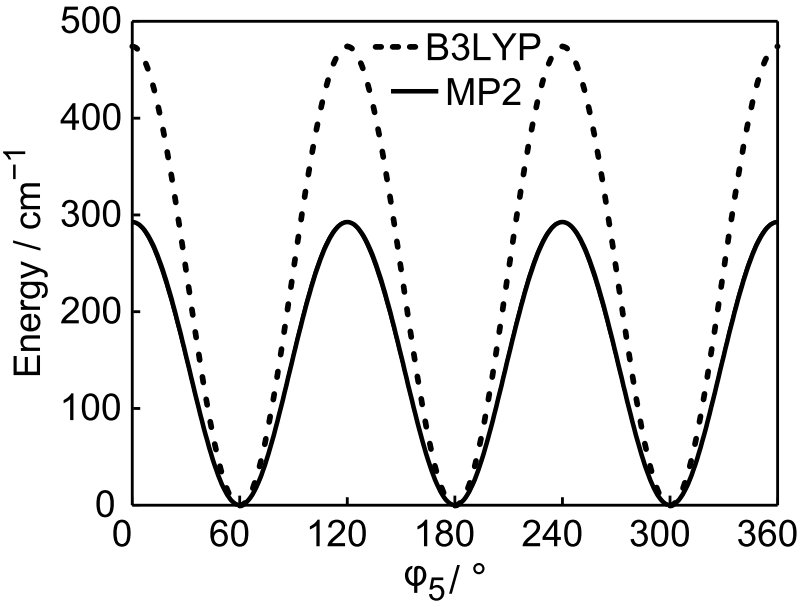

Figure 16.4. The potential energy curves of conformer I of CPC calculated at the MP2/6–311++G(d,p) and the B3LYP/6–311++G(d,p) level of theory obtained by varying the dihedral angle $\varphi_5 = \angle(H_1, C_{11}, O_{18}, C_{13})$ in a step width of 2°, corresponding to the rotations of one of the two equivalent methyl groups.

Finally, the B3LYP and MP2 methods in combination with various Pople and Dunning basis sets were used to re-optimize the geometry of conformer I given in Figure 16.1 to check for convergence and to compare the calculated rotational constants with the experimental values. Geometry optimizations to a first order transition state using the Berny algorithm [28] were performed to calculate more accurately the barriers to internal rotation. The results are listed in Table 17.85.

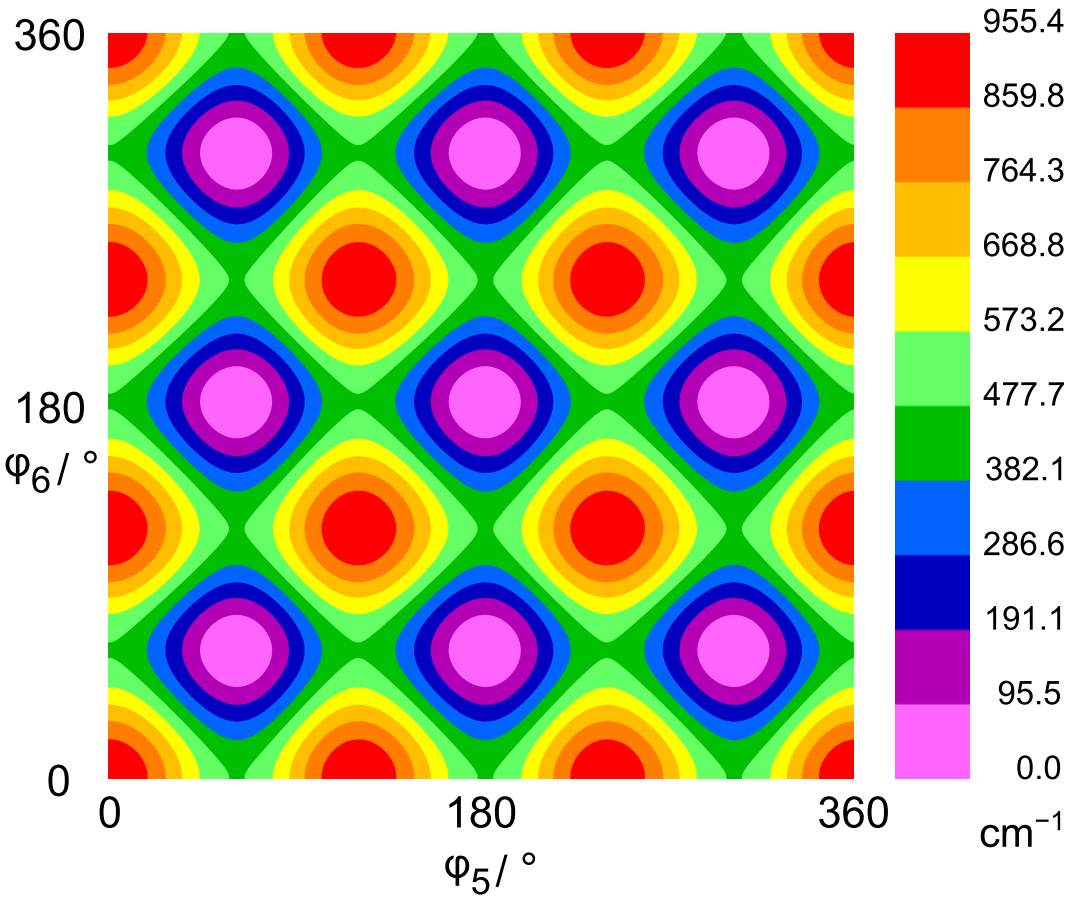

Figure 16.5. The potential energy surface of CPC calculated at the MP2/6–311++G(d,p) level of theory obtained by varying the dihedral angles $\varphi_5 = \angle(H_1, C_{11}, O_{18}, C_{13})$ and $\varphi_6 = \angle(H_4, C_{12}, O_{19}, C_{14})$ in a step width of 10°, corresponding to the rotations of the methyl groups. The global energy minimum is $E = -572.285795$ Hartree.

16.3 Group theory

16.3.1 Symmetry labels

CPC has an interesting and rather rare C_2 symmetry with two equivalent methyl rotors. In microwave spectroscopic studies, this type of symmetry has only been reported for dimethyl disulfide [133] and dimethyl diselenide [134]. It is known that the molecular symmetry group of such a system is G_{18} with the character table given in Table 16.2. [47]

For CPC the labeling scheme given in column S1 of Table 16.2 is used, for which G_{18} is written as the semi-direct product $(C_3^{\mathrm{I}} \times C_3^{\mathrm{I}}) \ltimes C_2$, as introduced by Ezra [81]. Details of the theoretical background can be found in the work of Altmann [82]. The direct product $C_3^{\mathrm{I}} \times C_3^{\mathrm{I}}$ of the two intrinsic (superscript I) C_3 groups of the internal rotors is an invariant subgroup of G_{18}, which decomposes into six orbits under the C_2 frame symmetry given in Table 16.3. One representative of each orbit provides the first part of the symmetry label, for example (01).

Table 16.2. Character table of the molecular symmetry group $(C_3^{\mathrm{I}} \times C_3^{\mathrm{I}}) \ltimes C_2$ of CPC.

G_{18} [a]	**E**	**a**	$\mathbf{a}^2$	**ab**	$\mathbf{a}^2\mathbf{b}^2$	$\mathbf{ab}^2$	**P**	**aP**	$\mathbf{a}^2$**P**	
S1[b]	[c]1	2	2	1	1	2	3	3	3	wt[d]
(00)·A	1	1	1	1	1	1	1	1	1	120
(00)·B	1	1	1	1	1	1	−1	−1	−1	136
(11)·A	1	ε	ε^2	ε^2	ε	1	1	ε	ε^2	28
(22)·A	1	ε^2	ε	ε	ε^2	1	1	ε^2	ε	28
(11)·B	1	ε	ε^2	ε^2	ε	1	−1	$-\varepsilon$	$-\varepsilon^2$	36
(22)·B	1	ε^2	ε	ε	ε^2	1	−1	$-\varepsilon^2$	$-\varepsilon$	36
(12)·A	2	−1	−1	2	2	−1	0	0	0	64
(01)·A	2	$-\varepsilon^2$	$-\varepsilon$	2ε	$2\varepsilon^2$	−1	0	0	0	128
(02)·A	2	$-\varepsilon$	$-\varepsilon^2$	$2\varepsilon^2$	2ε	−1	0	0	0	128

[a] **a** = (1 2 3), **b** = (4 5 6), **P** =(1 4)(2 5)(3 6)(7 8)(9 10)(11 12)(13 14)(15 16)(18 19)(20 21), for atom numbers see Figure 16.1, $\varepsilon = e^{i\cdot 2\pi/3}$. [b] Symmetry labels based on the semi-direct product $(C_3^{\mathrm{I}} \times C_3^{\mathrm{I}}) \ltimes C_2$. [c] Row between S1 and wt: number of elements in the respective class. [d] Spin statistical weight.

The numbers $\sigma = 0, 1, 2$ represent the three symmetry species A, E_a, E_b, respectively, of the group C_3. They correspond to the transformation properties of the C_3-adapted planar rotor wave functions $e^{i(3k+\sigma)\varphi}$ with $k \in \mathbb{Z}$ and the torsional angle φ. Each orbit is associated with its little co-set and forms a subgroup of C_2. The second part of the symmetry labels is the symmetry species of the little co-sets.

Table 16.3. Orbits of the irreducible representations of $(C_3^{\mathrm{I}} \times C_3^{\mathrm{I}})$ under C_2.

orbit	little co-set
(00)	C_2
(11)	C_2
(22)	C_2
(12), (21)	C_1
(01), (10)	C_1
(02), (20)	C_1

16.3.2 Nuclear spin statistics

The Pauli principle rules that the total wave function $\psi_{\text{tot}} = \psi_{\text{el}} \cdot \psi_{\text{vib}} \cdot \psi_{\text{rotors}} \cdot \psi_{\text{ns}}$ retains sign under an even number of fermion permutations (protons in the case of CPC) and changes sign under an odd number of permutations. By inspection of the character table, it is seen, that the classes labeled with E, a, a^2, ab, a^2b^2 and ab^2 correspond to an even number of proton permutations whereas P, aP, and a^2P correspond to an odd number. Therefore, the representation of the total wave function Γ_{tot} is $(00)\cdot$B. The 1024 nuclear spin functions arising from 10 protons in CPC has the representation

$$\begin{aligned}\Gamma_{ns} =& 136\ (00)\cdot\mathrm{A} + 120\ (00)\cdot\mathrm{B} + 36\ (11)\cdot\mathrm{A} + 36\ (22)\cdot\mathrm{A} + 28\ (11)\cdot\mathrm{B} + 28\ (22)\cdot\mathrm{B} \\ &+ 64\ (12)\cdot\mathrm{A} + 128\ (01)\cdot\mathrm{A} + 128\ (02)\cdot\mathrm{A}.\end{aligned}$$

The spin weights are determined by the number of allowed total wave functions, where only the vibronic ground state with $\Gamma_{el} = \Gamma_{vib} = (00)\cdot$A is considered. The results are indicated in the last column of Table 16.2 (under wt).

16.3.3 Selection rules

The dipole moment vector in space fixed coordinates is invariant under pure permutation operations but changes sign under inversion. Since only pure permutation operations and no inversions are present in the G_{18} group, it transforms as $\Gamma_\mu = (00)\cdot\mathrm{A}$. In the vibronic ground state, transitions between two rotorsional levels i and j are allowed, if $\Gamma_i \times \Gamma_\mu \times \Gamma_j \supset (00)\cdot\mathrm{A}$. The resulting four torsional components of two different types of b-type transitions, namely K_aK_c: ee $\leftrightarrow$ oo and eo$\leftrightarrow$ oe (e = even, o = odd) along with their spin statistical weights are given in Table 16.4. They were determined by correlation with the molecular symmetry group C_2(M) of the hypothetical rigid CPC.

The torsional state can be labeled conveniently by the first part $(\sigma_1\sigma_2)$ of the full symmetry label, if the quantum numbers K_a and K_c are known. This abbreviated notation will be used from now on in this chapter.

Table 16.4. Spin statistical weights of the torsional components for the allowed transitions in CPC.

ee $\leftrightarrow$ oo transitions			wt	eo $\leftrightarrow$ oe transitions			wt
(00)·A	$\leftrightarrow$	(00)·A	120	(00)·B	$\leftrightarrow$	(00)·B	136
(11)·A	$\leftrightarrow$	(11)·A	} 56	(11)·B	$\leftrightarrow$	(11)·B	} 72
(22)·A	$\leftrightarrow$	(22)·A		(22)·B	$\leftrightarrow$	(22)·B	
(12)·A	$\leftrightarrow$	(12)·A	64	(12)·A	$\leftrightarrow$	(12)·A	64
(01)·A	$\leftrightarrow$	(01)·A	} 256	(01)·A	$\leftrightarrow$	(01)·A	} 256
(02)·A	$\leftrightarrow$	(02)·A		(02)·A	$\leftrightarrow$	(02)·A	

16.4 Microwave spectroscopy

16.4.1 Spectral analysis

The quantum chemical calculations as well as symmetry considerations have shown that CPC has only a dipole moment in *b*-direction. Therefore, only *b*-type transitions are expected in the spectrum. At the beginning of the assignment process, the internal rotations of the two methyl tops were neglected and CPC was considered as a rigid rotor. Using the rotational constants of conformer I given in Table 16.1, the *b*-type transition frequencies are predicted with the program XIAM [45]. The prediction shows a high line density in the frequency range from 9.0 to 14.0 GHz. Thus, a broadband scan was recorded in this region, where overlapping spectra in a step width of 0.25 MHz with 50 co-added decays per step were automatically measured. The scan indicated line positions, which were subsequently remeasured with higher resolution, where all signals appeared as multiplets due to (i) the internal rotations of the two equivalent methyl tops and (ii) the Doppler effect. The average value of the line widths is about 13 kHz, corresponding to a measurement accuracy of 1.3 kHz. A typical spectrum is illustrated in Figure 16.6.

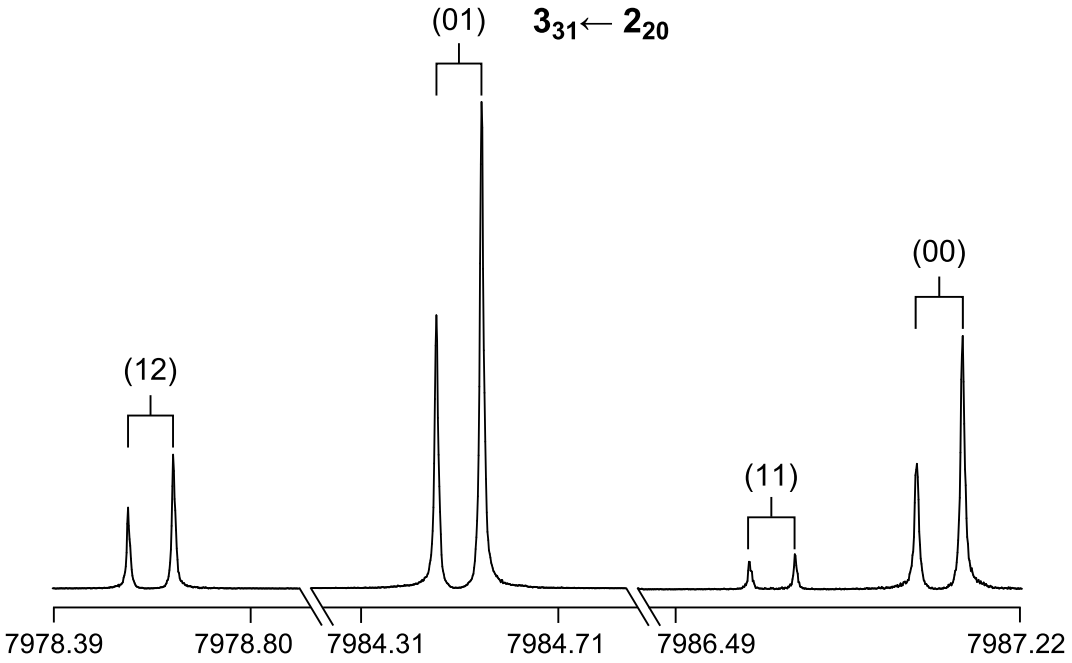

Figure 16.6. Typical spectra of the four torsional species (00), (10), (11), and (12) of the $3_{31} \leftarrow 2_{20}$ transition of conformer I of CPC. The experimental resolution is 1.3 kHz, the typical line width approximately 7 – 18 kHz (FWHH). The splitting indicated by brackets is due to the Doppler effect. For this spectrum 72 – 270 decays were co-added.

A spectrum with only *b*-type transitions is difficult to assign if the calculated *A* rotational constant is not sufficiently accurate. However, two *R*-branch series with the transitions $5_{33} \leftarrow 4_{22}$, $6_{34} \leftarrow 5_{23}$ and $4_{31} \leftarrow 3_{22}$, $5_{32} \leftarrow 4_{23}$ were assigned by trial and error. Further transitions in the scan were subsequently found and fitted. The rotational constants from this preliminary fit were used to predict the spectrum in the frequency range from $2-26.5$ GHz. The predicted transitions were directly measured in the high resolution mode.

As a next step, the internal rotations of both methyl groups were considered. For a prediction of the frequencies, the angles between the internal rotor axes and the principal axes of inertia, as well as the V_3 potentials were taken from the values calculated at the MP2/6-311++G(d,p) level. Based on this prediction and the intensities predicted with group theory, the (00), (01), (11), and (12) torsional transitions with $J \leq 10$ and $K_a \leq 4$ were successfully assigned. The largest splittings found in the scan were up to 20 MHz.

Table 16.5. Molecular parameters of conformer I of CPC under molecular beam conditions obtained by the XIAM program.

Par.[a]	Unit	Fit
A	GHz	1.441 866 55(41)
B	GHz	0.977 878 96(23)
C	GHz	0.674 701 576(53)
D_J	kHz	0.099 08(35)
D_{JK}	kHz	−0.1861(14)
D_K	kHz	0.3226(12)
d_1	kHz	−0.030 70(20)
d_2	kHz	−0.008 09(11)
V_3	cm^{-1}	407.02(34)
I_α	$uÅ^2$	3.1586(fixed)
∠(i,a)	°	144.58(32)
∠(i,b)	°	54.69(33)
∠(i,c)	°	87.669(64)
D_{pi2J}	kHz	−32.7(37)
D_{Dpi2K}	kHz	105(11)
D_{Dpi2-}	kHz	−17.4(37)
F_{12}	GHz	−0.640(derived)
σ^b	kHz	1.9
N[c]		245

[a] All parameters refer to the principal axis system and are given with one standard uncertainty in parentheses. Watson's S reduction in I^r representation was used. [b] Standard deviation of the fit. [c] Number of lines.

16.4.2 Results of the fit

The program XIAM was used to fit 252 torsional components of CPC with an excellent standard deviation of 1.9 kHz, which is within the measurement accuracy. The three rotational constants A, B, and C, as well as five centrifugal distortion constants D_J, D_{JK}, D_K, d_1, and d_2 were determined with very high accuracy. The V_3 potentials, the angles between the internal rotation axes and the a-principal axis (δ), and three higher order parameters D_{pi2J}, D_{pi2K}, and D_{pi2-} were also fitted. The fitted parameters are given in Table 16.5. A list of all frequencies along with their residuals can be found in Table 17.86.

16.5 Discussion

The experimentally deduced rotational constants were compared with those calculated by quantum chemistry. The best agreement was found at the MP2/6-31++G(df,pd) level of theory, as shown in Table 17.85. All levels of theory yielded B and C rotational constants, which are in very good agreement with the experimental values. The A rotational constant has larger deviations for all levels of theory. It should be noted here that the quantum chemical data refer to the equilibrium structure whereas the experimental data refer to the ground vibrational state.

The calculated barriers to internal rotation of the methyl groups vary in a wide range from $133.8 - 475.9$ cm^{-1}. The B3LYP method underestimates the barrier by over $100 - 200$ cm^{-1}, whereas the MP2 method yields deviations up to ± 70 cm^{-1}. The barrier of 410.6 cm^{-1} calculated at the MP2/6-311++G(d,p) level of theory matches the experimental value (407.0 cm^{-1}) quite well. The barrier to internal rotations of the two equivalent methyl groups of CPC is slightly lower than that of methyl hexanoate (414.0 cm^{-1}) [127]. Therefore, it is currently assumed that the increasing number of heavy atoms on the other side of the CH_3-O(C=O)-group decreases the barrier height of the methoxy methyl group.

16.6 Conclusion

The microwave spectrum of CPC was measured under molecular beam conditions and all lines were assigned to the lowest energy conformer which has a C_2 point group symmetry. This result is consistent with quantum chemical calculations at various levels of theory. The barrier to internal rotation of the two equivalent methyl groups was determined to be 407.02(34) cm^{-1}. Torsional symmetry labels were introduced for the molecular symmetry group G_{18} based on the more intuitive semi-direct product decomposition $(C_3^{\mathrm{I}} \times C_3^{\mathrm{I}}) \propto C_2$ rather than the older direct product decomposition $C_3^- \times C_3^+$. Moreover, the nuclear spin statistics of CPC was derived, which was used to obtain the correct intensity ratio of the four torsional species.

CHAPTER 17

Effects of Multiple Internal Rotations

In this part of the thesis, multiple internal rotations of methyl groups in planar five-membered ring systems have been investigated by a combination of Fourier transform microwave spectroscopy, group theory, and quantum chemical calculations. The molecular structures were determined by experimental rotational constants and compared to the results of quantum chemical calculations. The intramolecular dynamics and couplings of internal rotations were studied and supplemented by calculated transition states, potential energy curves and potential energy surfaces obtained by quantum chemistry. The results can be used in astrophysics and atmospheric chemistry as references.

First, a general tendency was found for the substitution of the heteroatom in planar ring molecules as shown in Figure 17.1. The torsional barriers increase in molecules with one and two methyl groups when sulfur is substituted with nitrogen or oxygen. This significant increase was already observed for the class of isothiazoles and isooxazoles [71]. Second, a tendency of decreasing torsional barriers was observed when the substituents were exchanged. The torsional barriers of the molecules 2,5-dimethylthiophene (**1**, see Chapter 10), 2,5-dimethylpyrrole (**2**, calculated at the MP2/6-311++G(d,p) level), and 2,5-dimethylfuran (**3**, see Chapter 11) with two methyl groups are higher than the ones of the molecules 2-methylthiophene (**4**) [20], 2-methylpyrrole (**5**, calculated at the MP2/6-311++G(d,p) level), and 2-methylfuran (**6**) [75] with one methyl group. A possible reason is a different electronic environment in the ring system due to the positive inductive effect of the second rotor. The reduced torsional barrier of the ring methyl groups in 2-acetyl-5-methylfuran (**7**, see Chapter 12) is a hint of this theory because the acetyl group as a substituent has a negative mesomeric as well as a negative inductive effect.

One the other hand, sometimes torsional barriers are unpredictable when only chemical intuition is applied as shown in Figure 17.2. Even though the torsional barriers in N-methylpyrrole (**8**) [72] and 2,5-dimethylpyrrole (**2**, calculated at the MP2/6-311++G(d,p) level) are known, the barriers in 1,2,5-trimethylpyrrole (**9**, see Chapter 14) are totally different and not comparable. Just due to a third methyl group added to 2,5-dimethylpyrrole (**2**), the torsional barriers of the two equivalent methyl groups are twice as high.

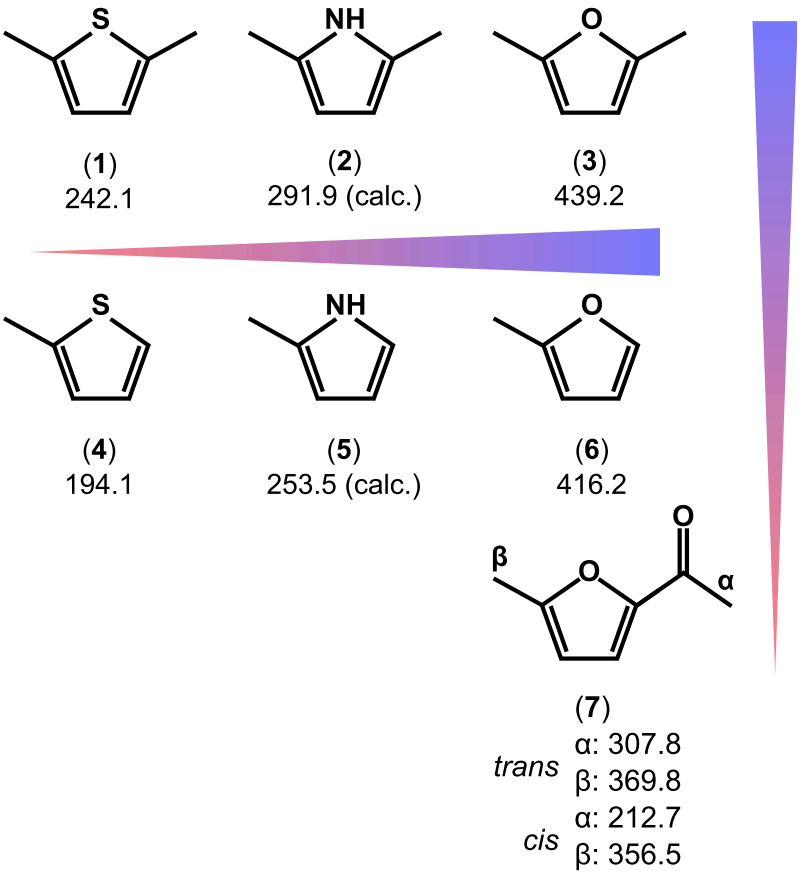

Figure 17.1. Tendencies of increasing torsional barriers (in cm^{-1}) from left to right and bottom up: 2,5-dimethylthiophene (**1**, see Chapter 10) , 2,5-dimethylpyrrole (**2**, calculated at the MP2/6-311++G(d,p) level), 2,5-dimethylfuran (**3**, see Chapter 11), 2-methylthiophene (**4**) [20], 2-methylpyrrole (**5**, calculated at the MP2/6-311++G(d,p) level), 2-methylfuran (**6**) [75], and 2-acetyl-5-methylfuran (**7**, see Chapter 12).

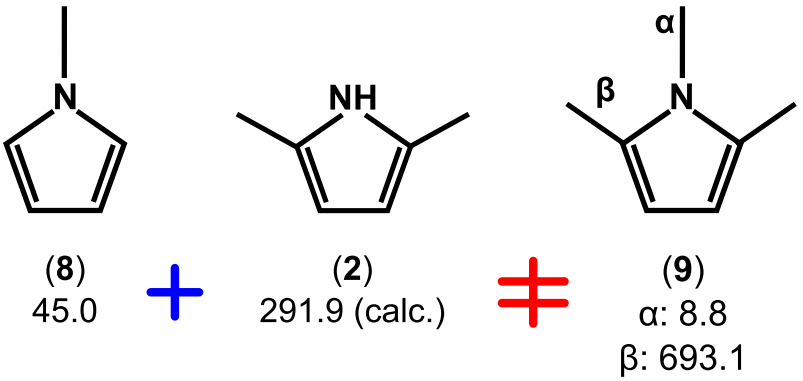

Figure 17.2. Unusual torsional barriers (in cm^{-1}) of 1,2,5-trimethylpyrrole (**9**, see Chapter 14) compared to N-methylpyrrole (**8**) [72] and 2,5-dimethylpyrrole (**2**, calculated at the MP2/6-311++G(d,p) level).

In the class of thiazoles (see Figure 17.3), the effect of coupled internal rotations was determined. The torsional barriers in 4,5-dimethylthiazole (**10**, see Chapter 13) are drastically smaller than the barriers in the monomethyl derivatives 4-methylthiazole (**12**) [117] and 5-methylthiazole (**13**) [118] just due to the coupling of the methyl groups. This effect was verified in the molecule 2,4-dimethylthiazole (**14**, preliminary results [135] as well as calculated at the MP2/6-311++G(d,p) level). Here, the torsional barriers are similar to the monomethyl derivatives 2-methylthiazole (**11**) [71] and 4-methylthiazole (**12**) [117]. The distance between the two methyl group is larger than in 4,5-dimethylthiazole (**10**). Therefore, the coupling between the internal rotors is smaller and the torsional barriers are less influenced.

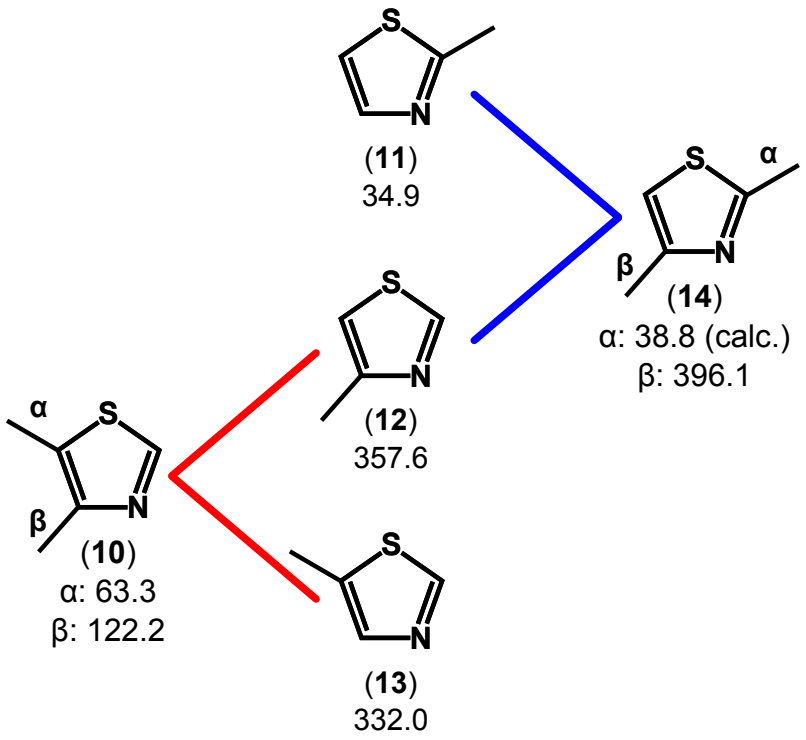

Figure 17.3. Left: Unusually small torsional barriers (in cm^{-1}) in 4,5-dimethylthiazole (**10**, see Chapter 13) due to the high coupling of the internal rotors when compared to 4-methylthiazole (**12**) [117] and 5-methylthiazole (**13**) [118]; right: similar torsional barriers (in cm^{-1}) in 2,4-dimethylthiazole (**14**, preliminary results [135] as well as calculated at the MP2/6-311++G(d,p) level) compared to 2-methylthiazole (**11**) [71] and 4-methylthiazole (**12**) [117].

To the best of my knowledge, the first molecule in microwave spectroscopy with four internal rotations was measured and assigned in this thesis. As shown in Figure 17.4, the bottom (β) methyl groups of 2,3,4,5-tetramethylthiophene (**16**, see Chapter 15) have similar torsional barriers as in the molecule 3-methylthiophene (**15**) [21]. On the other hand, the torsional barriers of the top (α) methyl groups are completely different than the ones of 2,5-dimethylthiophene (**1**, see Chapter 10) and 2-methylthiophene (**4**) [20]. However, a match of the torsional barriers of the top (α) methyl groups is found, when 2,3,4,5-tetramethylthiophene (**16**) is compared to 4,5-dimethylthiazole (**10**, see Chapter 13). Here, the α methyl groups of both molecules have the same direct surrounding and therefore similar barrier heights due to the high coupling between the methyl groups.

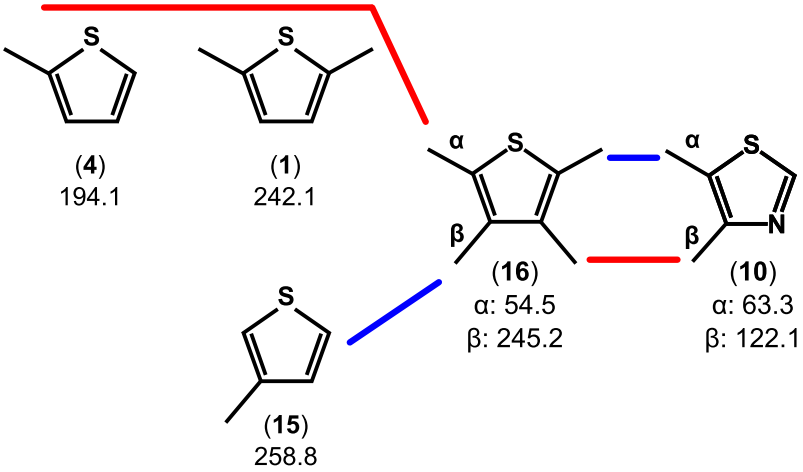

Figure 17.4. Center: 2,3,4,5-tetramethylthiophene (**16**, see Chapter 15) with similar torsional barriers (in cm^{-1}) of the bottom (β) methyl groups when compared to 3-methylthiophene (**15**) [21] but not when compared to 4,5-dimethylthiazole (**10**, see Chapter 13); unusual torsional barriers of the top (α) methyl groups when compared to 2,5-dimethylthiophene (**1**, see Chapter 10) and 2-methylthiophene (**4**) [20] but similar to the α methyl group of 4,5-dimethylthiazole (**10**, see Chapter 13).

All mentioned molecules are summarized in Figure 17.5 and their relations are marked by the same color.

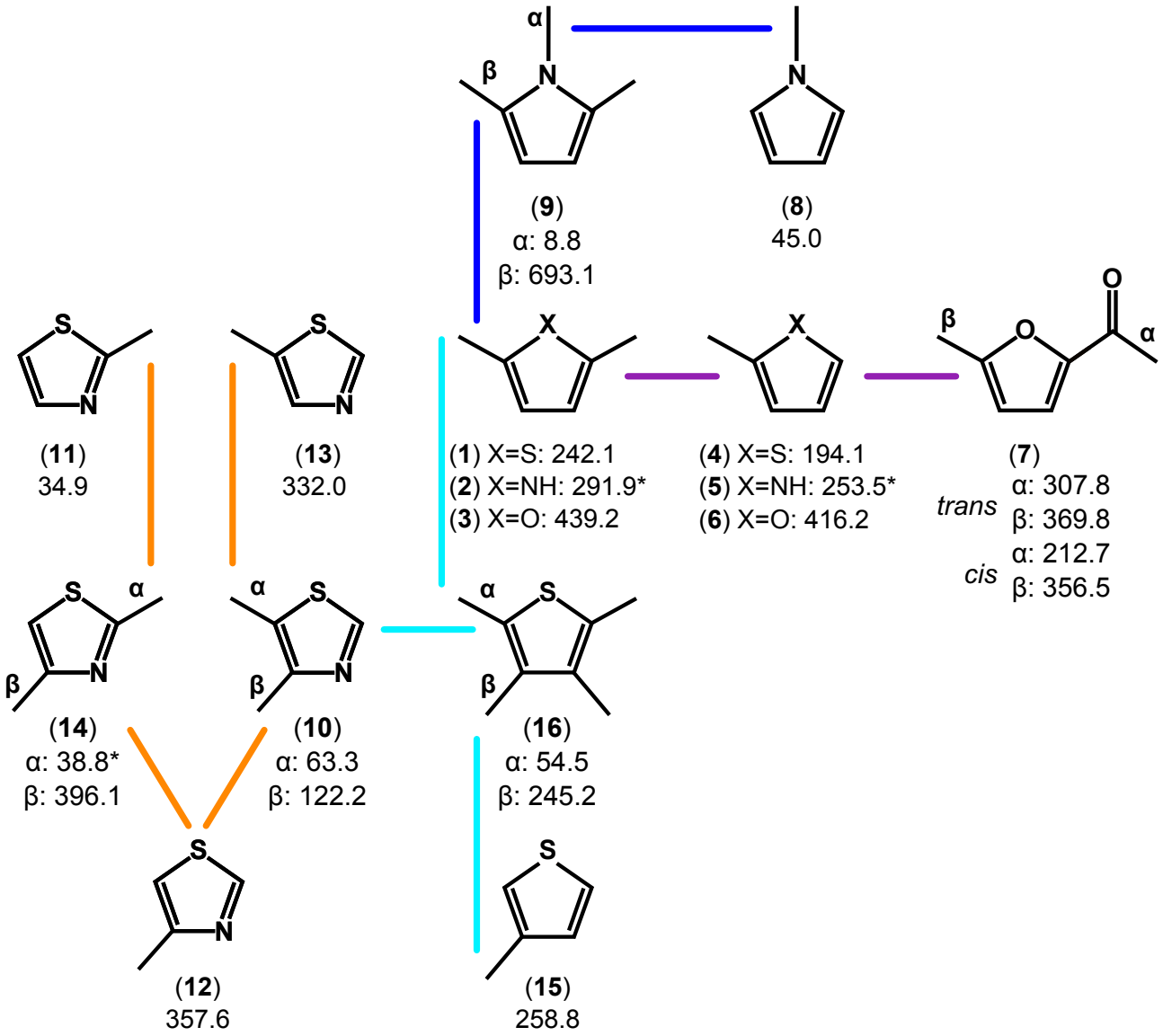

Figure 17.5. Torsional barriers (in cm^{-1}) of 2,5-dimethylthiophene (**1**, see Chapter 10) , 2,5-dimethylpyrrole (**2**, calculated at the MP2/6-311++G(d,p) level), 2,5-dimethylfuran (**3**, see Chapter 11), 2-methylthiophene (**4**) [20], 2-methylpyrrole (**5**, calculated at the MP2/6-311++G(d,p) level), 2-methylfuran (**6**) [75], 2-acetyl-5-methylfuran (**7**, see Chapter 12), N-methylpyrrole (**8**), 1,2,5-trimethylpyrrole (**9**, see Chapter 14), 4,5-dimethylthiazole (**10**, see Chapter 13), 2-methylthiazole (**11**) [71], 4-methylthiazole (**12**) [117], 5-methylthiazole (**13**) [118], 2,4-dimethylthiazole (**14**, preliminary results [135] or calculated at the MP2/6-311++G(d,p) level), 3-methylthiophene (**15**) [21], and 2,3,4,5-tetramethylthiophene (**16**, see Chapter 15). The stars mark calculated torsional barriers obtained at the MP2/6-311++G(d,p) level. Possible relations are given in the same color.

Bibliography

[1] C. Pérez, D. P. Zaleski, N. A. Seifert, B. Temelso, G. C. Shields, Z. Kisiel, B. H. Pate, *Angew. Chem. Int. Ed.* **2014,** *126,* 14596–14600.

[2] J.-U. Grabow, *Chemische Bindung und interne Dynamik in großen isolierten Molekülen: Rotationsspektroskopische Untersuchung;* Universität Hannover: 2004 Habilitation Dissertation.

[3] H. Mouhib, V. Van, W. Stahl, *J. Phys. Chem. A* **2013,** *117,* 6652–6656.

[4] M. Masuda, K.-I.-C. Nishimura, *J. Food Sci.* **1982,** *47,* 101–105.

[5] J. P. Walradt, A. O. Pittet, T. E. Kinlin, R. Muralidhara, A. Sanderson, *J. Agric. Food. Chem.* **1971,** *19,* 972–979.

[6] K. Umano, Y. Hagi, K. Nakahara, A. Shyoji, T. Shibamoto, *J. Agric. Food. Chem.* **1995,** *43,* 2212–2218.

[7] L. J. Farmer, D. S. Mottram, F. B. Whitfield, *J. Sci. Food Agric.* **1989,** *49,* 347–368.

[8] C. Fretz, S. Känel, J.-L. Luisier, R. Amadò, *Eur. Food Res. Technol.* **2005,** *221,* 504–510.

[9] Y. P. Zhao, J. M. Li, B. C. Zhang, Y. Yu, C. H. Shen, P. Song, *J. Inst. Brew.* **2012,** *118,* 315–324.

[10] G. J. Hartman, J. T. Carlin, J. D. Scheide, C. T. Ho, *J. Agric. Food. Chem.* **1984,** *32,* 1015–1018.

[11] V. Pace, P. Hoyos, L. Castoldi, P. Domínguez de María, A. R. Alcántara, *ChemSusChem* **2012,** *5,* 1369–1379.

[12] R. R. Peralta, M. Shimoda, Y. Osajima, *J. Agric. Food. Chem.* **1996,** *44,* 3606–3610.

[13] M. J. Cantalejo, *J. Agric. Food. Chem.* **1997,** *45,* 1853–1860.

[14] V. Garbusov, G. Rehfeld, G. Wölm, R. V. Golovnja, M. Rothe, *Mol. Nutr. Food Res.* **1976,** *20,* 235–241.

[15] T. Y. Chung, J. P. Eiserich, T. Shibamoto, *J. Agric. Food. Chem.* **1994,** *42,* 1743–1746.

[16] N. Yang, C. Liu, X. Liu, T. K. Degn, M. Munchow, I. Fisk, *Food Chem.* **2016,** *211,* 206–214.

[17] M. A. Gianturco, A. S. Giammarino, P. Friedel, V. Flanagan, *Tetrahedron* **1964,** *20,* 2951–2961.

[18] R. G. Buttery, R. M. Seifert, D. G. Guadagni, L. C. Ling, *J. Agric. Food. Chem.* **1971,** *19,* 524–529.

[19] D. S. Mottram, *J. Sci. Food Agric.* **1985,** *36,* 377–382.

[20] N. M. Pozdeev, L. N. Gunderova, A. A. Shapkin, *Opt. Spektrosk.* **1970,** *28*, 254–259.

[21] T. Ogata, K. Kozima, *J. Mol. Spectrosc.* **1972,** *42*, 38–46.

[22] U. Andresen, H. Dreizler, J. Grabow, W. Stahl, *Rev. Sci. Instrum.* **1990,** *61*, 3694–3699.

[23] J. Grabow, W. Stahl, H. Dreizler, *Rev. Sci. Instrum.* **1996,** *67*, 4072–4084.

[24] I. Merke, H. Dreizler, *Z. Naturforsch. A* **1994,** *49*, 490–496.

[25] SciFinder, SciFinder Scholar, version 2016; Chemical Abstracts Service: Columbus, OH, 2016 (accessed June 24, 2016); calculated using ACD/Labs software, V11.02; ACD/Labs 1994-2016.

[26] M. J. Frisch, G. W. Trucks, H. B. Schlegel, G. E. Scuseria, M. A. Robb, J. R. Cheeseman, G. Scalmani, V. Barone, B. Mennucci, G. A. Petersson, H. Nakatsuji, M. Caricato, X. Li, H. P. Hratchian, A. F. Izmaylov, J. Bloino, G. Zheng, J. L. Sonnenberg, M. Hada, M. Ehara, K. Toyota, R. Fukuda, J. Hasegawa, M. Ishida, T. Nakajima, Y. Honda, O. Kitao, H. Nakai, T. Vreven, J. A. Montgomery, Jr., J. E. Peralta, F. Ogliaro, M. Bearpark, J. J. Heyd, E. Brothers, K. N. Kudin, V. N. Staroverov, R. Kobayashi, J. Normand, K. Raghavachari, A. Rendell, J. C. Burant, S. S. Iyengar, J. Tomasi, M. Cossi, N. Rega, J. M. Millam, M. Klene, J. E. Knox, J. B. Cross, V. Bakken, C. Adamo, J. Jaramillo, R. Gomperts, R. E. Stratmann, O. Yazyev, A. J. Austin, R. Cammi, C. Pomelli, J. W. Ochterski, R. L. Martin, K. Morokuma, V. G. Zakrzewski, G. A. Voth, P. Salvador, J. J. Dannenberg, S. Dapprich, A. D. Daniels, Ö. Farkas, J. B. Foresman, J. V. Ortiz, J. Cioslowski, D. J. Fox, "Gaussian09 Revision E.01", Gaussian Inc. Wallingford CT 2009.

[27] H. Mouhib, W. Stahl, M. Lüthy, M. Büchel, P. Kraft, *Angew. Chem. Int. Ed.* **2011,** *50*, 5576–5580.

[28] H. B. Schlegel, *J. Comput. Chem.* **1982,** *3*, 214–218.

[29] W. Gordy, R. L. Cook, *Microwave molecular spectra;* Wiley: 1984.

[30] H. Dreizler, *Spektren und Molekülbau* **1968,** *10/1*, 59–155.

[31] J. K. Bragg, *Phys. Rev.* **1948,** *74*, 533.

[32] J. K. Bragg, S. Golden, *Phys. Rev.* **1949,** *75*, 735.

[33] H. Dreizler, H. D. Rudolph, H. Mäder, *Z. Naturforsch. A* **1970,** *25*, 25–35.

[34] C. H. Townes, A. L. Schawlow, *Microwave Spectroscopy;* volume 60 McGraw-Hill: 1955.

[35] J. Kraitchman, *Am. J. Phys* **1953,** *21*, 17–24.

[36] D. A. Lightner, J. E. Gurst, *Organic conformational analysis and stereochemistry from circular dichroism spectroscopy;* volume 23 John Wiley & Sons: 2000.

[37] D. Cremer, J. A. Pople, *J. Am. Chem. Soc.* **1975,** *97,* 1354–1358.

[38] D. Cremer, *Isr. J. Chem.* **1980,** *20,* 12–19.

[39] D. Cremer, *Quantum Chem. Program Exchange* **1975,** *288,* 1–8.

[40] C. Altona, M. Sundaralingam, *J. Am. Chem. Soc.* **1972,** *94,* 8205–8212.

[41] V. Van, C. Dindic, H. V. L. Nguyen, W. Stahl, *ChemPhysChem* **2015,** *16,* 291–294.

[42] J. L. Alonso, J. C. López, R. M. Villamañán, *J. Mol. Spectrosc.* **1987,** *126,* 348–355.

[43] L. Margulès, M. E. Sanz, S. Kassi, D. Petitprez, G. Wlodarczak, J. C. López, J. E. Boggs, *Chem. Phys.* **2001,** *263,* 19–31.

[44] S. Grimme, M. Steinmetz, *Phys. Chem. Chem. Phys.* **2013,** *15,* 16031–16042.

[45] H. Hartwig, H. Dreizler, *Z. Naturforsch. A* **1996,** *51,* 923–932.

[46] C. C. Costain, *Trans. Am. Crystallogr. Assoc* **1966,** *2,* 157–164.

[47] H. Dreizler, *Z. Naturforsch. A* **1961,** *16,* 1354–1367.

[48] V. Van, W. Stahl, H. V. L. Nguyen, *J. Mol. Struc.* **2016,** *1123,* 24–29.

[49] S. T. Shipman, J. L. Neill, R. D. Suenram, M. T. Muckle, B. H. Pate, *J. Phys. Chem. Lett.* **2011,** *2,* 443–448.

[50] J.-U. Grabow, S. Mata, J. L. Alonso, I. Peña, S. Blanco, J. C. López, C. Cabezas, *Phys. Chem. Chem. Phys.* **2011,** *13,* 21063–21069.

[51] T. Attig, L. W. Sutikdja, R. Kannengießer, I. Kleiner, W. Stahl, *J. Mol. Spectrosc.* **2013,** *284–285,* 8–15.

[52] O. Martinez, K. N. Crabtree, C. A. Gottlieb, J. F. Stanton, M. C. McCarthy, *Angew. Chem. Int. Ed.* **2015,** *54,* 1808–1811.

[53] D. F. Aycock, *Org. Process Res. Dev.* **2007,** *11,* 156–159.

[54] M. Smoleń, M. Kędziorek, K. Grela, *Catal. Commun.* **2014,** *44,* 80–84.

[55] Z.-Q. Duan, F. Hu, *J. Biotechnol.* **2013,** *163,* 45–49.

[56] Z. Kisiel, PROSPE-Programs for ROtational SPEctroscopy, http://info.ifpan.edu.pl/kisiel/prospe.htm.

[57] E. Fischer, *Ber. Dtsch. Chem. Ges.* **1894,** *27,* 2985–2993.

[58] L. M. Gregoret, S. D. Rader, R. J. Fletterick, F. E. Cohen, *Proteins* **1991,** *9,* 99–107.

[59] H. V. L. Nguyen, H. Mouhib, S. Klahm, W. Stahl, I. Kleiner, *Phys. Chem. Chem. Phys.* **2013,** *15,* 10012–10018.

[60] L. W. Sutikdja, D. Jelisavac, W. Stahl, I. Kleiner, *Mol. Phys.* **2012,** *110,* 2883–2893.

[61] H. Mouhib, W. Stahl, *ChemPhysChem* **2012,** *13,* 1297–1301.

[62] H. Mouhib, W. Stahl, *Chem. Biodivers.* **2014,** *11,* 1554–1566.

[63] E. Hirota, K. Sakieda, Y. Kawashima, *Phys. Chem. Chem. Phys.* **2010,** *12,* 8398–8404.

[64] Y. Zhao, H. Mouhib, W. Stahl, *J. Phys. Chem. A* **2012,** *117,* 311–314.

[65] H. V. L. Nguyen, R. Kannengießer, W. Stahl, *Phys. Chem. Chem. Phys.* **2012,** *14,* 11753–11758.

[66] G. Feng, Q. Gou, L. Evangelisti, W. Caminati, *Angew. Chem. Int. Ed.* **2014,** *53,* 530–534.

[67] M. J. Tubergen, A. R. Conrad, R. E. Chavez, I. Hwang, R. D. Suenram, J. J. Pajski, B. H. Pate, *J. Mol. Spectrosc.* **2008,** *251,* 330–338.

[68] C. Cabezas, I. Peña, A. M. Daly, J. L. Alonso, *Chem. Commun.* **2013,** *49,* 10826–10828.

[69] L. Maeztu, C. Sanz, S. Andueza, M. Paz de Pena, J. Bello, C. Cid, *J. Agric. Food. Chem.* **2001,** *49,* 5437–5444.

[70] V. Van, W. Stahl, H. V. L. Nguyen, *Phys. Chem. Chem. Phys.* **2015,** *17,* 32111–32114.

[71] J.-U. Grabow, H. Hartwig, N. Heineking, W. Jäger, H. Mäder, H. W. Nicolaisen, W. Stahl, *J. Mol. Struct.* **2002,** *612,* 349–356.

[72] W. Arnold, H. Dreizler, H. D. Rudolph, *Z. Naturforsch. A* **1968,** *23,* 301–306.

[73] H.-W. Nicolaisen, J.-U. Grabow, N. Heineking, W. Stahl, *Z. Naturforsch. A* **1991,** *46,* 635–638.

[74] E. Fliege, H. Dreizler, M. Meyer, K. Iqbal, J. Sheridan, *Z. Naturforsch. A* **1986,** *41,* 623–636.

[75] W. G. Norris, L. C. Krisher, *J. Chem. Phys.* **1969,** *51,* 403–406.

[76] T. Ogata, K. Kozima, *Bull. Chem. Soc. Jpn.* **1971,** *44,* 2344–2346.

[77] B. Bak, D. Christensen, L. Hansen-Nygaard, J. Rastrup-Andersen, *J. Mol. Spectrosc.* **1961,** *7,* 58–63.

[78] M. Tanabe, N. Kuze, H. Fujiwara, H. Takeuchi, S. Konaka, *J. Mol. Struct. THEOCHEM* **1995,** *372,* 173–180.

[79] D. Moran, A. C. Simmonett, F. E. Leach, W. D. Allen, P. v. R. Schleyer, H. F. Schaefer, *J. Am. Chem. Soc.* **2006,** *128,* 9342–9343.

[80] P. R. Bunker, P. Jensen, *Molecular symmetry and spectroscopy;* volume 2 NRC Research Press: 1998.

[81] G. S. Ezra, G. Berthier, M. J. S. Dewar, H. Fisher, K. Fukui, G. G. Hall, H. Hartmann, H. H. Jaffé, J. Jortner, W. Kutzelnigg, *Lecture Notes in Chemistry;* Springer: 1982.

[82] S. L. Altmann, N. O. Folland, *Phys. Today* **1979,** *32,* 73.

[83] P. Jensen, P. R. Bunker, *J. Mol. Spectrosc.* **1994,** *164,* 315–317.

[84] H. V. L. Nguyen, A. Jabri, V. Van, W. Stahl, *J. Phys. Chem. A* **2014,** *118,* 12130–12136.

[85] H. V. L. Nguyen, W. Stahl, *J. Mol. Spectrosc.* **2010,** *264,* 120–124.

[86] Y. Román-Leshkov, C. J. Barrett, Z. Y. Liu, J. A. Dumesic, *Nature* **2007,** *447,* 982–985.

[87] M. Chidambaram, A. T. Bell, *Green Chem.* **2010,** *12,* 1253–1262.

[88] T. Thananatthanachon, T. B. Rauchfuss, *Angew. Chem. Int. Ed.* **2010,** *49,* 6616–6618.

[89] J. B. Binder, R. T. Raines, *J. Am. Chem. Soc.* **2009,** *131,* 1979–1985.

[90] R. Ditchfield, W. J. Hehre, J. A. Pople, *J. Chem. Phys.* **1971,** *54,* 724–728.

[91] A. D. McLean, G. S. Chandler, *J. Chem. Phys.* **1980,** *72,* 5639–5648.

[92] G. A. Petersson, A. Bennett, T. G. Tensfeldt, M. A. Al-Laham, W. A. Shirley, J. Mantzaris, *J. Chem. Phys.* **1988,** *89,* 2193–2218.

[93] T. H. Dunning Jr, *J. Chem. Phys.* **1989,** *90,* 1007–1023.

[94] R. A. Kendall, T. H. Dunning Jr, R. J. Harrison, *J. Chem. Phys.* **1992,** *96,* 6796–6806.

[95] D. E. Woon, T. H. Dunning Jr, *J. Chem. Phys.* **1993,** *98,* 1358–1371.

[96] E. R. Davidson, *Chem. Phys. Lett.* **1996,** *260,* 514–518.

[97] A. Jabri, V. Van, H. V. L. Nguyen, W. Stahl, I. Kleiner, *ChemPhysChem* **2016,** *17,* 2660–2665.

[98] V. Van, W. Stahl, H. V. L. Nguyen, *ChemPhysChem* **2016,** *17,* 3228–3228.

[99] R. Kannengießer, S. Klahm, H. V. L. Nguyen, A. Lüchow, W. Stahl, *J. Chem. Phys.* **2014,** *141,* 204308.

[100] J.-U. Grabow, W. Stahl, *Z. Naturforsch. A* **1990,** *45,* 1043–1044.

[101] M. Tudorie, I. Kleiner, M. Jahn, J.-U. Grabow, M. Goubet, O. Pirali, *J. Phys. Chem. A* **2013,** *117,* 13636–13647.

[102] W. Fan, M. C. Qian, *J. Agric. Food. Chem.* **2006,** *54,* 2695–2704.

[103] V. Varlet, C. Knockaert, C. Prost, T. Serot, *J. Agric. Food. Chem.* **2006,** *54,* 3391–3401.

[104] D. Ryan, R. Shellie, P. Tranchida, A. Casilli, L. Mondello, P. Marriott, *J. Chromatogr. A* **2004,** *1054,* 57–65.

[105] Y. Zhao, J. Jin, W. Stahl, I. Kleiner, *J. Mol. Spectrosc.* **2012,** *281,* 4–8.

[106] D. Jelisavac, D. C. Cortés-Gómez, H. V. L. Nguyen, L. W. Sutikdja, W. Stahl, I. Kleiner, *J. Mol. Spectrosc.* **2009,** *257,* 111–115.

[107] H. V. L. Nguyen, H. Mouhib, W. Stahl, I. Kleiner, *Mol. Phys.* **2010,** *108,* 763–770.

[108] R. Kannengießer, M. J. Lach, W. Stahl, H. V. L. Nguyen, *ChemPhysChem* **2015,** *16,* 1906–1911.

[109] D. S. Wilcox, A. J. Shirar, O. L. Williams, B. C. Dian, *Chem. Phys. Lett.* **2011,** *508,* 10–16.

[110] H. V. L. Nguyen, V. Van, W. Stahl, I. Kleiner, *J. Chem. Phys.* **2014,** *140,* 214303.

[111] L. Tulimat, H. Mouhib, I. Kleiner, W. Stahl, *J. Mol. Spectrosc.* **2015,** *312,* 46–50.

[112] Y. Zhao, W. Stahl, H. V. L. Nguyen, *Chem. Phys. Lett.* **2012,** *545,* 9–13.

[113] R. Peter, H. Dreizler, *Z. Naturforsch. A* **1965,** *20,* 301–312.

[114] P. L. Lee, R. H. Schwendeman, *J. Mol. Spectrosc.* **1972,** *41,* 84–94.

[115] M. Tudorie, I. Kleiner, J. T. Hougen, S. Melandri, L. W. Sutikdja, W. Stahl, *J. Mol. Spectrosc.* **2011,** *269,* 211–225.

[116] L. Nygaard, E. Asmussen, J. H. Høg, R. C. Maheshwari, C. H. Nielsen, I. B. Petersen, J. Rastrup-Andersen, G. O. Sørensen, *J. Mol. Struct.* **1971,** *8,* 225–233.

[117] W. Jäger, H. Mäder, *Z. Naturforsch. A* **1987,** *42,* 1405–1409.

[118] W. Jäger, H. Mäder, *J. Mol. Struct.* **1988,** *190,* 295–305.

[119] E. Fliege, *Z. Naturforsch. A* **1990,** *45,* 911–922.

[120] V. M. Gaware, N. S. Dighe, S. R. Pattan, H. V. Shinde, D. S. Musmade, P. A. Chavan, P. Patel, *Pharm Lett* **2010,** *2,* 35–40.

[121] R. Kannengießer, W. Stahl, H. V. L. Nguyen, W. C. Bailey, *J. Mol. Spectrosc.* **2015,** *317,* 50–53.

[122] Y. Zhao, H. V. L. Nguyen, W. Stahl, J. T. Hougen, *J. Mol. Spectrosc.* **2015,** *318,* 91–100.

[123] R. F. Curl Jr, *J. Chem. Phys.* **1959,** *30,* 1529–1536.

[124] H. V. L. Nguyen, W. Stahl, I. Kleiner, *Mol. Phys.* **2012,** *110,* 2035–2042.

[125] H. V. L. Nguyen, A. Hermann, M. Schwell, W. Stahl, *J. Mol. Spectrosc.* to be published.

[126] H. V. L. Nguyen, M. Andresen, M. Schwell, W. Stahl, *Phys. Chem. Chem. Phys.* to be published.

[127] H. V. L. Nguyen, S. Katendahl, W. Stahl, *J. Mol. Spectrosc.* to be published.

[128] S. L. Baughcum, Z. Smith, E. B. Wilson, R. W. Duerst, *J. Am. Chem. Soc.* **1984,** *106,* 2260–2265.

[129] Y.-C. Chou, J. T. Hougen, *J. Chem. Phys.* **2006,** *124,* 74319–74319.

[130] K. M. Marstokk, H. Mollendal, S. Samdalb, *Acta Chem. Scand.* **1991,** *45,* 37–45.

[131] M. Oki, H. Nakanishi, *Bull. Chem. Soc. Jpn.* **1970,** *43,* 2558–2566.

[132] H. Mouhib, D. Jelisavac, L. W. Sutikdja, E. Isaak, W. Stahl, *J. Phys. Chem. A* **2010,** *115,* 118–122.

[133] A. Jabri, V. Van, H. V. L. Nguyen, H. Mouhib, F. K. Tchana, L. Manceron, W. Stahl, I. Kleiner, *A & A* **2016,** *589,* A127.

[134] P. Groner, C. W. Gillies, J. Z. Gillies, Y. Zhang, E. Block, *J. Mol. Spectrosc.* **2004,** *226,* 169–181.

[135] L. Hoppe Alvarez, *Internal Rotation and Quadrupole Coupling in 2,4-Dimethylthiazole;* RWTH Aachen University: 2016 Research Project.

Part III

Appendix

17.1 Structure Determination of Non-Planar Ring Molecules

17.1.1 2-Methyltetrahydrothiophene

Table 17.1. Nuclear coordinates in the principal inertial axes of conformer I and II of 2-methyltetrahydrothiophene (MTTP) calculated at the MP2/6-311++G(d,p) level of theory.

	Conformer I			**Conformer II**		
	a /Å	b /Å	c /Å	a /Å	b /Å	c /Å
S1	0.100312	−1.228195	−0.058861	−0.362058	−1.228047	0.085137
C2	−0.884851	0.285105	−0.395879	0.958919	−0.013852	0.486450
C3	−0.044450	1.438041	0.152108	0.245974	1.340263	0.607775
C4	1.408755	1.117958	−0.188526	−0.877714	1.350923	−0.429204
C5	1.644360	−0.314337	0.297355	−1.638544	0.044422	−0.214731
C6	−2.272826	0.187881	0.225067	2.055362	−0.015225	−0.576729
H7	1.838529	−0.327705	1.373329	−2.229155	−0.241339	−1.087936
H8	2.478812	−0.792205	−0.220430	−2.299087	0.123240	0.653645
H9	2.109907	1.815538	0.281868	−1.534614	2.218948	−0.308454
H10	1.547661	1.170628	−1.274421	−0.457992	1.377484	−1.440323
H11	−0.975084	0.393964	−1.482843	1.386192	−0.299748	1.452271
H12	−2.844015	1.097971	0.008783	2.863593	0.667019	−0.287032
H13	−2.831277	−0.665135	−0.171250	2.478167	−1.015939	−0.702607
H14	−2.192235	0.069384	1.309824	1.654908	0.300744	−1.544523
H15	−0.167983	1.483965	1.242033	0.956647	2.161422	0.461490
H16	−0.372333	2.393790	−0.272717	−0.191437	1.440339	1.608086

Table 17.2. The rotational constants A, B, and C (in GHz) and the dipole moment components in the principal axis system (in Debye) of conformer I of MTTP calculated using various method (HF, B3LYP, MP2, CCSD) and basis set combinations with the program GAUSSIAN03. Harmonic frequency calculations were also carried out for the cases of the HF, B3LYP, and MP2 methods to verify the nature of the stationary points. Deviations between the calculated and the experimental rotational constants (Dev. = exp. – calc.) are given in MHz.

Method/basis set	***A***	**Dev.**	***B***	**Dev.**	***C***	**Dev.**	μ_a	μ_b	μ_c
CCSD									
cc-pVTZ	4.225	0	2.798	−8	1.850	−1	−0.39	2.13	0.00
cc-pVDZ	4.142	83	2.762	28	1.824	25	−0.36	2.08	0.02
6-311++G(d,p)	4.200	26	2.784	6	1.840	9	−0.41	2.22	0.00
MP2									
cc-pVQZ	4.272	−46	2.824	−34	1.870	−22	−0.40	2.13	0.00
cc-pVTZ	4.248	−22	2.815	−25	1.863	−15	−0.40	2.12	0.00
cc-pVDZ	4.168	58	2.782	8	1.839	10	−0.36	2.07	0.02
6-311++G(3df,2pd)	4.268	−43	2.819	−29	1.869	−20	−0.40	2.14	0.00
6-311++G(d,p)	4.228	−3	2.803	−13	1.854	−6	−0.42	2.21	0.00
6-311+G(d,p)	4.228	−2	2.802	−12	1.854	−6	−0.42	2.20	0.01
6-311G(d,p)	4.224	1	2.805	−15	1.856	−7	−0.40	2.21	0.02
6-31++G(d,p)	4.218	7	2.805	−15	1.852	−4	−0.42	2.25	0.00
6-31+G(d,p)	4.215	10	2.806	−16	1.853	−5	−0.41	2.25	0.01
6-31G(d,p)	4.222	3	2.810	−19	1.855	−6	−0.39	2.19	0.02
B3LYP									
cc-pVQZ	4.198	27	2.772	18	1.830	19	−0.35	2.02	−0.02
cc-pVTZ	4.187	39	2.769	21	1.827	22	−0.34	1.99	−0.02
cc-pVDZ	4.137	88	2.752	38	1.814	34	−0.31	1.89	−0.01
6-311++G(3df,2pd)	4.202	24	2.772	18	1.830	18	−0.35	2.04	−0.02
6-311++G(d,p)	4.160	65	2.757	33	1.818	31	−0.36	2.11	−0.01
6-311+G(d,p)	4.161	64	2.757	33	1.818	31	−0.36	2.10	−0.01
6-311G(d,p)	4.160	66	2.758	32	1.818	30	−0.35	2.13	0.00
6-31++G(d,p)	4.151	75	2.751	39	1.814	34	−0.38	2.14	−0.01
6-31+G(d,p)	4.150	75	2.751	39	1.814	35	−0.38	2.14	−0.01
6-31G(d,p)	4.153	73	2.754	36	1.815	33	−0.35	2.10	0.00
HF									
6-311++G(3df,2pd)	4.263	−37	2.795	−5	1.850	−2	−0.38	2.17	−0.01
6-311++G(d,p)	4.232	−7	2.784	6	1.841	8	−0.40	2.25	0.00
6-311+G(d,p)	4.233	−7	2.784	6	1.840	8	−0.40	2.24	0.00
6-311G(d,p)	4.232	−7	2.785	5	1.841	7	−0.39	2.26	0.01
6-31++G(d,p)	4.227	−2	2.785	5	1.840	9	−0.41	2.27	−0.01
6-31+G(d,p)	4.226	−1	2.785	5	1.840	9	−0.41	2.28	−0.01
6-31G(d,p)	4.227	−2	2.785	5	1.839	9	−0.39	2.21	0.00
Experiment	**4.225**		**2.790**		**1.848**				

Table 17.3. The rotational constants A, B, and C (in GHz) and the dipole moment components in the principal axis system (in Debye) of conformer II of MTTP calculated using various method (HF, B3LYP, MP2, CCSD) and basis set combinations with the program GAUSSIAN03. Harmonic frequency calculations were also carried out for the cases of the HF, B3LYP, and MP2 methods to verify the nature of the stationary points. Deviations between the calculated and the experimental rotational constants (Dev. = exp. – calc.) are given in MHz.

Method/basis set	***A***	**Dev.**	***B***	**Dev.**	***C***	**Dev.**	μ_a	μ_b	μ_c
CCSD									
cc-pVTZ	3.790	0	3.018	−9	2.033	−2	0.12	2.14	0.04
cc-pVDZ	3.723	66	2.979	30	2.003	28	−0.08	1.84	−0.02
6-311++G(d,p)	3.775	15	2.999	10	2.017	14	0.09	2.24	0.05
MP2									
cc-pVQZ	3.823	−33	3.053	−45	2.060	−29	0.13	2.15	0.05
cc-pVTZ	3.803	−13	3.043	−34	2.052	−21	0.13	2.14	0.04
cc-pVDZ	3.742	48	3.005	3	2.022	9	0.13	2.09	0.03
6-311++G(3df,2pd)	3.817	−27	3.051	−42	2.060	−28	0.14	2.16	0.05
6-311++G(d,p)	3.796	−7	3.024	−15	2.036	−5	0.10	2.23	0.06
6-311+G(d,p)	3.798	−8	3.023	−14	2.035	−4	0.10	2.23	0.05
6-311G(d,p)	3.790	0	3.031	−23	2.041	−10	0.13	2.24	0.03
6-31++G(d,p)	3.797	−8	3.022	−13	2.030	1	0.10	2.27	0.06
6-31+G(d,p)	3.797	−7	3.022	−13	2.030	1	0.10	2.27	0.06
6-31G(d,p)	3.796	−6	3.030	−22	2.037	−6	0.12	2.21	0.04
B3LYP									
cc-pVQZ	3.783	7	2.976	33	2.002	30	−0.08	2.02	−0.04
cc-pVTZ	3.772	18	2.973	36	1.999	33	−0.08	2.00	−0.04
cc-pVDZ	3.729	61	2.958	51	1.987	44	−0.08	1.90	−0.03
6-311++G(3df,2pd)	3.784	6	2.977	32	2.003	28	−0.08	2.05	−0.04
6-311++G(d,p)	3.746	43	2.963	46	1.991	40	−0.09	2.12	−0.03
6-311+G(d,p)	3.747	43	2.962	46	1.991	40	−0.09	2.12	−0.03
6-311G(d,p)	3.745	45	2.965	44	1.992	39	−0.11	2.15	−0.03
6-31++G(d,p)	3.741	49	2.955	54	1.986	46	−0.08	2.15	−0.04
6-31+G(d,p)	3.740	50	2.955	53	1.986	46	−0.07	2.16	−0.04
6-31G(d,p)	3.737	53	2.961	47	1.990	41	−0.10	2.11	−0.01
HF									
6-311++G(3df,2pd)	3.843	−53	2.998	11	2.021	11	−0.06	2.19	−0.05
6-311++G(d,p)	3.813	−23	2.989	20	2.012	19	−0.06	2.27	−0.04
6-311+G(d,p)	3.814	−24	2.988	21	2.012	19	−0.06	2.26	−0.04
6-311G(d,p)	3.812	−22	2.991	18	2.014	17	−0.08	2.28	−0.03
6-31++G(d,p)	3.810	−20	2.989	20	2.010	21	−0.06	2.29	−0.05
6-31+G(d,p)	3.810	−20	2.989	19	2.011	20	−0.06	2.30	−0.05
6-31G(d,p)	3.808	−18	2.991	18	2.012	19	−0.07	2.23	−0.03
Experiment	**3.790**		**3.009**		**2.031**				

Table 17.4. Nuclear coordinates in the principal inertial axes of the transition states TS1 and TS2 of MTTP calculated at the MP2/6-311++G(d,p) level of theory.

	TS1			**TS2**		
	a /Å	b /Å	c /Å	a /Å	b /Å	c /Å
S1	−0.121582	−1.211045	−0.136156	0.277051	−1.231758	−0.287724
C2	0.860179	0.218609	0.424165	−0.965635	0.091394	−0.457240
C3	0.085397	1.476073	−0.026879	−0.160078	1.402153	−0.587017
C4	−1.403406	1.115662	−0.251942	1.217558	1.240883	0.108823
C5	−1.635581	−0.306200	0.274569	1.291696	−0.150388	0.755669
C6	2.285944	0.165494	−0.109994	−1.937200	0.123637	0.722501
H7	−2.493441	−0.788847	−0.199924	0.904689	−0.140590	1.778538
H8	−1.784867	−0.310958	1.359716	2.313351	−0.536922	0.778780
H9	−1.624006	1.128580	−1.322704	1.382201	2.021903	0.858253
H10	−2.074809	1.828875	0.237947	2.011092	1.324876	−0.638536
H11	0.883135	0.183233	1.520316	−1.517078	−0.108246	−1.381344
H12	2.847607	1.038748	0.238463	−2.680041	0.916472	0.575622
H13	2.809876	−0.732761	0.229729	−2.459623	−0.830331	0.829953
H14	2.279749	0.172323	−1.204447	−1.406501	0.329572	1.657946
H15	0.524171	1.850619	−0.957709	−0.734899	2.225494	−0.148742
H16	0.197167	2.262263	0.727861	−0.009981	1.633990	−1.645031

Table 17.5. The rotational constants A, B, and C in GHz and the characterizing angles $\varphi = \angle(C_5,C_4,C_3,C_2)$, $\gamma = \angle(S,C_2,C_5,C_4)$, and $\gamma' = \angle(S,C_5,C_2,C_3)$ of the transition state TS1 of MTTP calculated using various method (HF, B3LYP, MP2) and basis set combinations with the program GAUSSIAN03 and the Berny algorithm.

Method/Basis set	***A***	***B***	***C***	φ	γ	γ'
MP2						
cc-pVTZ	4.208	2.838	1.876	20.56	−135.16	−147.52
cc-pVDZ	4.153	2.794	1.845	17.33	−134.75	−145.21
6-311++G(3df,2pd)	4.226	2.843	1.882	20.64	−135.02	−147.46
6-311++G(d,p)	4.235	2.800	1.855	9.28	−135.43	−141.06
6-311+G(d,p)	4.237	2.799	1.854	8.63	−135.46	−140.70
6-311G(d,p)	4.235	2.801	1.855	8.82	−135.30	−140.67
6-31++G(d,p)	4.235	2.802	1.853	9.31	−136.03	−141.66
6-31+G(d,p)	4.233	2.803	1.854	10.14	−135.85	−141.98
6-31G(d,p)	4.243	2.804	1.855	7.78	−136.02	−140.73
B3LYP						
cc-pVQZ	4.165	2.791	1.839	18.37	−138.60	−149.50
cc-pVTZ	4.161	2.785	1.835	17.37	−138.36	−148.67
cc-pVDZ	4.118	2.765	1.821	16.94	−137.71	−147.77
6-311++G(3df,2pd)	4.172	2.790	1.840	17.85	−138.36	−148.97
6-311++G(d,p)	4.146	2.768	1.823	15.26	−137.91	−146.99
6-311+G(d,p)	4.143	2.768	1.823	15.79	−137.93	−147.32
6-311G(d,p)	4.144	2.768	1.823	15.27	−137.85	−146.94
6-31++G(d,p)	4.136	2.762	1.820	15.56	−137.89	−147.15
6-31+G(d,p)	4.131	2.764	1.821	16.40	−137.99	−147.74
6-31G(d,p)	4.136	2.764	1.820	15.27	−137.98	−147.06
HF						
6-311++G(3df,2pd)	4.237	2.809	1.858	17.01	−137.98	−148.12
6-311++G(d,p)	4.215	2.793	1.845	15.10	−137.93	−146.94
6-311+G(d,p)	4.212	2.794	1.845	15.71	−137.95	−147.32
6-311G(d,p)	4.217	2.793	1.845	14.73	−137.79	−146.58
6-31++G(d,p)	4.207	2.796	1.845	16.21	−138.23	−147.90
6-31+G(d,p)	4.205	2.797	1.846	16.54	−138.25	−148.11
6-31G(d,p)	4.205	2.797	1.846	16.24	−138.29	−147.97

Table 17.6. The rotational constants A, B, and C in GHz and the characterizing angles $\varphi = \angle(C_5,C_4,C_3,C_2)$, $\gamma = \angle(S,C_2,C_5,C_4)$, and $\gamma' = \angle(S,C_5,C_2,C_3)$ of the transition state TS2 of MTTP calculated using various method (HF, B3LYP, MP2) and basis set combinations with the program GAUSSIAN03 and the Berny algorithm.

Method/Basis set	***A***	***B***	***C***	φ	γ	γ'
MP2						
cc-pVTZ	3.550	3.123	2.185	−2.99	139.01	137.20
cc-pVDZ	3.486	3.085	2.156	−1.07	138.64	138.00
6-311++G(3df,2pd)	3.566	3.128	2.190	−3.75	139.27	137.00
6-311++G(d,p)	3.543	3.097	2.161	−2.75	140.07	138.41
6-311+G(d,p)	3.545	3.096	2.161	−3.01	140.05	138.24
6-311G(d,p)	3.533	3.111	2.172	−2.16	139.60	138.29
6-31++G(d,p)	3.557	3.087	2.149	−3.17	140.70	138.80
6-31+G(d,p)	3.549	3.092	2.156	−1.84	140.07	138.96
6-31G(d,p)	3.539	3.108	2.169	−0.86	139.42	138.90
B3LYP						
cc-pVQZ	3.538	3.046	2.120	2.25	140.75	142.09
cc-pVTZ	3.529	3.042	2.116	2.20	140.75	142.06
cc-pVDZ	3.482	3.029	2.107	2.96	140.13	141.89
6-311++G(3df,2pd)	3.540	3.047	2.122	1.73	140.73	141.76
6-311++G(d,p)	3.508	3.030	2.106	1.73	140.74	141.77
6-311+G(d,p)	3.509	3.029	2.105	1.47	140.79	141.67
6-311G(d,p)	3.505	3.033	2.108	1.70	140.66	141.67
6-31++G(d,p)	3.499	3.024	2.102	2.19	140.68	141.98
6-31+G(d,p)	3.498	3.023	2.102	2.35	140.64	142.03
6-31G(d,p)	3.497	3.029	2.106	2.02	140.55	141.75
HF						
6-311++G(3df,2pd)	3.603	3.064	2.135	−0.47	141.64	141.36
6-311++G(d,p)	3.577	3.052	2.123	−0.11	141.72	141.65
6-311+G(d,p)	3.578	3.051	2.122	−0.36	141.79	141.58
6-311G(d,p)	3.576	3.055	2.125	−0.36	141.72	141.51
6-31++G(d,p)	3.578	3.050	2.120	−0.40	141.97	141.73
6-31+G(d,p)	3.578	3.050	2.120	−0.45	141.99	141.72
6-31G(d,p)	3.580	3.050	2.119	−1.11	142.14	141.48

Table 17.7. Observed frequencies ($\nu_{\mathrm{Obs.}}$) of the main ^{32}S-isotopologue of conformer I of MTTP. $\nu_{\mathrm{Obs.}} - \nu_{\mathrm{Calc.}}$ values as obtained after a fit with XIAM.

J'	K_a'	K_c'	J	K_a	K_c	$\nu_{\mathrm{Obs.}}$	$\nu_{\mathrm{Obs.}} - \nu_{\mathrm{Calc.}}$
upper level			lower level			GHz	kHz
2	0	2	1	0	1	8.9425410	0.0
2	0	2	1	1	1	7.5073575	−1.8
2	1	1	1	1	0	10.2185097	−0.8
2	1	2	1	0	1	9.7703151	1.2
2	1	2	1	1	1	8.3351318	−0.4
2	2	0	1	1	1	15.8000157	2.1
2	2	1	1	1	0	14.5240421	−0.1
2	2	1	2	1	2	7.1306054	4.7
3	0	3	2	0	2	12.7858157	0.3
3	0	3	2	1	2	11.9580418	−0.7
3	1	2	2	1	1	15.0656000	−0.3
3	1	3	2	0	2	13.1483007	0.4
3	1	3	2	1	2	12.3205278	0.4
3	2	1	2	1	2	22.5094998	2.4
3	2	1	2	2	0	15.0446168	0.8
3	2	2	2	1	1	18.2207456	−0.4
3	2	2	2	2	1	13.9152137	−0.5
3	3	0	2	2	1	23.7074204	−1.3
3	3	0	3	2	1	8.3285255	0.5
3	3	1	2	2	0	23.2931534	−0.5
3	3	1	3	2	2	9.7122208	0.3
4	0	4	3	0	3	16.4068255	1.1
4	0	4	3	1	3	16.0443394	−0.2
4	1	3	3	1	2	19.5084708	0.0
4	1	3	3	2	2	16.3533238	−1.4
4	1	3	4	0	4	9.0342721	−1.1
4	1	3	4	1	4	8.9031161	1.0
4	1	4	3	0	3	16.5379833	0.7
4	1	4	3	1	3	16.1754986	0.9
4	2	2	3	2	1	20.4163981	−0.2
4	2	3	3	1	2	21.4404912	0.4
4	2	3	3	2	2	18.2853457	0.6
4	2	3	3	3	0	8.4931334	−4.3
4	2	3	4	1	4	10.8351357	0.7
4	3	1	3	3	0	19.4820728	−0.5
4	3	2	3	3	1	19.0483132	−0.7
4	3	2	4	2	3	10.4751893	0.0
4	4	0	4	3	1	12.4353106	−0.2
4	4	1	4	3	2	12.9333411	0.1
5	0	5	4	0	4	20.0318190	1.1
5	0	5	4	1	4	19.9006604	0.6
5	1	4	4	1	3	23.4281351	0.1
5	1	4	4	2	3	21.4961151	0.0
5	1	4	5	0	5	12.4305897	−0.6
5	1	4	5	1	5	12.3881688	5.9

Table 17.7. (continued)

J'	K'_a	K'_c	J	K_a	K_c	$\nu_{\mathrm{Obs.}}$	$\nu_{\mathrm{Obs.}} - \nu_{\mathrm{Calc.}}$
upper level			lower level			GHz	kHz
5	1	5	4	0	4	20.074246 0	0.7
5	1	5	4	1	4	19.943088 2	1.0
5	2	3	4	3	2	18.618996 8	0.0
5	2	3	5	1	4	7.598069 7	−1.3
5	2	4	4	1	3	24.389386 7	0.9
5	2	4	4	2	3	22.457365 9	0.1
5	2	4	5	0	5	13.391843 4	2.4
5	3	2	4	3	1	24.976025 8	−0.5
5	3	3	4	3	2	23.755462 7	0.4
5	3	3	5	1	4	12.734533 6	−2.9
5	3	3	5	2	4	11.773286 5	0.8
5	4	1	4	4	0	24.044541 2	−2.7
5	4	1	5	3	2	11.503827 4	−0.9
5	4	2	4	4	1	23.926498 3	−2.8
5	4	2	5	3	3	13.104378 7	−1.0
5	5	0	5	4	1	16.351140 1	−0.8
5	5	1	5	4	2	16.482118 0	−0.7
6	0	6	5	0	5	23.695980 8	0.3
6	0	6	5	1	5	23.653553 4	0.2
6	1	5	6	0	6	15.738359 4	2.4
6	1	5	6	1	6	15.725545 3	5.4
6	1	6	5	0	5	23.708798 2	0.6
6	1	6	5	1	5	23.666370 8	0.5
6	2	4	5	3	3	24.970901 7	1.5
6	2	4	6	1	5	10.701692 2	2.8
6	2	4	6	2	5	10.302214 8	−3.8
6	2	5	6	0	6	16.137827 4	−0.4
6	2	5	6	1	6	16.125009 9	−0.8
6	3	3	5	4	2	19.209106 0	−0.1
6	3	3	6	2	4	7.342584 7	−0.9
6	3	4	5	4	1	15.054901 3	−1.1
6	3	4	6	1	5	14.023827 7	−2.7
6	3	4	6	2	5	13.624360 7	1.0
6	4	2	6	3	3	10.221819 2	1.3
6	4	3	6	3	4	13.640077 5	−0.4
6	5	1	6	4	2	15.786819 6	−0.5
6	5	2	6	4	3	16.359695 4	−0.7
6	6	0	6	5	1	20.119227 2	0.5
6	6	1	6	5	2	20.148073 2	−0.8
7	1	6	7	0	7	18.895948 9	−0.4
7	1	6	7	1	7	18.892251 7	1.2
7	2	5	7	1	6	14.293067 7	−0.2
7	2	5	7	2	6	14.146424 9	−0.3
7	2	6	7	0	7	19.042589 3	−2.7
7	2	6	7	1	7	19.038891 4	−1.9
7	3	4	7	2	5	9.116988 5	−1.5

Table 17.7. (continued)

J'	K'_a	K'_c	J	K_a	K_c	$\nu_{\mathrm{Obs.}}$	$\nu_{\mathrm{Obs.}} - \nu_{\mathrm{Calc.}}$
upper level			lower level			GHz	kHz
7	3	4	7	3	5	7.3109116	−1.7
7	3	5	6	4	2	18.3713192	0.2
7	3	5	7	1	6	16.0991423	−2.4
7	3	5	7	2	6	15.9525001	−1.9
7	4	3	6	5	2	19.1407035	0.3
7	4	3	7	3	4	9.2159820	−0.3
7	4	4	6	5	1	17.2708696	4.0
7	4	4	7	2	5	16.4924441	0.7
7	4	4	7	3	5	14.6863658	−0.9
7	5	2	7	4	3	14.6996154	−0.1
7	5	3	7	4	4	16.3764220	−0.2
7	6	1	7	5	2	19.7737837	0.2
7	6	2	7	5	3	19.9317224	1.1
7	7	0	7	6	1	23.8377930	4.9
7	7	1	7	6	2	23.8434940	−5.3
8	1	7	8	0	8	21.9644052	0.4
8	2	6	8	1	7	17.8429420	−0.8
8	2	7	8	1	8	22.0129910	−1.9
8	3	5	8	2	6	12.1334361	−1.0
8	3	5	8	3	6	11.3042062	0.0
8	3	6	7	4	3	20.1877104	−1.2
8	3	6	8	2	7	18.6225523	−0.5
8	4	4	8	3	5	9.1942402	−0.2
8	4	5	7	5	2	21.7917741	−0.5
8	4	5	8	2	6	17.1329092	−0.3
8	4	5	8	3	6	16.3036778	−0.7
8	5	3	7	6	2	19.3649214	0.9
8	5	4	7	6	1	18.7275439	−2.2
8	5	4	8	4	5	16.7095536	−1.4
8	6	2	8	5	3	19.1107910	0.5
8	6	3	8	5	4	19.7040769	0.1
8	7	1	8	6	2	23.5790939	0.5
8	7	2	8	6	3	23.6163325	−0.7
9	1	8	9	0	9	24.9928894	0.7
9	2	7	9	1	8	21.1762221	−1.1
9	2	8	9	1	9	25.0084761	2.1
9	3	6	9	2	7	15.8722925	0.2
9	3	7	8	4	4	20.1367523	−2.2
9	4	5	9	3	6	10.5797551	−1.2
9	4	5	9	4	6	7.6663941	−0.5
9	4	6	9	3	7	18.4511756	−0.5
9	5	4	9	4	5	11.6949173	0.9
9	5	5	8	6	2	23.8555362	2.6
9	5	5	9	4	6	17.5247694	−1.1
9	6	3	9	5	4	17.9189939	−0.4
9	6	4	8	7	1	19.8557185	−0.4

Table 17.7. (continued)

J'	K'_a	K'_c	J	K_a	K_c	$\nu_{\text{Obs.}}$	$\nu_{\text{Obs.}} - \nu_{\text{Calc.}}$
upper level			lower level			GHz	kHz
9	6	4	9	5	5	19.5792800	1.3
9	7	2	9	6	3	23.1519528	1.1
9	7	3	9	6	4	23.3200859	0.9
10	5	5	10	4	6	11.1434234	0.1
11	5	6	11	4	7	12.0564285	1.8
13	6	7	13	5	8	13.6045134	1.6

Table 17.8. Observed frequencies ($\nu_{\text{Obs.}}$) of the ^{34}S-isotopologue of conformer I of MTTP. $\nu_{\text{Obs.}} - \nu_{\text{Calc.}}$ values as obtained after a fit with XIAM.

J'	K'_a	K'_c	J	K_a	K_c	$\nu_{\text{Obs.}}$	$\nu_{\text{Obs.}} - \nu_{\text{Calc.}}$
upper level			lower level			GHz	kHz
2	0	2	1	0	1	8.8728699	0.7
2	1	1	1	1	0	10.1975116	−1.4
2	1	2	1	0	1	9.6093919	0.2
2	1	2	1	1	1	8.2753475	−1.9
2	2	0	1	1	1	15.5242749	2.0
2	2	1	1	1	0	14.1996270	−0.2
3	0	3	2	1	2	11.9121873	0.9
3	1	2	2	1	1	15.0057603	−0.1
3	1	3	2	0	2	12.9526927	−0.6
3	1	3	2	1	2	12.2161700	−0.8
3	2	1	2	1	2	22.3094782	2.8
3	2	1	2	2	0	15.0605515	−0.3
3	2	2	2	1	1	17.8567424	−0.7
3	2	2	2	2	1	13.8546284	−0.4
3	3	0	2	2	1	23.2179673	−0.8
3	3	0	3	2	1	7.7938498	−4.1
3	3	1	2	2	0	22.7607573	0.0
4	0	4	3	0	3	16.2224502	0.8
4	0	4	3	1	3	15.9184649	0.0
4	1	3	3	1	2	19.3665442	−0.1
4	1	3	3	2	2	16.5155624	0.8
4	1	4	3	0	3	16.3258296	−0.2
4	1	4	3	1	3	16.0218451	−0.2
4	2	2	3	2	1	20.4103917	0.8
4	2	3	3	1	2	21.0308039	−1.1
4	2	3	4	1	4	10.6817980	1.9
4	3	2	3	3	1	19.0016195	0.1
4	3	2	4	2	3	10.0914903	2.2
4	4	0	4	3	1	11.6957631	−2.2
4	4	1	4	3	2	12.2692185	−4.6
5	0	5	4	0	4	19.8136345	1.2
5	0	5	4	1	4	19.7102538	0.9
5	1	4	4	1	3	23.1804253	0.7
5	1	4	4	2	3	21.5161635	−0.4

Table 17.8. (continued)

J'	K'_a	K'_c	J	K_a	K_c	$\nu_{\mathrm{Obs.}}$	$\nu_{\mathrm{Obs.}} - \nu_{\mathrm{Calc.}}$
upper level			lower level			GHz	kHz
5	1	5	4	0	4	19.8450929	0.6
5	1	5	4	1	4	19.7417121	0.2
5	2	3	4	3	2	19.1320648	−2.9
5	2	3	5	1	4	7.7073925	0.6
5	2	4	4	2	3	22.2932883	0.4
5	3	2	4	4	1	13.3615924	−1.2
5	3	3	5	2	4	11.4728854	−0.8
5	4	1	5	3	2	10.6939510	1.3
5	4	2	5	3	3	12.4831631	−0.1
5	5	0	5	4	1	15.4398760	1.1
5	5	1	5	4	2	15.6030277	1.9
6	0	6	5	0	5	23.4433305	1.8
6	1	5	6	0	6	15.7332045	−3.5
6	1	6	5	1	5	23.4208163	0.6
6	2	4	6	1	5	10.9265919	−1.6
6	2	5	6	1	6	16.0263586	1.6
6	3	4	5	4	1	15.5059202	−2.4
6	3	4	6	2	5	13.4150910	2.4
6	4	2	6	3	3	9.4229843	−2.0
6	5	1	6	4	2	14.7949650	0.4
6	5	2	6	4	3	15.4933278	−2.9
6	6	0	6	5	1	19.0273629	1.7
6	6	1	6	5	2	19.0661038	−0.1
7	1	6	7	0	7	18.8373488	−0.1
7	2	5	7	1	6	14.5068283	−1.1
7	2	6	7	1	7	18.9388989	2.5
7	3	4	7	2	5	9.2748517	−2.4
7	3	5	7	2	6	15.8202640	−1.7
7	4	4	7	3	5	14.2721971	−0.9
7	5	2	7	4	3	13.5924591	−1.0
7	5	3	7	4	4	15.5629634	−0.2
7	6	1	7	5	2	18.6313579	−0.5
8	2	6	8	1	7	17.9659376	2.8
8	3	5	8	2	6	12.5144937	−1.8
8	3	6	8	2	7	18.5381169	−0.2
8	4	5	8	3	6	16.0262870	−1.0
8	5	4	8	4	5	16.0040728	2.5
8	6	2	8	5	3	17.8588101	−2.5
8	6	3	8	5	4	18.6249055	1.7
9	4	5	9	3	6	10.7453992	2.4
9	5	4	9	4	5	10.7704088	0.5

Table 17.9. Observed frequencies ($\nu_{\text{Obs.}}$) of the ^{32}S-isotopologue of conformer II of MTTP. $\nu_{\text{Obs.}} - \nu_{\text{Calc.}}$ values as obtained after a fit with XIAM.

J'	K'_a	K'_c	J	K_a	K_c	$\nu_{\text{Obs.}}$	$\nu_{\text{Obs.}} - \nu_{\text{Calc.}}$
upper level			lower level			GHz	kHz
2	0	2	1	0	1	9.566 966 0	−0.3
2	0	2	1	1	1	8.785 687 7	−0.3
2	1	2	1	0	1	9.883 302 0	0.2
2	1	2	1	1	1	9.102 022 5	−1.0
2	2	0	1	1	1	14.890 827 8	0.4
2	2	1	1	1	0	13.400 809 8	0.7
3	0	3	2	0	2	13.612 874 9	0.2
3	0	3	2	1	2	13.296 540 3	1.1
3	1	2	2	1	1	16.119 719 2	0.2
3	1	2	2	2	1	13.775 894 4	−1.0
3	1	3	2	0	2	13.701 173 1	1.7
3	1	3	2	1	2	13.384 835 9	0.0
3	2	1	2	1	2	22.414 388 7	0.6
3	2	1	2	2	0	16.625 583 0	−1.2
3	2	2	2	1	1	17.463 061 6	−0.7
3	2	2	3	1	3	7.010 670 3	−1.3
3	3	0	2	2	1	21.934 983 8	−1.4
3	3	1	2	2	0	21.224 899 7	−0.8
4	0	4	3	0	3	17.599 027 3	−0.2
4	0	4	3	1	3	17.510 731 1	0.3
4	1	3	3	1	2	20.525 654 1	0.1
4	1	3	3	2	2	19.182 309 8	−0.8
4	1	3	4	0	4	8.682 253 1	1.6
4	1	4	3	0	3	17.619 242 1	0.4
4	1	4	3	1	3	17.530 945 4	0.5
4	2	2	3	3	1	17.629 989 0	1.0
4	2	3	3	1	2	21.075 373 4	−0.1
4	2	3	4	1	4	9.211 756 8	0.0
4	3	2	3	2	1	25.431 290 2	1.1
4	3	2	4	2	3	7.718 141 4	1.8
4	4	0	4	3	1	7.325 488 9	−3.0
4	4	1	4	3	2	8.375 623 2	−1.2
5	0	5	4	1	4	21.612 784 9	0.2
5	1	4	4	2	3	23.919 462 2	−0.6
5	1	4	5	0	5	11.518 437 1	2.2
5	1	5	4	0	4	21.637 161 7	0.3
5	2	3	4	3	2	24.031 426 5	−0.5
5	2	3	5	1	4	7.830 103 9	0.1
5	2	4	4	1	3	24.637 603 8	−0.2
5	2	4	5	1	5	11.682 695 3	1.3
5	3	3	5	2	4	9.424 356 7	0.3
5	4	2	5	3	3	8.890 853 3	0.3
5	5	0	5	4	1	9.969 706 6	−1.3
5	5	1	5	4	2	10.434 543 2	1.0
6	1	5	6	0	6	14.224 776 3	−0.3

Table 17.9. (continued)

J'	K'_a	K'_c	J	K_a	K_c	$\nu_{\mathrm{Obs.}}$	$\nu_{\mathrm{Obs.}} - \nu_{\mathrm{Calc.}}$
upper level			lower level			GHz	kHz
6	2	4	6	1	5	10.9275969	−0.1
6	2	5	6	1	6	14.2671467	−1.1
6	3	4	6	2	5	11.6114327	0.8
6	4	3	6	3	4	9.9985762	−0.6
6	5	1	6	4	2	8.8813102	1.1
6	5	2	6	4	3	10.5128959	0.9
6	6	0	6	5	1	12.4979669	2.6
6	6	1	6	5	2	12.6671771	0.2
7	1	6	7	0	7	16.8769528	−0.1
7	2	5	7	1	6	13.8573841	−0.8
7	2	6	7	1	7	16.8867412	−1.0
7	3	4	7	2	5	9.8787861	−0.5
7	3	5	7	2	6	14.0818782	−1.2
7	4	4	7	3	5	11.7225415	−0.5
7	5	2	7	4	3	7.5628245	−1.4
7	5	3	7	4	4	11.0373653	0.2
7	6	2	7	5	3	12.4865854	−0.3
8	1	7	8	0	8	19.5118261	1.0
8	2	6	8	1	7	16.6128421	0.5
8	3	6	8	2	7	16.6751425	−0.1
8	4	5	8	3	6	13.9291316	0.1
8	5	4	8	4	5	12.1789417	−0.6
8	6	2	8	5	3	10.2907756	1.1
8	6	3	8	5	4	12.5488548	−0.7
8	7	1	8	6	2	14.3647054	−0.7
9	2	7	9	1	8	19.2911571	−0.5
9	3	7	9	2	8	19.3067002	0.9
9	4	5	9	3	6	11.9188357	−1.3
9	5	5	9	4	6	13.9442130	−0.6
9	6	4	9	5	5	13.0990665	1.0
9	7	2	9	6	3	13.2775427	−0.7
11	6	5	11	5	6	9.4321516	1.6

17.1.2 2-Methyltetrahydrofuran

Table 17.10. Nuclear coordinates in the principal inertial axes of the stable conformers and the transition states of 2-methyltetrahydrofuran (MTHF) calculated at the MP2/6-311++G(d,p) level of theory. The atoms are numbered according to Figure 6.1.

	***equatorial* conformer**			***axial* conformer**		
	a /Å	b /Å	c /Å	a /Å	b /Å	c /Å
O1	0.042233	−1.078513	−0.164183	0.012577	−1.093290	−0.137344
C2	0.723104	0.054846	0.371842	0.746236	0.008047	0.403309
C3	−0.106556	1.234211	−0.132217	−0.113469	1.261819	0.113807
C4	−1.545881	0.703287	0.000489	−1.497119	0.684084	−0.263103
C5	−1.352061	−0.834856	0.029800	−1.351707	−0.791461	0.121616
C6	2.164577	0.020354	−0.087965	2.127568	0.023190	−0.217049
H7	0.673774	0.017865	1.474567	0.823760	−0.133716	1.493636
H8	0.068557	2.152838	0.434577	−0.164302	1.909989	0.993051
H9	0.148147	1.411784	−1.182315	0.313665	1.842302	−0.709221
H10	−2.005424	1.051441	0.929629	−2.324782	1.174843	0.255401
H11	−2.179457	1.022962	−0.829954	−1.665769	0.764721	−1.339871
H12	−1.668013	−1.249319	0.996701	−1.574339	−0.940080	1.190235
H13	−1.885751	−1.354584	−0.768542	−1.965380	−1.472960	−0.470324
H14	2.703101	0.894308	0.291373	2.716373	0.849731	0.192998
H15	2.663421	−0.882132	0.274424	2.651515	−0.914572	−0.014393
H16	2.202297	0.027260	−1.181188	2.043293	0.153364	−1.299967

	Transition state $^2\mathbf{T}_3$			**Transition state $\mathbf{E}_1$**		
	a /Å	b /Å	c /Å	a /Å	b /Å	c /Å
O1	0.068453	−1.138123	−0.408443	0.009489	−1.058221	−0.562626
C2	−0.811110	−0.012215	−0.511110	−0.799296	0.121435	−0.504710
C3	0.126949	1.195253	−0.541531	0.197075	1.281086	−0.299760
C4	1.202621	0.781567	0.471668	1.448063	0.599973	0.308407
C5	1.261250	−0.746375	0.290262	1.044574	−0.881434	0.399719
C6	−1.801428	0.018739	0.648003	−1.834258	0.032801	0.612495
H7	−1.352665	−0.134495	−1.454546	−1.304949	0.182910	−1.472574
H8	0.562305	1.292285	−1.541050	0.440059	1.749506	−1.256551
H9	−0.375837	2.130949	−0.282348	−0.220950	2.049817	0.356181
H10	2.167989	1.255694	0.279124	2.309097	0.720624	−0.352979
H11	0.894607	1.043576	1.487509	1.712225	1.008213	1.287287
H12	2.115800	−1.051329	−0.322445	1.850729	−1.570469	0.140784
H13	1.313278	−1.273006	1.249396	0.681110	−1.129481	1.406198
H14	−2.509415	0.845395	0.524083	−2.501490	0.900224	0.574747
H15	−2.360286	−0.920019	0.684306	−2.431332	−0.876644	0.504234
H16	−1.283576	0.145418	1.604037	−1.353762	0.021195	1.596241

Table 17.11. The rotational constants A, B, and C in GHz, the deviations (Dev.) between the experimental and calculated rotational constants in MHz and the barrier to internal rotation V_3 of MTHF in cm^{-1} calculated using various methods and basis sets. Harmonic frequency calculations were carried out to verify the nature of the stationary points.

Method/Basis set	A	Dev.	B	Dev.	C	Dev.	V_3
CCSD(T)/cc-pVTZ[a]	6.649	−58	3.172	−2	2.367	0	1070
CCSD/cc-pVDZ	6.516	75	3.170	1	2.381	−14	
CCSD/6-311++G(d,p)	6.628	−37	3.160	10	2.357	10	
MP2/cc-pVQZ	6.672	−80	3.208	−38	2.396	−29	
MP2/cc-pVTZ	6.675	−84	3.196	−26	2.385	−17	1116
MP2/cc-pVDZ	6.520	72	3.188	−17	2.398	−31	
MP2/6-311++G(3df,2pd)	6.673	−81	3.197	−27	2.387	−20	1109
MP2/6-311++G(d,p)	6.649	−58	3.172	−2	2.367	0	1142
MP2/6-311+G(d,p)	6.648	−57	3.172	−2	2.367	0	1152
MP2/6-311G(d,p)	6.657	−65	3.180	−9	2.374	−7	1138
MP2/6-31++G(d,p)	6.619	−28	3.178	−8	2.384	−17	1183
MP2/6-31+G(d,p)	6.610	−18	3.181	−10	2.388	−21	1195
MP2/6-31G(d,p)	6.617	−25	3.195	−25	2.398	−31	1276
M06-2X/cc-pVQZ	6.641	−50	3.203	−33	2.392	−25	1089
M06-2X/cc-pVTZ	6.640	−48	3.201	−31	2.390	−23	1067
M06-2X/cc-pVDZ	6.593	−1	3.194	−24	2.386	−19	1099
M06-2X/6-311++G(3df,2pd)	6.641	−49	3.200	−30	2.390	−23	1080
M06-2X/6-311++G(d,p)	6.618	−27	3.191	−20	2.382	−15	1077
M06-2X/6-311+G(d,p)	6.617	−25	3.191	−21	2.383	−15	1087
M06-2X/6-311G(d,p)	6.606	−14	3.203	−32	2.405	−38	1093
M06-2X/6-31++G(d,p)	6.605	−13	3.185	−15	2.379	−12	1089
M06-2X/6-31+G(d,p)	6.604	−13	3.185	−15	2.379	−12	1093
M06-2X/6-31G(d,p)	6.608	−16	3.193	−22	2.383	−16	1106
B3LYP/cc-pVQZ	6.591	1	3.168	3	2.363	4	1025
B3LYP/cc-pVTZ	6.590	2	3.166	4	2.361	6	1017
B3LYP/cc-pVDZ	6.528	64	3.159	12	2.358	9	
B3LYP/6-311++G(3df,2pd)	6.594	−2	3.165	6	2.360	7	1020
B3LYP/6-311++G(d,p)	6.566	25	3.153	18	2.352	16	1032
B3LYP/6-311+G(d,p)	6.563	29	3.153	17	2.352	15	1040
B3LYP/6-311G(d,p)	6.549	43	3.166	4	2.373	−6	1057
B3LYP/6-31++G(d,p)	6.544	48	3.147	24	2.348	19	1049
B3LYP/6-31+G(d,p)	6.544	47	3.146	24	2.348	19	1049
B3LYP/6-31G(d,p)	6.554	38	3.156	14	2.353	14	1089
HF/6-311++G(3df,2pd)	6.699	−107	3.213	−43	2.412	−45	1265
HF/6-311++G(d,p)	6.680	−89	3.202	−31	2.402	−35	1268
HF/6-311+G(d,p)	6.681	−90	3.201	−31	2.402	−35	1272
HF/6-311G(d,p)	6.660	−68	3.211	−41	2.412	−45	1280
HF/6-31++G(d,p)	6.671	−79	3.200	−29	2.402	−34	1251
HF/6-31+G(d,p)	6.670	−78	3.200	−29	2.402	−34	1254
HF/6-31G(d,p)	6.665	−74	3.207	−37	2.407	−40	1278
Experiment	**6.592**		**3.170**		**2.367**		

[a] Single point calculations using the optimized structures calculated at the MP2/6-311++G(d,p) level.

Table 17.12. Observed frequencies ($\nu_{\text{Obs.}}$) of the main isotopologue of MTHF. $\nu_{\text{Obs.}} - \nu_{\text{Calc.}}$ values as obtained after a fit with XIAM.

J'	K_a'	K_c'	J	K_a	K_c	$\nu_{\text{Obs.}}$	$\nu_{\text{Obs.}} - \nu_{\text{Calc.}}$
upper level			lower level			GHz	kHz
1	1	0	0	0	0	9.761 934 5	1.9
1	1	1	0	0	0	8.958 679 9	−1.2
2	0	2	1	0	1	10.949 409 4	0.3
2	1	1	1	0	1	16.102 661 6	2.2
2	1	1	1	1	0	11.878 210 1	−1.7
2	1	2	1	0	1	13.692 906 8	−0.8
2	1	2	1	1	1	10.271 709 8	−1.7
2	2	0	1	1	0	22.267 319 4	−0.7
2	2	0	1	1	1	23.070 572 7	1.1
2	2	0	2	1	1	10.389 106 9	−1.5
2	2	0	2	1	2	12.798 862 9	2.7
2	2	1	1	1	0	22.141 767 7	0.5
2	2	1	1	1	1	22.945 019 0	0.2
2	2	1	2	1	1	10.263 555 3	−0.2
2	2	1	2	1	2	12.673 310 1	2.8
3	0	3	2	0	2	16.129 290 3	1.5
3	0	3	2	1	1	10.976 036 3	−2.2
3	0	3	2	1	2	13.385 790 6	0.3
3	1	2	2	0	2	22.884 926 6	2.4
3	1	2	2	1	1	17.731 673 7	−0.1
3	1	3	2	0	2	18.077 877 2	0.7
3	1	3	2	1	2	15.334 379 7	1.7
3	2	1	2	2	0	17.095 553 8	−1.6
3	2	1	3	1	2	9.752 987 5	−2.5
3	2	1	3	1	3	14.560 039 1	1.4
3	2	2	2	2	1	16.612 420 9	−0.4
3	2	2	3	1	2	9.144 302 2	−0.7
3	2	2	3	1	3	13.951 352 7	2.1
3	3	0	3	2	1	18.590 871 3	−0.2
3	3	0	3	2	2	19.199 559 5	1.0
3	3	1	3	2	1	18.578 421 6	−2.4
3	3	1	3	2	2	19.187 110 3	−0.7
4	0	4	3	0	3	21.044 000 9	2.5
4	0	4	3	1	2	14.288 362 2	−0.9
4	0	4	3	1	3	19.095 411 6	0.8
4	1	3	3	1	2	23.464 814 8	0.2
4	1	3	3	2	1	13.711 825 2	0.6
4	1	3	3	2	2	14.320 511 2	−0.4
4	1	3	4	0	4	9.176 450 7	−0.8
4	1	4	3	0	3	22.273 880 3	2.3
4	1	4	3	1	3	20.325 292 7	2.4
4	2	2	3	2	1	23.156 458 0	−0.7
4	2	2	4	1	3	9.444 631 9	−2.2
4	2	2	4	1	4	17.391 205 8	−0.3
4	2	3	3	2	2	22.051 618 7	0.7

Table 17.12. (continued)

J'	K'_a	K'_c	J	K_a	K_c	$\nu_{\mathrm{Obs.}}$	$\nu_{\mathrm{Obs.}} - \nu_{\mathrm{Calc.}}$
upper level			lower level			GHz	kHz
4	2	3	4	1	4	15.677 678 5	0.2
4	3	1	3	3	0	22.441 386 4	−3.0
4	3	1	4	2	2	17.875 802 3	0.1
4	3	1	4	2	3	19.589 330 4	0.5
4	3	2	3	3	1	22.367 933 1	−2.6
4	3	2	4	2	2	17.789 901 4	0.5
4	3	2	4	2	3	19.503 427 1	−1.6
5	0	5	4	1	3	16.593 672 1	−1.0
5	1	4	4	2	2	19.566 704 0	1.4
5	1	4	4	2	3	21.280 229 3	−1.0
5	1	4	5	0	5	12.417 666 1	2.5
5	2	3	5	1	4	9.751 214 7	−1.0
5	2	4	5	1	5	17.843 382 9	0.9
5	3	2	5	2	3	16.810 124 6	−0.8
5	3	2	5	2	4	20.432 710 0	−1.1
5	3	3	5	2	3	16.476 278 2	−0.2
5	3	3	5	2	4	20.098 862 8	−1.3
6	1	5	6	0	6	16.289 702 3	2.3
6	2	4	5	3	2	18.620 555 2	−2.3
6	2	4	5	3	3	18.954 402 5	−1.9
6	2	4	6	1	5	10.882 468 2	−0.3
6	2	5	6	1	6	20.414 802 0	1.3
6	3	3	6	2	4	15.621 086 2	−1.7
6	3	3	6	2	5	22.005 225 3	−5.4
6	3	4	6	2	4	14.670 303 6	−0.1
6	3	4	6	2	5	21.054 444 9	−1.6
6	4	2	6	3	3	25.637 407 8	1.1
7	1	6	7	0	7	20.490 020 0	2.9
7	2	5	7	1	6	12.974 111 1	−3.7
7	2	5	7	2	6	9.941 471 8	−1.0
7	2	6	6	3	4	16.769 676 6	0.9
7	2	6	7	1	7	23.334 481 3	−3.2
7	3	4	7	2	5	14.671 146 8	3.7
7	3	5	7	2	5	12.487 196 8	−0.4
7	3	5	7	2	6	22.428 666 3	−3.7
7	4	3	7	3	4	24.665 248 6	−4.7
8	2	6	8	1	7	16.046 128 3	−3.4
8	2	6	8	2	7	14.164 445 0	6.1
8	3	5	7	4	4	22.253 381 6	1.5
8	3	5	8	2	6	14.332 376 6	1.3
8	3	6	7	4	3	17.846 214 3	−0.5
8	3	6	8	2	6	10.085 057 7	0.8

Table 17.13. Observed frequencies ($\nu_{\text{Obs.}}$) of the ^{13}C(2)-isotopologue of MTHF. $\nu_{\text{Obs.}} - \nu_{\text{Calc.}}$ values as obtained after a fit with XIAM.

J'	K'_a	K'_c	J	K_a	K_c	$\nu_{\text{Obs.}}$	$\nu_{\text{Obs.}} - \nu_{\text{Calc.}}$
upper level			lower level			GHz	kHz
1	1	0	0	0	0	9.7368370	−1.3
1	1	1	0	0	0	8.9410138	−1.7
2	0	2	1	0	1	10.9135433	1.1
2	1	1	1	0	1	16.0510930	−0.3
2	1	1	1	1	0	11.8326967	−0.3
2	1	2	1	0	1	13.6636273	−0.9
2	1	2	1	1	1	10.2410553	0.8
2	2	0	2	1	1	10.3910233	2.7
2	2	1	1	1	0	22.1003813	−2.5
2	2	1	2	1	1	10.2676859	−1.0
3	0	3	2	0	2	16.0804038	1.1
3	0	3	2	1	2	13.3303164	−0.3
3	1	2	2	1	1	17.6649839	0.3
3	1	3	2	0	2	18.0397345	−0.1
3	1	3	2	1	2	15.2896501	1.5
3	2	1	3	1	2	9.7562209	−0.5
4	0	4	3	0	3	20.9853429	1.3
4	0	4	3	1	3	19.0260103	0.5
4	1	3	3	1	2	23.3793030	1.1
4	1	4	3	0	3	22.2269232	3.9
4	1	4	3	1	3	20.2675900	2.5
4	2	2	3	2	1	23.0645521	−3.0
4	2	2	4	1	3	9.4414737	−0.8
4	2	3	3	2	2	21.9771886	−5.3
5	0	5	4	1	4	24.4607015	−1.0
5	1	4	5	0	5	12.3245484	4.3
5	2	3	5	1	4	9.7312690	−0.3
5	3	2	5	2	3	16.8286525	−0.1
5	3	3	5	2	4	20.0708796	−0.2
6	1	5	6	0	6	16.1639893	−0.9
6	2	4	6	1	5	10.8340474	0.9
6	3	3	6	2	4	15.6447179	1.6
6	3	4	6	2	5	21.0116760	−0.8

Table 17.14. Observed frequencies ($\nu_{\mathrm{Obs.}}$) of the ^{13}C(3)-isotopologue of MTHF. $\nu_{\mathrm{Obs.}} - \nu_{\mathrm{Calc.}}$ values as obtained after a fit with XIAM.

J'	K'_a	K'_c	J	K_a	K_c	$\nu_{\mathrm{Obs.}}$	$\nu_{\mathrm{Obs.}} - \nu_{\mathrm{Calc.}}$
upper level			lower level			GHz	kHz
1	1	0	0	0	0	9.631 874 2	1.8
1	1	1	0	0	0	8.811 816 0	0.4
2	0	2	1	0	1	10.904 871 4	−0.5
2	1	1	1	1	0	11.859 940 1	−1.3
2	1	2	1	0	1	13.511 701 5	2.2
2	1	2	1	1	1	10.219 828 8	−2.1
2	2	0	2	1	1	10.010 583 6	−3.1
3	0	3	2	0	2	16.042 350 2	0.7
3	1	2	2	1	1	17.697 337 4	0.4
3	1	3	2	0	2	17.858 128 3	−0.3
3	1	3	2	1	2	15.251 300 6	−0.6
3	2	1	3	1	2	9.390 519 7	1.9
4	0	4	3	0	3	20.904 574 9	0.4
4	0	4	3	1	3	19.088 795 5	0.2
4	1	3	3	1	2	23.403 789 2	−1.0
4	1	4	3	0	3	22.022 551 0	1.4
4	1	4	3	1	3	20.206 772 0	1.5
4	2	2	3	2	1	23.147 904 0	−2.3
4	2	2	4	1	3	9.134 632 3	−1.6
4	3	1	4	2	2	17.197 201 5	−2.1
4	3	2	4	2	3	18.926 290 2	−1.2
5	0	5	4	1	4	24.464 306 8	−0.1
5	1	4	5	0	5	12.545 592 4	1.5
5	2	3	5	1	4	9.535 854 5	0.8
5	2	4	5	1	5	17.625 626 3	1.0
5	3	2	5	2	3	16.103 708 1	−1.1
5	3	3	5	2	3	15.726 856 6	4.7
5	3	3	5	2	4	19.560 869 1	0.8
6	1	5	6	0	6	16.474 404 8	2.7
6	2	5	6	1	6	20.247 861 1	−3.8
6	3	3	6	2	4	14.931 500 3	−0.2

Table 17.15. Observed frequencies ($\nu_{\text{Obs.}}$) of the ^{13}C(4)-isotopologue of MTHF. $\nu_{\text{Obs.}} - \nu_{\text{Calc.}}$ values as obtained after a fit with XIAM.

J'	K'_a	K'_c	J	K_a	K_c	$\nu_{\text{Obs.}}$	$\nu_{\text{Obs.}} - \nu_{\text{Calc.}}$
upper level			lower level			GHz	kHz
1	1	0	0	0	0	9.674800 8	3.0
1	1	1	0	0	0	8.887185 9	−2.2
2	0	2	1	0	1	10.798881 1	−0.1
2	1	1	1	0	1	15.922420	−0.8
2	1	1	1	1	0	11.707288 3	−1.4
2	1	2	1	0	1	13.559417 7	1.3
2	1	2	1	1	1	10.132073 9	0.9
2	2	0	2	1	1	10.402797 8	−0.5
2	2	1	2	1	2	12.644822 0	−2.4
3	0	3	2	0	2	15.914016 8	−1.3
3	0	3	2	1	2	13.153482 2	−0.6
3	1	2	2	1	1	17.478680 5	−0.2
3	1	3	2	0	2	17.888147 4	4.1
3	1	3	2	1	2	15.127608 8	0.8
3	2	1	2	2	0	16.844982 4	−3.3
3	2	1	3	1	2	9.769103 3	0.0
3	2	2	3	1	3	13.896715 3	−2.6
4	0	4	3	0	3	20.770918 0	1.4
4	0	4	3	1	3	18.796791 0	−0.4
4	1	3	3	1	2	23.134790 6	−2.8
4	1	3	4	0	4	9.051907 1	6.1
4	1	4	3	0	3	22.027863 2	0.9
4	1	4	3	1	3	20.053739 1	2.0
4	2	2	3	2	1	22.812236 2	0.1
4	2	2	4	1	3	9.446546 6	0.6
4	2	3	3	2	2	21.744797 8	−1.0
4	3	1	4	2	2	17.908290 8	−1.0
4	3	2	4	2	3	19.480909 9	−2.9
5	1	4	5	0	5	12.223793 5	3.3
5	2	3	5	1	4	9.716619 7	−0.5
5	3	2	5	2	3	16.866280 5	4.5
5	3	3	5	2	3	16.550729 2	3.1
6	1	5	6	0	6	16.027274 5	0.6
6	2	4	6	1	5	10.786386 8	0.0
6	2	5	6	1	6	20.232309 7	−2.9
6	3	3	6	2	4	15.687734 2	−2.7
6	3	4	6	2	5	20.979599 5	0.6

Table 17.16. Observed frequencies ($\nu_{\mathrm{Obs.}}$) of the ^{13}C(5)-isotopologue of MTHF. $\nu_{\mathrm{Obs.}} - \nu_{\mathrm{Calc.}}$ values as obtained after a fit with XIAM.

J'	K'_a	K'_c	J	K_a	K_c	$\nu_{\mathrm{Obs.}}$	$\nu_{\mathrm{Obs.}} - \nu_{\mathrm{Calc.}}$
upper level			lower level			GHz	kHz
1	1	0	0	0	0	9.668887	0.3
1	1	1	0	0	0	8.874363	−1.5
2	0	2	1	0	1	10.825873	0.2
2	1	1	1	0	1	15.938185	1.3
2	1	1	1	1	0	11.744080	−1.3
2	1	2	1	0	1	13.554618	−2.0
2	1	2	1	1	1	10.155039	0.1
2	2	0	1	1	0	22.066477	−3.0
2	2	0	2	1	1	10.322401	2.8
2	2	1	2	1	1	10.198714	2.5
3	0	3	2	0	2	15.948225	1.1
3	1	2	2	1	1	17.531784	−0.7
3	1	3	2	0	2	17.889185	−0.6
3	1	3	2	1	2	15.160439	0.0
3	2	1	3	1	2	9.691028	−2.7
4	0	4	3	0	3	20.808660	0.9
4	0	4	3	1	3	18.867697	−0.8
4	1	3	3	1	2	23.201060	−2.6
4	1	4	3	0	3	22.036032	0.9
4	1	4	3	1	3	20.095071	1.8
4	2	2	3	2	1	22.891686	2.6
4	2	2	4	1	3	9.381651	−0.7
4	2	3	3	2	2	21.802286	3.6
5	0	5	4	1	4	24.254632	−3.0
5	2	3	5	1	4	9.678306	0.4
5	3	2	5	2	3	16.709459	−0.8
5	3	3	5	2	4	19.954871	4.4
6	2	4	6	1	5	10.788758	1.0
6	3	3	6	2	4	15.530525	0.3
6	3	4	6	2	5	20.897247	−3.9

Table 17.17. Observed frequencies ($\nu_{\text{Obs.}}$) of the ^{13}C(6)-isotopologue of MTHF. $\nu_{\text{Obs.}} - \nu_{\text{Calc.}}$ values as obtained after a fit with XIAM.

J'	K'_a	K'_c	J	K_a	K_c	$\nu_{\text{Obs.}}$	$\nu_{\text{Obs.}} - \nu_{\text{Calc.}}$
upper level			lower level			GHz	kHz
1	1	1	0	0	0	8.907293 2	−2.2
2	0	2	1	0	1	10.684088 9	1.6
2	1	1	1	0	1	15.832857 8	−1.4
2	1	1	1	1	0	11.559588 6	0.3
2	1	2	1	0	1	13.541312 1	−1.7
2	1	2	1	1	1	10.031891 0	−1.2
2	2	0	1	1	0	22.199468 9	−1.4
2	2	0	1	1	1	22.963316 1	−3.4
2	2	0	2	1	1	10.639880 6	−1.3
2	2	1	1	1	0	22.087818 4	0.7
2	2	1	1	1	1	22.851667 4	0.4
2	2	1	2	1	1	10.528233 7	4.3
3	0	3	2	0	2	15.761944 0	2.9
3	0	3	2	1	2	12.904718 7	4.1
3	1	2	2	1	1	17.263692 4	0.1
3	1	3	2	0	2	17.839713 1	−0.3
3	1	3	2	1	2	14.982489 0	2.1
3	2	1	2	2	0	16.625242 0	−0.1
3	2	1	3	1	2	10.001428 6	−3.1
3	2	2	3	1	2	9.458134 2	4.2
3	3	0	3	2	1	18.988913 2	0.0
4	0	4	3	0	3	20.594086 4	1.8
4	0	4	3	1	3	18.516313 8	1.5
4	1	3	3	1	2	22.862356 2	−2.1
4	1	3	3	2	2	13.404228 5	0.2
4	1	3	4	0	4	8.918796 0	−0.8
4	1	4	3	1	3	19.868093 2	1.9
4	2	2	3	2	1	22.500666 2	−1.4
4	2	2	4	1	3	9.639738 9	−2.1
4	2	3	3	2	2	21.504121 1	−5.2
4	2	3	4	1	4	15.666920 5	4.6
4	3	1	4	2	2	18.336416 1	−1.0
4	3	2	4	2	3	19.804822 1	−0.1
5	0	5	4	1	4	23.887208 0	0.5
5	1	4	4	2	3	20.198214 5	−0.3
5	1	4	5	0	5	11.977923 7	0.5
5	2	3	5	1	4	9.827163 6	2.6

Table 17.18. Observed frequencies ($\nu_{\text{Obs.}}$) of the ^{18}O-isotopologue of MTHF. $\nu_{\text{Obs.}} - \nu_{\text{Calc.}}$ values as obtained after a fit with XIAM.

J'	K'_a	K'_c	J	K_a	K_c	$\nu_{\text{Obs.}}$	$\nu_{\text{Obs.}} - \nu_{\text{Calc.}}$
upper level			lower level			GHz	kHz
1	1	0	0	0	0	9.565 888 7	3.7
1	1	1	0	0	0	8.738 520 0	−2.3
2	0	2	1	0	1	10.884 207 0	−0.4
2	1	1	1	1	0	11.851 258 4	−1.8
2	1	2	1	0	1	13.423 103 4	−2.6
2	1	2	1	1	1	10.196 540 8	3.0
3	0	3	2	0	2	16.001 555 5	−0.1
3	1	2	2	1	1	17.680 855 1	0.0
3	1	3	2	0	2	17.752 675 4	1.0
3	1	3	2	1	2	15.213 776 0	0.2
3	2	1	3	1	2	9.208 613 7	0.9
4	0	4	3	1	3	19.088 160 9	−0.3
4	2	2	4	1	3	8.979 890 4	−1.5
5	2	3	5	1	4	9.428 342 9	0.6

17.1.3 2-Methyl-1,3-dithiolane

Table 17.19. Nuclear coordinates in the principal inertial axes of the stable conformer of 2-methyl-1,3-dithiolane (MDT) calculated at the MP2/6-311++G(d,p) level of theory. The atoms are numbered according toFigure 7.3.

	Conformer E_4		
	a /Å	b /Å	c /Å
S1	−1.413 042	−0.513 477	−0.159 430
C2	−1.201 751	1.274 779	0.056 612
S3	1.356 713	0.594 673	−0.309 563
C4	0.158 766	1.501 441	0.696 937
C5	0.360 606	−0.929 381	−0.401 558
C6	0.789 521	−1.985 052	0.613 071
H7	0.488 787	−1.308 790	−1.418 772
H8	0.167 487	1.152 704	1.733 173
H9	0.440 234	2.558 445	0.668 508
H10	−2.009 111	1.622 502	0.708 637
H11	−1.258 331	1.790 235	−0.904 741
H12	1.823 481	−2.292 125	0.428 983
H13	0.714 972	−1.586 275	1.628 160
H14	0.143 704	−2.866 876	0.543 501

Table 17.20. The rotational constants A, B, and C in GHz, the deviations (Dev.) between the experimental and calculated rotational constants in MHz, the energy differences ΔE_1 between the stable conformer $^3T_4$ and $^1T_5$, ΔE_2 between the transition state E_2 and the global minimum, and ΔE_3 between the transition state ^2E and the global minimum of MDT in kJ·mol^{-1} calculated using various methods and basis sets. Harmonic frequency calculations were carried out to verify the nature of the stationary points.

Method/Basis set	***A***	**Dev.**	***B***	**Dev.**	***C***	**Dev.**	ΔE_1	ΔE_2	ΔE_3
CCSD/cc-pVDZ	2.737	42	2.652	54	1.581	44	-[a]		
MP2/cc-pVTZ	2.808	−29	2.694	12	1.640	−15	−0.89	11.51	11.63
MP2/cc-pVDZ	2.768	11	2.655	51	1.603	22	-[a]	14.79	12.51
MP2/6-311++G(3df,2pd)	2.827	−47	2.700	5	1.656	−31	−1.13	11.38	11.35
MP2/6-311++G(d,p)	2.780	−1	2.724	−18	1.605	20	-[a]	12.48	12.80
MP2/6-311+G(d,p)	2.779	0	2.725	−19	1.603	21	-[a]	12.38	12.73
MP2/6-311G(d,p)	2.803	−24	2.693	13	1.624	0	-[a]	13.65	12.66
MP2/6-31++G(d,p)	2.766	13	2.736	−31	1.585	40	-[a]	11.90	11.81
MP2/6-31+G(d,p)	2.767	13	2.737	−31	1.584	40	-[a]	11.81	12.02
MP2/6-31G(d,p)	2.773	6	2.732	−26	1.592	33	-[a]	12.97	12.91
M06-2X/cc-pVQZ	2.801	−22	2.698	7	1.638	−13	−0.75	10.14	10.61
M06-2X/cc-pVTZ	2.796	−17	2.691	14	1.634	−9	−0.99	10.84	10.74
M06-2X/cc-pVDZ	2.779	0	2.659	46	1.620	5	-[a]	13.10	11.68
M06-2X/6-311++G(3df,2pd)	2.803	−24	2.699	6	1.639	−14	−0.88	10.43	10.41
M06-2X/6-311++G(d,p)	2.783	−4	2.678	28	1.620	5	−1.26	11.84	11.01
M06-2X/6-311+G(d,p)	2.783	−3	2.678	28	1.619	5	-[a]	11.80	11.06
M06-2X/6-311G(d,p)	2.787	−8	2.672	33	1.623	2	−1.57[b]	12.23	11.06
M06-2X/6-31++G(d,p)	2.778	1	2.672	33	1.617	8	−1.27[b]	11.66	11.13
M06-2X/6-31+G(d,p)	2.777	2	2.672	33	1.616	9	-[a]	11.53	11.10
M06-2X/6-31G(d,p)	2.781	−2	2.670	35	1.618	7	-[a]	11.95	11.19
B3LYP/cc-pVQZ	2.745	34	2.696	10	1.568	57	0.05	8.48	11.09
B3LYP/cc-pVTZ	2.739	40	2.689	17	1.561	63	−0.05	8.95	11.21
B3LYP/cc-pVDZ	2.704	75	2.663	43	1.556	69	-[a]	11.76	11.99
B3LYP/6-311++G(3df,2pd)	2.743	36	2.699	6	1.578	47	−0.06	8.45	10.81
B3LYP/6-311++G(d,p)	2.719	60	2.678	27	1.554	71	-[a]	10.34	11.94
B3LYP/6-311+G(d,p)	2.719	60	2.678	28	1.554	71	-[a]	10.25	11.97
B3LYP/6-311G(d,p)	2.716	64	2.676	30	1.562	62	-[a]	10.54	11.87
B3LYP/6-31++G(d,p)	2.719	60	2.671	35	1.541	84	-[a]	10.35	12.28
B3LYP/6-31+G(d,p)	2.719	60	2.670	35	1.541	84	-[a]	10.28	12.26
B3LYP/6-31G(d,p)	2.714	65	2.674	32	1.545	80	-[a]	10.65	12.15
HF/6-311++G(3df,2pd)	2.966	−187	2.647	59	1.515	110	-[a]	10.15	12.82
HF/6-311++G(d,p)	2.826	−47	2.686	20	1.545	80	-[a]	11.11	13.04
HF/6-311+G(d,p)	2.816	−37	2.691	14	1.551	74	-[a]	11.08	13.12
HF/6-311G(d,p)	2.787	−8	2.707	−2	1.568	56	-[a]	11.45	12.88
HF/6-31++G(d,p)	2.883	−104	2.658	47	1.517	108	-[a]	10.46	12.73
HF/6-31+G(d,p)	2.901	−122	2.650	55	1.511	114	-[a]	10.47	12.80
HF/6-31G(d,p)	2.882	−102	2.659	46	1.517	108	-[a]	10.68	12.79
Experiment	**2.779**		**2.705**		**1.625**				

[a] No second conformer computable. Optimized structures correspond to first conformer. [b] The second conformer has an imaginary frequency.

Table 17.21. Nuclear coordinates in the principal inertial axes of the transition states of MDT calculated at the MP2/6-311++G(d,p) level of theory. The atoms are numbered according to Figure 7.3.

	Transition state E_2			**Transition state ^2E**		
	a /Å	b /Å	c /Å	a /Å	b /Å	c /Å
S1	0.011743	−1.453458	−0.179167	−1.453731	−0.047382	−0.464807
C2	0.873337	0.000000	0.474797	0.000001	1.024305	−0.297977
S3	0.011743	1.453458	−0.179167	1.453731	−0.047384	−0.464807
C4	−1.644512	0.777242	0.133171	0.775930	−1.342853	0.618455
C5	−1.644512	−0.777241	0.133171	−0.775932	−1.342851	0.618455
C6	2.329853	0.000000	0.027379	0.000003	1.843697	0.988754
H7	0.816219	0.000000	1.567858	0.000001	1.682784	−1.172456
H8	−2.299368	1.163990	−0.651040	1.137670	−1.200405	1.638787
H9	−2.011476	1.137299	1.096875	1.164671	−2.293974	0.247411
H10	−2.299369	−1.163990	−0.651040	−1.137670	−1.200401	1.638788
H11	−2.011475	−1.137299	1.096876	−1.164676	−2.293971	0.247413
H12	2.844674	0.885442	0.410713	0.891451	2.476064	1.036069
H13	2.393068	−0.000001	−1.063816	0.000002	1.189565	1.866211
H14	2.844674	−0.885442	0.410714	−0.891445	2.476066	1.036070

Table 17.22. Nuclear coordinates in the principal inertial axes of the stable conformers of MDT calculated at the M06-2X/cc-pVQZ level of theory. The atoms are numbered according to Figure 7.1.

	Conformer $^3T_4$			**Conformer $^1T_5$**		
	a /Å	b /Å	c /Å	a /Å	b /Å	c /Å
S1	−1.424270	−0.460749	−0.205977	0.003209	−1.464049	−0.111835
C2	0.335308	−0.951916	−0.384611	0.935652	−0.015016	0.440552
S3	1.357009	0.548775	−0.355977	−0.038709	1.486672	0.035404
C4	0.229842	1.460435	0.724609	−1.617379	0.662023	−0.341742
C5	−1.160506	1.302839	0.141630	−1.595338	−0.722881	0.282332
C6	0.727069	−1.964362	0.679656	2.309592	0.025147	−0.204626
H7	0.456692	−1.376899	−1.378015	1.030631	−0.059014	1.523312
H8	0.277293	1.066350	1.738067	−1.737189	0.592440	−1.419441
H9	0.552233	2.499743	0.731711	−2.420331	1.269528	0.070895
H10	−1.929137	1.613213	0.847213	−2.373575	−1.362353	−0.129098
H11	−1.258681	1.877834	−0.775534	−1.718721	−0.665520	1.362476
H12	1.747443	−2.308052	0.516644	2.858489	0.903304	0.131307
H13	0.661134	−1.518360	1.670326	2.215953	0.066852	−1.287417
H14	0.058527	−2.824560	0.649700	2.883647	−0.858937	0.070889

Table 17.23. Nuclear coordinates in the principal inertial axes of the transition states of MDT calculated at the M06-2X/cc-pVQZ level of theory. The atoms are numbered according to Figure 7.1.

	Transition state E_2			**Transition state ^2E**		
	a /Å	b /Å	c /Å	a /Å	b /Å	c /Å
S1	−0.008 874	1.447 132	−0.175 298	−1.445 644	−0.046 749	−0.458 747
C2	−0.885 285	−0.000 001	0.469 810	0.000 001	1.033 389	−0.299 375
S3	−0.008 868	−1.447 132	−0.175 298	1.445 641	−0.046 755	−0.458 751
C4	1.646 527	−0.773 128	0.129 804	0.771 587	−1.353 216	0.610 340
C5	1.646 524	0.773 134	0.129 803	−0.771 588	−1.353 223	0.610 332
C6	−2.335 458	−0.000 004	0.022 064	0.000 005	1.853 084	0.981 513
H7	−0.820 445	−0.000 002	1.556 777	0.000 002	1.676 254	−1.177 724
H8	2.294 033	−1.167 183	−0.648 571	1.137 426	−1.215 081	1.623 941
H9	2.011 813	−1.135 004	1.087 047	1.167 140	−2.292 583	0.234 277
H10	2.294 029	1.167 190	−0.648 574	−1.137 438	−1.215 106	1.623 931
H11	2.011 811	1.135 012	1.087 044	−1.167 132	−2.292 585	0.234 251
H12	−2.847 198	−0.882 125	0.402 638	0.887 404	2.481 919	1.029 471
H13	−2.394 943	−0.000 004	−1.064 502	0.000 001	1.197 934	1.852 490
H14	−2.847 201	0.882 115	0.402 638	−0.887 391	2.481 926	1.029 469

Table 17.24. Observed frequencies ($\nu_{\text{Obs.}}$) of MDT. $\nu_{\text{Obs.}} - \nu_{\text{Calc.}}$ values as obtained after a fit with the program XIAM.

J'	K'_a	K'_c	J	K_a	K_c	$\nu_{\text{Obs.}}$	$\nu_{\text{Obs.}} - \nu_{\text{Calc.}}$
upper level			lower level			GHz	kHz
2	1	1	1	0	1	10.895 630 8	1.3
2	1	1	1	1	0	9.741 271 0	1.8
2	2	0	1	1	0	10.972 973 2	−0.1
2	2	0	1	1	1	12.053 631 3	1.8
2	2	1	1	1	0	9.962 388 4	0.3
2	2	1	1	1	1	11.043 045 1	0.7
3	0	3	2	1	2	10.864 106 4	0.3
3	1	2	2	0	2	16.439 467 6	0.7
3	1	2	2	1	1	13.193 861 8	1.3
3	1	2	2	2	1	12.972 740 4	−1.2
3	1	3	2	0	2	10.867 864 5	0.3
3	2	1	2	1	1	16.345 722 3	−0.4
3	2	2	2	1	1	13.212 028 4	−0.7
3	2	2	2	1	2	16.453 990 7	0.4
3	3	0	2	2	0	16.468 460 8	−0.1
3	3	0	2	2	1	17.479 048 0	2.0
3	3	1	2	2	0	15.556 163 3	−0.1
3	3	1	2	2	1	16.566 748 4	−0.1
4	0	4	3	0	3	14.115 540 5	5.2
4	0	4	3	1	3	14.115 421 4	−0.9
4	1	3	3	0	3	21.930 986 2	0.7
4	1	3	3	2	2	16.341 101 5	0.3
4	1	4	3	0	3	14.115 540 5	2.3

Table 17.24. (continued)

J'	K'_a	K'_c	J	K_a	K_c	$\nu_{\text{Obs.}}$	$\nu_{\text{Obs.}} - \nu_{\text{Calc.}}$
upper level			lower level			GHz	kHz
4	1	4	3	1	3	14.115421 4	−3.8
4	2	2	3	1	2	21.905467 9	0.0
4	2	2	3	3	1	18.311460 2	−0.7
4	2	3	3	1	2	16.360060 1	0.4
4	2	3	3	1	3	21.931663 4	1.0
4	3	1	3	2	1	21.798711 1	−0.5
4	3	2	3	2	1	18.807707 4	−0.7
4	3	2	3	2	2	21.941401 5	−0.3
4	4	0	3	3	0	21.974418 0	0.0
4	4	0	3	3	1	22.886715 4	0.0
4	4	1	3	3	0	21.180618 8	−1.0
4	4	1	3	3	1	22.092917 3	0.0
5	0	5	4	0	4	17.365002 3	−0.5
5	0	5	4	1	4	17.365002 3	2.4
5	1	4	4	2	3	19.598887 3	0.0
5	1	4	5	0	5	10.050127 8	3.1
5	1	5	4	0	4	17.365002 3	−0.5
5	2	3	4	1	3	27.409385 7	0.0
5	2	3	4	3	2	21.809085 3	0.2
5	2	4	4	1	3	19.599703 5	0.1
5	2	4	5	1	5	10.050152 2	1.4
5	3	2	4	2	2	27.360795 3	−1.3
5	3	3	4	2	2	21.866337 6	−2.1
5	3	3	4	2	3	27.411746 7	−1.2
5	4	1	4	3	1	27.255833 8	0.0
5	4	1	4	3	2	30.246837 8	0.7
5	4	2	4	3	1	24.440159 6	−1.0
5	4	2	4	3	2	27.431164 5	0.4
5	5	0	4	4	0	27.493327 8	−0.1
5	5	0	4	4	1	28.287127 3	1.2
5	5	1	4	4	0	26.828325 7	−0.7
5	5	1	4	4	1	27.622124 6	0.1
6	0	6	5	0	5	20.614477 1	0.6
6	0	6	5	1	5	20.614477 1	0.6
6	1	5	5	0	5	32.898738 7	1.3
6	1	5	5	1	4	22.848614 0	1.2
6	1	5	5	2	4	22.848587 2	0.6
6	1	5	6	0	6	12.284262 2	1.2
6	1	6	5	0	5	20.614477 1	0.6
6	2	4	5	1	4	32.895211 3	−0.8
6	2	4	6	1	5	10.046598 5	−0.8
6	2	5	5	1	4	22.848614 0	0.5
6	2	5	5	1	5	32.898738 7	0.6
6	2	5	5	2	4	22.848587 2	−0.2
6	2	5	6	1	6	12.284262 2	0.5
6	3	3	5	2	3	32.884249 3	−1.4

Table 17.24. (continued)

J'	K'_a	K'_c	J	K_a	K_c	$\nu_{\text{Obs.}}$	$\nu_{\text{Obs.}} - \nu_{\text{Calc.}}$
upper level			lower level			GHz	kHz
6	3	3	5	4	2	27.262 170 8	−1.0
6	3	4	5	2	4	32.895 315 3	−1.3
6	3	4	6	2	5	10.046 732 2	3.0
6	4	2	5	3	2	32.805 071 9	0.0
6	4	2	5	5	1	28.762 286 8	−0.9
6	4	3	5	3	2	27.396 056 0	−0.8
6	4	3	5	3	3	32.890 513 1	−0.7
6	5	1	5	4	1	32.718 558 6	−1.1
6	5	1	5	4	2	35.534 226 7	−6.2
6	5	2	5	4	1	30.108 178 0	1.1
6	5	2	5	4	2	32.923 849 8	−0.3
6	6	0	5	5	0	33.026 166 8	0.2
6	6	0	5	5	1	33.691 166 8	−1.3
6	6	1	5	3	2	37.197 533 8	−2.9
6	6	1	5	5	0	32.489 751 8	0.8
6	6	1	5	5	1	33.154 753 0	0.5
7	0	7	6	0	6	23.863 883 0	1.1
7	0	7	6	1	6	23.863 883 0	1.1
7	1	6	6	0	6	38.382 244 9	1.6
7	1	6	7	0	7	14.518 362 6	1.1
7	1	7	6	0	6	23.863 883 0	1.1
7	2	5	6	1	5	38.379 246 0	1.4
7	2	5	7	1	6	12.281 264 3	2.1
7	2	6	6	1	6	38.382 244 9	1.5
7	2	6	7	1	7	14.518 362 6	1.1
7	3	4	6	2	4	38.373 620 9	−0.8
7	3	4	6	4	3	30.565 460 3	0.8
7	3	4	7	2	5	10.040 976 5	0.2
7	3	5	6	2	4	28.332 652 3	2.5
7	3	5	6	2	5	38.379 246 0	−2.3
7	3	5	7	2	6	12.281 264 3	−2.4
7	4	3	6	3	3	38.354 255 9	−0.5
7	4	3	6	5	2	32.692 577 3	−0.8
7	4	4	6	3	3	30.575 353 3	0.5
7	4	4	6	3	4	38.373 967 9	−1.3
7	4	4	7	3	5	10.041 449 0	−1.1
7	5	2	6	4	2	38.239 970 7	−0.2
7	5	2	6	6	1	33.847 507 6	1.4
7	5	3	6	4	2	32.959 195 9	0.2
7	5	3	6	4	3	38.368 211 4	0.5
7	6	1	6	5	1	38.188 631 7	−0.4
7	6	2	6	5	1	35.809 627 5	−0.4
7	6	2	6	5	2	38.420 010 2	−0.4
7	7	0	6	6	0	38.571 885 0	−1.5
7	7	0	6	6	1	39.108 301 8	−0.4
7	7	1	6	6	0	38.154 559 4	1.6

Table 17.24. (continued)

J'	K'_a	K'_c	J	K_a	K_c	$\nu_{\text{Obs.}}$	$\nu_{\text{Obs.}} - \nu_{\text{Calc.}}$
upper level			lower level			GHz	kHz
7	7	1	6	6	1	38.690973 7	0.3
8	2	6	8	1	7	14.515595 8	0.3
8	3	5	8	2	6	12.276864 6	−2.3
8	3	6	8	2	7	14.515595 8	0.2
8	4	4	8	3	5	10.032416 7	0.5
8	4	5	8	3	6	12.276887 7	1.6
8	5	4	8	4	5	10.033826 5	−0.6
9	3	6	9	2	7	14.511755 9	−2.8
9	4	5	9	3	6	12.270671 9	−0.4
9	4	6	9	3	7	14.511760 0	0.6
9	5	4	9	4	5	10.019794 9	0.8
9	5	5	9	4	6	12.270739 0	−0.4
9	6	4	9	5	5	10.023428 5	1.0
10	4	6	10	3	7	14.506593 1	1.8
10	5	5	10	4	6	12.262206 6	1.3
10	5	6	10	4	7	14.506593 1	−0.9
10	6	4	10	5	5	10.001582 0	0.9
10	6	5	10	5	6	12.262405 2	−0.2
10	7	4	10	6	5	10.009957 7	1.5
11	6	5	11	5	6	12.250904 8	1.7
11	7	5	11	6	6	12.251433 8	1.2

17.1.4 Coffee Furanone (2-Methyltetrahydrofuran-3-one)

Table 17.25. The rotational constants A, B and C in GHz, and the deviations (Dev.) between the experimental and the calculated rotational constants in MHz of conformer I of coffee furanone (2-methyltetrahydrofuran-3-one) calculated at various levels of theory. Harmonic frequency calculations were carried out to verify the nature of the stationary points.

Method/Basis set	*A*	Dev.	*B*	Dev.	*C*	Dev.
CCSD/cc-pVTZ	3.500	39	3.098	13	1.790	6
MP2/cc-pVDZ	3.508	32	3.104	7	1.796	0
MP2/6-311++G(3df,2pd)	3.556	−16	3.137	−25	1.812	−16
MP2/6-311++G(d,p)	3.530	10	3.119	−8	1.802	−5
MP2/6-311+G(d,p)	3.531	9	3.119	−8	1.802	−5
MP2/6-311G(d,p)	3.531	9	3.125	−14	1.810	−13
MP2/6-31++G(d,p)	3.520	20	3.111	0	1.796	0
MP2/6-31+G(d,p)	3.521	19	3.111	0	1.796	0
MP2/6-31G(d,p)	3.532	8	3.116	−5	1.804	−7
B3LYP/cc-pVQZ	3.524	16	3.113	−2	1.791	5
B3LYP/cc-pVDZ	3.505	35	3.095	16	1.785	11
B3LYP/cc-pVDZ	3.523	16	3.111	0	1.791	5
B3LYP/6-311++G(3df,2pd)	3.522	17	3.112	−1	1.790	6
B3LYP/6-311++G(d,p)	3.507	33	3.102	9	1.784	12
B3LYP/6-311+G(d,p)	3.507	33	3.102	9	1.784	12
B3LYP/6-311G(d,p)	3.511	29	3.104	7	1.789	7
B3LYP/6-31++G(d,p)	3.494	45	3.093	18	1.779	18
B3LYP/6-31+G(d,p)	3.494	45	3.093	18	1.778	18
B3LYP/6-31G(d,p)	3.506	34	3.095	16	1.785	11
HF/6-311++G(3df,2pd)	3.578	−38	3.170	−59	1.826	−30
HF/6-311++G(d,p)	3.567	−28	3.162	−51	1.821	−25
HF/6-311+G(d,p)	3.567	−28	3.162	−51	1.821	−25
HF/6-311G(d,p)	3.569	−30	3.164	−53	1.825	−29
HF/6-31++G(d,p)	3.561	−22	3.156	−44	1.818	−22
HF/6-31+G(d,p)	3.562	−22	3.155	−44	1.818	−21
HF/6-31G(d,p)	3.567	−27	3.157	−46	1.822	−26
M06-2X/6-31++G(d,p)	3.554	−14	3.119	−8	1.805	−9
M06-2X/6-31+G(d,p)	3.554	−15	3.119	−8	1.805	−8
M06-2X/6-311++G(3df,2pd)	3.578	−39	3.134	−23	1.814	−18
M06-2X/6-311++G(d,p)	3.564	−25	3.127	−16	1.809	−13
M06-2X/6-311+G(d,p)	3.564	−24	3.127	−16	1.809	−13
M06-2X/6-311G(d,p)	3.567	−27	3.129	−18	1.814	−18
M06-2X/6-31G(d,p)	3.564	−24	3.120	−9	1.809	−13
M06-2X/cc-pVDZ	3.562	−23	3.121	−10	1.810	−14
M06-2X/cc-pVQZ	3.580	−40	3.135	−24	1.814	−18
M06-2X/cc-pVTZ	3.580	−41	3.133	−22	1.814	−18
Experiment	**3.540**		**3.111**		**1.796**	

Table 17.26. The rotational constants *A*, *B* and *C* in GHz of conformer II of coffee furanone calculated at various levels of theory. Harmonic frequency calculations were carried out to verify the nature of the stationary points.

Method/Basis set	*A*	*B*	*C*
CCSD/cc-pVDZ	3.433	3.133	1.887
MP2/cc-pVTZ	3.514	3.134	1.931
MP2/cc-pVDZ	3.459	3.126	1.897
MP2/6-311++G(3df,2pd)	3.517	3.132	1.937
MP2/6-311++G(d,p)	3.486	3.116	1.921
MP2/6-311+G(d,p)	3.484	3.117	1.920
MP2/6-311G(d,p)	3.486	3.140	1.916
MP2/6-31++G(d,p)	3.468	3.113	1.908
MP2/6-31+G(d,p)	3.466	3.114	1.907
MP2/6-31G(d,p)	3.474	3.136	1.906
M06-2X/cc-pVQZ	3.511	3.156	1.936
M06-2X/cc-pVTZ	3.510	3.158	1.933
M06-2X/cc-pVDZ	3.487	3.160	1.914
M06-2X/6-311++G(3df,2pd)	3.513	3.153	1.937
M06-2X/6-311++G(d,p)	3.497	3.146	1.929
M06-2X/6-311+G(d,p)	3.496	3.146	1.929
M06-2X/6-311G(d,p)	3.495	3.162	1.923
M06-2X/6-31++G(d,p)	3.485	3.137	1.922
M06-2X/6-31+G(d,p)	3.484	3.138	1.922
M06-2X/6-31G(d,p)	3.490	3.151	1.920
B3LYP/cc-pVQZ	3.439	3.142	1.890
B3LYP/cc-pVTZ	3.438	3.142	1.887
B3LYP/cc-pVDZ	3.424	3.135	1.873
B3LYP/6-311++G(3df,2pd)	3.439	3.140	1.892
B3LYP/6-311++G(d,p)	3.425	3.127	1.886
B3LYP/6-311+G(d,p)	3.425	3.128	1.885
B3LYP/6-311G(d,p)	3.428	3.141	1.880
B3LYP/6-31++G(d,p)	3.415	3.116	1.880
B3LYP/6-31+G(d,p)	3.414	3.116	1.880
B3LYP/6-31G(d,p)	3.425	3.130	1.877
HF/6-311++G(3df,2pd)	3.481	3.221	1.922
HF/6-311++G(d,p)	3.470	3.212	1.917
HF/6-311+G(d,p)	3.470	3.213	1.917
HF/6-311G(d,p)	3.472	3.222	1.913
HF/6-31++G(d,p)	3.464	3.204	1.913
HF/6-31+G(d,p)	3.464	3.204	1.913
HF/6-31G(d,p)	3.470	3.212	1.911

Table 17.27. Nuclear coordinates in the principal inertial axes of conformer I and II of coffee furanone calculated at the MP2/6-311++G(d,p) level of theory. The atoms are numbered according to Figure 8.1.

	Conformer I			**Conformer II**		
	a /Å	b /Å	c /Å	a /Å	b /Å	c /Å
C1	−0.339384	0.825578	0.054696	0.830273	0.396530	−0.113037
C2	−0.438691	−0.665626	0.392468	−0.038216	−0.810319	−0.477949
O3	0.795369	−1.217198	−0.055284	−1.371070	−0.303574	−0.527322
C4	1.784838	−0.199490	0.137083	−1.443033	0.800060	0.386958
C5	1.111258	1.089772	−0.330470	−0.120018	1.541611	0.213148
C6	−1.606930	−1.359598	−0.275749	0.133137	−1.927387	0.547958
O7	−1.252515	1.622776	0.094599	2.042550	0.406432	−0.072171
H8	2.663850	−0.485600	−0.440563	−1.557428	0.437543	1.417536
H9	2.054125	−0.135213	1.201447	−2.323264	1.383527	0.116315
H10	1.166247	1.185763	−1.420407	0.223205	2.104521	1.083257
H11	1.481044	2.008606	0.129116	−0.158925	2.208211	−0.655690
H12	−2.540459	−0.891376	0.047306	1.174898	−2.261081	0.555052
H13	−1.622866	−2.418714	−0.008815	−0.516252	−2.768009	0.292746
H14	−1.521224	−1.268846	−1.361798	−0.124508	−1.577615	1.552530
H15	−0.510951	−0.747888	1.491375	0.220248	−1.165425	−1.480382

Table 17.28. Observed frequencies ($\nu_{\text{Obs.}}$) of conformer I of coffee furanone. $\nu_{\text{Obs.}} - \nu_{\text{Calc.}}$ values as obtained after a fit with XIAM.

J'	K'_a	K'_c	J	K_a	K_c	$\nu_{\text{Obs.}}$	$\nu_{\text{Obs.}} - \nu_{\text{Calc.}}$
upper level			lower level			GHz	kHz
2	0	2	1	0	1	8.8395076	0.4
2	1	1	1	0	1	12.8726143	1.3
2	1	1	1	1	0	11.1293041	−3.2
2	1	2	1	0	1	8.9282973	0.1
2	2	0	1	0	1	15.1332269	0.9
2	2	0	1	1	0	13.3899204	0.1
2	2	0	1	1	1	14.7046968	3.2
2	2	1	1	1	0	12.4148936	1.1
2	2	1	1	1	1	13.7296668	1.0
3	0	3	2	0	2	12.3327526	0.6
3	0	3	2	1	2	12.2439636	1.7
3	1	2	2	0	2	19.6191259	1.3
3	1	2	2	1	1	15.5860189	0.2
3	1	2	2	2	1	14.3004322	−1.5
3	1	3	2	0	2	12.3445543	1.9
3	1	3	2	1	2	12.2557628	0.5
3	2	1	2	0	2	23.4045452	1.6
3	2	1	2	1	1	19.3714374	−0.3
3	2	1	2	1	2	23.3157547	1.3
3	2	1	2	2	0	17.1108237	−1.1
3	2	2	2	1	1	16.0073774	0.7
3	2	2	2	1	2	19.9516941	1.5

Table 17.28. (continued)

J'	K'_a	K'_c	J	K_a	K_c	$\nu_{\text{Obs.}}$	$\nu_{\text{Obs.}} - \nu_{\text{Calc.}}$
upper level			lower level			GHz	kHz
3	2	2	2	2	1	14.721 790 8	−1.0
3	3	0	2	1	1	22.544 816 6	−1.7
3	3	0	2	2	0	20.284 203 6	−1.8
3	3	0	2	2	1	21.259 232 1	−1.2
3	3	1	2	2	0	19.670 157 8	−0.9
3	3	1	2	2	1	20.645 185 2	−1.3
4	0	4	3	0	3	15.890 459 1	1.6
4	0	4	3	1	3	15.878 658 7	1.6
4	1	3	3	1	2	19.099 446 0	0.6
4	1	3	3	2	2	18.678 087 9	0.6
4	1	3	3	3	0	12.140 637 6	−8.2
4	1	3	4	0	4	10.495 364 6	4.2
4	1	3	4	1	4	10.494 068 3	3.3
4	1	4	3	0	3	15.891 755 4	2.4
4	1	4	3	1	3	15.879 954 7	2.2
4	2	2	3	2	1	22.163 346 5	−0.6
4	2	2	3	3	1	19.604 012 0	−1.3
4	2	3	3	1	2	19.179 939 2	1.3
4	2	3	3	2	2	18.758 579 4	−0.4
4	2	3	4	0	4	10.575 857 0	4.1
4	2	3	4	1	4	10.574 558 1	0.6
4	3	1	3	3	0	22.788 128 8	−1.6
4	3	2	3	2	1	23.307 904 6	−1.7
4	3	2	3	3	1	20.748 571 2	−1.3
5	0	5	4	0	4	19.477 603 1	3.2
5	1	4	4	1	3	22.550 631 0	0.1
5	1	4	4	2	3	22.470 138 0	−0.3
5	1	4	5	1	5	13.568 271 0	8.1
5	1	5	4	1	4	19.476 433 8	0.8
5	2	3	4	2	2	25.976 098 5	−0.8
5	2	3	4	3	2	24.831 539 3	−0.8
5	2	3	4	4	0	17.639 492 7	−1.6
5	2	3	5	1	4	10.274 789 4	0.1
5	2	3	5	2	4	10.263 325 5	−0.5
5	2	4	4	1	3	22.562 095 0	0.9
5	2	4	4	2	3	22.481 601 9	0.3
5	2	4	5	0	5	13.579 858 1	3.5
5	3	3	4	3	2	25.136 884 6	−1.3
5	3	3	5	1	4	10.580 133 7	−1.3
5	3	3	5	2	4	10.568 671 4	−0.4
5	4	2	5	2	3	8.617 601 6	1.0
5	5	1	5	3	2	10.341 638 7	−1.8
6	0	6	5	0	5	23.069 266 8	−0.4
6	1	5	6	1	6	16.606 736 6	2.3
6	1	6	5	0	5	23.069 266 8	−12.4[a]
6	1	6	5	1	5	23.069 151 9	1.2

Table 17.28. (continued)

J'	K'_a	K'_c	J	K_a	K_c	$\nu_{\mathrm{Obs.}}$	$\nu_{\mathrm{Obs.}} - \nu_{\mathrm{Calc.}}$
upper level			lower level			GHz	kHz
6	2	4	6	1	5	13.462845 7	−2.3
6	2	4	6	2	5	13.461450 3	−3.6
6	2	5	6	0	6	16.608 144 9	4.4
6	3	3	6	2	4	9.846408 1	−3.2
6	3	3	6	3	4	9.790787 0	−3.1
6	3	4	6	1	5	13.518468 3	−0.8
6	3	4	6	2	5	13.517072 0	−3.0
6	4	3	6	2	4	10.679666 9	−1.0
6	4	3	6	3	4	10.624043 6	−3.2
6	5	2	6	3	3	9.766411 5	−3.6
6	5	2	6	4	3	8.933 156 3	−2.1
6	6	1	6	5	2	9.376 1100	−1.7
7	1	6	7	1	7	19.638 4524	13.9[a]
7	2	5	7	2	6	16.534 186 5	8.5
7	2	6	7	0	7	19.638 588 9	−4.2
7	3	4	7	2	5	13.258 982 9	−0.5
7	3	4	7	3	5	13.250 790 8	−3.8
7	3	5	7	1	6	16.542 524 7	4.3
7	4	3	7	3	4	9.191 436 7	−1.9
7	4	3	7	4	4	8.997 461 7	−2.5
7	4	4	7	2	5	13.452 954 2	−3.6
7	4	4	7	3	5	13.444 767 2	−1.8
7	5	3	7	3	4	10.991 427 3	−0.3
7	5	3	7	4	4	10.797 448 6	−4.5
7	6	2	7	4	3	11.595 582 9	−5.9
7	6	2	7	5	3	9.795 597 0	−2.7
7	7	0	7	6	1	10.220 892 3	3.7
7	7	1	7	6	2	10.881 910 4	−0.8
8	2	6	8	2	7	19.577 313 2	−3.2
8	3	5	8	2	6	16.416 496 7	−1.8
8	3	5	8	3	6	16.415 435 6	−5.8
8	3	6	8	1	7	19.578 393 5	4.2
8	4	4	8	3	5	12.887 225 3	−0.2
8	4	4	8	4	5	12.852 873 4	−1.8
8	4	5	8	2	6	16.450 845 7	−3.1
8	4	5	8	3	6	16.449 792 6	0.9
8	5	4	8	3	5	13.424 199 6	−0.7
8	6	3	8	4	4	11.683 566 0	−0.6
8	6	3	8	5	4	11.146 593 0	1.2
8	7	2	8	6	3	10.894 743 8	4.8
9	4	5	9	3	6	16.223 624 4	0.1
9	4	5	9	4	6	16.218 466 8	0.1
9	5	4	9	4	5	12.277 301 2	0.8
9	5	5	9	3	6	16.338 208 3	0.8
9	6	4	9	4	5	13.511 816 4	1.4
9	6	4	9	5	5	13.397 232 2	0.3

Table 17.28. (continued)

J'	K'_a	K'_c	J	K_a	K_c	$\nu_{\text{Obs.}}$	$\nu_{\text{Obs.}} - \nu_{\text{Calc.}}$
upper level			lower level			GHz	kHz
10	4	6	10	4	7	19.357 999 6	−4.4
10	5	5	10	4	6	15.905 582 9	2.5
10	5	5	10	5	6	15.885 642 8	0.0
10	5	6	10	3	7	19.378 634 1	0.1
10	6	4	10	5	5	11.425 766 6	2.4
10	6	4	10	6	5	11.105 265 7	−0.9
10	6	5	10	4	6	16.226 086 3	8.3
10	7	4	10	5	5	13.844 629 6	3.9

[a] Not included in the fit.

17.1.5 2-Methylcyclopentanon

Table 17.29. Nuclear coordinates in the principal inertial axes of conformer I and II of 2-methylcyclopentanone calculated at the MP2/6-311++G(d,p) level of theory.

	Conformer I			**Conformer II**		
	a /Å	b /Å	c /Å	a /Å	b /Å	c /Å
C1	0.250 622	0.811 769	−0.060 331	−0.785 057	−0.430 031	−0.126 673
C2	0.512 965	−0.664 718	−0.370 378	−0.041 378	0.856 061	−0.499 728
C3	−0.752 803	−1.361 538	0.142 856	1.425 669	0.413 162	−0.604 631
C4	−1.873 443	−0.344 677	−0.143 144	1.550 378	−0.738 243	0.414 717
C5	−1.237 273	0.998 437	0.236 326	0.234 661	−1.506 142	0.243 623
C6	1.841 709	−1.158 324	0.187 372	−0.277 219	1.897 050	0.604 358
O7	1.095 409	1.685 399	−0.035 749	−1.993 878	−0.558 176	−0.108 939
H8	−1.329 007	1.184 799	1.314 582	−0.100 050	−2.078 020	1.112 432
H9	−1.631 040	1.873 996	−0.286 031	0.296 394	−2.195 468	−0.609 589
H10	−2.792 568	−0.556 591	0.409 101	2.434 609	−1.356 977	0.241 657
H11	−2.113 106	−0.357 463	−1.212 993	1.621 319	−0.335 064	1.430 959
H12	0.524 902	−0.732 149	−1.470 351	−0.444 493	1.236 992	−1.443 949
H13	2.018 111	−2.202 064	−0.089 481	0.236 599	2.831 895	0.360 313
H14	2.666 325	−0.548 710	−0.191 094	0.101 636	1.541 012	1.568 562
H15	1.842 258	−1.087 062	1.280 311	−1.346 413	2.099 249	0.713 025
H16	−0.664 401	−1.520 205	1.226 356	2.126 746	1.230 905	−0.410 394
H17	−0.924 965	−2.334 621	−0.326 135	1.629 620	0.027 682	−1.611 105

Table 17.30. Nuclear coordinates in the principal inertial axes of the transition states TS1 and TS2 of 2-methylcyclopentanone calculated at the MP2/6-311++G(d,p) level of theory.

	TS1			**TS2**		
	a /Å	b /Å	c /Å	a /Å	b /Å	c /Å
C1	−0.186174	0.831454	0.102860	−0.780704	−0.420585	−0.091376
C2	−0.573637	−0.609478	0.429860	−0.073091	0.879377	−0.458467
C3	0.634585	−1.441899	−0.045089	1.412751	0.495389	−0.586777
C4	1.826753	−0.455153	−0.261818	1.593077	−0.903886	0.088860
C5	1.330163	0.934612	0.174215	0.215107	−1.316461	0.634605
C6	−1.920249	−1.015138	−0.154242	−0.322073	1.891592	0.671234
O7	−0.958470	1.723879	−0.188450	−1.943561	−0.685052	−0.328487
H8	1.700515	1.764973	−0.430067	0.124809	−1.095851	1.706059
H9	1.588580	1.133889	1.222675	−0.036211	−2.369521	0.491606
H10	2.102206	−0.432298	−1.320070	2.348929	−0.871915	0.876979
H11	2.713576	−0.765039	0.295678	1.932647	−1.632642	−0.652311
H12	−0.625388	−0.645175	1.529027	−0.495444	1.265728	−1.390717
H13	−2.175543	−2.039590	0.132799	0.164222	2.843700	0.437409
H14	−1.887316	−0.961511	−1.247363	0.094045	1.525125	1.616657
H15	−2.710360	−0.343924	0.192099	−1.393106	2.068943	0.807983
H16	0.384445	−1.942901	−0.986355	2.050385	1.248735	−0.113801
H17	0.887163	−2.223981	0.675888	1.705204	0.443141	−1.639443

Table 17.31. The rotational constants A, B, and C in GHz and the dipole moment components in the principal axis system (in Debye) of conformer I of 2-methylcyclopentanone calculated using various method (HF, B3LYP, MP2) and basis set combinations. Harmonic frequency calculations were also carried out for the cases of the HF, B3LYP, and MP2 methods to verify the nature of the stationary points. Deviations between the calculated and the experimental rotational constants (Dev. = exp. − calc.) are given in MHz.

Method/Basis set	***A***	**Dev.**	***B***	**Dev.**	***C***	**Dev.**	μ_a	μ_b	μ_c
MP2									
6-311++G(3df,2pd)	3.574	−31	2.882	−23	1.727	−16	−2.38	−2.60	−0.11
6-311++G(d,p)	3.539	3	2.864	−5	1.715	−4	−2.42	−2.65	−0.08
6-311+G(d,p)	3.540	2	2.863	−5	1.715	−4	−2.42	−2.65	−0.08
6-311G(d,p)	3.557	−14	2.858	1	1.715	−4	−2.30	−2.43	−0.11
6-31++G(d,p)	3.537	6	2.868	−9	1.714	−3	−2.49	−2.69	−0.09
6-31+G(d,p)	3.537	6	2.868	−9	1.714	−3	−2.50	−2.70	−0.09
6-31G(d,p)	3.559	−16	2.864	−5	1.716	−5	−2.34	−2.43	−0.10
B3LYP									
6-311++G(3df,2pd)	3.526	17	2.862	−3	1.705	6	−2.03	−2.34	−0.10
6-311++G(d,p)	3.511	32	2.850	9	1.698	13	−2.06	−2.37	−0.10
6-311+G(d,p)	3.512	31	2.850	9	1.698	13	−2.06	−2.37	−0.10
6-311G(d,p)	3.526	17	2.845	14	1.698	13	−1.92	−2.08	−0.11
6-31++G(d,p)	3.499	44	2.842	17	1.693	18	−2.09	−2.39	−0.10
6-31+G(d,p)	3.499	44	2.841	18	1.693	19	−2.09	−2.40	−0.10
6-31G(d,p)	3.519	24	2.838	21	1.695	16	−1.89	−2.03	−0.09
HF									
6-311++G(3df,2pd)	3.570	−27	2.893	−34	1.726	−15	−2.13	−2.57	−0.10
6-311++G(d,p)	3.560	−17	2.884	−25	1.721	−10	−2.16	−2.62	−0.10
6-311+G(d,p)	3.560	−17	2.884	−25	1.721	−10	−2.16	−2.62	−0.10
6-311G(d,p)	3.571	−28	2.881	−22	1.722	−11	−2.06	−2.41	−0.11
6-31++G(d,p)	3.554	−11	2.881	−22	1.719	−8	−2.21	−2.63	−0.10
6-31+G(d,p)	3.554	−11	2.881	−22	1.719	−8	−2.21	−2.63	−0.10
6-31G(d,p)	3.566	−24	2.878	−19	1.720	−9	−2.08	−2.39	−0.11
Experiment [42]	3.543		2.859		1.711				

Table 17.32. The rotational constants A, B, and C in GHz and the dipole moment components in the principal axis system (in Debye) of conformer II of 2-methylcyclopentanone calculated using various method (HF, B3LYP, MP2) and basis set combinations. Harmonic frequency calculations were also carried out for the cases of the HF, B3LYP, and MP2 methods to verify the nature of the stationary points.

Method/Basis set	A	B	C	μ_a	μ_b	μ_c
MP2						
6-311++G(d,p)	3.350	2.963	1.886	−3.58	−0.54	−0.01
6-311+G(d,p)	3.349	2.964	1.885	−3.58	−0.54	−0.01
6-311G(d,p)	3.352	2.973	1.881	−3.32	−0.58	−0.07
6-31++G(d,p)	3.345	2.969	1.875	−3.64	−0.64	−0.03
6-31+G(d,p)	3.342	2.971	1.874	−3.64	−0.65	−0.03
6-31G(d,p)	3.350	2.983	1.873	−3.32	−0.68	−0.08
B3LYP						
6-311++G(3df,2pd)	3.309	2.983	1.855	−3.00	−0.77	−0.03
6-311++G(d,p)	3.294	2.970	1.847	−3.04	−0.77	−0.02
6-311+G(d,p)	3.294	2.970	1.847	−3.04	−0.78	−0.02
6-311G(d,p)	3.300	2.978	1.839	−2.69	−0.83	−0.09
6-31++G(d,p)	3.283	2.961	1.840	−3.08	−0.79	−0.03
6-31+G(d,p)	3.282	2.961	1.840	−3.09	−0.79	−0.03
6-31G(d,p)	3.294	2.970	1.835	−2.66	−0.82	−0.08
HF						
6-311++G(3df,2pd)	3.332	3.034	1.875	−3.20	−0.96	−0.05
6-311++G(d,p)	3.320	3.022	1.871	−3.27	−0.95	−0.04
6-311+G(d,p)	3.320	3.023	1.870	−3.27	−0.95	−0.04
6-311G(d,p)	3.326	3.027	1.867	−3.02	−0.97	−0.08
6-31++G(d,p)	3.316	3.018	1.866	−3.31	−0.96	−0.04
6-31+G(d,p)	3.315	3.018	1.866	−3.31	−0.96	−0.04
6-31G(d,p)	3.322	3.021	1.862	−3.01	−0.99	−0.08

Table 17.33. The rotational constants A, B, and C in GHz and the characterizing angles $\varphi = \angle(C_5,C_4,C_3,C_2)$, $\gamma = \angle(O,C_2,C_5,C_4)$, and $\gamma' = \angle(O,C_2,C_5,C_3)$ of the transition state TS1 of 2-methylcyclopentanone calculated using various method (HF, B3LYP, MP2) and basis set combinations.

Method/Basis set	***A***	***B***	***C***	φ	γ	γ'
MP2						
6-311++G(3df,2pd)	3.555	2.868	1.735	3.72	−145.58	−147.95
6-311++G(d,p)	3.519	2.852	1.718	3.50	−147.31	−149.53
6-311+G(d,p)	3.520	2.851	1.719	3.59	−147.09	−149.36
6-311G(d,p)	3.532	2.849	1.722	3.71	−146.58	−148.93
6-31++G(d,p)	3.508	2.862	1.716	3.82	−149.30	−151.71
6-31+G(d,p)	3.509	2.861	1.716	4.04	−149.00	−151.56
6-31G(d,p)	3.526	2.860	1.720	4.11	−148.43	−151.03
B3LYP						
6-311++G(3df,2pd)	3.487	2.864	1.707	5.09	−152.71	−155.92
6-311++G(d,p)	3.472	2.852	1.699	4.86	−153.19	−156.25
6-311+G(d,p)	3.471	2.852	1.699	4.99	−153.10	−156.25
6-311G(d,p)	3.485	2.848	1.702	5.02	−152.23	−155.40
6-31++G(d,p)	3.456	2.845	1.693	4.87	−153.90	−156.96
6-31+G(d,p)	3.456	2.845	1.693	4.93	−153.87	−156.98
6-31G(d,p)	3.476	2.841	1.697	4.92	−152.73	−155.83
HF						
6-311++G(3df,2pd)	3.548	2.886	1.731	4.83	−149.11	−152.17
HF/6-311++G(d,p)	3.535	2.878	1.724	4.57	−149.93	−152.81
HF/6-311+G(d,p)	3.534	2.879	1.725	4.74	−149.82	−152.82
HF/6-311G(d,p)	3.543	2.877	1.727	4.72	−149.40	−152.39
HF/6-31++G(d,p)	3.522	2.879	1.721	4.74	−151.23	−154.23
HF/6-31+G(d,p)	3.521	2.879	1.721	4.90	−151.22	−154.32
HF/6-31G(d,p)	3.531	2.877	1.723	5.06	−150.79	−153.99

Table 17.34. The rotational constants A, B, and C in GHz and the characterizing angles $\varphi = \angle(C_5,C_4,C_3,C_2)$, $\gamma = \angle(O,C_2,C_5,C_4)$, and $\gamma' = \angle(O,C_2,C_5,C_3)$ of the transition state TS2 of 2-methylcyclopentanone calculated using various method (HF, B3LYP, MP2) and basis set combinations.

Method/Basis set	***A***	***B***	***C***	φ	γ	γ'
MP2						
6-311++G(3df,2pd)	3.285	2.917	1.923	−0.98	150.82	151.44
6-311++G(d,p)	3.255	2.903	1.895	−1.16	152.07	152.80
6-311+G(d,p)	3.253	2.904	1.895	−1.17	151.91	152.66
6-311G(d,p)	3.261	2.901	1.897	−0.72	152.39	152.85
6-31++G(d,p)	3.266	2.908	1.874	−0.95	154.96	155.56
6-31+G(d,p)	3.264	2.908	1.874	−0.55	155.06	155.41
6-31G(d,p)	3.272	2.907	1.879	−0.12	155.17	155.25
B3LYP						
6-311++G(3df,2pd)	3.266	2.919	1.824	1.46	162.67	161.76
6-311++G(d,p)	3.261	2.907	1.802	1.42	164.92	164.03
6-311+G(d,p)	3.257	2.907	1.808	1.43	163.93	163.04
HF						
6-311++G(3df,2pd)	3.268	2.962	1.879	0.92	157.03	156.44
HF/6-311++G(d,p)	3.263	2.952	1.866	0.78	157.98	157.49
HF/6-311+G(d,p)	3.262	2.953	1.867	0.80	157.79	157.29
HF/6-311G(d,p)	3.271	2.951	1.862	0.87	158.83	158.28
HF/6-31++G(d,p)	3.269	2.948	1.849	0.84	160.30	159.77
HF/6-31+G(d,p)	3.270	2.948	1.848	0.87	160.42	159.88
HF/6-31G(d,p)	3.286	2.945	1.834	1.15	163.02	162.30

17.1.6 Methylcyclopentane

Table 17.35. Nuclear coordinates in the principal inertial axes of conformer I, II, and III of methylcyclopentane calculated at the MP2/6-311++G(d,p) level of theory.

	Conformer I			**Conformer II**			**Conformer III**		
	a /Å	b /Å	c /Å	a /Å	b /Å	c /Å	a /Å	b /Å	a /Å
C1	−0.040574	1.188063	0.176139	−0.100204	−1.191015	0.550680	−0.055739	−1.194731	0.382209
C2	0.767082	−0.000046	−0.358808	0.869807	0.000018	0.532339	0.818238	0.085455	0.479648
C3	−0.040611	−1.188014	0.176372	−0.100215	1.191025	0.550651	−0.118748	1.246745	0.047051
C4	−1.511459	−0.778617	−0.038676	−1.237359	0.777447	−0.410482	−1.533141	0.648635	0.014307
C5	−1.511518	0.778599	−0.038379	−1.237323	−0.777474	−0.410490	−1.274583	−0.785923	−0.457811
C6	2.234597	0.000002	0.051597	1.746608	0.000000	−0.722085	2.065121	0.004257	−0.401791
H7	0.695736	−0.000167	−1.457372	1.515267	0.000027	1.418883	1.135830	0.234995	1.518045
H8	−2.166746	−1.191577	0.733712	−1.045626	1.160940	−1.417317	−2.218083	1.208368	−0.630271
H9	−1.869780	−1.157710	−1.001214	−2.199833	1.187786	−0.091796	−1.960264	0.627826	1.025001
H10	−1.870453	1.158058	−1.000540	−1.045510	−1.160948	−1.417316	−1.015564	−0.779017	−1.524441
H11	−2.166399	1.191171	0.734561	−2.199797	−1.187863	−0.091868	−2.130103	−1.455171	−0.323567
H12	2.754178	−0.885940	−0.328809	2.388348	0.887102	−0.749466	2.617080	0.950628	−0.393201
H13	2.754150	0.885903	−0.328942	2.388360	−0.887094	−0.749418	2.741092	−0.788959	−0.065168
H14	2.319931	0.000086	1.144706	1.137123	−0.000025	−1.632341	1.779923	−0.208812	−1.439049
H15	0.170852	−1.293832	1.249385	0.377102	2.133331	0.260413	0.155632	1.574183	−0.964412
H16	0.213848	−2.136771	−0.307920	−0.496897	1.316646	1.565400	−0.034028	2.117181	0.705262
H17	0.213768	2.136657	−0.308532	−0.496903	−1.316606	1.565426	−0.394346	−1.497676	1.380056
H18	0.171160	1.294271	1.249055	0.377140	−2.133315	0.260477	0.499854	−2.036379	−0.045683

Table 17.36. Nuclear coordinates in the principal inertial axes of the transition states TS1 and TS2 of methylcyclopentane calculated at the MP2/6-311++G(d,p) level of theory.

	TS1			**TS2**		
	a /Å	b /Å	c /Å	a /Å	b /Å	c /Å
C1	0.057001	1.213842	0.290386	0.140900	1.267296	0.307386
C2	−0.809132	−0.070370	0.449170	−0.851141	0.097202	0.525313
C3	0.099138	−1.228529	−0.028165	0.060281	−1.140289	0.595063
C4	1.526582	−0.681082	0.079808	1.135505	−0.857697	−0.461145
C5	1.353455	0.762001	−0.407027	1.444480	0.639345	−0.263132
C6	−2.123083	−0.002843	−0.327617	−1.857788	−0.006470	−0.623979
H7	−1.040099	−0.217469	1.511223	−1.404942	0.227763	1.462272
H8	2.254683	−1.254703	−0.502305	0.733048	−1.038495	−1.463719
H9	1.852463	−0.682123	1.128014	2.023683	−1.486698	−0.347414
H10	2.205786	1.409727	−0.179811	2.259160	0.752743	0.459964
H11	1.215881	0.759170	−1.495625	1.766671	1.122295	−1.190203
H12	−2.672384	−0.948394	−0.259104	−2.508046	−0.879549	−0.501536
H13	−2.770290	0.795667	0.050342	−2.489718	0.887017	−0.666210
H14	−1.922894	0.195253	−1.387375	−1.346972	−0.095362	−1.588944
H15	−0.119957	−1.449382	−1.081857	−0.485410	−2.074742	0.424039
H16	−0.064352	−2.148274	0.542817	0.530347	−1.199369	1.585364
H17	0.294764	1.633607	1.274180	0.346893	1.779154	1.253004
H18	−0.471459	1.990060	−0.273890	−0.284821	2.012531	−0.373281

Table 17.37. The rotational constants A, B, and C in GHz, the dipole moment components in the principal axis system (in Debye), and the characterizing angles $\varphi = \angle(C_3,C_4,C_5,C_1)$, $\gamma = \angle(C_2,C_1,C_3,C_4)$, and $\gamma' = \angle(C_2,C_1,C_3,C_5)$ of conformer I of methylcyclopentane calculated using various methods (HF, B3LYP, MP2) and basis set combinations. Harmonic frequency calculations were also carried out for the cases of the HF, B3LYP, and MP2 methods to verify the nature of the stationary points.

Method/Basis set	A	B	C	μ_a	μ_b	μ_c	φ	γ	γ'
MP2									
6-311++G(d,p)	6.268	2.935	2.218	−0.01	0.00	−0.08	0.03	−138.16	−138.18
6-311+G(d,p)	6.268	2.935	2.218	−0.01	0.00	−0.08	0.03	−138.19	−138.21
6-311G(d,p)	6.270	2.935	2.218	−0.01	0.00	−0.08	0.03	−138.24	−138.26
6-31++G(d,p)	6.287	2.944	2.222	−0.02	0.00	−0.09	0.02	−138.77	−138.78
6-31+G(d,p)	6.287	2.944	2.222	−0.02	0.00	−0.09	0.03	−138.79	−138.81
6-31G(d,p)	6.300	2.947	2.226	−0.02	0.00	−0.07	0.03	−138.58	−138.60
B3LYP									
6-311++G(3df,2pd)	6.249	2.925	2.203	−0.01	0.00	−0.10	0.02	−140.60	−140.62
6-311++G(d,p)	6.221	2.912	2.194	0.00	0.00	−0.10	0.02	−140.61	−140.62
6-311+G(d,p)	6.221	2.912	2.194	0.00	0.00	−0.10	0.02	−140.62	−140.64
6-311G(d,p)	6.222	2.912	2.194	0.00	0.00	−0.09	0.02	−140.58	−140.60
6-31++G(d,p)	6.208	2.905	2.189	−0.01	0.00	−0.10	0.02	−140.49	−140.51
6-31+G(d,p)	6.207	2.904	2.189	−0.02	0.00	−0.10	0.02	−140.51	−140.52
6-31G(d,p)	6.216	2.908	2.192	−0.01	0.00	−0.07	0.02	−140.32	−140.33
HF									
6-311++G(3df,2pd)	6.302	2.944	2.219	−0.02	0.00	−0.09	0.02	−139.94	−139.95
6-311++G(d,p)	6.280	2.935	2.212	−0.01	0.00	−0.08	0.02	−139.99	−140.01
6-311+G(d,p)	6.280	2.935	2.212	−0.02	0.00	−0.08	0.02	−140.01	−140.03
6-311G(d,p)	6.281	2.935	2.212	−0.01	0.00	−0.08	0.02	−139.97	−139.98
6-31++G(d,p)	6.276	2.934	2.211	−0.02	0.00	−0.09	0.02	−140.15	−140.16
6-31+G(d,p)	6.276	2.934	2.211	−0.02	0.00	−0.09	0.02	−140.14	−140.15
6-31G(d,p)	6.277	2.934	2.212	−0.02	0.00	−0.07	0.02	−140.04	−140.06

Table 17.38. The rotational constants A, B, and C in GHz, the dipole moment components in the principal axis system (in Debye), and the characterizing angles $\varphi = \angle(C_3,C_4,C_5,C_1)$, $\gamma = \angle(C_2,C_1,C_3,C_4)$, and $\gamma' = \angle(C_2,C_1,C_3,C_5)$ of conformer II of methylcyclopentane calculated using various methods (HF, B3LYP, MP2) and basis set combinations. Harmonic frequency calculations were also carried out for the cases of the HF, B3LYP, and MP2 methods to verify the nature of the stationary points. Re-optimizations of the *twist* conformers III/III* at different levels of theory starting from the optimized geometries obtained at the MP2/6-311++G(d,p) level yielded the stable *envelope* conformers I and II.

Method/Basis set	A	B	C	μ_a	μ_b	μ_c	φ	γ	γ'
MP2									
6-311++G(d,p)	4.844	3.450	2.825	0.00	0.00	0.09	0.00	−138.71	−138.71
6-311+G(d,p)	4.846	3.448	2.822	0.00	0.00	0.08	0.00	−138.78	−138.78
6-311G(d,p)	4.844	3.454	2.829	0.01	0.00	0.07	0.00	−138.65	−138.65
6-31++G(d,p)	4.882	3.443	2.811	−0.01	0.00	0.09	0.00	−139.48	−139.48
6-31+G(d,p)	4.882	3.443	2.811	−0.01	0.00	0.09	0.00	−139.44	−139.44
6-31G(d,p)	4.881	3.458	2.828	−0.01	0.00	0.06	0.00	−139.02	−139.02
B3LYP									
6-311++G(3df,2pd)	4.913	3.379	2.740	0.01	0.00	0.10	0.00	−141.60	−141.60
6-311++G(d,p)	4.891	3.364	2.729	0.01	0.00	0.09	0.00	−141.59	−141.59
6-311+G(d,p)	4.891	3.364	2.728	0.01	0.00	0.09	0.00	−141.60	−141.60
6-311G(d,p)	4.891	3.366	2.730	0.01	0.00	0.08	0.00	−141.56	−141.56
6-31++G(d,p)	4.879	3.356	2.723	0.00	0.00	0.09	0.00	−141.52	−141.52
6-31+G(d,p)	4.879	3.356	2.723	0.00	0.00	0.09	0.00	−141.51	−141.51
6-31G(d,p)	4.880	3.365	2.732	−0.01	0.00	0.04	0.00	−141.23	−141.23
HF									
6-311++G(3df,2pd)	4.950	3.401	2.762	0.01	0.00	0.10	0.00	−141.27	−141.27
6-311++G(d,p)	4.933	3.390	2.753	0.00	0.00	0.09	0.00	−141.32	−141.32
6-311+G(d,p)	4.933	3.390	2.753	0.00	0.00	0.09	0.00	−141.31	−141.32
6-311G(d,p)	4.931	3.393	2.756	0.01	0.00	0.08	0.00	−141.24	−141.24
6-31++G(d,p)	4.933	3.389	2.751	−0.01	0.00	0.09	0.00	−141.44	−141.44
6-31+G(d,p)	4.932	3.390	2.751	−0.01	0.00	0.09	0.00	−141.41	−141.42
6-31G(d,p)	4.931	3.392	2.754	−0.01	0.00	0.07	0.00	−141.33	−141.33

Table 17.39. The rotational constants A, B, and C in GHz and the characterizing angles $\varphi = \angle(C_5,C_4,C_3,C_2)$, $\gamma = \angle(C_3,C_4,C_2,C_1)$, and $\gamma' = \angle(C_3,C_4,C_2,C_5)$ of the transition state TS2 of methylcyclopentane calculated using various various method (HF, B3LYP, MP2) and basis set combinations. The transition states TS1/1* could only be obtained at the MP2/6-311++G(d,p) level of theory. Calculations carried out at all other levels lead to non-optimized geometries.

Method/Basis set	***A***	***B***	***C***	φ	γ	γ'
MP2						
6-311++G(d,p)	5.101	3.336	2.666	4.21	140.94	138.23
6-311+G(d,p)	5.104	3.334	2.664	4.38	141.01	138.19
6-311G(d,p)	5.102	3.339	2.670	4.33	140.82	138.03
6-31++G(d,p)	5.146	3.330	2.654	5.03	141.90	138.67
6-31+G(d,p)	5.127	3.337	2.664	3.65	141.28	138.93
6-31G(d,p)	5.123	3.350	2.678	3.18	140.73	138.68
B3LYP						
6-311++G(3df,2pd)	5.057	3.317	2.654	−3.29	140.73	142.84
6-311++G(d,p)	5.039	3.301	2.640	−2.93	140.84	142.71
6-311+G(d,p)	5.041	3.300	2.639	−2.81	140.88	142.68
6-311G(d,p)	5.042	3.301	2.640	−2.66	140.87	142.58
6-31++G(d,p)	5.014	3.297	2.642	−4.11	140.45	143.08
6-31+G(d,p)	5.015	3.297	2.641	−4.00	140.45	143.01
6-31G(d,p)	5.011	3.307	2.652	−4.54	140.06	142.97
HF						
6-311++G(3df,2pd)	5.129	3.327	2.657	−0.65	141.24	141.66
6-311++G(d,p)	5.114	3.314	2.647	−0.43	141.38	141.66
6-311+G(d,p)	5.115	3.314	2.646	−0.37	141.41	141.65
6-311G(d,p)	5.119	3.314	2.645	0.13	141.48	141.40
6-31++G(d,p)	5.122	3.310	2.640	0.36	141.75	141.52
6-31+G(d,p)	5.123	3.310	2.640	0.42	141.75	141.48
6-31G(d,p)	5.128	3.310	2.639	0.86	141.81	141.26

17.1.7 Comparison of Non-Planar Rings

Table 17.40. The angles α of the twist conformers of 2-methyltetrahydrothiophen-3-one (**1**), 2-methyltetrahydrothiophene (**2**), 2-methyl-1,3-dithiolane (**4**), and 2-methylcyclopentanone (**6**) calculated at different levels of theory.

Method/ basis set	(**1**)		(**2**)		(**4**)		(**6**)	
	I	II	I	II	I	II	I	II
CCSD/cc-pVTZ			27.51	−27.18				
CCSD/cc-pVDZ			27.50	−27.13	−24.58	–[a]		
CCSD/6-311++G(d,p)			27.33	−27.00	−23.76	–[a]		
MP2/cc-pVQZ			28.06		−25.83	−10.97		
MP2/cc-pVTZ			28.12	−27.84	−25.73	−12.42		
MP2/cc-pVDZ			28.00	−27.72	−25.29	–[a]		
MP2/6-311++G(3df,2pd)	27.46	−25.98	28.30	−27.97	−25.99	−11.05	25.21	
MP2/6-311++G(d,p)	26.10	−25.01	27.83	−27.55	−24.50	–[a]	24.79	−24.00
MP2/6-311+G(d,p)	26.32	−24.99	27.82	−27.54	−24.48	–[a]	24.81	−23.98
MP2/6-311G(d,p)	26.17	−24.18	27.83	−27.63	−25.22	–[a]	24.76	−24.07
MP2/6-31++G(d,p)	25.71	−24.21	27.35	−27.11	−23.60	–[a]	24.17	−23.39
MP2/6-31+G(d,p)	25.86	−24.36	27.37	−27.12	−23.59	–[a]	24.25	−23.47
MP2/6-31G(d,p)	25.77	−22.49	27.47	−27.25	−23.91	–[a]	24.32	−23.63
B3LYP/cc-pVQZ			26.48	−26.14	−23.10	−13.12		
B3LYP/cc-pVTZ			26.51	−26.16	−22.97	−14.54		
B3LYP/cc-pVDZ			26.82	−26.45	−23.56	–[a]		
B3LYP/6-311++G(3df,2pd)	24.15	−20.69	26.53	−26.20	−23.53	−12.92	22.76	−22.01
B3LYP/6-311++G(d,p)	24.13	−20.51	26.58	−26.29	−23.10	–[a]	22.76	−21.99
B3LYP/6-311+G(d,p)	24.19	−20.31	26.59	−26.29	−23.10	–[a]	22.76	−21.99
B3LYP/6-311G(d,p)	24.38	−17.16	26.63	−26.35	−23.49	–[a]	22.74	−21.90
B3LYP/6-31++G(d,p)	23.72	−19.97	26.58	−26.26	−22.60	–[a]	22.79	−22.00
B3LYP/6-31+G(d,p)	23.79	−20.00	26.57	−26.26	−22.57	–[a]	22.78	−21.99
B3LYP/6-31G(d,p)	23.79	−16.13	26.65	−26.37	−22.79	–[a]	22.89	−22.03
HF/6-311++G(3df,2pd)	24.36	−20.91	26.66	−26.04	−12.94	–[a]	23.41	−22.43
HF/6-311++G(d,p)	24.27	−21.05	26.62	−26.06	−20.46	–[a]	23.34	−22.38
HF/6-311+G(d,p)	24.33	−20.92	26.63	−26.06	−20.96	–[a]	23.34	−22.38
HF/6-311G(d,p)	24.53	−19.74	26.67	−26.13	−22.15	–[a]	23.34	−22.36
HF/6-31++G(d,p)	24.05	−20.85	26.50	−25.94	−16.87	–[a]	23.14	−22.19
HF/6-31+G(d,p)	24.09	−20.75	26.51	−25.96	−15.58	–[a]	23.13	−22.19
HF/6-31G(d,p)	24.11	−18.93	26.53	−25.99	−16.89	–[a]	23.14	−22.11

[a] No second conformer computable. The optimized structures correspond to the first conformer.

Table 17.41. The angles γ of the *envelope* conformers of 2-methyltetrahydrothiophene (**2**), 2-methyltetrahydrofuran (**3**), 2-methyl-1,3-dithiolane (**4**), 2-methylcyclopentanone (**6**), and methylcyclopentane (**7**) calculated at different levels of theory.

Method/ basis set	(**2**)		(**3**)		(**4**)		(**6**)		(**7**)		
	TS1	TS2	I	TS1	TS1	TS2	TS1	TS2	I	II	TS2
MP2											
cc-pVTZ	−135.16	137.20			−131.30	130.84					
cc-pVDZ	−134.75	138.00			−131.67	131.21					
6-311++G(3df,2pd)	−135.02	137.00			−131.33	130.70	−145.58	150.82			
6-311++G(d,p)	−135.43	138.41	−139.90	141.53	−132.12	131.25	−147.31	152.07	−138.16	−138.71	138.23
6-311+G(d,p)	−135.46	138.24	−139.98	141.56	−132.06	131.14	−147.09	151.91	−138.19	−138.78	138.19
6-311G(d,p)	−135.30	138.29	−137.26	141.93	−132.09	131.33	−146.58	152.39	−138.24	−138.65	138.03
6-31++G(d,p)	−136.03	138.80	−140.44	141.67	−132.37	131.82	−149.30	154.96	−138.77	−139.48	138.67
6-31+G(d,p)	−135.85	138.96	−141.15	141.74	−132.54	131.84	−149.00	155.06	−138.79	−139.44	138.93
6-31G(d,p)	−136.02	138.90	−140.11	142.16	−133.10	132.21	−148.43	155.17	−138.58	−139.02	138.68
B3LYP											
cc-pVQZ	−138.60	142.09			−134.91	136.40					
cc-pVTZ	−138.36	142.06			−134.94	136.46					
cc-pVDZ	−137.71	141.89			−134.73	135.94					
6-311++G(3df,2pd)	−138.36	141.76	−151.85	146.98	−134.77	136.04	−152.71	162.67	−140.60	−141.60	142.84
6-311++G(d,p)	−137.91	141.77	−151.32	146.60	−134.66	135.79	−153.19	164.92	−140.61	−141.59	142.71
6-311+G(d,p)	−137.93	141.67	−151.85	146.64	−134.56	135.73	−153.10	163.93	−140.62	−141.60	142.68
6-311G(d,p)	−137.85	141.67	−144.10	146.57	−134.66	135.78	−152.23		−140.58	−141.56	142.58
6-31++G(d,p)	−137.89	141.98	−152.22	147.01	−134.74	136.07	−153.90		−140.49	−141.52	143.08
6-31+G(d,p)	−137.99	142.03	−152.22	146.98	−134.80	136.07	−153.87		−140.51	−141.51	143.01
6-31G(d,p)	−137.98	141.75	−143.56	146.83	−135.19	136.33	−152.73		−140.32	−141.23	142.97
HF											
6-311++G(3df,2pd)	−137.98	141.36	−144.07	146.77	−136.47	137.43	−149.11	157.03	−139.94	−141.27	141.66
6-311++G(d,p)	−137.93	141.65	−143.53	146.68	−136.59	137.44	−149.93	157.98	−139.99	−141.32	141.66
6-311+G(d,p)	−137.95	141.58	−143.54	146.65	−136.45	137.29	−149.82	157.79	−140.01	−141.31	141.65
6-311G(d,p)	−137.79	141.51	−144.66	146.56	−136.58	137.28	−149.40	158.83	−139.97	−141.24	141.40
6-31++G(d,p)	−138.23	141.73	−143.92	146.77	−136.59	137.56	−151.23	160.30	−140.15	−141.44	141.52
6-31+G(d,p)	−138.25	141.72	−143.93	146.68	−136.58	137.56	−151.22	160.42	−140.14	−141.41	141.48
6-31G(d,p)	−138.29	141.48	−144.10	146.57	−136.81	137.64	−150.79	163.02	−140.04	−141.33	141.26

Table 17.42. The angles φ of the *envelope* conformers of 2-methyltetrahydrothiophene (**2**), 2-methyltetrahydrofuran (**3**), 2-methyl-1,3-dithiolane (**4**), 2-methylcyclopentanone (**6**), and methylcyclopentane (**7**) calculated at different levels of theory.

Method/ basis set	(2)		(3)		(4)		(6)		(7)		
	TS1	TS2	I	TS1	TS1	TS2	TS1	TS2	I	II	TS2
MP2											
cc-pVTZ	20.56	−2.99			0.00	0.00					
cc-pVDZ	17.33	−1.07			0.00	0.00					
6-311++G(3df,2pd)	20.64	−3.75			0.00	0.00	3.72	−0.98			
6-311++G(d,p)	9.28	−2.75	−3.66	−0.29	0.00	0.00	3.50	−1.16	0.03	0.00	4.21
6-311+G(d,p)	8.63	−3.01	−3.65	−0.21	0.00	0.00	3.59	−1.17	0.03	0.00	4.38
6-311G(d,p)	8.82	−2.16	5.70	0.93	0.00	0.00	3.71	−0.72	0.03	0.00	4.33
6-31++G(d,p)	9.31	−3.17	23.68	−0.24	0.00	0.00	3.82	−0.95	0.02	0.00	5.03
6-31+G(d,p)	10.14	−1.84	25.38	0.12	0.00	0.00	4.04	−0.55	0.03	0.00	3.65
6-31G(d,p)	7.78	−0.86	23.44	1.56	0.00	0.00	4.11	−0.12	0.03	0.00	3.18
B3LYP											
cc-pVQZ	18.37	2.25			0.00	0.00					
cc-pVTZ	17.37	2.20			0.00	0.00					
cc-pVDZ	16.94	2.96			0.00	0.00					
6-311++G(3df,2pd)	17.85	1.73	−17.94	5.49	0.00	0.00	5.09	1.46	0.02	0.00	−3.29
6-311++G(d,p)	15.26	1.73	−17.81	5.53	0.00	0.00	4.86	1.42	0.02	0.00	−2.93
6-311+G(d,p)	15.79	1.47	−18.50	5.66	0.00	0.00	4.99	1.43	0.02	0.00	−2.81
6-311G(d,p)	15.27	1.70	24.76	5.44	0.00	0.00	5.02		0.02	0.00	−2.66
6-31++G(d,p)	15.56	2.19	−19.04	6.51	0.00	0.00	4.87		0.02	0.00	−4.11
6-31+G(d,p)	16.40	2.35	−19.04	6.40	0.00	0.00	4.93		0.02	0.00	−4.00
6-31G(d,p)	15.27	2.02	23.91	6.45	0.00	0.00	4.92		0.02	0.00	−4.54
HF											
6-311++G(3df,2pd)	17.01	−0.47	24.18	2.93	0.00	0.00	4.83	0.92	0.02	0.00	−0.65
6-311++G(d,p)	15.10	−0.11	23.39	3.33	0.00	0.00	4.57	0.78	0.02	0.00	−0.43
6-311+G(d,p)	15.71	−0.36	23.31	3.35	0.00	0.00	4.74	0.80	0.02	0.00	−0.37
6-311G(d,p)	14.73	−0.36	26.00	2.95	0.00	0.00	4.72	0.87	0.02	0.00	0.13
6-31++G(d,p)	16.21	−0.40	23.83	3.16	0.00	0.00	4.74	0.84	0.02	0.00	0.36
6-31+G(d,p)	16.54	−0.45	23.74	3.03	0.00	0.00	4.90	0.87	0.02	0.00	0.42
6-31G(d,p)	16.24	−1.11	24.59	2.84	0.00	0.00	5.06	1.15	0.02	0.00	0.86

17.2 Multiple Internal Rotations of Methyl Groups in Planar Ring Systems

17.2.1 2,5-Dimethylthiophene

Table 17.43. Fourier coefficients of the potential energy curves of 2,5-dimethylthiophene (DMTP) obtained by rotating one methyl group around the C_{12}-C_{10} bond (for atom number see Figure 10.2). The dihedral angle $\varphi_1 = \angle(S_{15},C_{12},C_{10},H_4)$ was varied in a step width of 1°. Calculations were performed using different methods and the cc-pVTZ basis set (see Figure 10.3). The potential is expanded as $V(\varphi) = a_0 + \sum_{n=3}^{15} a_n \cdot \cos(n \cdot \varphi)$.

	MP2/ cc-pVTZ		**B3LYP/cc-pVTZ**		**M06-2X/cc-pVTZ**	
	Hartree	cm^{-1}	Hartree	cm^{-1}	Hartree	cm^{-1}
a_0	−630.645 711 484		−631.761 436 484		−631.616 516 796	
a_3	−0.000 492 240	−108.0	−0.000 560 540	−123.0	−0.000 584 515	−128.3
a_6	0.000 022 517	4.9	0.000 010 775	2.4	0.000 012 199	2.7
a_9	0.000 000 942	0.2	0.000 001 992	0.4	−0.000 004 691	−1.0
a_{12}	0.000 000 497	0.1	0.000 000 433	0.1	0.000 000 805	0.2
a_{15}			0.000 000 981	0.2	0.000 001 996	0.4

Table 17.44. Cartesian nuclear coordinates of DMTP calculated at the MP2/6-311++G(d,p) level of theory. The atoms are numbered according to Figure 10.2.

	a /Å	b /Å	c /Å
H1	−3.317337	−0.636278	0.000175
H2	−2.969253	0.856100	−0.885955
H3	−2.969284	0.856501	0.885641
H4	3.317340	−0.636284	−0.000151
H5	2.969248	0.856105	0.885958
H6	2.969292	0.856486	−0.885635
H7	−1.326284	−2.279910	0.000032
H8	1.326269	−2.279913	−0.000040
C9	−2.705099	0.269804	−0.000019
C10	2.705101	0.269796	0.000029
C11	−1.255167	−0.115027	0.000082
C12	1.255168	−0.115031	−0.000079
C13	−0.711617	−1.384921	0.000023
C14	0.711605	−1.384921	−0.000028
S15	0.000004	1.073062	−0.000005

Table 17.45. Coefficients of the two-dimensional Fourier expansion for the potential energy surface of DMTP calculated at the MP2/6-311++G(d,p) and B3LYP/6-311++G(d,p) level of theory in a grid of 10° (see Figure 10.4). Due to symmetry, only data points in the range from $\varphi_1 = 0°$ to 120° and $\varphi_2 = 0°$ to 120° were needed. The potential is expanded as $V(\varphi_1, \varphi_2) = \sum_{i=1}^{12} V_i \cdot f_i$.

		MP2/6-311++G(d,p)	**B3LYP/6-311++G(d,p)**
i	f_i	V_i/Hartree	V_i/Hartree
1	1	−630.445037756	−631.729233044
2	$\cos(3\varphi_1) + \sin(3\varphi_2)$	0.000006328	0.000005076
3	$\cos(3\varphi_1) + \cos(3\varphi_2)$	0.000538003	0.000620153
4	$\cos(6\varphi_1) + \sin(6\varphi_2)$	−0.000001196	−0.000001883
5	$\cos(6\varphi_1) + \cos(6\varphi_2)$	0.000054143	0.000015548
6	$\cos(3\varphi_1)\cos(3\varphi_2)$	−0.000010439	−0.000014867
7	$\sin(3\varphi_1)\sin(3\varphi_2)$	−0.000011985	0.000016431
8	$\cos(6\varphi_1)\cos(6\varphi_2)$	0.000002005	
9	$\sin(6\varphi_1)\sin(6\varphi_2)$	−0.000001900	0.000000231
10	$\cos(3\varphi_1)\sin(3\varphi_2) + \sin(3\varphi_1)\cos(3\varphi_2)$	0.000000705	0.000000279
11	$\cos(6\varphi_1)\cos(3\varphi_2) + \cos(3\varphi_1)\cos(6\varphi_2)$	0.000001777	
12	$\sin(6\varphi_1)\sin(3\varphi_2) + \sin(3\varphi_1)\sin(6\varphi_2)$	0.000002986	

Table 17.46. The rotational constants A, B, and C in GHz, the deviations (Dev.) between the experimental and calculated rotational constants in MHz, the angles between the internal rotor axis and the principal axes of inertia ∠(i,a), ∠(i,b), ∠(i,c) of the methyl group containing the C_{10} atom, and the barrier to internal rotation V_3 of the two equivalent methyl groups of DMTP calculated using various methods and basis sets. Additionally, harmonic frequency calculations were carried out to verify the nature of the stationary points.

Method/Basis set	A	Dev.	B	Dev.	C	Dev.	∠(i,a)	∠(i,b)	∠(i,c)	V_3/cm^{-1}
HF/6-31G(d,p)	5.024	−59	1.742	5	1.314	−1	14.89	75.11	90.00	382.5
HF/6-31+G(d,p)	5.019	−54	1.740	7	1.313	0	14.97	75.03	90.00	392.3
HF/6-31++G(d,p)	5.019	−54	1.740	7	1.313	0	14.97	75.03	90.00	393.5
HF/6-311G(d,p)	5.029	−64	1.743	4	1.315	−2	14.95	75.05	90.00	380.0
HF/6-311+G(d,p)	5.027	−62	1.742	5	1.314	−1	15.01	74.99	90.00	398.2
HF/6-311++G(d,p)	5.027	−62	1.742	5	1.314	−1	15.01	74.99	90.00	405.2
HF/6-311++G(3df,2pd)	5.077	−112	1.751	−4	1.323	−10	14.93	75.07	90.00	366.2
B3LYP/6-31G(d,p)	4.927	38	1.727	20	1.299	14	14.89	75.11	90.00	294.4
B3LYP/6-31+G(d,p)	4.920	44	1.725	22	1.298	16	14.96	75.04	90.00	292.9
B3LYP/6-31++G(d,p)	4.921	44	1.725	22	1.298	16	14.95	75.05	90.00	290.8
B3LYP/6-311G(d,p)	4.940	25	1.731	16	1.302	11	14.92	75.08	90.00	271.0
B3LYP/6-311+G(d,p)	4.940	25	1.730	17	1.302	11	14.98	75.02	90.00	275.4
B3LYP/6-311++G(d,p)	4.940	25	1.730	17	1.302	11	14.98	75.02	90.00	279.1
B3LYP/6-311++G(3df,2pd)	4.998	−33	1.741	6	1.312	1	14.88	75.12	90.00	230.7
B3LYP/cc-pVDZ	4.900	65	1.723	24	1.296	18	15.01	74.99	90.00	270.6
B3LYP/cc-pVTZ	4.979	−14	1.738	9	1.309	4	14.89	75.11	90.00	244.6
B3LYP/cc-pVQZ	4.991	−26	1.741	6	1.311	2	14.90	75.10	90.00	237.7
M06-2X/6-31G(d,p)	4.967	−2	1.745	1	1.313	1	15.06	74.94	90.00	298.8
M06-2X/6-31+G(d,p)	4.961	4	1.744	3	1.311	2	15.13	74.87	89.99	296.1
M06-2X/6-31++G(d,p)	4.962	3	1.744	3	1.311	2	15.12	74.88	89.99	295.2
M06-2X/6-311G(d,p)	4.977	−12	1.748	−1	1.315	−2	15.09	74.91	90.00	282.6
M06-2X/6-311+G(d,p)	4.977	−12	1.747	0	1.314	−1	15.16	74.84	90.00	290.5
M06-2X/6-311++G(d,p)	4.977	−12	1.747	0	1.314	−1	15.16	74.84	90.00	295.2
M06-2X/6-311++G(3df,2pd)	5.027	−62	1.756	−10	1.323	−10	15.09	74.91	90.00	255.2
M06-2X/cc-pVDZ	4.946	19	1.742	5	1.310	4	15.18	74.82	90.00	281.8
M06-2X/cc-pVTZ	5.014	−49	1.754	−7	1.321	−8	15.07	74.93	90.00	261.6
M06-2X/cc-pVQZ	5.026	−61	1.757	−10	1.323	−10	15.09	74.91	89.99	253.6
MP2/6-31G(d,p)	4.952	13	1.746	1	1.312	1	14.72	75.28	90.00	247.4
MP2/6-31+G(d,p)	4.941	24	1.744	3	1.310	4	14.85	75.18	89.17	
MP2/6-31++G(d,p)	4.941	24	1.744	3	1.310	4	14.87	75.16	89.06	
MP2/6-311G(d,p)	4.943	22	1.745	2	1.311	3	14.82	75.18	90.00	248.4
MP2/6-311+G(d,p)	4.941	24	1.743	4	1.309	4	14.86	75.14	90.00	238.9
MP2/6-311++G(d,p)[a]	4.941	24	1.742	4	1.309	4	14.90	75.10	89.96	241.2
MP2/cc-pVDZ	4.877	88	1.728	19	1.297	17	15.03	74.97	90.00	245.2
MP2/cc-pVTZ	4.980	−15	1.752	−5	1.317	−4	14.98	75.02	90.00	215.5
MP2/cc-pVQZ	5.006	−41	1.758	−11	1.322	−9	15.03	74.97	90.00	
CCSD/6-311++G(d,p)	4.924	41	1.733	14	1.303	10	14.97	75.03	90.00	
CCSD/cc-pVDZ	4.858	107	1.719	28	1.290	23	15.07	74.93	90.00	
CCSD(T)/cc-pVTZ[b]	4.980	−15	1.752	−5	1.317	−4	14.98	75.02	90.00	275.0
Experiment	4.965		1.747		1.313		14.59	75.41	90.00	248.0

[a] One imaginary frequency was obtained for the minimum structure (see text) [b] Single point calculations using the optimized structures calculated at the MP2/cc-pVTZ level.

Table 17.47. Observed frequencies ($\nu_{\text{Obs.}}$) of the (00), (01), (11), and (12) torsional species of DMTP. $\nu_{\text{Obs.}} - \nu_{\text{Calc.}}$ values as obtained after a fit with the program XIAM.

J'	K_a'	K_c'	J	K_a	K_c	$(\sigma_1\sigma_2)$	$\nu_{\text{Obs.}}$	$\nu_{\text{Obs.}} - \nu_{\text{Calc.}}$
upper level			lower level				GHz	kHz
2	2	1	2	1	2	(00)	10.9765365	−2.3
						(01)	10.7878122	6.4
						(12)	10.5955690	−1.8
						(11)	10.9440246	−0.5
3	1	3	2	0	2	(00)	11.3387590	1.4
						(01)	11.3295459	0.5
						(12)	11.3126677	0.3
						(11)	11.3281475	−0.1
3	2	1	3	1	2	(00)	9.2541060	0.6
						(01)	9.3559650	4.1
						(12)	9.5148455	0.9
						(11)	9.2224300	0.0
3	2	2	2	1	1	(00)	18.8568018	−6.8
						(01)	18.7112833	1.6
						(12)	18.4867022	−0.3
						(11)	18.8240931	0.2
3	2	2	3	1	3	(00)	11.6513380	2.3
						(01)	11.5173545	3.2
						(12)	11.3265087	−1.3
						(11)	11.6187890	−0.4
4	0	4	3	1	3	(00)	9.5343173	−0.2
						(01)	9.5423794	−0.1
						(12)	9.5579888	0.3
						(11)	9.5427464	−0.1
4	1	4	3	0	3	(00)	13.6180181	−0.2
						(01)	13.6105325	0.3
						(12)	13.5983489	0.2
						(11)	13.6078216	0.3
4	2	2	4	1	3	(00)	8.8326193	−4.4
						(01)	8.8742012	−2.6
						(12)	8.9877496	0.2
						(11)	8.8024198	0.1
4	2	3	4	1	4	(00)	12.5615812	1.1
						(01)	12.4886107	2.7
						(12)	12.3438966	−0.4
						(11)	12.5289805	−0.1
4	3	1	3	2	2	(11)	29.5137418	0.3
4	3	1	4	2	2	(00)	16.7680988	−10.1
						(01)	16.9710250	6.1
						(12)	17.1047684	0.0
						(11)	16.7130308	−0.3
4	3	2	3	2	1	(00)	29.3489770	2.1
						(11)	29.2943697	−0.1
4	3	2	4	2	3	(00)	17.3413095	0.7
						(01)	17.0838880	−5.8

Table 17.47. (continued)

J'	K'_a	K'_c	J	K_a	K_c	$(\sigma_1\sigma_2)$	$\nu_{\mathrm{Obs.}}$	$\nu_{\mathrm{Obs.}} - \nu_{\mathrm{Calc.}}$
upper level			lower level				GHz	kHz
						(12)	16.8956150	−0.9
						(11)	17.2877417	0.3
4	4	0	3	3	0	(12)	36.4610260	−1.0
4	4	0	3	3	1	(11)	36.2672629	−0.1
4	4	1	3	3	0	(00)	36.3402495	3.7
						(11)	36.2647106	−1.1
4	4	1	3	3	1	(00)	36.3427845	121.4[a]
						(01)	36.2059699	1.5
						(12)	36.0707866	0.8
5	0	5	4	1	4	(00)	12.8104635	−0.2
						(01)	12.8161123	−0.3
						(12)	12.8261327	0.2
						(11)	12.8173160	0.0
5	1	5	4	0	4	(00)	15.8274913	0.3
						(01)	15.8211763	0.3
						(12)	15.8117354	0.0
						(11)	15.8180447	0.3
5	2	3	5	1	4	(00)	8.5883523	0.6
						(01)	8.6002029	−0.2
						(12)	8.6573483	−0.2
						(11)	8.5606005	0.0
5	2	4	5	1	5	(00)	13.7100406	0.2
						(01)	13.6680106	−2.1
						(12)	13.5809972	0.1
						(11)	13.6773378	0.0
5	3	2	5	2	3	(00)	16.3000706	1.1
						(01)	16.5097668	3.6
						(12)	16.7006530	−2.1
						(11)	16.2441595	0.6
5	3	3	5	2	4	(00)	17.5487510	1.0
						(01)	17.2843342	1.1
						(12)	17.0385646	0.9
						(11)	17.4957106	−0.8
5	4	1	4	3	1	(01)	39.4707114	−1.7
						(12)	39.5305356	−1.4
5	4	1	4	3	2	(00)	39.4198024	−1.5
						(11)	39.3442656	−0.3
5	4	2	4	3	1	(00)	39.4019011	−2.3
						(11)	39.3262585	1.4
5	4	2	4	3	2	(01)	39.2752427	1.2
						(12)	39.1398133	−0.9
6	0	6	5	1	5	(00)	15.9609636	−0.3
						(01)	15.9648206	−0.7
						(12)	15.9713286	0.2
						(11)	15.9659788	0.4
6	1	5	5	2	4	(00)	11.9941358	−0.2

Table 17.47. (continued)

J'	K'_a	K'_c	J	K_a	K_c	$(\sigma_1\sigma_2)$	$\nu_{\mathrm{Obs.}}$	$\nu_{\mathrm{Obs.}} - \nu_{\mathrm{Calc.}}$
upper level			lower level				GHz	kHz
						(01)	12.0369669	0.9
						(12)	12.1303855	0.5
						(11)	12.0228012	−0.5
6	1	5	6	0	6	(00)	9.7432119	−0.6
						(01)	9.7401571	−0.3
						(11)	9.7341613	0.2
6	1	6	5	0	5	(00)	18.0476297	−0.3
						(01)	18.0423861	0.2
						(12)	18.0350255	0.3
						(11)	18.0393073	1.0
6	2	4	6	1	5	(00)	8.6453315	−0.4
						(01)	8.6459070	0.0
						(12)	8.6710172	−0.4
						(11)	8.6209081	0.3
6	2	5	6	1	6	(00)	15.0938338	−0.8
						(01)	15.0647072	−0.6
						(12)	15.0114780	0.2
						(11)	15.0609230	−0.2
6	3	3	6	2	4	(00)	15.6310127	1.1
						(01)	15.8006644	1.0
						(12)	16.0169060	−1.8
						(11)	15.5746017	1.2
6	3	4	6	2	5	(00)	17.8945907	1.3
						(01)	17.6703043	1.4
						(11)	17.8423639	−0.2
7	0	7	6	1	6	(00)	18.9719345	0.1
						(01)	18.9743628	0.5
						(12)	18.9784023	0.3
						(11)	18.9751414	−0.6
7	1	6	6	2	5	(00)	16.0695913	0.3
						(01)	16.0975961	−0.9
						(11)	16.0959109	0.0
7	1	6	7	0	7	(00)	12.1914914	0.3
						(01)	12.1879419	−0.7
						(12)	12.1871051	1.3
						(11)	12.1816922	0.1
7	1	7	6	0	6	(00)	20.3353917	0.2
						(01)	20.3311854	−0.2
						(12)	20.3255799	−0.6
						(11)	20.3284180	−1.1
7	2	5	7	1	6	(00)	9.1018196	0.0
						(01)	9.0986020	0.2
						(12)	9.1092128	−0.3
						(11)	9.0813360	0.9
7	2	6	6	1	5	(00)	27.2946495	−1.9
						(01)	27.2700520	0.9

Table 17.47. (continued)

J'	K'_a	K'_c	J	K_a	K_c	$(\sigma_1\sigma_2)$	$\nu_{\mathrm{Obs.}}$	$\nu_{\mathrm{Obs.}} - \nu_{\mathrm{Calc.}}$
upper level			lower level				GHz	kHz
						(12)	27.2279202	1.5
						(11)	27.2634222	−1.5
7	2	6	7	1	7	(00)	16.7024726	0.2
						(01)	16.6790225	−0.3
						(12)	16.6423931	1.3
						(11)	16.6691639	−1.8
7	3	4	7	2	5	(00)	14.8294534	0.0
						(01)	14.9308278	−1.3
						(11)	14.7736285	−0.1
7	3	5	6	2	4	(00)	37.0634786	1.3
						(01)	36.8830885	1.5
7	3	5	7	2	6	(00)	18.4141567	−1.0
						(01)	18.2589415	−1.5
						(11)	18.3630346	0.7
7	5	2	7	4	3	(00)	30.7867789	2.3
						(01)	30.8452546	1.3
						(12)	30.8942989	0.8
						(11)	30.6900419	−2.3
7	5	3	7	4	4	(00)	30.8056399	−2.2
						(12)	30.5045854	−0.5
						(11)	30.7090747	1.4

[a] Not included in the fit.

17.2.2 2,5-Dimethylfuran

Table 17.48. Nuclear coordinates in the principal inertial axes of 2,5-dimethylfuran (DMF) calculated at the MP2/6-311++G(d,p) level of theory. The atoms are numbered according to Figure 11.1.

	a /Å	b /Å	c /Å
C1	1.106248	0.015649	−0.000038
C2	0.716839	−1.299519	0.000005
C3	−0.716842	−1.299526	−0.000012
C4	−1.106247	0.015647	0.000045
H5	1.379731	−2.153549	−0.000011
H6	−1.379731	−2.153556	0.000025
C7	−2.428541	0.698708	0.000012
H8	−2.547499	1.329836	0.886384
H9	−2.547573	1.329595	−0.886521
H10	−3.222976	−0.051125	0.000147
C11	2.428542	0.698704	0.000035
H12	2.547543	1.329804	−0.886350
H13	2.547537	1.329618	0.886554
H14	3.222976	−0.051133	−0.000039
O15	0.000000	0.820726	−0.000047

Table 17.49. The rotational constants A, B, and C in GHz, the deviations (Dev.) between the experimental and calculated rotational constants in MHz, the angles between the internal rotor axis and the principal axes of inertia $\angle(i_1,a)$, $\angle(i_1,b)$, $\angle(i_1,c)$, and the barriers to internal rotation V_3 of the methyl rotor of DMF in cm^{-1} calculated using various methods and basis sets. Harmonic frequency calculations were carried out to verify the nature of the stationary points. The relations of the angles $\angle(i_2,a)$, $\angle(i_2,b)$, $\angle(i_2,c)$ between the internal rotor axis of inertia of the second rotor and the principal axes are: $\angle(i_2,a) = \pi - \angle(i_1,a)$, $\angle(i_2,b) = \angle(i_1,b)$, $\angle(i_2,c) = \angle(i_1,c)$.

Method/Basis set	A	Dev.	B	Dev.	C	Dev.	$\angle(i_1,a)$	$\angle(i_1,b)$	$\angle(i_1,c)$	V_3/cm^{-1}
CCSD-cc-pVDZ	6.079	85	2.113	18	1.600	15	27.25	62.75	90.00	
MP2/cc-pVTZ	6.172	−8	2.141	−11	1.622	−7	27.18	62.82	90.00	393.2
MP2/cc-pVDZ	6.056	108	2.118	12	1.601	14	27.21	62.79	90.00	356.3
MP2/6-311++G(3df,2pd)	6.166	−2	2.144	−13	1.623	−8	27.34	62.66	90.00	395.1
MP2/6-311++G(d,p)	6.113	51	2.129	1	1.611	4	27.32	62.68	90.00	404.1
MP2/6-311+G(d,p)	6.113	51	2.129	1	1.611	4	27.32	62.68	90.00	396.7
MP2/6-311G(d,p)	6.119	45	2.133	−3	1.614	1	27.25	62.75	90.00	366.9
MP2/6-31++G(d,p)[a]	6.117	47	2.125	6	1.609	6	27.43	62.57	90.00	
MP2/6-31+G(d,p)	6.116	48	2.125	6	1.609	6	27.45	62.55	90.00	387.0
MP2/6-31G(d,p)	6.130	34	2.132	−2	1.614	1	27.37	62.63	90.00	370.2
M06-2X/cc-pVQZ	6.250	−87	2.148	−17	1.631	−16	27.16	62.84	90.00	421.6
M06-2X/cc-pVTZ	6.237	−73	2.147	−17	1.630	−15	27.24	62.76	90.00	407.5
M06-2X/cc-pVDZ	6.166	−2	2.140	−9	1.621	−6	27.27	62.73	90.00	367.7
M06-2X/6-311++G(3df,2pd)	6.237	−73	2.149	−18	1.630	−16	27.28	62.72	90.00	417.2
M06-2X/6-311++G(d,p)	6.202	−38	2.142	−12	1.625	−10	27.37	62.63	90.00	410.9
M06-2X/6-311+G(d,p)	6.202	−38	2.142	−12	1.625	−10	27.37	62.63	90.00	406.3
M06-2X/6-311G(d,p)a	6.204	−40	2.144	−14	1.626	−11	27.33	62.67	90.00	375.3
M06-2X/6-31++G(d,p)	6.173	−9	2.138	−8	1.620	−6	27.45	62.55	90.00	404.5
M06-2X/6-31+G(d,p)	6.173	−9	2.138	−8	1.620	−6	27.45	62.55	90.00	401.4
M06-2X/6-31G(d,p)	6.187	−23	2.141	−10	1.623	−8	27.32	62.68	90.00	371.2
B3LYP/cc-pVQZ	6.226	−62	2.131	0	1.619	−5	27.10	62.90	90.00	404.7
B3LYP/cc-pVTZ	6.220	−56	2.130	1	1.618	−4	27.11	62.89	90.00	396.3
B3LYP/cc-pVDZ	6.137	26	2.118	12	1.607	8	27.14	62.86	90.00	362.2
B3LYP/6-311++G(3df,2pd)	6.221	−57	2.131	0	1.619	−4	27.15	62.85	90.00	403.9
B3LYP/6-311++G(d,p)	6.185	−21	2.123	8	1.612	3	27.22	62.78	90.00	404.1
B3LYP/6-311+G(d,p)	6.185	−21	2.123	8	1.612	3	27.21	62.79	90.00	400.0
B3LYP/6-311G(d,p)	6.185	−22	2.125	5	1.614	1	27.19	62.81	90.00	367.2
B3LYP/6-31++G(d,p)	6.149	15	2.117	14	1.606	8	27.31	62.69	90.00	396.2
B3LYP/6-31+G(d,p)	6.148	16	2.117	14	1.606	8	27.31	62.69	90.00	394.4
B3LYP/6-31G(d,p)	6.162	2	2.121	9	1.610	5	27.18	62.82	90.00	366.2
HF/6-311++G(3df,2pd)	6.326	−162	2.162	−31	1.643	−29	27.40	62.60	90.00	589.4
HF/6-311++G(d,p)	6.292	−128	2.155	−24	1.637	−23	27.48	62.52	90.00	574.1
HF/6-311+G(d,p)	6.292	−128	2.155	−24	1.637	−23	27.48	62.52	90.00	568.9
HF/6-311G(d,p)	6.296	−133	2.156	−25	1.638	−23	27.43	62.57	90.00	536.5
HF/6-31++G(d,p)	6.271	−107	2.151	−20	1.634	−19	27.55	62.45	90.00	554.8
HF/6-31+G(d,p)	6.270	−106	2.151	−20	1.634	−19	27.56	62.44	90.00	553.0
HF/6-31G(d,p)	6.288	−124	2.154	−23	1.637	−22	27.43	62.57	90.00	509.6
Experiment	6.161		2.131		1.615		27.31	62.70	90.00	440.8

[a] One imaginary frequency.

Table 17.50. Coefficients of the two-dimensional Fourier expansion for the potential energy surface of DMF calculated with the methods MP2 and B3LYP and the basis set 6-311++G(d,p) level of theory in a grid of 10° (Figure 11.2). Due to symmetry, only data points in the range from $\varphi_1 = 0°$ to 120° and $\varphi_2 = 0°$ to 120° are needed. The potential is expanded as $V(\varphi_2, \varphi_3) = \sum_{i=1}^{9} V_i \cdot f_i$.

		MP2	**B3LYP**
i	f_i	V_i/Hartree	V_i/Hartree
1	1	−307.842 143 925	−308.751 570 425
2	$\cos(3\varphi_1) + \cos(3\varphi_2)$	−0.000 889 120	−0.000 909 450
3	$\sin(3\varphi_1) + \sin(3\varphi_2)$	−0.000 004 592	−0.000 003 595
4	$\cos(6\varphi_1) + \cos(6\varphi_2)$	0.000 118 414	0.000 058 627
5	$\sin(6\varphi_1) + \sin(6\varphi_2)$	0.000 006 830	0.000 004 449
6	$\cos(3\varphi_1)\cos(3\varphi_2)$	−0.000 005 903	−0.000 003 101
7	$\sin(3\varphi_1)\sin(3\varphi_2)$	−0.000 145 094	−0.000 043 885
8	$\sin(3\varphi_1)\sin(6\varphi_2) + \sin(6\varphi_1)\sin(3\varphi_2)$	0.000 018 629	0.000 004 982
9	$\cos(6\varphi_1)\cos(6\varphi_2)$	0.000 012 997	–

Table 17.51. Observed frequencies ($\nu_{\text{Obs.}}$) of the (00), (01), (11), and (12) torsional species of DMF. $\nu_{\text{Obs.}} - \nu_{\text{Calc.}}$ values as obtained after a fit with XIAM.

J'	K'_a	K'_c	J	K_a	K_c	$(\sigma_1\sigma_2)$	$\nu_{\text{Obs.}}$	$\nu_{\text{Obs.}} - \nu_{\text{Calc.}}$
upper level			lower level				GHz	kHz
1	1	1	0	0	0	(00)	7.776 504 50	0.5
						(01)	7.775 746 03	0.0
						(11)	7.775 331 41	0.0
						(12)	7.774 645 35	−0.2
2	1	2	1	0	1	(00)	11.006 583 46	−0.8
						(01)	11.005 940 84	−0.6
						(11)	11.005 414 36	0.4
						(12)	11.005 183 99	0.5
2	2	0	1	1	1	(00)	20.661 518 90	−0.6
						(01)	20.666 547 55	1.8
						(11)	20.657 976 70	0.3
						(12)	20.679 545 90	0.1
2	2	0	2	1	1	(01)	12.143 275 50	3.4
						(11)	12.135 001 68	−1.0
						(12)	12.155 662 29	−0.4
2	2	1	1	1	0	(00)	20.099 386 22	−2.1
						(01)	20.090 834 73	1.3
						(11)	20.095 874 70	0.1
						(12)	20.074 305 31	−0.3
2	2	1	2	1	2	(00)	13.639 223 76	−3.2
						(01)	13.630 905 80	4.7
						(11)	13.635 714 60	−0.7
						(12)	13.615 056 54	−1.0
3	0	3	2	1	2	(00)	7.492 991 75	−0.6
						(01)	7.493 524 53	−2.1
						(11)	7.493 942 55	0.1
						(12)	7.494 179 40	0.5
3	1	3	2	0	2	(00)	13.997 384 47	−2.1

Table 17.51. (continued)

J'	K'_a	K'_c	J	K_a	K_c	$(\sigma_1\sigma_2)$	$\nu_{\mathrm{Obs.}}$	$\nu_{\mathrm{Obs.}} - \nu_{\mathrm{Calc.}}$
upper level			lower level				GHz	kHz
						(01)	13.996 783 20	−0.9
						(11)	13.996 242 16	1.0
						(12)	13.996 123 00	0.9
3	2	1	3	1	2	(00)	11.578 339 10	−0.3
						(01)	11.578 159 50	1.6
						(11)	11.575 022 99	−0.8
						(12)	11.580 815 80	−0.3
3	2	2	2	1	1	(00)	23.329 466 27	−0.9
						(01)	23.326 148 90	−0.6
						(11)	23.325 952 50	0.0
						(12)	23.319 826 35	1.0
3	2	2	3	1	3	(00)	14.440 635 56	0.8
						(01)	14.437 380 70	3.6
						(11)	14.437 070 29	−1.5
						(12)	14.431 281 50	0.1
4	0	4	3	1	3	(00)	11.597 267 50	−0.9
						(01)	11.597 704 87	−0.1
						(11)	11.598 081 32	0.7
						(12)	11.598 203 59	1.6
4	1	3	4	0	4	(00)	7.408 199 80	0.8
						(01)	7.407 578 77	1.1
						(11)	7.406 928 19	0.1
						(12)	7.406 983 50	−1.2
4	1	4	3	0	3	(00)	16.809 415 83	−2.1
						(01)	16.808 852 49	−0.4
						(11)	16.808 327 23	1.6
						(12)	16.808 250 80	0.6
4	2	2	4	1	3	(00)	11.054 592 69	−1.1
						(01)	11.053 491 14	−0.1
						(11)	11.051 414 50	−0.1
						(12)	11.053 355 28	−3.0
5	0	5	4	1	4	(00)	15.627 382 30	−1.2
						(01)	15.627 721 13	−0.1
						(11)	15.628 023 65	0.9
						(12)	15.628 096 50	1.2
5	1	4	4	2	3	(00)	9.404 570 25	1.6
						(01)	9.406 552 47	−1.1
						(11)	9.407 508 31	2.2
						(12)	9.409 566 40	1.0
5	1	4	5	0	5	(00)	9.298 567 36	−0.7
						(01)	9.297 910 56	−1.2
						(11)	9.297 233 98	−0.6
						(12)	9.297 275 73	−0.8
5	1	5	4	0	4	(00)	19.531 406 79	−2.2
						(01)	19.530 893 10	−0.3
						(11)	19.530 405 90	1.7

Table 17.51. (continued)

J'	K'_a	K'_c	J	K_a	K_c	$(\sigma_1\sigma_2)$	$\nu_{\mathrm{Obs.}}$	$\nu_{\mathrm{Obs.}} - \nu_{\mathrm{Calc.}}$
upper level			lower level				GHz	kHz
						(12)	19.530 353 65	2.0
5	2	3	5	1	4	(00)	10.725 377 51	−0.1
						(01)	10.724 089 20	0.5
						(11)	10.722 393 19	−0.1
						(12)	10.723 206 26	−0.1
5	2	4	5	1	5	(00)	16.885 104 79	0.3
						(01)	16.883 038 29	−1.2
						(11)	16.881 385 03	0.0
						(12)	16.880 564 80	−0.4
6	0	6	5	1	5	(00)	19.514 363 40	−2.1
						(01)	19.514 601 38	−0.4
						(11)	19.514 813 58	−1.6
						(12)	19.514 861 94	1.3
6	1	5	5	2	4	(00)	14.354 577 14	−0.9
						(01)	14.356 165 30	−1.2
6	1	5	6	0	6	(00)	11.725 317 53	0.5
						(01)	11.724 604 30	0.0
						(11)	11.723 870 54	−1.2
						(12)	11.723 910 44	−1.2
6	2	4	6	1	5	(00)	10.737 735 54	−0.1
						(01)	10.736 462 06	0.4
						(11)	10.734 994 00	0.0
						(12)	10.735 381 62	0.1
6	2	5	6	1	6	(01)	18.527 300 90	1.5
6	3	3	6	2	4	(00)	19.613 177 60	−1.0
						(01)	19.613 679 80	0.8
7	1	6	6	2	5	(01)	19.342 735 40	1.1
						(01)	14.634 077 36	0.9
7	2	5	7	1	6	(00)	11.210 046 98	0.9
						(01)	11.208 861 55	0.6
						(11)	11.207 578 15	1.9
						(12)	11.207 770 43	−5.3[a]
8	2	6	8	1	7	(00)	12.232 434 91	−0.3
						(01)	12.231 367 47	−1.4
						(11)	12.230 254 26	7.0[a]
						(12)	12.230 353 27	−4.8[a]

[a] Not included in the fit.

17.2.3 2-Acetyl-5-Methylfuran

Table 17.52. Fourier coefficients of the potential energy curve of 2-acetyl-5-methylfuran (AMF) obtained by varying the dihedral angle $\varphi_1 = \angle(O_{11},C_4,C_{12},O_{13})$ in a grid of 2°, while all other parameters were optimized at the MP2/6-311++G(d,p) level of theory. The potential is expanded as $V(\varphi) = \sum_{n=1}^{15} a_n \cdot \cos(n \cdot \varphi)$.

	Hartree	cm^{-1}
a_0	−420.923 233 570	
a_1	0.000 929 801	204.1
a_2	−0.006 984 709	−1533.0
a_3	−0.000 194 641	−42.7
a_4	0.000 570 572	125.2
a_5	0.000 054 936	12.1
a_6	0.000 019 398	4.3
a_7	−0.000 011 200	−2.5
a_8	0.000 044 615	9.8
a_{10}	0.000 010 989	2.4
a_{11}	−0.000 011 325	−2.5
a_{12}	0.000 009 100	2.0
a_{13}	−0.000 009 773	−2.1
a_{15}	−0.000 011 416	−2.5

Table 17.53. The calculated rotational constants A, B, and C in GHz, the deviations (Dev.) between the experimental and the calculated rotational constants in MHz, the angles between the internal rotor axes and the principal axes of inertia $\angle(i_1,a)$, $\angle(i_1,b)$, $\angle(i_1,c)$ and $\angle(i_2,a)$, $\angle(i_2,b)$, $\angle(i_2,c)$ in degrees, and the barriers to internal rotation $V_{3,1}$ and $V_{3,2}$ in cm^{-1} of the ring methyl group and the acetyl methyl group, respectively, of the *trans* conformer of AMF calculated at various levels of theory. Harmonic frequency calculations were carried out to verify the nature of the stationary points.

Method/Basis set	A	Dev.	B	Dev.	C	Dev.	$\angle(i_1,a)$	$\angle(i_1,b)$	$\angle(i_1,c)$	$\angle(i_2,a)$	$\angle(i_2,b)$	$\angle(i_2,c)$	$V_{3,1}$	$V_{3,2}$
CCSD/cc-pVDZ	3.654	45	1.116	10	0.864	9	143.41	126.59	90.00	78.20	168.20	90.00		
CCSD/6-311++G(d,p)[a]	3.675	25	1.124	2	0.870	3	143.08	126.92	90.00	78.43	168.43	90.00		
MP2/cc-pVTZ	3.697	3	1.134	−9	0.877	−5	143.37	126.63	90.00	78.64	168.64	89.97	331	
MP2/cc-pVDZ	3.643	56	1.120	6	0.866	7	143.45	126.55	90.00	78.39	168.39	89.96	310	283
MP2/6-311++G(3df,2pd)	3.691	9	1.137	−11	0.878	−6	143.09	126.91	90.00	78.71	168.71	89.97		
MP2/6-311++G(d,p)	3.662	37	1.127	−2	0.871	1	143.11	126.89	90.00	78.59	168.59	89.99	340	241
MP2/6-311+G(d,p)	3.662	37	1.127	−2	0.871	1	143.11	126.89	90.00	78.59	168.59	89.99	335	260
MP2/6-311G(d,p)	3.670	29	1.128	−2	0.872	1	143.29	126.71	90.00	78.45	168.45	89.98	322	240
MP2/6-31++G(d,p)	3.665	35	1.124	2	0.870	3	143.07	126.93	90.00	78.35	168.35	90.00	325	
MP2/6-31+G(d,p)	3.665	35	1.124	2	0.870	3	143.05	126.95	90.00	78.33	168.33	90.00	327	
MP2/6-31G(d,p)	3.677	23	1.127	−1	0.872	1	143.27	126.73	90.00	78.25	168.25	89.98	322	299
M06-2X/cc-pVQZ	3.740	−40	1.137	−11	0.881	−9	143.55	126.45	90.00	78.38	168.38	90.00	358	292
M06-2X/cc-pVTZ	3.736	−37	1.137	−11	0.881	−8	143.54	126.46	90.00	78.45	168.45	90.00	352	292
M06-2X/cc-pVDZ	3.705	−5	1.132	−6	0.876	−3	143.56	126.44	90.00	78.36	168.36	89.96	317	269
M06-2X/6-311++G(3df,2pd)	3.733	−34	1.138	−12	0.881	−9	143.44	126.56	90.00	78.51	168.51	90.00	356	300
M06-2X/6-311++G(d,p)	3.717	−17	1.134	−9	0.879	−6	143.36	126.64	90.00	78.59	168.59	90.00	352	264
M06-2X/6-311+G(d,p)	3.717	−17	1.134	−9	0.879	−6	143.35	126.65	90.00	78.59	168.59	90.00	347	265
M06-2X/6-311G(d,p)	3.720	−21	1.135	−9	0.879	−6	143.45	126.55	90.00	78.54	168.54	90.00	326	255
M06-2X/6-31++G(d,p)	3.700	−1	1.132	−6	0.876	−3	143.22	126.78	90.00	78.38	168.38	90.00	339	248
M06-2X/6-31+G(d,p)	3.700	−1	1.132	−6	0.876	−3	143.22	126.78	90.00	78.39	168.39	90.00	335	246
M06-2X/6-31G(d,p)	3.709	−9	1.133	−7	0.877	−4	143.44	126.56	90.00	78.37	168.37	90.00	315	269
B3LYP/cc-pVQZ	3.726	−26	1.126	0	0.874	−1	143.78	126.22	90.00	77.62	167.62	90.00	326	192
B3LYP/cc-pVTZ	3.724	−24	1.125	1	0.873	−1	143.79	126.21	90.00	77.63	167.63	90.00	321	190
B3LYP/cc-pVDZ	3.686	14	1.119	7	0.868	5	143.80	126.20	90.00	77.63	167.63	90.00	297	201
B3LYP/6-311++G(3df,2pd)	3.723	−23	1.126	0	0.874	−1	143.72	126.28	90.00	77.66	167.66	90.00	322	193
B3LYP/6-311++G(d,p)	3.704	−4	1.122	4	0.870	3	143.65	126.35	90.00	77.74	167.74	90.00	323	165
B3LYP/6-311+G(d,p)	3.704	−4	1.122	4	0.870	3	143.65	126.35	90.00	77.73	167.73	90.00	320	166
B3LYP/6-311G(d,p)	3.707	−7	1.122	4	0.871	2	143.72	126.28	90.00	77.70	167.70	90.00	300	163
B3LYP/6-31++G(d,p)	3.685	14	1.118	8	0.867	6	143.55	126.45	90.00	77.56	167.56	90.00	315	163

Table 17.53. (continued)

Method/Basis set	*A*	Dev.	*B*	Dev.	*C*	Dev.	∠(i$_1$,a)	∠(i$_1$,b)	∠(i$_1$,c)	∠(i$_2$,a)	∠(i$_2$,b)	∠(i$_2$,c)	$V_{3,1}$	$V_{3,2}$
B3LYP/6-31+G(d,p)	3.685	14	1.118	8	0.867	6	143.54	126.46	90.00	77.56	167.56	90.00	312	162
B3LYP/6-31G(d,p)	3.693	6	1.120	6	0.869	4	143.75	126.25	90.00	77.55	167.55	90.00	295	192
HF/6-311++G(3df,2pd)	3.783	−83	1.141	−15	0.886	−13	143.25	126.75	90.00	77.76	167.76	90.00	501	349
HF/6-311++G(d,p)	3.766	−66	1.138	−12	0.883	−11	143.19	126.81	90.00	77.87	167.87	90.00	492	319
HF/6-311+G(d,p)	3.766	−66	1.138	−12	0.883	−11	143.18	126.82	90.00	77.86	167.86	90.00	486	321
HF/6-311G(d,p)	3.770	−71	1.139	−13	0.884	−11	143.27	126.73	90.00	77.81	167.81	90.00	462	314
HF/6-31++G(d,p)	3.755	−56	1.136	−10	0.882	−9	143.12	126.88	90.00	77.75	167.75	90.00	474	313
HF/6-31+G(d,p)	3.755	−56	1.136	−10	0.882	−9	143.11	126.89	90.00	77.75	167.75	90.00	472	
HF/6-31G(d,p)	3.764	−64	1.137	−11	0.883	−10	143.28	126.72	90.00	77.67	167.67	90.00	435	
Experiment	3.700		1.126		0.873		143.56	126.44	90.00	75.17	165.17	90.00	370	308

[a] No frequency calculation at the CCSD/6-311++G(d,p) level.

Table 17.54. The calculated rotational constants *A*, *B*, and *C* in GHz, the deviations (Dev.) between the experimental and the calculated rotational constants in MHz, the angles between the internal rotor axes and the principal axes of inertia ∠(i$_1$,a), ∠(i$_1$,b), ∠(i$_1$,c) and ∠(i$_2$,a), ∠(i$_2$,b), ∠(i$_2$,c) in degrees, and the barriers to internal rotation $V_{3,1}$ and $V_{3,2}$ in cm^{-1} of the ring methyl group and the acetyl methyl group, respectively, of the *cis* conformer of AMF calculated at various levels of theory. ΔE is the relative energy in kJ·mol^{-1} with respect to the *trans* conformer. Harmonic frequency calculations were carried out to verify the nature of the stationary points.

Method/Basis set	*A*	Dev.	*B*	Dev.	*C*	Dev.	∠(i$_1$,a)	∠(i$_1$,b)	∠(i$_1$,c)	∠(i$_2$,a)	∠(i$_2$,b)	∠(i$_2$,c)	ΔE	$V_{3,1}$	$V_{3,2}$
CCSD/cc-pVDZ[a]	3.861	53	1.086	9	0.857	9	146.49	123.51	90.00	−44.23	45.77	89.99	6.6		
CCSD/6-311++G(d,p)[a]	3.898	16	1.091	4	0.862	4	146.45	123.55	90.00	−44.22	45.78	90.00	4.0		
MP2/cc-pVTZ	3.902	12	1.104	−8	0.870	−4	146.58	123.42	90.00	−44.68	45.32	89.99	4.7	322	190
MP2/cc-pVDZ	3.833	81	1.092	4	0.859	6	146.37	123.63	90.00	−44.50	45.50	90.00	6.6	297	311
MP2/6-311++G(3df,2pd)	3.903	11	1.104	−9	0.870	−5	146.41	123.59	90.00	−44.57	45.43	89.99	3.9		
MP2/6-311++G(d,p)	3.870	44	1.097	−1	0.864	2	146.36	123.64	90.00	−44.48	45.52	90.00	3.9	334	207
MP2/6-311+G(d,p)	3.870	44	1.097	−1	0.864	2	146.36	123.64	90.00	−44.48	45.52	90.00	3.9	326	200
MP2/6-311G(d,p)	3.871	43	1.098	−3	0.865	1	146.36	123.64	90.00	−44.45	45.55	89.98	5.9	308	244
MP2/6-31++G(d,p)[b]	3.866	47	1.094	1	0.862	3	146.14	123.86	90.00	−43.95	46.05	90.00	6.1		
MP2/6-31+G(d,p)[b]	3.866	47	1.094	1	0.862	3	146.13	123.87	90.00	−43.93	46.07	90.00	6.0		
MP2/6-31G(d,p)	3.871	43	1.098	−2	0.865	1	146.14	123.86	90.00	−43.92	46.08	89.98	6.9	309	273
M06-2X/cc-pVQZ[b]	3.963	−50	1.105	−9	0.873	−8	146.87	123.13	90.00	−44.42	45.58	90.00	4.2		
M06-2X/cc-pVTZ	3.956	−43	1.105	−9	0.873	−7	146.77	123.23	90.00	−44.39	45.61	90.00	5.2	330	210
M06-2X/cc-pVDZ	3.910	3	1.102	−6	0.869	−4	146.49	123.51	90.00	−44.14	45.86	90.00	7.5	302	256

Table 17.54. (continued)

Method/Basis set	*A*	Dev.	*B*	Dev.	*C*	Dev.	∠(i_1,a)	∠(i_1,b)	∠(i_1,c)	∠(i_2,a)	∠(i_2,b)	∠(i_2,c)	Δ*E*	$V_{3,1}$	$V_{3,2}$
M06-2X/6-311++G(3df,2pd)	3.958	−44	1.105	−9	0.873	−8	146.74	123.26	90.00	−44.37	45.63	90.00	3.6	335	217
M06-2X/6-311++G(d,p)[b]	3.938	−25	1.102	−6	0.870	−5	146.60	123.40	90.00	−44.30	45.70	90.00	5.3		194
M06-2X/6-311+G(d,p)[b]	3.938	−24	1.102	−6	0.870	−5	146.59	123.41	90.00	−44.29	45.71	90.00	5.3		191
M06-2X/6-311G(d,p)	3.936	−22	1.103	−8	0.871	−6	146.56	123.44	90.00	−44.25	45.75	90.00	7.4	307	218
M06-2X/6-31++G(d,p)	3.918	−4	1.100	−4	0.868	−2	146.38	123.62	90.00	−43.92	46.08	90.00	5.6		165
M06-2X/6-31+G(d,p)[b]	3.918	−4	1.100	−4	0.868	−2	146.38	123.62	90.00	−43.91	46.09	90.00	5.6		166
M06-2X/6-31G(d,p)[b]	3.919	−6	1.102	−6	0.869	−4	146.46	123.54	90.00	−44.06	45.94	90.00	7.0	300	234
B3LYP/cc-pVQZ	3.944	−30	1.096	0	0.867	−1	146.86	123.14	90.00	−43.76	46.24	90.00	5.2	311	94
B3LYP/cc-pVTZ	3.939	−25	1.095	0	0.866	−1	146.83	123.17	90.00	−43.70	46.30	90.00	6.1	308	104
B3LYP/cc-pVDZ	3.888	26	1.091	5	0.861	5	146.67	123.33	90.00	−43.79	46.21	90.00	8.4	284	192
B3LYP/6-311++G(3df,2pd)	3.942	−28	1.095	0	0.866	−1	146.85	123.15	90.00	−43.83	46.17	90.00	5.0	310	95
B3LYP/6-311++G(d,p)	3.920	−7	1.091	4	0.863	3	146.74	123.26	90.00	−43.79	46.21	90.00	6.0	313	87
B3LYP/6-311+G(d,p)	3.920	−6	1.091	4	0.863	3	146.74	123.26	90.00	−43.78	46.22	90.00	6.0	309	86
B3LYP/6-311G(d,p)	3.917	−3	1.093	3	0.864	2	146.68	123.32	90.00	−43.70	46.30	90.00	8.4	287	126
B3LYP/6-31++G(d,p)	3.898	16	1.088	7	0.860	6	146.60	123.40	90.00	−43.58	46.42	90.00	6.6		71
B3LYP/6-31+G(d,p)	3.898	16	1.088	7	0.860	6	146.60	123.40	90.00	−43.58	46.42	90.00	6.6	302	71
B3LYP/6-31G(d,p)	3.899	15	1.091	4	0.862	4	146.64	123.36	90.00	−43.65	46.35	90.00	7.7	283	147
HF/6-311++G(3df,2pd)	4.035	−121	1.107	−11	0.878	−12	146.70	123.30	90.00	−43.37	46.63	90.00	4.1	487	215
HF/6-311++G(d,p)	4.015	−101	1.104	−8	0.875	−10	146.58	123.42	90.00	−43.36	46.64	90.00	6.2	477	200
HF/6-311+G(d,p)	4.015	−101	1.104	−8	0.875	−10	146.57	123.43	90.00	−43.35	46.65	90.00	6.2	472	198
HF/6-311G(d,p)	4.014	−101	1.105	−10	0.876	−11	146.56	123.44	90.00	−43.30	46.70	90.00	8.1	450	217
HF/6-31++G(d,p)	4.001	−87	1.102	−7	0.874	−8	146.46	123.54	90.00	−43.17	46.83	90.00	7.0	462	184
HF/6-31+G(d,p)	4.001	−87	1.102	−7	0.874	−8	146.46	123.54	90.00	−43.17	46.83	90.00	6.9	458	188
HF/6-31G(d,p)	4.005	−91	1.104	−9	0.875	−9	146.53	123.47	90.00	−43.22	46.78	90.00	8.6	422	250
Experiment	3.914		1.096		0.866		146.45	123.55	90.00	−41.01	48.99	90.00		356	213

[a] No frequency calculations. [b] One imaginary frequency obtained for the optimized structure.

Table 17.55. Nuclear coordinates in the principal inertial axes of the *trans* and the *cis* conformer of AMF calculated at the MP2/6-311++G(d,p) level of theory. The atoms are numbered according to Figure 12.2.

	***trans* conformer**			***cis* conformer**		
	a /Å	b /Å	c /Å	a /Å	b /Å	c /Å
C1	−1.787897	−0.088905	−0.000011	−1.807956	−0.040424	0.000007
C2	−1.628567	1.280107	0.000075	−1.573845	1.317660	−0.000074
C3	−0.228803	1.530325	0.000057	−0.161010	1.480881	−0.000045
C4	0.381373	0.292666	0.000044	0.375231	0.205457	−0.000011
H5	−2.431238	2.004390	0.000028	−2.331403	2.088827	−0.000130
H6	0.290714	2.477897	0.000237	0.397853	2.406380	−0.000060
C7	−2.977803	−0.982065	−0.000076	−3.046471	−0.864667	0.000060
H8	−2.987432	−1.623334	−0.886845	−3.087960	−1.505296	−0.885943
H9	−2.987279	−1.623642	0.886471	−3.087995	−1.505132	0.886180
H10	−3.886294	−0.375945	0.000105	−3.920538	−0.209973	−0.000018
O11	−0.567414	−0.692556	−0.000019	−0.628418	−0.714080	0.000036
C12	1.798494	−0.104789	−0.000060	1.759498	−0.293726	0.000009
O13	2.674296	0.752302	−0.000123	2.009943	−1.491916	−0.000101
C14	2.097818	−1.587540	0.000107	2.841357	0.768674	0.000105
H15	1.656167	−2.061168	0.882013	2.748335	1.405244	−0.885091
H16	1.654839	−2.061790	−0.880780	2.748294	1.405123	0.885383
H17	3.178844	−1.730564	−0.000595	3.815659	0.279136	0.000095

Table 17.56. Fourier coefficients of the potential energy curve of AMF obtained by varying the dihedral angle $\varphi_2 = \angle(C_2,C_1,C_7,H_8)$ in a grid of 2°, while all other parameters were optimized at the MP2/6-311++G(d,p) level of theory. The potential is expanded as $V(\varphi) = \sum_{n=1}^{9} a_n \cdot \cos(n \cdot \varphi)$.

	trans		***cis***	
	Hartree	cm^{-1}	Hartree	cm^{-1}
a_0	−420.929578459		−420.928086253	
a_3	−0.000770474	−169.1	−0.000760299	−166.9
a_6	0.000040522	8.9	0.000034940	7.7
a_9	−0.000002772	−0.6	−0.000001371	−0.3

Table 17.57. Fourier coefficients of the potential energy curve of the *cis* conformer of AMF obtained by varying the dihedral angle $\varphi_3 = \angle(O_{13},C_{12},C_{14},H_{15})$ in a grid of 2°, while all other parameters were optimized at the MP2/6-311++G(d,p) level of theory. The data set of the *trans* conformer was not fitted. The potential is expanded as $V(\varphi) = \sum_{n=1}^{9} a_n \cdot \cos(n \cdot \varphi)$.

	Hartree	cm^{-1}
a_0	−420.928 419 702	
a_3	−0.000 467 771	−102.7
a_6	0.000 074 398	16.3
a_9	−0.000 001 907	−0.4

Table 17.58. Coefficients of the two-dimensional Fourier expansion for the potential energy surfaces of the *trans* and the *cis* conformer of AMF as given in Figure 12.6. The potential is expanded as $V(\varphi_2, \varphi_3) = \sum_{i=1}^{16} V_i \cdot f_i$.

		trans	***cis***
i	f_i	V_i/Hartree	V_i/Hartree
1	1	−420.927 685 702	−420.929 124 788
2	$\cos(3\varphi_2)$	−0.000 757 134	−0.000 790 372
3	$\sin(3\varphi_2)$	−0.000 003 554	–
4	$\cos(3\varphi_3)$	0.000 468 843	0.000 573 306
5	$\sin(3\varphi_3)$	0.000 003 869	−0.000 006 001
6	$\cos(6\varphi_2)$	0.000 033 322	0.000 040 093
7	$\sin(6\varphi_2)$	0.000 002 719	0.000 003 704
8	$\cos(6\varphi_3)$	0.000 064 646	0.000 083 988
9	$\sin(6\varphi_3)$	0.000 006 993	0.000 008 902
10	$\cos(3\varphi_2)\cos(3\varphi_3)$	0.000 001 472	0.000 021 137
11	$\sin(3\varphi_2)\sin(3\varphi_3)$	−0.000 004 108	–
12	$\cos(6\varphi_2)\cos(3\varphi_3)$	–	−0.000 005 100
13	$\cos(3\varphi_2)\cos(6\varphi_3)$	−0.000 001 438	−0.000 016 960
14	$\sin(3\varphi_2)\sin(6\varphi_3)$	0.000 001 003	−0.000 007 216
15	$\cos(6\varphi_2)\cos(6\varphi_3)$	0.000 001 031	0.000 003 477
16	$\cos(6\varphi_2)\sin(6\varphi_3)$	–	0.000 003 429

Table 17.59. Observed frequencies ($\nu_{\mathrm{Obs.}}$) of the (00), (01), (10), (11), and (12) torsional species of the *trans* conformer of AMF. $\nu_{\mathrm{Obs.}} - \nu_{\mathrm{Calc.}}$ values as obtained after a fit with XIAM.

J'	K_a'	K_c'	J	K_a	K_c	$(\sigma_1\sigma_2)$	$\nu_{\mathrm{Obs.}}$	$\nu_{\mathrm{Obs.}} - \nu_{\mathrm{Calc.}}$
upper level			lower level				GHz	kHz
2	2	0	1	1	1	(00)	12.243 628 1	−2.8
						(10)	12.257 447 1	4.3
						(01)	12.252 270 7	−8.5
						(11)	12.272 518 1	−7.5
						(12)	12.244 173 4	−8.1
2	2	1	1	1	0	(00)	11.972 713 0	−3.0
						(10)	11.956 697 2	8.2
						(01)	11.963 394 2	9.8
						(12)	11.969 259 6	−3.5
3	2	1	2	1	2	(00)	14.566 197 7	7.1
						(10)	14.570 163 8	3.0
						(01)	14.568 195 2	4.3
						(11)	14.578 155 4	7.7
						(12)	14.564 879 8	0.7
3	2	2	2	1	1	(00)	13.718 485 3	0.2
						(10)	13.712 260 5	−1.2
						(01)	13.715 529 5	−0.8
						(11)	13.703 323 5	−5.9
						(12)	13.716 580 5	0.8
4	1	4	3	0	3	(00)	9.474 638 2	−1.9
						(10)	9.474 259 3	−2.1
						(01)	9.474 748 5	−0.7
						(12)	9.474 482 1	0.9
4	2	3	3	1	2	(00)	15.335 363 6	−1.7
						(10)	15.332 455 3	−2.3
						(01)	15.334 173 2	0.7
						(11)	15.328 797 5	0.6
						(12)	15.333 797 9	1.0
5	0	5	4	0	4	(00)	9.662 907 7	0.5
						(10)	9.662 820 2	0.0
						(01)	9.662 643 0	−0.1
						(11)	9.662 563 3	1.9
						(12)	9.662 551 4	0.4
5	1	4	4	1	3	(00)	10.541 205 5	−0.3
						(10)	10.541 050 5	0.5
						(01)	10.540 453 0	−1.3
						(11)	10.540 297 5	−1.2
5	1	5	4	0	4	(00)	10.943 368 0	5.9
						(10)	10.943 021 9	−4.8
						(01)	10.943 579 6	−0.1
						(11)	10.943 146 1	0.3
						(12)	10.943 343 0	0.1
5	1	5	4	1	4	(00)	9.291 739 2	0.9
						(10)	9.291 709 4	1.5
						(01)	9.291 546 0	−0.9

Table 17.59. (continued)

J'	K'_a	K'_c	J	K_a	K_c	$(\sigma_1\sigma_2)$	$\nu_{\text{Obs.}}$	$\nu_{\text{Obs.}} - \nu_{\text{Calc.}}$
upper level			lower level				GHz	kHz
						(12)	9.2914891	0.9
5	2	3	4	2	2	(00)	10.2865337	−1.1
						(10)	10.2854504	−0.4
						(01)	10.2853326	−0.7
						(11)	10.2828899	0.0
						(12)	10.2856687	−0.3
5	2	4	4	1	3	(00)	16.8264967	−3.4
						(10)	16.8246267	−4.1
						(01)	16.8259365	0.3
						(11)	16.8229865	2.3
						(12)	16.8251555	1.4
5	2	4	4	2	3	(00)	9.9551015	−0.7
						(10)	9.9559997	0.1
						(01)	9.9551213	0.6
						(11)	9.9573629	1.1
						(12)	9.9546138	−0.5
5	3	2	4	3	1	(00)	10.0641000	−0.5
						(10)	10.0574671	−0.6
						(01)	10.0576360	−0.2
						(11)	10.0561709	−1.9
5	3	3	4	3	2	(00)	10.0478458	−1.1
						(10)	10.0542956	−0.2
						(01)	10.0531997	2.0
						(11)	10.0544736	2.1
						(12)	10.0507791	1.3
6	0	6	5	0	5	(00)	11.4495360	−0.1
						(10)	11.4494396	0.1
						(01)	11.4493273	−1.0
						(11)	11.4492272	−0.6
						(12)	11.4492371	1.3
6	0	6	5	1	5	(00)	10.1690822	1.0
						(10)	10.1692336	0.5
						(01)	10.1683910	−0.7
						(11)	10.1686437	0.2
						(12)	10.1684429	−1.1
6	1	5	5	1	4	(00)	12.5883089	0.5
						(10)	12.5881295	0.0
						(01)	12.5874446	−0.3
						(11)	12.5872950	2.8
						(12)	12.5872381	−1.6
6	1	6	5	0	5	(00)	12.3927864	73.3[a]
						(10)	12.3924246	4.6
						(01)	12.3929916	−0.3
						(11)	12.3926132	0.2
6	1	6	5	1	5	(00)	11.1122576	−0.7
						(10)	11.1122146	1.1

Table 17.59. (continued)

J'	K'_a	K'_c	J	K_a	K_c	$(\sigma_1\sigma_2)$	$\nu_{\mathrm{Obs.}}$	$\nu_{\mathrm{Obs.}} - \nu_{\mathrm{Calc.}}$
upper level			lower level				GHz	kHz
						(01)	11.1120526	−2.8
						(12)	11.1119921	−0.5
6	2	4	5	2	3	(00)	12.4567089	0.0
						(10)	12.4562153	0.2
						(01)	12.4556169	−0.2
						(12)	12.4556739	−0.6
6	2	5	5	1	4	(00)	18.1990855	−3.8
						(10)	18.1976523	12.2[a]
						(01)	18.1989126	1.2
						(11)	18.1969109	2.8
						(12)	18.1980183	1.9
6	2	5	5	2	4	(00)	11.9137951	0.1
						(10)	11.9140597	0.5
						(01)	11.9134284	−1.2
						(11)	11.9142222	−0.5
						(12)	11.9131600	−0.7
6	2	5	6	1	6	(00)	10.8623020	3.7
						(10)	10.8606804	−4.5
						(01)	10.8608509	−1.6
						(11)	10.8587079	−0.1
						(12)	10.8597710	0.6
6	3	3	5	3	2	(00)	12.1135451	1.7
						(10)	12.1035235	−1.3
						(01)	12.1056028	−1.2
						(11)	12.0988086	−1.4
						(12)	12.1105571	1.0
6	3	4	5	3	3	(00)	12.0707426	0.3
						(10)	12.0805406	0.8
						(01)	12.0773075	2.4
						(11)	12.0838730	2.5
						(12)	12.0721383	−1.3
7	0	7	6	0	6	(00)	13.1969892	0.0
						(10)	13.1968890	1.4
						(11)	13.1967224	−1.0
						(12)	13.1967433	2.2
7	0	7	6	1	6	(00)	12.2538119	−0.3
						(10)	12.2539079	0.8
						(01)	12.2531695	−0.9
						(11)	12.2533373	−0.9
7	1	6	6	1	5	(00)	14.5954429	0.1
						(10)	14.5952395	1.1
						(01)	14.5945180	−1.7
						(11)	14.5943528	−1.0
						(12)	14.5942750	−2.1
7	1	7	6	0	6	(00)	13.8609490	−0.4
						(10)	13.8606989	1.1

Table 17.59. (continued)

J'	K'_a	K'_c	J	K_a	K_c	$(\sigma_1\sigma_2)$	$\nu_{\text{Obs.}}$	$\nu_{\text{Obs.}} - \nu_{\text{Calc.}}$
upper level			lower level				GHz	kHz
						(01)	13.8612315	−0.9
						(11)	13.8609124	1.2
						(12)	13.8610524	2.0
7	1	7	6	1	6	(00)	12.9177717	−0.6
						(10)	12.9177186	1.2
						(01)	12.9175674	−1.4
						(12)	12.9175011	−0.7
7	2	5	6	2	4	(00)	14.6473443	0.9
						(10)	14.6470269	0.2
						(01)	14.6461566	0.7
						(11)	14.6455833	−1.0
						(12)	14.6460949	0.7
7	2	6	6	2	5	(00)	13.8553467	0.7
						(10)	13.8553852	0.4
						(01)	13.8548169	−0.4
						(11)	13.8550970	0.0
						(12)	13.8546127	−2.3
7	3	4	6	3	3	(00)	14.1895524	−1.1
						(10)	14.1823348	−0.7
						(01)	14.1846041	−0.9
						(11)	14.1740440	−3.6
						(12)	14.1877634	−1.0
7	3	5	6	3	4	(00)	14.0952803	0.8
						(10)	14.1022387	−0.4
						(01)	14.0985665	0.6
						(11)	14.1088578	3.0
						(12)	14.0951577	−0.7
7	4	3	6	4	2	(00)	14.0829256	−1.6
						(10)	14.0810816	0.6
						(01)	14.0804585	−2.2
						(11)	14.0801937	−3.1
						(12)	14.0805173	4.7
7	4	4	6	4	3	(00)	14.0795448	−0.7
						(10)	14.0811337	−1.2
						(01)	14.0804472	4.1
						(11)	14.0804585	12.6[a]
						(12)	14.0801344	−4.6
8	0	8	7	0	7	(00)	14.9233251	−0.3
						(10)	14.9232245	1.9
						(01)	14.9232039	−1.1
						(11)	14.9230931	0.4
						(12)	14.9231138	1.7
8	0	8	7	1	7	(00)	14.2593652	0.0
						(10)	14.2594126	0.2
						(01)	14.2588055	−1.1
						(11)	14.2589056	0.6

Table 17.59. (continued)

J'	K'_a	K'_c	J	K_a	K_c	$(\sigma_1\sigma_2)$	$\nu_{\mathrm{Obs.}}$	$\nu_{\mathrm{Obs.}} - \nu_{\mathrm{Calc.}}$
upper level			lower level				GHz	kHz
8	1	7	7	1	6	(00)	16.552 110 3	1.2
						(10)	16.551 877 8	−1.9
						(01)	16.551 193 0	−0.4
						(11)	16.550 999 5	−1.0
						(12)	16.550 926 3	−1.1
8	1	8	7	0	7	(00)	15.373 412 7	−2.5
						(10)	15.373 205 3	2.7
						(01)	15.373 656 2	−0.7
						(11)	15.373 384 5	−7.2
						(12)	15.373 498 8	1.9
8	1	8	7	1	7	(00)	14.709 454 7	−0.4
						(10)	14.709 393 7	1.3
8	2	6	7	2	5	(00)	16.836 299 8	1.2
						(10)	16.836 027 8	−0.7
						(01)	16.834 967 4	1.0
						(11)	16.834 572 1	1.5
						(12)	16.834 822 6	0.6
8	2	7	7	2	6	(00)	15.777 576 8	0.0
						(10)	15.777 515 7	0.7
						(01)	15.776 963 2	−0.1
						(11)	15.777 027 3	0.7
8	3	5	7	3	4	(00)	16.300 334 0	−0.8
						(10)	16.296 919 5	−0.9
						(01)	16.297 559 5	0.9
						(11)	16.290 512 2	−0.1
						(12)	16.298 826 8	0.2
8	3	6	7	3	5	(00)	16.118 066 7	0.4
						(10)	16.121 183 4	−1.1
						(01)	16.118 870 7	0.4
						(11)	16.125 607 8	0.8
						(12)	16.117 320 3	0.5
8	4	4	7	4	3	(00)	16.121 565 9	1.0
						(01)	16.116 629 8	−2.4
						(11)	16.115 950 3	−6.4
						(12)	16.117 463 8	5.2
8	4	5	7	4	4	(10)	16.116 442 4	0.6
						(01)	16.115 457 8	3.5
						(11)	16.115 833 7	3.2
9	0	9	8	0	8	(00)	16.643 243 4	−1.0
						(10)	16.643 144 3	0.7
9	0	9	8	1	8	(00)	16.193 153 2	−1.3
						(10)	16.193 165 3	1.6
						(01)	16.192 688 6	−0.6
						(11)	16.192 732 8	0.0
						(12)	16.192 663 8	−0.2
9	1	8	8	1	7	(00)	18.449 299 0	0.0

Table 17.59. (continued)

J'	K'_a	K'_c	J	K_a	K_c	$(\sigma_1\sigma_2)$	$\nu_{\text{Obs.}}$	$\nu_{\text{Obs.}} - \nu_{\text{Calc.}}$
upper level			lower level				GHz	kHz
						(10)	18.4490453	−0.4
						(01)	18.4484557	−0.5
						(11)	18.4482257	−1.3
						(12)	18.4481795	0.6
9	1	9	8	0	8	(00)	16.9392734	−1.5
						(10)	16.9390978	1.5
						(01)	16.9394500	−1.7
						(11)	16.9392435	7.9
						(12)	16.9393039	−6.6
9	1	9	8	1	8	(00)	16.4891846	−0.5
						(10)	16.4891174	1.1
						(01)	16.4890000	0.2
						(11)	16.4889390	2.5
						(12)	16.4889247	−1.0
9	2	7	8	2	6	(00)	19.0039577	−0.2
						(10)	19.0036844	−0.2
						(01)	19.0024829	1.0
						(11)	19.0021588	1.6
						(12)	19.0022600	0.1
9	2	8	8	2	7	(00)	17.6788612	−2.1
						(10)	17.6787468	−0.3
						(01)	17.6782037	−0.9
						(11)	17.6781620	1.3
						(12)	17.6780175	1.3
9	3	6	8	3	5	(00)	18.4525131	−1.4
						(10)	18.4509192	−1.0
						(01)	18.4504769	−0.3
						(11)	18.4469501	−0.1
9	3	7	8	3	6	(00)	18.1350337	−2.4
						(10)	18.1362957	0.4
						(01)	18.1347688	−1.1
						(11)	18.1379447	0.4
						(12)	18.1339971	2.4
10	0	10	9	0	9	(00)	18.3650810	−0.8
						(10)	18.3649843	0.2
						(11)	18.3648812	1.8
10	0	10	9	1	9	(00)	18.0690512	−0.1
						(10)	18.0690317	0.2
						(01)	18.0686713	−1.7
						(12)	18.0686319	1.1
10	1	9	9	1	8	(00)	20.2830532	−0.2
						(10)	20.2827796	0.4
						(01)	20.2823281	−1.7
						(11)	20.2820669	4.1
						(12)	20.2820485	−0.1
10	1	10	9	0	9	(00)	18.5552025	−0.4

Table 17.59. (continued)

J'	K'_a	K'_c	J	K_a	K_c	$(\sigma_1\sigma_2)$	$\nu_{\mathrm{Obs.}}$	$\nu_{\mathrm{Obs.}} - \nu_{\mathrm{Calc.}}$
upper level			lower level				GHz	kHz
						(10)	18.555052 4	0.8
						(01)	18.555309 3	−1.7
						(11)	18.555134 9	0.7
						(12)	18.555184 5	−0.8
10	1	10	9	1	9	(00)	18.259172 1	−0.3
						(10)	18.259100 4	1.4
						(01)	18.258999 2	−1.2
						(12)	18.258923 2	−0.4

[a] Not included in the fit.

Table 17.60. Observed frequencies ($\nu_{\mathrm{Obs.}}$) of the (00), (01), (10), (11), and (12) torsional species of the *cis* conformer of AMF. $\nu_{\mathrm{Obs.}} - \nu_{\mathrm{Calc.}}$ values as obtained after a fit with XIAM.

J'	K'_a	K'_c	J	K_a	K_c	$(\sigma_1\sigma_2)$	$\nu_{\mathrm{Obs.}}$	$\nu_{\mathrm{Obs.}} - \nu_{\mathrm{Calc.}}$
upper level			lower level				GHz	kHz
2	2	0	1	1	1	(00)	12.858409 9	2.6
						(10)	12.879958 7	5.2
						(01)	13.077185 1	8.7
						(11)	13.038513 5	2.4
						(12)	13.113334 6	0.5
2	2	1	1	1	0	(00)	12.614706 5	1.5
						(01)	12.375499 7	12.4[a]
						(11)	12.410993 3	−6.8
						(12)	12.336145 9	−6.9
3	2	1	2	1	2	(00)	15.103568 1	2.5
						(10)	15.112466 7	3.1
						(01)	15.274434 0	−3.6
						(11)	15.241407 3	−2.1
						(12)	15.304761 8	−7.9
3	2	2	2	1	1	(00)	14.345725 9	−0.9
						(10)	14.333620 2	−2.2
						(01)	14.153939 3	−0.3
						(11)	14.183798 8	5.8
						(12)	14.120386 1	4.3
3	3	0	2	2	1	(00)	20.571259 5	−0.8
4	1	4	3	0	3	(00)	9.663173 2	−2.2
						(10)	9.662642 4	44.3[a]
						(01)	9.656426 1	−1.6
						(11)	9.656939 8	0.0
						(12)	9.654769 7	1.4
4	2	3	3	1	2	(00)	15.959843 8	−0.3
						(10)	15.954269 1	−1.8
						(01)	15.821169 2	−2.2
						(11)	15.846167 0	2.7
						(12)	15.792096 2	3.4
4	2	3	4	1	4	(10)	9.976184 8	−5.6

Table 17.60. (continued)

J'	K'_a	K'_c	J	K_a	K_c	$(\sigma_1\sigma_2)$	$\nu_{\text{Obs.}}$	$\nu_{\text{Obs.}} - \nu_{\text{Calc.}}$
upper level			lower level				GHz	kHz
5	0	5	4	0	4	(00)	9.548661 5	−0.1
						(01)	9.547670 5	−0.3
						(11)	9.547626 0	−0.7
						(12)	9.547524 1	−0.2
5	1	4	4	1	3	(00)	10.316938 0	−0.3
						(10)	10.316771 4	0.6
						(01)	10.313967 2	0.2
						(11)	10.314237 9	0.2
						(12)	10.313362 5	−0.8
5	1	5	4	0	4	(00)	11.127239 8	−0.7
						(10)	11.126722 6	−0.4
						(01)	11.122360 5	−3.3
						(11)	11.122485 8	−4.5
						(12)	11.121208 5	1.0
5	1	5	4	1	4	(00)	9.176406 6	0.8
						(10)	9.176388 4	0.5
						(01)	9.177297 1	0.0
						(11)	9.176904 9	0.9
						(12)	9.177652 1	0.2
5	2	3	4	2	2	(00)	10.033213 9	−0.5
						(10)	10.030952 4	−0.4
						(01)	9.983331 8	0.7
						(11)	9.990543 8	1.6
						(12)	9.976714 4	1.4
5	2	4	4	1	3	(00)	17.459230 6	−1.0
						(10)	17.455911 3	−0.3
						(01)	17.372620 1	−1.7
						(11)	17.389549 6	2.2
						(12)	17.350994 8	3.0
5	2	4	4	2	3	(00)	9.775980 2	−0.7
						(10)	9.778069 3	1.0
						(01)	9.824161 3	1.0
						(11)	9.816711 5	−0.2
						(12)	9.830665 4	−2.0
6	0	6	5	0	5	(00)	11.338091 3	−1.8
						(10)	11.337982 9	0.4
						(01)	11.337127 2	−0.8
						(11)	11.337049 5	0.1
6	0	6	5	1	5	(00)	9.759514 1	−0.1
						(10)	9.759826 7	1.1
						(01)	9.762434 5	−0.7
						(11)	9.762187 0	1.2
						(12)	9.763300 9	−1.5
6	1	5	5	1	4	(00)	12.335306 2	−0.2
						(10)	12.335119 2	−0.3
						(01)	12.332446 2	−3.8

Table 17.60. (continued)

J'	K'_a	K'_c	J	K_a	K_c	$(\sigma_1\sigma_2)$	$\nu_{\mathrm{Obs.}}$	$\nu_{\mathrm{Obs.}} - \nu_{\mathrm{Calc.}}$
upper level			lower level				GHz	kHz
						(11)	12.3325853	3.8
						(12)	12.3319439	−1.6
6	1	6	5	0	5	(00)	12.5602239	−1.8
						(10)	12.5597646	0.3
						(01)	12.5565600	1.0
						(11)	12.5564908	2.6
						(12)	12.5557125	1.3
6	1	6	5	1	5	(00)	10.9816457	−1.0
						(10)	10.9816082	0.9
						(01)	10.9818653	−0.8
						(12)	10.9820292	1.2
6	2	4	5	2	3	(00)	12.1350939	−0.3
						(10)	12.1341545	−0.1
						(01)	12.1020217	−0.3
						(11)	12.1088542	1.0
						(12)	12.0948204	2.2
6	2	5	5	2	4	(00)	11.7065194	−0.3
						(10)	11.7072489	1.6
						(01)	11.7375162	−0.1
						(11)	11.7303905	−0.8
						(12)	11.7445891	−0.8
7	0	7	6	0	6	(00)	13.0880842	−0.4
						(10)	13.0879632	0.4
						(01)	13.0871527	−0.7
						(12)	13.0870138	0.3
8	0	8	7	0	7	(00)	14.8116132	−0.8
						(10)	14.8114877	1.3
						(01)	14.8107151	−1.3
						(11)	14.8106005	0.9
						(12)	14.8105788	0.4

[a] Not included in the fit.

Table 17.61. Correlation matrix of the fit in Table 12.2 of the *trans* conformer of AMF.

	B_-	B_K	B_J	D_J	D_{JK}	D_K	d_1	d_2	$V_{3,1}$	$V_{3,2}$	δ_1	δ_2	$D_{pi2K,2}$	$D_{pi2J,2}$
B_-	1.000													
B_K	0.491	1.000												
B_J	0.417	0.118	1.000											
D_J	0.210	−0.261	0.697	1.000										
D_{JK}	0.304	0.409	0.326	−0.111	1.000									
D_K	0.519	0.954	0.213	−0.211	0.377	1.000								
d_1	−0.810	−0.177	−0.371	−0.479	−0.014	−0.212	1.000							
d_2	−0.413	−0.326	−0.212	−0.095	−0.209	−0.375	0.490	1.000						
$V_{3,1}$	0.122	−0.022	0.047	0.015	0.010	0.018	−0.027	−0.004	1.000					
$V_{3,2}$	0.089	0.050	0.386	−0.020	−0.013	0.139	0.007	−0.003	−0.080	1.000				
δ_1	0.114	−0.024	0.043	0.010	0.008	0.016	−0.017	0.006	0.996	−0.079	1.000			
δ_2	−0.084	−0.048	−0.383	0.021	0.015	−0.137	−0.012	−0.002	0.076	−0.995	0.076	1.000		
$D_{pi2K,2}$	0.076	−0.148	0.204	−0.011	0.015	0.084	−0.013	−0.008	0.087	0.339	0.085	−0.337	1.000	
$D_{pi2J,2}$	−0.061	−0.014	−0.468	0.018	0.030	−0.113	−0.024	0.014	0.005	−0.739	0.005	0.735	−0.391	1.000

Table 17.62. Correlation matrix of the fit in Table 12.1 of the *trans* conformer of AMF.

	B_-	B_K	B_J	D_J	D_{JK}	D_K	d_1	d_2	$V_{3,1}$	$V_{3,2}$	δ_1	δ_2	$D_{pi2K,2}$	$D_{pi2J,2}$	$F_{0,1}$	$F_{0,2}$
B_-	1.000															
B_K	0.509	1.000														
B_J	0.374	0.102	1.000													
D_J	0.177	−0.272	0.699	1.000												
D_{JK}	0.290	0.399	0.325	−0.110	1.000											
D_K	0.570	0.917	0.152	−0.226	0.331	1.000										
d_1	−0.795	−0.188	−0.362	−0.469	−0.013	−0.225	1.000									
d_2	−0.386	−0.314	−0.214	−0.097	−0.209	−0.319	0.486	1.000								
$V_{3,1}$	−0.013	0.069	−0.014	−0.030	−0.032	0.088	−0.014	0.009	1.000							
$V_{3,2}$	−0.274	−0.177	0.109	0.084	0.008	−0.446	0.081	−0.031	−0.212	1.000						
δ_1	0.101	0.005	0.029	−0.005	−0.007	0.050	−0.023	0.006	0.454	−0.093	1.000					
δ_2	−0.293	−0.188	−0.021	0.088	0.012	−0.473	0.075	−0.030	−0.184	0.944	−0.060	1.000				
$D_{pi2K,2}$	0.268	0.042	0.065	−0.072	0.006	0.396	−0.071	0.018	0.084	−0.746	0.091	−0.792	1.000			
$D_{pi2J,2}$	0.034	0.041	−0.468	−0.009	0.025	0.047	−0.048	0.023	0.063	−0.365	0.031	−0.122	0.008	1.000		
$F_{0,1}$	−0.032	0.072	−0.020	−0.031	−0.033	0.084	−0.010	0.010	0.989	−0.209	0.320	−0.184	0.073	0.062	1.000	
$F_{0,2}$	−0.280	−0.181	0.084	0.086	0.009	−0.456	0.081	−0.031	−0.209	0.998	−0.087	0.964	−0.762	−0.319	−0.207	1.000

Table 17.63. Correlation matrix of the fit in Table 12.2 of the *cis* conformer of AMF.

	B_-	B_K	B_J	D_J	D_{JK}	D_K	d_1	d_2	$V_{3,1}$	$V_{3,2}$	δ_1	$D_{pi2K,2}$	$D_{pi2J,2}$
B_-	1.000												
B_K	−0.052	1.000											
B_J	0.577	−0.318	1.000										
D_J	0.680	−0.324	0.907	1.000									
D_{JK}	−0.419	0.422	−0.109	−0.340	1.000								
D_K	0.254	0.631	0.008	0.001	−0.033	1.000							
d_1	−0.915	0.218	−0.677	−0.829	0.470	−0.119	1.000						
$V_{3,1}$	0.141	0.073	0.027	0.015	−0.018	0.220	−0.060	1.000					
$V_{3,2}$	−0.001	−0.485	0.165	0.070	−0.123	0.077	−0.058	−0.070	1.000				
δ_1	0.140	0.071	0.026	0.014	−0.019	0.220	−0.059	0.999	−0.070	1.000			
δ_2	−0.008	−0.486	0.160	0.065	−0.124	0.074	−0.052	−0.078	1.000	−0.078	1.000		
$D_{pi2K,2}$	−0.011	−0.658	0.160	0.044	−0.140	−0.086	−0.039	0.042	0.806	0.044	0.806	1.000	
$D_{pi2J,2}$	−0.023	0.338	−0.308	−0.052	0.068	−0.012	0.043	−0.009	−0.460	−0.010	−0.460	−0.557	1.000

Table 17.64. Correlation matrix of the fit in Table 12.1 of the *cis* conformer of AMF.

	B_-	B_K	B_J	D_J	D_{JK}	D_K	d_1	$V_{3,1}$	$V_{3,2}$	δ_1	δ_2	$D_{pi2K,2}$	$D_{pi2J,2}$	$F_{0,1}$	$F_{0,2}$
B_-	1.000														
B_K	0.250	1.000													
B_J	0.612	0.364	1.000												
D_J	0.673	0.024	0.855	1.000											
D_{JK}	−0.312	0.358	0.030	−0.300	1.000										
D_K	0.231	0.021	−0.035	−0.006	−0.063	1.000									
d_1	−0.914	−0.128	−0.675	−0.828	0.395	−0.107	1.000								
$V_{3,1}$	−0.051	0.034	0.053	0.010	0.047	−0.165	0.019	1.000							
$V_{3,2}$	0.264	0.982	0.425	0.084	0.289	−0.087	−0.170	0.033	1.000						
δ_1	0.040	0.049	0.063	0.019	0.032	−0.012	−0.021	0.840	0.041	1.000					
δ_2	−0.217	−0.868	−0.274	−0.032	−0.308	0.129	0.109	−0.102	−0.820	−0.116	1.000				
$D_{pi2K,2}$	−0.262	−0.991	−0.404	−0.077	−0.304	0.083	0.163	−0.050	−0.992	−0.052	0.877	1.000			
$D_{pi2J,2}$	−0.193	−0.612	−0.489	−0.094	−0.149	0.053	0.145	−0.037	−0.675	−0.044	0.372	0.619	1.000		
$F_{0,1}$	−0.069	0.029	0.048	0.008	0.048	−0.190	0.027	0.993	0.030	0.772	−0.095	−0.047	−0.034	1.000	
$F_{0,2}$	0.264	0.985	0.421	0.082	0.292	−0.090	−0.169	0.037	1.000	0.046	−0.836	−0.995	−0.665	0.034	1.000

17.2.4 4,5-Dimethylthiazole

Table 17.65. Nuclear coordinates in the principal inertial axes of 4,5-dimethylthiazole (DMTA) calculated at the MP2/6-311++G(d,p) level of theory. The atoms are numbered according to Figure 13.2.

	a /Å	b /Å	c /Å
S1	1.509874	0.318035	0.000084
C2	1.076626	−1.347444	0.000000
N3	−0.215591	−1.588311	−0.000013
C4	−0.927700	−0.408767	−0.000150
C5	−0.160704	0.746268	−0.000337
H6	1.835438	−2.121034	−0.000045
C7	−2.425419	−0.496627	0.000133
H8	−2.893258	0.489828	−0.000661
H9	−2.768837	−1.043367	−0.882938
H10	−2.768576	−1.041611	0.884402
C11	−0.598942	2.181310	0.000067
H12	−0.227921	2.712565	−0.881858
H13	−1.688918	2.240540	−0.007752
H14	−0.240625	2.708325	0.889793

Table 17.66. Fourier coefficients of the potential function of DMTA for a rotation of the γ methyl group around the dihedral angle $\varphi_1 = \angle(S_1,C_5,C_{11},H_{12})$ calculated in 2° steps calculated with the methods MP2, B3LYP, M06-2X, and CCSD and the basis set 6-311++G(d,p). The potential is expanded as $V(\varphi) = \sum_{n=1}^{15} a_n \cdot \cos(n \cdot \varphi)$.

	MP2		B3LYP		M06-2X		CCSD	
	Hartree	cm^{-1}	Hartree	cm^{-1}	Hartree	cm^{-1}	Hartree	cm^{-1}
a0	−646.481 472 247		−647.779 985 719		−647.632 511 305		−646.524 991 792	
a3	0.000 143 666	31.5	0.000 377 211	82.8	0.000 223 924	49.1	0.000 361 796	79.4
a6	0.000 006 338	1.4	−0.000 002 022	−0.4	−0.000 026 480	−5.8	0.000 011 830	2.6
a9			0.000 003 002	0.7	0.000 002 941	0.6	−0.000 004 511	−1.0
a12					−0.000 002 748	−0.6	0.000 001 527	0.3
a15			0.000 001 531	0.3	0.000 002 303	0.5		

Table 17.67. Fourier coefficients of the potential function of DMTA for a rotation of the δ methyl group around the dihedral angle $\varphi_2 = \angle(N_3,C_4,C_7,H_8)$ calculated in 2° steps calculated with the methods MP2, B3LYP, M06-2X, and CCSD and the basis set 6-311++G(d,p). The potential is expanded as $V(\varphi) = \sum_{n=1}^{15} a_n \cdot \cos(n \cdot \varphi)$.

	MP2		B3LYP		M06-2X		CCSD	
	Hartree	cm^{-1}	Hartree	cm^{-1}	Hartree	cm^{-1}	Hartree	cm^{-1}
a0	−646.481 563 028		−647.780 093 023		−647.632 619 447		−646.525 173 892	
a3	0.000 038 027	8.3	0.000 291 349	63.9	0.000 160 919	35.3	0.000 197 135	43.3
a6	0.000 041 323	9.1	0.000 012 409	2.7	−0.000 002 023	−0.4	0.000 029 485	6.5
a9	−0.000 006 783	−1.5					−0.000 005 172	−1.1
a12	0.000 002 882	0.6	0.000 001 196	0.3	0.000 003 477	0.8	0.000 001 375	0.3
a15	−0.000 001 158	−0.3						

Table 17.68. The rotational constants A, B, and C in GHz, the deviations (Dev.) between the experimental and calculated rotational constants in MHz, the angles between the internal rotor axis and the principal axes of inertia $\angle(i_1,a)$, $\angle(i_1,b)$, $\angle(i_1,c)$ of the γ methyl rotor, the angles between the internal rotor axis and the principal axes of inertia $\angle(i_2,a)$, $\angle(i_2,b)$, $\angle(i_2,c)$ of δ methyl rotor, and the barriers to internal rotation $V_{3,1}$ of the γ methyl rotor and $V_{3,2}$ of the δ methyl rotor of DMTA in cm^{-1} calculated using various methods and basis sets. Harmonic frequency calculations were carried out to verify the nature of the stationary points.

Method/Basis set	A	Dev.	B	Dev.	C	Dev.	$\angle(i_1,a)$	$\angle(i_1,b)$	$\angle(i_1,c)$	$\angle(i_2,a)$	$\angle(i_2,b)$	$\angle(i_2,c)$	$V_{3,1}/cm^{-1}$	$V_{3,2}/cm^{-1}$
CCSD/cc-pVDZ	3.131	61	2.416	41	1.388	24	176.53	93.47	90.00	106.15	16.15	89.99		
MP2/cc-pVTZ	3.195	−3	2.466	−10	1.416	−4	176.56	93.44	90.00	107.23	17.23	89.99	73.5	43.0
MP2/cc-pVDZ	3.143	49	2.427	29	1.394	18	177.27	92.73	90.00	106.24	16.24	89.98	20.1	40.4
MP2/6-311++G(3df,2pd)	3.203	−12	2.473	−17	1.420	−8	176.40	93.60	89.90	107.54	17.54	89.60		
MP2/6-311++G(d,p)	3.185	6	2.447	9	1.408	4	176.11	93.89	89.84	108.47	18.49	89.34	64.3	27.2
MP2/6-311+G(d,p)	3.185	6	2.447	9	1.408	4	176.10	93.89	89.77	108.46	18.47	89.26	64.2	24.1
MP2/6-311G(d,p)	3.184	8	2.451	5	1.409	3	176.66	93.34	89.97	107.44	17.46	89.27	15.9	34.9
MP2/6-31++G(d,p)	3.185	6	2.445	11	1.407	5	176.21	93.79	90.14	107.98	18.00	89.23	63.1	
MP2/6-31+G(d,p)	3.185	7	2.445	11	1.408	4	176.23	93.77	90.14	107.90	17.93	89.05	60.7	
MP2/6-31G(d,p)	3.185	6	2.450	6	1.409	3	176.56	93.44	89.89	107.18	17.20	89.26	50.1	47.0
M06-2X/cc-pVQZ	3.210	−18	2.478	−22	1.423	−11	175.57	94.43	90.00	107.44	17.44	90.00	113.1	66.5
M06-2X/cc-pVTZ	3.205	−13	2.473	−17	1.420	−8	175.64	94.36	90.00	107.33	17.33	90.00	101.1	69.3
M06-2X/cc-pVDZ	3.178	14	2.452	4	1.408	4	176.14	93.86	90.00	106.96	16.96	89.99	92.7	92.2
M06-2X/6-311++G(3df,2pd)	3.208	−17	2.478	−22	1.423	−11	175.65	94.35	90.01	107.32	17.32	89.99	98.6	53.5
M06-2X/6-311++G(d,p)	3.189	3	2.461	−5	1.413	−1	175.92	94.08	90.00	106.81	16.81	89.99	103.2	72.4
M06-2X/6-311+G(d,p)	3.189	3	2.461	−5	1.413	−1	175.91	94.09	90.00	106.83	16.83	89.99	98.6	68.3
M06-2X/6-311G(d,p)	3.190	2	2.462	−6	1.414	−2	176.06	93.94	90.00	106.71	16.71	89.99	64.5	71.5
M06-2X/6-31++G(d,p)	3.183	8	2.455	1	1.410	2	175.99	94.01	90.00	106.91	16.91	89.99	109.8	88.1
M06-2X/6-31+G(d,p)	3.183	8	2.455	1	1.410	2	175.99	94.01	90.00	106.91	16.91	89.99	109.4	87.5
M06-2X/6-31G(d,p)	3.185	6	2.457	−1	1.411	1	176.03	93.97	90.00	106.93	16.93	89.99	94.0	109.1
B3LYP/cc- pVQZ	3.187	5	2.457	−1	1.412	0	175.60	94.40	90.00	107.27	17.27	89.99	153.6	98.3
B3LYP/cc-pVTZ	3.182	10	2.452	4	1.409	3	175.65	94.35	90.00	107.16	17.16	89.99	147.4	105.7
B3LYP/cc-pVDZ	3.148	43	2.426	30	1.394	18	176.15	93.85	90.00	106.83	16.83	89.99	119.7	121.5
B3LYP/6-311++G(3df,2pd)	3.189	3	2.459	−3	1.412	0	175.59	94.41	90.00	107.35	17.35	89.99	149.7	91.5
B3LYP/6-311++G(d,p)	3.166	25	2.437	19	1.401	11	175.77	94.23	89.99	107.02	17.02	89.99	168.0	127.0
B3LYP/6-311+G(d,p)	3.166	25	2.437	19	1.401	11	175.77	94.23	89.99	107.02	17.02	89.99	164.9	124.0
B3LYP/6-311G(d,p)	3.167	24	2.439	17	1.402	10	175.98	94.02	90.00	106.84	16.84	89.99	129.8	135.2
B3LYP/6-31++G(d,p)	3.156	36	2.430	27	1.397	15	175.95	94.05	90.00	106.89	16.89	89.99	162.7	141.1
B3LYP/6-31+G(d,p)	3.155	36	2.430	26	1.397	16	175.95	94.05	90.00	106.88	16.88	89.99	162.6	141.7

Table 17.68. (continued)

Method/Basis set	*A*	Dev.	*B*	Dev.	*C*	Dev.	∠(i$_1$,a)	∠(i$_1$,b)	∠(i$_1$,c)	∠(i$_2$,a)	∠(i$_2$,b)	∠(i$_2$,c)	$V_{3,1}$/cm^{-1}	$V_{3,2}$/cm^{-1}
B3LYP/6-31G(d,p)	3.158	34	2.432	24	1.398	14	176.00	94.00	90.00	106.92	16.92	89.99	149.0	167.0
HF/6-311++G(3df,2pd)	3.212	−21	2.491	−34	1.427	−15	174.61	95.39	90.00	106.98	16.98	89.99	264.2	152.9
HF/6-311++G(d,p)	3.193	−2	2.473	−17	1.418	−6	174.77	95.23	90.00	106.63	16.63	89.99	271.6	174.1
HF/6-311+G(d,p)	3.193	−2	2.473	−17	1.418	−6	174.77	95.23	90.00	106.64	16.64	89.99	266.8	170.4
HF/6-311G(d,p)	3.196	−4	2.475	−19	1.419	−7	174.89	95.11	90.00	106.57	16.57	89.99	237.4	164.9
HF/6-31++G(d,p)	3.192	0	2.470	−14	1.417	−5	174.90	95.10	89.99	106.59	16.59	89.99	241.0	166.3
HF/6-31+G(d,p)	3.192	0	2.470	−14	1.417	−5	174.90	95.10	89.99	106.58	16.58	89.99	237.7	162.2
HF/6-31G(d,p)	3.194	−2	2.472	−16	1.418	−6	174.90	95.10	89.99	106.63	16.63	89.99	220.2	167.9
Experiment	3.192		2.456		1.412		184.93	85.06	90.00	108.92	18.92	90.00	61.5	126.5

Table 17.69. Coefficients of the two-dimensional Fourier expansion for the potential energy surface of DMTA calculated with the methods MP2, B3LYP, M06-2X, and CCSD and the basis set 6-311++G(d,p) in a grid of 10° (Figure 13.5). Due to symmetry, only data points in the range from $\varphi_1 = 0°$ to 120° and $\varphi_2 = 0°$ to 120° were needed. The potential is expanded as $V(\varphi_2, \varphi_3) = \sum_{i=1}^{20} V_i \cdot f_i$.

		MP2	**B3LYP**	**M06-2X**	**CCSD**
i	f_i	V_i/Hartree	V_i/Hartree	V_i/Hartree	V_i/Hartree
1	1	−646.481 423 123	−647.779 753 558	−647.632 331 393	−646.524 833 279
2	$\cos(3\varphi_1)$	−0.000 164 881	−0.000 338 604	−0.000 262 066	−0.000 372 103
3	$\sin(3\varphi_1)$	−0.000 002 952	−0.000 005 745	−0.000 004 252	−0.000 006 108
4	$\cos(3\varphi_2)$	−0.000 044 684	−0.000 247 732	−0.000 187 329	−0.000 209 613
5	$\sin(3\varphi_2)$		−0.000 004 704	−0.000 003 849	−0.000 002 752
6	$\cos(6\varphi_1)$	0.000 025 073	−0.000 003 585	−0.000 015 962	0.000 022 584
7	$\sin(6\varphi_1)$		−0.000 001 058	−0.000 001 678	
8	$\cos(6\varphi_2)$	0.000 048 167	0.000 015 987	0.000 003 373	0.000 043 379
9	$\sin(6\varphi_2)$	0.000 001 455	0.000 000 521		
10	$\cos(3\varphi_1)\cos(3\varphi_2)$	0.000 025 286	−0.000 040 146	0.000 037 562	0.000 028 470
11	$\sin(3\varphi_1)\sin(3\varphi_2)$	−0.000 034 950	0.000 096 390	0.000 008 074	−0.000 025 703
12	$\cos(3\varphi_1)\sin(3\varphi_2)$	0.000 001 294	−0.000 001 311	0.000 001 702	0.000 001 782
13	$\sin(3\varphi_1)\cos(3\varphi_2)$		−0.000 004 236	−0.000 001 776	−0.000 002 218
14	$\cos(6\varphi_1)\cos(3\varphi_2)$	−0.000 014 472	−0.000 002 423	−0.000 011 398	−0.000 013 389
15	$\sin(6\varphi_1)\sin(3\varphi_2)$	0.000 011 994		0.000 009 230	0.000 009 719
16	$\cos(3\varphi_1)\cos(6\varphi_2)$	−0.000 019 570		−0.000 004 856	−0.000 016 253
17	$\sin(3\varphi_1)\sin(6\varphi_2)$	0.000 014 361	−0.000 001 811	0.000 007 608	0.000 010 676
18	$\cos(3\varphi_1)\sin(6\varphi_2)$	−0.000 001 437			−0.000 001 138
19	$\cos(6\varphi_1)\cos(6\varphi_2)$	0.000 015 745	0.000 002 322	0.000 005 936	0.000 013 547
20	$\sin(6\varphi_1)\sin(6\varphi_2)$	−0.000 013 875	−0.000 002 163	−0.000 002 687	−0.000 011 694

Table 17.70. Observed frequencies ($\nu_{\text{Obs.}}$) of the (00), (10), (01), (11), and (12) torsional species of DMTA. $\nu_{\text{Obs.}} - \nu_{\text{Calc.}}$ values as obtained after a fit with the program XIAM.

J'	K_a'	K_c'	F'	J	K_a	K_c	F	$(\sigma_1\sigma_2)$	$\nu_{\text{Obs.}}$	$\nu_{\text{Obs.}} - \nu_{\text{Calc.}}$
upper level				lower level					GHz	kHz
2	1	1	1	1	1	1	0	(01)	9.665 566 2	42.1
2	1	1	1	1	1	1	1	(01)	9.666 739 1	43.5
2	1	1	2	1	1	1	1	(01)	9.667 088 6	45.1
2	1	1	2	1	1	1	1	(01)	9.667 088 6	45.1
2	1	1	3	1	1	1	2	(01)	9.666 394 6	43.1
2	1	1	1	1	1	1	0	(11)	9.570 341 4	−2.6
2	1	1	1	1	1	1	1	(11)	9.572 523 8	−11.9
2	1	1	2	1	1	1	1	(11)	9.572 974 8	−13.0
2	1	1	2	1	1	1	1	(11)	9.572 974 8	−13.0
2	1	1	3	1	1	1	2	(11)	9.571 813 4	−7.3
2	1	1	1	1	1	1	0	(12)	9.752 492 5	30.3
2	1	1	1	1	1	1	1	(12)	9.752 674 3	44.8
2	1	1	2	1	1	1	1	(12)	9.752 877 9	40.2
2	1	1	2	1	1	1	1	(12)	9.752 877 9	40.2
2	1	1	3	1	1	1	2	(12)	9.752 674 3	37.2
2	2	0	1	1	1	0	0	(01)	12.220 514 7	52.4[a]
2	2	0	2	1	1	0	1	(01)	12.219 651 1	59.4[a]
2	2	0	3	1	1	0	2	(01)	12.219 957 4	54.6[a]
2	2	0	3	1	1	0	2	(11)	11.873 907 4	−22.5
2	2	0	1	1	1	0	0	(12)	12.608 904 0	−117.7
2	2	0	2	1	1	0	1	(12)	12.608 226 2	−112.4
2	2	0	2	1	1	0	2	(12)	12.608 448 2	−112.9
2	2	0	3	1	1	0	2	(12)	12.608 527 7	−115.6
2	2	0	1	1	1	1	0	(00)	12.673 467 8	9.3
2	2	0	1	1	1	1	1	(00)	12.675 860 8	10.1
2	2	0	2	1	1	1	1	(00)	12.676 590 3	12.3
2	2	0	2	1	1	1	2	(00)	12.675 632 8	10.9
2	2	0	3	1	1	1	2	(00)	12.675 166 9	12.6
2	2	1	1	1	1	0	0	(00)	11.014 957 0	14.6
2	2	1	1	1	1	0	1	(00)	11.013 031 8	11.7
2	2	1	2	1	1	0	1	(00)	11.012 724 7	17.1
2	2	1	2	1	1	0	2	(00)	11.013 490 6	14.1
2	2	1	3	1	1	0	2	(00)	11.013 695 3	18.0
2	2	1	1	1	1	0	0	(01)	10.174 294 0	−322.5[a]
2	2	1	1	1	1	0	1	(01)	10.173 266 8	−325.1[a]
2	2	1	2	1	1	0	1	(01)	10.174 238 3	−328.8[a]
2	2	1	2	1	1	0	2	(01)	10.174 646 3	−331.0[a]
2	2	1	3	1	1	0	2	(01)	10.174 027 5	−323.0[a]
2	2	1	1	1	1	0	0	(10)	10.238 862 7	0.7
2	2	1	1	1	1	0	1	(10)	10.237 414 4	−2.1
2	2	1	2	1	1	0	1	(10)	10.237 490 9	1.9
2	2	1	2	1	1	0	2	(10)	10.238 066 3	−1.2
2	2	1	3	1	1	0	2	(10)	10.238 021 9	1.1
2	2	1	1	1	1	0	0	(11)	10.593 399 0	−11.5
2	2	1	1	1	1	0	1	(11)	10.591 850 2	−13.4

Table 17.70. (continued)

J'	K'_a	K'_c	F'	J	K_a	K_c	F	$(\sigma_1\sigma_2)$	$\nu_{\mathrm{Obs.}}$	$\nu_{\mathrm{Obs.}} - \nu_{\mathrm{Calc.}}$
upper level				lower level					GHz	kHz
2	2	1	2	1	1	0	1	(11)	10.591748 8	−6.8
2	2	1	2	1	1	0	2	(11)	10.592364 2	−10.3
2	2	1	3	1	1	0	2	(11)	10.592435 1	−9.0
2	2	1	1	1	1	0	0	(12)	9.475725 2	−51.5
2	2	1	1	1	1	0	1	(12)	9.475166 2	−55.5
2	2	1	2	1	1	0	1	(12)	9.476701 4	−65.5
2	2	1	2	1	1	0	2	(12)	9.476922 9	−66.5
2	2	1	3	1	1	0	2	(12)	9.475938 9	−57.1
3	0	3	2	2	1	2	1	(00)	9.684863 6	−4.0
3	0	3	2	2	1	2	2	(00)	9.686145 8	−3.4
3	0	3	3	2	1	2	2	(00)	9.684935 5	−2.8
3	0	3	3	2	1	2	3	(00)	9.684110 9	−3.6
3	0	3	4	2	1	2	3	(00)	9.685010 2	−1.2
3	0	3	2	2	1	2	1	(01)	9.397431 5	−15.9
3	0	3	2	2	1	2	2	(01)	9.398643 4	−16.3
3	0	3	3	2	1	2	2	(01)	9.397690 4	−16.8
3	0	3	3	2	1	2	3	(01)	9.396912 0	−15.9
3	0	3	4	2	1	2	3	(01)	9.397617 4	−16.1
3	0	3	2	2	1	2	1	(10)	9.718772 5	−12.6
3	0	3	2	2	1	2	2	(10)	9.720008 8	−8.8
3	0	3	3	2	1	2	2	(10)	9.718790 8	−8.1
3	0	3	3	2	1	2	3	(10)	9.717996 8	−9.8
3	0	3	4	2	1	2	3	(10)	9.718900 4	−9.0
3	0	3	2	2	1	2	1	(11)	9.386595 4	−32.1
3	0	3	2	2	1	2	2	(11)	9.387831 6	−32.0
3	0	3	3	2	1	2	2	(11)	9.386930 3	−34.1
3	0	3	3	2	1	2	3	(11)	9.386135 4	−34.4
3	0	3	4	2	1	2	3	(11)	9.386804 0	−31.9
3	0	3	2	2	1	2	1	(12)	9.426129 4	−1.7
3	0	3	2	2	1	2	2	(12)	9.427307 6	−2.7
3	0	3	3	2	1	2	2	(12)	9.426286 5	−5.7
3	0	3	3	2	1	2	3	(12)	9.425531 7	−2.5
3	0	3	4	2	1	2	3	(12)	9.426286 5	−1.8
3	1	3	2	2	0	2	2	(00)	10.017715 5	1.4
3	1	3	3	2	0	2	2	(00)	10.016401 2	1.3
3	1	3	3	2	0	2	3	(00)	10.015934 1	1.8
3	1	3	4	2	0	2	3	(00)	10.016907 7	1.9
3	1	3	2	2	0	2	1	(01)	10.334139 0	6.3
3	1	3	2	2	0	2	2	(01)	10.334406 9	9.6
3	1	3	3	2	0	2	2	(01)	10.333167 9	10.4
3	1	3	3	2	0	2	3	(01)	10.332993 6	6.4
3	1	3	4	2	0	2	3	(01)	10.333914 1	8.6
3	1	3	2	2	0	2	1	(10)	9.982227 1	−5.6
3	1	3	2	2	0	2	2	(10)	9.982968 4	−10.1
3	1	3	3	2	0	2	2	(10)	9.981664 7	−8.0
3	1	3	3	2	0	2	3	(10)	9.981182 9	−10.2

Table 17.70. (continued)

J'	K'_a	K'_c	F'	J	K_a	K_c	F	$(\sigma_1\sigma_2)$	$\nu_{\text{Obs.}}$	$\nu_{\text{Obs.}} - \nu_{\text{Calc.}}$
upper level				lower level					GHz	kHz
3	1	3	4	2	0	2	3	(10)	9.982 151 9	−8.4
3	1	3	2	2	0	2	1	(11)	10.328 149 8	18.3
3	1	3	2	2	0	2	2	(11)	10.328 248 4	20.6
3	1	3	3	2	0	2	2	(11)	10.327 029 5	21.7
3	1	3	4	2	0	2	3	(11)	10.327 869 2	19.8
3	1	3	2	2	0	2	1	(12)	10.310 471 9	34.1
3	1	3	2	2	0	2	2	(12)	10.310 918 3	34.2
3	1	3	3	2	0	2	2	(12)	10.309 661 7	35.6
3	1	3	3	2	0	2	3	(12)	10.309 373 5	34.5
3	1	3	4	2	0	2	3	(12)	10.310 305 9	35.0
3	2	1	2	2	2	1	1	(01)	14.807 562 7	8.4
3	2	1	2	2	2	1	2	(01)	14.806 601 6	22.5
3	2	1	3	2	2	1	2	(01)	14.807 219 7	31.2
3	2	1	4	2	2	1	3	(01)	14.807 377 2	13.3
3	2	1	2	2	2	1	1	(11)	14.318 898 2	−107.9[a]
3	2	1	3	2	2	1	2	(11)	14.319 763 6	−113.0[a]
3	2	1	4	2	2	1	3	(11)	14.319 133 6	−108.7[a]
3	2	2	2	2	1	1	1	(00)	13.837 623 2	8.1
3	2	2	2	2	1	1	2	(00)	13.836 031 2	10.1
3	2	2	3	2	1	1	2	(00)	13.836 031 2	10.1
3	2	2	3	2	1	1	3	(00)	13.837 054 5	8.7
3	2	2	4	2	1	1	3	(00)	13.837 054 5	8.8
3	2	2	2	2	1	1	1	(01)	13.867 800 0	16.5
3	2	2	3	2	1	1	2	(01)	13.867 483 7	15.7
3	2	2	4	2	1	1	3	(01)	13.867 684 8	17.1
3	2	2	2	2	1	1	1	(11)	13.935 740 6	32.3
3	2	2	3	2	1	1	2	(11)	13.935 168 6	34.8
3	2	2	4	2	1	1	3	(11)	13.935 549 3	34.2
3	2	2	3	2	1	1	2	(12)	13.692 757 9	148.4[a]
3	2	2	4	2	1	1	3	(12)	13.692 783 6	171.7[a]
3	3	0	2	2	2	0	1	(01)	18.455 228 6	−36.9
3	3	0	3	2	2	0	2	(01)	18.454 736 0	−38.0
3	3	0	4	2	2	0	3	(01)	18.455 083 9	−39.2
3	3	0	2	2	2	0	1	(11)	17.792 010 9	5.4
3	3	0	3	2	2	0	2	(11)	17.791 268 8	10.4
3	3	0	4	2	2	0	3	(11)	17.791 722 5	7.4
3	3	0	2	2	2	0	1	(12)	18.874 210 3	−341.8[a]
3	3	0	3	2	2	0	2	(12)	18.873 945 0	−339.1[a]
3	3	0	4	2	2	0	3	(12)	18.874 154 7	−340.4[a]
3	3	0	2	2	2	1	1	(00)	18.512 710 4	8.1
3	3	0	3	2	2	1	2	(00)	18.513 230 6	7.4
3	3	0	4	2	2	1	3	(00)	18.512 875 8	7.8
3	3	1	2	2	2	0	1	(00)	17.657 265 7	10.8
3	3	1	3	2	2	0	2	(00)	17.656 419 9	12.6
3	3	1	4	2	2	0	3	(00)	17.656 981 5	17.4
4	0	4	3	3	1	3	2	(00)	12.635 923 2	1.7

Table 17.70. (continued)

J'	K'_a	K'_c	F'	J	K_a	K_c	F	$(\sigma_1\sigma_2)$	$\nu_{\mathrm{Obs.}}$	$\nu_{\mathrm{Obs.}} - \nu_{\mathrm{Calc.}}$
upper level				lower level					GHz	kHz
4	0	4	3	3	1	3	3	(00)	12.6372352	−0.5
4	0	4	4	3	1	3	3	(00)	12.6358345	0.8
4	0	4	4	3	1	3	4	(00)	12.6348605	0.3
4	0	4	5	3	1	3	4	(00)	12.6359771	1.7
4	0	4	3	3	1	3	2	(01)	12.5546818	−20.1
4	0	4	3	3	1	3	3	(01)	12.5559220	−19.6
4	0	4	4	3	1	3	3	(01)	12.5546270	−19.3
4	0	4	4	3	1	3	4	(01)	12.5537068	−21.1
4	0	4	5	3	1	3	4	(01)	12.5547377	−20.7
4	0	4	3	3	1	3	2	(10)	12.6395447	−8.3
4	0	4	3	3	1	3	3	(10)	12.6408512	−7.6
4	0	4	4	3	1	3	3	(10)	12.6394453	−9.5
4	0	4	4	3	1	3	4	(10)	12.6384773	−10.2
4	0	4	5	3	1	3	4	(10)	12.6395962	−8.2
4	0	4	3	3	1	3	2	(11)	12.5486838	−19.2
4	0	4	3	3	1	3	3	(11)	12.5499033	−19.9
4	0	4	4	3	1	3	3	(11)	12.5486281	−19.5
4	0	4	4	3	1	3	4	(11)	12.5477230	−20.9
4	0	4	5	3	1	3	4	(11)	12.5487391	−19.4
4	0	4	3	3	1	3	2	(12)	12.5608328	−7.5
4	0	4	3	3	1	3	3	(12)	12.5620890	−9.4
4	0	4	4	3	1	3	3	(12)	12.5607694	−7.6
4	0	4	4	3	1	3	4	(12)	12.5598364	−8.7
4	0	4	5	3	1	3	4	(12)	12.5608881	−8.1
4	1	3	3	3	2	2	2	(00)	14.6137728	6.3
4	1	3	3	3	2	2	3	(00)	14.6137728	6.3
4	1	3	4	3	2	2	3	(00)	14.6139731	−6.6
4	1	3	4	3	2	2	4	(00)	14.6139731	−6.6
4	1	3	5	3	2	2	4	(00)	14.6138041	−6.1
4	1	3	3	3	2	2	2	(01)	13.5586006	92.8[a]
4	1	3	4	3	2	2	3	(01)	13.5590580	94.4[a]
4	1	3	5	3	2	2	4	(01)	13.5586947	95.4[a]
4	1	3	4	3	2	2	3	(10)	14.8244231	−15.4
4	1	3	5	3	2	2	4	(10)	14.8243825	−14.3
4	1	3	3	3	2	2	2	(11)	13.4954786	19.5
4	1	3	4	3	2	2	3	(11)	13.4961646	17.7
4	1	3	5	3	2	2	4	(11)	13.4956284	21.9
4	1	3	3	3	2	2	2	(12)	13.7073608	185.3[a]
4	1	3	4	3	2	2	3	(12)	13.7075739	182.8[a]
4	1	3	5	3	2	2	4	(12)	13.7073935	183.6[a]
4	1	3	3	4	0	4	3	(00)	9.2481755	7.1
4	1	3	4	4	0	4	3	(00)	9.2484960	114.3[a]
4	1	3	4	4	0	4	4	(00)	9.2497924	8.8
4	1	3	5	4	0	4	4	(00)	9.2497823	168.3[a]
4	1	3	5	4	0	4	5	(00)	9.2485093	10.5
4	1	3	3	4	0	4	3	(10)	9.2443363	−7.1

Table 17.70. (continued)

J'	K'_a	K'_c	F'	J	K_a	K_c	F	$(\sigma_1\sigma_2)$	$\nu_{\text{Obs.}}$	$\nu_{\text{Obs.}} - \nu_{\text{Calc.}}$
upper level				lower level					GHz	kHz
4	1	3	4	4	0	4	4	(10)	9.245 943 0	7.3
4	1	3	5	4	0	4	5	(10)	9.244 679 1	10.0
4	1	4	3	3	0	3	2	(00)	12.715 210 6	1.1
4	1	4	3	3	0	3	3	(00)	12.716 422 0	1.7
4	1	4	4	3	0	3	3	(00)	12.715 003 3	1.7
4	1	4	4	3	0	3	4	(00)	12.714 104 6	0.0
4	1	4	5	3	0	3	4	(00)	12.715 234 8	1.5
4	1	4	3	3	0	3	2	(01)	12.832 101 2	8.1
4	1	4	3	3	0	3	3	(01)	12.833 054 9	9.2
4	1	4	4	3	0	3	3	(01)	12.831 702 4	8.8
4	1	4	4	3	0	3	4	(01)	12.830 996 5	8.5
4	1	4	5	3	0	3	4	(01)	12.832 073 4	10.0
4	1	4	3	3	0	3	2	(10)	12.701 480 0	−14.0
4	1	4	3	3	0	3	3	(10)	12.702 697 6	−15.1
4	1	4	4	3	0	3	3	(10)	12.701 280 0	−14.8
4	1	4	4	3	0	3	4	(10)	12.700 376 4	−15.7
4	1	4	5	3	0	3	4	(10)	12.701 505 3	−14.6
4	1	4	3	3	0	3	2	(11)	12.824 754 0	−1.2
4	1	4	3	3	0	3	3	(11)	12.825 655 9	1.5
4	1	4	4	3	0	3	3	(11)	12.824 319 4	1.5
4	1	4	4	3	0	3	4	(11)	12.823 651 5	−0.3
4	1	4	5	3	0	3	4	(11)	12.824 715 6	0.7
4	1	4	3	3	0	3	2	(12)	12.817 106 5	31.0
4	1	4	3	3	0	3	3	(12)	12.818 119 9	26.4
4	1	4	4	3	0	3	3	(12)	12.816 751 9	27.5
4	1	4	4	3	0	3	4	(12)	12.815 996 1	25.8
4	1	4	5	3	0	3	4	(12)	12.817 085 7	26.3
4	2	2	3	3	2	2	2	(01)	19.466 439 6	−11.9
4	2	2	4	3	2	2	3	(01)	19.467 044 7	−11.0
4	2	2	5	3	2	2	4	(01)	19.466 565 5	−7.7
4	2	2	3	3	2	2	2	(11)	19.336 066 2	−4.1
4	2	2	4	3	2	2	3	(11)	19.336 888 5	−6.7
4	2	2	5	3	2	2	4	(11)	19.336 242 2	−3.5
4	2	2	3	3	2	2	2	(12)	19.596 044 8	201.1[a]
4	2	2	4	3	2	2	3	(12)	19.596 429 9	203.6[a]
4	2	2	5	3	2	2	4	(12)	19.596 116 5	204.2[a]
4	2	3	3	3	1	2	2	(00)	16.191 653 4	3.6
4	2	3	4	3	1	2	3	(00)	16.190 574 0	4.6
4	2	3	5	3	1	2	4	(00)	16.191 382 2	5.2
4	2	3	3	3	1	2	2	(01)	16.880 399 1	−6.1
4	2	3	4	3	1	2	3	(01)	16.879 526 1	−1.9
4	2	3	5	3	1	2	4	(01)	16.880 184 1	−2.5
4	2	3	3	3	1	2	2	(10)	16.045 610 9	−17.0
4	2	3	4	3	1	2	3	(10)	16.044 581 4	−17.2
4	2	3	5	3	1	2	4	(10)	16.045 357 4	−9.4
4	2	3	3	3	1	2	2	(11)	16.875 249 6	14.1

Table 17.70. (continued)

J'	K'_a	K'_c	F'	J	K_a	K_c	F	$(\sigma_1\sigma_2)$	$\nu_{\mathrm{Obs.}}$	$\nu_{\mathrm{Obs.}} - \nu_{\mathrm{Calc.}}$
upper level				lower level					GHz	kHz
4	2	3	4	3	1	2	3	(11)	16.8742469	16.9
4	2	3	5	3	1	2	4	(11)	16.8749995	15.2
4	2	3	3	3	1	2	2	(12)	16.7977765	70.5
4	2	3	4	3	1	2	3	(12)	16.7970335	72.2
4	2	3	5	3	1	2	4	(12)	16.7975935	72.4
4	2	3	3	4	1	4	3	(00)	9.6552819	5.5
4	2	3	4	4	1	4	4	(00)	9.6565668	7.1
4	2	3	5	4	1	4	5	(00)	9.6555412	2.3
4	2	3	3	4	1	4	3	(10)	9.5630955	−8.4
4	2	3	4	4	1	4	4	(10)	9.5644073	−8.8
4	2	3	5	4	1	4	5	(10)	9.5633656	−6.7
4	3	1	4	3	2	2	3	(00)	24.2907442	−4.7
4	3	1	4	3	2	2	4	(00)	24.2907442	−4.7
4	3	1	5	3	2	2	4	(00)	24.2898251	−6.6
4	3	2	3	3	2	1	2	(00)	20.6055824	7.6
4	3	2	4	3	2	1	3	(00)	20.6044079	4.9
4	3	2	5	3	2	1	4	(00)	20.6052586	5.2
4	3	2	3	3	2	1	2	(10)	19.6779818	−0.3
4	3	2	4	3	2	1	3	(10)	19.6772166	1.0
4	3	2	5	3	2	1	4	(10)	19.6777506	−0.6
4	4	0	4	3	3	0	3	(01)	24.8743762	−260.8[a]
4	4	0	5	3	3	0	4	(01)	24.8745103	−259.3[a]
4	4	0	3	3	3	0	2	(11)	24.1864627	10.2
4	4	0	4	3	3	0	3	(11)	24.1858448	15.2
4	4	0	5	3	3	0	4	(11)	24.1863248	12.8
4	4	0	4	3	3	1	3	(00)	24.6304535	−11.7
4	4	0	5	3	3	1	4	(00)	24.6303972	−10.0
4	4	1	3	3	3	1	2	(01)	23.7969168	4.7
4	4	1	4	3	3	1	3	(01)	23.7965519	5.7
4	4	1	5	3	3	1	4	(01)	23.7967793	6.2
4	4	1	3	3	3	1	2	(11)	24.3247284	10.6
4	4	1	4	3	3	1	3	(11)	24.3249221	11.0
4	4	1	5	3	3	1	4	(11)	24.3247484	13.4
4	4	1	3	3	3	1	2	(12)	23.0933398	210.5[a]
4	4	1	4	3	3	1	3	(12)	23.0931567	520.6[a]
4	4	1	5	3	3	1	4	(12)	23.0928516	−91.4[a]
5	0	5	4	4	1	4	3	(00)	15.4890102	6.8
5	0	5	4	4	1	4	4	(00)	15.4904268	4.6
5	0	5	5	4	1	4	4	(00)	15.4889257	4.7
5	0	5	5	4	1	4	5	(00)	15.4877960	3.6
5	0	5	6	4	1	4	5	(00)	15.4890446	5.0
5	0	5	4	4	1	4	3	(01)	15.4667561	−12.6
5	0	5	4	4	1	4	4	(01)	15.4681080	−12.7
5	0	5	5	4	1	4	4	(01)	15.4666619	−13.5
5	0	5	5	4	1	4	5	(01)	15.4655853	−14.6
5	0	5	6	4	1	4	5	(01)	15.4667871	−13.6

Table 17.70. (continued)

J'	K'_a	K'_c	F'	J	K_a	K_c	F	$(\sigma_1\sigma_2)$	$\nu_{\mathrm{Obs.}}$	$\nu_{\mathrm{Obs.}} - \nu_{\mathrm{Calc.}}$
upper level				lower level					GHz	kHz
5	0	5	4	4	1	4	3	(10)	15.485 230 7	−7.6
5	0	5	4	4	1	4	4	(10)	15.486 646 5	−9.6
5	0	5	5	4	1	4	4	(10)	15.485 144 5	−9.4
5	0	5	5	4	1	4	5	(10)	15.484 015 0	−11.2
5	0	5	6	4	1	4	5	(10)	15.485 264 3	−9.7
5	0	5	4	4	1	4	3	(11)	15.460 888 3	−16.4
5	0	5	4	4	1	4	4	(11)	15.462 224 0	−17.2
5	0	5	5	4	1	4	4	(11)	15.460 789 7	−16.6
5	0	5	5	4	1	4	5	(11)	15.459 726 4	−16.7
5	0	5	6	4	1	4	5	(11)	15.460 918 7	−16.5
5	0	5	4	4	1	4	3	(12)	15.464 559 4	−2.0
5	0	5	4	4	1	4	4	(12)	15.465 927 0	−3.6
5	0	5	5	4	1	4	4	(12)	15.464 468 3	−3.1
5	0	5	5	4	1	4	5	(12)	15.463 379 2	−3.1
5	0	5	6	4	1	4	5	(12)	15.464 591 3	−3.2
5	1	4	4	4	2	3	3	(00)	18.016 200 2	9.0
5	1	4	5	4	2	3	4	(00)	18.016 058 2	6.4
5	1	4	6	4	2	3	5	(00)	18.016 176 9	4.5
5	1	4	4	4	2	3	3	(01)	17.548 871 5	−11.8
5	1	4	5	4	2	3	4	(01)	17.548 961 4	−4.4
5	1	4	6	4	2	3	5	(01)	17.548 899 2	−3.7
5	1	4	4	4	2	3	3	(10)	18.063 708 4	1.0
5	1	4	5	4	2	3	4	(10)	18.063 528 3	2.4
5	1	4	6	4	2	3	5	(10)	18.063 683 4	3.0
5	1	4	4	4	2	3	3	(11)	17.529 469 4	18.3
5	1	4	5	4	2	3	4	(11)	17.529 592 4	16.5
5	1	4	6	4	2	3	5	(11)	17.529 496 8	18.4
5	1	4	4	4	2	3	3	(12)	17.600 399 7	62.3
5	1	4	5	4	2	3	4	(12)	17.600 422 0	65.6
5	1	4	6	4	2	3	5	(12)	17.600 410 3	64.4
5	1	5	4	4	0	4	3	(00)	15.504 852 8	7.0
5	1	5	4	4	0	4	4	(00)	15.506 253 3	5.5
5	1	5	5	4	0	4	4	(00)	15.504 748 9	4.9
5	1	5	5	4	0	4	5	(00)	15.503 631 9	3.1
5	1	5	6	4	0	4	5	(00)	15.504 882 7	4.6
5	1	5	4	4	0	4	3	(01)	15.528 593 2	0.2
5	1	5	4	4	0	4	4	(01)	15.529 889 9	1.5
5	1	5	5	4	0	4	4	(01)	15.528 435 4	1.8
5	1	5	5	4	0	4	5	(01)	15.527 404 2	1.1
5	1	5	6	4	0	4	5	(01)	15.528 614 1	2.3
5	1	5	4	4	0	4	3	(10)	15.497 379 6	−11.4
5	1	5	4	4	0	4	4	(10)	15.498 782 2	−12.9
5	1	5	5	4	0	4	4	(10)	15.497 278 6	−12.3
5	1	5	5	4	0	4	5	(10)	15.496 159 7	−14.3
5	1	5	6	4	0	4	5	(10)	15.497 411 1	−12.6
5	1	5	4	4	0	4	4	(12)	15.521 751 6	63.8

Table 17.70. (continued)

J'	K'_a	K'_c	F'	J	K_a	K_c	F	$(\sigma_1\sigma_2)$	$\nu_{\text{Obs.}}$	$\nu_{\text{Obs.}} - \nu_{\text{Calc.}}$
upper level				lower level					GHz	kHz
5	1	5	5	4	0	4	4	(12)	15.5202382	17.5
5	1	5	5	4	0	4	5	(12)	15.5191846	15.0
5	1	5	6	4	0	4	5	(12)	15.5204044	16.0
5	2	4	4	4	1	3	3	(00)	18.5501763	0.6
5	2	4	5	4	1	3	4	(00)	18.5496013	2.4
5	2	4	6	4	1	3	5	(00)	18.5500719	1.4
5	2	4	4	4	1	3	3	(01)	19.1302341	−30.0
5	2	4	5	4	1	3	4	(01)	19.1294069	−30.0
5	2	4	6	4	1	3	5	(01)	19.1300764	−30.4
5	2	4	4	4	1	3	3	(10)	18.4801800	−30.3
5	2	4	5	4	1	3	4	(10)	18.4796311	−31.2
5	2	4	6	4	1	3	5	(10)	18.4800789	−31.9
5	2	4	4	4	1	3	3	(11)	19.1089301	−24.2
5	2	4	5	4	1	3	4	(11)	19.1080369	−21.1
5	2	4	6	4	1	3	5	(11)	19.1087591	−23.5
5	2	4	4	4	1	3	3	(12)	19.0635090	24.4
5	2	4	5	4	1	3	4	(12)	19.0627646	24.8
5	2	4	6	4	1	3	5	(12)	19.0633692	24.5
5	3	3	5	4	2	2	4	(00)	22.8778326	−3.1
5	3	3	4	4	2	2	3	(01)	23.1782759	193.4[a]
5	3	3	5	4	2	2	4	(01)	23.1779447	191.7[a]
5	3	3	6	4	2	2	5	(01)	23.1781955	191.3[a]
5	3	3	4	4	2	2	3	(11)	23.2399502	51.1
5	3	3	5	4	2	2	4	(11)	23.2394863	54.1
5	3	3	6	4	2	2	5	(11)	23.2398484	53.1
5	3	3	4	4	2	2	3	(12)	22.9624632	259.7[a]
5	3	3	5	4	2	2	4	(12)	22.9622790	259.8[a]
5	3	3	6	4	2	2	5	(12)	22.9624136	261.0[a]
5	4	2	6	5	3	3	6	(00)	8.8974024	−15.1
6	0	6	5	5	1	5	4	(00)	18.3179390	12.4
6	0	6	5	5	1	5	5	(00)	18.3194415	11.1
6	0	6	6	5	1	5	5	(00)	18.3178768	12.2
6	0	6	6	5	1	5	6	(00)	18.3166253	10.0
6	0	6	7	5	1	5	6	(00)	18.3179669	12.0
6	0	6	5	5	1	5	4	(01)	18.3062469	−6.6
6	0	6	5	5	1	5	5	(01)	18.3077011	−7.3
6	0	6	6	5	1	5	5	(01)	18.3061715	−7.1
6	0	6	6	5	1	5	6	(01)	18.3049616	−8.3
6	0	6	7	5	1	5	6	(01)	18.3062720	−6.7
6	0	6	5	5	1	5	4	(10)	18.3124440	−7.2
6	0	6	6	5	1	5	5	(10)	18.3123814	−7.5
6	0	6	7	5	1	5	6	(10)	18.3124722	−7.3
6	0	6	5	5	1	5	4	(11)	18.3001691	−15.3
6	0	6	6	5	1	5	5	(11)	18.3000901	−16.1
6	0	6	7	5	1	5	6	(11)	18.3001923	−16.6
6	0	6	5	5	1	5	4	(12)	18.3015202	2.5

Table 17.70. (continued)

J'	K'_a	K'_c	F'	J	K_a	K_c	F	$(\sigma_1\sigma_2)$	$\nu_{\mathrm{Obs.}}$	$\nu_{\mathrm{Obs.}} - \nu_{\mathrm{Calc.}}$
upper level				lower level					GHz	kHz
6	0	6	6	5	1	5	5	(12)	18.301 448 1	2.0
6	0	6	7	5	1	5	6	(12)	18.301 545 5	1.8
6	1	5	5	5	2	4	4	(00)	21.024 812 0	13.5
6	1	5	6	5	2	4	5	(00)	21.024 613 8	9.4
6	1	5	7	5	2	4	6	(00)	21.024 789 2	9.7
6	1	5	5	5	2	4	4	(01)	20.875 497 5	−39.3
6	1	5	6	5	2	4	5	(01)	20.875 362 7	−42.2
6	1	5	7	5	2	4	6	(01)	20.875 482 9	−43.2
6	1	5	6	5	2	4	5	(10)	21.023 998 1	−5.5
6	1	5	7	5	2	4	6	(10)	21.024 181 3	−5.5
6	1	5	5	5	2	4	4	(11)	20.860 055 9	−6.2
6	1	5	6	5	2	4	5	(11)	20.859 925 1	−8.0
6	1	5	7	5	2	4	6	(11)	20.860 043 1	−8.6
6	1	5	5	5	2	4	4	(12)	20.882 168 8	11.6
6	1	5	6	5	2	4	5	(12)	20.882 022 8	9.6
6	1	5	7	5	2	4	6	(12)	20.882 154 5	9.4
6	1	6	5	5	0	5	4	(00)	18.320 810 2	12.5
6	1	6	5	5	0	5	5	(00)	18.322 309 0	10.0
6	1	6	6	5	0	5	5	(00)	18.320 744 0	11.2
6	1	6	6	5	0	5	6	(00)	18.319 495 3	9.7
6	1	6	7	5	0	5	6	(00)	18.320 837 1	11.6
6	1	6	5	5	0	5	4	(01)	18.318 271 2	−0.8
6	1	6	6	5	0	5	5	(01)	18.318 183 7	−2.4
6	1	6	7	5	0	5	6	(01)	18.318 294 5	−0.9
6	1	6	5	5	0	5	4	(10)	18.314 606 0	−7.9
6	1	6	5	5	0	5	5	(10)	18.316 108 1	−7.9
6	1	6	6	5	0	5	5	(10)	18.314 540 7	−8.5
6	1	6	7	5	0	5	6	(10)	18.314 633 5	−8.2
6	2	5	5	5	1	4	4	(00)	21.164 030 4	3.8
6	2	5	6	5	1	4	5	(00)	21.163 730 6	5.5
6	2	5	7	5	1	4	6	(00)	21.163 994 6	4.9
6	2	5	5	5	1	4	4	(01)	21.381 727 3	−16.0
6	2	5	6	5	1	4	5	(01)	21.381 269 6	−16.3
6	2	5	7	5	1	4	6	(01)	21.381 662 4	−16.8
6	2	5	5	5	1	4	4	(10)	21.131 099 3	−28.6
6	2	5	6	5	1	4	5	(10)	21.130 809 8	−27.1
6	2	5	5	5	1	4	4	(11)	21.359 130 3	−36.8
6	2	5	6	5	1	4	5	(11)	21.358 651 3	−36.2
6	2	5	7	5	1	4	6	(11)	21.359 062 0	−37.0
6	2	5	5	5	1	4	4	(12)	21.340 063 2	42.8
6	2	5	6	5	1	4	5	(12)	21.339 643 9	43.6
6	2	5	7	5	1	4	6	(12)	21.340 005 7	42.8
6	4	3	5	6	3	4	5	(00)	10.240 240 9	−34.6
6	4	3	6	6	3	4	6	(00)	10.240 573 6	−35.0
6	4	3	7	6	3	4	7	(00)	10.240 289 3	−34.3
7	0	7	6	6	1	6	5	(00)	21.142 014 8	19.5

Table 17.70. (continued)

J'	K'_a	K'_c	F'	J	K_a	K_c	F	$(\sigma_1\sigma_2)$	$\nu_{\mathrm{Obs.}}$	$\nu_{\mathrm{Obs.}} - \nu_{\mathrm{Calc.}}$
upper level				lower level					GHz	kHz
7	0	7	7	6	1	6	6	(00)	21.1419709	21.9
7	0	7	8	6	1	6	7	(00)	21.1420407	22.4
7	0	7	6	6	1	6	5	(01)	21.1301521	−0.6
7	0	7	7	6	1	6	6	(01)	21.1300967	−0.5
7	0	7	8	6	1	6	7	(01)	21.1301735	−0.4
7	0	7	6	6	1	6	5	(10)	21.1360886	−1.5
7	0	7	7	6	1	6	6	(10)	21.1360430	−0.8
7	0	7	8	6	1	6	7	(10)	21.1361125	−0.6
7	1	6	6	6	2	5	5	(00)	23.8938442	17.8
7	1	6	7	6	2	5	6	(00)	23.8936737	15.5
7	1	6	8	6	2	5	7	(00)	23.8938304	14.6
7	1	6	6	6	2	5	5	(01)	23.8419300	−41.0
7	1	6	7	6	2	5	6	(01)	23.8417645	−43.6
7	1	6	8	6	2	5	7	(01)	23.8419166	−43.8
7	1	6	6	6	2	5	5	(10)	23.8802918	−7.7
7	1	6	7	6	2	5	6	(10)	23.8801207	−9.0
7	1	6	8	6	2	5	7	(10)	23.8802788	−9.9
7	1	6	6	6	2	5	5	(11)	23.8251710	−26.4
7	1	6	7	6	2	5	6	(11)	23.8250037	−28.4
7	1	6	8	6	2	5	7	(11)	23.8251581	−28.2
7	1	7	6	6	0	6	5	(01)	21.1323174	0.9
7	1	7	7	6	0	6	6	(01)	21.1322603	1.0
7	1	7	8	6	0	6	7	(01)	21.1323389	1.5
7	2	6	6	6	1	5	5	(00)	23.9248416	15.3
7	2	6	7	6	1	5	6	(00)	23.9246496	13.4
7	2	6	8	6	1	5	7	(00)	23.9248233	10.7
7	2	6	6	6	1	5	5	(01)	23.9670603	−11.0
7	2	6	7	6	1	5	6	(01)	23.9668117	−18.5
7	2	6	8	6	1	5	7	(01)	23.9670310	−18.6
7	2	6	6	6	1	5	5	(12)	23.9425466	41.1
7	2	6	7	6	1	5	6	(12)	23.9423166	39.6
7	2	6	8	6	1	5	7	(12)	23.9425256	39.8
8	0	8	7	7	1	7	6	(01)	23.9518282	3.6
8	0	8	8	7	1	7	7	(01)	23.9517913	8.5
8	0	8	9	7	1	7	8	(01)	23.9518519	9.5
8	1	8	7	7	0	7	6	(01)	23.9521990	3.9
8	1	8	8	7	0	7	7	(01)	23.9521615	8.4
8	1	8	9	7	0	7	8	(01)	23.9522226	9.7

[a] Not included in the fit.

17.2.5 1,2,5-Trimethylpyrrole

Table 17.71. Nuclear coordinates in the principal inertial axes of 1,2,5-trimethylpyrrole (TMP) calculated at the MP2/cc-pVTZ level of theory. The atoms are numbered according to Figure 14.2.

	a /Å	b /Å	c /Å
H1	−3.224402	−0.493362	0.025782
H2	−2.708179	0.903085	−0.908980
H3	−2.686009	0.963092	0.852556
H4	3.224456	−0.493091	0.025224
H5	2.708010	0.903917	−0.908553
H6	2.686200	0.962824	0.853033
H7	−0.001769	2.337273	1.059369
H8	−0.880810	2.363810	−0.476686
H9	0.881701	2.363881	−0.474123
H10	−1.360278	−2.429551	0.022613
H11	1.360667	−2.429341	0.021971
N12	−0.000036	0.533611	−0.028678
C13	−2.502529	0.319302	−0.009587
C14	2.502554	0.319576	−0.009483
C15	−1.128873	−0.254772	−0.006910
C16	1.128933	−0.254592	−0.006923
C17	−0.707108	−1.573037	0.014752
C18	0.707361	−1.572928	0.014403
C19	−0.000264	1.977827	0.029470

Table 17.72. The rotational constants A, B, and C in GHz, the deviations (Dev.) between the experimental and calculated rotational constants in MHz, the angles between the internal rotor axis and the principal axes of inertia $\angle(i_1,a)$, $\angle(i_1,b)$, $\angle(i_1,c)$ of the nitrogen rotor, the angles between the internal rotor axis and the principal axes of inertia $\angle(i_2,a)$, $\angle(i_2,b)$, $\angle(i_2,c)$ of one carbon rotor, and the barriers to internal rotation $V_{3,1}$ of the nitrogen rotor and $V_{3,2}$ of the carbon rotors of TMP in cm^{-1} calculated using various methods and basis sets. Harmonic frequency calculations were carried out to verify the nature of the stationary points. The relations of the angles $\angle(i_3,a)$, $\angle(i_3,b)$, $\angle(i_3,c)$ between the internal rotor axis of inertia of the second equivalent carbon rotor and the principal axes are: $\angle(i_3,a) = \pi - \angle(i_2,a)$, $\angle(i_3,b) = \angle(i_2,b)$, $\angle(i_3,c) = \angle(i_2,c)$.

Method/Basis set	A	Dev.	B	Dev.	C	Dev.	$\angle(i_1,a)$	$\angle(i_1,b)$	$\angle(i_1,c)$	$\angle(i_2,a)$	$\angle(i_2,b)$	$\angle(i_2,c)$	$V_{3,1}/cm^{-1}$	$V_{3,1}/cm^{-1}$
CCSD/cc-pVDZ	3.285	33	1.960	23	1.258	14	90.01	3.16	86.84	22.49	67.51	90.20		
CCSD/6-311++G(d,p)	3.308	9	1.972	10	1.266	5	90.01	4.48	85.52	22.61	67.40	90.47		
MP2/cc-pVTZ	3.331	−13	1.996	−13	1.278	−7	90.01	2.31	87.69	22.68	67.32	90.10		
MP2/cc-pVDZ	3.284	34	1.967	15	1.260	11	90.01	2.77	87.23	22.62	67.38	90.12	24	615
MP2/6-311++G(3df,2pd)	3.331	−13	1.996	−14	1.278	−7	90.01	2.37	87.63	22.77	67.23	90.11		576
MP2/6-311++G(d,p)	3.306	12	1.979	3	1.268	3	90.01	4.29	85.71	22.72	67.28	90.41	92	659
MP2/6-311+G(d,p)	3.306	12	1.979	3	1.268	3	90.01	4.13	85.87	22.72	67.29	90.34	95	659
MP2/6-311G(d,p)	3.310	8	1.981	1	1.269	2	90.01	3.26	86.74	22.67	67.34	90.30	72	649
MP2/6-31++G(d,p)	3.311	7	1.980	2	1.269	2	90.01	3.78	86.22	22.65	67.35	90.24		671
MP2/6-31+G(d,p)	3.311	7	1.980	2	1.269	2	90.01	3.62	86.38	22.63	67.37	90.23	87	666
MP2/6-31G(d,p)	3.320	−2	1.985	−2	1.272	−1	90.01	2.91	87.09	22.60	67.40	90.27	38	626
B3LYP/cc-pVQZ	3.336	−18	1.983	−1	1.273	−2	90.01	2.22	87.78	22.07	67.93	90.16	17	580
B3LYP/cc-pVTZ	3.334	−17	1.982	0	1.273	−2	90.01	2.17	87.83	22.06	67.94	90.14	17	583
B3LYP/cc-pVDZ	3.304	14	1.967	15	1.263	8	90.01	2.33	87.67	22.16	67.84	90.10	8	600
B3LYP/6-311++G(3df,2pd)	3.334	−16	1.982	0	1.273	−2	90.01	2.23	87.77	22.09	67.91	90.16	15	576
B3LYP/6-311++G(d,p)	3.317	1	1.973	10	1.267	5	90.01	2.50	87.50	22.13	67.87	90.21	26	586
B3LYP/6-311+G(d,p)	3.317	1	1.973	10	1.267	4	90.01	2.51	87.49	22.14	67.86	90.21	26	583
B3LYP/6-311G(d,p)	3.319	−2	1.973	9	1.267	4	90.01	2.40	87.60	22.07	67.93	90.18	21	581
B3LYP/6-31++G(d,p)	3.307	11	1.968	14	1.263	8	90.01	2.45	87.55	22.20	67.80	90.18	24	589
B3LYP/6-31+G(d,p)	3.307	11	1.968	14	1.263	8	90.01	2.45	87.55	22.21	67.79	90.17	23	591
B3LYP/6-31G(d,p)	3.313	5	1.972	11	1.266	6	90.01	2.39	87.61	22.16	67.84	90.19	17	576
M06-2X/cc-pVQZ	3.351	−33	2.005	−22	1.284	−13	90.01	2.28	87.72	22.78	67.22	90.15	23	612
M06-2X/cc-pVTZ	3.347	−29	2.003	−21	1.284	−12	90.01	2.29	87.71	22.81	67.19	90.15	30	613
M06-2X/cc-pVDZ[a]	3.324	−6	1.990	−8	1.275	−4	90.02	2.17	87.83	22.79	67.21	90.09	14	
M06-2X/6-311++G(3df,2pd)	3.348	−30	2.003	−21	1.283	−12	90.01	2.32	87.68	22.80	67.20	90.16	21	613
M06-2X/6-311+G(d,p)	3.332	−15	1.994	−12	1.278	−7	90.01	2.62	87.38	22.81	67.19	90.20	43	619
M06-2X/6-311G(d,p)	3.335	−17	1.995	−12	1.278	−7	90.01	2.49	87.51	22.75	67.25	90.16	35	612
M06-2X/6-31++G(d,p)[a]	3.326	−8	1.991	−9	1.276	−4	90.01	2.34	87.66	22.85	67.16	90.13	29	

Table 17.72. (continued)

Method/Basis set	*A*	Dev.	*B*	Dev.	*C*	Dev.	∠(i$_1$,a)	∠(i$_1$,b)	∠(i$_1$,c)	∠(i$_2$,a)	∠(i$_2$,b)	∠(i$_2$,c)	$V_{3,1}$/cm^{-1}	$V_{3,1}$/cm^{-1}
M06-2X/6-31+G(d,p)[a]	3.326	−8	1.991	−9	1.276	−4	90.01	2.35	87.65	22.85	67.15	90.12	29	
M06-2X/6-31G(d,p)[a]	3.331	−14	1.994	−11	1.277	−6	90.01	2.26	87.74	22.81	67.19	90.14	21	
HF/6-311++G(3df,2pd)	3.388	−70	1.999	−17	1.287	−16	90.01	2.93	87.07	21.89	68.11	90.23	23	763
HF/6-311++G(d,p)	3.371	−53	1.991	−8	1.282	−11	90.01	3.10	86.90	21.93	68.07	90.28	33	764
HF/6-311+G(d,p)	3.371	−53	1.991	−8	1.282	−11	90.01	3.13	86.87	21.94	68.07	90.28	31	757
HF/6-311G(d,p)	3.373	−56	1.991	−9	1.282	−11	90.01	2.98	87.02	21.86	68.14	90.23	27	743
HF/6-31++G(d,p)	3.366	−49	1.990	−8	1.281	−9	90.01	2.74	87.26	21.97	68.03	90.20	18	755
HF/6-31+G(d,p)	3.366	−49	1.990	−8	1.281	−9	90.01	2.80	87.20	21.98	68.02	90.22	19	751
HF/6-31G(d,p)	3.372	−54	1.991	−9	1.282	−11	90.01	2.77	87.23	21.88	68.12	90.20	17	723
Experiment	3.318		1.982		1.271		90.00	0.00	90.00	16.62	73.38	90.00	9	693

[a] obtained from scan.

Table 17.73. Fourier coefficients of the potential function of TMP about a rotation of the nitrogen methyl group around the dihedral angle $\varphi_1 = \angle(C_{15},N_{12},C_{19},H_7)$ calculated in 2° steps. The potential is expanded as $V(\varphi_1) = \sum_{n=1}^{15} a_n \cdot \cos(n \cdot \varphi_1)$.

	MP2/6-311++G(d,p)		MP2/cc-pVTZ		M06-2X/cc-pVTZ		B3LYP/cc-pVTZ	
	Hartree	cm^{-1}	Hartree	cm^{-1}	Hartree	cm^{-1}	Hartree	cm^{-1}
a_0	−327.193 459 788		−327.403 972 983		−328.081 309 910		−328.235 207 541	
a_3	0.000 057 568	12.6	0.000 008 719	1.9	0.000 007 738	1.7	0.000 004 192	0.9
a_6	0.000 179 906	39.5	0.000 068 314	15.0	0.000 063 903	14.0	0.000 038 485	8.4
a_9	−0.000 028 270	−6.2	−0.000 007 413	−1.6	−0.000 005 594	−1.2	−0.000 004 264	−0.9
a_{12}	0.000 026 871	5.9	0.000 005 005	1.1	0.000 009 038	2.0		
a_{15}	−0.000 008 487	−1.9	−0.000 001 081	−0.2				

Table 17.74. Coefficients of the two-dimensional Fourier expansion for the potential energy surface of TMP calculated at the MP2/6-311++G(d,p) level of theory in a grid of 10° (Figure 14.4). Due to symmetry, only data points in the range from $\varphi_1 = 0°$ to 120° and $\varphi_2 = 0°$ to 120° were needed. The potential is expanded as

$$V(\varphi_1, \varphi_2) = \sum_{i=1}^{25} V_i \cdot f_i.$$

i	f_i	V_i/Hartree
1	1	−327.191 939 674
2	$\cos(3\varphi_1)$	0.000 206 630
3	$\sin(3\varphi_1)$	0.000 002 171
4	$\cos(3\varphi_2)$	0.001 567 997
5	$\sin(3\varphi_2)$	0.000 065 494
6	$\cos(6\varphi_1)$	0.000 112 136
7	$\sin(6\varphi_1)$	0.000 001 660
8	$\cos(6\varphi_2)$	0.000 062 785
9	$\sin(6\varphi_2)$	−0.000 005 469
10	$\cos(3\varphi_1)\cos(3\varphi_2)$	0.000 162 970
11	$\sin(3\varphi_1)\sin(3\varphi_2)$	−0.000 141 464
12	$\cos(3\varphi_1)\sin(3\varphi_2)$	0.000 025 984
13	$\sin(3\varphi_1)\cos(3\varphi_2)$	0.000 011 905
14	$\cos(6\varphi_1)\cos(3\varphi_2)$	−0.000 058 150
15	$\sin(6\varphi_1)\sin(3\varphi_2)$	0.000 048 242
16	$\cos(6\varphi_1)\sin(3\varphi_2)$	−0.000 008 871
17	$\sin(6\varphi_1)\cos(3\varphi_2)$	−0.000 004 192
18	$\cos(3\varphi_1)\cos(6\varphi_2)$	0.000 025 126
19	$\sin(3\varphi_1)\sin(6\varphi_2)$	−0.000 017 635
20	$\cos(3\varphi_1)\sin(6\varphi_2)$	0.000 003 095
21	$\sin(3\varphi_1)\cos(6\varphi_2)$	0.000 001 958
22	$\cos(6\varphi_1)\cos(6\varphi_2)$	0.000 015 139
23	$\sin(6\varphi_1)\sin(6\varphi_2)$	−0.000 012 210
24	$\cos(6\varphi_1)\sin(6\varphi_2)$	0.000 001 683
25	$\sin(6\varphi_1)\cos(6\varphi_2)$	0.000 001 534

Table 17.75. Coefficients of the two-dimensional Fourier expansion for the potential energy surface of TMP calculated at the MP2/6-311++G(d,p) level of theory in a grid of 10° (Figure 14.5). Due to symmetry, only data points in the range from $\varphi_2 = 0°$ to 120° and $\varphi_3 = 0°$ to 120° were needed. The potential is expanded as

$$V(\varphi_2, \varphi_3) = \sum_{i=1}^{25} V_i \cdot f_i.$$

i	f_i	V_i/Hartree
1	1	−327.190 655 185
2	$\cos(3\varphi_2)$	−0.001 587 073
3	$\sin(3\varphi_2)$	−0.000 076 336
4	$\cos(3\varphi_3)$	0.001 581 471
5	$\sin(3\varphi_3)$	0.000 028 682
6	$\cos(6\varphi_2)$	0.000 074 474
7	$\sin(6\varphi_2)$	0.000 003 724
8	$\cos(6\varphi_3)$	0.000 046 759
9	$\sin(6\varphi_3)$	0.000 001 651
10	$\cos(3\varphi_2)\cos(3\varphi_3)$	−0.000 146 435
11	$\sin(3\varphi_2)\sin(3\varphi_3)$	−0.000 127 229
12	$\cos(3\varphi_2)\sin(3\varphi_3)$	−0.000 074 054
13	$\sin(3\varphi_2)\cos(3\varphi_3)$	0.000 067 601
14	$\cos(6\varphi_2)\cos(3\varphi_3)$	0.000 038 346
15	$\sin(6\varphi_2)\sin(3\varphi_3)$	0.000 044 845
16	$\cos(6\varphi_2)\sin(3\varphi_3)$	−0.000 002 550
17	$\sin(6\varphi_2)\cos(3\varphi_3)$	0.000 023 923
18	$\cos(3\varphi_2)\cos(6\varphi_3)$	−0.000 031 801
19	$\sin(3\varphi_2)\sin(6\varphi_3)$	−0.000 040 473
20	$\cos(3\varphi_2)\sin(6\varphi_3)$	0.000 026 039
21	$\sin(3\varphi_2)\cos(6\varphi_3)$	−0.000 009 509
22	$\cos(6\varphi_2)\cos(6\varphi_3)$	0.000 011 384
23	$\sin(6\varphi_2)\sin(6\varphi_3)$	−0.000 013 256
24	$\cos(6\varphi_2)\sin(6\varphi_3)$	0.000 014 827
25	$\sin(6\varphi_2)\cos(6\varphi_3)$	−0.000 014 510

Table 17.76. Observed frequencies ($\nu_{\text{Obs.}}$) of the (000), (100), (001), (011), (012), (101), (102), (111), (112), and (122) torsional species of TMP. $\nu_{\text{Obs.}} - \nu_{\text{Calc.}}$ values as obtained after a fit with the program XIAM.

J'	K_a'	K_c'	F'	J	K_a	K_c	F	$(\sigma_1\sigma_2\sigma_3)$	$\nu_{\text{Obs.}}$	$\nu_{\text{Obs.}} - \nu_{\text{Calc.}}$
upper level				lower level					GHz	kHz
2	1	1	1	1	1	1	0	(100)	8.971475 9	−0.6
2	1	1	1	1	1	1	1	(100)	8.969 949 4	0.4
2	1	1	2	1	1	1	1	(100)	8.970 711 1	−1.1
2	1	1	2	1	1	1	2	(100)	8.971 325 9	2.7
2	1	1	3	1	1	1	2	(100)	8.970 835 2	2.7
2	1	1	1	1	1	1	0	(101)	8.971 465 1	0.8
2	1	1	1	1	1	1	1	(101)	8.969 936 7	−0.1
2	1	1	2	1	1	1	1	(101)	8.970 698 9	−1.1
2	1	1	2	1	1	1	2	(101)	8.971 312 6	1.6
2	1	1	3	1	1	1	2	(101)	8.970 822 5	2.2
2	1	1	1	1	1	1	0	(111)	8.971 452 3	0.2
2	1	1	1	1	1	1	1	(111)	8.969 924 2	−0.4
2	1	1	2	1	1	1	1	(111)	8.970 684 8	−3.0
2	1	1	2	1	1	1	2	(111)	8.971 298 7	−0.1
2	1	1	3	1	1	1	2	(111)	8.970 809 1	1.0
2	1	1	1	1	1	1	0	(112)	8.971 435 2	−6.5
2	1	1	1	1	1	1	1	(112)	8.969 911 6	−2.6
2	1	1	2	1	1	1	1	(112)	8.970 674 5	−2.9
2	1	1	2	1	1	1	2	(112)	8.971 287 3	−1.2
2	1	1	3	1	1	1	2	(112)	8.970 796 3	−1.4
2	2	0	1	1	1	1	0	(000)	12.196 022 6	18.2
2	2	0	1	1	1	1	1	(000)	12.194 493 1	16.2
2	2	0	2	1	1	1	1	(000)	12.193 399 1	14.7
2	2	0	2	1	1	1	2	(000)	12.194 014 1	18.7
2	2	0	3	1	1	1	2	(000)	12.194 711 4	13.7
2	2	0	1	1	1	1	0	(100)	16.549 514 6	−8.5
2	2	0	1	1	1	1	1	(100)	16.547 996 6	1.0
2	2	0	2	1	1	1	1	(100)	16.546 599 8	−7.2
2	2	0	2	1	1	1	2	(100)	16.547 214 1	−3.9
2	2	0	3	1	1	1	2	(100)	16.548 106 4	−4.2
2	2	0	1	1	1	1	0	(102)	16.549 417 9	11.0
2	2	0	2	1	1	1	1	(102)	16.546 501 4	10.6
2	2	0	3	1	1	1	2	(102)	16.547 996 6	2.0
2	2	0	1	1	1	1	0	(111)	16.549 623 1	−73.3[a]
2	2	0	3	1	1	1	2	(111)	16.548 211 9	−72.1[a]
2	2	1	1	1	1	0	0	(000)	11.223 172 8	−4.9
2	2	1	1	1	1	0	1	(000)	11.225 579 4	−14.1
2	2	1	2	1	1	0	1	(000)	11.224 984 5	−16.8
2	2	1	2	1	1	0	2	(000)	11.224 025 4	−9.6
2	2	1	3	1	1	0	2	(000)	11.224 409 4	−6.3
2	2	1	1	1	1	0	0	(101)	10.125 158 5	16.3
2	2	1	2	1	1	0	1	(101)	10.126 164 3	11.5
2	2	1	3	1	1	0	2	(101)	10.125 805 5	12.7
2	2	1	1	1	1	0	0	(102)	10.125 117 5	−46.7[a]

Table 17.76. (continued)

J'	K'_a	K'_c	F'	J	K_a	K_c	F	$(\sigma_1\sigma_2\sigma_3)$	$\nu_{\text{Obs.}}$	$\nu_{\text{Obs.}} - \nu_{\text{Calc.}}$
upper level				lower level					GHz	kHz
2	2	1	2	1	1	0	1	(102)	10.126122 9	−51.8[a]
2	2	1	3	1	1	0	2	(102)	10.125763 8	−51.0[a]
2	2	1	2	1	1	0	1	(111)	10.126078 9	−30.3[a]
2	2	1	3	1	1	0	2	(111)	10.125715 2	−34.0[a]
2	2	1	1	1	1	0	0	(112)	10.125117 4	−3.0
2	2	1	2	1	1	0	1	(112)	10.126142 7	11.7
2	2	1	3	1	1	0	2	(112)	10.125763 8	−7.2
3	1	2	2	2	1	2	1	(100)	12.617892 5	2.3
3	1	2	2	2	1	2	2	(100)	12.616693 9	3.9
3	1	2	3	2	1	2	2	(100)	12.617567 7	2.6
3	1	2	3	2	1	2	3	(100)	12.618339 3	2.7
3	1	2	4	2	1	2	3	(100)	12.617689 5	1.0
3	1	2	2	2	1	2	1	(101)	12.617879 0	4.2
3	1	2	2	2	1	2	2	(101)	12.616679 4	4.8
3	1	2	3	2	1	2	2	(101)	12.617554 4	4.7
3	1	2	3	2	1	2	3	(101)	12.618324 5	3.3
3	1	2	4	2	1	2	3	(101)	12.617689 5	16.5
3	1	2	2	2	1	2	1	(112)	12.617865 2	17.3
3	1	2	2	2	1	2	2	(112)	12.616665 3	17.7
3	1	2	3	2	1	2	2	(112)	12.617539 6	16.8
3	1	2	3	2	1	2	3	(112)	12.618310 9	16.7
3	1	2	4	2	1	2	3	(112)	12.617662 9	16.8
3	1	3	2	2	0	2	1	(000)	9.410676 9	40.8[a]
3	1	3	2	2	0	2	2	(000)	9.409540 4	−3.3
3	1	3	3	2	0	2	2	(000)	9.411238 6	−6.6
3	1	3	3	2	0	2	3	(000)	9.411936 8	−10.6
3	1	3	4	2	0	2	3	(000)	9.410694 6	7.5
3	1	3	2	2	0	2	1	(100)	11.364345 3	−15.9
3	1	3	3	2	0	2	2	(100)	11.365836 0	−3.6
3	1	3	3	2	0	2	3	(100)	11.365578 9	−8.0
3	1	3	4	2	0	2	3	(100)	11.364777 7	−5.2
3	1	3	2	2	0	2	2	(001)	9.409532 4	−0.5
3	1	3	4	2	0	2	3	(001)	9.410682 4	6.1
3	1	3	2	2	0	2	2	(011)	9.409520 2	−1.9
3	1	3	4	2	0	2	3	(011)	9.410662 3	−3.2
3	1	3	2	2	0	2	2	(012)	9.409528 2	6.2
3	1	3	4	2	0	2	3	(012)	9.410673 5	8.1
3	1	3	2	2	0	2	1	(101)	11.364377 8	9.2
3	1	3	3	2	0	2	2	(101)	11.365855 8	8.8
3	1	3	3	2	0	2	3	(101)	11.365602 7	8.3
3	1	3	4	2	0	2	3	(101)	11.364799 7	9.4
3	1	3	2	2	0	2	1	(102)	11.364325 0	2.0
3	1	3	3	2	0	2	2	(102)	11.365803 1	1.7
3	1	3	3	2	0	2	3	(102)	11.365550 2	1.4
3	1	3	4	2	0	2	3	(102)	11.364746 9	2.2
3	1	3	2	2	0	2	1	(112)	11.364345 2	14.8

Table 17.76. (continued)

J'	K'_a	K'_c	F'	J	K_a	K_c	F	$(\sigma_1\sigma_2\sigma_3)$	$\nu_{\text{Obs.}}$	$\nu_{\text{Obs.}} - \nu_{\text{Calc.}}$
upper level				lower level					GHz	kHz
3	1	3	3	2	0	2	2	(112)	11.365 823 0	14.2
3	1	3	4	2	0	2	3	(112)	11.364 776 4	24.3
3	2	1	2	2	1	2	1	(000)	17.023 330 1	−6.2
3	2	1	2	2	1	2	2	(000)	17.021 725 3	−0.5
3	2	1	3	2	1	2	2	(000)	17.020 798 6	−2.0
3	2	1	3	2	1	2	3	(000)	17.021 828 0	−7.9
3	2	1	4	2	1	2	3	(000)	17.022 516 4	−4.8
3	2	1	4	2	1	2	3	(001)	17.022 492 6	2.6
3	2	1	4	2	1	2	3	(011)	17.022 479 9	21.8
3	2	1	4	2	1	2	3	(012)	17.022 472 3	12.7
3	2	1	3	2	2	1	2	(100)	13.769 711 9	−1.4
3	2	1	4	2	2	1	3	(100)	13.769 727 7	0.1
3	2	1	3	2	2	1	2	(101)	13.769 727 7	7.6
3	2	1	4	2	2	1	3	(101)	13.769 745 2	10.8
3	2	1	3	2	2	1	2	(111)	13.769 764 0	37.3[a]
3	2	1	3	2	2	1	3	(111)	13.769 657 4	47.5[a]
3	2	1	4	2	2	1	3	(111)	13.769 780 3	39.3[a]
3	2	2	2	2	1	1	1	(000)	13.766 376 4	−22.0
3	2	2	3	2	1	1	2	(000)	13.767 394 8	−22.0
3	2	2	4	2	1	1	3	(000)	13.766 737 8	−24.3
3	2	2	2	2	1	1	2	(100)	13.374 515 2	−9.8
3	2	2	3	2	1	1	2	(100)	13.375 044 1	−9.7
3	2	2	3	2	1	1	3	(100)	13.375 533 3	−11.1
3	2	2	4	2	1	1	3	(100)	13.375 142 5	−10.3
3	2	2	2	2	1	1	2	(101)	13.374 497 1	−5.2
3	2	2	3	2	1	1	2	(101)	13.375 025 0	−6.0
3	2	2	3	2	1	1	3	(101)	13.375 515 5	−6.2
3	2	2	4	2	1	1	3	(101)	13.375 124 4	−5.6
3	2	2	2	2	1	1	2	(111)	13.374 484 0	4.5
3	2	2	3	2	1	1	2	(111)	13.375 013 9	5.6
3	2	2	3	2	1	1	3	(111)	13.375 503 5	4.6
3	2	2	4	2	1	1	3	(111)	13.375 113 3	6.0
3	2	2	3	2	1	1	2	(112)	13.374 996 3	−4.9
3	2	2	3	2	1	1	3	(112)	13.375 484 8	−7.2
3	2	2	4	2	1	1	3	(112)	13.375 093 9	−6.4
3	3	0	2	2	2	1	1	(000)	18.406 353 7	−0.6
3	3	0	2	2	2	1	2	(000)	18.406 942 3	−4.2
3	3	0	3	2	2	1	2	(000)	18.406 088 1	−2.3
3	3	0	3	2	2	1	3	(000)	18.405 702 5	−7.2
3	3	0	4	2	2	1	3	(000)	18.406 337 7	−6.1
3	3	0	4	2	2	1	3	(001)	18.406 260 6	−46.1[a]
3	3	0	4	2	2	1	3	(011)	18.406 009 8	−219.8[a]
3	3	1	2	2	2	0	1	(000)	18.122 730 7	−44.7[a]
3	3	1	2	2	2	0	2	(000)	18.123 817 5	−50.4[a]
3	3	1	3	2	2	0	2	(000)	18.123 033 8	−49.1[a]
3	3	1	3	2	2	0	3	(000)	18.122 335 2	−45.5[a]

Table 17.76. (continued)

J'	K'_a	K'_c	F'	J	K_a	K_c	F	$(\sigma_1\sigma_2\sigma_3)$	$\nu_{\text{Obs.}}$	$\nu_{\text{Obs.}} - \nu_{\text{Calc.}}$
upper level				lower level					GHz	kHz
3	3	1	4	2	2	0	3	(000)	18.122917 7	−44.4[a]
4	0	4	3	3	1	3	2	(000)	11.130376 2	−15.8
4	0	4	3	3	1	3	3	(000)	11.128676 9	−13.6
4	0	4	4	3	1	3	3	(000)	11.130390 9	−12.2
4	0	4	4	3	1	3	4	(000)	11.131647 5	−16.0
4	0	4	5	3	1	3	4	(000)	11.130287 7	−13.5
4	1	3	3	3	1	3	2	(100)	16.193057 7	−17.6
4	1	3	3	3	1	3	3	(100)	16.191971 3	−18.4
4	1	3	4	3	1	3	3	(100)	16.192701 0	−17.8
4	1	3	4	3	1	3	4	(100)	16.193504 4	−18.4
4	1	3	5	3	1	3	4	(100)	16.192924 8	−18.1
4	1	3	5	3	1	3	4	(111)	16.192868 8	−24.5
4	1	3	5	3	1	3	4	(112)	16.192889 4	−5.4
4	1	3	3	4	0	4	3	(100)	8.930574 4	−13.6
4	1	3	4	4	0	4	4	(100)	8.931382 9	−12.8
4	1	3	3	4	0	4	3	(101)	8.930605 4	−48.9[a]
4	1	3	5	4	0	4	5	(101)	8.930771 9	−47.6[a]
4	1	3	3	4	0	4	3	(102)	8.930473 9	26.9
4	1	3	4	4	0	4	4	(102)	8.931275 6	20.9
4	1	3	5	4	0	4	5	(102)	8.930638 5	26.3
4	1	3	4	4	0	4	4	(111)	8.931515 4	−12.8
4	1	3	5	4	0	4	5	(111)	8.930875 2	−10.4
4	1	4	3	3	0	3	2	(000)	11.674119 7	−1.5
4	1	4	3	3	0	3	3	(000)	11.672660 3	−2.6
4	1	4	4	3	0	3	3	(000)	11.674466 0	2.5
4	1	4	4	3	0	3	4	(000)	11.675541 0	−2.7
4	1	4	5	3	0	3	4	(000)	11.674108 3	−3.1
4	1	4	3	3	0	3	2	(100)	14.001844 9	1.8
4	1	4	3	3	0	3	3	(100)	14.002148 8	−0.5
4	1	4	4	3	0	3	3	(100)	14.003247 2	0.0
4	1	4	5	3	0	3	4	(100)	14.002148 8	1.8
4	1	4	3	3	0	3	2	(101)	14.001870 6	6.8
4	1	4	3	3	0	3	3	(101)	14.002172 6	2.6
4	1	4	4	3	0	3	3	(101)	14.003276 6	8.7
4	1	4	5	3	0	3	4	(101)	14.002172 6	4.9
4	1	4	3	3	0	3	2	(102)	14.001790 7	−0.2
4	1	4	3	3	0	3	3	(102)	14.002095 9	−1.1
4	1	4	4	3	0	3	3	(102)	14.003194 5	−0.4
4	1	4	5	3	0	3	4	(102)	14.002095 9	1.1
4	1	4	3	3	0	3	2	(122)	14.001741 6	3.1
4	1	4	3	3	0	3	3	(122)	14.002043 9	−0.8
4	1	4	4	3	0	3	3	(122)	14.003149 3	6.6
4	2	2	3	3	2	2	2	(100)	17.601465 0	−1.2
4	2	2	4	3	2	2	3	(100)	17.601293 0	4.5
4	2	2	5	3	2	2	4	(100)	17.601405 7	4.8
4	2	2	3	3	2	2	2	(101)	17.601457 6	8.3

Table 17.76. (continued)

J'	K'_a	K'_c	F'	J	K_a	K_c	F	$(\sigma_1\sigma_2\sigma_3)$	$\nu_{\text{Obs.}}$	$\nu_{\text{Obs.}} - \nu_{\text{Calc.}}$
upper level				lower level					GHz	kHz
4	2	2	4	3	2	2	3	(101)	17.601 278 7	7.2
4	2	2	5	3	2	2	4	(101)	17.601 391 2	7.3
4	2	2	3	3	2	2	2	(102)	17.601 428 3	0.7
4	2	2	4	3	2	2	3	(102)	17.601 254 0	4.2
4	2	2	5	3	2	2	4	(102)	17.601 367 7	5.4
4	2	2	4	3	2	2	3	(112)	17.601 238 0	5.2
4	2	2	5	3	2	2	4	(112)	17.601 353 1	7.7
4	2	3	3	3	1	2	2	(100)	16.902 234 4	−3.6
4	2	3	3	3	1	2	3	(100)	16.901 360 7	−2.2
4	2	3	4	3	1	2	3	(100)	16.902 070 5	−2.8
4	2	3	4	3	1	2	4	(100)	16.902 720 6	−0.9
4	2	3	5	3	1	2	4	(100)	16.902 154 6	−1.8
4	2	3	3	3	1	2	3	(101)	16.901 325 1	−18.4
4	2	3	4	3	1	2	3	(101)	16.902 034 8	−19.1
4	2	3	4	3	1	2	4	(101)	16.902 683 2	−19.0
4	2	3	5	3	1	2	4	(101)	16.902 119 0	−18.1
4	2	3	3	3	1	2	2	(112)	16.902 154 6	−28.3
4	2	3	3	3	1	2	3	(112)	16.901 291 0	−16.9
4	2	3	4	3	1	2	3	(112)	16.902 001 8	−16.4
4	2	3	5	3	1	2	4	(112)	16.902 087 0	−14.3
4	3	1	3	3	2	2	2	(000)	22.315 032 5	−145.1[a]
4	3	1	3	3	2	2	3	(000)	22.315 032 5	−145.1[a]
4	3	1	4	3	2	2	3	(000)	22.314 358 7	−144.7[a]
4	3	1	4	3	2	2	4	(000)	22.314 358 7	−144.7[a]
4	3	1	5	3	2	2	4	(000)	22.314 894 7	−144.9[a]
4	3	2	3	3	2	1	2	(001)	20.944 131 6	17.5
4	3	2	4	3	2	1	3	(001)	20.944 623 8	4.6
4	3	2	5	3	2	1	4	(001)	20.944 282 6	14.5
4	3	2	3	3	2	1	2	(011)	20.944 052 9	−3.0
4	3	2	4	3	2	1	3	(011)	20.944 551 8	−9.2
4	3	2	5	3	2	1	4	(011)	20.944 197 4	−12.5
4	4	0	4	3	3	1	3	(000)	24.929 880 4	129.0[a]
4	4	0	5	3	3	1	4	(000)	24.929 955 9	129.9[a]
4	4	0	4	3	3	1	3	(011)	24.929 761 5	171.8[a]
4	4	0	5	3	3	1	4	(011)	24.929 836 2	171.8[a]
4	4	0	4	3	3	1	3	(012)	24.930 360 1	2.6
4	4	0	5	3	3	1	4	(012)	24.930 434 1	2.4
4	4	1	3	3	3	0	2	(000)	24.871 553 0	−255.2[a]
4	4	1	4	3	3	0	3	(000)	24.871 582 8	−265.9[a]
4	4	1	5	3	3	0	4	(000)	24.871 608 3	−255.0[a]
4	4	1	3	3	3	0	2	(012)	24.870 915 9	38.0[a]
4	4	1	4	3	3	0	3	(012)	24.870 951 4	33.7[a]
4	4	1	5	3	3	0	4	(012)	24.870 971 1	38.2[a]
5	0	5	4	4	1	4	3	(000)	13.841 728 4	−20.4
5	0	5	4	4	1	4	4	(000)	13.839 929 6	−18.7
5	0	5	5	4	1	4	4	(000)	13.841 790 0	−19.9

Table 17.76. (continued)

J'	K'_a	K'_c	F'	J	K_a	K_c	F	$(\sigma_1\sigma_2\sigma_3)$	$\nu_{\text{Obs.}}$	$\nu_{\text{Obs.}} - \nu_{\text{Calc.}}$
upper level				lower level					GHz	kHz
5	0	5	5	4	1	4	5	(000)	13.843 221 0	−21.1
5	0	5	6	4	1	4	5	(000)	13.841 676 0	−19.5
5	0	5	4	4	1	4	3	(100)	11.339 317 5	−14.1
5	0	5	5	4	1	4	4	(100)	11.338 542 7	−11.7
5	0	5	6	4	1	4	5	(100)	11.339 145 8	−15.5
5	0	5	4	4	1	4	3	(102)	11.339 446 3	11.8
5	0	5	5	4	1	4	4	(102)	11.338 667 6	10.2
5	0	5	6	4	1	4	5	(102)	11.339 276 5	12.2
5	0	5	4	4	1	4	3	(122)	11.339 548 5	11.0
5	0	5	5	4	1	4	4	(122)	11.338 773 0	12.7
5	0	5	6	4	1	4	5	(122)	11.339 378 4	11.2
5	1	4	4	4	1	4	3	(100)	19.986 303 8	5.3
5	1	4	5	4	1	4	4	(100)	19.985 648 6	6.8
5	1	4	6	4	1	4	5	(100)	19.986 155 3	6.7
5	1	4	4	4	1	4	3	(101)	19.986 254 9	4.9
5	1	4	5	4	1	4	4	(101)	19.985 598 5	5.2
5	1	4	6	4	1	4	5	(101)	19.986 105 6	5.5
5	1	4	4	4	1	4	3	(102)	19.986 303 8	8.4
5	1	4	5	4	1	4	4	(102)	19.985 648 6	10.0
5	1	4	6	4	1	4	5	(102)	19.986 155 3	9.9
5	1	4	4	4	1	4	3	(112)	19.986 254 9	8.0
5	1	4	5	4	1	4	4	(112)	19.985 598 5	8.4
5	1	4	6	4	1	4	5	(112)	19.986 105 6	8.6
5	1	5	4	4	0	4	3	(000)	14.052 398 7	−18.0
5	1	5	4	4	0	4	4	(000)	14.050 706 6	2.5
5	1	5	5	4	0	4	4	(000)	14.052 598 4	4.9
5	1	5	5	4	0	4	5	(000)	14.053 959 8	4.1
5	1	5	6	4	0	4	5	(000)	14.052 391 7	5.6
5	1	5	4	4	0	4	3	(100)	16.183 406 1	1.9
5	1	5	4	4	0	4	4	(100)	16.183 483 5	0.6
5	1	5	5	4	0	4	4	(100)	16.184 672 8	−1.0
5	1	5	5	4	0	4	5	(100)	16.184 607 0	−4.3
5	1	5	6	4	0	4	5	(100)	16.183 620 0	−1.9
5	1	5	4	4	0	4	3	(101)	16.183 429 8	−7.2
5	1	5	5	4	0	4	4	(101)	16.184 715 1	8.6
5	1	5	6	4	0	4	5	(101)	16.183 661 4	6.8
5	1	5	4	4	0	4	3	(102)	16.183 339 2	−0.9
5	1	5	5	4	0	4	4	(102)	16.184 607 0	−2.7
5	1	5	6	4	0	4	5	(102)	16.183 555 0	−2.7
5	1	5	5	4	0	4	4	(111)	16.184 754 7	15.5
5	1	5	4	4	0	4	3	(112)	16.183 380 4	7.7
5	1	5	4	4	0	4	4	(112)	16.183 448 9	−2.5
5	1	5	5	4	0	4	4	(112)	16.184 647 9	5.5
5	1	5	5	4	0	4	5	(112)	16.184 542 6	−37.2[a]
5	1	5	6	4	0	4	5	(112)	16.183 592 8	2.4
5	1	5	5	4	0	4	4	(122)	16.184 543 8	−1.6

Table 17.76. (continued)

J'	K'_a	K'_c	F'	J	K_a	K_c	F	$(\sigma_1\sigma_2\sigma_3)$	$\nu_{\text{Obs.}}$	$\nu_{\text{Obs.}} - \nu_{\text{Calc.}}$
upper level				lower level					GHz	kHz
5	2	3	4	4	2	3	3	(100)	21.2147296	−3.2
5	2	3	5	4	2	3	4	(100)	21.2145467	−2.9
5	2	3	6	4	2	3	5	(100)	21.2146742	−2.5
5	2	3	4	4	2	3	3	(101)	21.2147078	−0.2
5	2	3	5	4	2	3	4	(101)	21.2145257	0.9
5	2	3	6	4	2	3	5	(101)	21.2146547	2.8
5	2	3	4	4	2	3	3	(102)	21.2146912	−1.4
5	2	3	5	4	2	3	4	(102)	21.2145071	−2.3
5	2	3	6	4	2	3	5	(102)	21.2146341	−2.4
5	2	3	6	4	2	3	5	(122)	21.2145942	−2.1
5	2	4	4	4	1	3	3	(000)	17.8538770	8.0
5	2	4	4	4	1	3	4	(000)	17.8540378	−29.8[a]
5	2	4	5	4	1	3	4	(000)	17.8546086	−5.3
5	2	4	5	4	1	3	5	(000)	17.8545796	123.8[a]
5	2	4	6	4	1	3	5	(000)	17.8539954	−6.6
5	2	4	5	4	1	3	4	(100)	20.3189176	−22.0
5	2	4	6	4	1	3	5	(100)	20.3188865	−19.3
5	2	4	4	4	1	3	3	(001)	17.8538343	−2.1
5	2	4	4	4	1	3	4	(001)	17.8540105	−24.6
5	2	4	5	4	1	3	4	(001)	17.8545796	−1.8
5	2	4	6	4	1	3	5	(001)	17.8539681	−1.4
5	2	4	5	4	1	3	4	(102)	20.3188995	3.5
5	2	4	6	4	1	3	5	(102)	20.3188679	5.8
5	2	4	5	4	1	3	4	(111)	20.3188865	−21.8
5	2	4	6	4	1	3	5	(111)	20.3188546	−19.7
5	2	4	5	4	1	3	4	(122)	20.3188546	2.3
5	2	4	6	4	1	3	5	(122)	20.3188242	5.8
5	2	4	4	5	1	5	4	(000)	10.9947096	−119.7[a]
5	2	4	5	5	1	5	5	(000)	10.9933615	−124.7[a]
5	2	4	6	5	1	5	6	(000)	10.9944811	−120.9[a]
5	3	3	4	4	2	2	3	(102)	22.0018185	10.1
5	3	3	5	4	2	2	4	(102)	22.0017190	11.1
5	3	3	6	4	2	2	5	(102)	22.0017904	11.4
5	3	3	5	4	2	2	4	(111)	22.0016901	9.0
5	3	3	6	4	2	2	5	(111)	22.0017621	9.9
5	3	3	6	4	2	2	5	(112)	22.0017466	2.5
5	3	3	4	4	2	2	3	(122)	22.0016758	−89.7[a]
5	3	3	6	4	2	2	5	(122)	22.0016477	−88.4[a]
6	0	6	5	5	1	5	4	(000)	16.4499420	−13.2
6	0	6	5	5	1	5	5	(000)	16.4480544	−11.4
6	0	6	6	5	1	5	5	(000)	16.4500086	−11.0
6	0	6	6	5	1	5	6	(000)	16.4515773	−11.9
6	0	6	7	5	1	5	6	(000)	16.4499079	−9.8
6	0	6	5	5	1	5	4	(100)	15.1615522	17.1
6	0	6	6	5	1	5	5	(100)	15.1611998	20.8
6	0	6	7	5	1	5	6	(100)	15.1614675	13.4

Table 17.76. (continued)

J'	K'_a	K'_c	F'	J	K_a	K_c	F	$(\sigma_1\sigma_2\sigma_3)$	$\nu_{\text{Obs.}}$	$\nu_{\text{Obs.}} - \nu_{\text{Calc.}}$
upper level				lower level					GHz	kHz
6	0	6	5	5	1	5	4	(102)	15.161 620 4	14.4
6	0	6	6	5	1	5	5	(102)	15.161 266 7	16.7
6	0	6	7	5	1	5	6	(102)	15.161 539 6	14.5
6	1	5	5	5	1	5	4	(100)	24.402 853 3	5.4
6	1	5	6	5	1	5	5	(100)	24.401 768 4	6.1
6	1	5	7	5	1	5	6	(100)	24.402 668 9	7.4
6	1	5	5	5	1	5	4	(101)	24.402 754 1	−5.6
6	1	5	6	5	1	5	5	(101)	24.401 668 1	−6.0
6	1	5	7	5	1	5	6	(101)	24.402 567 4	−6.0
6	1	5	5	5	1	5	4	(102)	24.402 890 5	5.7
6	1	5	6	5	1	5	5	(102)	24.401 805 5	6.4
6	1	5	7	5	1	5	6	(102)	24.402 705 5	7.1
6	1	5	5	5	2	4	4	(000)	18.182 582 4	−363.3[a]
6	1	5	6	5	2	4	5	(000)	18.182 634 5	−363.9[a]
6	1	5	7	5	2	4	6	(000)	18.182 582 4	−357.4[a]
6	1	5	6	6	0	6	6	(100)	9.240 573 9	−9.4
6	1	5	7	6	0	6	7	(100)	9.241 196 9	−10.5
6	1	5	5	6	0	6	5	(101)	9.241 269 9	−6.7
6	1	5	6	6	0	6	6	(101)	9.240 540 3	−6.8
6	1	5	7	6	0	6	7	(101)	9.241 164 4	−6.8
6	1	5	5	6	0	6	5	(112)	9.241 236 8	−5.7
6	1	5	6	6	0	6	6	(112)	9.240 507 5	−5.5
6	1	5	7	6	0	6	7	(112)	9.241 131 6	−5.5
6	1	6	5	5	0	5	4	(000)	16.523 811 1	5.6
6	1	6	5	5	0	5	5	(000)	16.521 953 6	9.7
6	1	6	6	5	0	5	5	(000)	16.523 915 1	9.3
6	1	6	6	5	0	5	6	(000)	16.525 458 7	6.4
6	1	6	7	5	0	5	6	(000)	16.523 783 7	9.9
6	1	6	5	5	0	5	4	(100)	18.053 687 8	5.1
6	1	6	6	5	0	5	5	(100)	18.054 694 0	1.7
6	1	6	7	5	0	5	6	(100)	18.053 823 6	3.0
6	1	6	5	5	0	5	4	(101)	18.053 729 0	10.1
6	1	6	6	5	0	5	5	(101)	18.054 741 2	12.6
6	1	6	7	5	0	5	6	(101)	18.053 869 1	12.3
6	1	6	5	5	0	5	4	(102)	18.053 616 1	−0.7
6	1	6	6	5	0	5	5	(102)	18.054 626 8	0.4
6	1	6	7	5	0	5	6	(102)	18.053 757 3	2.7
6	1	6	6	5	0	5	5	(111)	18.054 785 8	21.0
6	1	6	5	5	0	5	4	(112)	18.053 660 2	7.2
6	1	6	6	5	0	5	5	(112)	18.054 671 4	8.8
6	1	6	7	5	0	5	6	(112)	18.053 798 9	8.1
6	1	6	6	5	0	5	5	(122)	18.054 561 5	1.1
6	2	5	5	5	1	4	4	(000)	19.770 045 0	21.5
6	2	5	6	5	1	4	5	(000)	19.770 577 4	23.6
6	2	5	7	5	1	4	6	(000)	19.770 121 3	26.7
6	3	4	5	6	2	5	5	(000)	11.377 625 7	−417.8[a]

Table 17.76. (continued)

J'	K'_a	K'_c	F'	J	K_a	K_c	F	$(\sigma_1\sigma_2\sigma_3)$	$\nu_{\text{Obs.}}$	$\nu_{\text{Obs.}} - \nu_{\text{Calc.}}$
upper level				lower level					GHz	kHz
6	3	4	5	6	2	5	6	(000)	11.376 867 2	−421.5[a]
6	3	4	6	6	2	5	5	(000)	11.377 555 2	−441.1[a]
6	3	4	6	6	2	5	6	(000)	11.376 783 9	−457.6[a]
6	3	4	6	6	2	5	7	(000)	11.377 468 2	−419.0[a]
6	3	4	7	6	2	5	6	(000)	11.376 827 0	−454.9[a]
6	3	4	7	6	2	5	7	(000)	11.377 468 3	−459.3[a]
7	0	7	6	6	1	6	5	(000)	19.015 377 0	6.0
7	0	7	6	6	1	6	6	(000)	19.013 410 9	1.8
7	0	7	7	6	1	6	6	(000)	19.015 433 2	7.3
7	0	7	7	6	1	6	7	(000)	19.017 110 0	5.6
7	0	7	8	6	1	6	7	(000)	19.015 347 1	5.3
7	0	7	6	6	1	6	5	(100)	18.496 992 8	−22.7
7	0	7	7	6	1	6	6	(100)	18.496 940 8	−18.9
7	0	7	7	6	1	6	7	(100)	18.498 092 2	−5.7
7	0	7	8	6	1	6	7	(100)	18.496 976 3	−7.7
7	0	7	6	6	1	6	5	(102)	18.497 044 5	−6.9
7	0	7	7	6	1	6	6	(102)	18.496 976 3	−19.3
7	0	7	7	6	1	6	7	(102)	18.498 125 5	−8.2
7	0	7	8	6	1	6	7	(102)	18.497 011 2	−8.6
7	0	7	6	6	1	6	5	(122)	18.497 079 1	−8.1
7	0	7	7	6	1	6	6	(122)	18.497 011 2	−20.2
7	0	7	7	6	1	6	7	(122)	18.498 161 8	−7.8
7	0	7	8	6	1	6	7	(122)	18.497 044 5	−11.2
7	1	7	6	6	0	6	5	(000)	19.039 689 1	16.9
7	1	7	6	6	0	6	6	(000)	19.037 736 9	18.5
7	1	7	7	6	0	6	6	(000)	19.039 756 4	18.7
7	1	7	7	6	0	6	7	(000)	19.041 425 7	16.5
7	1	7	8	6	0	6	7	(000)	19.039 662 6	18.1
7	1	7	6	6	0	6	5	(100)	19.905 174 2	−15.5
7	1	7	7	6	0	6	6	(100)	19.905 837 0	−1.9
7	1	7	8	6	0	6	7	(100)	19.905 251 9	−4.3
7	1	7	6	6	0	6	5	(101)	19.905 202 9	−13.3
7	1	7	7	6	0	6	6	(101)	19.905 854 8	−10.6
7	1	7	8	6	0	6	7	(101)	19.905 272 7	−10.0
7	1	7	6	6	0	6	5	(111)	19.905 251 8	9.1
7	1	7	7	6	0	6	6	(111)	19.905 890 3	−1.6
7	1	7	8	6	0	6	7	(111)	19.905 307 8	−1.3
7	1	7	6	6	0	6	5	(112)	19.905 153 9	−11.0
7	1	7	7	6	0	6	6	(112)	19.905 803 4	−10.8
7	1	7	8	6	0	6	7	(112)	19.905 222 4	−9.0
7	2	6	6	6	1	5	5	(000)	21.878 455 8	−6.1
7	2	6	7	6	1	5	6	(000)	21.878 799 1	−1.9
7	2	6	8	6	1	5	7	(000)	21.878 491 5	−2.2

[a] Not included in the fit.

17.2.6 2,3,4,5-Tetramethylpthiophene

Table 17.77. Nuclear coordinates in the principal inertial axes of 2,3,4,5-tetramethylpthiophene (TMTP) calculated with the methods MP2, B3LYP, M06-2X, and CCSD with the basis set 6-311++G(d,p). The atoms are numbered according to Figure 15.2.

	MP2			**B3LYP**		
	a /Å	b /Å	c /Å	a /Å	b /Å	c /Å
H1	2.819783	−1.875782	0.248753	2.999698	−1.208714	−0.988839
H2	3.273484	−0.240101	0.728424	2.882832	−1.635921	0.718939
H3	3.149816	−0.656829	−0.989830	3.360439	−0.006686	0.251341
H4	−2.819677	−1.875984	−0.248471	−2.882826	−1.636020	−0.718815
H5	−3.273384	−0.240415	−0.728613	−3.360418	−0.006702	−0.251494
H6	−3.149830	−0.656671	0.989748	−2.999760	−1.208546	0.988888
H7	2.588524	1.918211	0.188114	2.591366	1.953329	0.040093
H8	1.180124	2.830754	0.749903	1.257600	2.772405	0.852219
H9	1.467143	2.624157	−0.981391	1.321109	2.723084	−0.906135
H10	−2.588461	1.918062	−0.189696	−2.591352	1.953371	−0.040212
H11	−1.179455	2.831308	−0.748749	−1.257486	2.772495	−0.852114
H12	−1.468746	2.623058	0.981977	−1.321174	2.722993	0.906231
C13	2.700601	−0.818234	−0.003440	2.698715	−0.835887	−0.003660
C14	−2.700541	−0.818375	0.003435	−2.698723	−0.835876	0.003664
C15	1.532620	2.122770	−0.008148	1.517521	2.137303	−0.001368
C16	−1.532835	2.122571	0.008181	−1.517507	2.137312	0.001381
C17	1.252197	−0.417247	0.017520	1.262897	−0.400117	0.011424
C18	−1.252153	−0.417346	−0.017515	−1.262897	−0.400126	−0.011434
C19	0.715283	0.860625	0.011505	0.724365	0.857943	0.004764
C20	−0.715314	0.860544	−0.011575	−0.724373	0.857941	−0.004790
S21	0.000074	−1.601881	0.000009	−0.000001	−1.610435	0.000004

Table 17.78. Nuclear coordinates in the principal inertial axes of TMTP calculated with the methods MP2, B3LYP, M06-2X, and CCSD with the basis set 6-311++G(d,p). The atoms are numbered according to Figure 15.2.

	M06-2X			**CCSD**		
	a /Å	b /Å	c /Å	a /Å	b /Å	c /Å
H1	2.961090	−1.360414	−0.882484	2.967916	−1.372198	−0.886187
H2	2.961201	−1.360165	0.882568	2.968328	−1.371197	0.886565
H3	3.360823	0.111940	−0.000192	3.372246	0.105017	−0.000791
H4	−2.898379	−1.480840	−0.882561	−2.909439	−1.482724	−0.886283
H5	−3.322095	−0.011580	−0.000106	−3.339008	−0.010488	−0.000076
H6	−2.898401	−1.480563	0.882792	−2.909418	−1.482299	0.886772
H7	2.537580	2.018902	0.000077	2.557327	2.015578	0.002212
H8	1.212627	2.774779	0.881341	1.232108	2.784190	0.884309
H9	1.212739	2.774676	−0.881405	1.235137	2.782781	−0.885770
H10	−2.261621	2.089599	−0.881952	−2.268222	2.106761	−0.884656
H11	−1.017935	2.970196	−0.000846	−1.017744	2.988157	−0.002901
H12	−2.260428	2.090416	0.882748	−2.264577	2.109613	0.886925
C13	2.714467	−0.764968	−0.000025	2.722990	−0.774300	−0.000093
C14	−2.663138	−0.880757	0.000023	−2.675561	−0.880623	0.000097
C15	1.460244	2.176399	0.000016	1.477203	2.182450	0.000175
C16	−1.616541	2.059321	−0.000029	−1.620448	2.075637	−0.000154
C17	1.270266	−0.363486	0.000024	1.271153	−0.369494	−0.000033
C18	−1.232475	−0.438750	−0.000005	−1.236396	−0.437439	0.000001
C19	0.703127	0.877975	0.000052	0.709947	0.881491	0.000023
C20	−0.741321	0.832607	−0.000039	−0.744524	0.840179	−0.000056
S21	0.052561	−1.601039	−0.000006	0.047727	−1.609523	0.000012

Table 17.79. The rotational constants A, B, and C in GHz, the deviations (Dev.) between the experimental and calculated rotational constants in MHz, the angles $\angle(i_1,a)$, $\angle(i_1,b)$, and $\angle(i_1,c)$ between the top internal rotor axis and the principal axes of inertia, the angles $\angle(i_3,a)$, $\angle(i_3,b)$, and $\angle(i_3,c)$ between the bottom internal rotor axis and the principal axes of inertia, the barriers to internal rotation $V_{3,1}$ of the top methyl rotors, the barriers to internal rotation $V_{3,2}$ of the bottom methyl rotor of TMTP in cm^{-1} calculated using various methods and basis sets. Harmonic frequency calculations were carried out to verify the nature of the stationary points. The relations of the angles $\angle(i_x,a)$, $\angle(i_x,b)$, $\angle(i_x,c)$ with x = 1,2,3,4 between the internal rotor axis of inertia of the second and fourth rotor and the principal axes are: $\angle(i_2,a) = \pi - \angle(i_1,a)$, $\angle(i_2,b) = \angle(i_1,b)$, $\angle(i_2,c) = \angle(i_1,c)$ and $\angle(i_4,a) = \pi - \angle(i_3,a)$, $\angle(i_4,b) = \angle(i_3,b)$, $\angle(i_4,c) = \angle(i_3,c)$.

Method/Basis set	A	Dev.	B	Dev.	C	Dev.	$\angle(i_1,a)$	$\angle(i_1,b)$	$\angle(i_1,c)$	$\angle(i_3,a)$	$\angle(i_3,b)$	$\angle(i_3,c)$	$V_{3,1}/cm^{-1}$	$V_{3,2}/cm^{-1}$
MP2/cc-pVDZ	1.789	31	1.370	16	0.791	9	15.48	74.52	90.00	56.98	146.98	90.00	76	164
MP2/6-311++G(d,p)	1.805	15	1.381	5	0.798	2	15.49	74.53	90.80	57.08	147.07	90.75	93	172
MP2/6-311+G(d,p)	1.805	15	1.381	5	0.798	2	15.49	74.53	90.77	57.06	147.05	90.78	100	179
MP2/6-311G(d,p)	1.808	12	1.382	4	0.799	1	15.38	74.64	90.75	57.00	146.99	90.77	81	158
MP2/6-31++G(d,p)	1.801	19	1.386	0	0.799	1	15.83	74.22	91.32	57.30	147.29	90.84	93	194
MP2/6-31+G(d,p)	1.803	17	1.385	1	0.799	1	15.75	74.31	88.61	57.19	147.17	89.11	103	192
MP2/6-31G(d,p)	1.808	12	1.387	−1	0.800	0	15.62	74.41	89.14	57.18	147.18	89.57	81	174
B3LYP/cc-pVQZ	1.814	6	1.384	2	0.801	−1	15.98	74.03	89.29	57.71	147.71	89.75	24	200
B3LYP/cc-pVTZ	1.806	14	1.385	1	0.799	1	16.27	73.74	90.62	57.59	147.59	90.28	17	207
B3LYP/cc-pVDZ	1.770	50	1.381	5	0.791	9	16.92	73.08	90.35	58.33	148.33	90.13		243
B3LYP/6-311++G(3df,2pd)	1.817	3	1.383	3	0.801	−1	15.94	74.06	90.00	57.20	147.20	90.00	41	197
B3LYP/6-311++G(d,p)	1.782	38	1.384	2	0.794	6	16.89	73.12	90.58	58.20	148.20	90.23	15	246
B3LYP/6-311+G(d,p)	1.785	35	1.383	3	0.795	5	16.77	73.24	89.31	58.10	148.10	89.68		241
B3LYP/6-311G(d,p)	1.784	36	1.384	2	0.795	5	16.81	73.20	90.65	58.12	148.12	90.28		249
B3LYP/6-31++G(d,p)	1.773	47	1.382	4	0.792	8	16.99	73.01	90.28	58.33	148.33	90.11		265
B3LYP/6-31+G(d,p)	1.773	47	1.382	4	0.792	8	16.99	73.01	90.28	58.33	148.33	90.11		263
B3LYP/6-31G(d,p)	1.775	45	1.384	2	0.793	7	16.98	73.02	89.85	58.35	148.35	89.95		
HF/6-311++G(3df,2pd)	1.816	4	1.399	−13	0.806	−6	17.01	73.00	90.60	58.36	148.36	90.40		332
HF/6-311++G(d,p)	1.794	26	1.396	−10	0.800	0	17.48	72.52	90.00	58.80	148.80	90.00	45	
HF/6-311+G(d,p)	1.794	26	1.395	−9	0.800	0	17.47	72.53	90.00	58.80	148.80	90.00	38	
HF/6-311G(d,p)	1.799	21	1.395	−9	0.801	−1	17.31	72.70	90.41	58.65	148.65	90.26		
HF/6-31++G(d,p)	1.792	28	1.395	−9	0.800	0	17.43	72.57	89.99	58.82	148.82	90.01	37	
HF/6-31+G(d,p)	1.792	28	1.395	−9	0.800	0	17.43	72.57	90.00	58.81	148.81	90.00	32	
HF/6-31G(d,p)	1.794	26	1.396	−10	0.800	0	17.40	72.60	90.00	58.79	148.79	90.00	40	
Experiment	1.820		1.386		0.800		16.84	73.15	90.00	57.03	147.03	90.00	54	245

Table 17.80. Observed frequencies ($\nu_{\mathrm{Obs.}}$) of the (0000), (0100), (0001), (0011), (0012), (0110), (0120), (0101), (0102), (0111) and (0122) torsional species of TMTP. $\nu_{\mathrm{Obs.}} - \nu_{\mathrm{Calc.}}$ values as obtained after a fit with XIAM. The frequency list is separated into the transitions used for the different fits.

J'	K'_a	K'_c	J	K_a	K_c	$(\sigma_1\sigma_2\sigma_3\sigma_4)$	$\nu_{\mathrm{Obs.}}$	$\nu_{\mathrm{Obs.}} - \nu_{\mathrm{Calc.}}$
upper level			lower level				GHz	kHz
2	2	0	1	1	1	(0000)	7.197 274 5	1.0
3	0	3	2	1	2	(0000)	5.469 202 9	0.7
3	1	3	2	0	2	(0000)	5.689 578 5	1.5
3	3	0	2	2	1	(0000)	10.541 751 0	−1.0
3	3	1	2	2	0	(0000)	10.099 324 9	−1.3
4	0	4	3	1	3	(0000)	7.152 839 6	0.1
4	1	4	3	0	3	(0000)	7.209 618 8	−1.8
4	2	3	3	1	2	(0000)	9.228 085 5	−8.4
4	3	1	3	2	2	(0000)	13.714 729 0	0.5
4	3	2	3	2	1	(0000)	11.779 586 0	8.1
4	4	0	3	3	1	(0000)	14.054 182 9	−1.4
4	4	1	3	3	0	(0000)	13.886 382 7	−1.2
5	0	5	4	1	4	(0000)	8.774 020 8	0.1
5	1	4	4	2	3	(0000)	10.165 039 9	1.6
5	1	5	4	0	4	(0000)	8.786 271 7	1.0
5	2	4	4	1	3	(0000)	10.543 329 2	−0.3
5	3	3	4	2	2	(0000)	13.078 759 8	2.5
5	4	1	4	3	2	(0000)	16.788 550 5	−1.1
5	4	2	4	3	1	(0000)	15.771 423 6	−0.9
5	5	0	4	4	1	(0000)	17.660 799 4	0.3
5	5	1	4	4	0	(0000)	17.607 064 7	0.6
6	0	6	5	1	5	(0000)	10.378 516 6	−0.2
6	1	5	5	2	4	(0000)	11.894 752 5	1.7
6	1	6	5	0	5	(0000)	10.380 913 4	0.1
6	2	5	5	1	4	(0000)	12.001 589 0	−1.2
6	3	4	5	2	3	(0000)	14.186 921 5	−0.7
7	0	7	6	1	6	(0000)	11.979 361 6	0.5
7	1	6	6	2	5	(0000)	13.529 946 2	−1.0
7	1	7	6	0	6	(0000)	11.979 802 0	−0.1
7	2	6	6	1	5	(0000)	13.555 672 6	0.4
8	0	8	7	1	7	(0000)	13.579 533 2	−0.1
8	1	7	7	2	6	(0000)	15.137 371 1	−0.9
8	2	7	7	1	6	(0000)	15.142 982 0	0.8
3	2	1	2	1	1	(1000)	9.179 379 5	−12.3
3	3	0	2	2	0	(0100)	11.461 345 5	−16.0
3	3	1	2	2	1	(0100)	10.150 971 8	−24.8
4	2	3	3	1	2	(0100)	9.385 254 1	10.7
4	3	1	3	2	1	(0100)	12.529 611 0	−19.9[a]
4	3	1	3	2	2	(0100)	13.738 365 1	−30.4
4	3	2	3	2	1	(0100)	11.644 447 4	−12.2
4	4	0	3	3	0	(0100)	15.089 209 4	−16.7
4	4	1	3	3	1	(0100)	13.763 358 8	−59.8[a]
5	0	5	4	1	4	(0100)	8.775 252 7	7.0

Table 17.80. (continued)

J'	K'_a	K'_c	J	K_a	K_c	$(\sigma_1\sigma_2\sigma_3\sigma_4)$	$\nu_{\mathrm{Obs.}}$	$\nu_{\mathrm{Obs.}} - \nu_{\mathrm{Calc.}}$
upper level			lower level				GHz	kHz
5	1	4	4	2	3	(0100)	10.131 101 0	−2.3
5	1	5	4	0	4	(0100)	8.792 547 9	9.7
5	2	3	4	3	2	(0100)	10.189 914 2	73.6[a]
5	2	4	4	1	3	(0100)	10.642 451 6	12.2
5	3	2	4	2	3	(0100)	17.689 171 4	27.7
5	3	3	4	2	2	(0100)	13.141 726 2	−31.1[a]
5	4	1	4	3	1	(0100)	16.137 698 1	50.8[a]
5	5	0	4	4	0	(0100)	18.717 366 3	−1.9
5	5	1	4	4	1	(0100)	17.393 340 3	−87.1[a]
6	0	6	5	1	5	(0100)	10.378 365 5	6.7
6	1	5	5	2	4	(0100)	11.887 923 6	−6.6
6	1	6	5	0	5	(0100)	10.381 634 0	8.3
6	2	4	5	3	3	(0100)	12.737 934 9	−3.8
6	2	5	5	1	4	(0100)	12.033 458 4	10.4
6	3	4	5	2	3	(0100)	14.351 268 9	−18.4
6	4	3	5	3	2	(0100)	16.966 327 3	−126.4[a]
6	5	1	5	4	1	(0100)	19.860 800 6	151.8[a]
6	5	2	5	4	2	(0100)	19.701 962 7	−187.7[a]
6	6	0	5	5	0	(0100)	22.345 130 6	37.2
6	6	1	5	5	1	(0100)	21.023 403 7	−94.9[a]
7	0	7	6	1	6	(0100)	11.977 762 3	4.9
7	1	6	6	2	5	(0100)	13.526 240 0	−6.1
7	1	7	6	0	6	(0100)	11.978 344 4	4.9
7	2	6	6	1	5	(0100)	13.560 606 9	0.0
7	3	5	6	2	4	(0100)	15.485 222 5	4.6
8	0	8	7	1	7	(0100)	13.576 943 8	2.5
8	1	7	7	2	6	(0100)	15.131 032 7	−11.6
8	2	7	7	1	6	(0100)	15.138 342 4	−8.0
9	0	9	8	1	8	(0100)	15.176 385 0	−3.2
9	1	9	8	0	8	(0100)	15.176 402 1	−2.6
2	1	2	1	0	1	(0110)	4.365 102 2	9.0
3	0	3	2	1	2	(0110)	5.434 357 6	−13.0
3	1	3	2	0	2	(0110)	5.777 357 8	3.6
3	2	1	2	1	1	(0110)	9.186 136 8	1.3
3	3	0	2	2	0	(0110)	11.481 285 5	−32.7
3	3	1	2	2	1	(0110)	10.171 470 7	3.5
4	0	4	3	1	3	(0110)	7.149 546 6	−13.7
4	1	4	3	0	3	(0110)	7.237 582 9	−2.9
4	2	3	3	1	2	(0110)	9.406 542 9	15.9
4	3	1	3	2	1	(0110)	12.513 441 9	15.1
4	3	1	3	2	2	(0110)	13.716 812 9	−7.2
4	3	2	3	2	1	(0110)	11.672 009 5	31.3
4	4	0	3	3	0	(0110)	15.108 416 8	10.6
4	4	1	3	3	1	(0110)	13.782 604 0	−17.4
5	0	5	4	1	4	(0110)	8.775 065 7	−15.7

Table 17.80. (continued)

J'	K'_a	K'_c	J	K_a	K_c	$(\sigma_1\sigma_2\sigma_3\sigma_4)$	$\nu_{\text{Obs.}}$	$\nu_{\text{Obs.}} - \nu_{\text{Calc.}}$
upper level			lower level				GHz	kHz
5	1	4	4	2	3	(0110)	10.120154 2	−24.2
5	1	5	4	0	4	(0110)	8.793453 6	−11.0
5	2	3	4	3	2	(0110)	10.119043 5	54.3
5	2	4	4	1	3	(0110)	10.658461 1	20.6
5	3	3	4	2	2	(0110)	13.161815 6	7.2
5	4	1	4	3	1	(0110)	16.092964 7	121.0[a]
5	4	1	4	3	2	(0110)	16.934281 0	−11.2
5	5	0	4	4	0	(0110)	18.735932 5	−7.6
5	5	1	4	4	1	(0110)	17.411800 8	−50.6[a]
6	0	6	5	1	5	(0110)	10.378375 8	−18.9
6	1	5	5	2	4	(0110)	11.885209 2	−22.8
6	2	4	5	3	3	(0110)	12.701180 1	−24.8
6	2	5	5	1	4	(0110)	12.039462 7	12.3
6	3	4	5	2	3	(0110)	14.381457 1	22.3
6	4	3	5	3	2	(0110)	16.989356 8	−42.5[a]
6	5	1	5	4	1	(0110)	19.824430 5	213.6[a]
6	5	2	5	4	2	(0110)	19.729908 7	−154.7[a]
6	6	0	5	5	0	(0110)	22.363115 2	−24.7
7	1	6	6	2	5	(0110)	13.525762 6	−13.0
7	2	6	6	1	5	(0110)	13.562288 2	0.5
7	3	5	6	2	4	(0110)	15.505578 4	38.3
8	1	7	7	2	6	(0110)	15.130894 8	−13.5
8	2	7	7	1	6	(0110)	15.138673 8	−8.5
2	1	2	1	0	1	(0120)	4.345 148 9	9.2
3	0	3	2	1	2	(0120)	5.448 121 2	−15.1
3	1	3	2	0	2	(0120)	5.758 682 1	2.3
3	2	1	2	1	1	(0120)	9.172 038 9	−21.6
3	3	0	2	2	0	(0120)	11.440 630 6	32.1
3	3	1	2	2	1	(0120)	10.130 044 2	20.7
4	0	4	3	1	3	(0120)	7.152 081 4	83.3
4	1	4	3	0	3	(0120)	7.230 741 8	−4.8
4	2	3	3	1	2	(0120)	9.364 150 1	11.3
4	3	1	3	2	1	(0120)	12.543 719 6	−14.3
4	3	1	3	2	2	(0120)	13.760 000 0	−306.6[a]
4	3	2	3	2	1	(0120)	11.610 033 0	70.6
4	4	0	3	3	0	(0120)	15.068 266 8	15.5
4	4	1	3	3	1	(0120)	13.742 602 9	−5.7
5	1	4	4	2	3	(0120)	10.138 905 5	−23.4
5	2	3	4	3	2	(0120)	10.253 736 0	20.5
5	2	4	4	1	3	(0120)	10.627 101 7	11.3
5	3	3	4	2	2	(0120)	13.118 406 9	4.7
5	4	1	4	3	1	(0120)	16.172 106 5	63.0
5	5	0	4	4	0	(0120)	18.696 094 4	19.8
5	5	1	4	4	1	(0120)	17.372 336 5	−39.8
6	2	4	5	3	3	(0120)	12.767 762 8	−16.9

Table 17.80. (continued)

J'	K'_a	K'_c	J	K_a	K_c	$(\sigma_1\sigma_2\sigma_3\sigma_4)$	$\nu_{\mathrm{Obs.}}$	$\nu_{\mathrm{Obs.}} - \nu_{\mathrm{Calc.}}$
upper level			lower level				GHz	kHz
6	2	5	5	1	4	(0120)	12.026 884 9	3.8
6	3	4	5	2	3	(0120)	14.321 659 4	5.0
6	4	3	5	3	2	(0120)	16.934 280 1	−48.0
6	5	1	5	4	1	(0120)	19.885 448 8	142.6[a]
6	5	2	5	4	2	(0120)	19.674 328 2	−116.1[a]
6	6	0	5	5	0	(0120)	22.323 433 1	−22.8
7	1	6	6	2	5	(0120)	13.525 013 6	−61.9[a]
7	2	6	6	1	5	(0120)	13.557 671 0	−7.1
7	3	5	6	2	4	(0120)	15.465 392 1	19.4
8	1	7	7	2	6	(0120)	15.129 592 6	−17.9
8	2	7	7	1	6	(0120)	15.136 525 2	−15.7
2	1	2	1	0	1	(0101)	4.355 072 7	18.4
3	0	3	2	1	2	(0101)	5.437 271 6	−14.2
3	1	3	2	0	2	(0101)	5.771 755 0	4.3
3	2	1	2	1	1	(0101)	9.204 011 5	42.9
3	3	0	2	2	0	(0101)	11.441 599 6	26.0
3	3	1	2	2	1	(0101)	10.130 801 2	53.3
4	0	4	3	1	3	(0101)	7.149 578 7	−19.1
4	1	4	3	0	3	(0101)	7.235 583 6	−12.5
4	2	3	3	1	2	(0101)	9.392 857 7	28.2
4	3	1	3	2	1	(0101)	12.553 320 6	−10.2
4	3	1	3	2	2	(0101)	13.801 309 4	−11.8
4	3	2	3	2	1	(0101)	11.593 211 1	107.3[a]
4	4	0	3	3	0	(0101)	15.068 605 7	−4.8
4	4	1	3	3	1	(0101)	13.741 296 5	7.3
5	1	4	4	2	3	(0101)	10.123 381 6	3.7
5	2	4	4	1	3	(0101)	10.650 946 9	17.7
5	3	3	4	2	2	(0101)	13.133 429 9	23.8
5	4	1	4	3	1	(0101)	16.161 005 4	−19.9
5	5	0	4	4	0	(0101)	18.696 098 2	−45.1
5	5	1	4	4	1	(0101)	17.371 254 4	−41.4
6	2	4	5	3	3	(0101)	12.718 144 9	55.3
6	2	5	5	1	4	(0101)	12.036 271 0	5.1
6	3	4	5	2	3	(0101)	14.366 178 3	8.2
6	5	1	5	4	1	(0101)	19.878 060 7	57.9
7	2	5	6	3	4	(0101)	14.840 737 0	12.9
7	2	6	6	1	5	(0101)	13.560 836 3	−8.3
7	3	5	6	2	4	(0101)	15.497 309 6	19.6
2	1	2	1	0	1	(0102)	4.355 793 3	6.5
3	0	3	2	1	2	(0102)	5.445 686 8	−22.6
3	1	3	2	0	2	(0102)	5.763 788 9	−5.0
3	2	1	2	1	1	(0102)	9.151 711 5	10.4
3	3	0	2	2	0	(0102)	11.481 285 5	35.0
3	3	1	2	2	1	(0102)	10.171 470 7	−35.5

Table 17.80. (continued)

J'	K'_a	K'_c	J	K_a	K_c	$(\sigma_1\sigma_2\sigma_3\sigma_4)$	$\nu_{\mathrm{Obs.}}$	$\nu_{\mathrm{Obs.}} - \nu_{\mathrm{Calc.}}$
upper level			lower level				GHz	kHz
4	0	4	3	1	3	(0102)	7.152 100 2	−7.4
4	1	4	3	0	3	(0102)	7.232 506 5	−18.0
4	2	3	3	1	2	(0102)	9.377 427 0	18.8
4	3	1	3	2	1	(0102)	12.500 293 1	0.5
4	3	1	3	2	2	(0102)	13.666 777 0	−33.9
4	3	2	3	2	1	(0102)	11.696 867 7	54.2
4	4	0	3	3	0	(0102)	15.108 958 0	9.9
4	4	1	3	3	1	(0102)	13.784 777 5	−6.6
5	1	4	4	2	3	(0102)	10.136 319 7	−25.4
5	2	4	4	1	3	(0102)	10.633 579 4	5.2
5	3	3	4	2	2	(0102)	13.149 085 2	0.7
5	4	1	4	3	1	(0102)	16.102 721 2	52.9
5	5	0	4	4	0	(0102)	18.736 732 0	−21.4
5	5	1	4	4	1	(0102)	17.413 793 4	−53.4
6	2	4	5	3	3	(0102)	12.752 066 0	−10.0
6	2	5	5	1	4	(0102)	12.029 612 3	−11.7
6	3	4	5	2	3	(0102)	14.335 661 4	−2.3
6	5	1	5	4	1	(0102)	19.832 003 3	139.7[a]
7	2	5	6	3	4	(0102)	14.856 307 9	−40.9
7	2	6	6	1	5	(0102)	13.558 969 1	−28.2
7	3	5	6	2	4	(0102)	15.472 185 6	3.4
2	1	2	1	0	1	(0001)	4.231 515 7	−2.4
2	2	0	1	1	1	(0001)	7.201 747 9	8.2
2	2	1	1	1	0	(0001)	6.288 284 4	6.5
3	0	3	2	1	2	(0001)	5.468 837 7	5.5
3	1	3	2	0	2	(0001)	5.689 515 6	−4.6
3	2	2	2	1	1	(0001)	7.892 802 2	8.3
3	3	0	2	2	1	(0001)	10.566 852 3	5.0
3	3	1	2	2	0	(0001)	10.071 391 5	−6.1
3	3	1	2	2	1	(0001)	10.396 509 4	−1.6
4	0	4	3	1	3	(0001)	7.152 542 3	2.5
4	1	4	3	0	3	(0001)	7.209 438 9	−0.1
4	2	3	3	1	2	(0001)	9.227 757 9	−0.9
4	3	1	3	2	2	(0001)	13.718 012 4	0.7
4	3	2	3	2	1	(0001)	11.773 098 3	0.9
4	4	0	3	3	0	(0001)	13.962 963 5	−0.5
4	4	0	3	3	1	(0001)	14.133 303 7	3.3
4	4	1	3	3	0	(0001)	13.803 480 8	−6.0
4	4	1	3	3	1	(0001)	13.973 820 3	−2.8
5	0	5	4	1	4	(0001)	8.773 751 9	0.4
5	1	4	4	2	3	(0001)	10.164 029 0	2.7
5	1	5	4	0	4	(0001)	8.786 032 8	−0.1
5	2	4	4	1	3	(0001)	10.542 984 2	−1.1
5	3	3	4	2	2	(0001)	13.076 773 5	−5.9
5	4	1	4	3	2	(0001)	16.806 082 2	−9.3

Table 17.80. (continued)

J'	K'_a	K'_c	J	K_a	K_c	$(\sigma_1\sigma_2\sigma_3\sigma_4)$	$\nu_{\text{Obs.}}$	$\nu_{\text{Obs.}} - \nu_{\text{Calc.}}$
upper level			lower level				GHz	kHz
5	4	2	4	3	1	(0001)	15.749261 5	3.9
5	5	0	4	4	0	(0001)	17.648765 7	−2.7
5	5	1	4	4	1	(0001)	17.614407 4	−0.9
6	0	6	5	1	5	(0001)	10.378255 3	0.4
6	1	5	5	2	4	(0001)	11.893882 3	−0.8
6	1	6	5	0	5	(0001)	10.380658 0	−0.6
6	2	4	5	3	3	(0001)	12.858326 5	−27.3[a]
6	2	5	5	1	4	(0001)	12.000982 5	2.4
6	3	4	5	2	3	(0001)	14.186480 0	−1.8
6	4	3	5	3	2	(0001)	17.161974 4	11.5
6	5	2	5	4	1	(0001)	19.635020 3	9.9
6	6	0	5	5	0	(0001)	21.314421 5	0.2
7	0	7	6	1	6	(0001)	11.979100 0	−0.1
7	1	6	6	2	5	(0001)	13.529139 9	0.3
7	1	7	6	0	6	(0001)	11.979542 2	−0.3
7	2	5	6	3	4	(0001)	14.895506 2	−33.6[a]
7	2	6	6	1	5	(0001)	13.554939 2	0.6
7	3	5	6	2	4	(0001)	15.386922 5	2.1
8	0	8	7	1	7	(0001)	13.579270 9	−1.1
8	1	7	7	2	6	(0001)	15.136579 6	1.4
8	2	7	7	1	6	(0001)	15.142206 9	1.2
9	0	9	8	1	8	(0001)	15.179352 4	−1.7
9	1	8	8	2	7	(0001)	16.737435 0	1.8
2	1	2	1	0	1	(0011)	4.232471 1	−2.8
2	2	0	1	1	1	(0011)	7.197475 6	11.2
2	2	1	1	1	0	(0011)	6.291574 8	−2.3
3	0	3	2	1	2	(0011)	5.467861 7	5.2
3	1	3	2	0	2	(0011)	5.690125 9	−2.5
3	2	2	2	1	1	(0011)	7.893608 4	4.4
3	3	0	2	2	1	(0011)	10.540013 4	2.6
3	3	1	2	2	0	(0011)	10.095350 9	−2.3
4	0	4	3	1	3	(0011)	7.152101 4	0.5
4	1	4	3	0	3	(0011)	7.209469 3	−1.2
4	2	3	3	1	2	(0011)	9.229609 9	−1.5
4	3	1	3	2	2	(0011)	13.714111 7	3.9
4	3	2	3	2	1	(0011)	11.774930 2	−0.5
4	4	0	3	3	1	(0011)	14.050814 2	−0.1
4	4	1	3	3	0	(0011)	13.882064 3	−3.1
5	0	5	4	1	4	(0011)	8.773463 0	1.1
5	1	4	4	2	3	(0011)	10.162027 4	0.3
5	2	4	4	1	3	(0011)	10.543877 6	−0.3
5	3	3	4	2	2	(0011)	13.078359 6	−1.7
5	4	1	4	3	2	(0011)	16.785924 3	−9.0
5	4	2	4	3	1	(0011)	15.764700 1	0.2
5	5	1	4	4	0	(0011)	17.602186 2	−1.5

Table 17.80. (continued)

J'	K'_a	K'_c	J	K_a	K_c	$(\sigma_1\sigma_2\sigma_3\sigma_4)$	$\nu_{\text{Obs.}}$	$\nu_{\text{Obs.}} - \nu_{\text{Calc.}}$
upper level			lower level				GHz	kHz
6	1	5	5	2	4	(0011)	11.892 772 9	−2.1
7	0	7	6	1	6	(0011)	11.978 846 3	2.2
7	2	6	6	1	5	(0011)	13.554 342 6	1.6
8	0	8	7	1	7	(0011)	13.579 015 5	0.9
2	1	2	1	0	1	(0012)	4.230 292 5	−1.7
2	2	0	1	1	1	(0012)	7.214 408 9	11.5
2	2	1	1	1	0	(0012)	6.273 477 4	−0.1
3	0	3	2	1	2	(0012)	5.469 077 4	−0.9
3	1	3	2	0	2	(0012)	5.688 789 6	−1.6
3	3	0	2	2	1	(0012)	10.623 006 6	3.2
3	3	1	2	2	0	(0012)	10.012 447 4	−4.6
3	3	1	2	2	1	(0012)	10.361 851 2	2.1
4	0	4	3	1	3	(0012)	7.152 382 4	0.7
4	1	4	3	0	3	(0012)	7.209 042 1	−0.2
4	2	3	3	1	2	(0012)	9.225 205 8	−1.9
4	3	1	3	2	2	(0012)	13.728 336 7	−2.6
4	3	2	3	2	1	(0012)	11.758 439 6	−0.8
4	4	0	3	3	0	(0012)	13.991 567 7	−4.3
4	4	1	3	3	0	(0012)	13.680 386 3	−1.7
4	4	1	3	3	1	(0012)	13.941 542 8	0.5
5	0	5	4	1	4	(0012)	8.773 502 2	−0.4
5	2	4	4	1	3	(0012)	10.541 396 7	0.8
5	3	3	4	2	2	(0012)	13.071 191 0	−1.3
5	4	1	4	3	2	(0012)	16.854 568 1	−23.7[a]
5	4	2	4	3	1	(0012)	15.696 205 8	9.9
5	5	0	4	4	0	(0012)	17.667 521 0	−4.0
6	1	5	5	2	4	(0012)	11.893 252 2	−3.9
6	2	5	5	1	4	(0012)	11.999 939 9	1.6
7	0	7	6	1	6	(0012)	11.978 829 7	−2.8
7	2	6	6	1	5	(0012)	13.554 071 9	0.4
8	0	8	7	1	7	(0012)	13.579 003 4	−1.6
2	1	2	1	0	1	(0111)	4.365 492 0	35.7
3	0	3	2	1	2	(0111)	5.428 960 4	−29.2
3	1	3	2	0	2	(0111)	5.781 973 1	20.6
3	2	1	2	1	1	(0111)	9.210 454 4	23.0
3	3	0	2	2	0	(0111)	11.461 659 8	87.6
3	3	1	2	2	1	(0111)	10.151 501 8	94.2
4	0	4	3	1	3	(0111)	7.147 806 4	−18.8
4	1	4	3	0	3	(0111)	7.239 257 6	−1.9
4	2	3	3	1	2	(0111)	9.415 288 3	61.0
4	3	1	3	2	1	(0111)	12.535 660 0	−54.6
4	3	1	3	2	2	(0111)	13.776 509 3	−101.9
4	3	2	3	2	1	(0111)	11.624 906 4	162.9
4	4	0	3	3	0	(0111)	15.087 844 9	66.7

Table 17.80. (continued)

J'	K'_a	K'_c	J	K_a	K_c	$(\sigma_1\sigma_2\sigma_3\sigma_4)$	$\nu_{\mathrm{Obs.}}$	$\nu_{\mathrm{Obs.}} - \nu_{\mathrm{Calc.}}$
upper level			lower level				GHz	kHz
4	4	1	3	3	1	(0111)	13.7605789	59.2
5	1	4	4	2	3	(0111)	10.1114325	−20.3
5	2	4	4	1	3	(0111)	10.6680222	45.0
5	3	3	4	2	2	(0111)	13.1554932	59.2
5	4	1	4	3	1	(0111)	16.1173492	−100.5
5	5	0	4	4	0	(0111)	18.7146802	39.4
5	5	1	4	4	1	(0111)	17.3897023	17.8
6	1	5	5	2	4	(0111)	11.8820946	−13.5
6	2	4	5	3	3	(0111)	12.6782380	−20.1
6	2	5	5	1	4	(0111)	12.0427671	19.7
6	3	4	5	2	3	(0111)	14.3980842	61.2
6	5	1	5	4	1	(0111)	19.8433179	−2.0
7	1	6	6	2	5	(0111)	13.5244992	−14.8
7	2	5	6	3	4	(0111)	14.8259318	−25.3
7	2	6	6	1	5	(0111)	13.5626756	−1.4
7	3	5	6	2	4	(0111)	15.5191567	58.0
2	1	2	1	0	1	(0122)	4.3445870	33.8
3	0	3	2	1	2	(0122)	5.4439704	−8.0
3	1	3	2	0	2	(0122)	5.7622475	−14.7
3	2	1	2	1	1	(0122)	9.1968681	21.2
3	3	0	2	2	0	(0122)	11.4207708	−45.4
3	3	1	2	2	1	(0122)	10.1096405	−35.8
4	0	4	3	1	3	(0122)	7.1506448	77.2
4	1	4	3	0	3	(0122)	7.2319452	−17.8
4	2	3	3	1	2	(0122)	9.3706445	−23.2
4	3	1	3	2	1	(0122)	12.5682962	23.6
4	3	1	3	2	2	(0122)	13.8255967	69.3
4	3	2	3	2	1	(0122)	11.5555068	−61.1
4	4	0	3	3	0	(0122)	15.0475728	−70.3
4	4	1	3	3	1	(0122)	13.7204484	−76.0
5	1	4	4	2	3	(0122)	10.1320764	4.0
5	2	4	4	1	3	(0122)	10.6346177	−16.6
5	3	3	4	2	2	(0122)	13.1081824	−64.3
5	4	1	4	3	1	(0122)	16.1943213	72.0
5	5	0	4	4	0	(0122)	18.6747235	−97.1
5	5	1	4	4	1	(0122)	17.3501928	−111.9
6	2	4	5	3	3	(0122)	12.7508230	77.6
6	2	5	5	1	4	(0122)	12.0292638	−12.3
6	3	4	5	2	3	(0122)	14.3348785	−55.0
6	5	1	5	4	1	(0122)	19.9019613	105.9
7	1	6	6	2	5	(0122)	13.5238579	−24.8
7	2	6	6	1	5	(0122)	13.5576718	−102.5

[a] Not included in the fit.

17.2.7 Dimethylcyclopropane-1,1-Dicarboxylate

Table 17.81. Nuclear coordinates in the principal inertial axes of the conformers of dimethylcyclopropane-1,1-dicarboxylate (CPC) calculated at the MP2/6-311++G(d,p) level of theory. The atoms are numbered according to Figure 16.1.

	Conformer I			**Conformer II**			**Conformer III**		
	a /Å	b /Å	c /Å	a /Å	b /Å	c /Å	a /Å	b /Å	c /Å
H1	−2.687490	−2.100941	0.537934	−3.526075	−0.996479	−0.936883	3.738912	−0.529190	0.981489
H2	−2.350818	−2.662119	−1.132130	−4.206035	−0.432994	0.625224	4.346082	0.331705	−0.471252
H3	−3.356778	−1.204364	−0.847612	−3.131962	−1.867919	0.563860	3.599724	−1.292609	−0.619901
H4	2.687499	−2.100985	−0.537896	3.255574	−1.573788	−0.630530	−3.739042	−0.529225	−0.981414
H5	2.350744	−2.662177	1.132141	2.893244	−2.462782	0.883700	−4.346023	0.331692	0.471389
H6	3.356720	−1.204428	0.847684	3.600741	−0.814561	0.943688	−3.599611	−1.292601	0.619979
H7	−0.695907	2.395467	1.400171	−1.139589	1.833126	1.510028	0.937708	2.031130	−1.247087
H8	0.695992	2.395430	−1.400192	0.488131	2.531185	−1.062911	−0.937849	2.030799	1.247185
H9	−1.123862	2.414954	−1.074898	−1.323973	2.174632	−0.972063	0.907368	2.025748	1.261119
H10	1.123991	2.414824	1.074942	0.665945	2.203325	1.416112	−0.907488	2.026098	−1.260796
C11	−2.509223	−1.794566	−0.494312	−3.347681	−0.888256	0.134505	3.585107	−0.342868	−0.083040
C12	2.509171	−1.794614	0.494341	2.927627	−1.485379	0.406512	−3.585086	−0.342876	0.083092
C13	−1.281405	0.081240	0.172328	−1.084848	−0.380410	−0.189133	1.254218	−0.361543	0.136786
C14	1.281394	0.081210	−0.172352	1.401813	0.202348	−0.125214	−1.254203	−0.361604	−0.136864
C15	0.126947	2.155057	0.737335	−0.229566	1.839352	0.924158	0.013158	1.774413	−0.746753
C16	−0.126838	2.155072	−0.737311	−0.333527	2.042329	−0.553096	−0.013224	1.774217	0.746905
C17	−0.000004	0.829789	−0.000008	−0.021844	0.652306	−0.013667	−0.000029	0.441712	−0.000084
O18	−1.294334	−1.032014	−0.584550	−2.253178	0.012825	0.371905	2.334294	0.332249	−0.298159
O19	1.294285	−1.032063	0.584522	1.578863	−0.992201	0.460520	−2.334267	0.332285	0.298002
O20	−2.222558	0.462329	0.837891	−0.953501	−1.412196	−0.810589	1.319740	−1.462283	0.634961
O21	2.222570	0.462273	−0.837887	2.296733	0.866971	−0.607480	−1.319710	−1.462415	−0.634881

Table 17.82. Coefficients of the two-dimensional Fourier expansion for the potential energy surface of CPC calculated at the MP2/6-311++G(d,p) level of theory in a grid of 10° around the dihedral angles $\varphi_1 = \angle(O_{18},C_{13},C_{17},C_{14})$ and $\varphi_2 = \angle(O_{19},C_{14},C_{17},C_{13})$ (see Figure 16.3). The dihedral angles $\varphi_3 = \angle(C_{11},O_{18},C_{13},C_{17})$ and $\varphi_4 = \angle(C_{12},O_{19},C_{14},C_{17})$ were allowed to relax starting from the value of 180°. The potential is expanded as $V(\varphi_1,\varphi_2) = \sum_{i=1}^{46} V_i \cdot f_i$.

i	f_i	V_i/Hartree
1	1	−57.2800850
2	$\cos(1\varphi_1)+\cos(1\varphi_2)$	−0.0012040
3	$\cos(2\varphi_1)+\cos(2\varphi_2)$	−0.0021183
4	$\cos(3\varphi_1)+\cos(3\varphi_2)$	0.0003985
5	$\cos(4\varphi_1)+\cos(4\varphi_2)$	−0.0001791
6	$\cos(5\varphi_1)+\cos(5\varphi_2)$	0.0000198
7	$\cos(6\varphi_1)+\cos(6\varphi_2)$	−0.0000333
8	$\cos(1\varphi_1)\cos(1\varphi_2)$	0.0003930
9	$\sin(1\varphi_1)\sin(1\varphi_2)$	−0.0000987
10	$\cos(2\varphi_1)\cos(1\varphi_2)+\cos(1\varphi_1)\cos(2\varphi_2)$	0.0001450
11	$\sin(2\varphi_1)\sin(1\varphi_2)+\sin(1\varphi_1)\sin(2\varphi_2)$	0.0000186
12	$\cos(3\varphi_1)\cos(1\varphi_2)+\cos(1\varphi_1)\cos(3\varphi_2)$	−0.0000219
13	$\sin(3\varphi_1)\sin(1\varphi_2)+\sin(1\varphi_1)\sin(3\varphi_2)$	−0.0000298
14	$\cos(4\varphi_1)\cos(1\varphi_2)+\cos(1\varphi_1)\cos(4\varphi_2)$	−0.0000425
15	$\cos(5\varphi_1)\cos(1\varphi_2)+\cos(1\varphi_1)\cos(5\varphi_2)$	0.0000182
16	$\cos(5\varphi_1)\cos(1\varphi_2)+\cos(1\varphi_1)\cos(5\varphi_2)$	0.0000177
17	$\sin(5\varphi_1)\sin(1\varphi_2)+\sin(1\varphi_1)\sin(5\varphi_2)$	−0.0000051
18	$\cos(6\varphi_1)\cos(1\varphi_2)+\cos(1\varphi_1)\cos(6\varphi_2)$	−0.0000031
19	$\sin(6\varphi_1)\sin(1\varphi_2)+\sin(1\varphi_1)\sin(6\varphi_2)$	0.0000109
20	$\cos(2\varphi_1)\cos(2\varphi_2)$	0.0026965
21	$\sin(2\varphi_1)\sin(2\varphi_2)$	−0.0028250
22	$\cos(3\varphi_1)\cos(2\varphi_2)+\cos(2\varphi_1)\cos(3\varphi_2)$	0.0001231
23	$\sin(3\varphi_1)\sin(2\varphi_2)+\sin(2\varphi_1)\sin(3\varphi_2)$	−0.0001289
24	$\cos(4\varphi_1)\cos(2\varphi_2)+\cos(2\varphi_1)\cos(4\varphi_2)$	0.0000848
25	$\sin(4\varphi_1)\sin(2\varphi_2)+\sin(2\varphi_1)\sin(4\varphi_2)$	−0.0002538
26	$\cos(5\varphi_1)\cos(2\varphi_2)+\cos(2\varphi_1)\cos(5\varphi_2)$	−0.0000807
27	$\sin(5\varphi_1)\sin(2\varphi_2)+\sin(2\varphi_1)\sin(5\varphi_2)$	0.0001111
28	$\cos(6\varphi_1)\cos(2\varphi_2)+\cos(2\varphi_1)\cos(6\varphi_2)$	−0.0000047
29	$\sin(3\varphi_1)\sin(3\varphi_2)$	0.0000059
30	$\cos(4\varphi_1)\cos(3\varphi_2)+\cos(3\varphi_1)\cos(4\varphi_2)$	0.0000150
31	$\sin(4\varphi_1)\sin(3\varphi_2)+\sin(3\varphi_1)\sin(4\varphi_2)$	0.0000199
32	$\cos(5\varphi_1)\cos(3\varphi_2)+\cos(3\varphi_1)\cos(5\varphi_2)$	−0.0000200
33	$\sin(5\varphi_1)\sin(3\varphi_2)+\sin(3\varphi_1)\sin(5\varphi_2)$	0.0000158
34	$\cos(6\varphi_1)\cos(3\varphi_2)+\cos(3\varphi_1)\cos(6\varphi_2)$	−0.0000032
35	$\sin(6\varphi_1)\sin(3\varphi_2)+\sin(3\varphi_1)\sin(6\varphi_2)$	0.0000046
36	$\cos(4\varphi_1)\cos(4\varphi_2)$	−0.0000086
37	$\sin(4\varphi_1)\sin(4\varphi_2)$	−0.0000066
38	$\cos(5\varphi_1)\cos(4\varphi_2)+\cos(4\varphi_1)\cos(5\varphi_2)$	−0.0000354
39	$\sin(5\varphi_1)\sin(4\varphi_2)+\sin(4\varphi_1)\sin(5\varphi_2)$	0.0000395
40	$\cos(6\varphi_1)\cos(4\varphi_2)+\cos(4\varphi_1)\cos(6\varphi_2)$	0.0000056
41	$\sin(6\varphi_1)\sin(4\varphi_2)+\sin(4\varphi_1)\sin(6\varphi_2)$	−0.0000078
42	$\cos(5\varphi_1)\cos(5\varphi_2)$	−0.0000021
43	$\sin(5\varphi_1)\sin(5\varphi_2)$	0.0000044
44	$\sin(6\varphi_1)\sin(5\varphi_2)+\sin(5\varphi_1)\sin(6\varphi_2)$	0.0000032
45	$\cos(6\varphi_1)\cos(6\varphi_2)$	0.0000125
46	$\sin(6\varphi_1)\sin(6\varphi_2)$	−0.0000108

Table 17.83. Fourier coefficients of the potential function for a rotation of the methyl group of conformer I of CPC around the dihedral angle $\varphi_5 = \angle(H_1,C_{11},O_{18},C_{13})$ calculated in 2° steps calculated with the basis set 6-311++G(d,p) and different methods (see Figure 16.4). The potential is expanded as $V(\varphi) = a_0 + \sum_{n=3}^{6} a_n \cdot \cos(n \cdot \varphi)$.

	MP2		**B3YLP**		**HF**	
	Hartree	cm^{-1}	Hartree	cm^{-1}	Hartree	cm^{-1}
a_0	−572.284 700 042		−573.817 179 083		−570.498 947 710	
a_3	0.001 080 807	237.2	0.000 666 352	146.2	0.001 063 384	233.4
a_6	−0.000 015 584	−3.4	−0.000 018 919	−4.2	−0.000 022 820	−5.0

Table 17.84. Coefficients of the two-dimensional Fourier expansion for the potential energy surface of conformer I of CPC calculated at the MP2/6-311++G(d,p) level of theory obtained by rotating the two methyl groups in a step width of 10° around the dihedral angles $\varphi_5 = \angle(H_1,C_{11},O_{18},C_{13})$ and $\varphi_6 = \angle(H_4,C_{12},O_{19},C_{14})$ (see Figure 16.5). Due to symmetry, only data points in the range from $\varphi_1 = 0°$ to 120° and $\varphi_2 = 0°$ to 120° were needed. The potential is expanded as $V(\varphi_5,\varphi_6) = \sum_{i=1}^{10} V_i \cdot f_i$.

i	f_i	V_i/Hartree
1	1	−572.283 595 915
2	$\sin(3\varphi_5) + \sin(3\varphi_6)$	0.000 081 284
3	$\cos(3\varphi_5) + \cos(3\varphi_6)$	0.001 084 607
4	$\sin(6\varphi_5) + \sin(6\varphi_6)$	−0.000 020 995
5	$\cos(6\varphi_5) + \cos(6\varphi_6)$	−0.000 011 780
6	$\cos(3\varphi_5)\cos(3\varphi_6)$	0.000 010 673
7	$\sin(3\varphi_5)\sin(3\varphi_6)$	0.000 007 992
8	$\cos(3\varphi_5)\sin(3\varphi_6) + \sin(3\varphi_5)\cos(3\varphi_6)$	0.000 002 768
9	$\cos(3\varphi_5)\sin(6\varphi_6) + \sin(3\varphi_5)\cos(6\varphi_6)$	−0.000 000 584
10	$\cos(6\varphi_5)\sin(3\varphi_6) + \sin(6\varphi_5)\cos(3\varphi_6)$	−0.000 000 601

Table 17.85. The rotational constants A, B, and C in GHz, the deviations (Dev.) between the experimental and calculated rotational constants in MHz, the angles between the internal rotor axis and the principal axes of inertia $\angle(i_1,a)$, $\angle(i_1,b)$, $\angle(i_1,c)$ of one methyl rotor, the deviations (Dev.) between the experimental and calculated internal rotor axis, and the barriers to internal rotation V_3 of conformer I of CPC in cm^{-1} calculated using various methods and basis sets. The angle relations are: $\angle(i_2,a) = 180° - \angle(i_1,a)$, $\angle(i_2,b) = \angle(i_1,b)$, $\angle(i_2,c) = 180° - \angle(i_1,c)$. Harmonic frequency calculations were carried out to verify the nature of the stationary points.

Method/Basis set	*A*	Dev.	*B*	Dev.	*C*	Dev.	$\angle(i_1,a)$	Dev.	$\angle(i_1,b)$	Dev.	$\angle(i_1,c)$	Dev.	V_3/cm^{-1}
B3LYP													
cc-pVTZ	1.434	8	0.977	1	0.671	4	32.30	3.11	57.84	−3.15	87.28	0.39	202
cc-pVDZ	1.436	6	0.975	3	0.659	16	31.07	4.35	59.05	−4.37	87.54	0.13	293
6-311++G(3df,3pd)	1.432	10	0.975	3	0.674	1	32.69	2.72	57.46	−2.77	87.22	0.45	283
6-311++G(df,pd)	1.425	17	0.976	2	0.674	1	33.08	2.33	57.07	−2.39	87.13	0.54	291
6-311++G(d,p)	1.421	21	0.973	4	0.673	2	33.08	2.33	57.09	−2.40	87.07	0.60	196
6-311++G	1.372	70	0.969	8	0.669	6	34.78	0.63	55.42	−0.73	86.70	0.97	294
6-311+G(3df,3pd)	1.432	10	0.975	3	0.674	1	32.68	2.73	57.46	−2.78	87.22	0.45	283
6-311+G(df,pd)	1.425	17	0.976	1	0.674	1	33.09	2.32	57.06	−2.37	87.14	0.53	291
6-311+G(d,p)	1.421	21	0.974	4	0.673	2	33.08	2.33	57.08	−2.40	87.09	0.58	203
6-311+G	1.371	70	0.970	8	0.669	6	34.81	0.61	55.39	−0.70	86.74	0.93	292
6-311G(3df,3pd)	1.436	6	0.979	−1	0.671	4	32.27	3.14	57.86	−3.17	87.34	0.33	300
6-311G(df,pd)	1.436	6	0.980	−2	0.667	8	32.07	3.34	58.07	−3.38	87.33	0.34	293
6-311G(d,p)	1.433	9	0.977	1	0.666	9	32.03	3.39	58.12	−3.43	87.25	0.42	189
6-311G	1.377	65	0.971	7	0.666	9	34.47	0.95	55.75	−1.06	86.61	1.06	291
6-31++G(3df,3pd)	1.428	14	0.972	6	0.672	3	32.53	2.88	57.62	−2.93	87.23	0.44	298
6-31++G(df,pd)	1.422	20	0.971	6	0.668	7	32.59	2.82	57.55	−2.87	87.27	0.40	289
6-31++G(d,p)	1.422	20	0.970	8	0.667	8	32.42	2.99	57.73	−3.04	87.20	0.47	141
6-31++G	1.371	71	0.965	12	0.665	9	34.57	0.84	55.62	−0.93	86.80	0.87	257
6-31+G(df,pd)	1.422	20	0.971	6	0.668	7	32.61	2.81	57.54	−2.85	87.28	0.39	234
6-31+G(d,p)	1.421	21	0.970	8	0.667	8	32.44	2.97	57.71	−3.02	87.21	0.46	134
6-31+G	1.370	72	0.966	12	0.665	9	34.63	0.78	55.56	−0.87	86.80	0.87	301
6-31G(3df,3pd)	1.435	7	0.977	1	0.668	6	31.97	3.44	58.16	−3.47	87.36	0.31	246
6-31G(df,pd)	1.441	1	0.973	5	0.661	14	30.94	4.47	59.16	−4.48	87.67	0.00	245
6-31G(d,p)	1.440	2	0.971	7	0.660	15	30.79	4.62	59.33	−4.64	87.56	0.11	257
6-31G	1.381	61	0.965	13	0.662	13	33.65	1.76	56.54	−1.86	86.82	0.85	277

Table 17.85. (continued)

Method/Basis set	*A*	Dev.	*B*	Dev.	*C*	Dev.	∠(i$_1$,a)	Dev.	∠(i$_1$,b)	Dev.	∠(i$_1$,c)	Dev.	V_3/cm^{-1}
MP2													
cc-pVTZ	1.470	−28	0.977	1	0.671	3	30.01	5.40	60.17	−5.48	87.04	0.63	
cc-pVDZ	1.454	−12	0.971	6	0.662	13	29.74	5.67	60.41	−5.72	87.28	0.39	
6-311++G(df,pd)	1.454	−12	0.979	−1	0.683	−8	31.70	3.72	58.54	−3.85	86.51	1.16	397
6-311++G(d,p)	1.438	4	0.975	3	0.681	−6	32.29	3.12	57.96	−3.27	86.41	1.26	411
6-311++G	1.351	91	0.970	8	0.677	−2	36.22	−0.80	54.04	0.65	86.29	1.37	266
6-311+G(df,pd)	1.453	−11	0.979	−1	0.683	−9	31.76	3.66	58.48	−3.79	86.53	1.14	
6-311+G(d,p)	1.437	5	0.975	3	0.682	−7	32.33	3.08	57.91	−3.22	86.43	1.24	386
6-311+G	1.349	93	0.970	8	0.677	−3	36.12	−0.71	54.21	0.48	85.74	1.93	399
6-311G(3df,3pd)	1.469	−28	0.982	−4	0.673	2	30.35	5.06	59.81	−5.12	87.16	0.51	
6-311G(df,pd)	1.480	−39	0.979	−1	0.668	6	29.30	6.11	60.84	−6.15	87.37	0.30	476
6-311G(d,p)	1.463	−21	0.974	4	0.667	7	29.94	5.47	60.22	−5.53	87.22	0.45	
6-311G	1.367	75	0.954	24	0.676	−2	36.45	−1.04	53.67	1.02	87.38	0.29	
6-31++G(3df,3pd)	1.463	−22	0.980	−2	0.676	−2	30.75	4.66	59.44	−4.75	86.93	0.74	
6-31++G(df,pd)	1.443	−1	0.981	−3	0.681	−6	32.10	3.31	58.13	−3.44	86.57	1.10	474
6-31++G(d,p)	1.427	15	0.977	1	0.679	−4	32.57	2.84	57.67	−2.98	86.44	1.23	
6-31++G	1.340	101	0.959	19	0.669	6	35.72	−0.30	54.59	0.09	85.90	1.77	
6-31+G(3df,3pd)	1.463	−21	0.979	−1	0.677	−2	30.75	4.66	59.43	−4.75	86.93	0.74	
6-31+G(df,pd)	1.442	0	0.981	−3	0.682	−7	32.13	3.28	58.09	−3.41	86.59	1.08	433
6-31+G(d,p)	1.426	16	0.977	1	0.680	−5	32.66	2.76	57.59	−2.90	86.41	1.26	218
6-31+G	1.339	103	0.959	19	0.670	5	35.87	−0.46	54.45	0.24	85.84	1.83	
6-31G(3df,3pd)	1.476	−34	0.983	−5	0.669	5	29.60	5.81	60.54	−5.85	87.43	0.24	
6-31G(df,pd)	1.472	−30	0.980	−2	0.670	5	29.57	5.84	60.57	−5.88	87.38	0.29	353
6-31G(d,p)	1.454	−12	0.974	4	0.669	6	30.22	5.19	59.95	−5.26	87.10	0.57	409
6-31G	1.355	87	0.951	27	0.666	9	34.57	0.84	55.76	−1.08	85.78	1.89	
Experiment	1.442		0.978		0.675		35.41		54.69		87.67		407

Table 17.86. Observed frequencies ($\nu_{\mathrm{Obs.}}$) of the (00), (01), (11), and (12) torsional species of conformer I of CPC. $\nu_{\mathrm{Obs.}} - \nu_{\mathrm{Calc.}}$ values as obtained after a fit with XIAM.

J'	K_a'	K_c'	J	K_a	K_c	$(\sigma_1\sigma_2)$	$\nu_{\mathrm{Obs.}}$	$\nu_{\mathrm{Obs.}} - \nu_{\mathrm{Calc.}}$
upper level			lower level				GHz	kHz
2	2	0	1	1	1	(00)	5.4109297	−0.4
						(01)	5.4110850	2.6
						(11)	5.4107171	−2.7
						(12)	5.4117430	−0.6
2	2	1	1	1	0	(00)	5.0004350	−1.7
						(01)	5.0000773	−0.5
						(11)	5.0002327	−1.3
						(12)	4.9992083	−1.7
3	0	3	2	1	2	(00)	4.3267608	−1.8
						(01)	4.3267612	0.0
						(12)	4.3267780	2.0
3	1	3	2	0	2	(00)	4.7126480	−0.1
						(01)	4.7126154	−0.6
						(12)	4.7125751	2.5
3	2	1	2	1	2	(01)	7.7294791	2.7
						(11)	7.7292994	−0.9
						(12)	7.7294917	−15.3[a]
3	2	2	2	1	1	(00)	6.3498411	−0.1
						(01)	6.3496860	−0.2
						(11)	6.3496387	−0.3
						(12)	6.3494236	0.2
3	3	0	2	2	1	(00)	8.1199254	0.5
						(01)	8.1221081	0.3
						(11)	8.1195884	−0.3
						(12)	8.1276847	0.2
3	3	1	2	2	0	(00)	7.9870259	0.5
						(01)	7.9845048	0.1
						(11)	7.9866850	−0.9
						(12)	7.9785897	−0.8
4	0	4	3	1	3	(00)	5.8023213	0.9
						(01)	5.8023077	1.1
						(12)	5.8022993	−2.2
4	1	3	3	2	2	(00)	5.8975142	8.6
						(01)	5.8975599	3.4
4	1	4	3	0	3	(00)	5.9627730	−0.3
						(11)	5.9627465	15.2[a]
						(12)	5.9627150	0.6
4	2	3	3	1	2	(00)	7.5456382	−0.6
						(01)	7.5455256	−0.2
						(12)	7.5453686	−0.7
4	3	1	3	2	2	(00)	10.0703167	−1.3
						(01)	10.0705192	0.7
						(11)	10.0699678	2.0
						(12)	10.0714638	−0.3
4	3	2	3	2	1	(00)	9.4357023	−0.7

Table 17.86. (continued)

J'	K'_a	K'_c	J	K_a	K_c	$(\sigma_1\sigma_2)$	$\nu_{\text{Obs.}}$	$\nu_{\text{Obs.}} - \nu_{\text{Calc.}}$
upper level			lower level				GHz	kHz
						(01)	9.435 146 3	−0.8
						(11)	9.435 343 0	−1.4
						(12)	9.433 844 5	−1.4
4	4	0	3	3	1	(00)	10.952 254 0	0.9
						(01)	10.962 174 5	0.6
						(11)	10.951 786 2	0.8
						(12)	10.977 075 7	−0.1
4	4	1	3	3	0	(00)	10.921 651 3	−0.1
						(01)	10.911 262 5	0.6
						(11)	10.921 182 5	0.8
						(12)	10.895 893 0	1.5
5	0	5	4	1	4	(00)	7.203 546 2	−0.9
						(01)	7.203 528 2	6.4
5	1	5	4	0	4	(00)	7.260 122 3	−0.5
						(01)	7.260 100 3	−6.6
5	2	4	4	1	3	(00)	8.653 834 8	−1.2
						(01)	8.653 744 2	0.2
						(11)	8.653 677 2	−0.6
5	3	2	4	2	3	(00)	12.381 565 8	−2.7
						(01)	12.381 478 7	0.1
						(11)	12.381 194 7	0.1
						(12)	12.381 568 7	−13.8[a]
5	3	3	4	2	2	(00)	10.670 395 7	−0.7
						(01)	10.670 117 8	−0.5
						(11)	10.670 038 8	−1.0
						(12)	10.669 640 1	−0.6
5	4	1	4	3	2	(00)	12.719 377 6	−0.2
						(01)	12.721 714 2	0.3
						(11)	12.718 895 3	0.5
						(12)	12.728 179 9	−0.7
5	4	2	4	3	1	(00)	12.512 252 4	−0.7
						(01)	12.509 428 0	−0.5
						(11)	12.511 758 6	0.1
						(12)	12.502 474 8	0.9
5	5	0	4	4	1	(00)	13.824 473 8	1.5
						(01)	13.844 603 4	0.9
						(11)	13.823 874 2	1.0
5	5	1	4	4	0	(00)	13.818 578 0	0.8
						(01)	13.797 848 5	0.9
						(11)	13.817 977 6	0.1
6	0	6	5	1	5	(00)	8.571 241 7	−0.4
						(01)	8.571 184 3	−1.2
6	1	5	5	2	4	(00)	9.339 273 3	−2.4
						(01)	9.339 242 8	0.2
						(11)	9.339 194 9	2.8
						(12)	9.339 220 9	−5.9

Table 17.86. (continued)

J'	K'_a	K'_c	J	K_a	K_c	$(\sigma_1\sigma_2)$	$\nu_{\mathrm{Obs.}}$	$\nu_{\mathrm{Obs.}} - \nu_{\mathrm{Calc.}}$
upper level			lower level				GHz	kHz
6	1	6	5	0	5	(00)	8.589296 0	−0.8
6	2	4	5	3	3	(01)	8.986039 0	0.6
6	2	5	5	1	4	(00)	9.782336 6	0.1
						(01)	9.782259 3	−0.7
						(11)	9.782196 1	−3.2
						(12)	9.782169 6	1.8
6	3	3	5	2	4	(01)	15.153174 4	−2.0
						(11)	15.152927 3	−0.9
						(12)	15.153059 4	−1.6
6	3	4	5	2	3	(00)	11.729133 7	−0.3
						(01)	11.728931 2	−0.2
						(11)	11.728811 0	3.1
						(12)	11.728649 1	−0.9
6	4	2	5	3	3	(00)	14.660982 8	−0.3
						(01)	14.661306 3	0.6
						(11)	14.660491 5	−1.2
						(12)	14.662749 4	0.0
6	4	3	5	3	2	(00)	13.913009 2	0.1
						(01)	13.912180 9	−0.5
						(11)	13.912488 1	−1.0
						(12)	13.910233 4	0.6
6	5	1	5	4	2	(00)	15.530831 8	0.7
						(01)	15.541603 1	0.4
						(11)	15.530214 7	0.5
						(12)	15.559276 1	0.1
6	5	2	5	4	1	(00)	15.478848 4	0.0
						(01)	15.467458 0	0.3
						(11)	15.478227 1	0.5
						(12)	15.449166 6	1.0
6	6	0	5	5	1	(00)	16.706141 1	0.4
						(01)	16.733480 3	−9.9[a]
						(11)	16.705411 8	1.2
6	6	1	5	5	0	(00)	16.705111 6	0.9
						(01)	16.704381 0	0.5
7	0	7	6	1	6	(00)	9.926388 9	−0.1
7	1	6	6	2	5	(00)	10.818643 4	−2.9
						(01)	10.818599 1	2.2
7	1	7	6	0	6	(00)	9.931802 2	0.8
7	2	5	6	3	4	(00)	11.027429 2	5.6
						(01)	11.027427 6	−1.7
7	2	6	6	1	5	(00)	10.996988 4	0.8
						(01)	10.996921 0	−2.8
						(12)	10.996848 9	1.4
7	3	4	6	2	5	(00)	18.357500 5	−1.3
						(01)	18.357248 5	−0.6
7	3	5	6	2	4	(00)	12.694597 6	1.1

Table 17.86. (continued)

J'	K'_a	K'_c	J	K_a	K_c	$(\sigma_1\sigma_2)$	$\nu_{\text{Obs.}}$	$\nu_{\text{Obs.}} - \nu_{\text{Calc.}}$
upper level			lower level				GHz	kHz
						(01)	12.694431 8	−0.2
						(11)	12.694315 0	2.5
						(12)	12.694223 5	0.8
7	4	3	6	3	4	(00)	16.943391 5	−0.1
						(01)	16.943306 9	−0.3
						(11)	16.942896 2	−0.6
						(12)	16.943549 4	1.0
7	4	4	6	3	3	(00)	15.065290 7	1.1
						(01)	15.064861 7	−0.2
7	5	2	6	4	3	(00)	17.293208 9	0.3
						(01)	17.296175 4	0.0
						(11)	17.292580 0	0.1
						(12)	17.304407 3	0.3
7	5	3	6	4	2	(00)	17.048912 9	0.5
						(01)	17.045306 4	−0.3
						(11)	17.048262 7	0.3
						(12)	17.036437 6	0.6
7	6	1	6	5	2	(00)	18.397501 5	−0.1
						(01)	18.420323 6	−0.7
7	6	2	6	5	1	(00)	18.386353 5	0.8
						(01)	18.362780 7	0.2
7	7	0	6	6	1	(00)	19.589602 3	0.8
						(11)	19.588741 0	0.2
7	7	1	6	6	0	(00)	19.589432 3	0.0
8	0	8	7	1	7	(00)	11.277379 7	−0.3
8	1	7	7	2	6	(00)	12.220071 2	0.1
						(01)	12.220015 9	10.5[a]
8	1	8	7	0	7	(00)	11.278935 1	0.3
8	2	7	7	1	6	(00)	12.284347 8	−1.5
8	3	5	7	4	4	(00)	11.990246 0	0.8
						(01)	11.990424 6	0.0
8	3	6	7	2	5	(00)	13.684343 7	−1.5
						(01)	13.684208 5	0.2
8	4	4	7	3	5	(00)	19.697487 5	−2.0
						(01)	19.697283 7	0.6
						(11)	19.696964 0	0.0
8	4	5	7	3	4	(00)	16.006733 5	−0.6
						(01)	16.006425 1	−0.1
						(11)	16.006247 8	3.4
						(12)	16.005988 3	0.2
8	5	3	7	4	4	(00)	19.212122 5	0.1
						(01)	19.212649 8	0.5
						(11)	19.211493 4	−0.4
						(12)	19.214829 8	0.5
8	5	4	7	4	3	(00)	18.422803 6	0.6
						(01)	18.421619 3	−1.2

Table 17.86. (continued)

J'	K'_a	K'_c	J	K_a	K_c	$(\sigma_1\sigma_2)$	$\nu_{\mathrm{Obs.}}$	$\nu_{\mathrm{Obs.}} - \nu_{\mathrm{Calc.}}$
upper level			lower level				GHz	kHz
						(11)	18.422 119 0	−0.7
						(12)	18.418 784 4	−1.4
8	6	2	7	5	3	(00)	20.099 605 6	−0.2
						(01)	20.112 159 2	−0.2
						(11)	20.098 840 2	−0.2
						(12)	20.133 340 0	−0.4
8	6	3	7	5	2	(00)	20.035 400 0	0.7
						(01)	20.022 076 6	0.2
						(11)	20.034 625 7	0.1
						(12)	20.000 126 4	−0.4
8	7	1	7	6	2	(00)	21.278 364 2	0.3
						(11)	21.277 484 4	0.4
8	7	2	7	6	1	(00)	21.276 195 3	−0.4
						(11)	21.275 314 2	−1.2
8	8	0	7	7	1	(00)	22.473 310 1	0.0
						(11)	22.472 317 9	−1.1
8	8	1	7	7	0	(00)	22.473 284 2	0.7
						(11)	22.472 291 3	−1.0
9	1	8	8	2	7	(00)	13.587 619 2	−1.1
						(01)	13.587 509 3	−3.3
9	2	7	8	3	6	(00)	14.408 489 5	−1.5
						(01)	14.408 420 3	1.0
						(12)	14.408 364 1	0.3
9	2	8	8	1	7	(00)	13.609 127 9	−1.3
9	3	6	8	4	5	(00)	14.258 356 3	1.6
						(01)	14.258 389 8	0.3
9	3	7	8	2	6	(00)	14.789 168 2	−0.7
						(01)	14.789 051 8	−2.0
						(12)	14.788 921 4	−0.3
9	4	6	8	3	5	(00)	16.833 294 9	−0.5
						(01)	16.833 045 0	0.0
						(11)	16.832 863 1	−0.5
						(12)	16.832 725 9	0.0
9	5	4	8	4	5	(00)	21.450 089 3	0.4
						(01)	21.450 039 4	1.3
						(11)	21.449 474 2	1.8
						(12)	21.450 502 2	1.2
9	5	5	8	4	4	(00)	19.521 767 4	−0.3
						(01)	19.521 157 8	−0.7
9	6	3	8	5	4	(00)	21.850 120 9	−0.4
						(01)	21.854 065 3	0.3
						(11)	21.849 347 0	0.2
						(12)	21.864 740 3	0.6
9	6	4	8	5	3	(00)	21.593 196 6	−0.7
						(01)	21.588 463 0	−1.6
						(11)	21.592 394 6	2.1

Table 17.86. (continued)

J'	K'_a	K'_c	J	K_a	K_c	$(\sigma_1\sigma_2)$	$\nu_{\text{Obs.}}$	$\nu_{\text{Obs.}} - \nu_{\text{Calc.}}$
upper level			lower level				GHz	kHz
						(12)	21.5769990	−2.9
9	7	3	8	6	2	(00)	22.9509247	−1.1
						(11)	22.9500239	−1.2
10	0	10	9	1	9	(00)	13.9765038	2.2
10	1	9	9	2	8	(00)	14.9423987	0.2
10	2	8	9	3	7	(00)	15.8607281	−1.0
						(01)	15.8606451	6.0
						(12)	15.8605586	−8.0
10	2	9	9	1	8	(00)	14.9492278	0.7
10	3	7	9	4	6	(00)	16.2504025	−2.0
						(01)	16.2503628	0.0
10	3	8	9	2	7	(00)	16.0109726	−1.3
						(01)	16.0108704	−5.5
						(12)	16.0107682	8.9
10	4	7	9	3	6	(00)	17.6745506	8.1
						(01)	17.6743330	−1.2

[a] Not included in the fit.